BRITISH GEOLOGICAL SURVEY

TECHNICAL REPORT
WM/00/17R

Geomagnetism Series

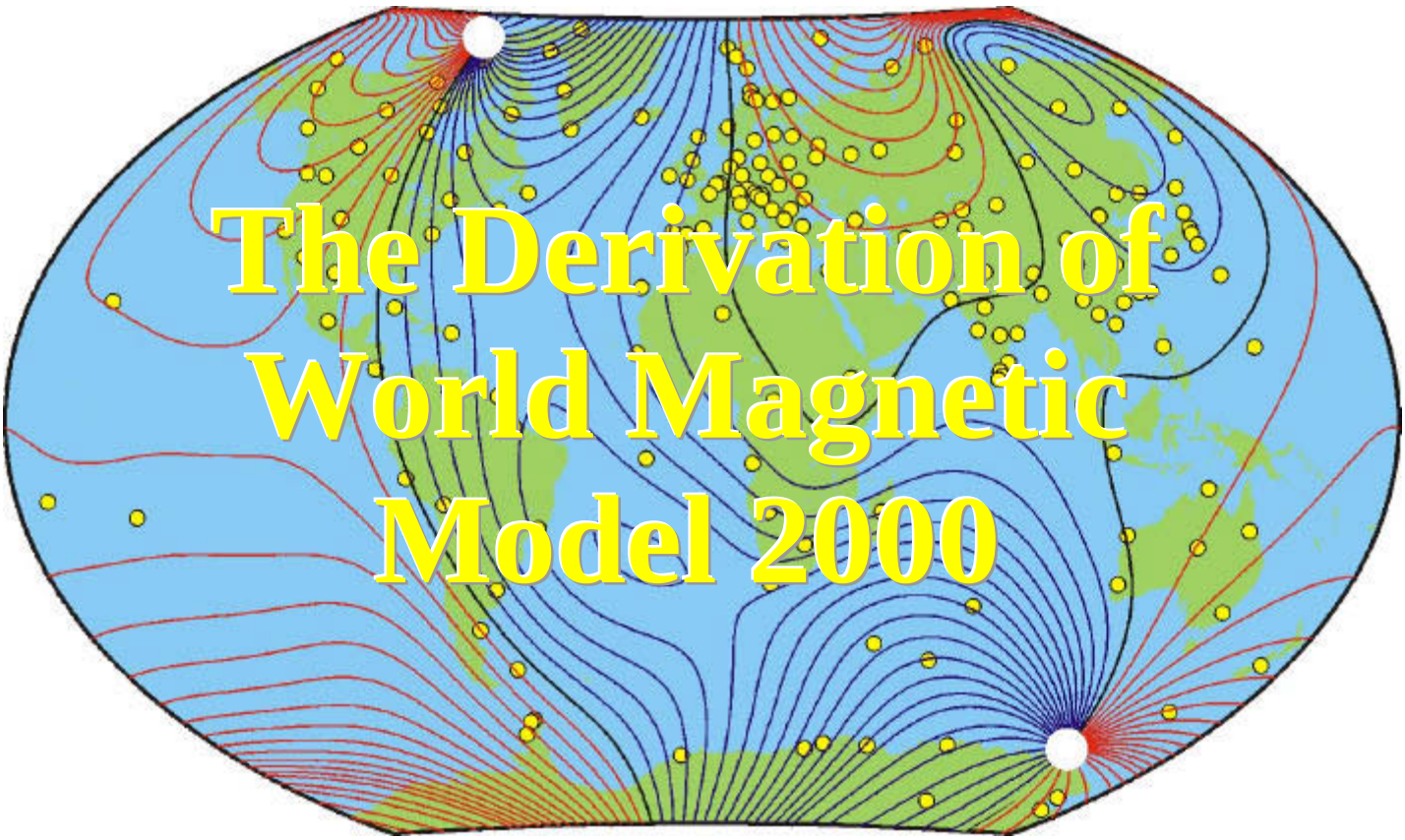

The Derivation of World Magnetic Model 2000

Susan Macmillan and John M. Quinn*
(* at United States Geological Survey)

British Geological Survey

USGS science for a changing world

BRITISH GEOLOGICAL SURVEY
TECHNICAL REPORT WM/00/17R

Geomagnetism Series

The Derivation of World Magnetic Model 2000

Susan Macmillan and John M. Quinn[*]
([*] at United States Geological Survey)

Bibliographic reference

Macmillan, S. and J. M. Quinn, 2000. The Derivation of World Magnetic Model 2000. *British Geological Survey Technical Report* WM/00/17R.

 British Geological Survey, Edinburgh, January 2000

Contents

Abstract

This report contains a detailed summary of the data used, the modelling techniques employed and the results obtained in the production of the World Magnetic Model 2000. This model is designed for use in air and sea navigation systems and is valid till 2005.0.

The derivation of World Magnetic Model 2000 has been the joint responsibility of the British Geological Survey (BGS) and the United States Geological Survey (USGS). The World Magnetic Model is the standard model in UK Ministry of Defence and US Department of Defense, the North Atlantic Treaty Organization (NATO), and the World Hydrographic Office (WHO) navigation and attitude/heading referencing systems. It is also used widely in civilian navigation systems.

1 Introduction

The earth's magnetic field is a vector quantity, **B**, dependent on position ***r*** and time *t*, and it may be expressed as the vector sum of the contributions from three main sources: the main field generated in the earth's core ($\mathbf{B}_m$), the crustal field from local rocks ($\mathbf{B}_c$), and a combined disturbance field from electrical currents flowing in the upper atmosphere and magnetosphere, which also induce electrical currents in the sea and the ground ($\mathbf{B}_d$), i.e.

$$\mathbf{B}(\boldsymbol{r}, t) = \mathbf{B}_m(\boldsymbol{r}, t) + \mathbf{B}_c(\boldsymbol{r}) + \mathbf{B}_d(\boldsymbol{r}, t) \quad (1)$$

$\mathbf{B}_m$ accounts for over 95% of the field strength at the earth's surface, and it varies slowly with time. It is this field that is represented by the World Magnetic Model, a series of spherical harmonic models designed for use in air and sea navigation systems. World Magnetic Model 2000 (WMM2000) comprises a main-field model for epoch 2000.0 and a predictive secular-variation model for the period 2000.0 to 2005.0. A revised 1995.0 epoch model has also been derived.

Three 5-year average secular-variation models were required for the production of the WMM2000 valid for the periods 1990.0-1995.0, 1995.0-2000.0 and 2000.0-2005.0 respectively. The first two models are used to reduce the main-field data to epoch and the last model allows computation of main-field values after 2000.0. The secular-variation models are based mainly on geomagnetic observatory data.

The main-field model for 2000.0 is based mainly on scalar data from the Danish satellite Ørsted. Vector data in the magnetic equatorial area are provided by a revised version of a model produced for WMM-95, reduced to epoch.

The field arising from magnetised crustal rocks, $\mathbf{B}_c$, has spatial variations with wavelengths of the order of metres to thousands of kilometres but is much smaller in magnitude than the main field. The magnetisation may be either induced (by the main magnetic field) or remanent or a combination of both. As the time scales used in the

production of the WMM2000 are of the order of years it is assumed that the crustal field does not vary with time.

The field arising from currents flowing in the ionosphere and magnetosphere and their resultant induced currents in the crust, $\mathbf{B}_d$, varies both with location and time. These various current systems are shown in Figure 1. The disturbance field can vary both regularly, with a fundamental period of one day, and irregularly on time scales of seconds to days. The regular variations are called diurnal variations and they are essentially generated by the daylit atmosphere in the region 100-130 km, ionised by the Sun's radiation, being moved in the earth's main field by winds and tides, thus producing the necessary conditions (motion of a conductor in a magnetic field) for a dynamo to operate. The irregular variations are called magnetic storms and these generally have three phases: an initial phase, often with sudden commencement, a main phase, and a recovery phase. The main phase is primarily caused by plasma within the magnetosphere resulting in ring currents lying in the equatorial plane. Magnetic storms are generally more severe at high geomagnetic latitudes where the ionised region of the upper atmosphere, the ionosphere, is coupled to the magnetosphere by field-aligned currents and is therefore strongly influenced by the interplanetary magnetic field and current systems in the magnetotail. Both the regular and irregular disturbance field variations are modulated by season and the solar cycle. The disturbance field is often called the external field as its main source, the ionosphere, is external to the surface of the earth where most geomagnetic measurements are made. However, this term can be confusing and is avoided when using satellite data as the ionosphere is below the altitude of these data and is therefore effectively internal to this observation surface.

For further information about the crustal and disturbance fields (and general information about geomagnetism) see Merrill *et al* (1996) and Parkinson (1983).

The geomagnetic field vector, **B**, is described by the orthogonal components X (northerly intensity), Y (easterly intensity) and Z (vertical intensity, positive downwards); total intensity F; horizontal intensity H; inclination (or dip) I (the angle between the horizontal plane and the field vector, measured positive downwards) and declination (or magnetic variation) D (the horizontal angle between true north and the

field vector, measured positive eastwards). Declination, inclination and total intensity can be computed from the orthogonal components using the equations

$$D = \arctan\frac{Y}{X} \qquad I = \arctan\frac{Z}{H} \qquad F = \sqrt{H^2 + Z^2} \tag{2}$$

where H is given by

$$H = \sqrt{X^2 + Y^2}\ .$$

2 Data acquisition and quality control

2.1 Observatories

A geomagnetic observatory is where vector observations of the earth's magnetic field are recorded accurately and continuously, with a time resolution of one minute or less, over a long period of time. The site of the observatory must be magnetically clean and remain so for the foreseeable future.

There are three categories of instruments at an observatory. The first category comprises variometers, which make continuous measurements of elements of the geomagnetic field vector. Both analogue and digital variometers require temperature-controlled environments and can generally operate without manual intervention. They are also required to be installed on extremely stable platforms. The most common type of variometer nowadays is the triaxial fluxgate magnetometer, an example of which is shown in Figure 2.

The second category comprises absolute instruments which can make measurements of the magnetic field in terms of absolute physical basic units or universal physical constants. The most common types of absolute instrument are the fluxgate theodolite for measuring D and I and the proton precession magnetometer for measuring F (see Figure 3). In the former the basic unit is an angle. The fluxgate sensor mounted on the telescope of a non-magnetic theodolite is used to detect when the it is perpendicular to the magnetic field vector. With the fluxgate sensor operating in null-field mode the stability of the sensor and its electronics is maximised. True north is determined by reference to a fixed mark of known azimuth. In a proton precession magnetometer the universal physical constant is the gyromagnetic ratio of the proton. Measurements with a fluxgate theodolite can only be made manually whilst a proton magnetometer can operate automatically.

The third category comprises semi-absolute measurements. These are instruments which measure deviations from a field, which is determined on a regular basis using an absolute instrument. An example is a proton vector magnetometer where artificial

bias fields are applied to a proton precession magnetometer sensor to obtain vector measurements (see Figure 4). Like variometers, they are temperature-sensitive and require stable platforms. For more information on magnetic instrumentation and operation of magnetic observatories the reader is referred to Jankowski and Sucksdorff (1996).

The locations of currently operating magnetic observatories are shown in Figure 5. It can be seen that the spatial distribution of the observatories is rather uneven, with a concentration in Europe and a dearth elsewhere in the world, particularly in the ocean areas. This uneven distribution is well demonstrated by plotting the number of observatory annual means for each year from 1900 onwards by hemisphere, as in Figure 6.

BGS and USGS operate nineteen observatories altogether. BGS operates Lerwick, Eskdalemuir and Hartland in the UK, Ascension Island in the Atlantic Ocean, Port Stanley in the Falkland Islands and Sable Island, offshore Nova Scotia, Canada. USGS operates Point Barrow, College and Sitka in Alaska; Boulder, Del Rio, Fredericksburg, Fresno, Newport, Tucson and Bay St Louis in conterminous USA; Honolulu in Hawaii; San Juan in Puerto Rico and Guam in the west Pacific. Two more will become operational in 2000 at Midway Island and at Adak, Alaska.

BGS and USGS also actively collect global observatory data through their involvement in INTERMAGNET. The objectives of INTERMAGNET are to establish a global network of cooperating digital magnetic observatories, to adopt modern standard specifications for measuring and recording equipment, and to facilitate data exchange and the production of geomagnetic products in close to real time. Both BGS and USGS operate INTERMAGNET GINs (Geomagnetic Information Nodes) of which there are six in total, and play a leading role in the INTERMAGNET organisation. BGS also actively collects observatory data through its involvement in the World Data Centre system which includes maintaining a database of global data suitable for secular-variation modelling, maintaining contacts with all organisations operating magnetic observatories and collaborating with the other World Data Centres for geomagnetism. Each year requests are sent to all

organisations operating observatories for the latest annual mean values and other relevant information.

The quality of the data an observatory produces is the responsibility of the operator and for global modelling purposes the most important aspect of this is the stability of the baselines. A baseline is the difference between the calibrated variometer data and the absolute observations. A baseline with many points, low scatter, few drifts and offsets is a sign of good quality.

Quality control measures, other than those carried out by the observatory operators, are also carried out by INTERMAGNET through its observatory standardisation programme and by BGS's and USGS's participation in IAGA (International Association of Geomagnetism and Aeronomy) Observatory Workshops. The BGS World Data Centre quality control procedures include checking the data from each observatory when they are added to the global database by looking for large internal inconsistencies (for example when $F^2 \neq X^2 + Y^2 + Z^2$) and making secular-variation plots (see Figure 7) in order to identify any jumps. If there are any problems the data are marked as preliminary and an enquiry is sent to the observatory operator.

2.2 Satellite data

The principal characteristic of satellite data is its global distribution within a relatively short time span. The inclination of the orbit (the angle between the plane containing the satellite's path and the earth's equatorial plane) determines the latitudinal extent of the data coverage; an inclination of 90° provides 100% coverage, an inclination of slightly less or slightly more than 90° results in small regions around the geographic poles absent of data. Another important characteristic of satellite data is that the crustal field is largely attenuated.

As the earth has an equatorial bulge the satellite orbit precesses very slowly in inertial space. However the orbital parameters can be chosen so that the earth's rotation brings each longitude under the orbital plane and the resulting data distribution, over a short period of time, is global. One drawback is that all observations at one latitude may have nearly the same local time for an extended period of time. A sun-

synchronous orbit is an orbit plane fixed relative to the sun and hence in local time. The implications of this type of orbit is that modelling the regular external fields, which are dependent on local time, is made more difficult although at least the contribution from these variations is approximately constant from one orbit to another. The satellite Magsat, which made an accurate vector magnetic survey in 1979 and 1980, is an example of a near sun-synchronous orbit with dawn and dusk being the local times sampled (Langel & Hinze, 1998).

2.2.1 Ørsted

The primary purpose of the Danish satellite Ørsted is to provide data for accurate global magnetic field modelling. It was successfully launched on 23 February 1999 from Vandenburg Air Force Base in California on a Delta II rocket along with the American ARGOS (Advanced Research Global Observation Satellite) and the South African micro-satellite SUNSAT.

The satellite has a mass of 62 kg and measures 34x45x72 cm when the boom is stowed. The main instruments carried are a Compact Spherical Coil (CSC) fluxgate magnetometer, a variometer measuring three orthogonal components of the magnetic field; an Overhauser magnetometer, an absolute instrument measuring the strength of the magnetic field; and a star imager camera for determining the orientation of the fluxgate magnetometer. These three instruments are mounted at the end of a 8 m boom to minimise magnetic disturbance from within the satellite body (see Figure 8). In the main body there are two other important instruments: a charged particle detector and a Global Positioning System (GPS) receiver. Attitude control is done passively by the boom and actively by magnetotorquer coils. Power is generated by solar panels and there are batteries on board for when the satellite is in the night sector. Accurate time is provided by GPS. Communication with ground control is by S-band (2.2 GHz) transmitter and receiver. The main receiving station is at the Danish Meteorological Institute in Copenhagen.

The satellite was launched into a retrograde orbit with the ascending node at start of mission being 14:11 local time, apogee ~850 km, perigee ~640 km, inclination 96.5°,

nodal period 99.6 minutes, longitude increment -24.9°/orbit and local time increment -0.88 minutes/day. The satellite velocity is approximately 7.5 km/second. It is hoped that the mission will last at least 14 months.

Although data recovery from the Overhauser magnetometer has been very high there have been a number of problems obtaining oriented vector data from the CSC fluxgate magnetometer and the star camera.. When the boom was deployed on 14th March its orientation relative to the satellite body was about 50° different from its intended orientation. Over the following two months this decreased to 40° as the boom extended further and tightened the boom release wire. One consequence of this was that the sun was in the star camera's field of view more often than anticipated, especially in the first few months of the mission, and orientation fixes were unobtainable. Faulty attitude data was therefore sent to the attitude control system and the satellite orbit was destabilised and the star camera was unable to obtain a star fix. The only solution to this negative feedback problem was manual intervention from ground control.

Radiation hits have had quite a significant effect as a result of the mission being close to solar maximum due to the three-year delay in the launch. This particularly affects passes over the so-called South Atlantic anomaly where the protection given to the satellite from damage due to exposure to charged particles in the radiation belts surrounding the earth, by the earth's main field, is weakest. The star camera is particularly sensitive to radiation hits and this leads to faulty data being transmitted to the attitude control system. Again, the satellite orbit is destabilised and the star camera is unable to obtain attitude data. By turning down the resolution of the star camera the impact of radiation hits over the South Atlantic anomaly has been reduced, however there has been some loss of accuracy with the attitude data.

Other problems with the vector data include uncertainty with the time stamp associated with the attitude data, thermal boom oscillations resulting in smearing of the images of the stars and a further loss of accuracy with the attitude data, and a 50% loss of so-called house-keeping data in the first six months of the mission. This includes important data such as temperature which is required for correcting the CSC fluxgate data.

As a result of all these problems with the vector data it was decided not to attempt to use them in the World Magnetic Model and to only use the Overhauser magnetometer data.

2.2.2 POGS

The Polar Orbiting Geomagnetic Survey (POGS) satellite was a project of the Naval Oceanographic Office and the U. S. Space Test Programme, and was launched from Vandenburg Air Force Base in April 1990. Instrumentation included a triaxial fluxgate magnetometer on a 8 ft boom and sun sensors for attitude determination. Its orbit was approximately circular with period 98.6 minutes, an average altitude 688 km and inclination 89.9° (Quinn *et al*, 1993). Useful data were collected between January 1991 and October 1993 and during this time all local times were sampled. However it has not been possible to use the vector data from this satellite because no provision was made for accurate attitude determination. Even the total intensity data derived from the magnetometer observations were far from ideal because no provision was made for in-flight calibration with an absolute instrument, due to cost. Consequently, ad-hoc methods, for example comparing the satellite data with high-quality ground-based data from West European geomagnetic observatories, were imposed to account for the fluxgate magnetometer thermal drift. The onboard crystal clock drift rate was not smooth. There were sporadic jumps in the drift rate associated with changes in the crystal's molecular-dislocation structure, making it difficult to calibrate. Other difficulties encountered during its three-year mission included the unexpected initial orientation of the satellite's antennae away from the earth, and the three-month communication blackout, and hence data loss, due to solar radiation damaging the part of the satellite's memory holding the down-link schedule. Although the orientation problem could have been corrected by using the satellite's torquer coils, it was felt that this might snap off the magnetometer boom which had already been deployed. So, a complete redesign of the ground station antennae pattern was performed, taking nine months, with much loss of data (Quinn *et al*, 1995).

2.3 Repeat stations

A repeat station is a permanently marked site where high-quality vector observations of the earth's magnetic field are made for a few hours (sometimes a few days), every few years, the more frequently the better. Their main purpose is to track secular variation and, if accurate observational techniques and careful reduction procedures are followed, they can be a cost-effective way of supplementing observatory data for secular-variation modelling.

The instrumentation used in the UK repeat station survey is shown in Figure 3. The instruments are essentially the same as those used at magnetic observatories for absolute observations though they include a gyro-attachment for the theodolite for the determination of true north.

An important aspect of repeat station data reduction procedures is the correction for the transient external field variations. As none of the UK repeat stations is significantly remote from any of the UK observatories these variations are observed and corrected for with observatory data. Elsewhere, especially for repeat stations in areas of complex external fields such as the auroral zones or remote from geomagnetic observatories, on-site variometers are sometimes run to monitor these variations.

BGS actively collects repeat station data from around the world as part of its World Data Centre activities. On receipt these data are checked by comparison with an existing model and with existing data for that site. Figure 9 shows the distribution of repeat stations with at least two occupations since 1990. For more information about repeat station practice see Newitt *et al*, 1996.

2.4 Other data

2.4.1 Aeromagnetic surveys

Most aeromagnetic surveys are designed for looking at the crustal field. As a result they are flown at altitudes lower than 300 m, they cover small areas, generally once only, with very high spatial resolution. Because of the difficulty in making accurately

oriented measurements of the magnetic field on a moving platform, these kinds of aeromagnetic surveys generally comprise total intensity data only. Their use in global main-field modelling has never really been explored for these reasons. However, between 1953 and 1994 the U.S. Navy under the Project MAGNET programme collected high-level three-component aeromagnetic data specifically for world magnetic modelling purposes. The surveys are mainly over the ocean areas of the earth, at mid to low latitudes, at altitudes up to 25,000 ft although low-level calibration flights over geomagnetic observatories were carried out at the beginning and end of each survey. A variety of platforms and instrumentation have been used but the most recent set-up included a fluxgate vector magnetometer mounted on a rigid beam in the magnetically clean rear part of the aircraft, a ring laser gyro fixed at the other end of the beam, and a scalar magnetometer located in the stinger extending several feet behind the aircraft's tail section (Coleman, 1991). Figure 10 shows the distribution of Project MAGNET data.

2.4.2 Marine surveys

Marine magnetic surveys are also invariably designed to look at the crustal field but with careful processing it is possible to obtain main-field information from them. In a marine magnetic survey a scalar magnetometer is towed some distance behind a ship, usually along with other geophysical equipment, as it makes either a systematic survey of an area or traverses an ocean. When two such magnetometers with a fixed separation are towed, one behind another, it is possible to isolate the temporal variations along the survey track to leave the main field and crustal field. Along-track filtering can then be used to reduce the crustal field signal. Figure 11 shows the distribution of marine magnetic data from 1990 onwards available in the public domain.

3 Data selection for WMM2000

In deriving the World Magnetic Model the main field and the secular variation are modelled separately. This strategy means that different data can be used for main-field and secular-variation modelling, thereby optimising their different strengths. As it is a model intended for navigation it is necessary that it gives magnetic field values for dates for some time into the future. Its ability to predict secular variation is therefore very important. Not all data types are suitable for secular-variation prediction and, in addition, some data types are better than others for minimising contributions from crustal and external field variations. BGS is primarily responsible for secular-variation modelling and USGS for main-field modelling. However, during the modelling process there is feedback between the two modelling groups.

3.1 Data for secular-variation modelling

Given that secular variation in many parts of the world is quite small the data requirements for secular-variation modelling and prediction in approximate order of importance are that

(1) they are based on high-quality absolute observations,
(2) if they are surface data, they have been measured at exactly the same location through time so that they are uncontaminated by crustal fields when differences are taken between data at different times,
(3) the most recent data are available to minimise the errors caused by prediction,
(4) they have been measured over continuous periods of time or near other data measured over continuous periods of time that are long relative to the periods of the disturbance field variations so that these effects can be evaluated and eliminated,
(5) they are evenly distributed over the globe, and
(6) they have been measured over a long period of time (greater than one year) so that future predictions can be more confidently made based on the historical records.

Data from magnetic observatories satisfy requirements (1), (2), (3), (4) and (6) and, to a lesser extent, so do repeat station data. The observatories and repeat stations, however, do not cover the ocean areas of the earth and even their distribution on land is far from ideal. To satisfy requirement (5) secular-variation information has been extracted from models based on satellite data. Particular emphasis is placed on requirement (3) for both observatories and repeat stations. The recent conversion of many magnetic observatories from analogue to digital operation, often through the INTERMAGNET programme, has helped considerably in this respect. The acquisition and data quality control procedures for global observatory and repeat station data at the World Data Centre for geomagnetism at BGS ensures, to some extent, that requirements (1) and (3) are met.

A total of 190 observatories was used and their positions are shown in Figure 12. The disturbance field variations are greatly reduced by using annual means of observatory data. This is demonstrated in the power spectral plot of 85 years of hourly mean values of the horizontal intensity from Eskdalemuir observatory (Figure 13). All the significant peaks in the power spectral plot occur at periods 1 year (corresponding to a frequency of 1.14×10^{-4} hour^{-1}) or less, and they are all attributable to disturbance field sources.

As regards recent data in the models, 70 observatories had their latest annual means for 1998, 76 for 1997, 11 for 1996 and the remainder for 1995 and before. The recent temporal distribution of observatory data is shown in Figure 14. Unfortunately the observatories in the areas of the world where there are few others are, in some cases, experiencing the greatest difficulties in producing timely data and this is demonstrated in Figure 15. If an observatory has moved for any reason, the data recorded at the original site can often be adjusted to the new site using measured site differences.

Repeat stations were also used for secular-variation modelling. Annual secular-variation estimates were made by taking the difference between the data from two consecutive occupations and dividing by the number of years. Outliers were identified and rejected by comparison of the secular-variation estimates with an existing global model. In an attempt to alleviate the very uneven global distribution, only three repeat station estimates were selected per equal-area tessera. The tesseral dimensions are

fixed in latitude at 5° but vary in longitude from 5° at the equator to 120° near the poles. The distribution of selected repeat stations is shown in Figure 16.

Equal-area tesserae with dimension 10° in latitude, which have neither observatory nor repeat-station data, were filled with secular-variation estimates derived from a secular-variation model incorporating satellite data. The data locations are shown in Figure 17. Details of the models used to compute these synthetic data are given later.

3.2 Data for main-field modelling

For a snapshot model of the present main field the data requirements are slightly different from those for secular-variation modelling. The main emphasis is the availability of recent data with a good global coverage and with minimal crustal field and disturbance field contamination. Ørsted satellite data satisfy these requirements. The crustal field is largely attenuated at the altitude of the satellite and, with the exception of the auroral and polar areas, disturbance field effects at these altitudes are small. By selecting data during the night-side passes and using global disturbance indices, the disturbance field effects can be further reduced. The time interval selected for modelling extended from 11 March 1999 through 31 May 1999 since this was the only time interval for which preliminary magnetic activity indices were available for data selection. The selected data were divided into eight 10-day or 11-day subsets depending on the number of days per month. Each subset had sufficient data to generate an independent model.

However there is a problem if only scalar data are available, as in the case of Ørsted, and that is the indeterminate nature of the sectorial harmonics. This is commonly called the Backus effect and results in spurious short-wavelength features around the dip equator. To overcome this problem vector data in the region of the dip equator must be incorporated into the model. Project MAGNET is a suitable source of data for this purpose. They are included by generating a 4-degree by 4-degree synthetic data set at the mean epoch of each of the eight satellite data subsets from a model that incorporates the Project MAGNET data. Four degrees is the approximate longitudinal separation at the equator of the satellite survey tracks in each of the eight data subsets.

4 Modelling method

4.1 Secular-variation prediction

Prediction of secular variation to 2005.0 was made using linear predictor filters applied to first differences of observatory annual means in *X*, *Y* and *Z*. The historic time series of secular-variation values is characterised in terms of frequencies present by using maximum entropy spectral analysis. The characterisation consists of a finite number of poles that best represents the power spectrum in the *z*-transform plane where *z* is mapped from complex frequency *f* by the relation $z \equiv e^{2\pi i f \Delta}$, Δ being the sampling interval in the time domain. The Nyquist interval on the real axis of the *f*-plane maps one-to-one onto the unit circle in the complex *z*-plane. These poles correspond to infinite power spectral density on the unit *z*-circle, i.e. at real frequencies in the Nyquist interval. Such poles provide an accurate representation of the underlying power spectrum, especially if it has sharp, discrete lines. The coefficients of a finite series in the *z*-transform plane which is representative of the power spectrum can be found by comparison of the series with the *z*-transform of the Fourier transform of the autocorrelations in the time domain. These coefficients form the coefficients of a linear filter. The filter is then used to extrapolate the time series beyond its last secular-variation value. Linear prediction is especially successful at extrapolating signals which are smooth and oscillatory, though not necessarily periodic. Any dominant frequencies in the original time series are therefore preserved in the forecast.

As this characterisation requires the secular-variation values to be evenly spaced, any missing values in the secular-variation records were replaced with estimates obtained by linear interpolation if the gap was no more than five years long; otherwise, the earlier part of the record was discarded. In addition, annual means which were not computed from a full twelve months of data were adjusted using the neighbouring annual means so that the resulting secular-variation values were at exactly one year intervals. Some very noisy parts of other records, especially in the vertical component (*Z*), were also discarded.

The predictions were plotted for each observatory and checked manually to see that they were reasonable. These plots are shown in Figures 18 – 187, ordered by latitude, north to south. In these plots the solid line is the observed secular variation, the middle dotted line is the output from the linear predictor, the two outer dotted lines indicate the estimated 1-σ error envelope, and the dashed line is the values synthesised from the final annual secular-variation spherical harmonic models. As many observatories started in the late 1950s with the International Geophysical Year in 1957, only the data after 1955 are shown. However, if earlier data exist they were also used to build the linear prediction filters. Along the top of each plot there is the IAGA code, the observatory name, the latitude, the longitude and the time span of data used.

Data from the 20 observatories which had time series too short for the application of linear prediction filters were used by simply computing average secular-variation estimates and assuming that these do not change with time.

Prediction of secular variation at the repeat stations was made either by taking a mean of the secular-variation estimates or, if there were enough recent estimates (more than three since 1988.0), making linear regression fits to the observed average annual secular-variation values at the mid-dates between occupations.

4.2 Model parameterisation

In a source-free region near the surface of the earth the magnetic field **B** is the negative gradient of a scalar potential *V*, i.e.

$$\mathbf{B} = -\nabla V(r, \theta, \lambda, t) \tag{3}$$

which satisfies Laplace's equation

$$\nabla^2 V(r, \theta, \lambda, t) = 0 \tag{4}$$

where the spherical coordinates (r, θ, λ) correspond to the radial distance from the centre of the earth, the geocentric colatitude (90° - latitude) and the longitude, and t is the time. A solution to Laplace's equation in spherical coordinates is

$$V(r,\theta,\lambda,t) = a\sum_{n=1}^{ni_{\max}}\left(\frac{a}{r}\right)^{n+1}\sum_{m=0}^{n}(g_n^m(t)\cdot\cos m\lambda + h_n^m(t)\cdot\sin m\lambda)\cdot P_n^m(\theta)$$
$$\Sigma \qquad + a\sum_{n=1}^{ne_{\max}}\left(\frac{r}{a}\right)^{n}\sum_{m=0}^{n}(q_n^m(t)\cdot\cos m\lambda + s_n^m(t)\cdot\sin m\lambda)\cdot P_n^m(\theta) \tag{5}$$

where a is the mean radius of the earth (6371.2 km); $g_n^m(t)$ and $h_n^m(t)$ are the internal Gauss coefficients at time t; $q_n^m(t)$ and $s_n^m(t)$ are the external Gauss coefficients at time t and $P_n^m(\theta)$ are the Schmidt-normalised associated Legendre functions of degree n and order m. The Gauss coefficients are functions of time and for navigation purposes the internal ones are assumed to vary at a constant rate for the next five-year period:

$$g_n^m(t) = g_n^m + \dot{g}_n^m\cdot(t-t_0) \qquad t_0 \le t \le t_0+5$$
$$h_n^m(t) = h_n^m + \dot{h}_n^m\cdot(t-t_0) \qquad t_0 \le t \le t_0+5 \tag{6}$$

where g_n^m and h_n^m are the main-field coefficients for the base epoch of the model, t_0, and $\dot{g}_n^m$ and $\dot{h}_n^m$ are the annual secular-variation coefficients for the 5-year period following the base epoch. Predictions of the main field for more than 5 years into the future are not sufficiently accurate for general navigation purposes and for this reason models and charts are revised every five years. The external coefficients are assumed not to vary with time over the time span of the input data for the model:

$$q_n^m(t) = q_n^m \qquad t \approx t_0$$
$$s_n^m(t) = s_n^m \qquad t \approx t_0 \tag{7}$$

An induction effect from the ring current is taken into account for the first three internal main-field coefficients by allowing them to vary linearly with the global disturbance index *Dst*:

$$g_1^0 = g_{1,0}^0 + g_{1,Dst}^0 \cdot Dst, \quad g_1^1 = g_{1,0}^1 + g_{1,Dst}^1 \cdot Dst, \quad h_1^1 = h_{1,0}^1 + h_{1,Dst}^1 \cdot Dst \tag{8}$$

In practice the main field/external field and secular variation are modelled separately (see discussion in Section 3). The maximum degree for the main field, ni_{max}, is set at 12, for the external field, ne_{max}, 5 and for the secular variation of the main field, 8. There is a distinct change in slope of the power spectral density of the internal coefficients at degree 12-15 and this is interpreted to mean that the low-degree harmonics corresponding to n≤12 are dominated by the main field and the high-degree harmonics associated with n≥15 are dominated by the crustal field. The secular variation cannot be modelled to the same maximum degree as the main field because there are insufficient data. The equations for observations of the magnetic field are

$$\begin{aligned} B_r = -\frac{\partial V}{\partial r} = \sum_{n=1}^{12}(n+1)\left(\frac{a}{r}\right)^{n+2}\sum_{m=0}^{n}(g_n^m \cdot \cos m\lambda + h_n^m \cdot \sin m\lambda)\cdot P_n^m(\theta) \\ -\sum_{n=1}^{5} n\left(\frac{r}{a}\right)^{n-1}\sum_{m=0}^{n}(q_n^m \cdot \cos m\lambda + s_n^m \cdot \sin m\lambda)\cdot P_n^m(\theta) \end{aligned} \tag{9}$$

$$\begin{aligned} B_\theta = -\frac{1}{r}\frac{\partial V}{\partial \theta} = -\sum_{n=1}^{12}\left(\frac{a}{r}\right)^{n+2}\sum_{m=0}^{n}(g_n^m \cdot \cos m\lambda + h_n^m \cdot \sin m\lambda)\cdot \frac{dP_n^m(\theta)}{d\theta} \\ -\sum_{n=1}^{5}\left(\frac{r}{a}\right)^{n-1}\sum_{m=0}^{n}(q_n^m \cdot \cos m\lambda + s_n^m \cdot \sin m\lambda)\cdot \frac{dP_n^m(\theta)}{d\theta} \end{aligned} \tag{10}$$

$$\begin{aligned} B_\lambda = -\frac{1}{r\sin\theta}\frac{\partial V}{\partial \lambda} = \frac{1}{\sin\theta}\sum_{n=1}^{12}\left(\frac{a}{r}\right)^{n+2}\sum_{m=0}^{n} m\cdot(g_n^m \cdot \sin m\lambda - h_n^m \cdot \cos m\lambda)\cdot P_n^m(\theta) \\ +\frac{1}{\sin\theta}\sum_{n=1}^{5}\left(\frac{r}{a}\right)^{n-1}\sum_{m=0}^{n} m\cdot(q_n^m \cdot \sin m\lambda - s_n^m \cdot \cos m\lambda)\cdot P_n^m(\theta) \end{aligned} \tag{11}$$

and for secular-variation observations are

$$\dot{B}_r = -\frac{\partial \dot{V}}{\partial r} = \sum_{n=1}^{8} (n+1)\left(\frac{a}{r}\right)^{n+2} \sum_{m=0}^{n} (\dot{g}_n^m \cdot \cos m\lambda + \dot{h}_n^m \cdot \sin m\lambda) \cdot P_n^m(\theta) \qquad (12)$$

$$\dot{B}_\theta = -\frac{1}{r}\frac{\partial \dot{V}}{\partial \theta} = -\sum_{n=1}^{8}\left(\frac{a}{r}\right)^{n+2} \sum_{m=0}^{n} (\dot{g}_n^m \cdot \cos m\lambda + \dot{h}_n^m \cdot \sin m\lambda) \cdot \frac{dP_n^m(\theta)}{d\theta} \qquad (13)$$

$$\dot{B}_\lambda = -\frac{1}{r\sin\theta}\frac{\partial \dot{V}}{\partial \lambda} = \frac{1}{\sin\theta}\sum_{n=1}^{8}\left(\frac{a}{r}\right)^{n+2} \sum_{m=0}^{n} m \cdot (\dot{g}_n^m \cdot \sin m\lambda - \dot{h}_n^m \cdot \cos m\lambda) \cdot P_n^m(\theta) \qquad (14)$$

4.3 Model determination

The above equations, with the estimates of the true main field/external field or secular variation on the left-hand side, form the equations of condition. Thus, if there are *p* "observations", there are *p* linear equations with $N = n_{max}(n_{max} + 2)$ unknowns:

$$\mathbf{y} = \mathbf{Am} \qquad (15)$$

where is **y** the column vector (*p* x 1) of observations, **A** is the matrix (*p* x *N*) of coefficients to the unknowns which are functions of position, and **m** is the column vector (*N* x 1) of unknowns, the Gauss coefficients of the model. As there are many more observations than unknowns, i.e. as $p > N$, the system is over-determined and therefore does not have a unique solution. Suppose $\tilde{\mathbf{m}}$ is an estimate of **m**. Then

$$\tilde{\mathbf{y}} = \mathbf{A}\tilde{\mathbf{m}} \qquad (16)$$

where $\tilde{\mathbf{y}}$ are estimates of the observations. The residuals are $\mathbf{y} - \tilde{\mathbf{y}}$ and the least-squares method requires that $\tilde{\mathbf{m}}$ is chosen so as to minimise the weighted sum of the squares of the residuals, *S*, i.e.:

$$\text{minimise} \quad S = (\mathbf{y} - \tilde{\mathbf{y}})^{\mathbf{T}}\,\mathbf{W}(\mathbf{y} - \tilde{\mathbf{y}})$$
$$= (\mathbf{y} - \mathbf{A}\tilde{\mathbf{m}})^{\mathbf{T}}\,\mathbf{W}(\mathbf{y} - \mathbf{A}\tilde{\mathbf{m}}) \quad \text{with respect to } \tilde{\mathbf{m}}.$$

W is the weight matrix (p x p) of the data. It is required that $\frac{\partial S}{\partial \tilde{\mathbf{m}}} = 0$. Now

$$\begin{aligned}
\frac{\partial S}{\partial \tilde{\mathbf{m}}} &= \lim_{\delta\tilde{\mathbf{m}} \to \mathbf{0}} \frac{S(\tilde{\mathbf{m}} + \delta\tilde{\mathbf{m}}) - S(\tilde{\mathbf{m}})}{\delta\tilde{\mathbf{m}}} \\
&= \lim_{\delta\tilde{\mathbf{m}} \to \mathbf{0}} \frac{(\mathbf{y} - \mathbf{A}(\tilde{\mathbf{m}} + \delta\tilde{\mathbf{m}}))^{\mathbf{T}} \mathbf{W}(\mathbf{y} - \mathbf{A}(\tilde{\mathbf{m}} + \delta\tilde{\mathbf{m}})) - (\mathbf{y} - \mathbf{A}\tilde{\mathbf{m}})^{\mathbf{T}} \mathbf{W}(\mathbf{y} - \mathbf{A}\tilde{\mathbf{m}})}{\delta\tilde{\mathbf{m}}} \\
&= \lim_{\delta\tilde{\mathbf{m}} \to \mathbf{0}} \frac{(\mathbf{z} - \mathbf{A}\delta\tilde{\mathbf{m}})^{\mathbf{T}} \mathbf{W}(\mathbf{z} - \mathbf{A}\delta\tilde{\mathbf{m}}) - \mathbf{z}^{\mathbf{T}}\mathbf{W}\mathbf{z}}{\delta\tilde{\mathbf{m}}} \quad \text{where } \mathbf{z} = \mathbf{y} - \mathbf{A}\tilde{\mathbf{m}} \\
&= \lim_{\delta\tilde{\mathbf{m}} \to \mathbf{0}} \frac{-2\delta\tilde{\mathbf{m}}^{\mathbf{T}}\mathbf{A}^{\mathbf{T}}\mathbf{W}\mathbf{z} + \mathrm{O}(\delta\tilde{\mathbf{m}}^{\mathbf{2}})}{\delta\tilde{\mathbf{m}}} \\
&= 0 \quad \text{when } \mathbf{A}^{\mathbf{T}}\mathbf{W}\mathbf{z} = \mathbf{0}
\end{aligned}$$

i.e. when $\mathbf{A}^{\mathbf{T}}\mathbf{W}\mathbf{A}\tilde{\mathbf{m}} = \mathbf{A}^{\mathbf{T}}\mathbf{W}\mathbf{y}$.

These are the normal equations and the estimated unknowns $\tilde{\mathbf{m}}$ are found from

$$\tilde{\mathbf{m}} = (\mathbf{A}^{\mathbf{T}}\mathbf{W}\mathbf{A})^{-1}\mathbf{A}^{\mathbf{T}}\mathbf{W}\mathbf{y}. \tag{17}$$

4.4 Coordinate transformations

Satellite data are already located in a geocentric coordinate system but surface data are almost invariably located in a geodetic coordinate system, i.e. relative to the mean sea surface of the earth, which can be approximated by a spheroid. The locations of surface data, and the data themselves, must be transformed from geodetic to geocentric coordinates prior to spherical harmonic modelling.

When computing the model the locations (h, θ', λ), where h is the altitude above mean sea level and θ' is the geodetic colatitude, are transformed into (r, θ, λ) using

$$\tan\theta = \frac{(A^2 \sin^2\theta' + B^2 \cos^2\theta')^{1/2} h + A^2}{(A^2 \sin^2\theta' + B^2 \cos^2\theta')^{1/2} h + B^2} \tan\theta' \tag{18}$$

and

$$r^2 = h^2 + 2h(A^2 \sin^2\theta' + B^2 \cos^2\theta')^{1/2} + \frac{A^4 \sin^2\theta' + B^4 \cos^2\theta'}{A^2 \sin^2\theta' + B^2 \cos^2\theta'} \qquad (19)$$

where A is the equatorial radius of the spheroid and B is the polar radius.

The observations of the northerly, easterly and vertically down intensities *X*, *Y* and *Z*, relative to a spheroid, are transformed into the northerly, easterly and vertically down intensities relative to a sphere, B_θ, B_λ and B_r:

$$\begin{aligned} B_\theta &= -X\cos\psi + Z\sin\psi \\ B_\lambda &= Y \\ B_r &= -X\sin\psi - Z\cos\psi \end{aligned} \qquad (20)$$

where ψ is the difference between geocentric and geodetic colatitude in the sense $\theta - \theta'$.

Another coordinate system used in global magnetic field modelling is the geomagnetic coordinate system. This is used in the derivation of WMM2000 to identify data locations within a certain latitude band of the geomagnetic equator for which vector data values from a pre-determined model are required. This coordinate system is based on the internal centred dipolar field and is defined by the first three main-field coefficients of an existing global spherical harmonic model. Its reference axis is aligned along the dipole axis, which is tilted from the rotational axis of the earth by about 11° and cuts the surface of the earth at the geomagnetic poles. The geomagnetic equator is the great circle 90° from the geomagnetic poles and geomagnetic latitude varies from 0° at the geomagnetic equator to ±90° at the geomagnetic poles.

4.5 Data weighting schemes

For the main-field models the relative numbers of scalar and vector data in the equatorial region are not equal, but the vector data is more heavily weighted so as to give these synthetic data an overall weight equal to the scalar data contained in a fixed

equatorial band about the geomagnetic equator. All data are equal-area weighted using a factor of sin θ where θ is the geocentric colatitude. In the last iteration outliers are down-weighted using the factor

$$w_0 = e^{-\left(\frac{\Delta B}{3\bar{\sigma}}\right)^2}$$

where ΔB is the residual of the observation over the model from the first iteration and $\bar{\sigma}$ is the global root mean square (rms) error of the model from the first iteration. By the last iteration, the guess model is presumed to be close to the final model, so the net effect of this weight factor is to down-weight outliers, particularly those found in the auroral zones, which are most likely associated with field-aligned currents and the auroral electrojets, which are always present. Satellite orbits must penetrate the field-aligned currents in the polar regions. At such times the magnetic field is not source-free, and so does not strictly satisfy Laplace's equation. This weight factor provides some control over this situation.

For the secular-variation models error assignment is based on actual past prediction errors (up to a maximum lead time of 10 years) both globally and locally. For the observed values the errors are based on the rms residuals to quadratic fits made to data over a five-year period. The global mean 1-σ errors for each component are shown in Figure 188 – the values for lead time of 0 years are the means of the errors for the observed values. It can be seen that the errors for predicting secular variation in Z are higher than for X and Y. Also shown in Figure 188 is the number of observatories requiring predictions for each lead-time. As most observatories had annual mean values for 1997 the most common maximum lead-time is 8 years and this was for predictions for 2005.0.

Shown in Figure 189 is the mean error of the data (observed and predicted) by year. The diagonal terms of the weight matrix in the least squares analysis for determining the spherical harmonic coefficients are $1/\sigma^2$, while the off-diagonal terms were set to zero, i.e. secular-variation data were assumed not to be correlated.

For the secular-variation estimates derived from repeat stations the errors were set at five times greater than the mean observatory errors as shown in Figure 188. The

errors are increased by a further 50% if one or both observations making up a secular-variation estimate had not been reduced to a magnetically quiet level.

The satellite-based secular-variation values were assigned errors 70% greater than the mean errors of the observatory estimates.

4.6 Derivation of WMM2000

An iterative procedure was adopted for the derivation of the final WMM2000. The first step was the derivation of initial secular-variation models. Sixteen annual secular-variation models were computed, each valid from the mid-point of one year to the mid-point of the next year, for the period 1990 to 2005. The synthetic values at the locations shown in Figure 17 in these models were computed from a secular-variation model which included secular-variation information derived from POGS data and recent observatory and repeat station data. The three five-year average models were taken as weighted mean values of the annual coefficients. For example, for the secular-variation model for 2000.0-2005.0, a mean of the coefficients of the models for 2000.0, 2001.0, 2002.0, 2003.0, 2004.0 and 2005.0 was used with half weight being given to the 2000.0 and 2005.0 coefficients and unit weight to the others.

The next step was the computation of an initial main-field model for 2000.0. This step in itself was an iterative process as the bulk of the data for the main-field model was total intensity data from Ørsted and, being non-linear in the Gauss coefficients, an *a priori* or initial-guess model is required. In addition it was suspected that there were errors in the model used to generate the equatorial vector data but, by strengthening the influence of the Ørsted scalar data on these synthetic vector data at each iteration, it was hoped to minimise them.

Eight main-field models were generated, each based on data from 10 or 11 consecutive days, depending on the number of days in each month, from 11 March to 31 May 1999. Preliminary models with synthetic vector data within 20° of the geomagnetic equator were synthesised from the base epoch model of WMM-95 at 1992.5 (Quinn *et al*, 1995) updated to the base epoch of the selected Ørsted data using the initial secular-variation models for 1990.0-1995.0 and 1995.0-2000.0. Every 20th Ørsted data sample was selected resulting in a 20-second data series. This was further decimated by only selecting data from periods when local time was 12 pm – 6 am, $Kp \leq 2_+$ and $Dst \leq |30\ \text{nT}|$. The *a priori* model was the same model that was used to generate the equatorial vector data. For the next iteration the equatorial vector data were computed from the model from the previous iteration and combined with the

scalar data. For each of the eight models there were three iterations. One model was then calculated by taking the weighted mean of the eight models where the weights were the inverses of the root mean square (rms) fits of each model to the input data. These rms fits were of the order of 11 nT. This model was updated to 2000.0 using the initial secular-variation model for 1995.0-2000.0.

The next step was the computation of better secular-variation models using better synthetic data in the areas devoid of observatory and repeat station data, and some new observatory data. The synthetic data were computed from a model of secular variation derived from the difference between a POGS-based model at 1995.0 and the Ørsted-based model at 2000.0 just derived. The POGS-based model was the base epoch model of WMM-95 at 1992.5 updated to 1995.0 using the initial secular-variation models for 1990.0-1995.0. In Figure 190, 191 and 192 the differences in secular variation of *X*, *Y* and *Z* between this secular-variation model and the initial secular-variation model for 1995.0-2000.0 are shown. As the differences are predominantly in the areas where only the synthetic data have been used, any improvements to these synthetic data by using more recent and absolute satellite data will be passed on to the final secular-variation models. New predictions of secular variation at the observatories where new data had been received were made and the secular-variation errors were recomputed. Again, three five-year average secular-variation models were derived.

The final step is the recomputation of the main-field model for 2000.0 using the same method described above, but with revised secular-variation models for the two 5-year time intervals between 1990 and 2000 for reduction of satellite data to epoch, plus a revised predictive secular-variation model for the 5-year interval 2000-2005. This time, synthetic vector data only within 15° of the geomagnetic equator were included. Models with the larger band about the geomagnetic equator were also generated but were statistically indistinguishable from the narrow band models. The models with the least amount of synthetic data were considered the most desirable. So the narrow band was chosen for the final modelling sequence. The 1995.0 model was also recomputed using the new secular-variation models. Differences between the initial and final main-field model for 2000.0 are shown in Figure 193.

The fit of the model to the Ørsted data for each of the eight models generated in the final computation is given in Table 1. Included are the mean epoch of each model, the number of days used in each model, and the number of Ørsted scalar magnetic field observations (records) used in each model. An example of the satellite data distribution for one of these subsets is shown in Figure 194. The others are quite similar.

Table 1 Statistics of model residuals for Ørsted Overhauser magnetometer data

Model		**1**	**2**	**3**	**4**	**5**	**6**	**7**	**8**
	Month	March	March	April	April	April	May	May	May
	Day Begin	11	21	1	11	21	1	11	21
	Day End	20	31	10	20	30	10	20	31
	Mean Day	77.4	84.1	96.0	105.3	114.6	126.8	135.8	144.7
	Records	9890	15115	14111	13050	14664	16769	14591	13926
Iteration									
	(nT)								
1	Mean	0.0	-0.2	0.0	-0.1	-0.3	-0.3	-0.4	-0.4
	Rms	12.1	11.4	11.7	11.4	12.9	12.0	10.8	11.3
2	Mean	0.0	-0.2	0.2	0.2	-0.1	0.0	-0.2	-0.2
	Rms	10.7	9.8	10.4	10.0	11.8	10.8	9.5	9.9
3	Mean	0.5	0.3	0.8	0.5	0.9	0.7	0.2	0.2
	Rms	10.4	9.3	10.1	9.7	11.7	10.6	9.1	9.4

5 Modelling results

The coefficients of the final main-field models for 1995.0 and 2000.0, and the final secular-variation model for 2000.0-2005.0 are listed in Table 2.

Table 2 Gauss main-field coefficients for 1995.0 and 2000.0 and secular-variation (SV) coefficients for 2000.0-2005.0.

g/h	*n*	*m*	1995.0	2000.0	SV
g	1	0	-29686.6	-29616.0	14.7
g	1	1	-1781.9	-1722.7	11.1
h	1	1	5311.1	5194.5	-20.4
g	2	0	-2196.1	-2266.7	-13.6
g	2	1	3071.9	3070.2	-0.7
h	2	1	-2370.2	-2484.8	-21.5
g	2	2	1684.2	1677.6	-1.8
h	2	2	-420.4	-467.9	-9.6
g	3	0	1319.3	1322.4	0.3
g	3	1	-2267.9	-2291.5	-4.3
h	3	1	-254.6	-224.7	6.4
g	3	2	1251.4	1255.9	0.9
h	3	2	298.3	293.0	-1.3
g	3	3	765.5	724.8	-8.4
h	3	3	-418.9	-486.5	-13.3
g	4	0	938.2	932.1	-1.6
g	4	1	782.3	786.3	0.9
h	4	1	260.9	273.3	2.3
g	4	2	289.9	250.6	-7.6
h	4	2	-230.8	-227.9	0.7
g	4	3	-415.3	-401.5	2.2
h	4	3	99.5	120.9	3.7
g	4	4	118.8	106.2	-3.2
h	4	4	-302.8	-302.7	-0.5
g	5	0	-210.6	-211.9	-0.9
g	5	1	352.6	351.6	-0.2
h	5	1	42.8	42.0	0.0
g	5	2	235.5	220.8	-2.5
h	5	2	161.5	173.8	2.1
g	5	3	-123.7	-134.5	-2.7
h	5	3	-147.4	-135.0	2.3
g	5	4	-164.4	-168.8	-0.9
h	5	4	-56.2	-38.6	3.1
g	5	5	-21.9	-13.3	1.7
h	5	5	104.4	105.2	0.0
g	6	0	69.3	73.8	1.2
g	6	1	66.3	68.2	0.2
h	6	1	-17.0	-17.4	-0.3
g	6	2	66.8	74.1	1.7

g/h	*n*	*m*	**1995.0**	**2000.0**	**SV**
h	6	2	72.3	61.2	-1.7
g	6	3	-171.6	-163.5	1.6
h	6	3	68.5	63.2	-0.9
g	6	4	-0.3	-3.8	-0.1
h	6	4	-57.3	-62.9	-1.0
g	6	5	17.3	17.1	-0.3
h	6	5	1.6	0.2	-0.1
g	6	6	-89.2	-85.1	0.8
h	6	6	34.5	43.0	1.9
g	7	0	78.1	77.4	-0.4
g	7	1	-68.8	-73.9	-0.8
h	7	1	-73.4	-62.3	1.4
g	7	2	1.1	2.2	-0.2
h	7	2	-25.4	-24.5	0.2
g	7	3	31.5	35.7	1.1
h	7	3	3.5	8.9	0.7
g	7	4	3.3	7.3	0.4
h	7	4	20.5	23.4	0.4
g	7	5	6.8	5.2	0.0
h	7	5	17.4	15.0	-0.3
g	7	6	8.6	8.4	-0.2
h	7	6	-24.6	-27.6	-0.8
g	7	7	-2.3	-1.5	-0.2
h	7	7	-6.3	-7.8	-0.1
g	8	0	24.1	23.3	-0.3
g	8	1	5.2	7.3	0.6
h	8	1	13.1	12.4	-0.5
g	8	2	-3.2	-8.5	-0.8
h	8	2	-18.9	-20.8	0.1
g	8	3	-9.2	-6.6	0.3
h	8	3	6.9	8.4	-0.2
g	8	4	-15.4	-16.9	-0.2
h	8	4	-20.8	-21.2	0.0
g	8	5	4.0	8.6	0.5
h	8	5	13.0	15.5	0.1
g	8	6	3.1	4.9	0.0
h	8	6	8.2	9.1	-0.1
g	8	7	-5.0	-7.8	-0.6
h	8	7	-17.8	-15.5	0.3
g	8	8	-8.4	-7.6	0.1
h	8	8	-7.3	-5.4	0.2
g	9	0	2.9	5.7	0.0
g	9	1	7.7	8.5	0.0
h	9	1	-20.3	-20.4	0.0
g	9	2	0.5	2.0	0.0
h	9	2	14.1	13.9	0.0
g	9	3	-10.2	-9.8	0.0
h	9	3	11.3	12.0	0.0
g	9	4	9.5	7.6	0.0

g/h	*n*	*m*	1995.0	2000.0	SV
h	9	4	-7.2	-6.2	0.0
g	9	5	-2.5	-7.0	0.0
h	9	5	-7.2	-8.6	0.0
g	9	6	-2.3	-2.0	0.0
h	9	6	9.2	9.4	0.0
g	9	7	6.9	9.2	0.0
h	9	7	7.6	5.0	0.0
g	9	8	-0.4	-2.2	0.0
h	9	8	-8.1	-8.4	0.0
g	9	9	-6.5	-6.6	0.0
h	9	9	2.7	3.2	0.0
g	10	0	-3.0	-2.2	0.0
g	10	1	-3.5	-5.7	0.0
h	10	1	3.1	0.9	0.0
g	10	2	2.9	1.6	0.0
h	10	2	1.3	-0.7	0.0
g	10	3	-4.3	-3.7	0.0
h	10	3	2.9	3.9	0.0
g	10	4	-3.0	-0.6	0.0
h	10	4	5.6	4.8	0.0
g	10	5	2.7	4.1	0.0
h	10	5	-3.5	-5.3	0.0
g	10	6	2.9	2.2	0.0
h	10	6	-0.6	-1.0	0.0
g	10	7	1.0	2.2	0.0
h	10	7	-2.6	-2.4	0.0
g	10	8	4.0	4.6	0.0
h	10	8	2.4	1.3	0.0
g	10	9	3.6	2.3	0.0
h	10	9	-1.6	-2.3	0.0
g	10	10	0.6	0.1	0.0
h	10	10	-6.6	-6.4	0.0
g	11	0	1.8	3.3	0.0
g	11	1	-1.4	-1.1	0.0
h	11	1	-0.1	-1.5	0.0
g	11	2	-3.4	-2.4	0.0
h	11	2	1.1	0.7	0.0
g	11	3	1.3	2.6	0.0
h	11	3	-3.3	-1.1	0.0
g	11	4	-0.7	-1.3	0.0
h	11	4	-1.6	-2.3	0.0
g	11	5	-0.2	-1.7	0.0
h	11	5	1.6	1.3	0.0
g	11	6	-0.7	-0.6	0.0
h	11	6	0.1	-0.6	0.0
g	11	7	-0.7	0.4	0.0
h	11	7	-1.4	-2.8	0.0
g	11	8	1.4	0.7	0.0
h	11	8	-2.3	-1.6	0.0

g/h	*n*	*m*	1995.0	2000.0	SV
g	11	9	-0.3	-0.3	0.0
h	11	9	-0.7	-0.1	0.0
g	11	10	2.1	2.3	0.0
h	11	10	-2.1	-1.9	0.0
g	11	11	4.1	4.2	0.0
h	11	11	1.4	1.4	0.0
g	12	0	-1.8	-1.5	0.0
g	12	1	0.4	-0.2	0.0
h	12	1	0.3	-1.0	0.0
g	12	2	0.0	-0.3	0.0
h	12	2	1.2	0.7	0.0
g	12	3	-0.4	0.5	0.0
h	12	3	1.1	2.2	0.0
g	12	4	0.7	0.2	0.0
h	12	4	-2.9	-2.5	0.0
g	12	5	0.4	0.9	0.0
h	12	5	0.3	-0.2	0.0
g	12	6	0.5	-1.4	0.0
h	12	6	0.5	0.0	0.0
g	12	7	0.5	0.6	0.0
h	12	7	-0.8	-0.2	0.0
g	12	8	-0.5	-0.6	0.0
h	12	8	0.7	0.0	0.0
g	12	9	0.4	-1.0	0.0
h	12	9	0.2	0.2	0.0
g	12	10	0.2	-0.3	0.0
h	12	10	-1.4	-0.9	0.0
g	12	11	0.4	0.3	0.0
h	12	11	-0.4	-0.2	0.0
g	12	12	0.4	0.4	0.0
h	12	12	0.9	1.0	0.0

These coefficients can be used to compute values for B_θ, B_λ and B_r and their annual rates of change at any location near the surface of the earth and at any date between 1995.0 and 2005.0. On input the geodetic latitude and altitude must be transformed into geocentric colatitude and radial distance using equations (18) and (19) and on output, B_θ, B_λ and B_r must be transformed into X, Y and Z using:

$$\begin{aligned} X &= -B_\theta \cos\psi' - B_r \sin\psi' \\ Y &= B_\lambda \\ Z &= B_\theta \sin\psi' - B_r \cos\psi' \end{aligned} \qquad (21)$$

where ψ is the difference between geocentric and geodetic colatitude (θ') in the sense $\theta - \theta'$. The other magnetic field elements can be computed from X, Y and Z using equations (2). For secular variation the other elements are computed using

$$\dot{H} = \frac{X \cdot \dot{X} + Y \cdot \dot{Y}}{H}$$

$$\dot{F} = \frac{X \cdot \dot{X} + Y \cdot \dot{Y} + Z \cdot \dot{Z}}{F} \qquad (22)$$

$$\dot{D} = \frac{180}{\pi} \frac{X \cdot \dot{Y} - Y \cdot \dot{X}}{H^2}$$

$$\dot{I} = \frac{180}{\pi} \frac{H \cdot \dot{Z} - Z \cdot \dot{H}}{F^2}$$

where $\dot{D}$ and $\dot{I}$ are given in degrees/year.

Shown in Figures 195-201 are Mercator charts of D, I, F, H, X, Y, Z at the earth's surface for 2000.0, in Figures 202-208 polar stereographic charts for the north pole and in Figures 209-215 for the south pole. Mercator charts of annual secular variation of D, I, F, H, X, Y, Z at the earth's surface for the period 2000.0-2005.0 are shown in Figures 216-222, the north polar charts in Figures 223-229 and the south polar charts in Figures 230-236.

The geomagnetic poles, otherwise known as the dipole poles, can be computed from the first three Gauss coefficients. From the WMM2000 coefficients for 2000.0 the geomagnetic north pole is at longitude 71.65°W and geodetic latitude 79.60°N and the geomagnetic south pole is at longitude 108.35°E and geodetic latitude 79.60°S.

The magnetic poles, otherwise known as the dip poles, are computed from all the Gauss coefficients using an iterative method. At 2000.0 the north magnetic pole is located at longitude 109.37°W and geodetic latitude 80.81°N and the south magnetic pole is at longitude 138.31°E and geodetic latitude 64.67°S. In practice the geomagnetic field is not exactly vertical at these dip poles but on oval-shaped loci

traced on a daily basis, with considerable variation from one day to another, and approximately centred on the dip pole positions.

The location of the centre of the eccentric dipole, sometimes known as the magnetic centre, computed using the first eight Gauss coefficients for 2000.0, is (r, θ, λ) = (540.56 km, 21.77°, 143.17°E).

An estimate of the accuracy of WMM2000 can be made for land locations by comparing observatory annual means and repeat station data collected from 1995.0 onwards with values computed from the model. These data have the effects of disturbance fields reduced but are contaminated by crustal fields. This results in considerable contributions from the crustal fields to the residuals. The results of these comparisons are given in Table 3. Residuals > 1000 nT are excluded from the statistics.

Table 3 Statistics of WMM2000 residuals for observatory annual means and repeat station data.

	1995	**1996**	**1997**	**1998**
Observatories				
Mean *X* residual	-26	-23	-27	-50
RMS *X* residual	221	194	199	223
Mean *Y* residual	-16	-20	-19	-33
RMS *Y* residual	219	224	228	250
Mean *Z* residual	12	9	10	-11
RMS *Z* residual	231	217	228	240
Mean *F* residual	-16	-16	-19	-30
RMS *F* residual	249	225	222	239
Number of usable data locations	170	154	151	99
Repeat stations				
Mean *X* residual	-14	-1	-1	-12
RMS *X* residual	120	152	189	222
Mean *Y* residual	6	-2	20	0
RMS *Y* residual	103	145	138	163
Mean *Z* residual	0	-39	-78	2
RMS *Z* residual	159	219	186	221
Mean *F* residual	-6	-37	13	5
RMS *F* residual	143	205	183	219
Number of usable data locations	481	189	101	123

The spatial distributions of these residuals show no significant patterns. One possible explanation for the observatories having higher residuals than the repeat stations is that a number of the observatories are on volcanic islands which are likely to have considerable crustal fields. In ocean areas the errors are expected to be less.

Acknowledgements

The staff of magnetic observatories and survey organisations around the world are thanked for providing the data on which this model depends. The Ørsted satellite Overhauser data were kindly provided by the Danish Meteorological Institute. The preliminary *Dst* indices were provided by the University of Kyoto, Japan and the *Kp* indices were provided by the Adolf-Schmidt-Observatorium für Geomagnetismus, GeoForschungsZentrum, Potsdam, Germany. Both indices are based on 1-minute data from many observatories. This report is published with the permission of the Director, British Geological Survey (Natural Environment Research Council).

References

Coleman, 1991. Project MAGNET high-level vector survey data reduction. *NASA Conference Publication 3153.*

Jankowski, J. and C. Sucksdorff, 1996. *Guide for magnetic measurements and observatory practice.* International Association of Geomagnetism and Aeronomy.

Langel, R. A. and W. J. Hinze, 1998. *The magnetic field of the earth's lithosphere. The satellite perspective.* Cambridge University Press.

Merrill, R. T., M. W. McElhinny and P. L. McFadden, 1996. *The magnetic field of the earth.* Academic Press.

Newitt, L. R., C. E. Barton and J. Bitterly, 1996. *Guide to Magnetic Repeat Station Surveys*. International Association of Geomagnetism and Aeronomy.

Parkinson, W. D., 1983. *Introduction to geomagnetism.* Scottish Academic Press.

Quinn, J. M., D. L. Shiel, M. H. Acuña and J. Scheifle, 1993. Initial analysis and modeling results from the Polar Orbiting Geomagnetic Survey (POGS) satellite. Naval Oceanographic Office Technical Report TR 311.

Quinn, J. M., R. J. Coleman, D. L. Shiel, J. M. Nigro, 1995. The joint US/UK 1995 epoch World Magnetic Model. Naval Oceanographic Office Technical Report TR 314.

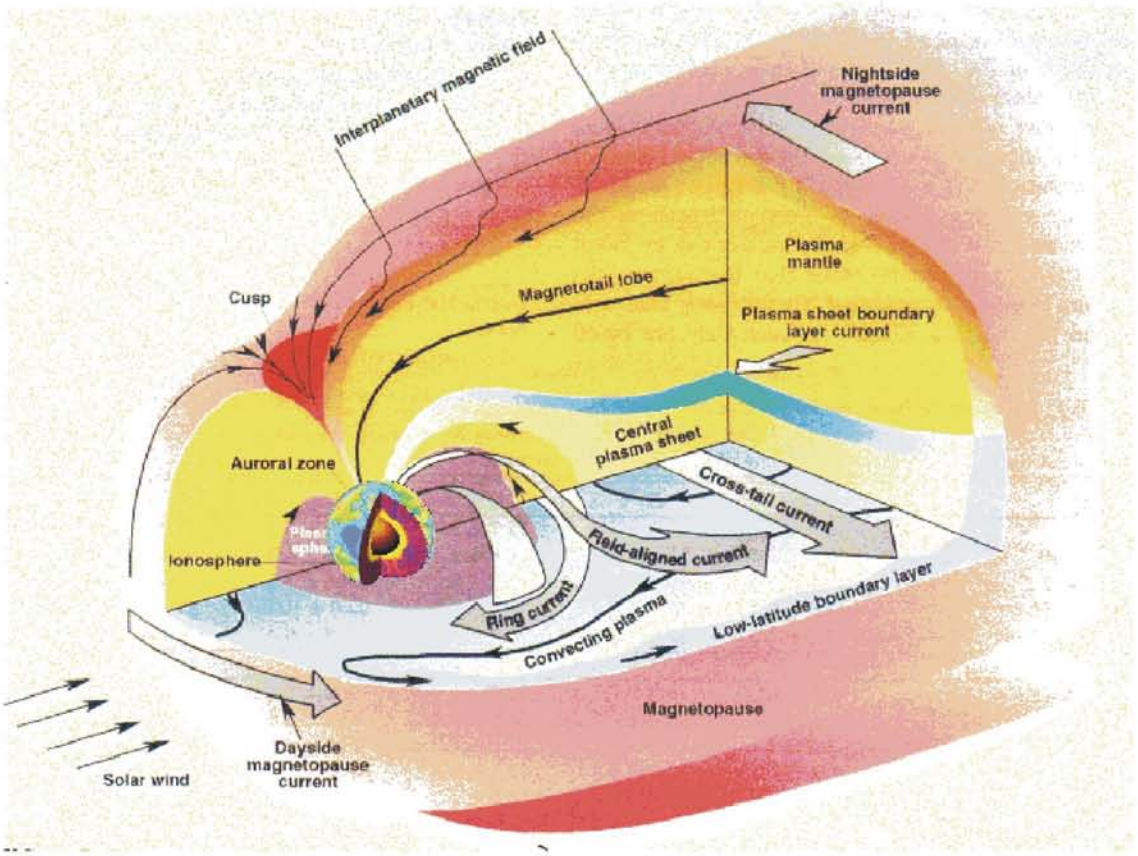

The main current systems in the magnetosphere

Figure 1

Danish Meteorological Institute triaxial fluxgate magnetometer

Figure 2

Geomagnetic absolute instruments.

From left to right
Control box for proton precession magnetometer
Fluxgate theodolite with gyro-attachment
Proton precession magnetometer
Control box and power supply for gyro- attachment
Palmtop PC

Figure 3

Proton vector magnetometer and control PC

Figure 4

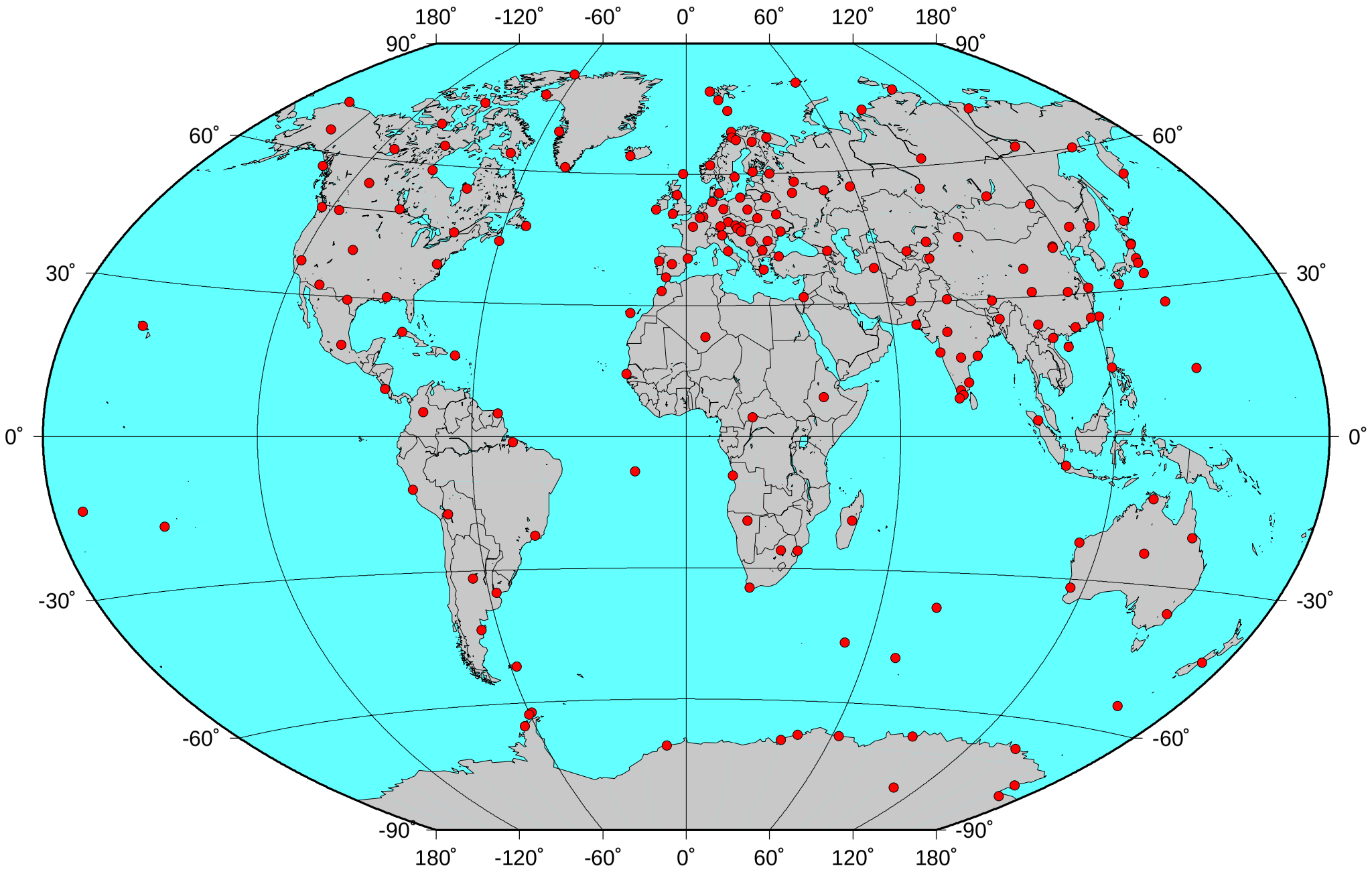

Figure 5

Locations of geomagnetic observatories

Number of observatory annual means from north and south hemispheres received by WDC for Geomagnetism (BGS, Edinburgh) by end of 1999

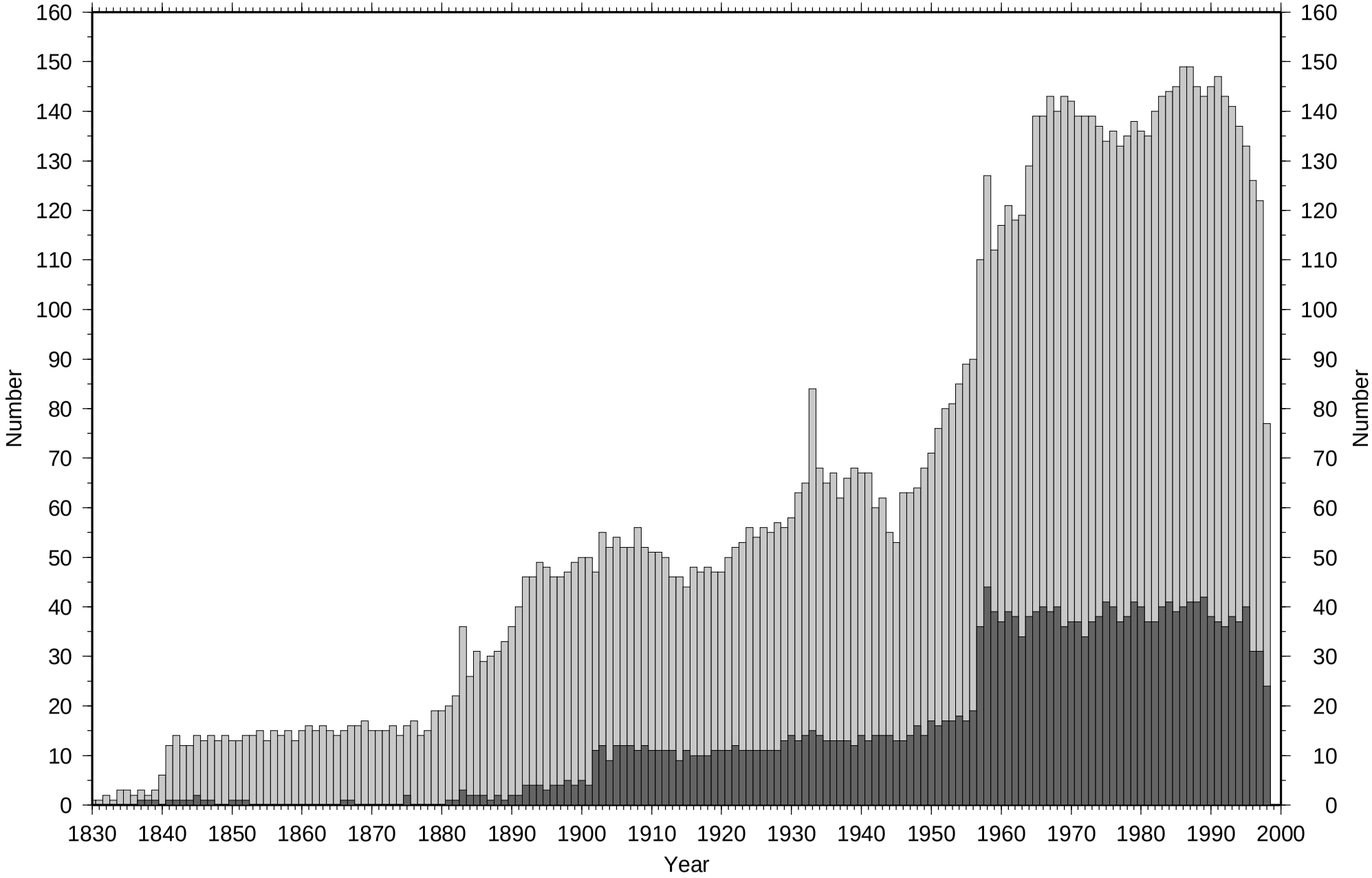

Figure 6

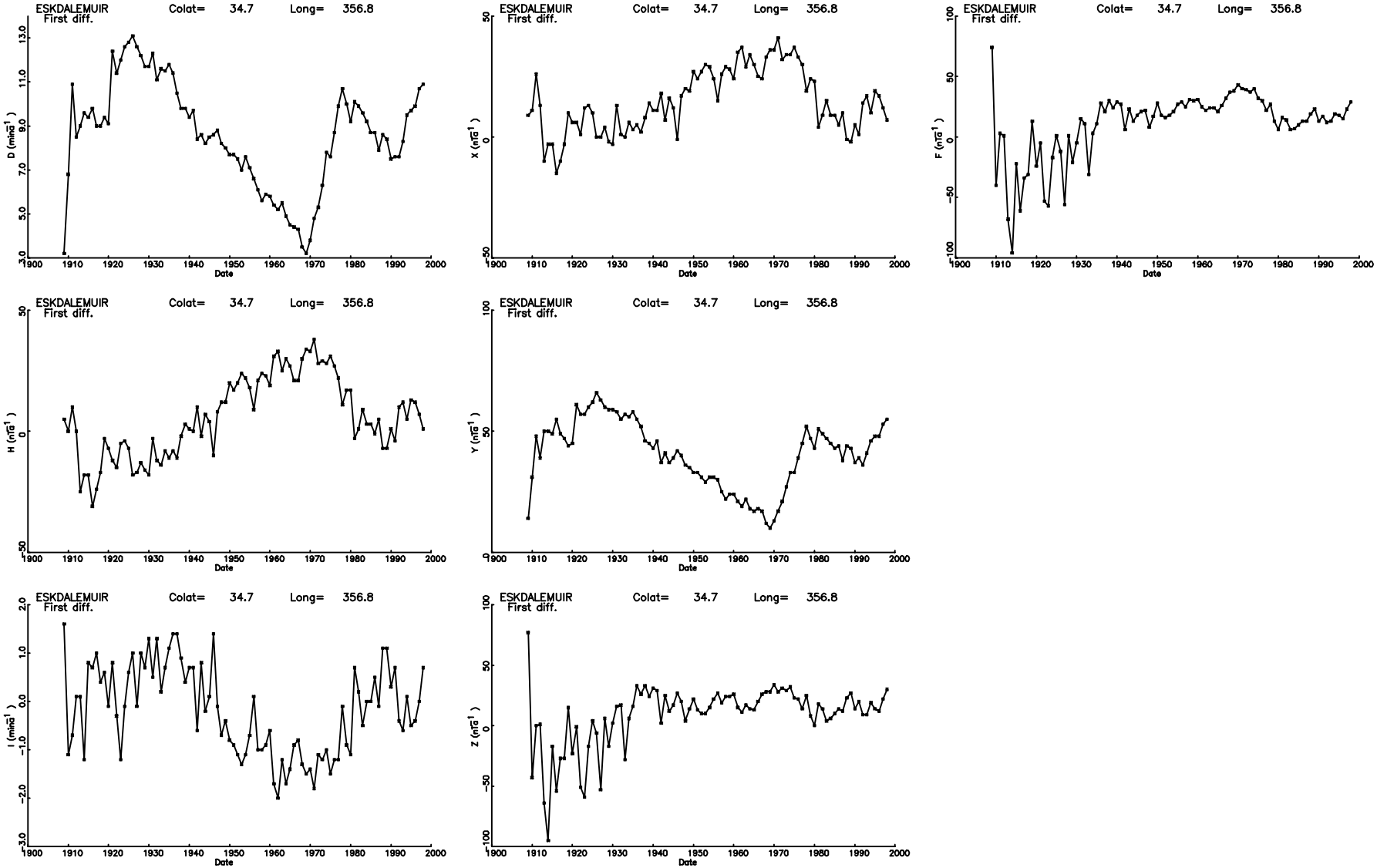
ESKDALEMUIR Colat= 34.7 Long= 356.8
First diff.
D (min yr⁻¹)
X (nT yr⁻¹)
F (nT yr⁻¹)
H (nT yr⁻¹)
Y (nT yr⁻¹)
I (min yr⁻¹)
Z (nT yr⁻¹)
Date

Figure 7

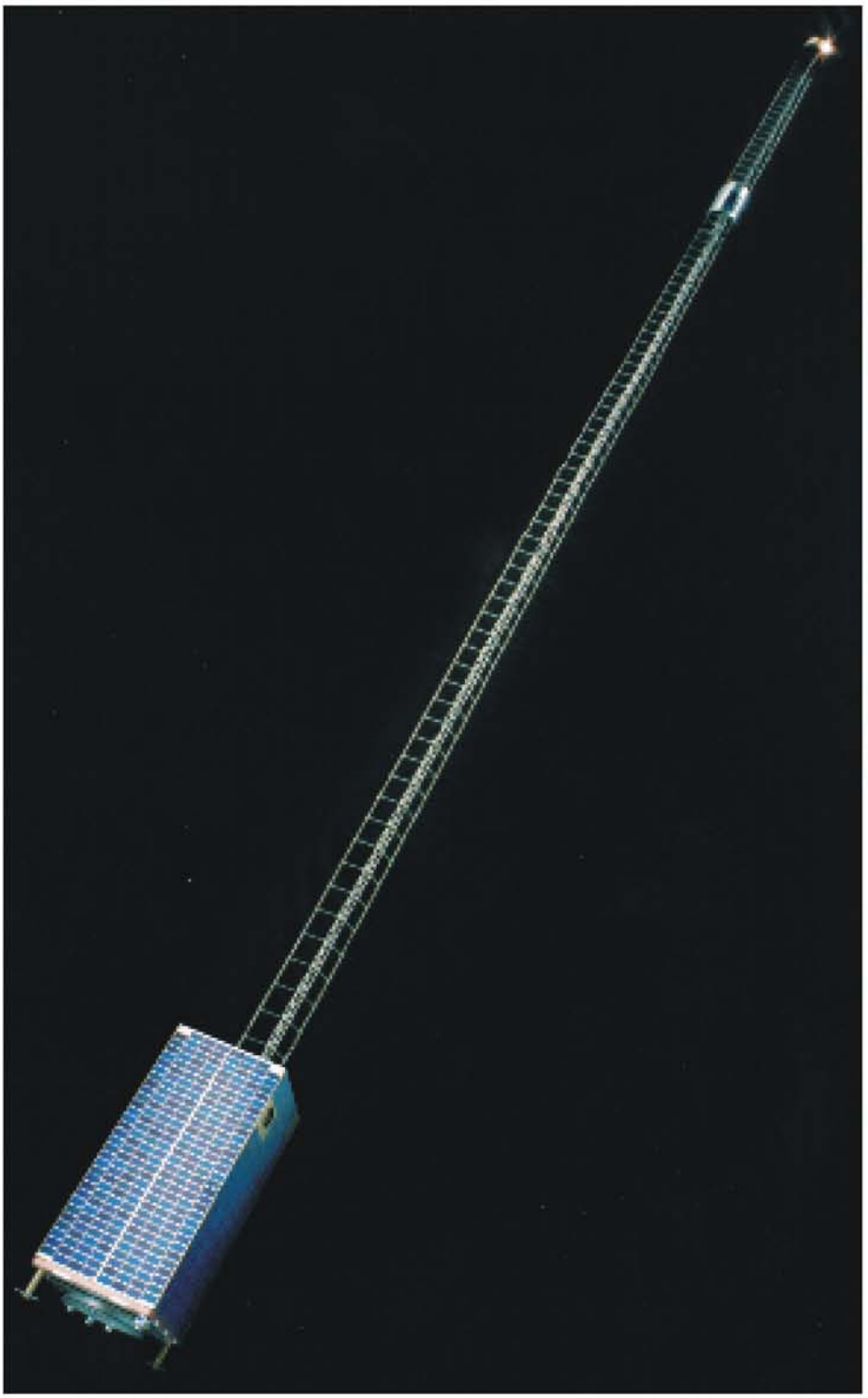

Oersted - Danish magnetic field survey satellite launched February 1999

Figure 8

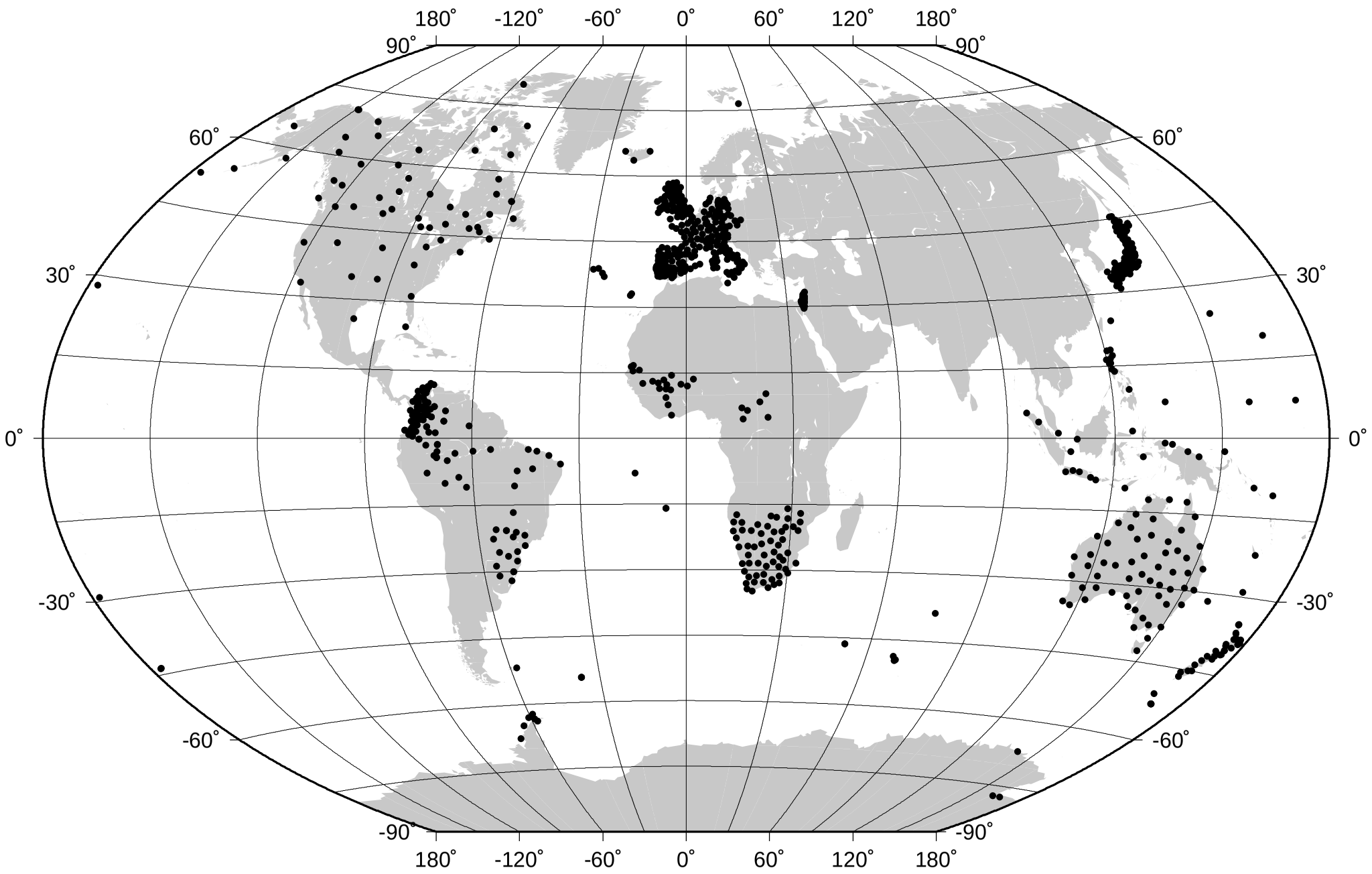

Figure 9

The 806 repeat stations with viable secular-variation information before tesseral selection

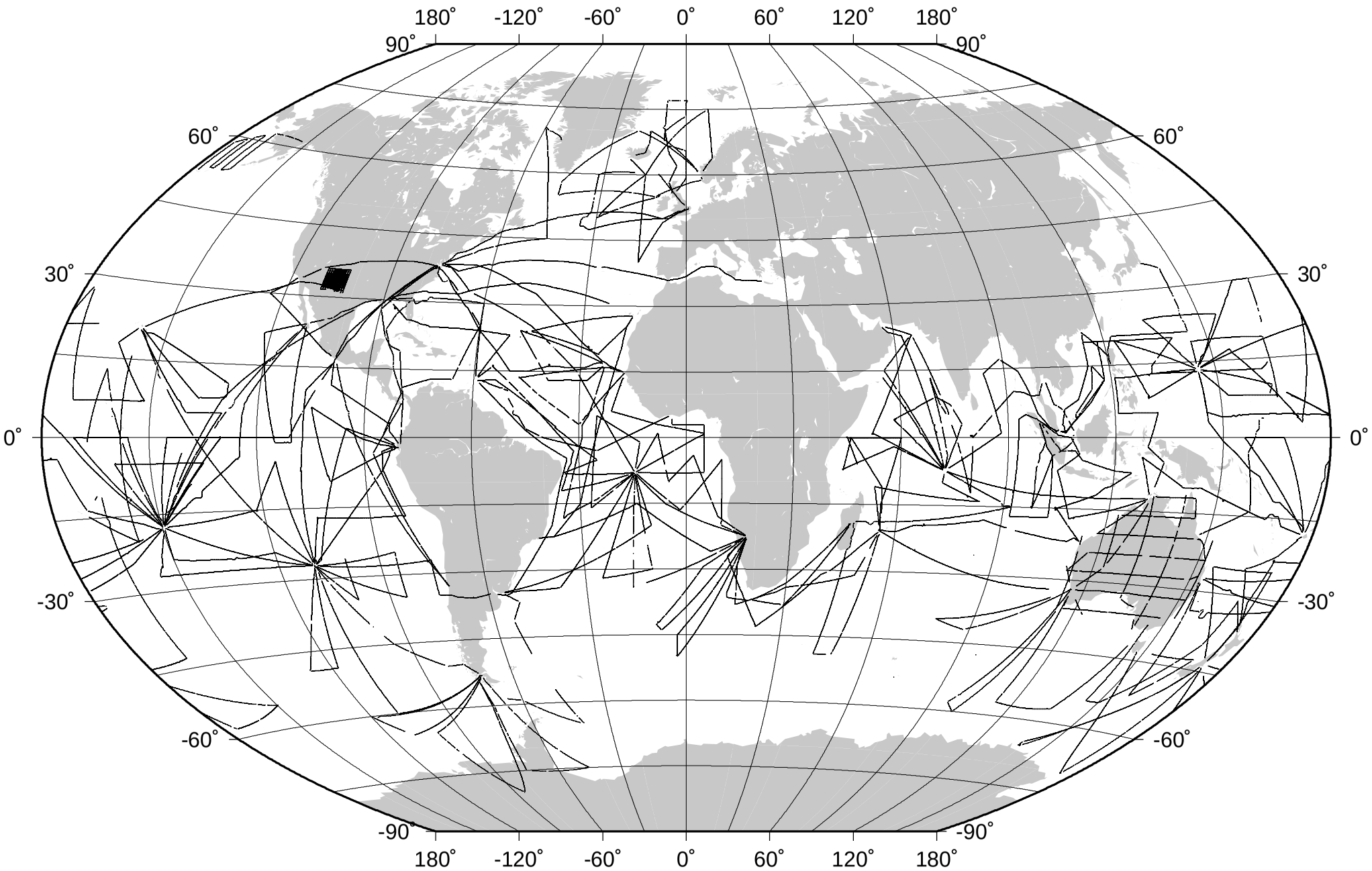

Figure 10

High-level Project MAGNET data 1988-1994

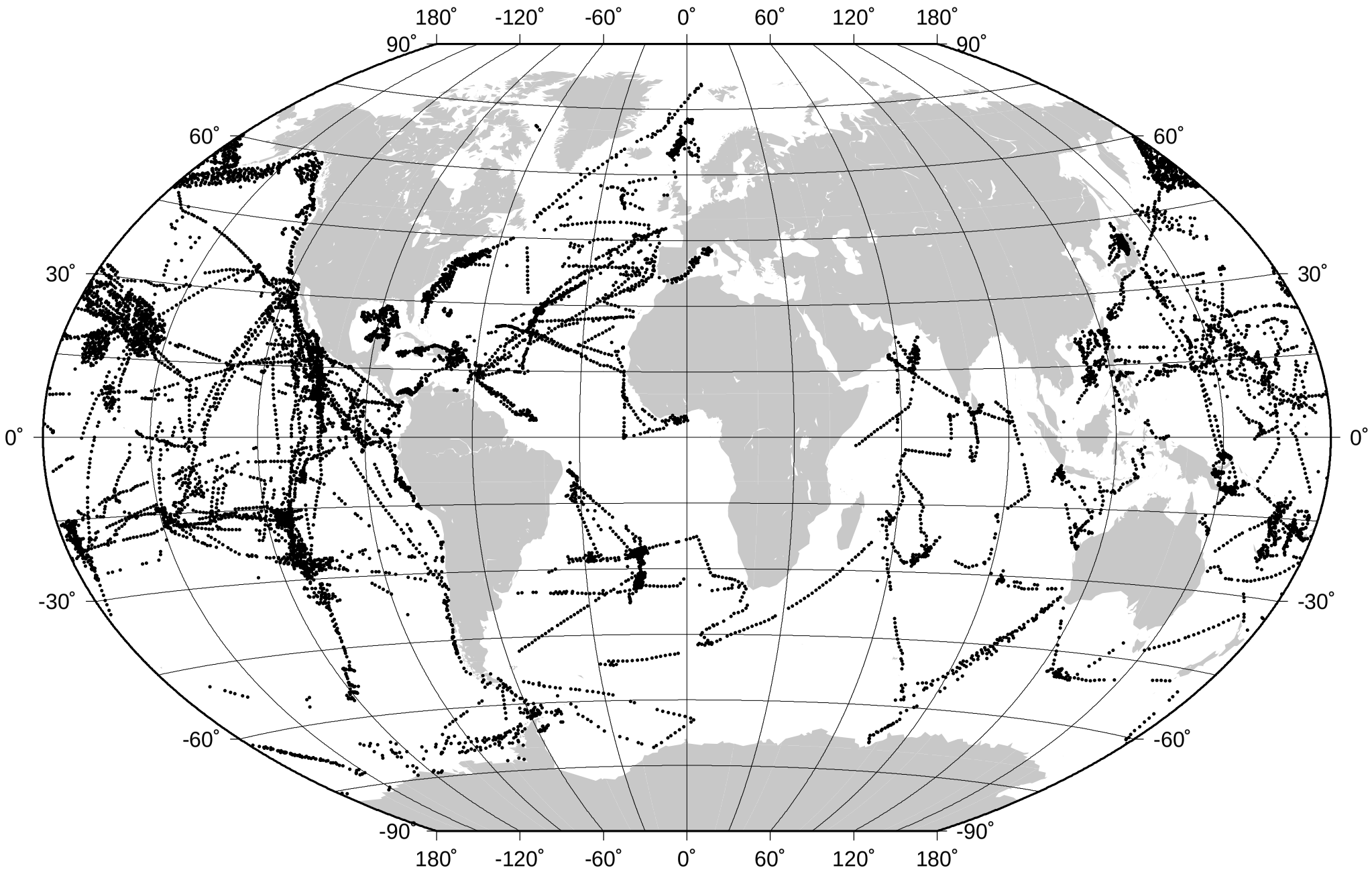

Figure 11

The 11779 marine data locations with viable MF information - 110km segment means comprising at least 25 data (every other data point sampled) with Kp =< 2+ and IGRF residual < 500 nT

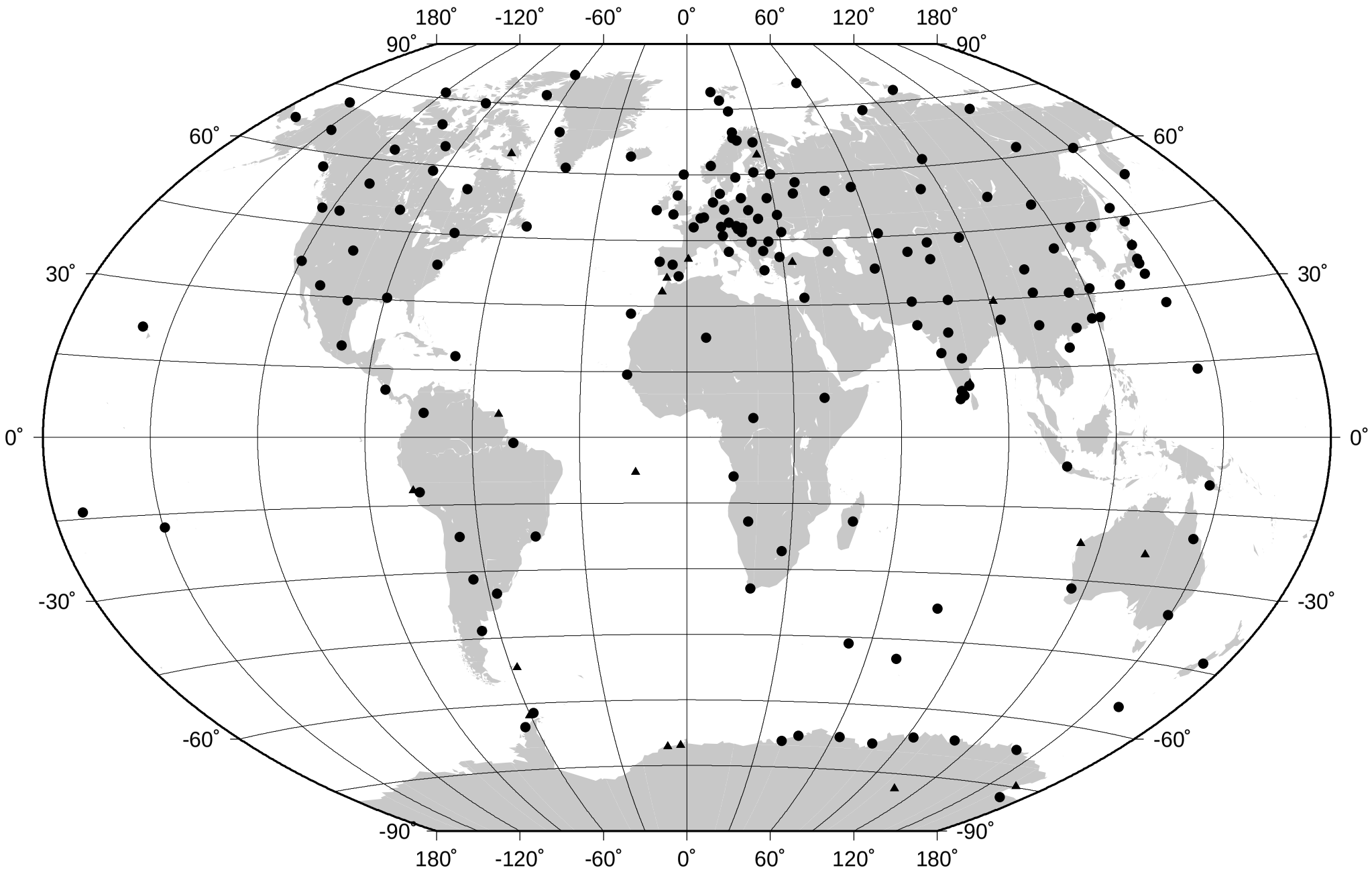

Figure 12

Observatories used for secular variation modelling. Dots - linear predictor applied at 170 observatories, triangles - 20 other observatories

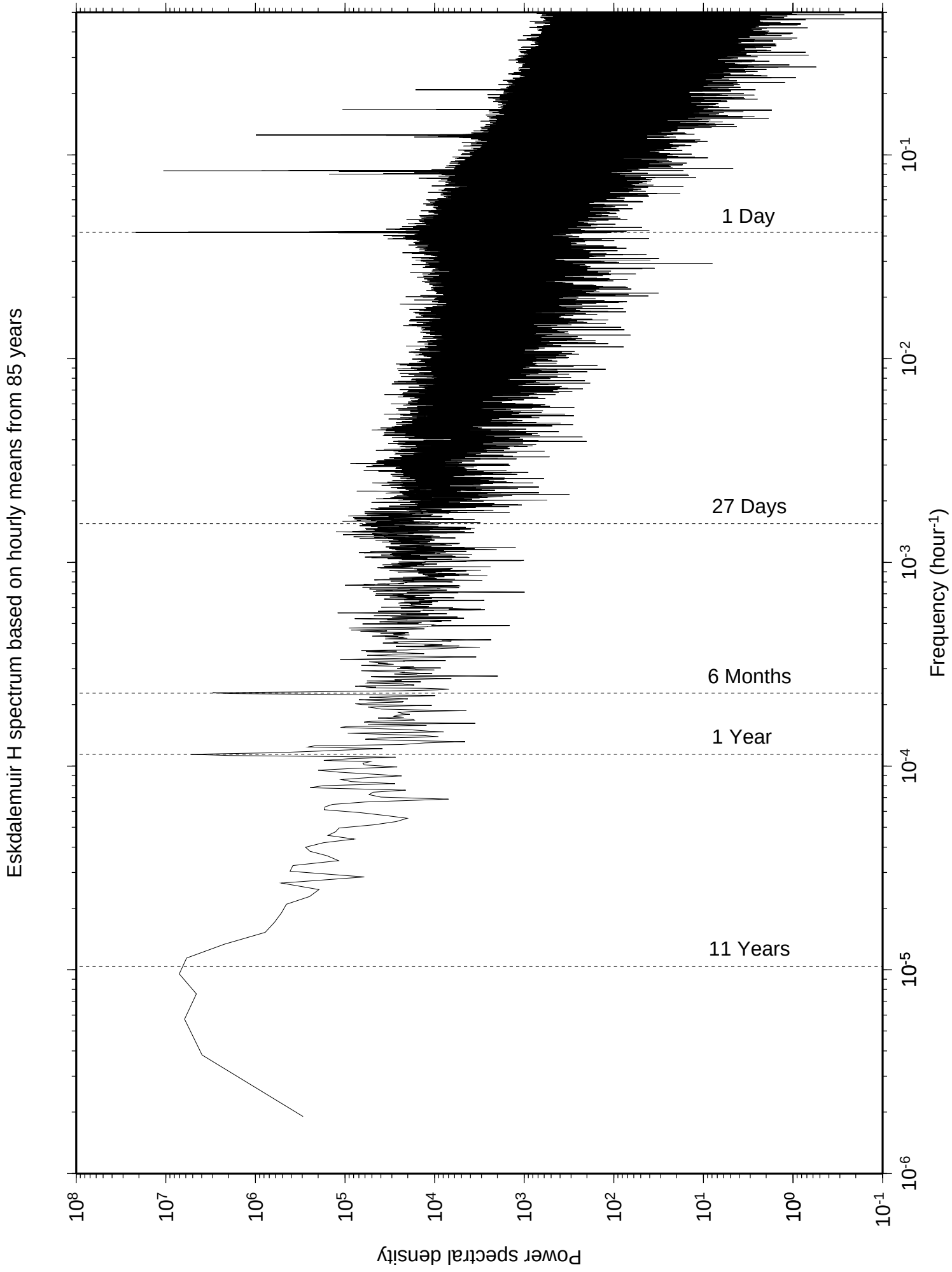
Eskdalemuir H spectrum based on hourly means from 85 years
Power spectral density
Frequency (hour-1)
1 Day
27 Days
6 Months
1 Year
11 Years
10-1
10-2
10-3
10-4
10-5
10-6
108
107
106
105
104
103
102
101
100
10-1

Figure 13

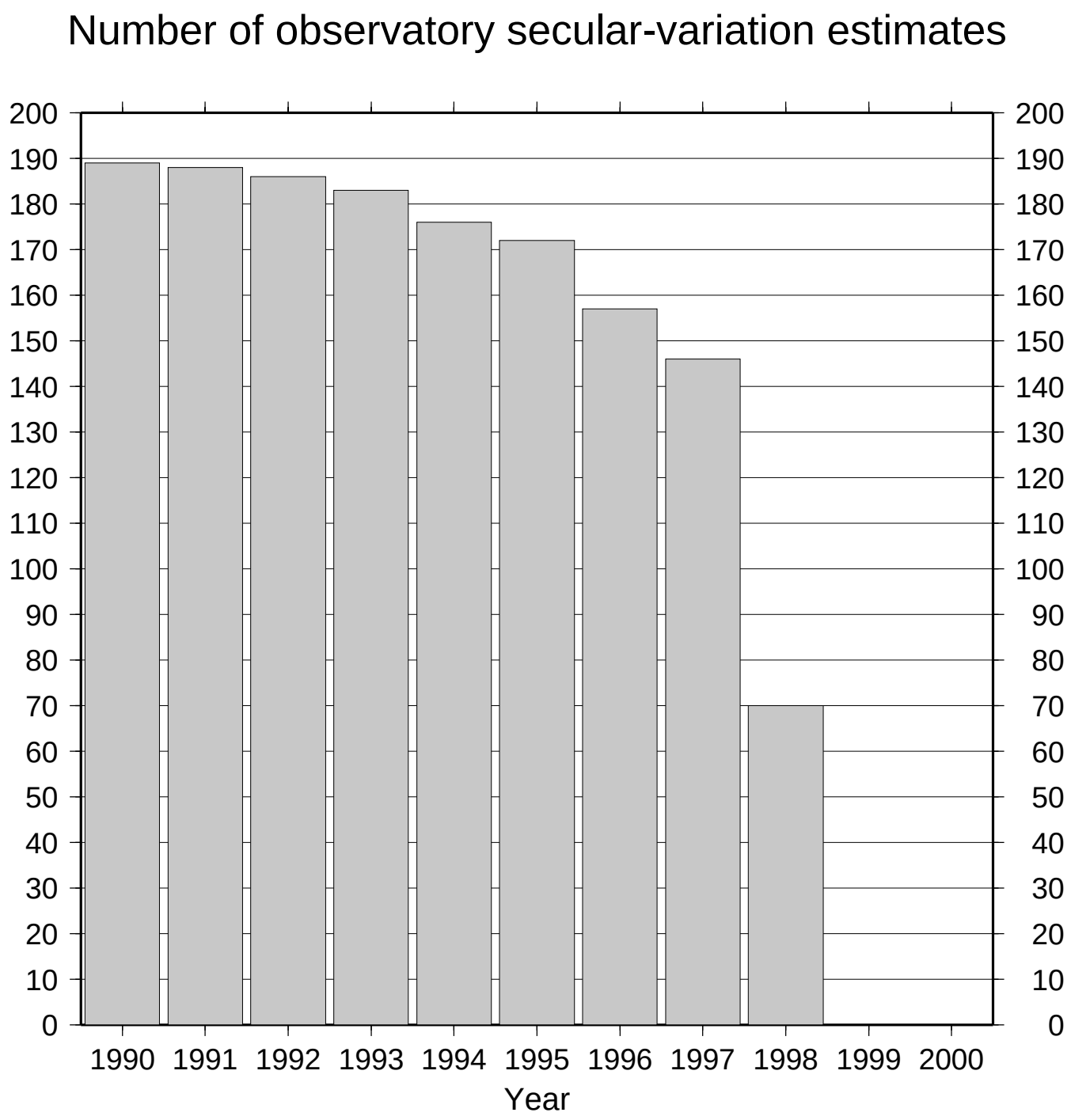
Number of observatory secular-variation estimates
200
190
180
170
160
150
140
130
120
110
100
90
80
70
60
50
40
30
20
10
0
1990
1991
1992
1993
1994
1995
1996
1997
1998
1999
2000
Year

Figure 14

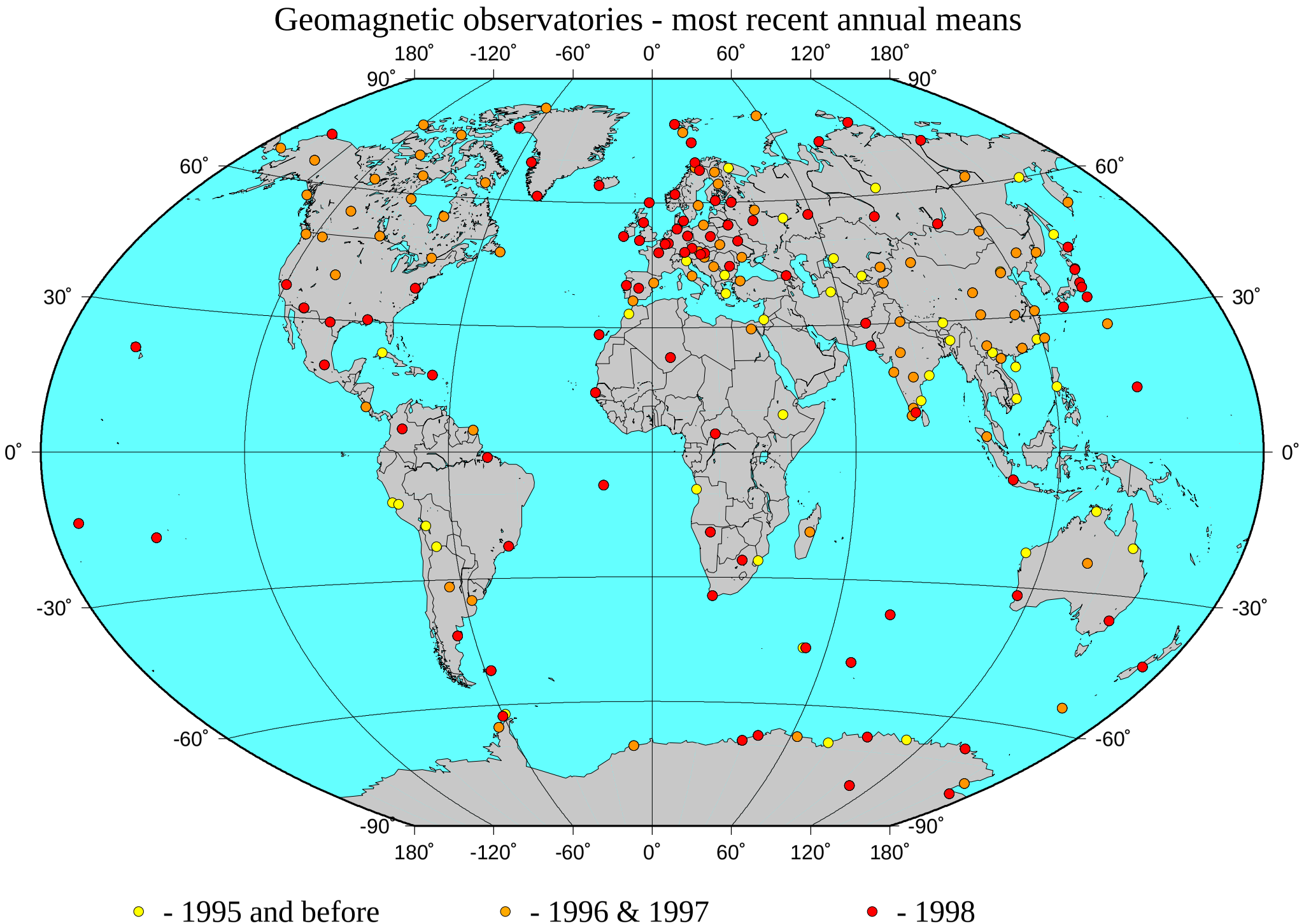
Geomagnetic observatories - most recent annual means
180° -120° -60° 0° 60° 120° 180°
90°
60°
30°
0°
-30°
-60°
-90°
- 1995 and before
- 1996 & 1997
- 1998

Figure 15

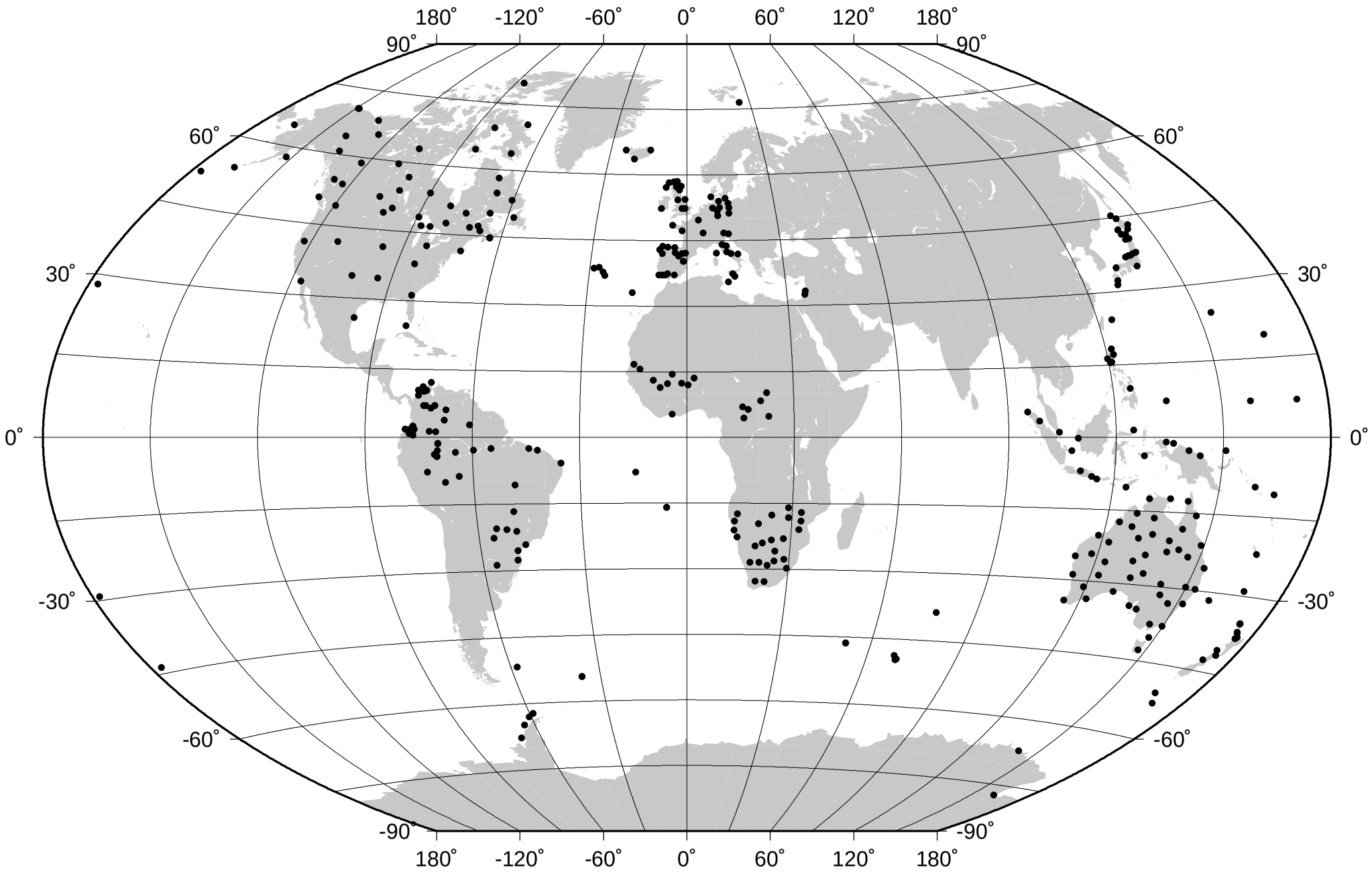

Figure 16

The 341 selected repeat stations with secular-variation information

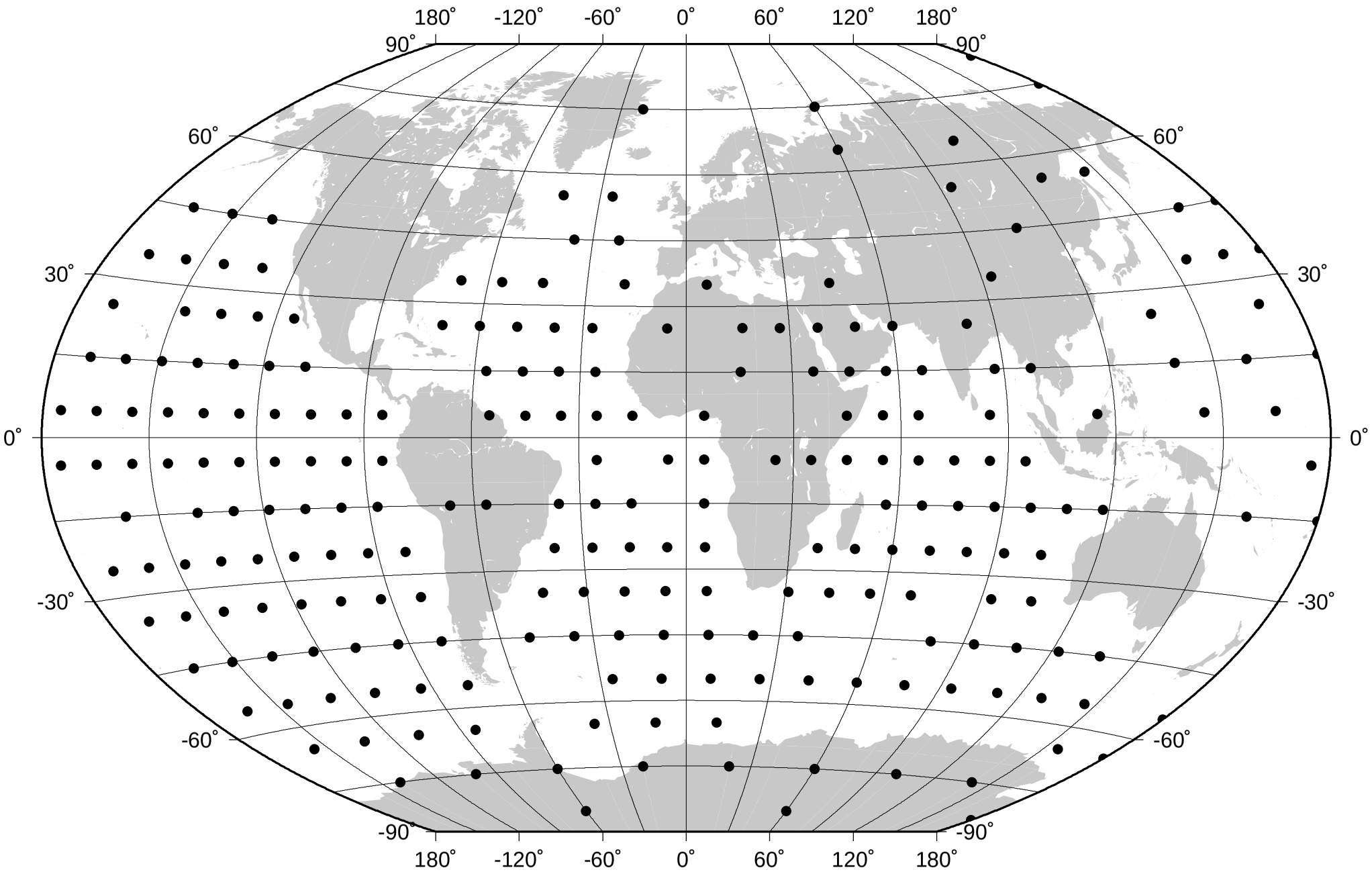

Figure 17

Locations where synthetic SV values from 5-year average SV models which incorporate data from POGS and Oersted satellites are used

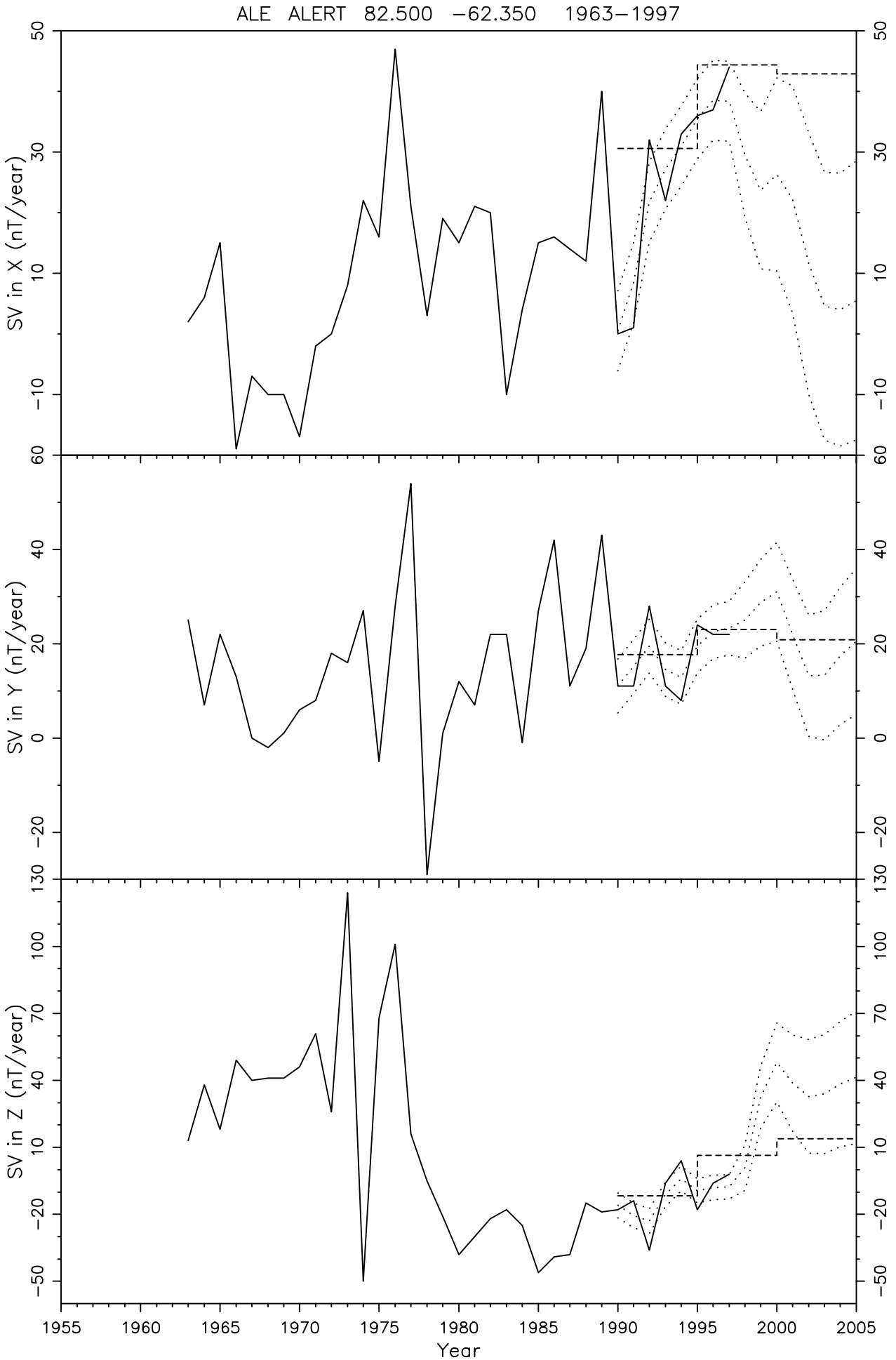
ALE ALERT 82.500 −62.350 1963−1997
SV in X (nT/year)
SV in Y (nT/year)
SV in Z (nT/year)
Year
1955
1960
1965
1970
1975
1980
1985
1990
1995
2000
2005

Figure 18

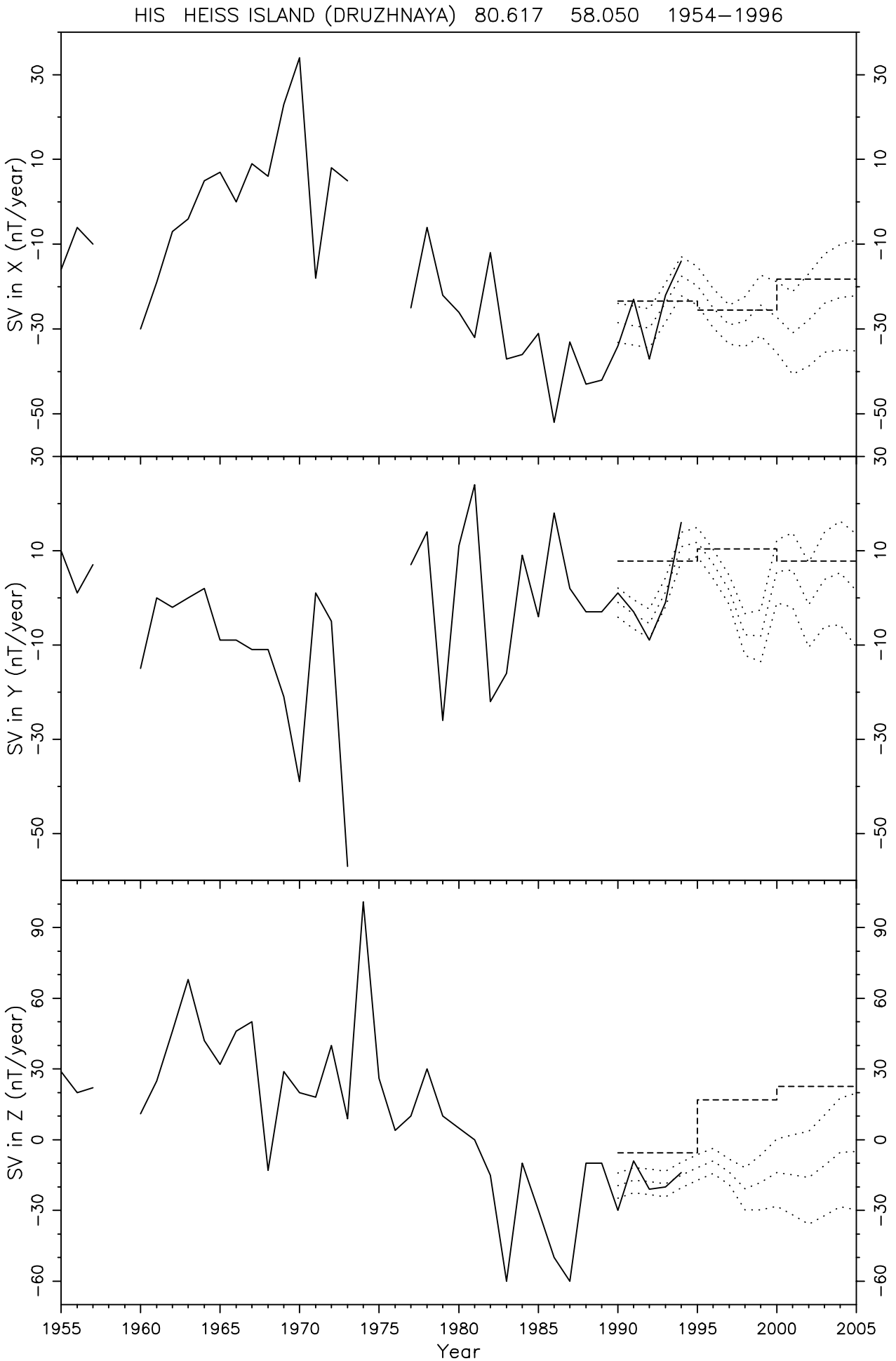
HIS HEISS ISLAND (DRUZHNAYA) 80.617 58.050 1954–1996
SV in X (nT/year)
SV in Y (nT/year)
SV in Z (nT/year)
Year
1955
1960
1965
1970
1975
1980
1985
1990
1995
2000
2005

Figure 19

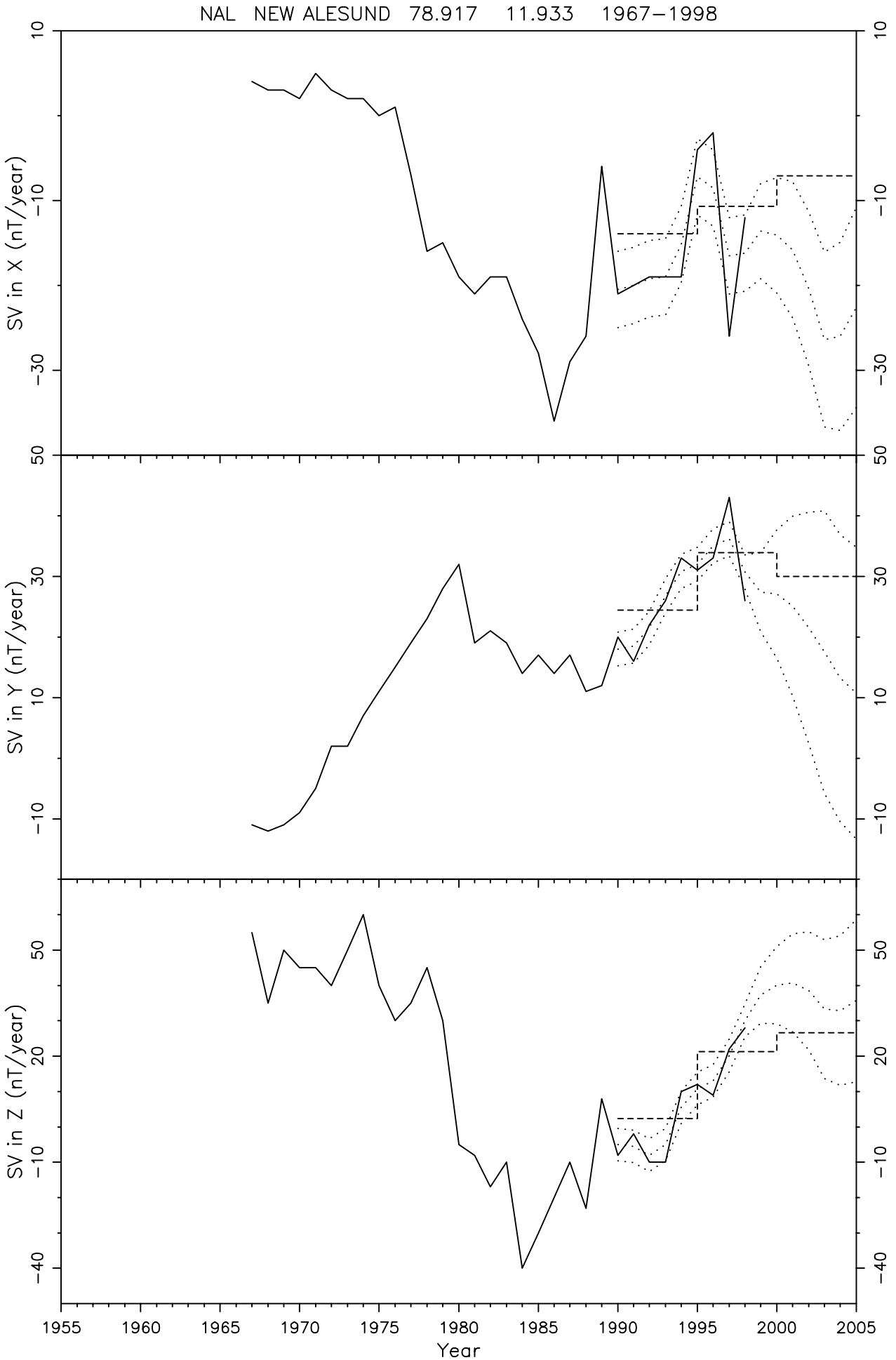
NAL NEW ALESUND 78.917 11.933 1967–1998
SV in X (nT/year)
SV in Y (nT/year)
SV in Z (nT/year)
10
−10
−30
50
30
−40
20
1955
1960
1965
1970
1975
1980
1985
1990
1995
2000
2005
Year

Figure 20

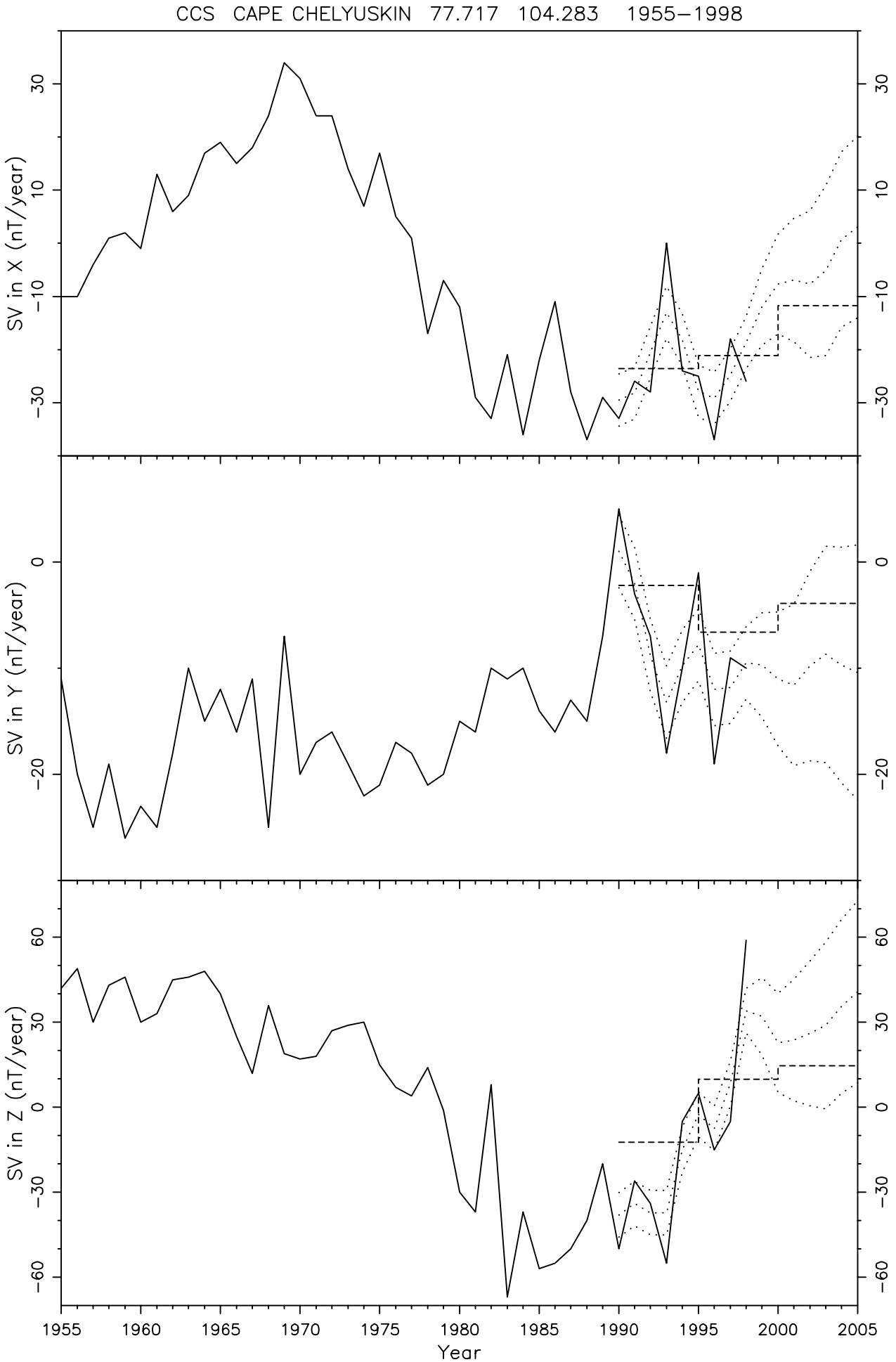
CCS CAPE CHELYUSKIN 77.717 104.283 1955–1998
SV in X (nT/year)
SV in Y (nT/year)
SV in Z (nT/year)
Year
1955
1960
1965
1970
1975
1980
1985
1990
1995
2000
2005

Figure 21

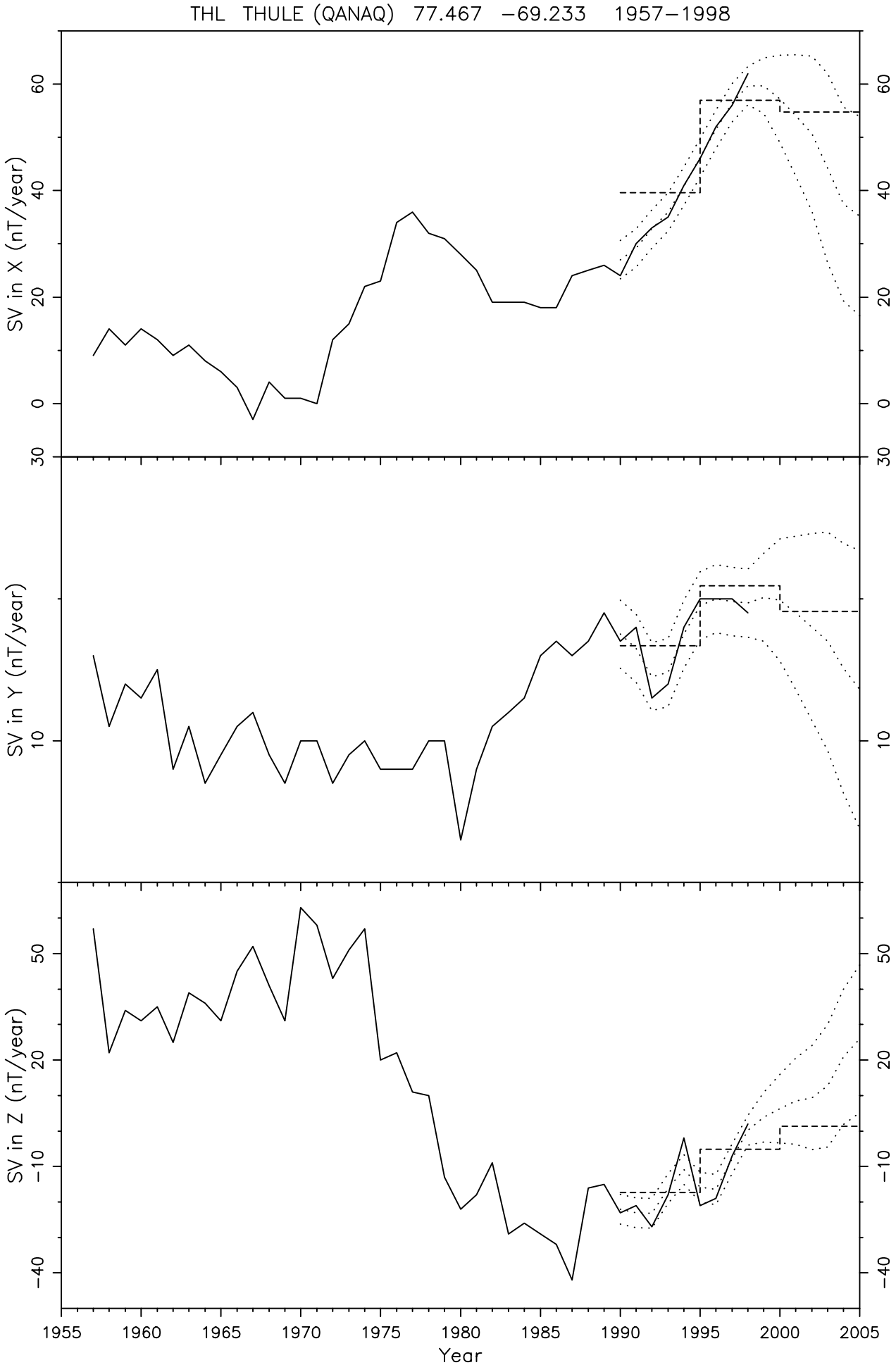
THL THULE (QANAQ) 77.467 −69.233 1957−1998
SV in X (nT/year)
SV in Y (nT/year)
SV in Z (nT/year)
60
40
20
0
30
10
50
−10
−40
1955
1960
1965
1970
1975
1980
1985
1990
1995
2000
2005
Year

Figure 22

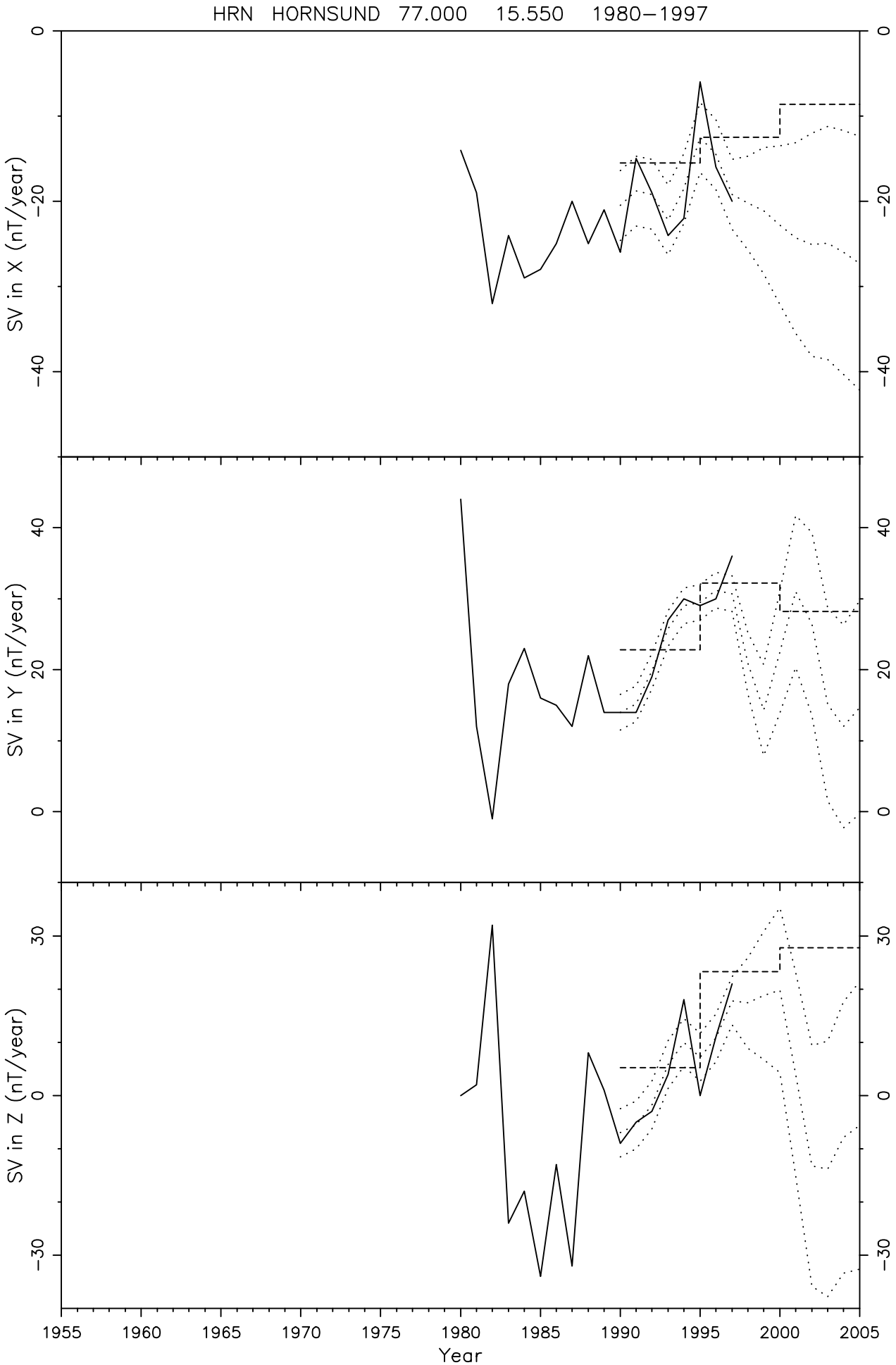
HRN HORNSUND 77.000 15.550 1980–1997
SV in X (nT/year)
SV in Y (nT/year)
SV in Z (nT/year)
0
−20
−40
40
20
30
−30
1955
1960
1965
1970
1975
1980
1985
1990
1995
2000
2005
Year

Figure 23

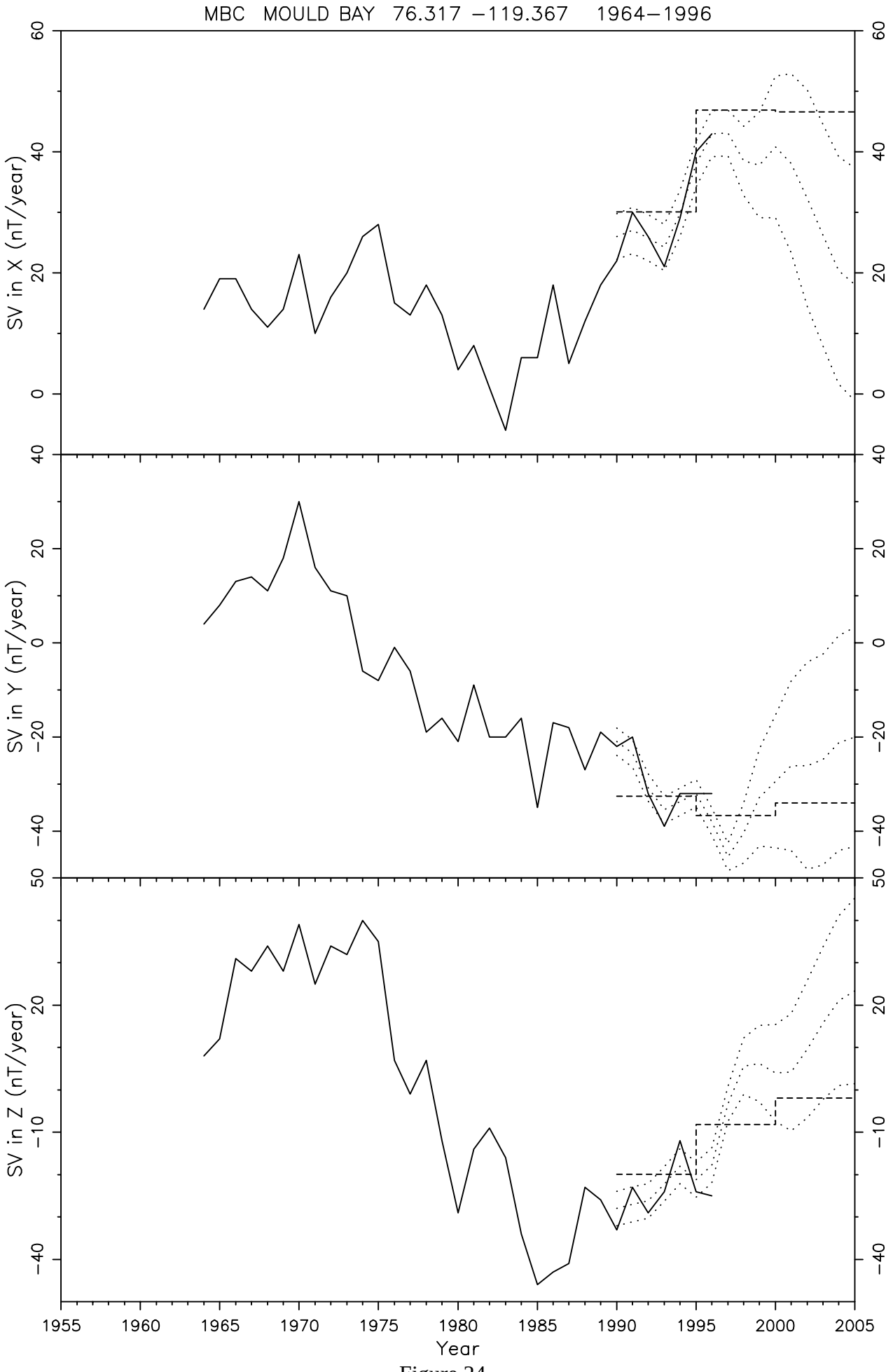
MBC MOULD BAY 76.317 −119.367 1964−1996
SV in X (nT/year)
SV in Y (nT/year)
SV in Z (nT/year)
Year
1955
1960
1965
1970
1975
1980
1985
1990
1995
2000
2005

Figure 24

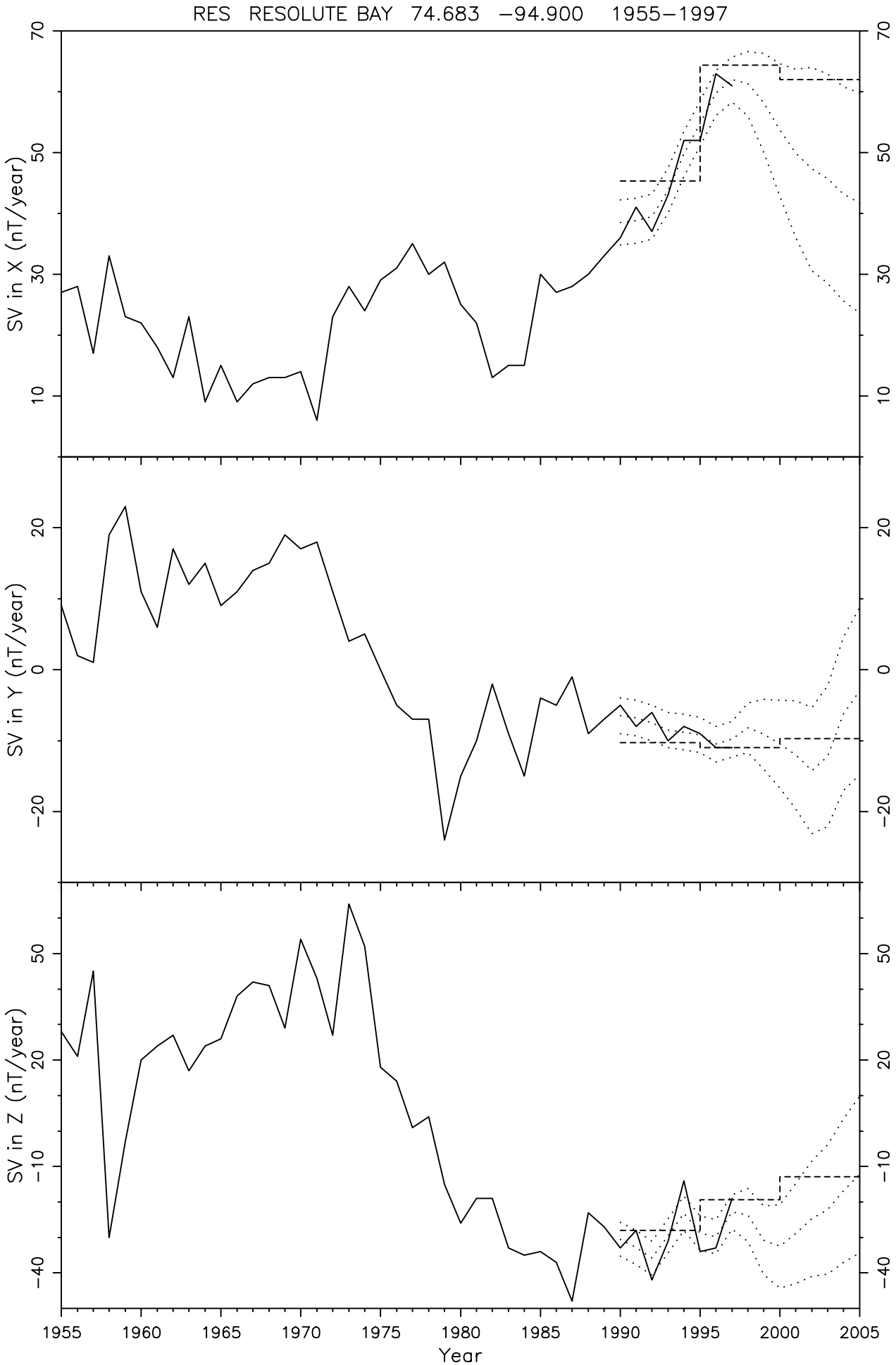
RES RESOLUTE BAY 74.683 −94.900 1955−1997
SV in X (nT/year)
SV in Y (nT/year)
SV in Z (nT/year)
Year
1955
1960
1965
1970
1975
1980
1985
1990
1995
2000
2005

Figure 25

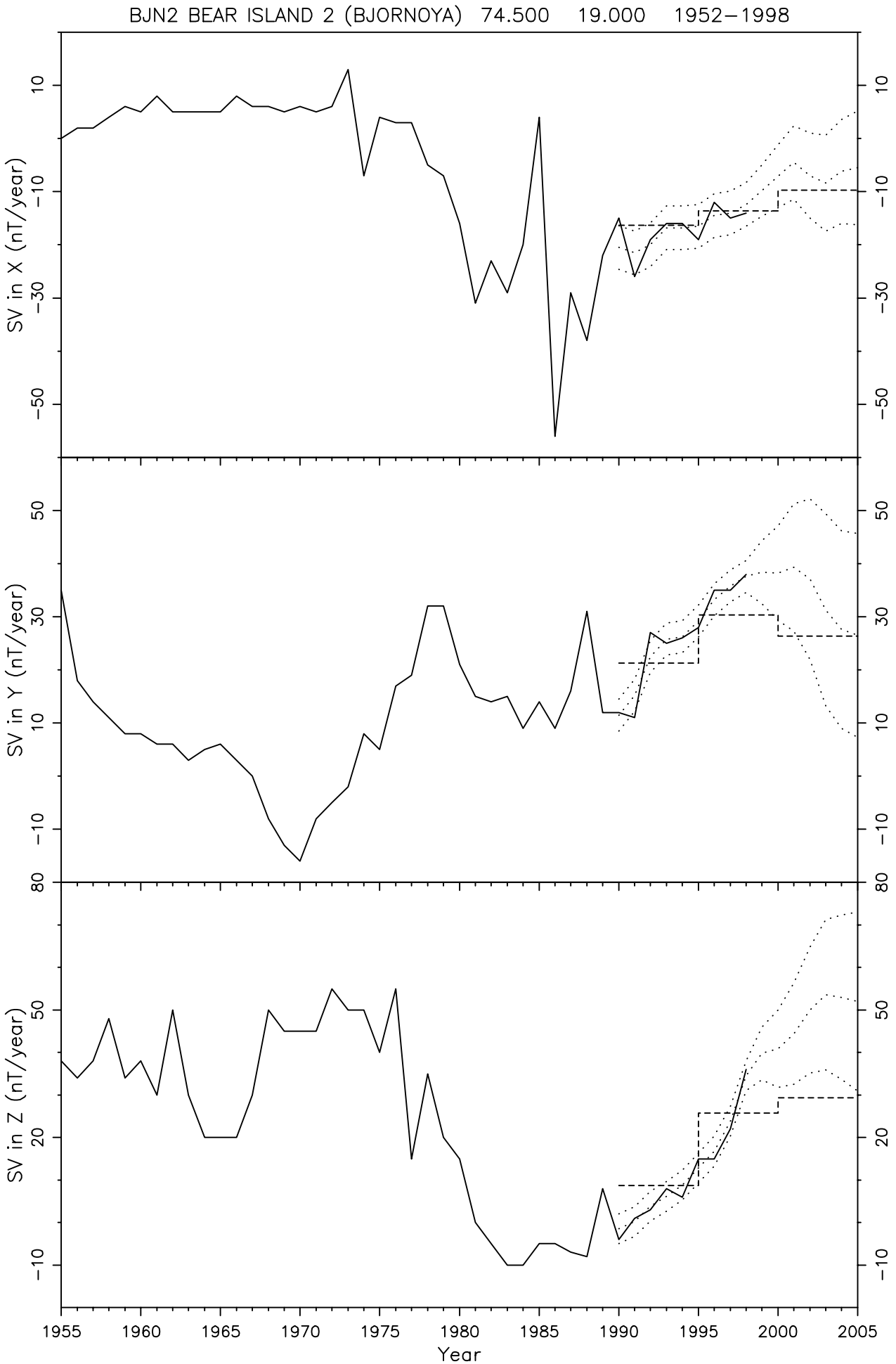
BJN2 BEAR ISLAND 2 (BJORNOYA) 74.500 19.000 1952–1998
SV in X (nT/year)
SV in Y (nT/year)
SV in Z (nT/year)
10
−10
−30
−50
50
30
10
−10
80
50
20
−10
1955
1960
1965
1970
1975
1980
1985
1990
1995
2000
2005
Year

Figure 26

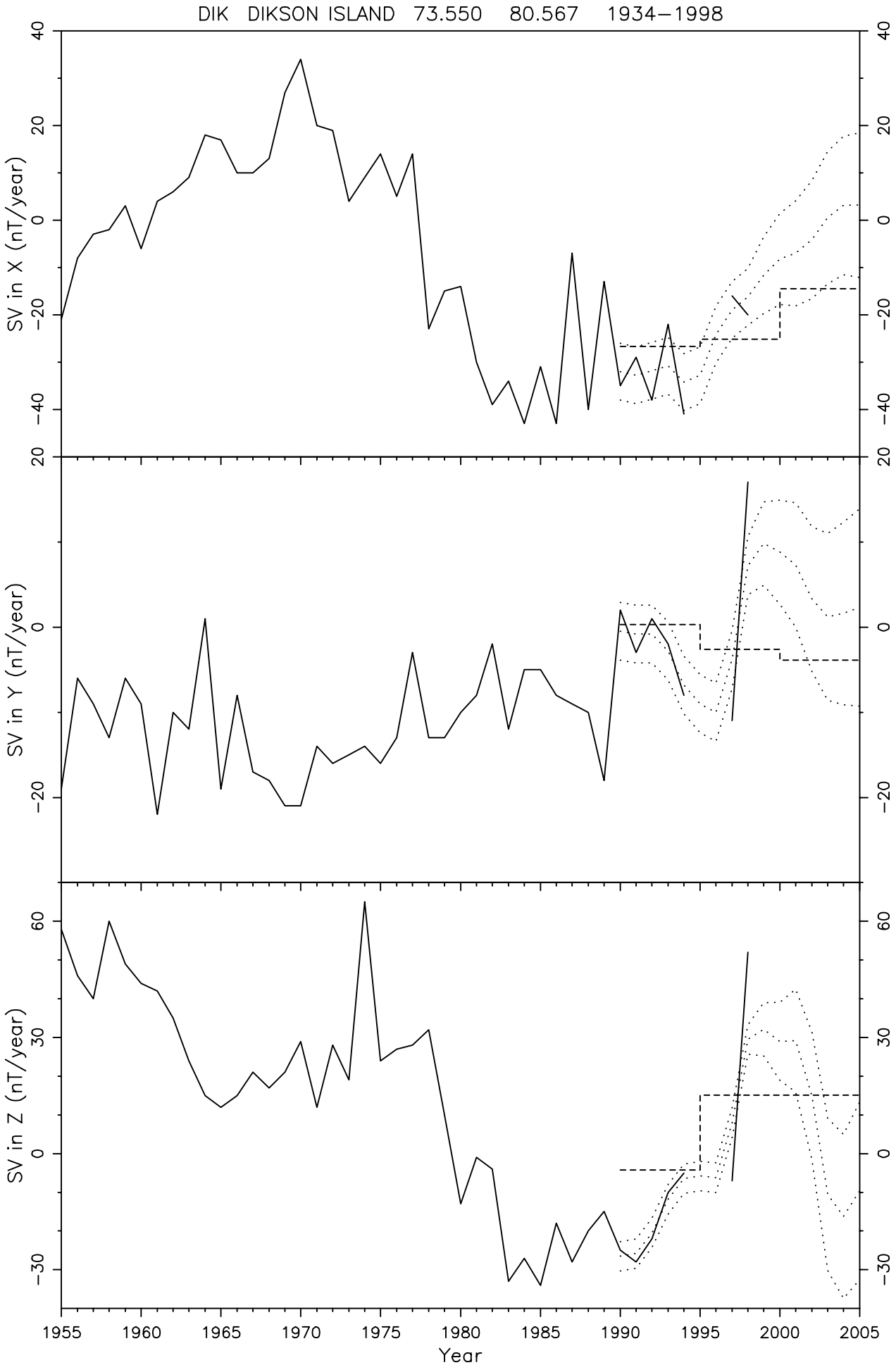
DIK DIKSON ISLAND 73.550 80.567 1934–1998
SV in X (nT/year)
SV in Y (nT/year)
SV in Z (nT/year)
Year
1955
1960
1965
1970
1975
1980
1985
1990
1995
2000
2005

Figure 27

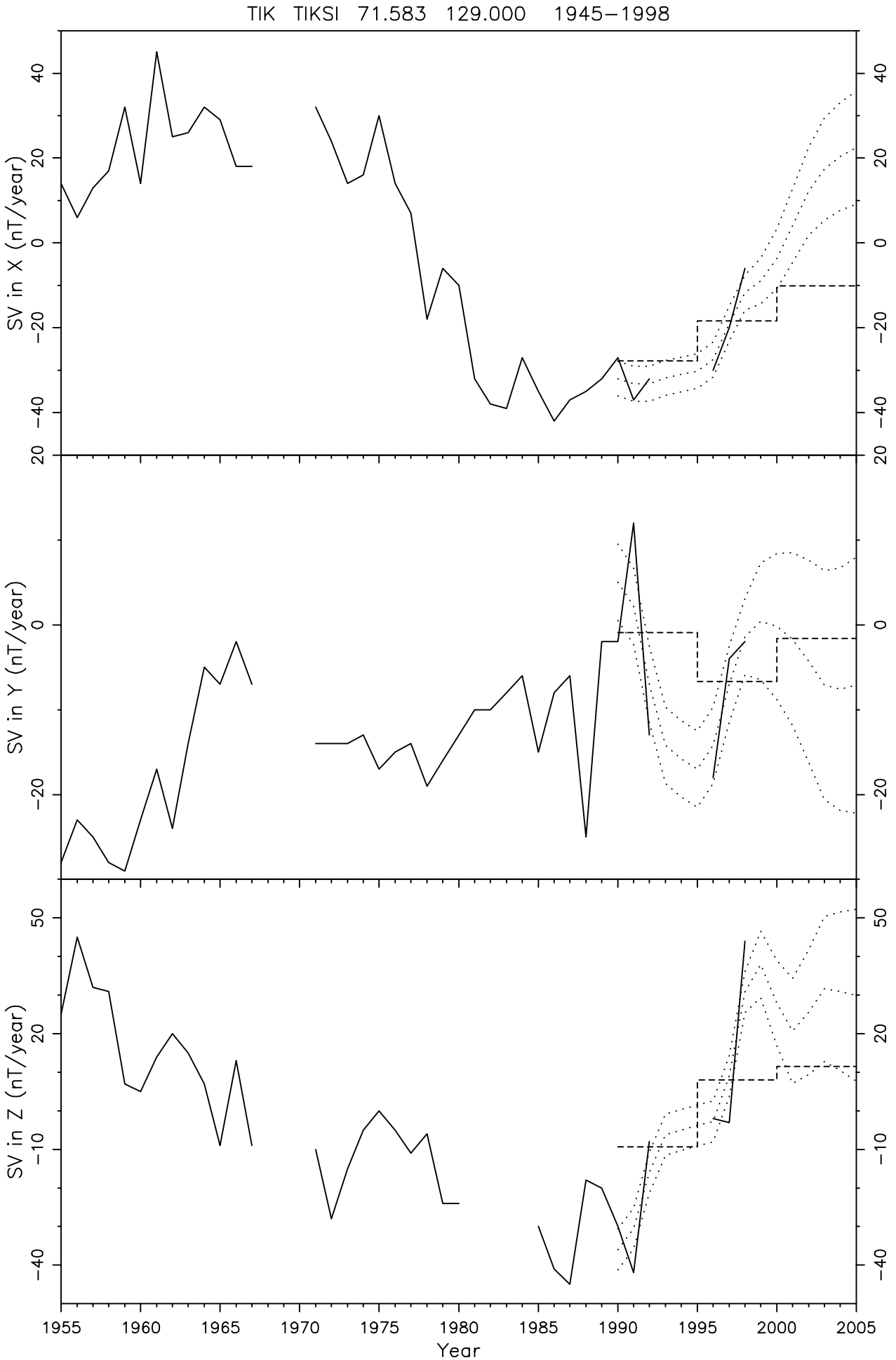
TIK TIKSI 71.583 129.000 1945–1998
SV in X (nT/year)
SV in Y (nT/year)
SV in Z (nT/year)
Year
1955
1960
1965
1970
1975
1980
1985
1990
1995
2000
2005

Figure 28

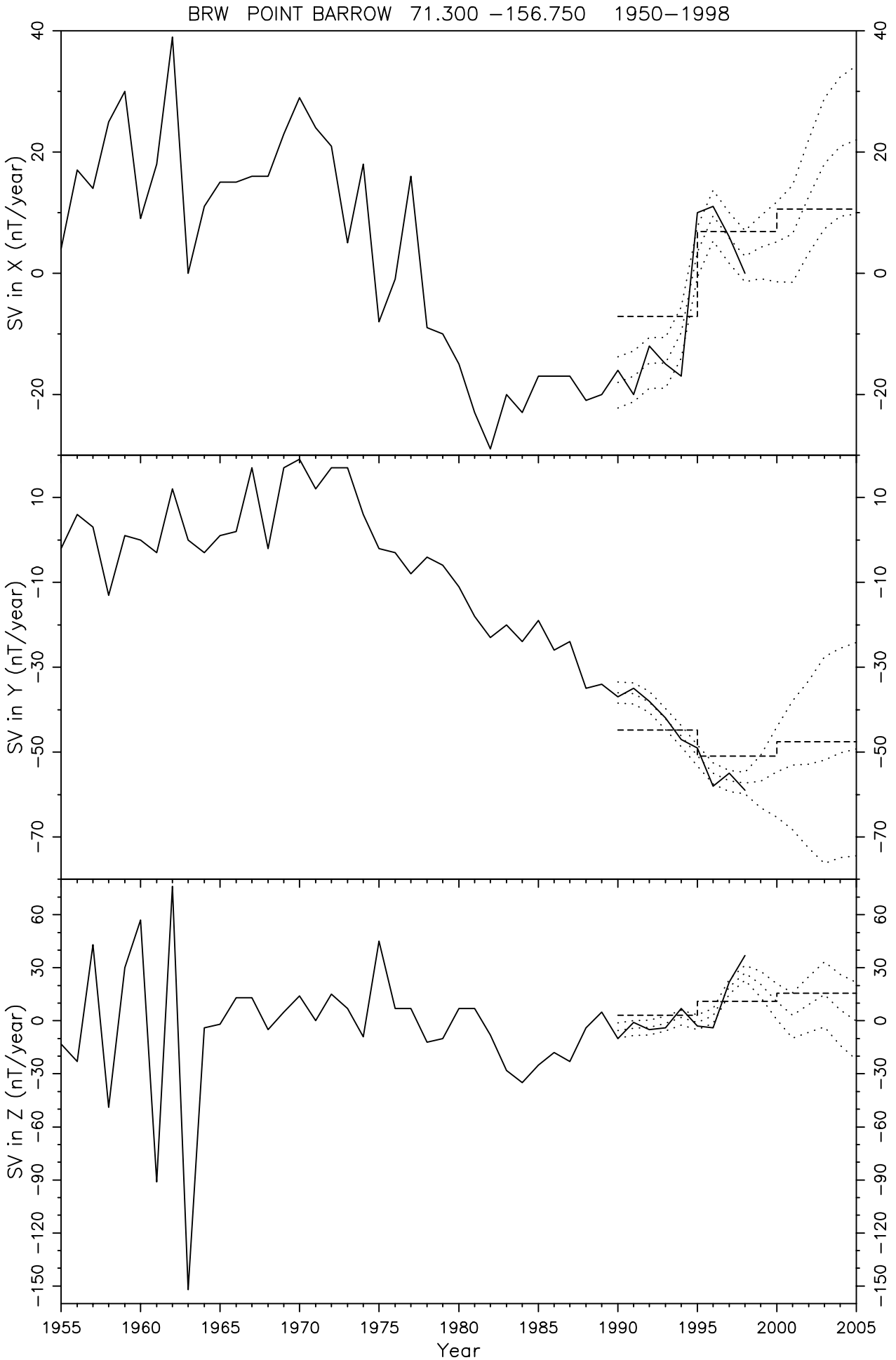
BRW POINT BARROW 71.300 −156.750 1950−1998
SV in X (nT/year)
SV in Y (nT/year)
SV in Z (nT/year)
Year
1955
1960
1965
1970
1975
1980
1985
1990
1995
2000
2005

Figure 29

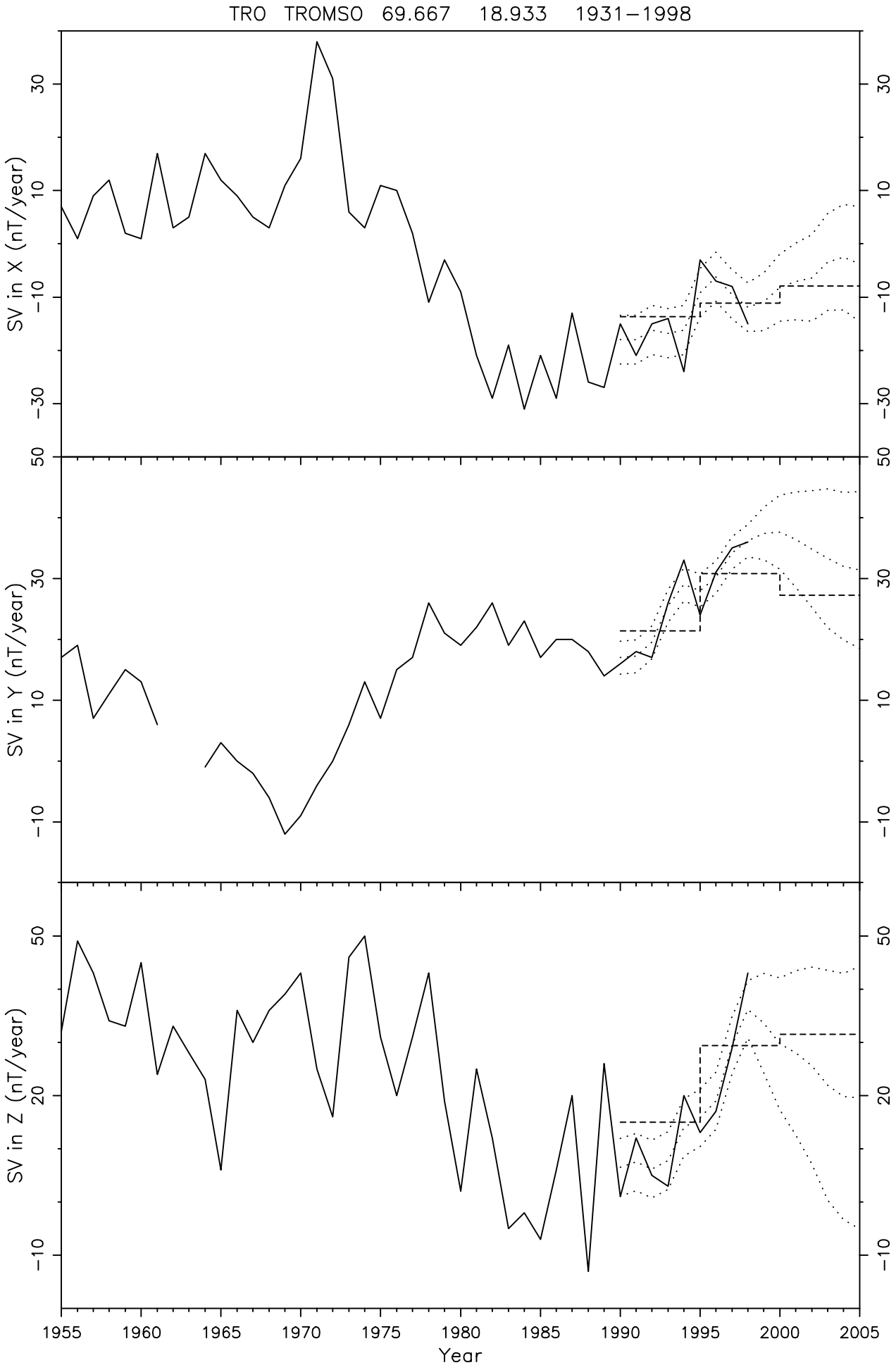
TRO TROMSO 69.667 18.933 1931–1998
SV in X (nT/year)
SV in Y (nT/year)
SV in Z (nT/year)
Year
1955
1960
1965
1970
1975
1980
1985
1990
1995
2000
2005

Figure 30

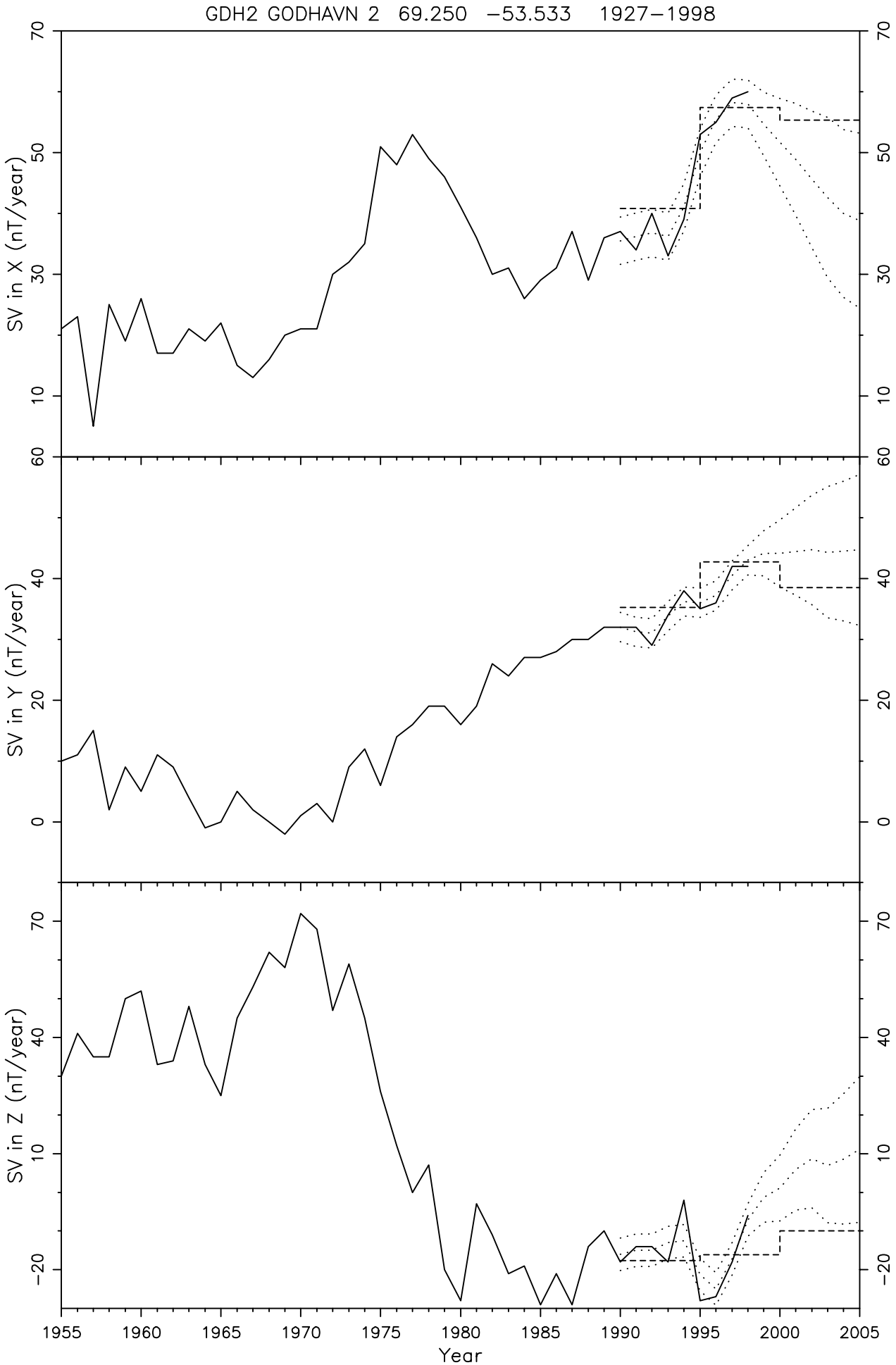
GDH2 GODHAVN 2 69.250 −53.533 1927−1998
SV in X (nT/year)
SV in Y (nT/year)
SV in Z (nT/year)
70
50
30
10
60
40
20
0
−20
1955
1960
1965
1970
1975
1980
1985
1990
1995
2000
2005
Year

Figure 31

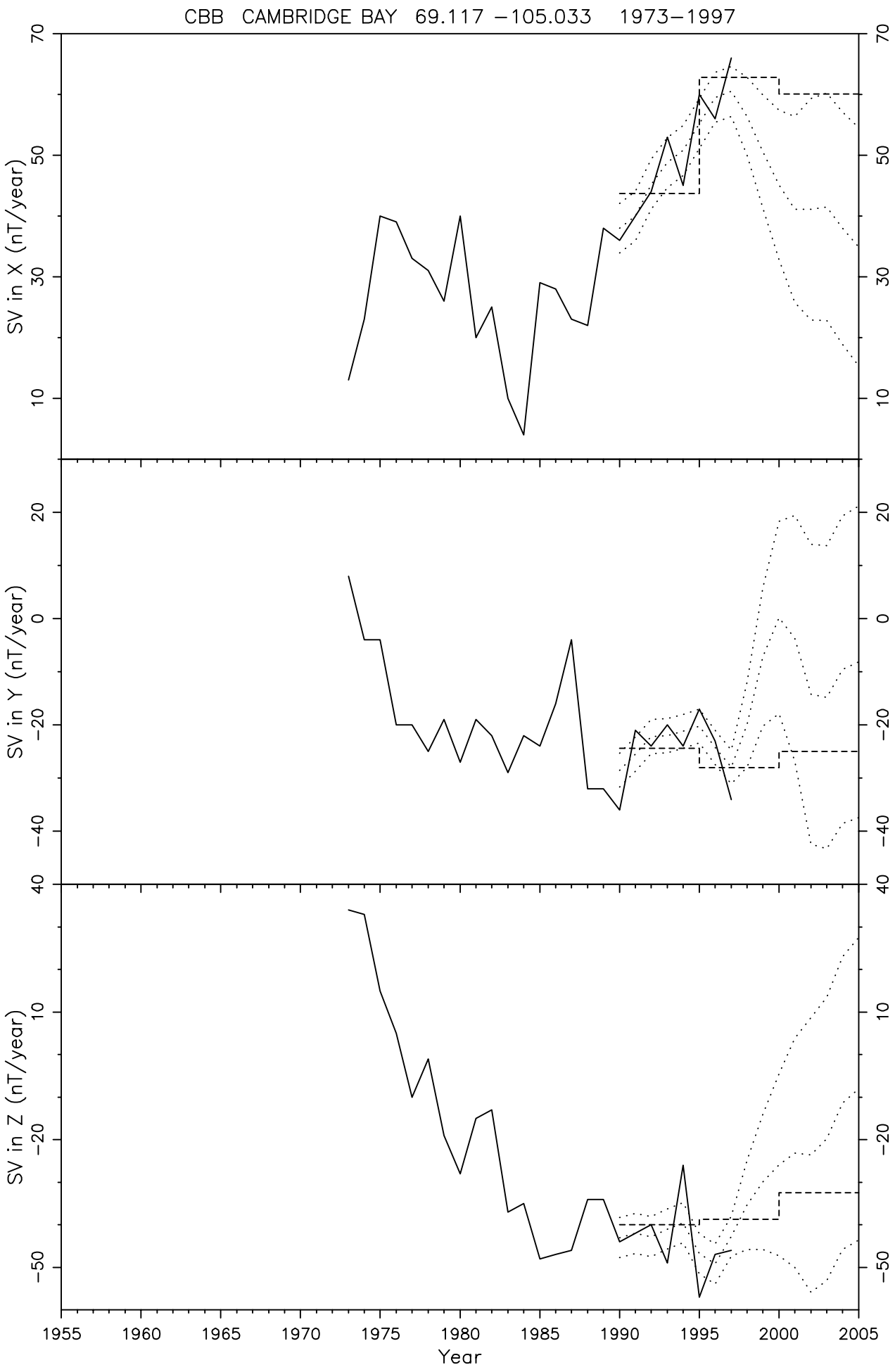
CBB CAMBRIDGE BAY 69.117 −105.033 1973−1997
SV in X (nT/year)
SV in Y (nT/year)
SV in Z (nT/year)
Year
1955
1960
1965
1970
1975
1980
1985
1990
1995
2000
2005

Figure 32

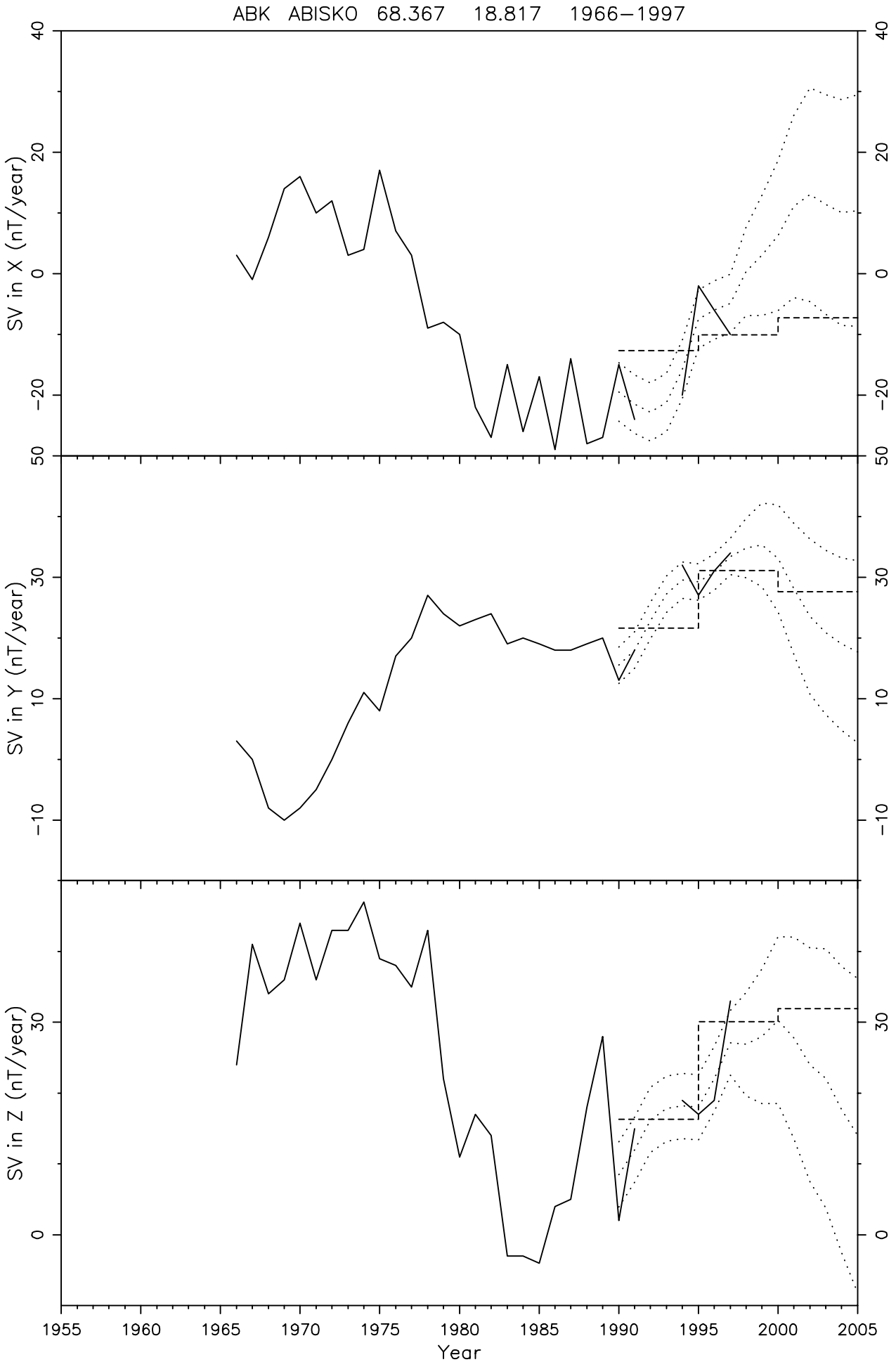
ABK ABISKO 68.367 18.817 1966–1997
SV in X (nT/year)
SV in Y (nT/year)
SV in Z (nT/year)
Year
1955
1960
1965
1970
1975
1980
1985
1990
1995
2000
2005

Figure 33

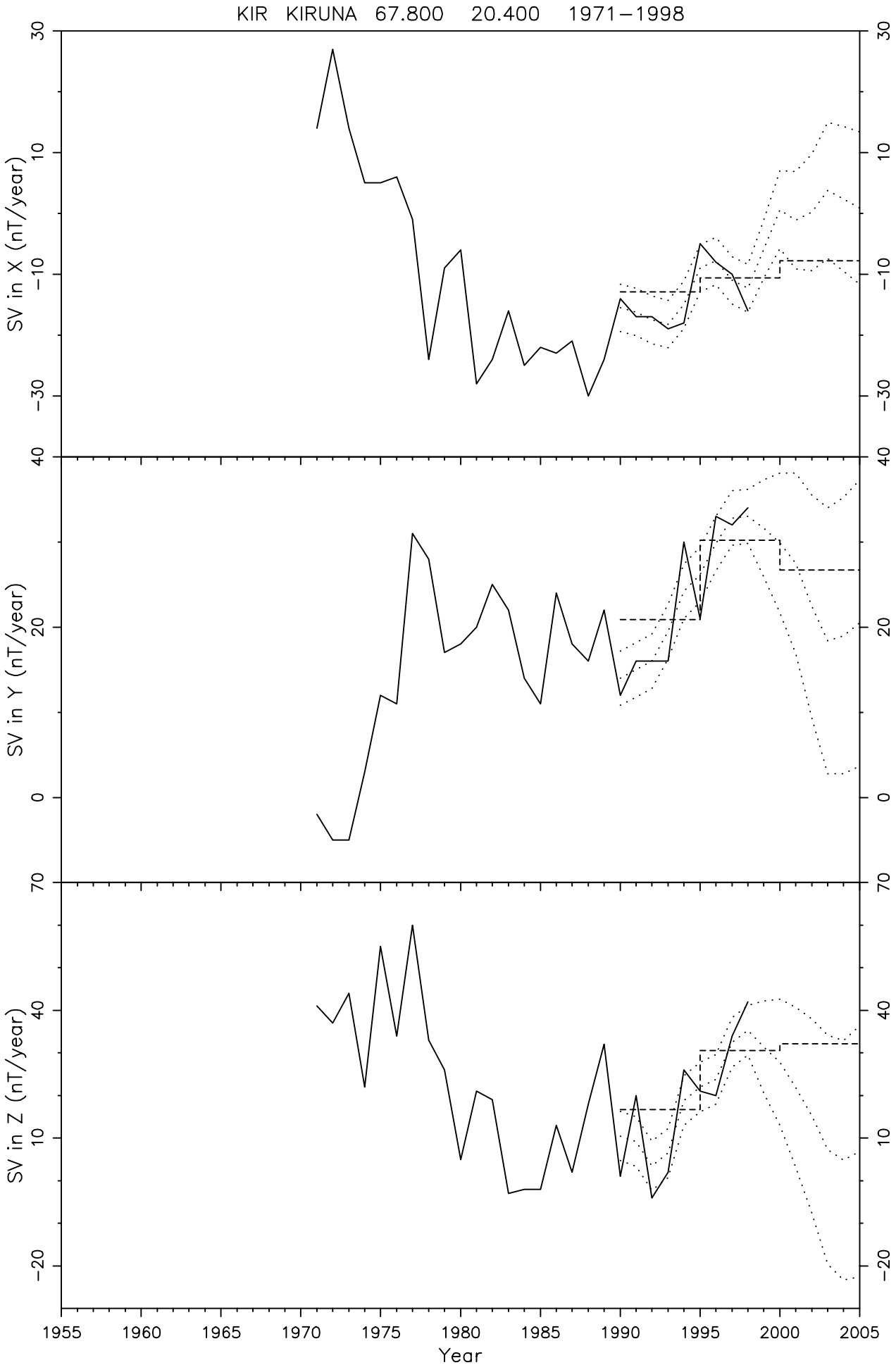
KIR KIRUNA 67.800 20.400 1971−1998
SV in X (nT/year)
SV in Y (nT/year)
SV in Z (nT/year)
30
10
−10
−30
40
20
0
70
−20
1955
1960
1965
1970
1975
1980
1985
1990
1995
2000
2005
Year

Figure 34

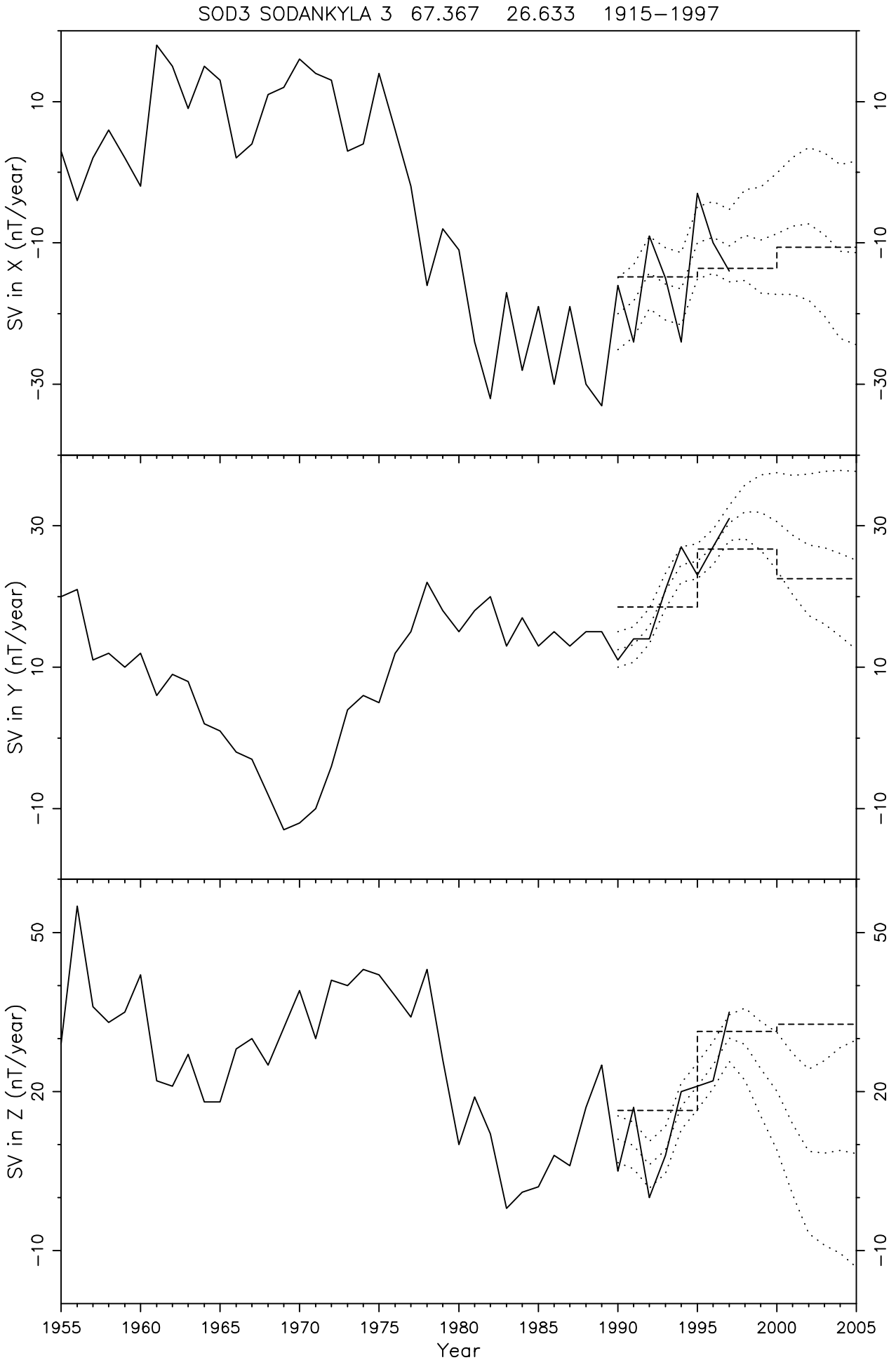
SOD3 SODANKYLA 3 67.367 26.633 1915–1997
SV in X (nT/year)
SV in Y (nT/year)
SV in Z (nT/year)
10
−10
−30
30
50
20
1955
1960
1965
1970
1975
1980
1985
1990
1995
2000
2005
Year

Figure 35

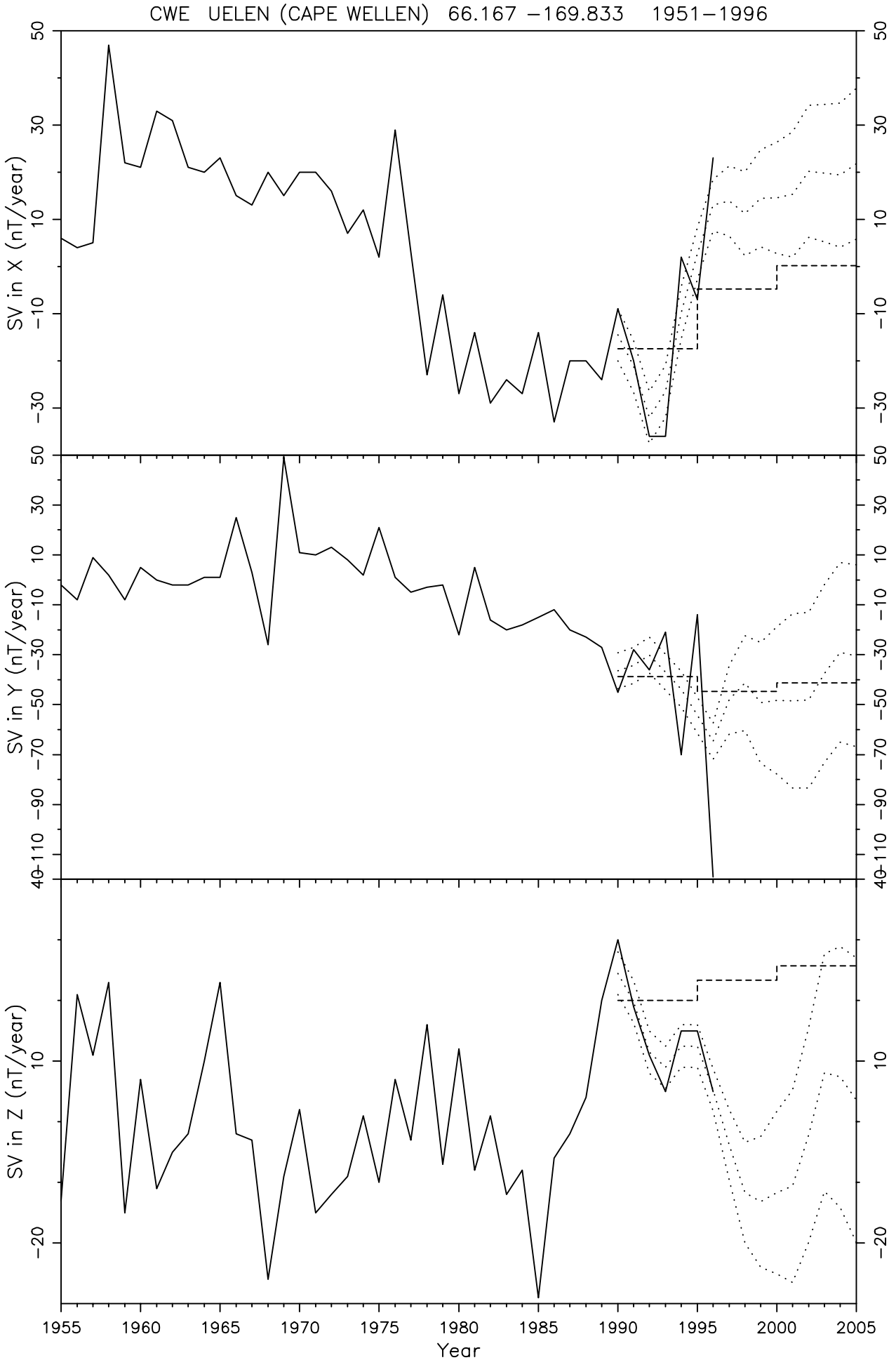
CWE UELEN (CAPE WELLEN) 66.167 −169.833 1951−1996
SV in X (nT/year)
SV in Y (nT/year)
SV in Z (nT/year)
Year
1955
1960
1965
1970
1975
1980
1985
1990
1995
2000
2005

Figure 36

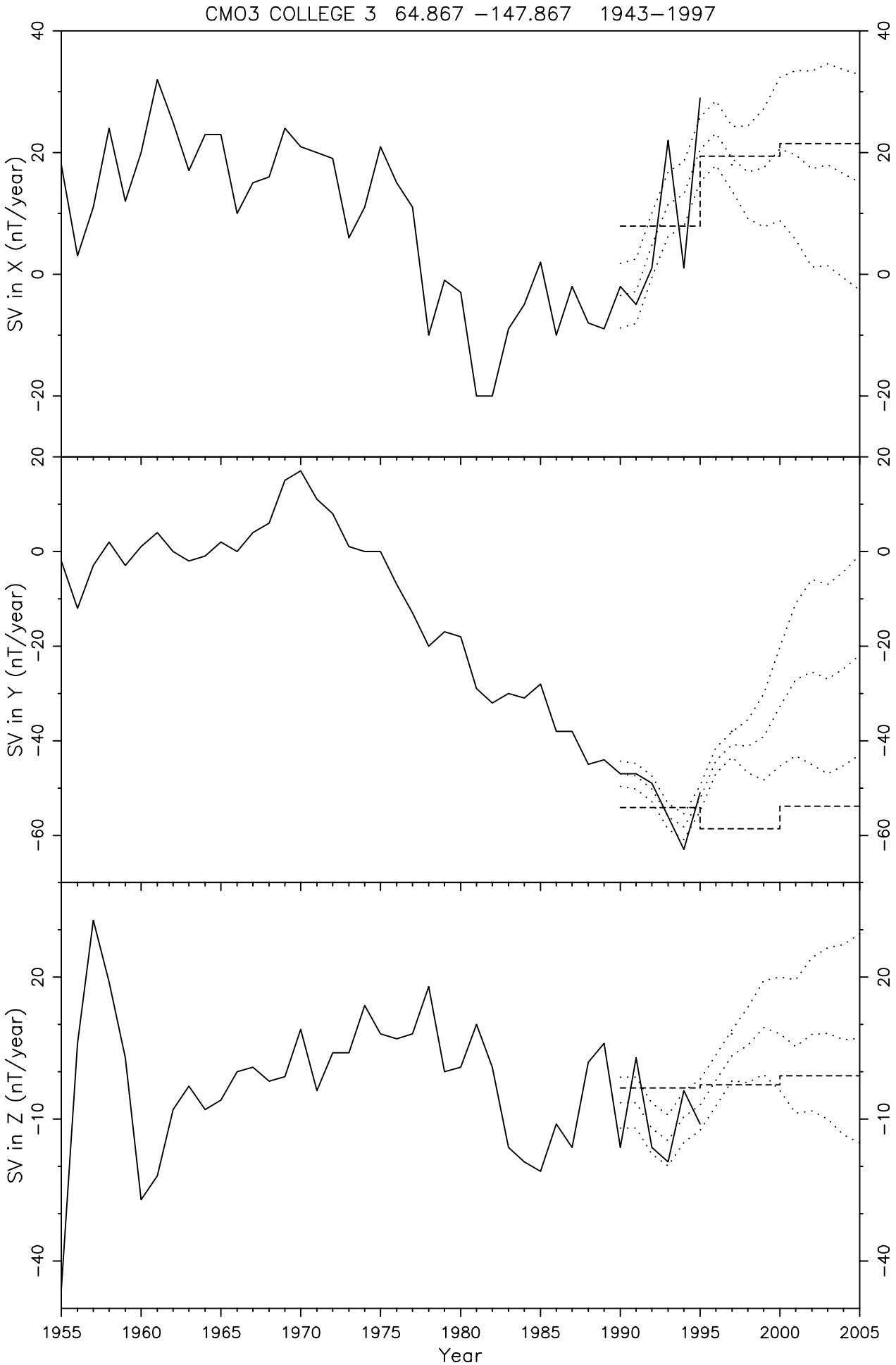
CMO3 COLLEGE 3 64.867 −147.867 1943−1997
SV in X (nT/year)
SV in Y (nT/year)
SV in Z (nT/year)
Year
1955
1960
1965
1970
1975
1980
1985
1990
1995
2000
2005

Figure 37

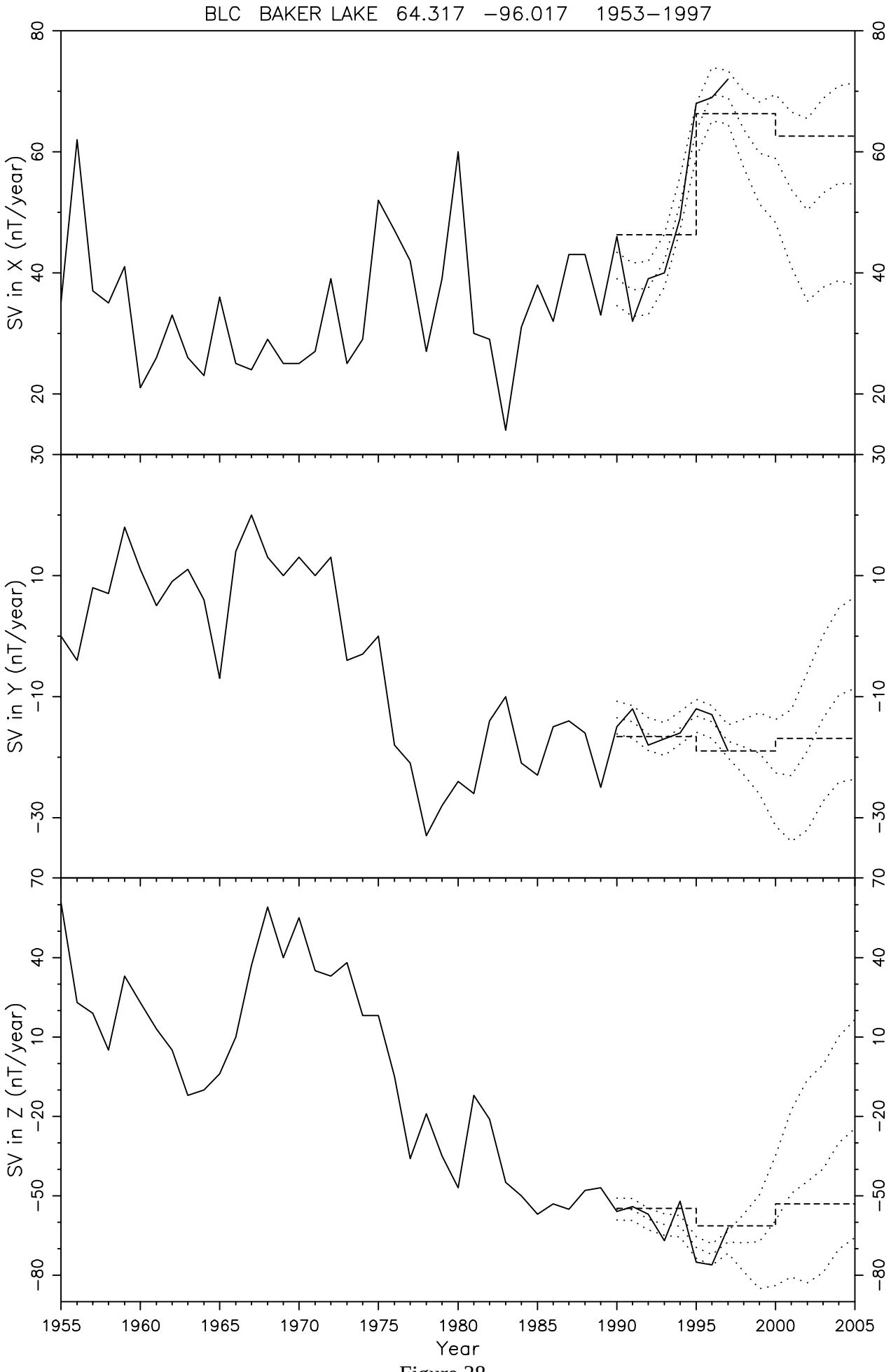
BLC BAKER LAKE 64.317 −96.017 1953−1997
SV in X (nT/year)
SV in Y (nT/year)
SV in Z (nT/year)
Year
1955
1960
1965
1970
1975
1980
1985
1990
1995
2000
2005

Figure 38

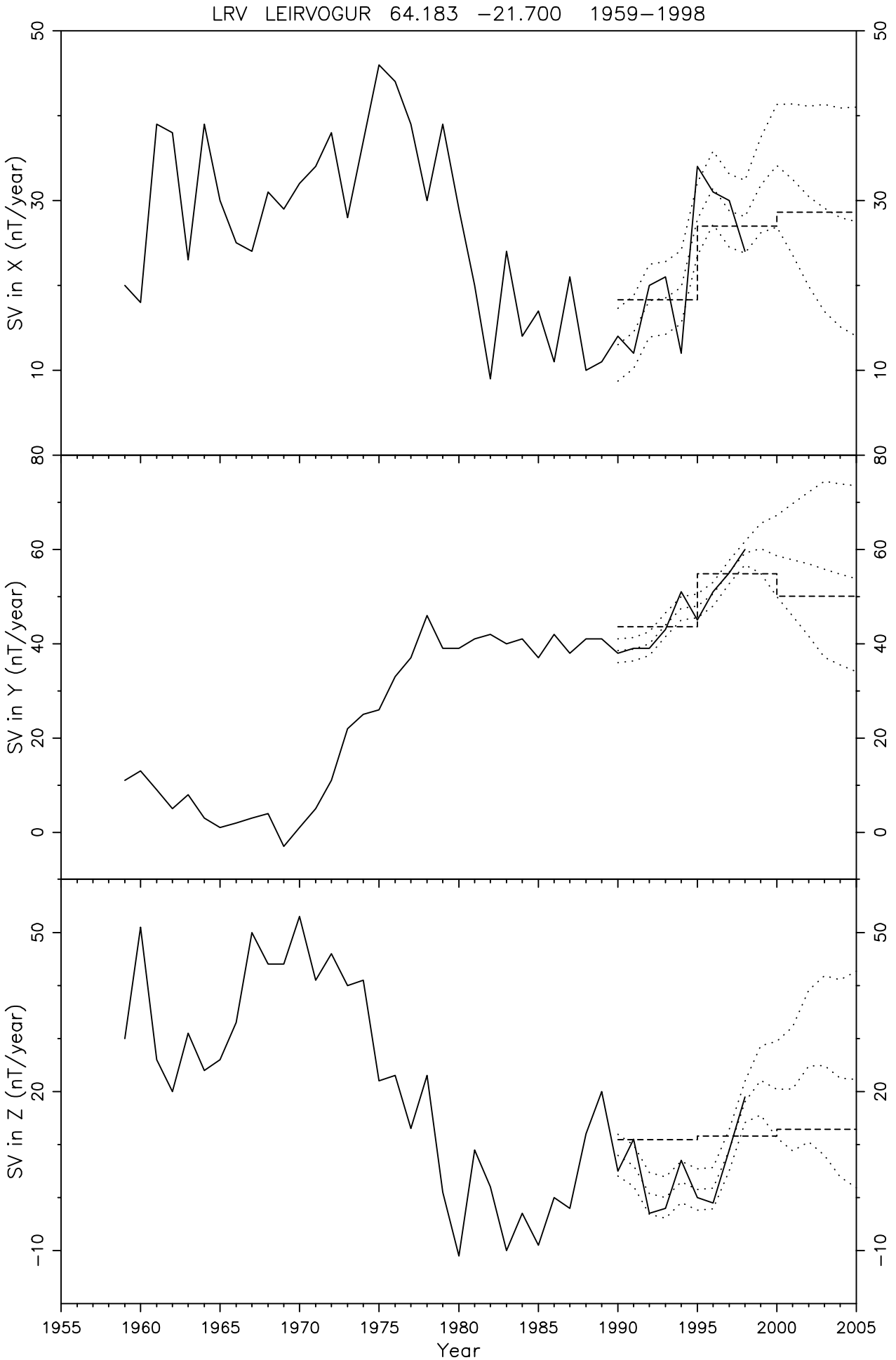
LRV LEIRVOGUR 64.183 −21.700 1959−1998
SV in X (nT/year)
SV in Y (nT/year)
SV in Z (nT/year)
Year
1955
1960
1965
1970
1975
1980
1985
1990
1995
2000
2005

Figure 39

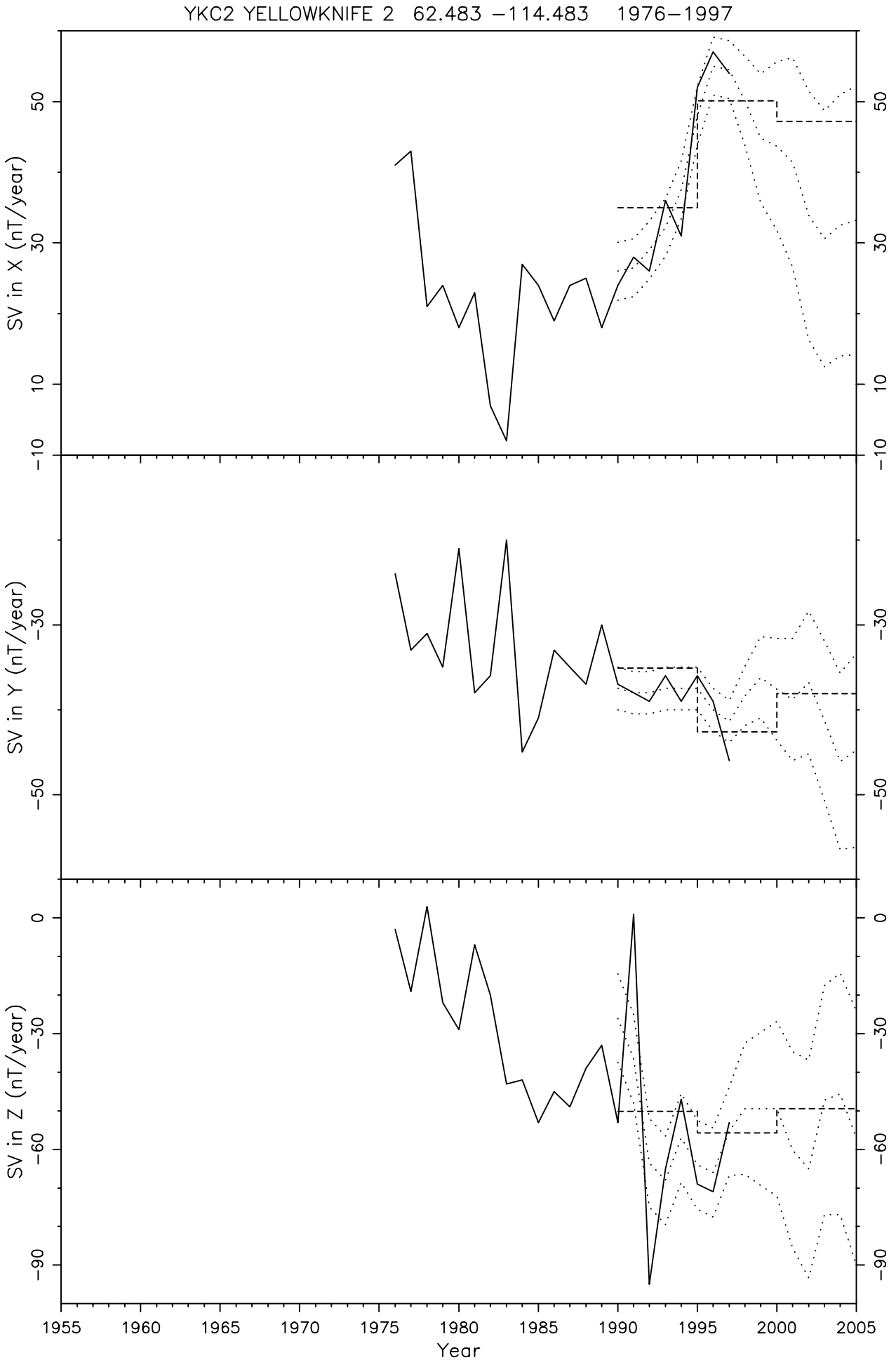
YKC2 YELLOWKNIFE 2 62.483 −114.483 1976−1997
SV in X (nT/year)
SV in Y (nT/year)
SV in Z (nT/year)
Year
1955
1960
1965
1970
1975
1980
1985
1990
1995
2000
2005

Figure 40

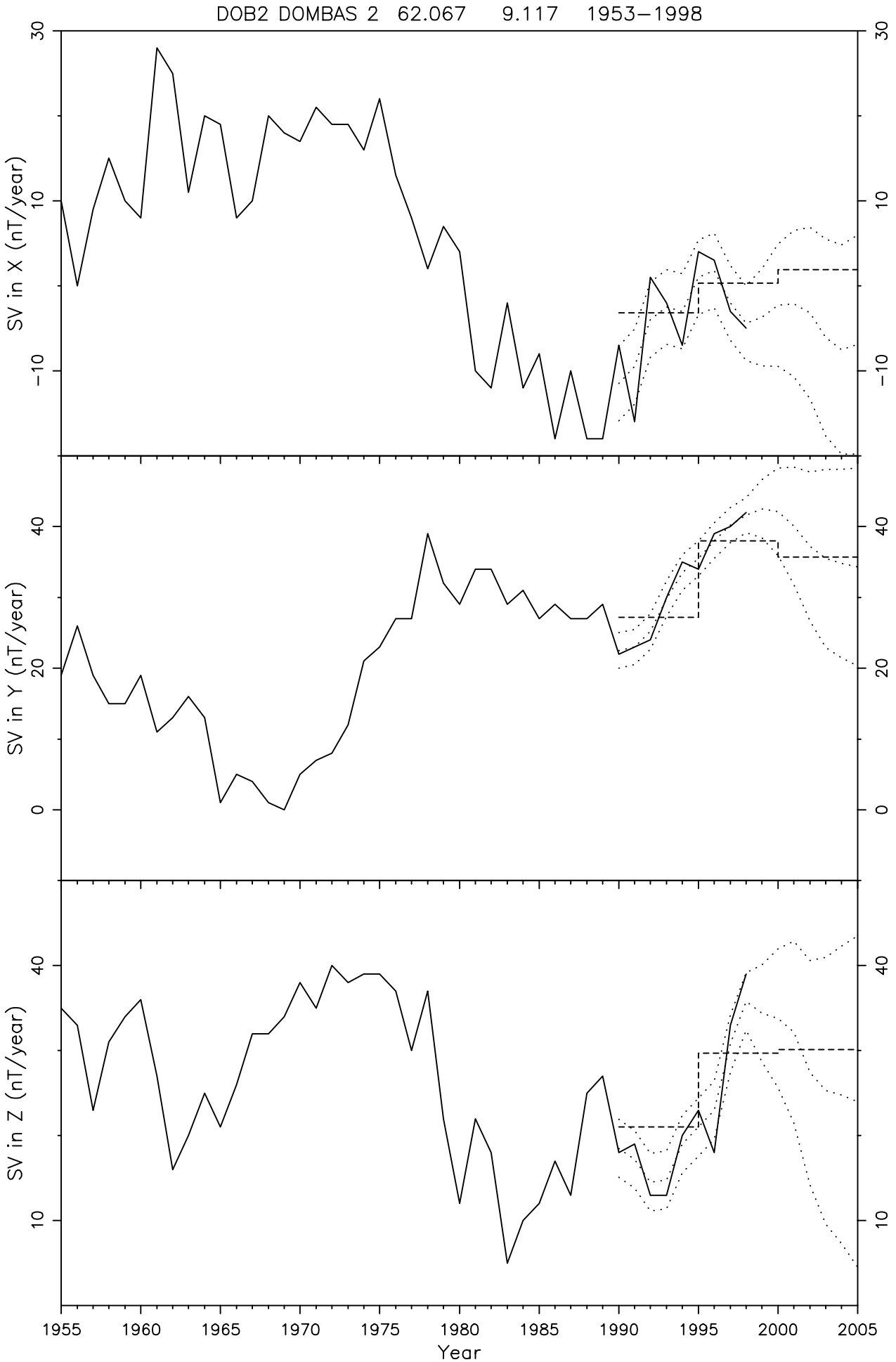
DOB2 DOMBAS 2 62.067 9.117 1953−1998
SV in X (nT/year)
SV in Y (nT/year)
SV in Z (nT/year)
Year
1955
1960
1965
1970
1975
1980
1985
1990
1995
2000
2005

Figure 41

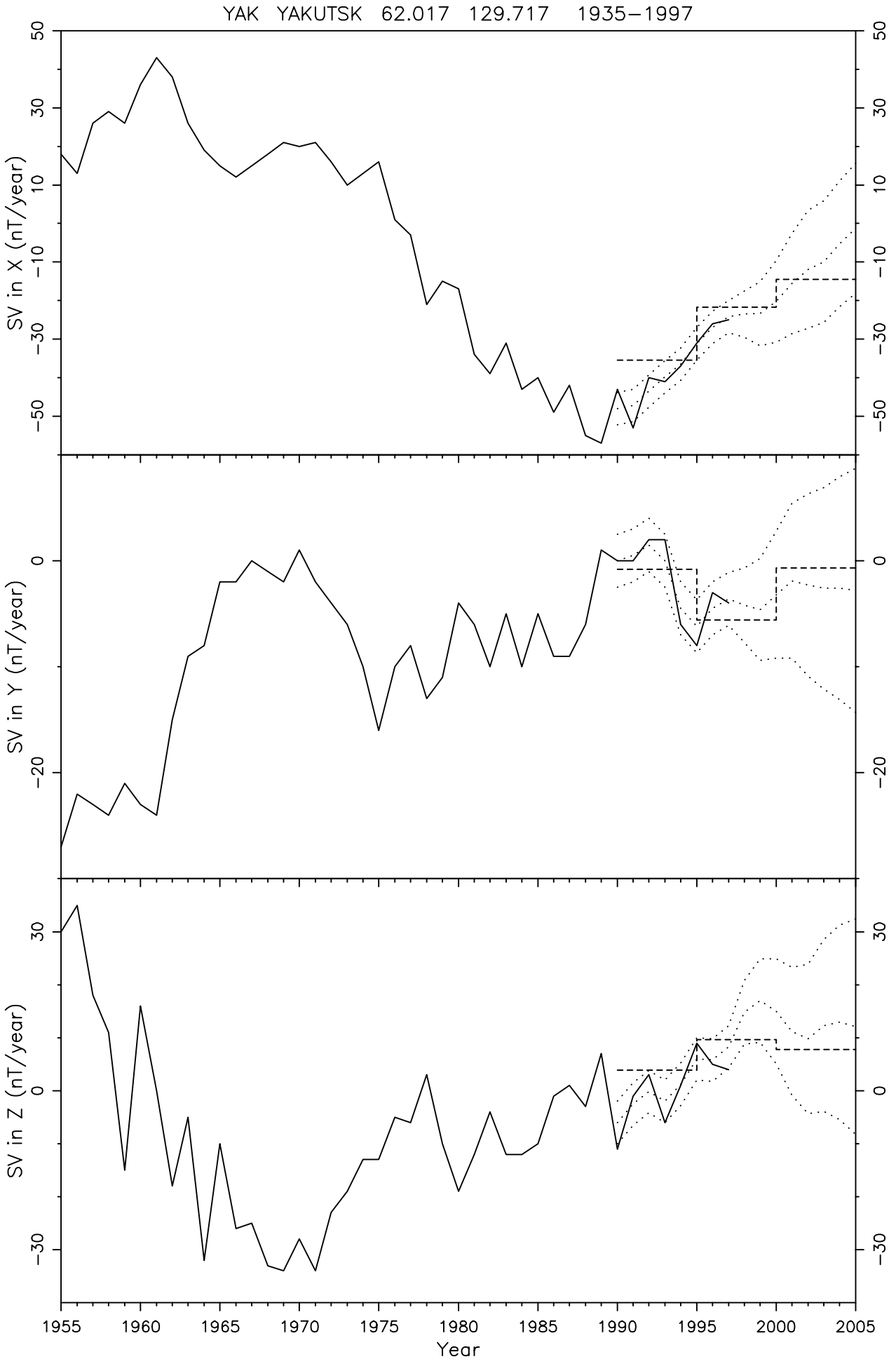
YAK YAKUTSK 62.017 129.717 1935–1997
SV in X (nT/year)
SV in Y (nT/year)
SV in Z (nT/year)
Year
1955
1960
1965
1970
1975
1980
1985
1990
1995
2000
2005

Figure 42

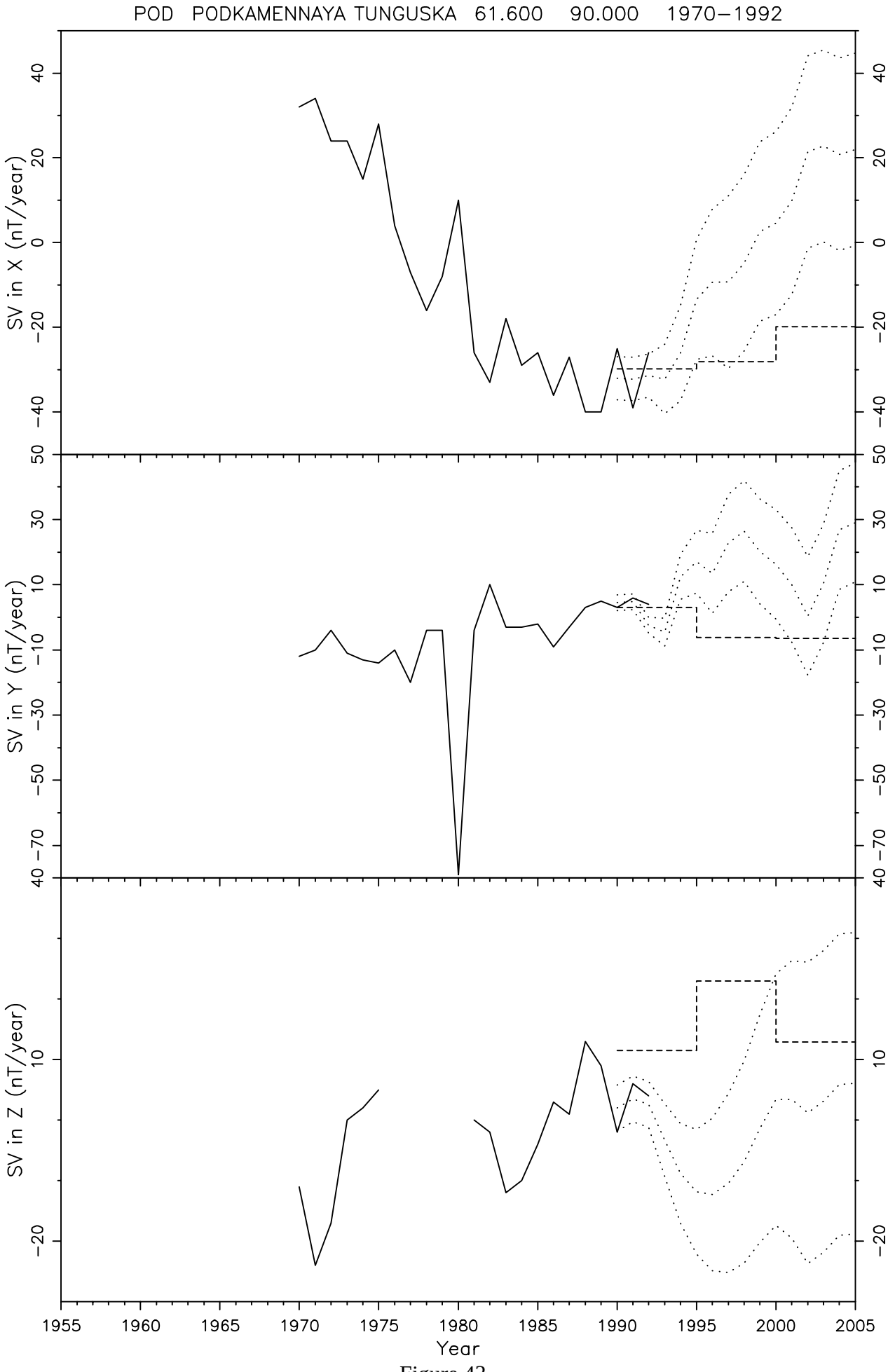
POD PODKAMENNAYA TUNGUSKA 61.600 90.000 1970–1992
SV in X (nT/year)
SV in Y (nT/year)
SV in Z (nT/year)
Year
1955
1960
1965
1970
1975
1980
1985
1990
1995
2000
2005

Figure 43

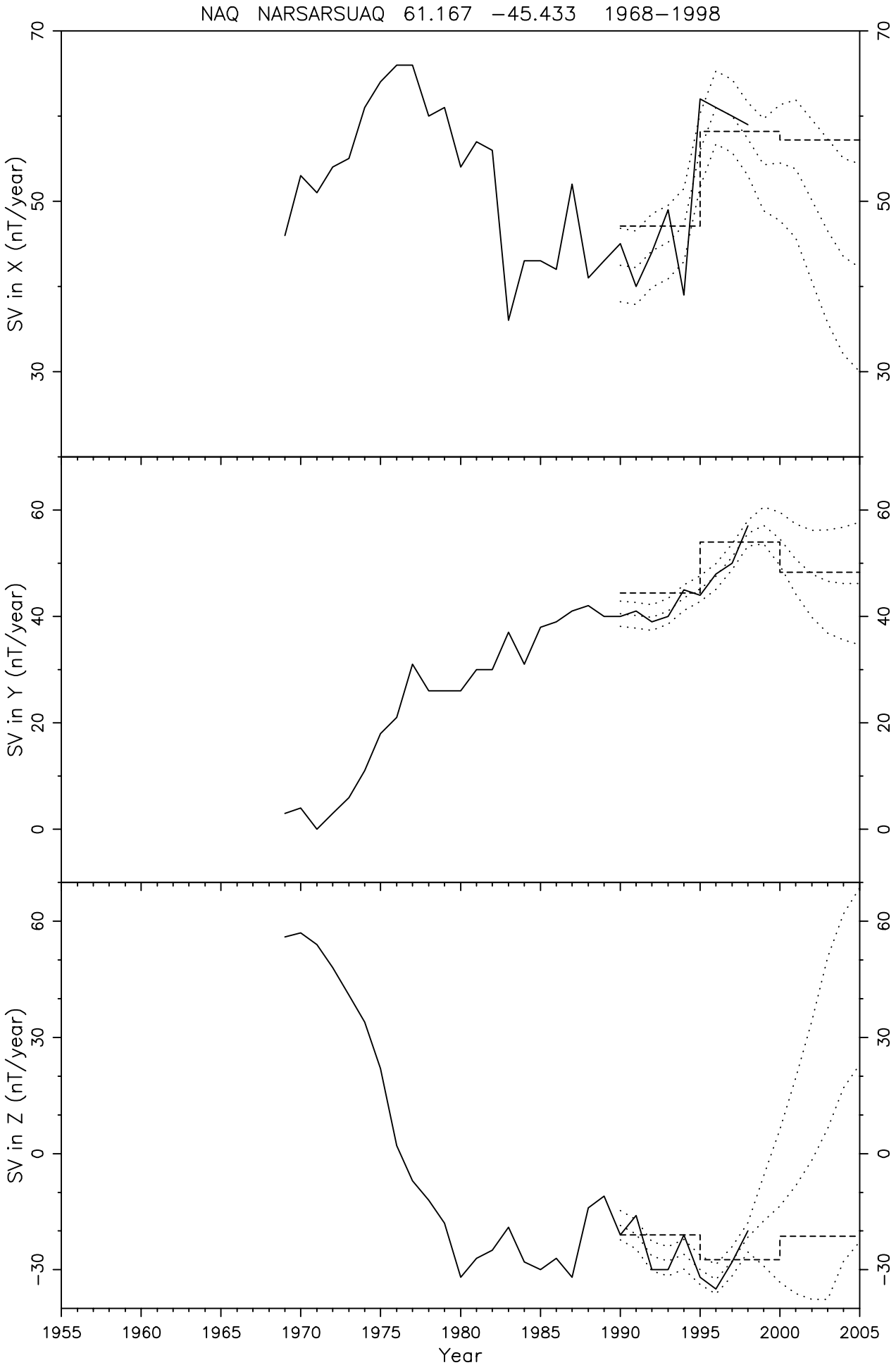
NAQ NARSARSUAQ 61.167 −45.433 1968−1998
SV in X (nT/year)
SV in Y (nT/year)
SV in Z (nT/year)
Year
1955
1960
1965
1970
1975
1980
1985
1990
1995
2000
2005

Figure 44

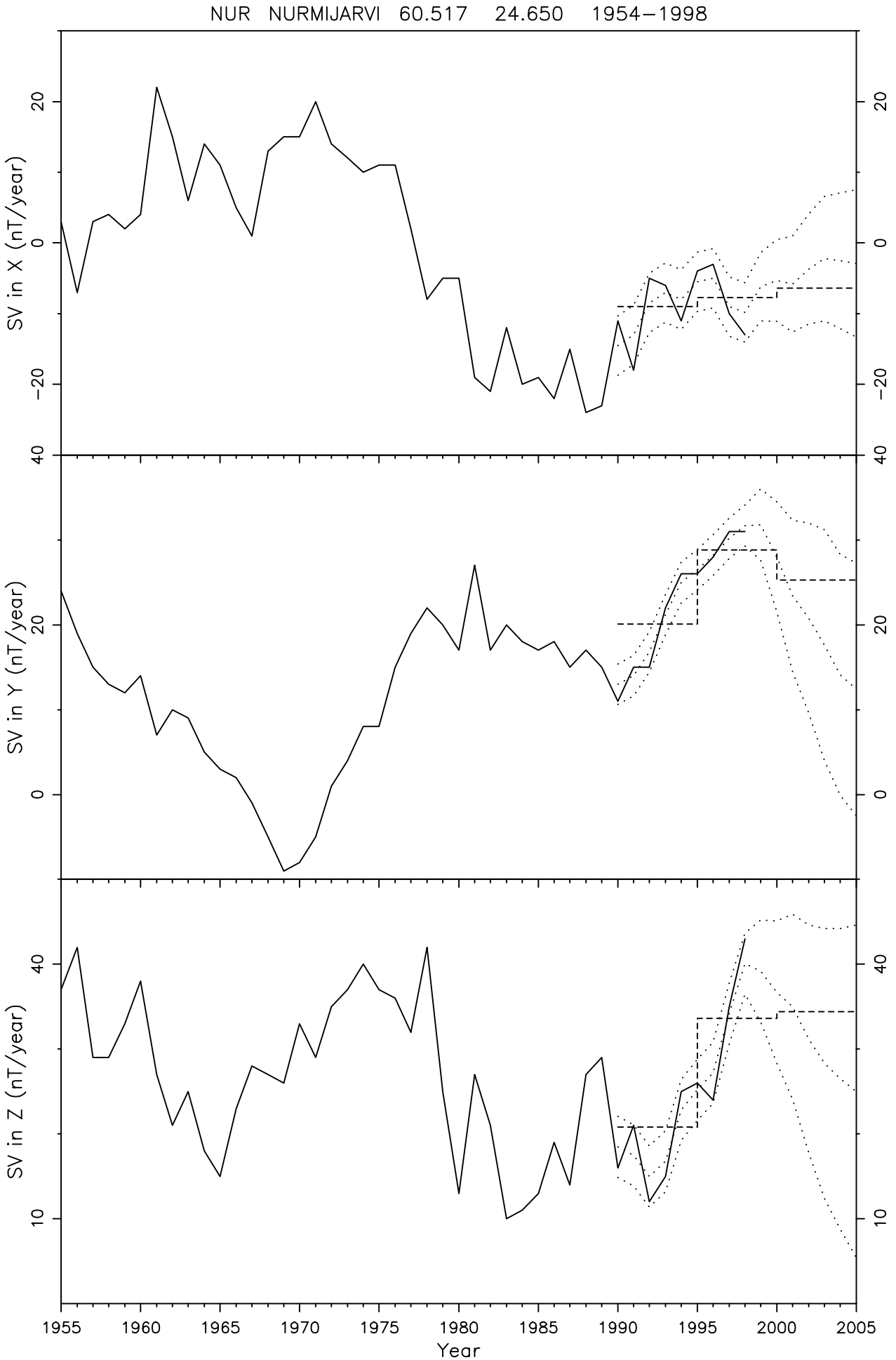
NUR NURMIJARVI 60.517 24.650 1954–1998
SV in X (nT/year)
SV in Y (nT/year)
SV in Z (nT/year)
Year
1955
1960
1965
1970
1975
1980
1985
1990
1995
2000
2005

Figure 45

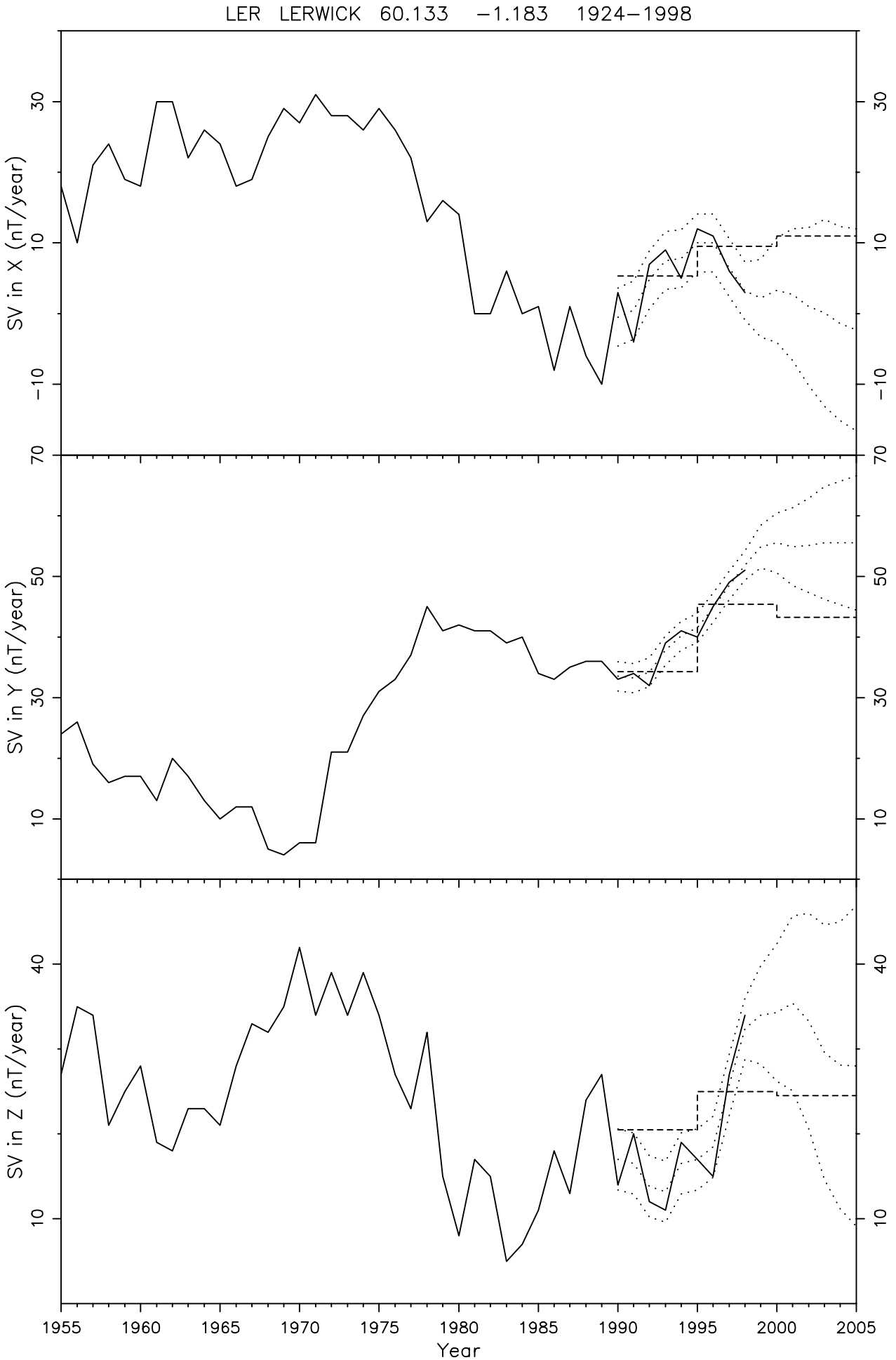
LER LERWICK 60.133 −1.183 1924−1998
SV in X (nT/year)
SV in Y (nT/year)
SV in Z (nT/year)
Year
1955
1960
1965
1970
1975
1980
1985
1990
1995
2000
2005

Figure 46

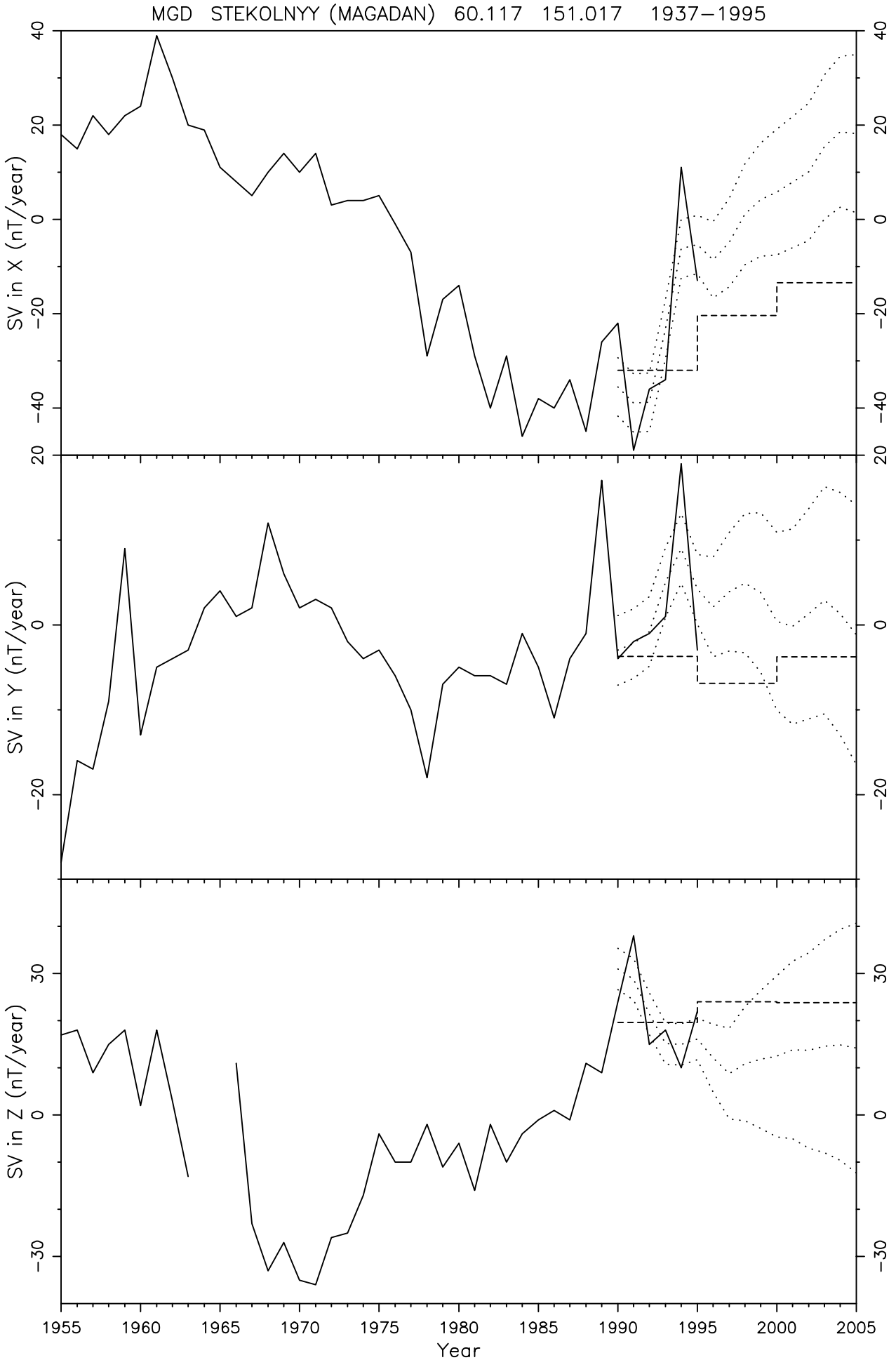
MGD STEKOLNYY (MAGADAN) 60.117 151.017 1937–1995
SV in X (nT/year)
SV in Y (nT/year)
SV in Z (nT/year)
Year
1955
1960
1965
1970
1975
1980
1985
1990
1995
2000
2005

Figure 47

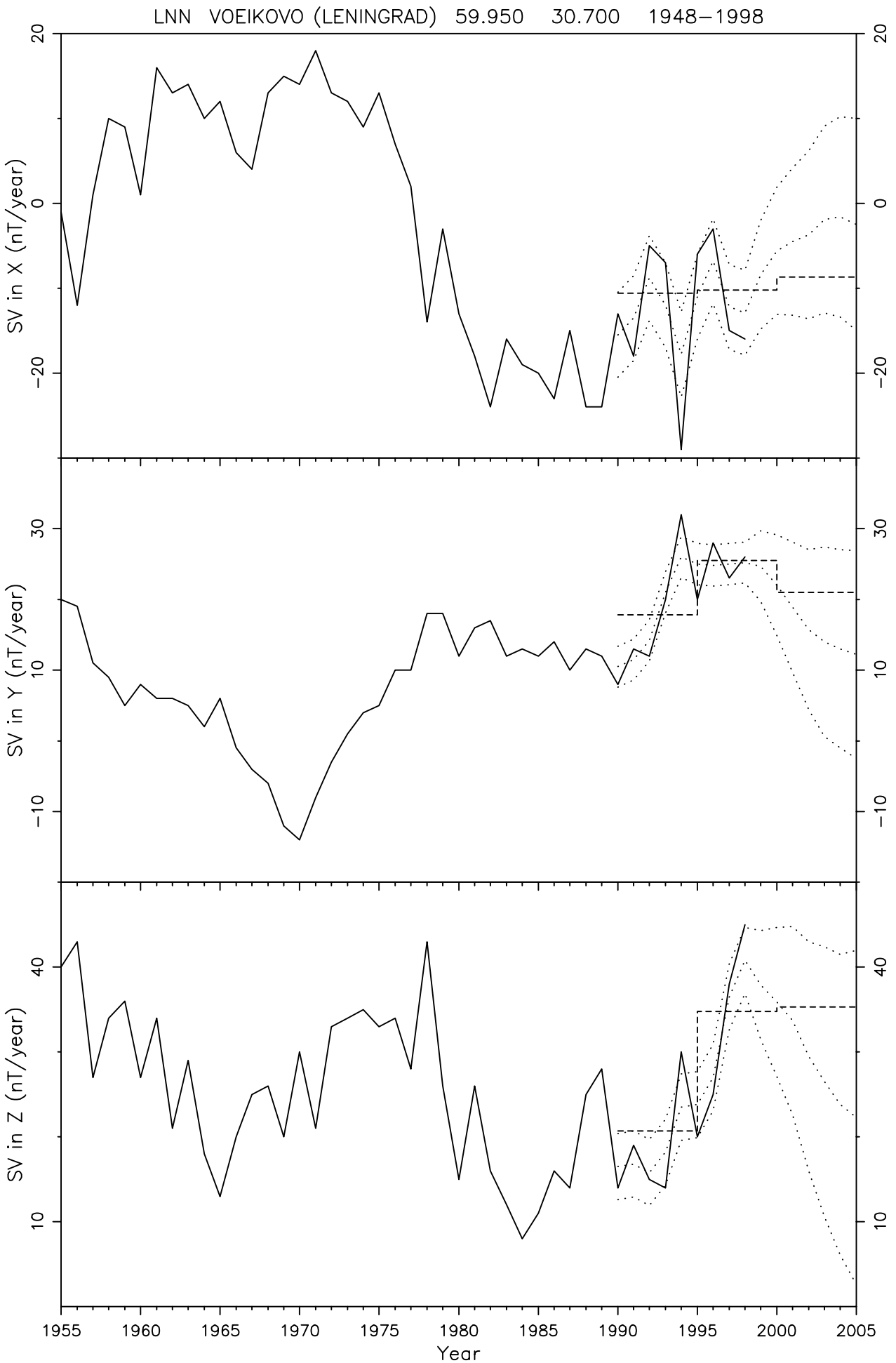
LNN VOEIKOVO (LENINGRAD) 59.950 30.700 1948–1998
SV in X (nT/year)
SV in Y (nT/year)
SV in Z (nT/year)
Year
1955
1960
1965
1970
1975
1980
1985
1990
1995
2000
2005

Figure 48

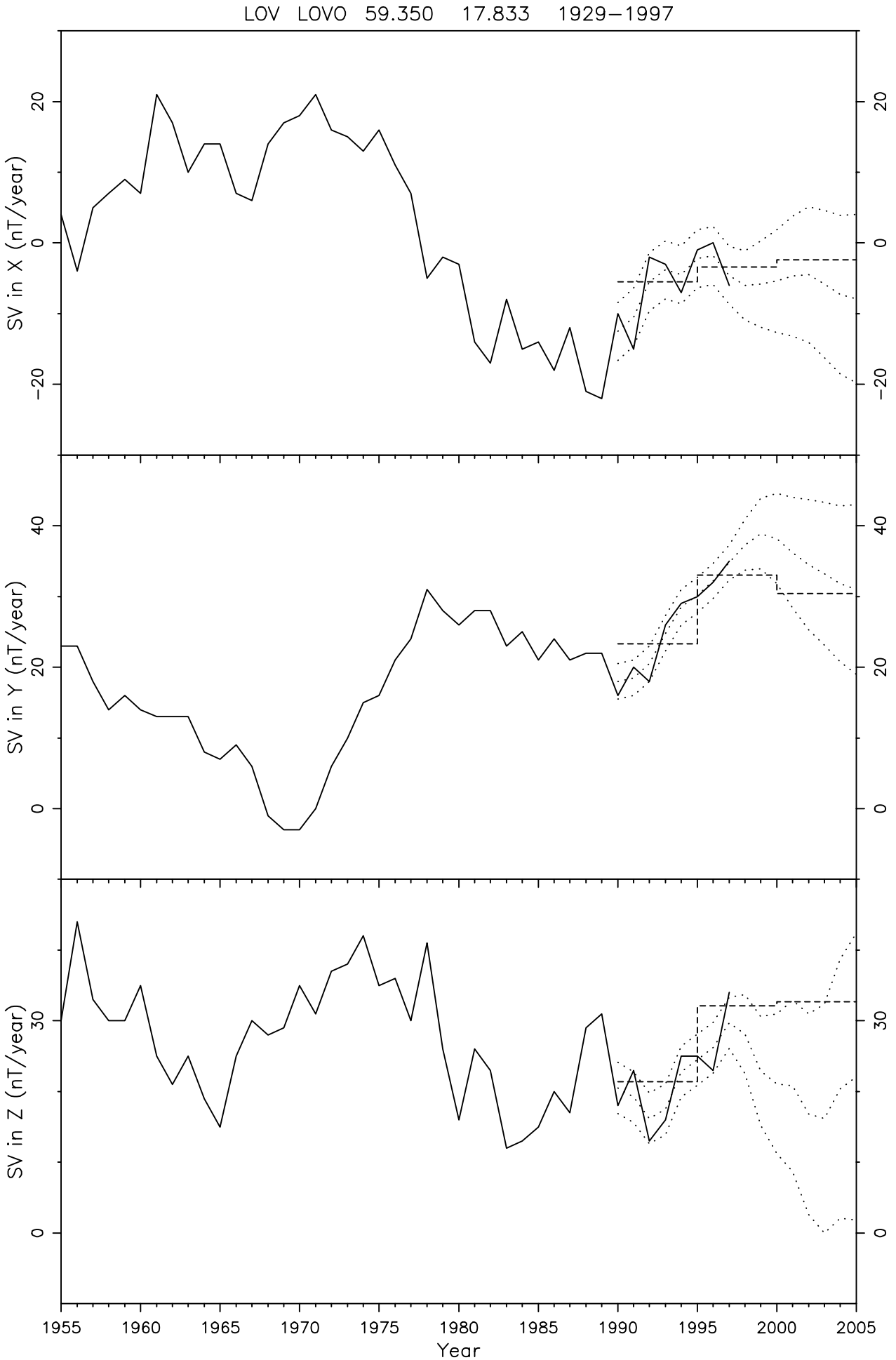
LOV LOVO 59.350 17.833 1929–1997
SV in X (nT/year)
SV in Y (nT/year)
SV in Z (nT/year)
Year
1955
1960
1965
1970
1975
1980
1985
1990
1995
2000
2005

Figure 49

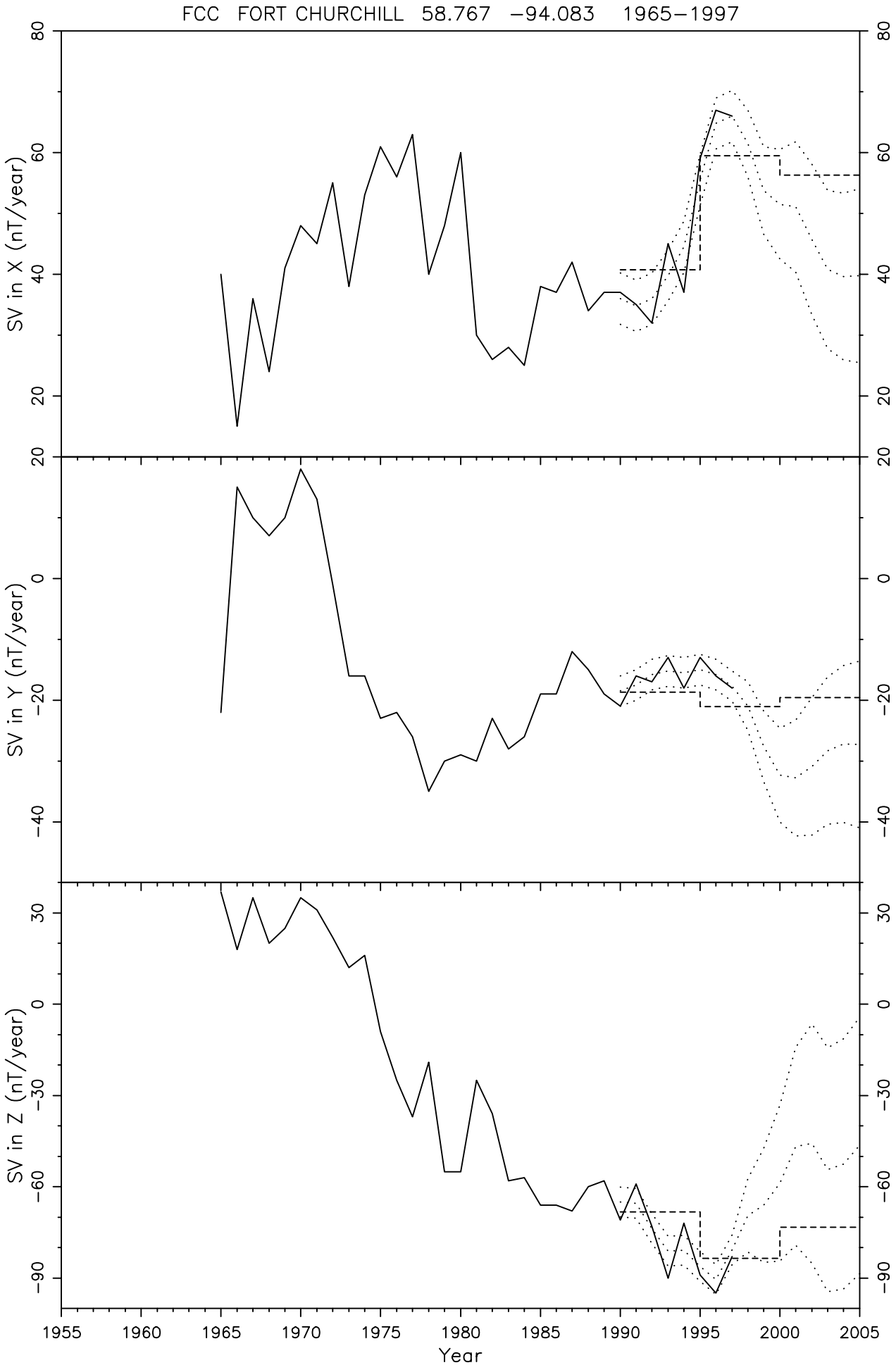
FCC FORT CHURCHILL 58.767 −94.083 1965−1997
SV in X (nT/year)
SV in Y (nT/year)
SV in Z (nT/year)
Year
1955
1960
1965
1970
1975
1980
1985
1990
1995
2000
2005

Figure 50

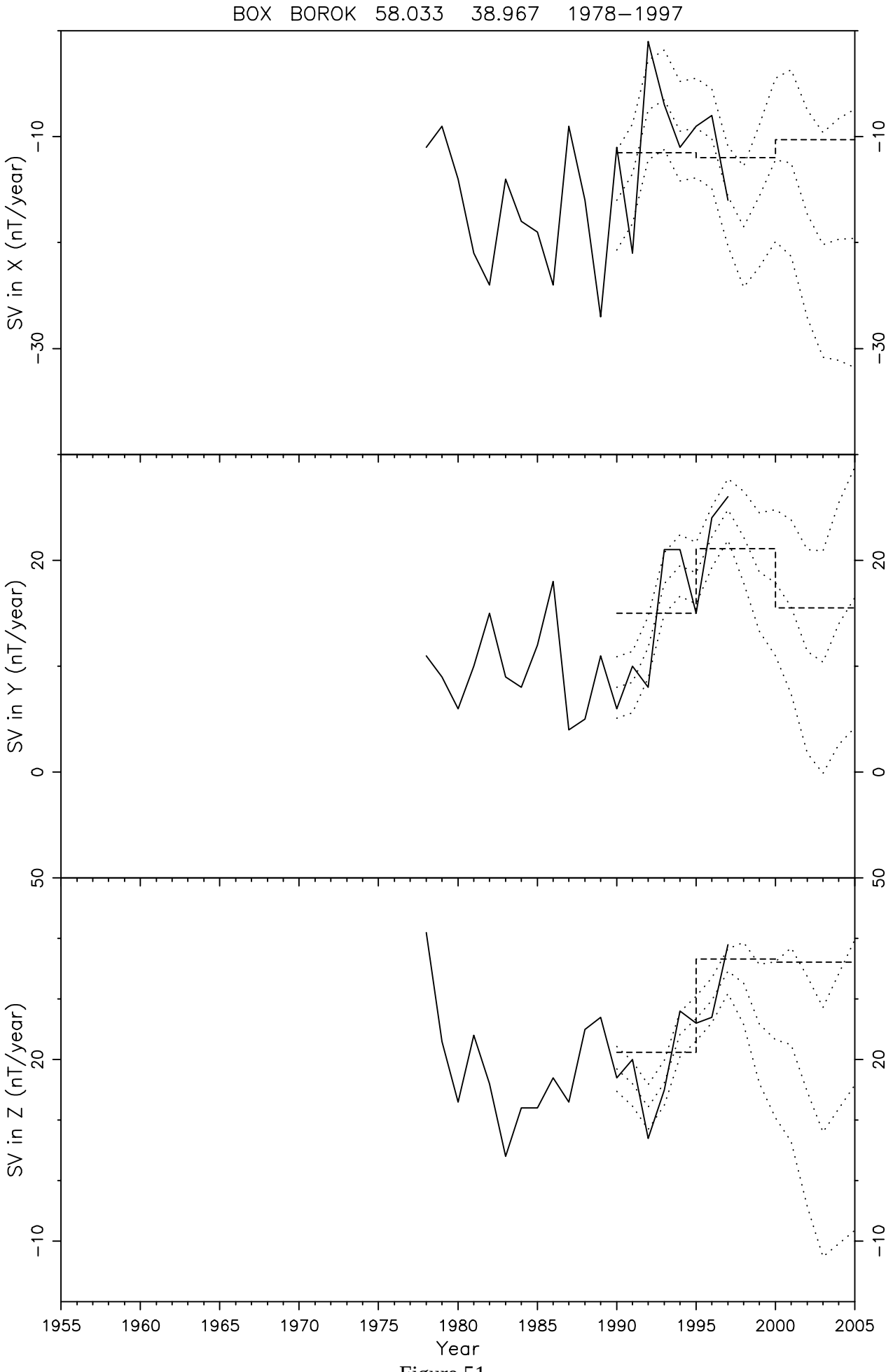
BOX BOROK 58.033 38.967 1978–1997
SV in X (nT/year)
−10
−30
SV in Y (nT/year)
20
0
50
SV in Z (nT/year)
20
−10
1955
1960
1965
1970
1975
1980
1985
1990
1995
2000
2005
Year

Figure 51

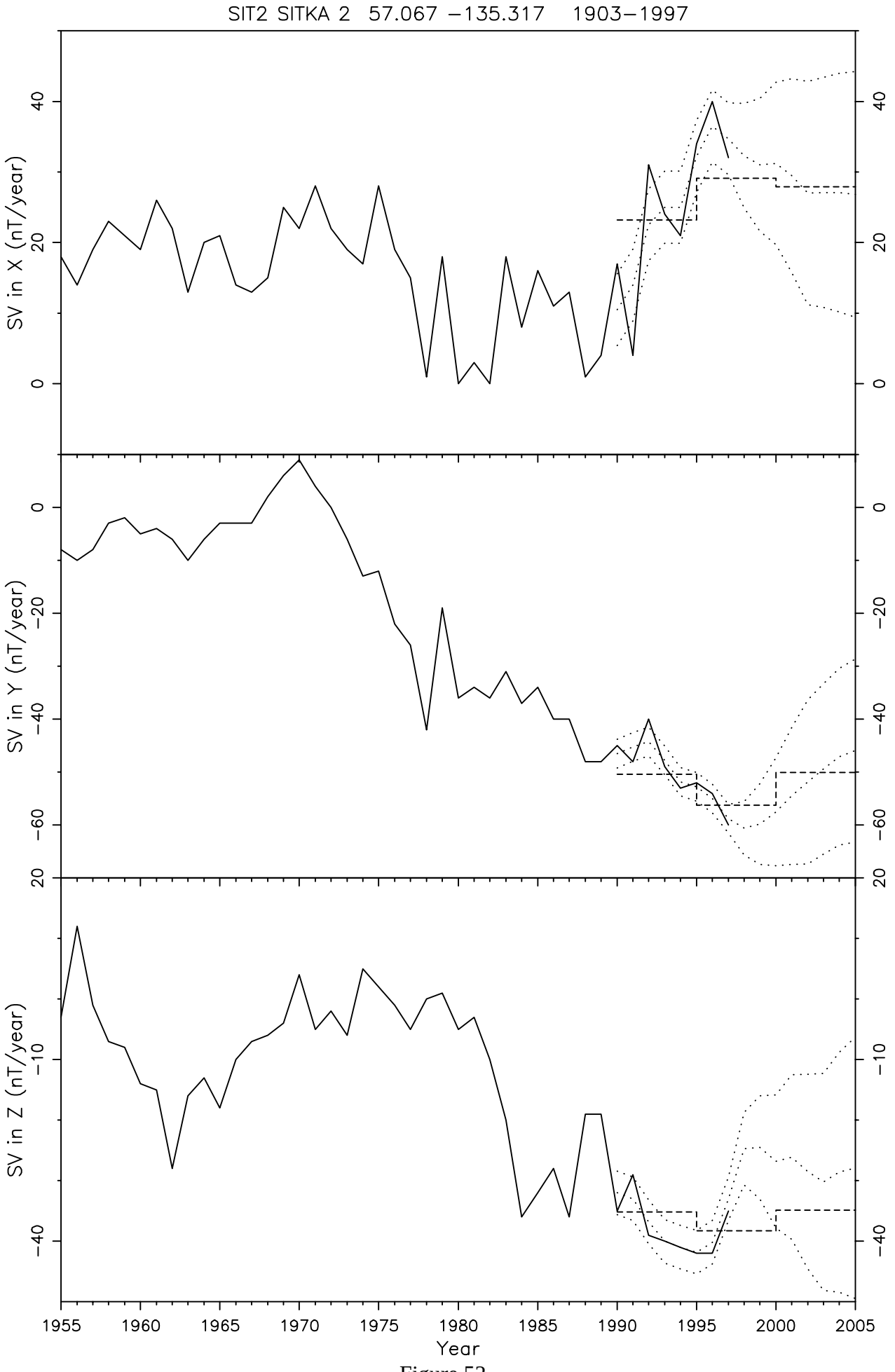
SIT2 SITKA 2 57.067 −135.317 1903−1997
SV in X (nT/year)
SV in Y (nT/year)
SV in Z (nT/year)
Year
1955
1960
1965
1970
1975
1980
1985
1990
1995
2000
2005

Figure 52

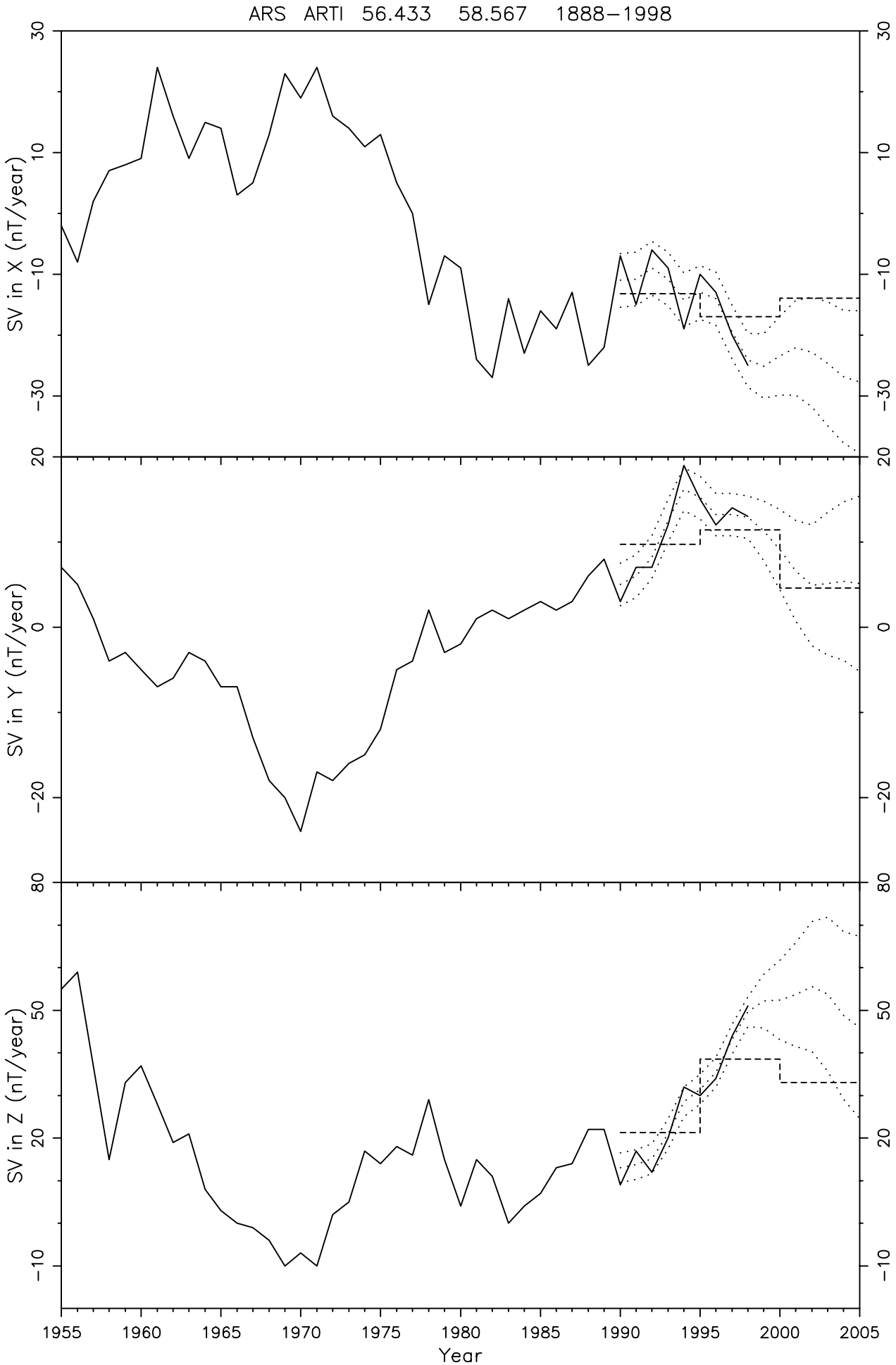
ARS ARTI 56.433 58.567 1888–1998
SV in X (nT/year)
SV in Y (nT/year)
SV in Z (nT/year)
30
10
−10
−30
20
0
−20
80
50
−10
1955
1960
1965
1970
1975
1980
1985
1990
1995
2000
2005
Year

Figure 53

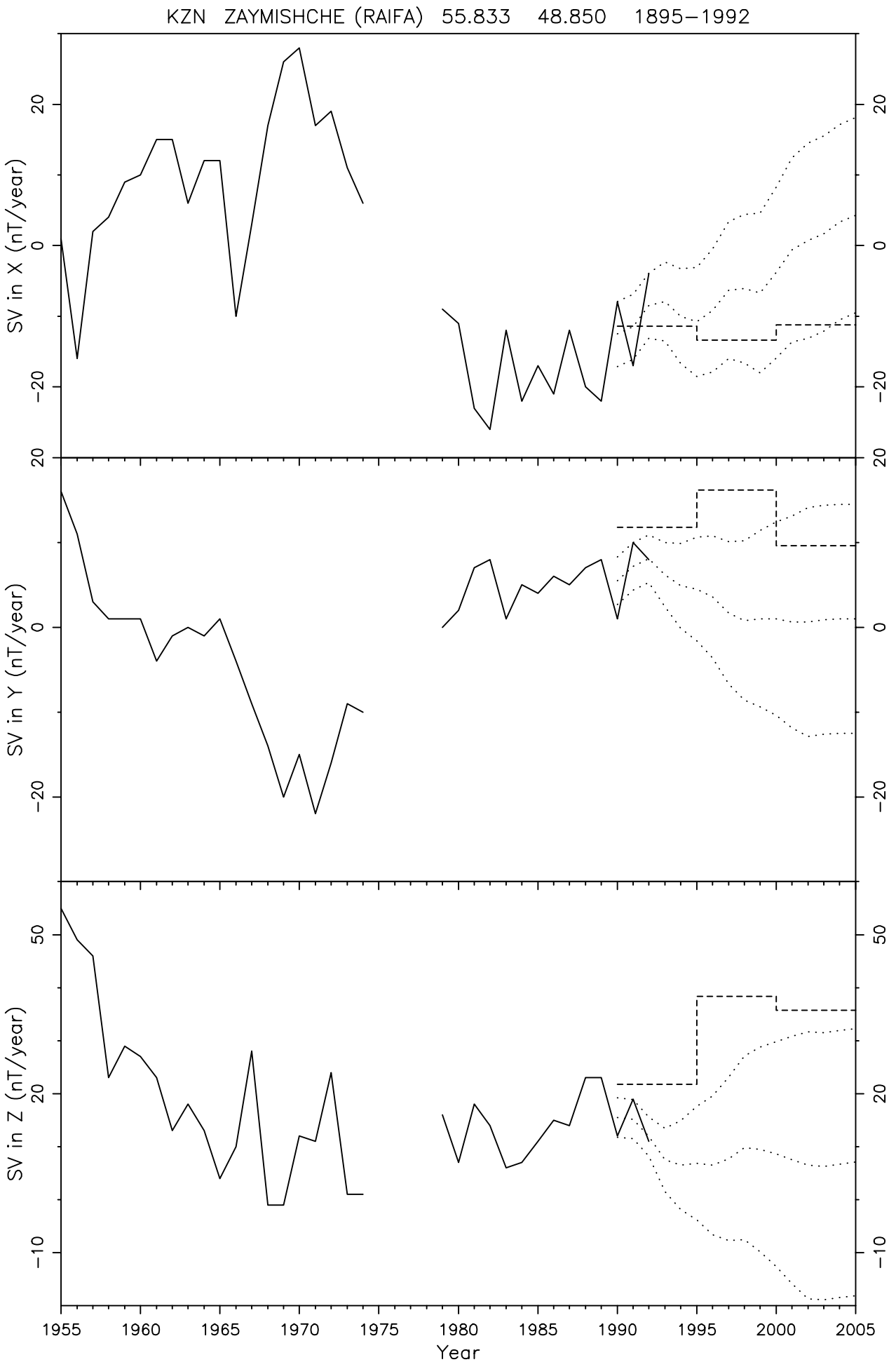
KZN ZAYMISHCHE (RAIFA) 55.833 48.850 1895–1992
SV in X (nT/year)
SV in Y (nT/year)
SV in Z (nT/year)
Year
1955
1960
1965
1970
1975
1980
1985
1990
1995
2000
2005

Figure 54

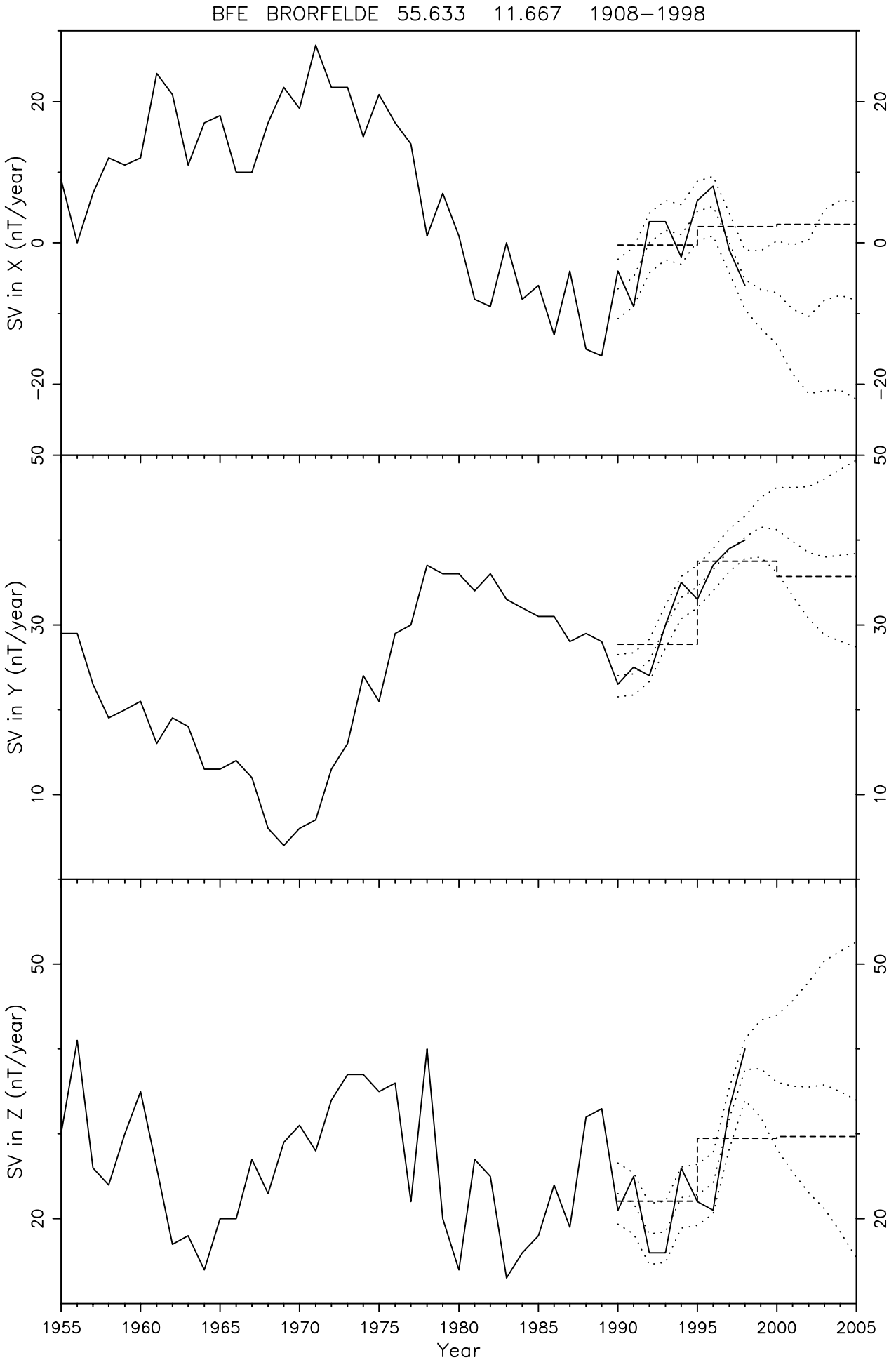
BFE BRORFELDE 55.633 11.667 1908–1998
SV in X (nT/year)
SV in Y (nT/year)
SV in Z (nT/year)
Year
1955
1960
1965
1970
1975
1980
1985
1990
1995
2000
2005

Figure 55

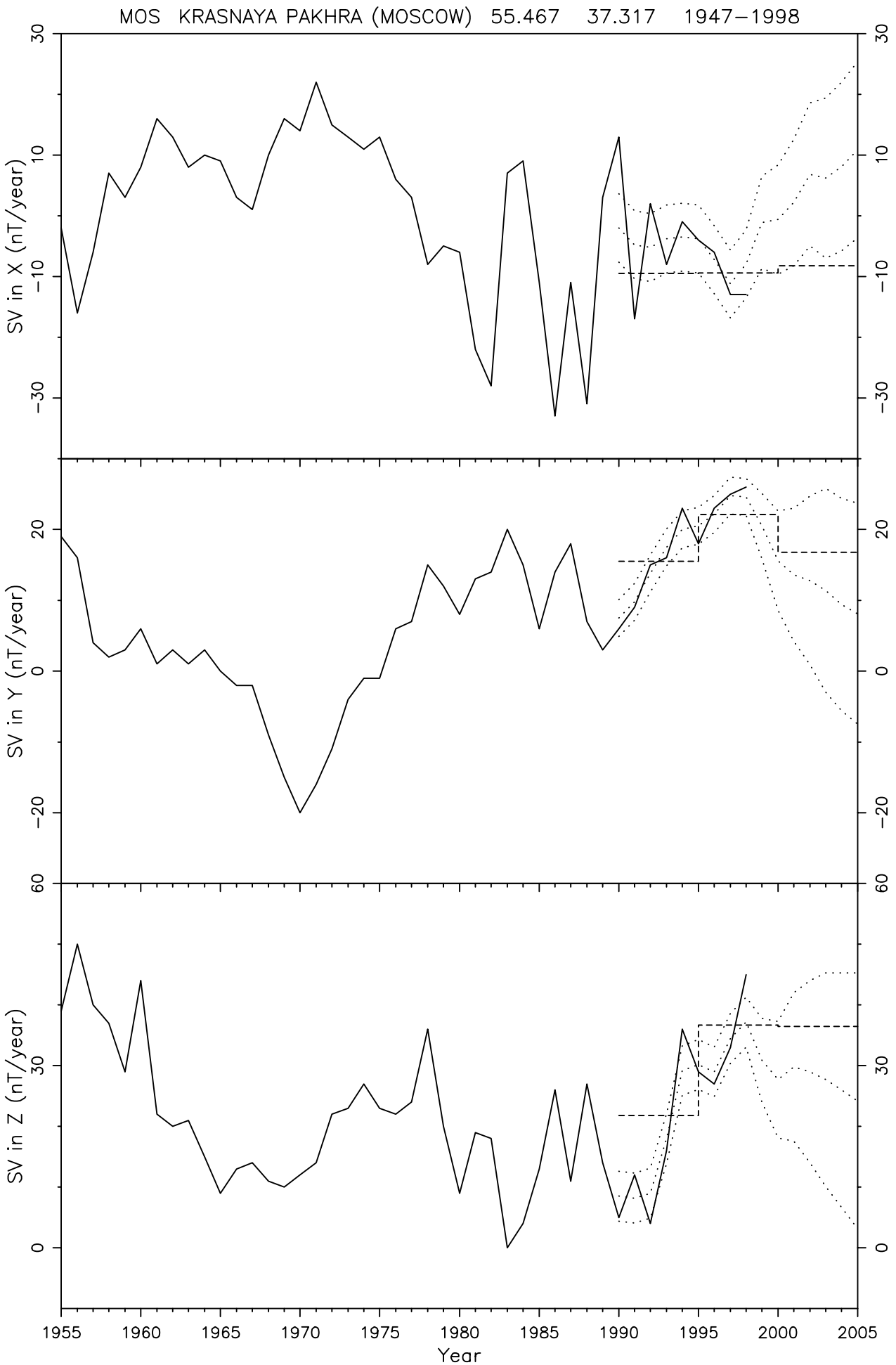
MOS KRASNAYA PAKHRA (MOSCOW) 55.467 37.317 1947–1998
SV in X (nT/year)
SV in Y (nT/year)
SV in Z (nT/year)
30
10
−10
−30
20
0
−20
60
1955
1960
1965
1970
1975
1980
1985
1990
1995
2000
2005
Year

Figure 56

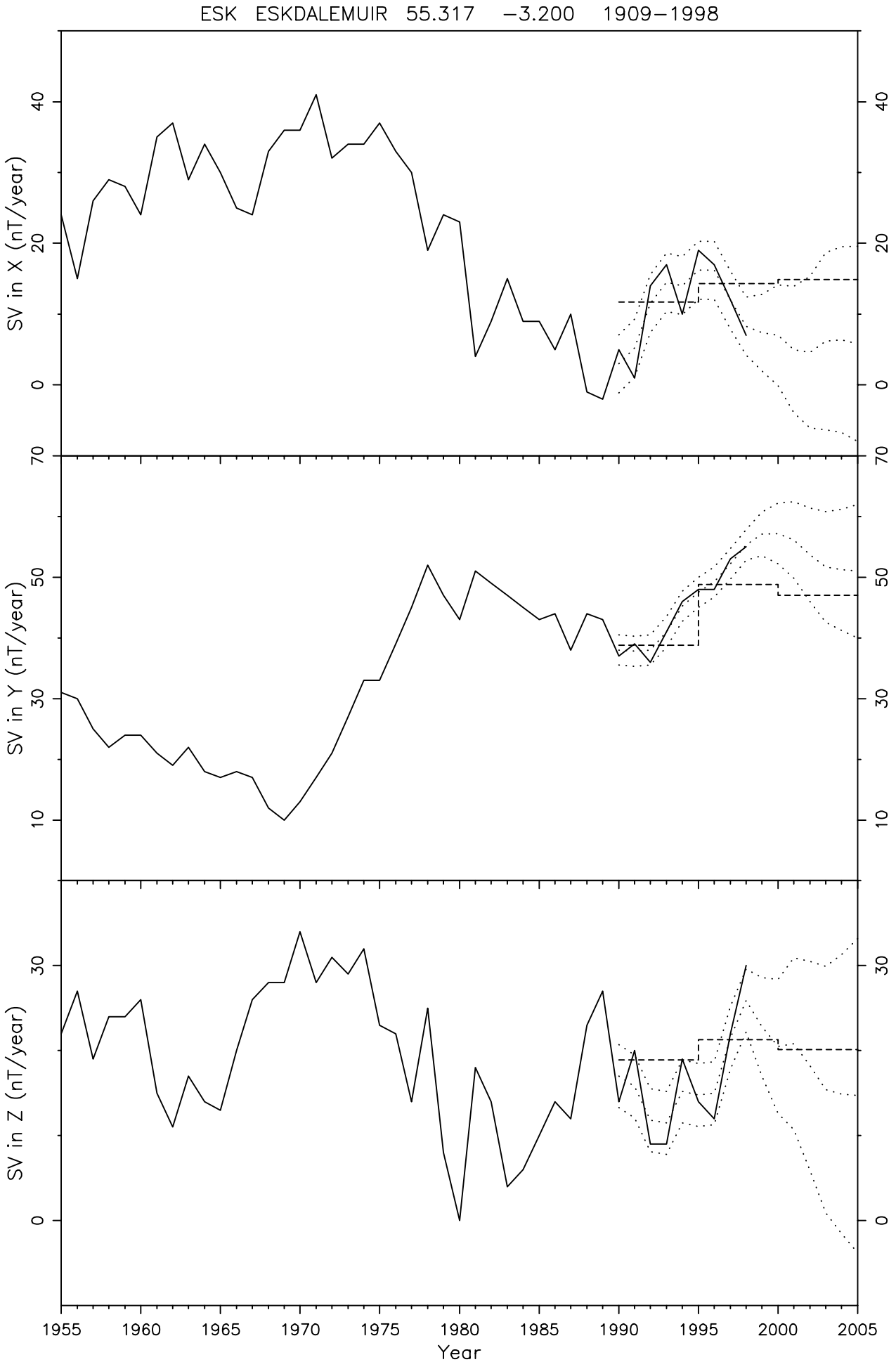
ESK ESKDALEMUIR 55.317 −3.200 1909−1998
SV in X (nT/year)
SV in Y (nT/year)
SV in Z (nT/year)
Year
1955
1960
1965
1970
1975
1980
1985
1990
1995
2000
2005

Figure 57

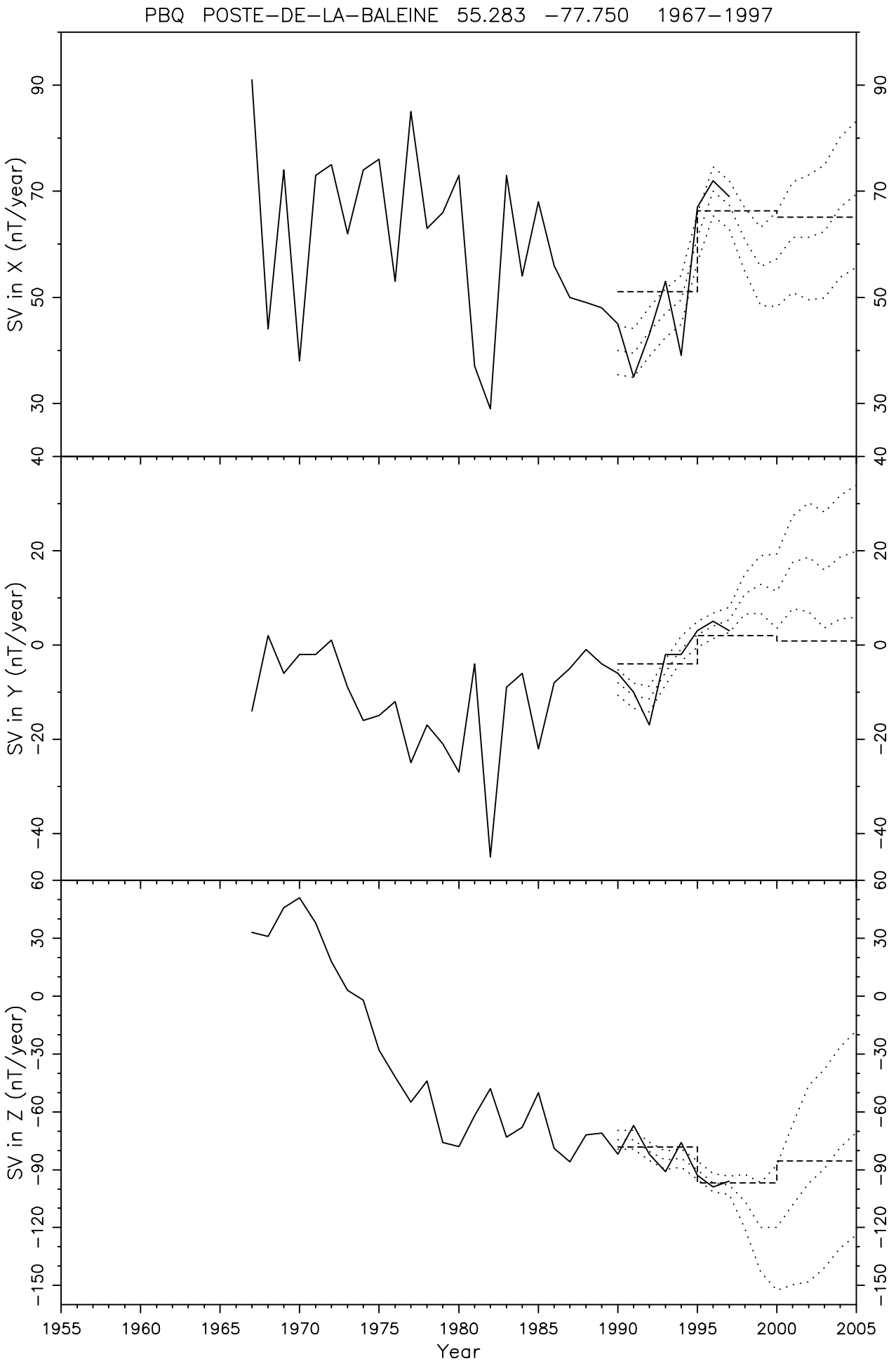
PBQ POSTE-DE-LA-BALEINE 55.283 -77.750 1967-1997
SV in X (nT/year)
SV in Y (nT/year)
SV in Z (nT/year)
Year
1955
1960
1965
1970
1975
1980
1985
1990
1995
2000
2005

Figure 58

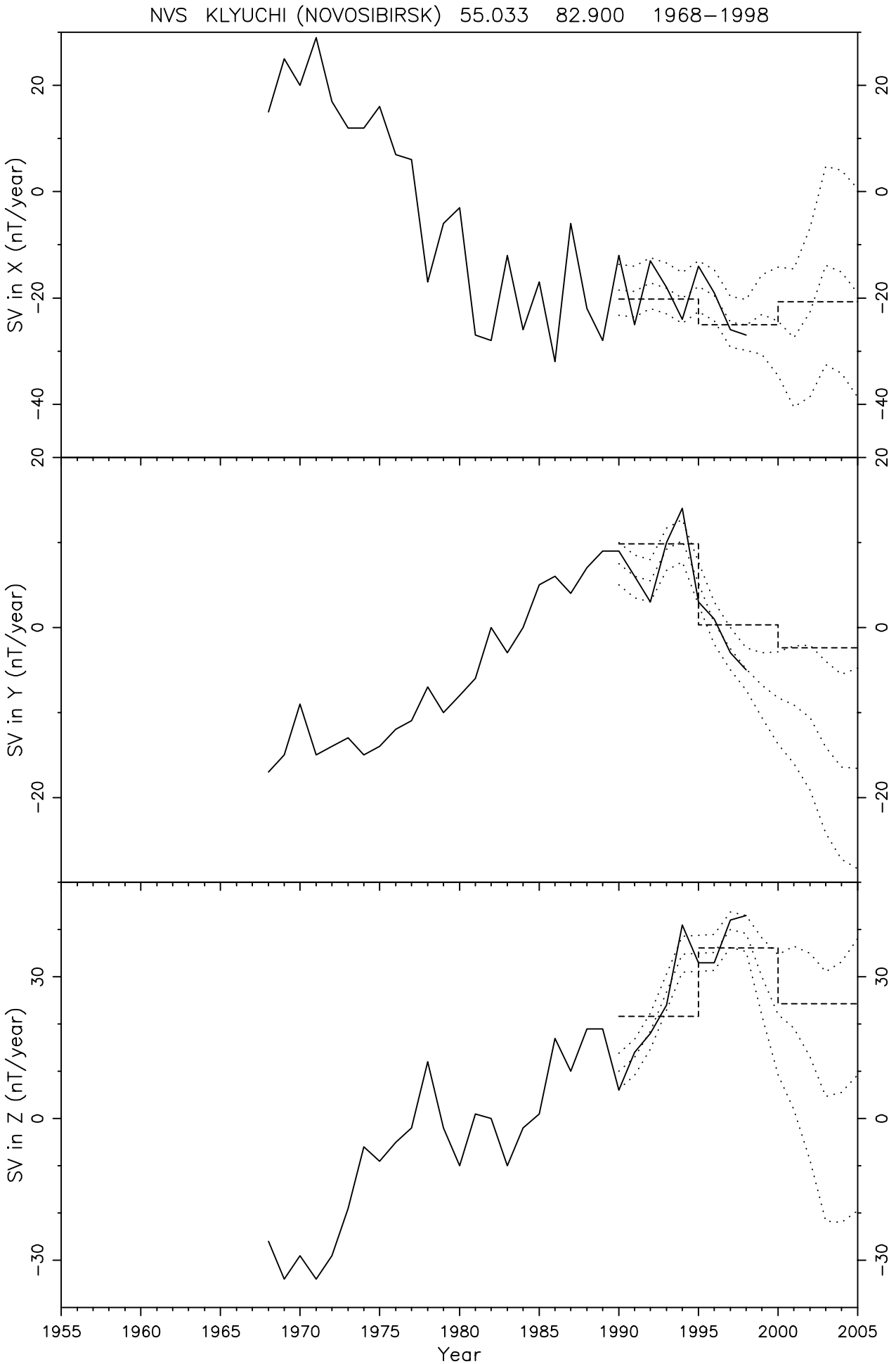
NVS KLYUCHI (NOVOSIBIRSK) 55.033 82.900 1968–1998
SV in X (nT/year)
SV in Y (nT/year)
SV in Z (nT/year)
Year
1955
1960
1965
1970
1975
1980
1985
1990
1995
2000
2005

Figure 59

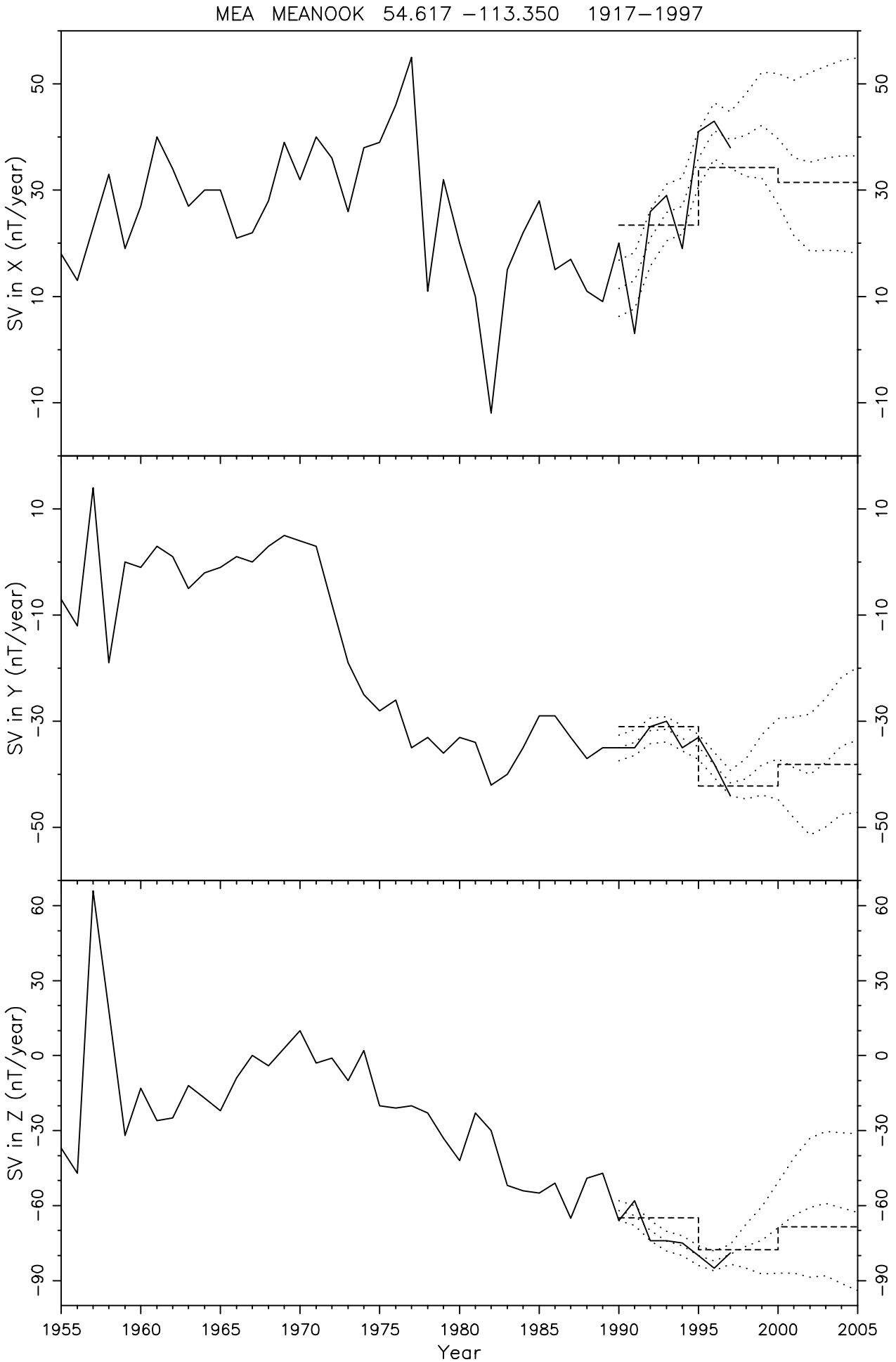
MEA MEANOOK 54.617 −113.350 1917−1997
SV in X (nT/year)
SV in Y (nT/year)
SV in Z (nT/year)
Year
1955
1960
1965
1970
1975
1980
1985
1990
1995
2000
2005

Figure 60

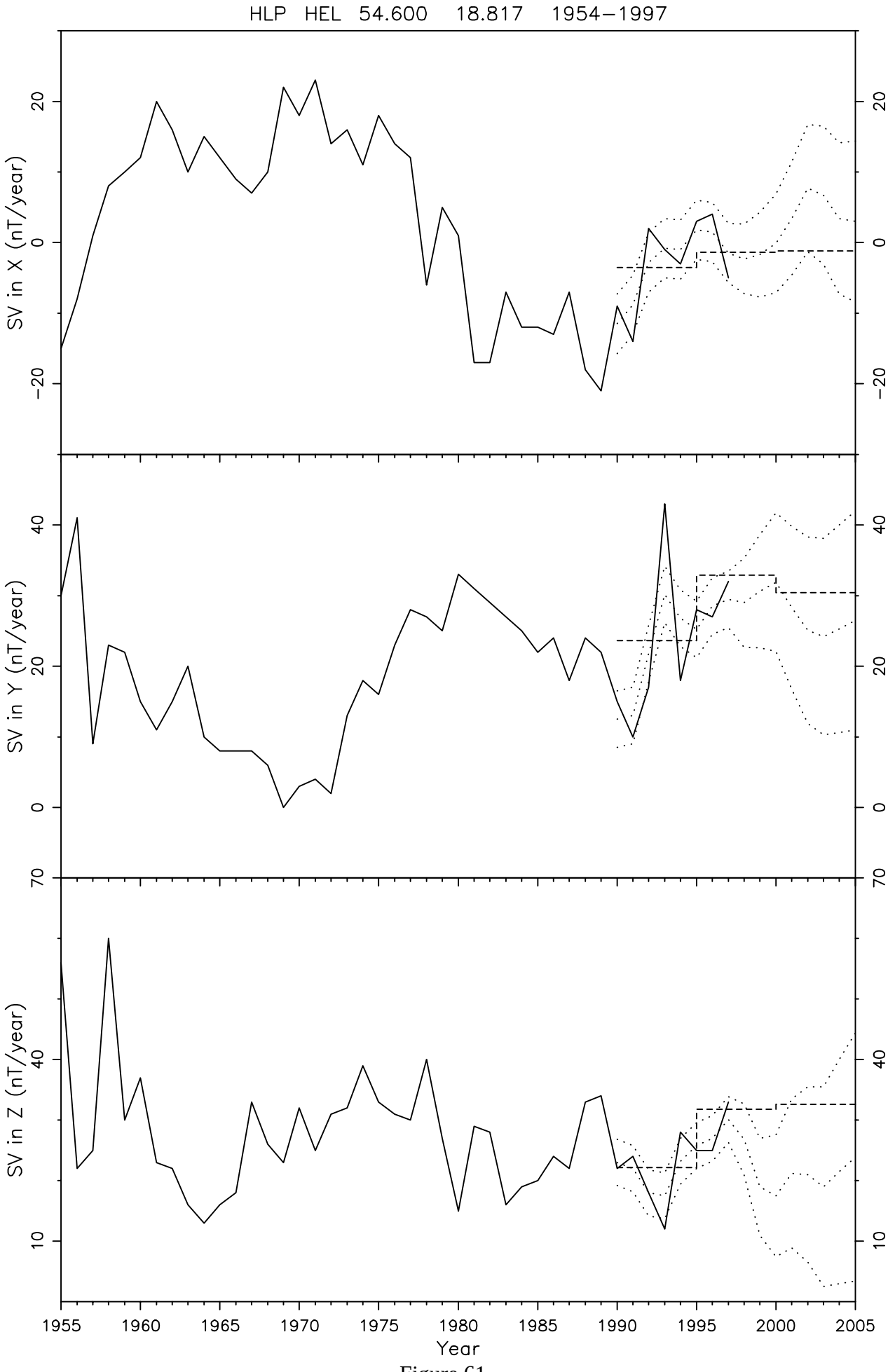
HLP HEL 54.600 18.817 1954–1997
SV in X (nT/year)
SV in Y (nT/year)
SV in Z (nT/year)
20
0
−20
40
70
10
1955
1960
1965
1970
1975
1980
1985
1990
1995
2000
2005
Year

Figure 61

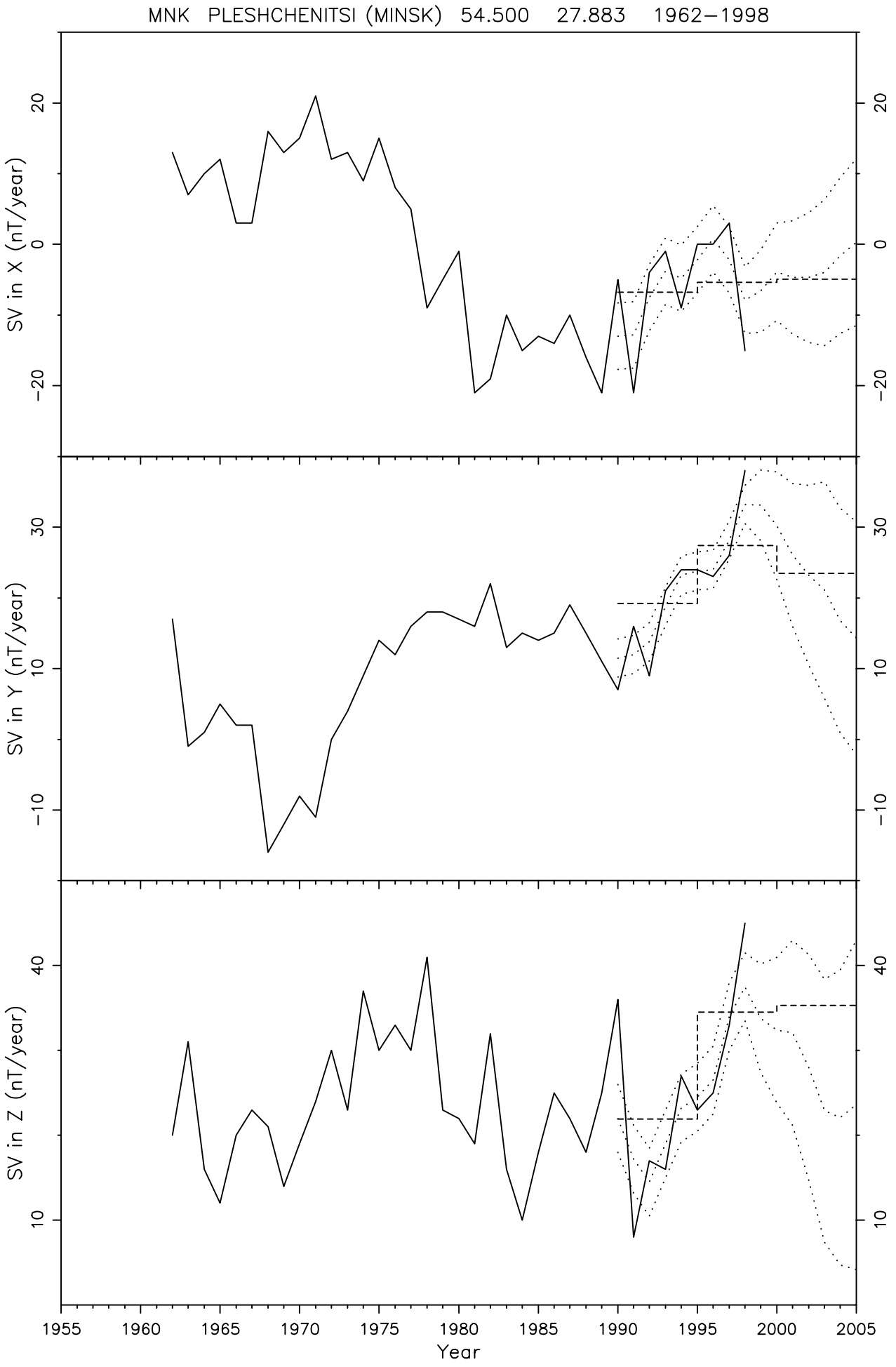
MNK PLESHCHENITSI (MINSK) 54.500 27.883 1962–1998
SV in X (nT/year)
SV in Y (nT/year)
SV in Z (nT/year)
Year
1955
1960
1965
1970
1975
1980
1985
1990
1995
2000
2005

Figure 62

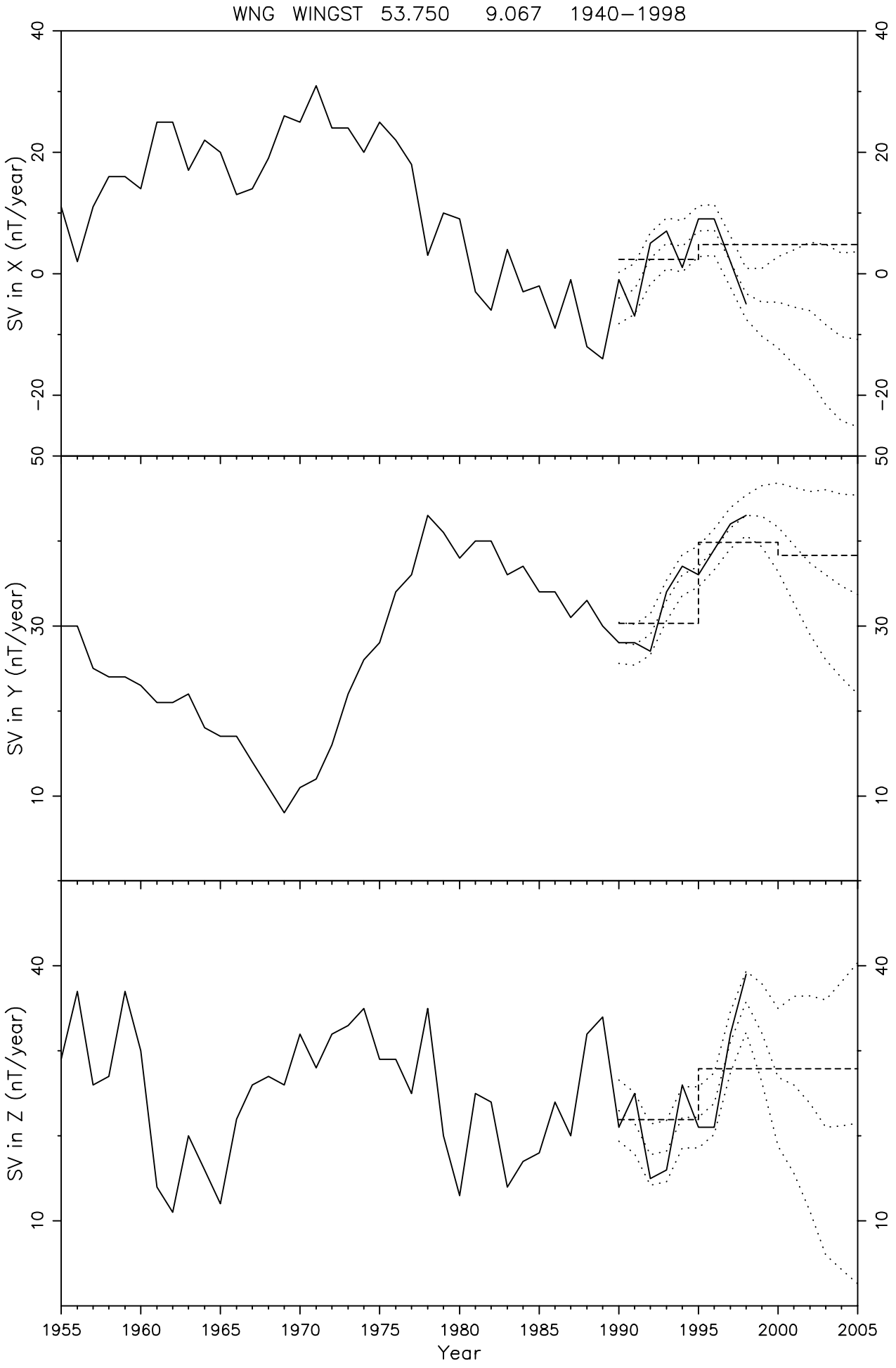
WNG WINGST 53.750 9.067 1940–1998
SV in X (nT/year)
SV in Y (nT/year)
SV in Z (nT/year)
40
20
0
−20
50
30
10
1955
1960
1965
1970
1975
1980
1985
1990
1995
2000
2005
Year

Figure 63

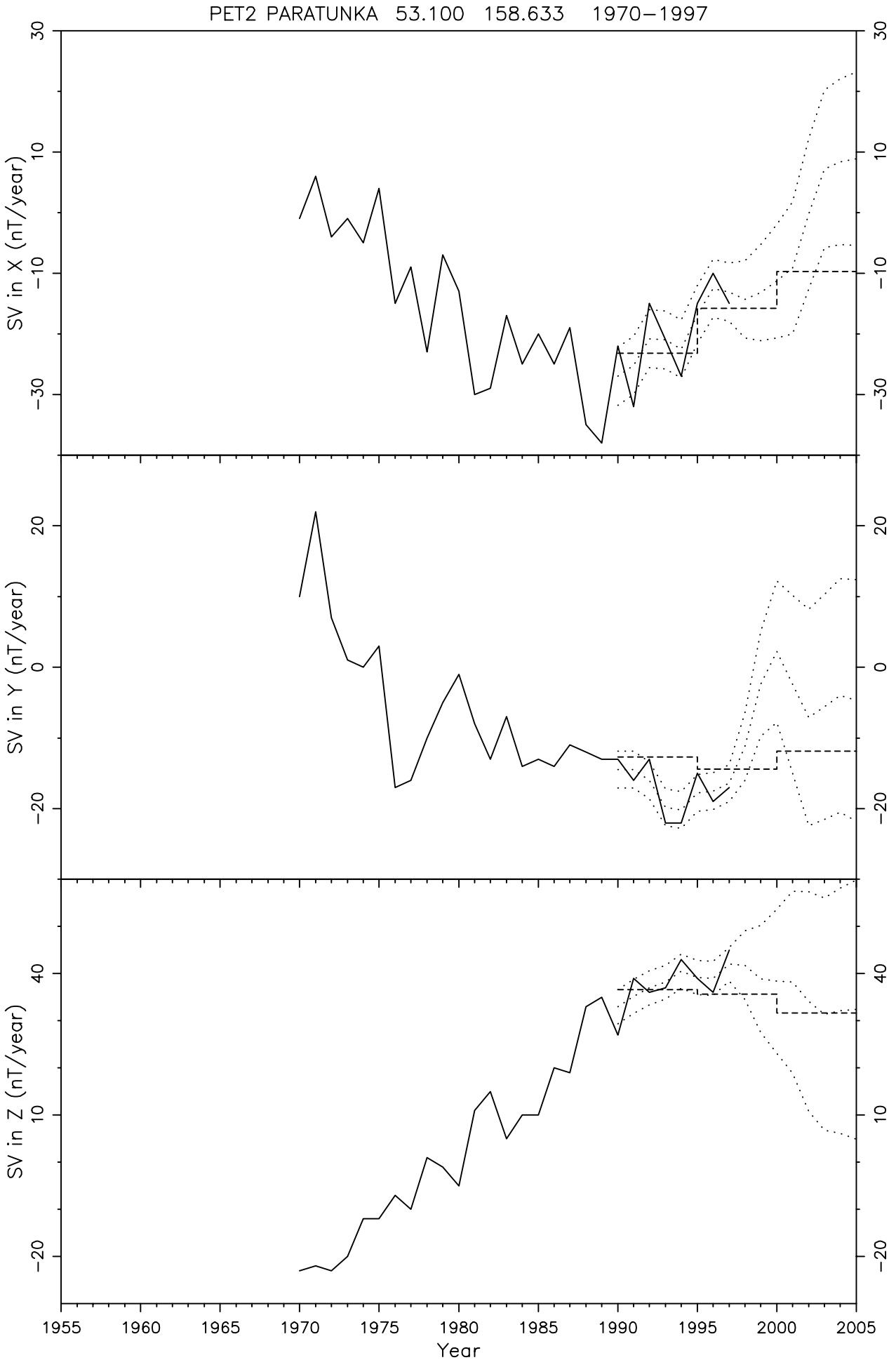
PET2 PARATUNKA 53.100 158.633 1970–1997
SV in X (nT/year)
SV in Y (nT/year)
SV in Z (nT/year)
30
10
−10
−30
20
0
−20
40
1955
1960
1965
1970
1975
1980
1985
1990
1995
2000
2005
Year

Figure 64

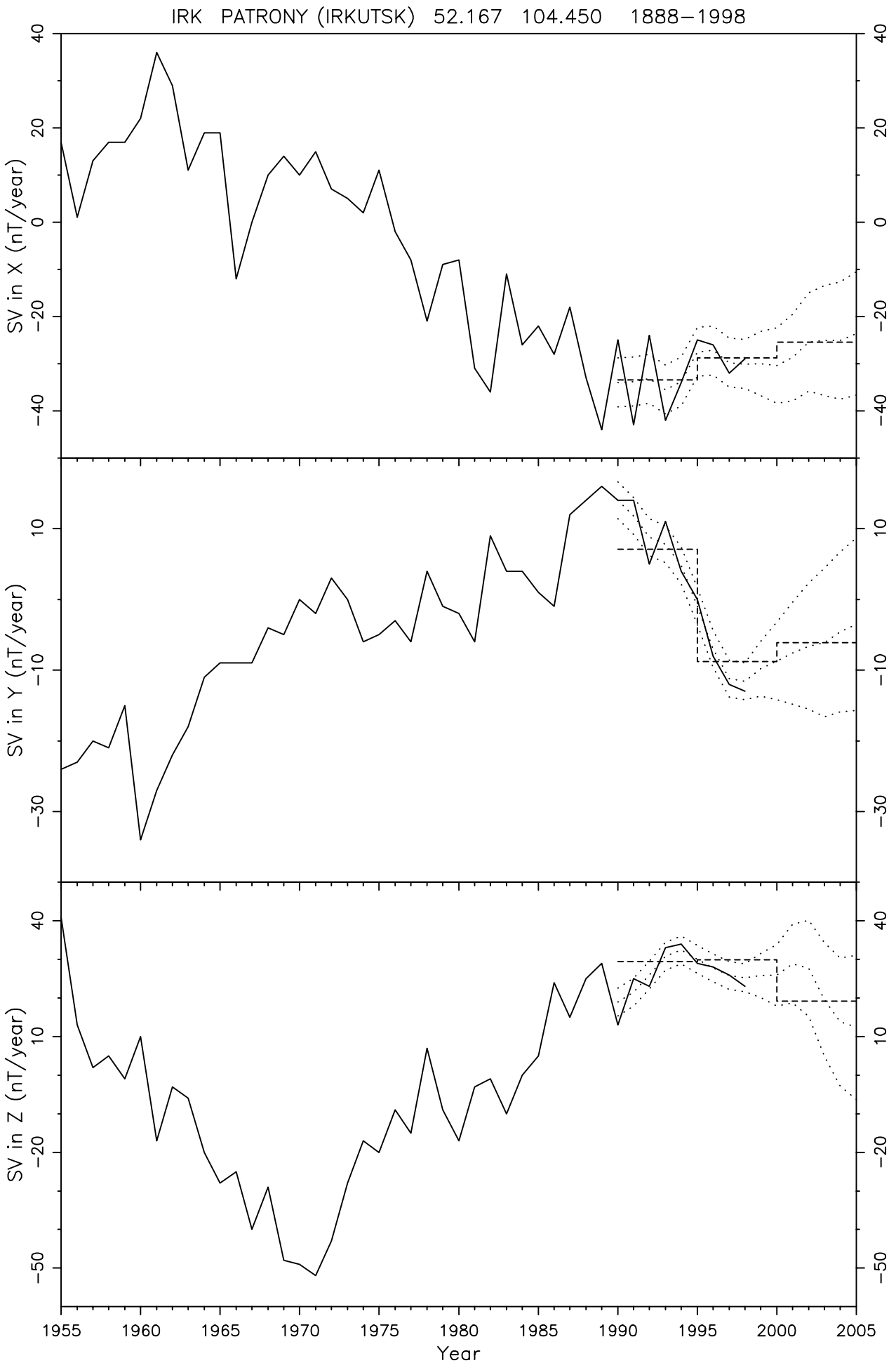
IRK PATRONY (IRKUTSK) 52.167 104.450 1888–1998
SV in X (nT/year)
SV in Y (nT/year)
SV in Z (nT/year)
Year
1955
1960
1965
1970
1975
1980
1985
1990
1995
2000
2005

Figure 65

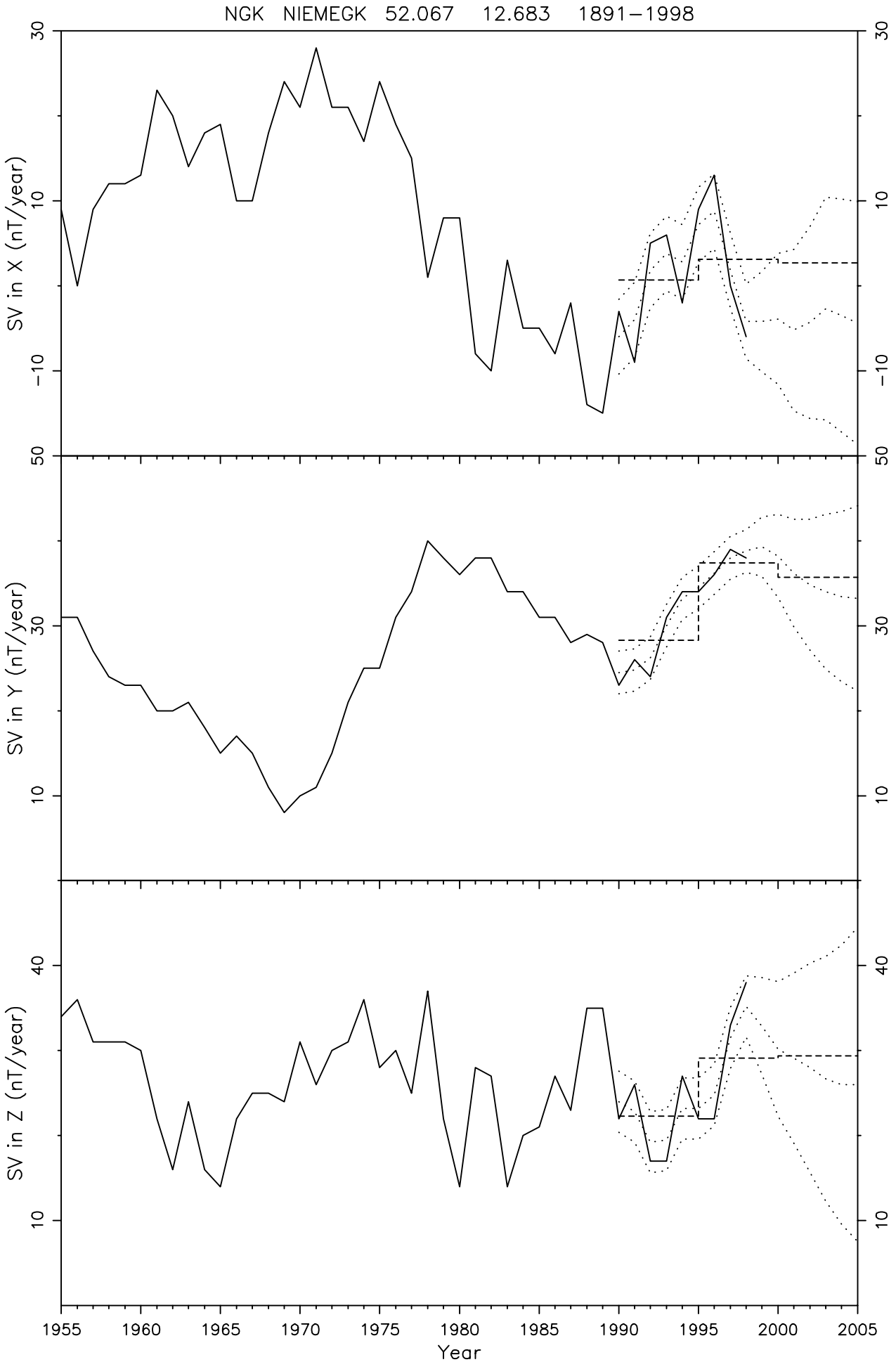
NGK NIEMEGK 52.067 12.683 1891–1998
SV in X (nT/year)
SV in Y (nT/year)
SV in Z (nT/year)
30
10
−10
50
40
1955
1960
1965
1970
1975
1980
1985
1990
1995
2000
2005
Year

Figure 66

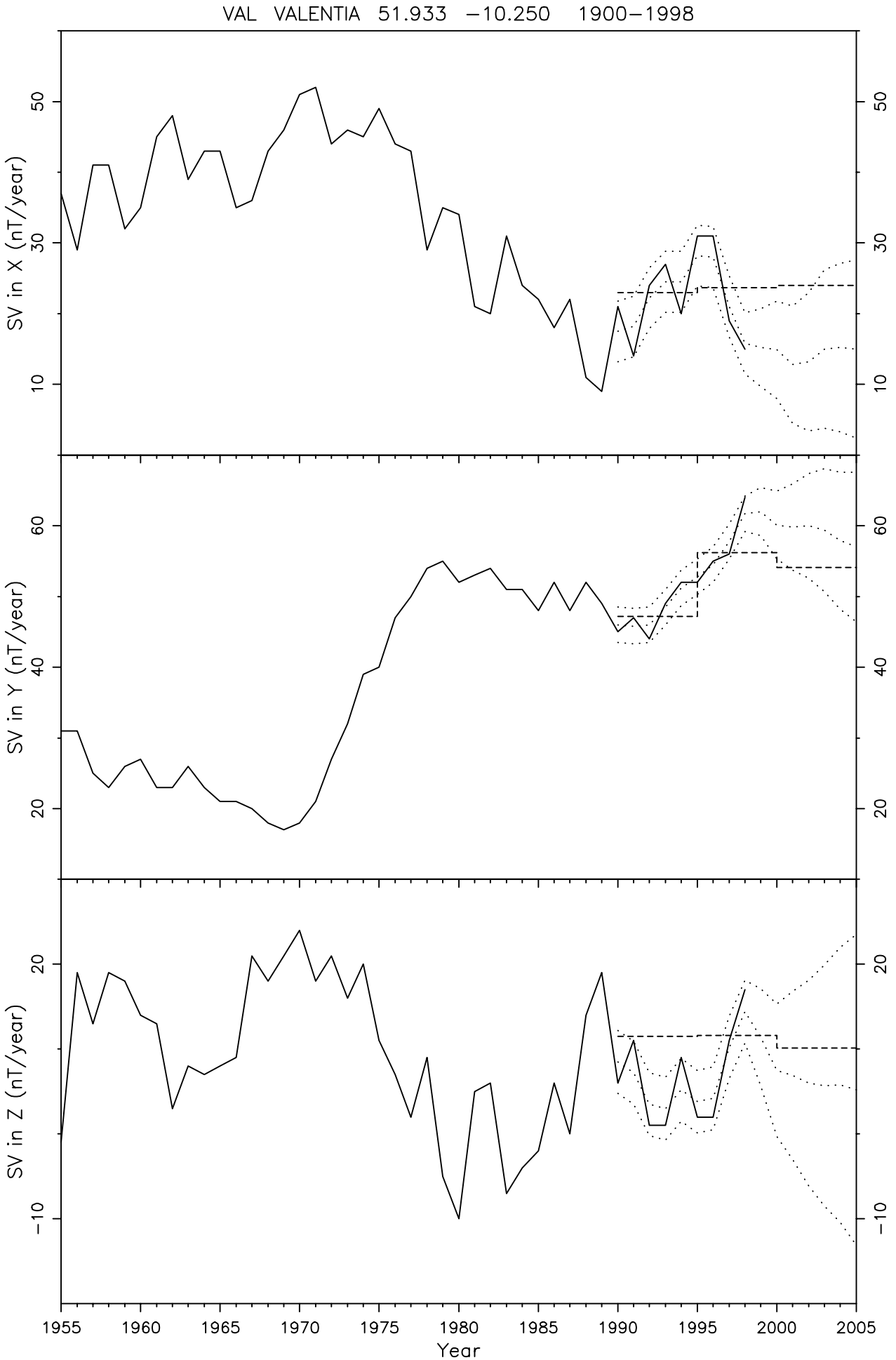
VAL VALENTIA 51.933 −10.250 1900−1998
SV in X (nT/year)
SV in Y (nT/year)
SV in Z (nT/year)
Year
1955
1960
1965
1970
1975
1980
1985
1990
1995
2000
2005

Figure 67

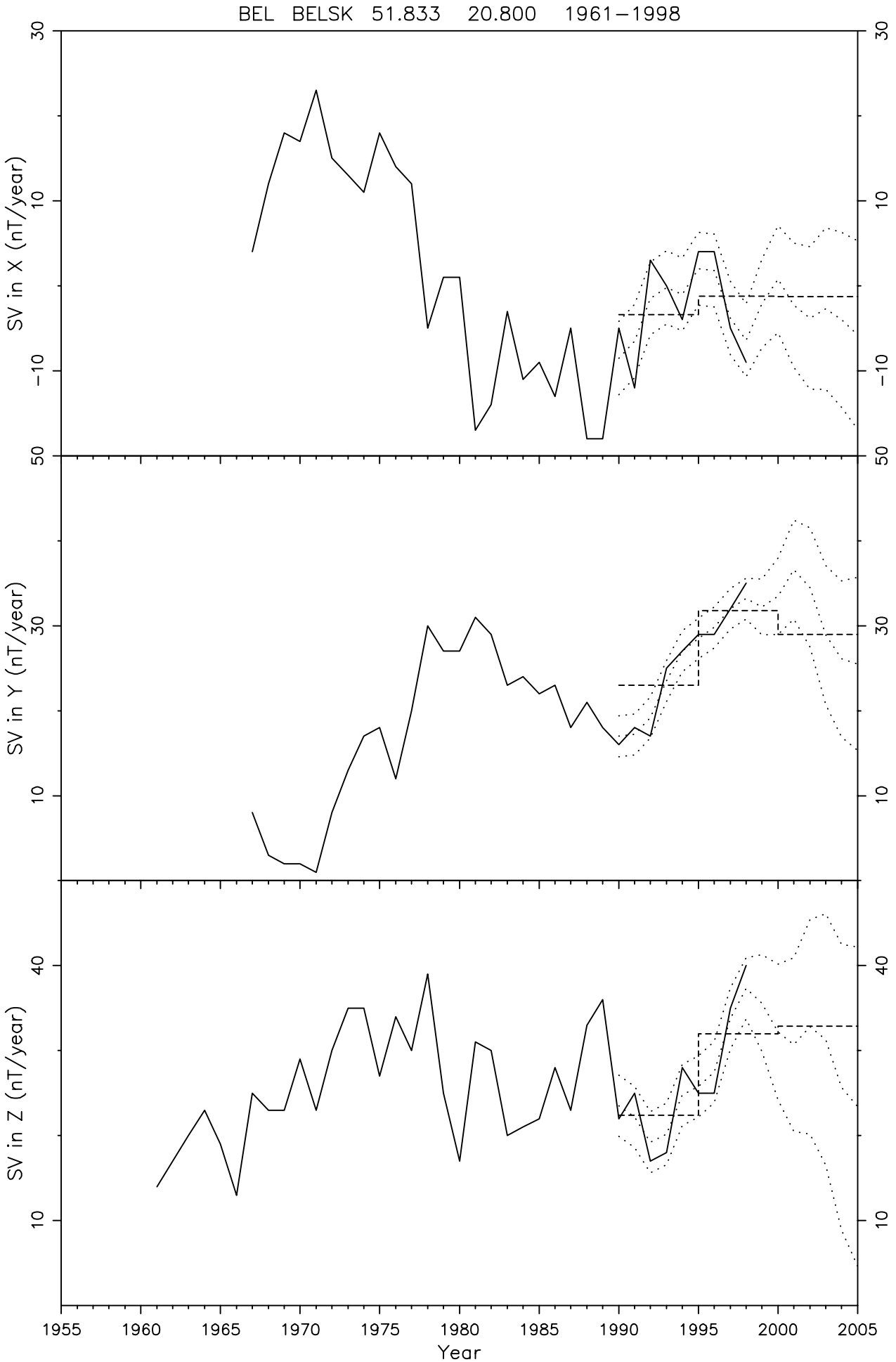
BEL BELSK 51.833 20.800 1961–1998
SV in X (nT/year)
SV in Y (nT/year)
SV in Z (nT/year)
30
10
−10
50
40
1955
1960
1965
1970
1975
1980
1985
1990
1995
2000
2005
Year

Figure 68

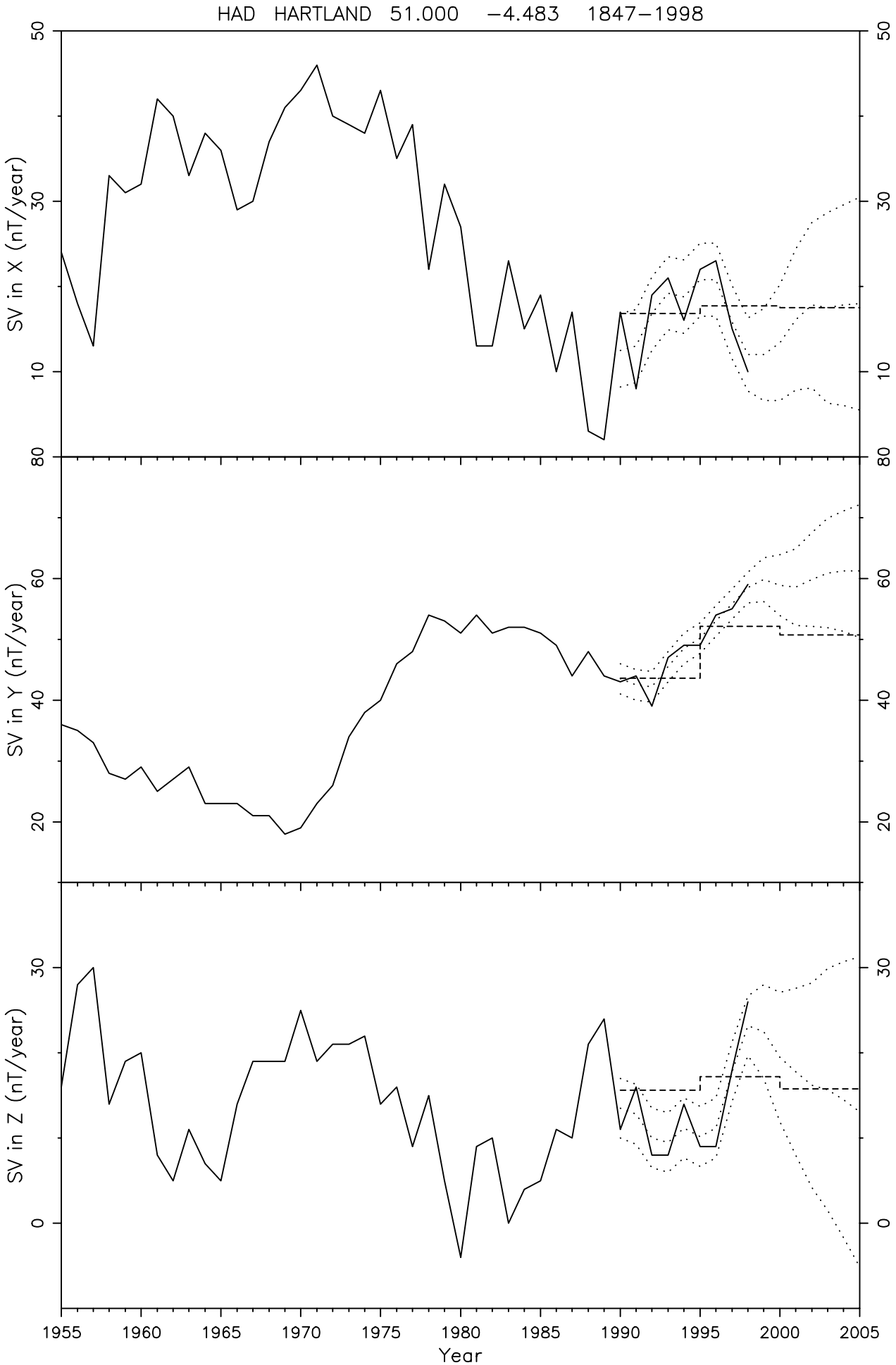
HAD HARTLAND 51.000 −4.483 1847−1998
SV in X (nT/year)
SV in Y (nT/year)
SV in Z (nT/year)
Year
1955
1960
1965
1970
1975
1980
1985
1990
1995
2000
2005

Figure 69

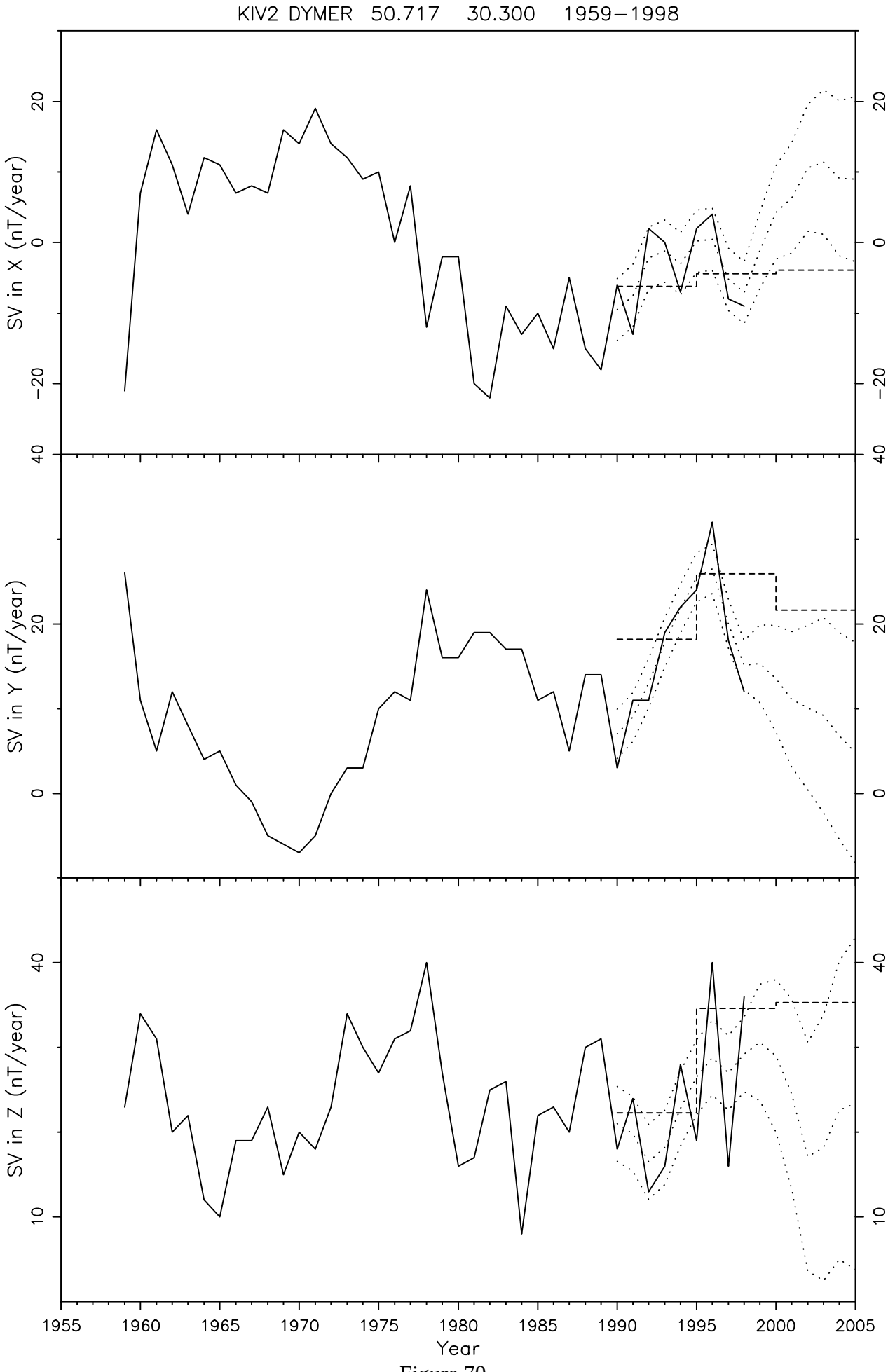
KIV2 DYMER 50.717 30.300 1959–1998
SV in X (nT/year)
SV in Y (nT/year)
SV in Z (nT/year)
Year
1955
1960
1965
1970
1975
1980
1985
1990
1995
2000
2005

Figure 70

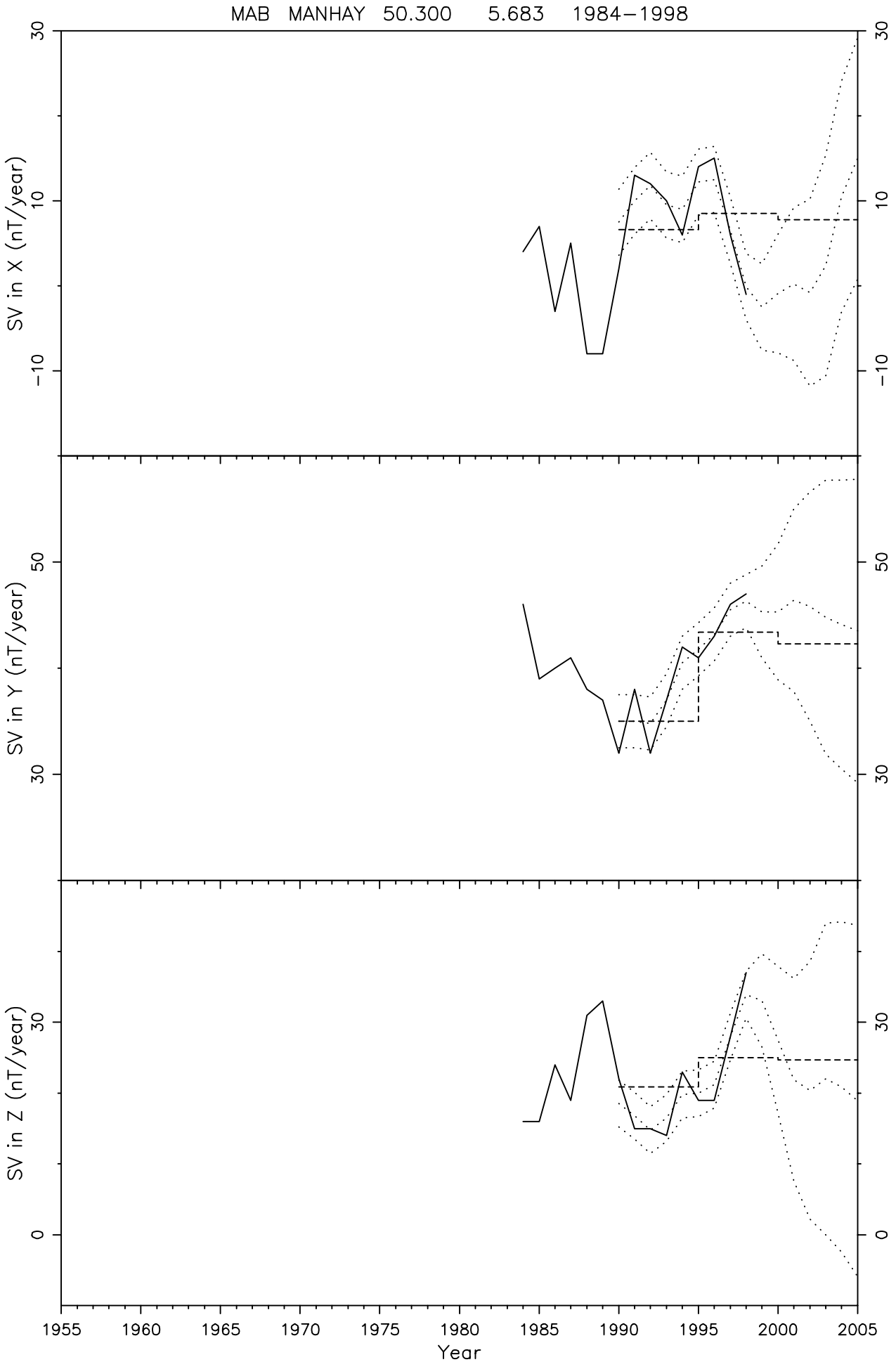
MAB MANHAY 50.300 5.683 1984−1998
SV in X (nT/year)
SV in Y (nT/year)
SV in Z (nT/year)
30
10
−10
50
30
30
0
1955
1960
1965
1970
1975
1980
1985
1990
1995
2000
2005
Year

Figure 71

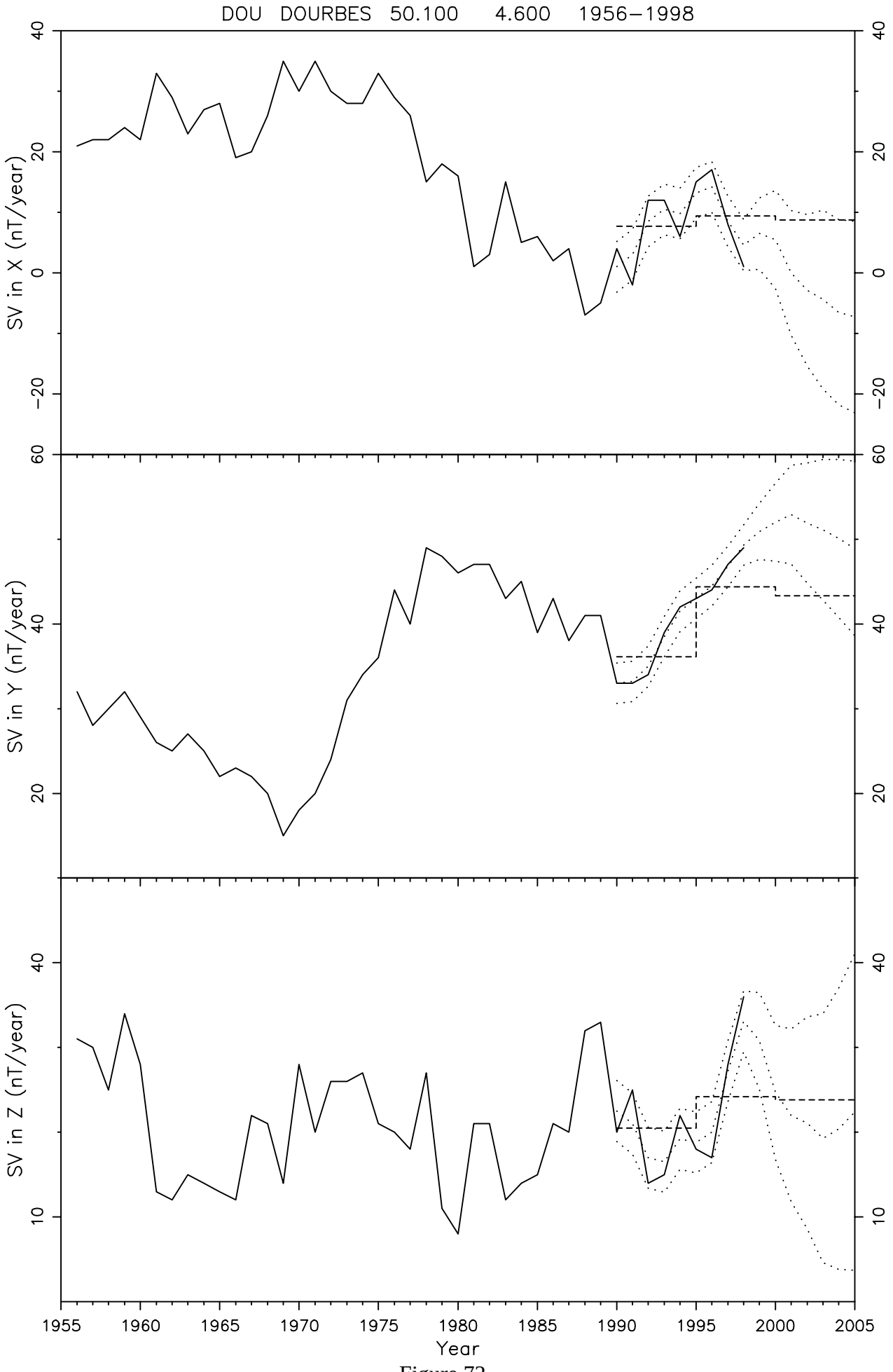
DOU DOURBES 50.100 4.600 1956–1998
SV in X (nT/year)
SV in Y (nT/year)
SV in Z (nT/year)
Year
1955
1960
1965
1970
1975
1980
1985
1990
1995
2000
2005

Figure 72

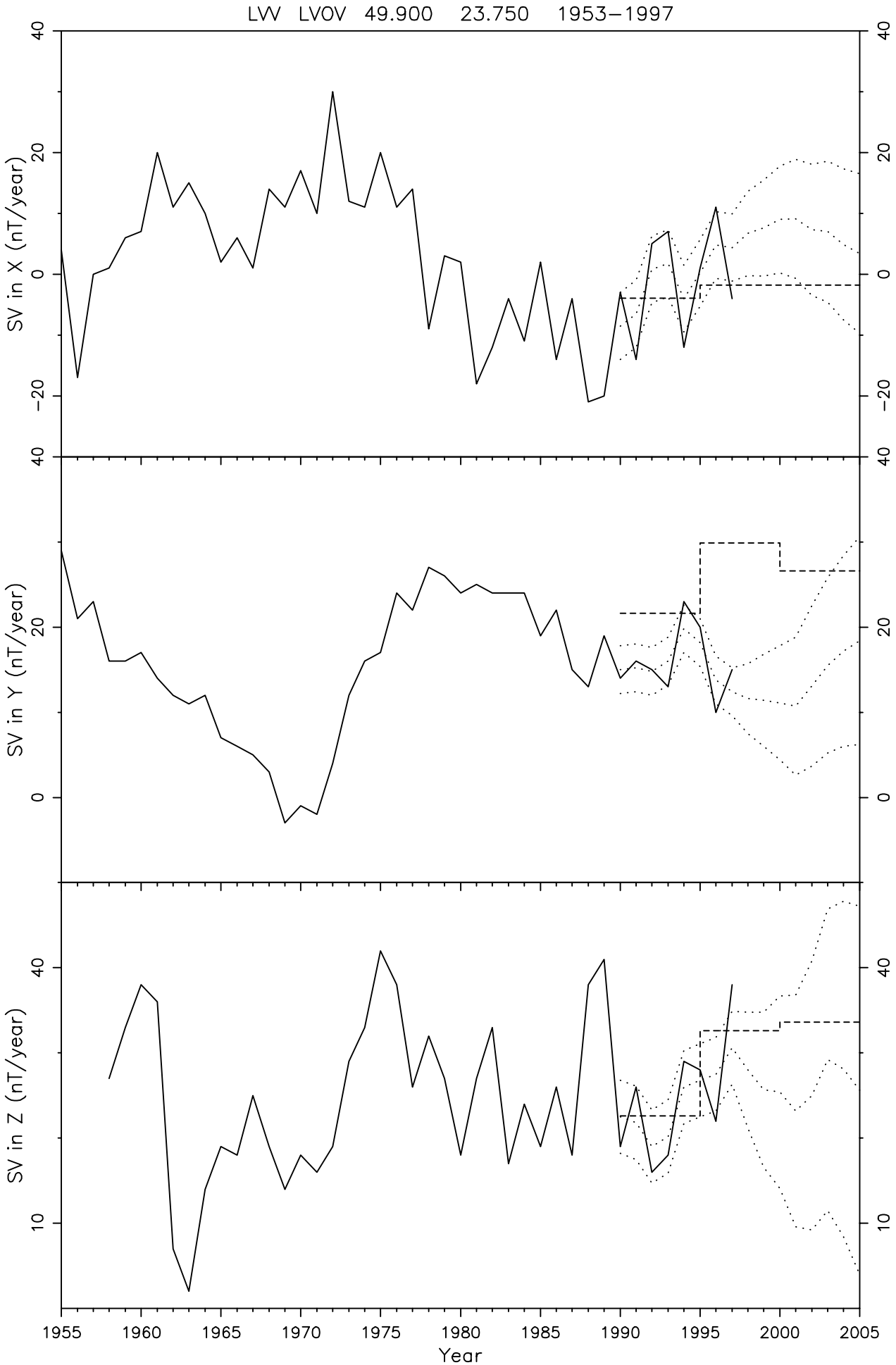
LVV LVOV 49.900 23.750 1953–1997
SV in X (nT/year)
SV in Y (nT/year)
SV in Z (nT/year)
Year
1955
1960
1965
1970
1975
1980
1985
1990
1995
2000
2005

Figure 73

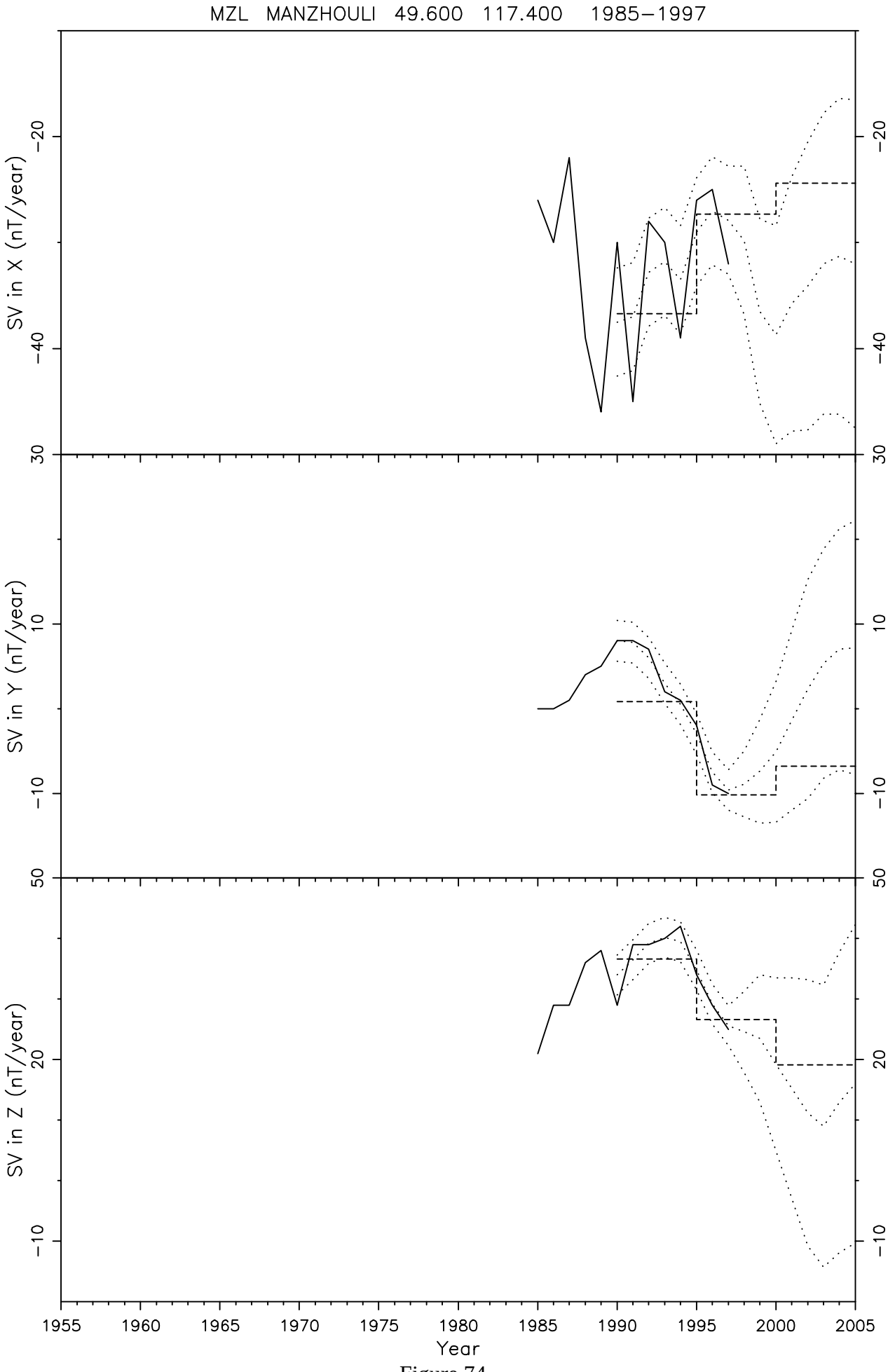
MZL MANZHOULI 49.600 117.400 1985–1997
SV in X (nT/year)
SV in Y (nT/year)
SV in Z (nT/year)
Year
1955
1960
1965
1970
1975
1980
1985
1990
1995
2000
2005

Figure 74

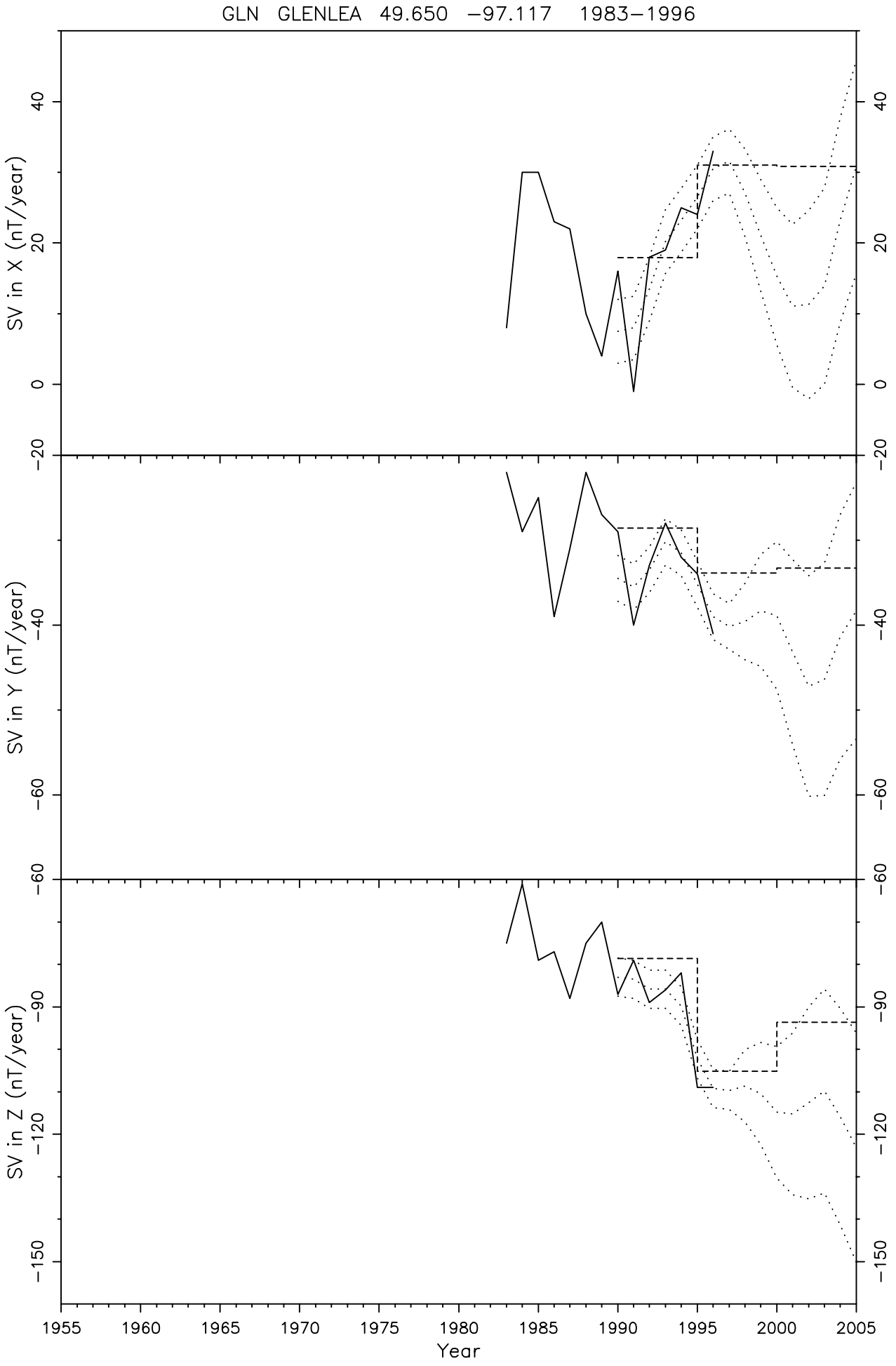
GLN GLENLEA 49.650 −97.117 1983−1996
SV in X (nT/year)
SV in Y (nT/year)
SV in Z (nT/year)
40
20
0
−20
−40
−60
−90
−120
−150
1955
1960
1965
1970
1975
1980
1985
1990
1995
2000
2005
Year

Figure 75

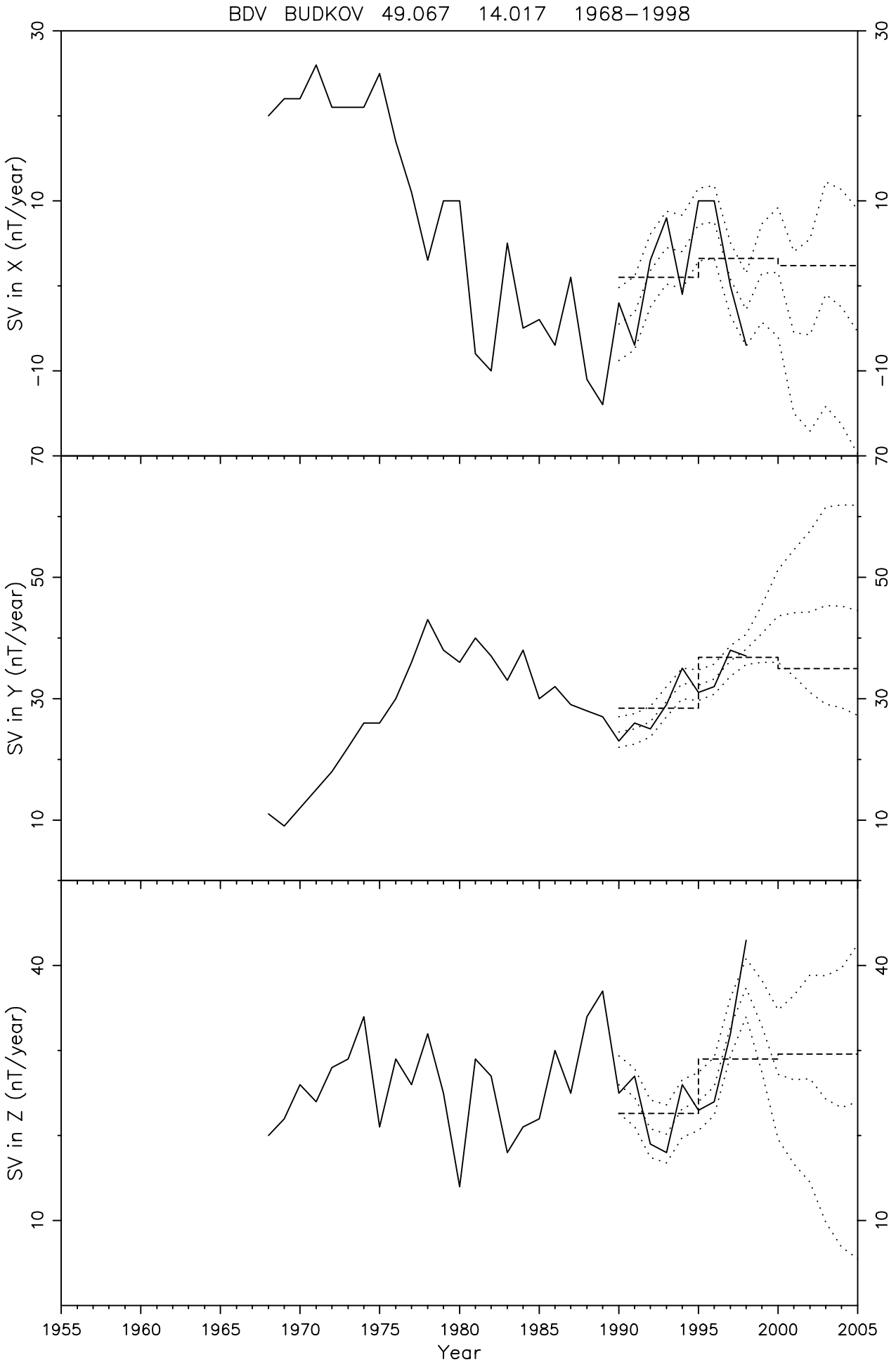
BDV BUDKOV 49.067 14.017 1968–1998
SV in X (nT/year)
SV in Y (nT/year)
SV in Z (nT/year)
Year
1955
1960
1965
1970
1975
1980
1985
1990
1995
2000
2005

Figure 76

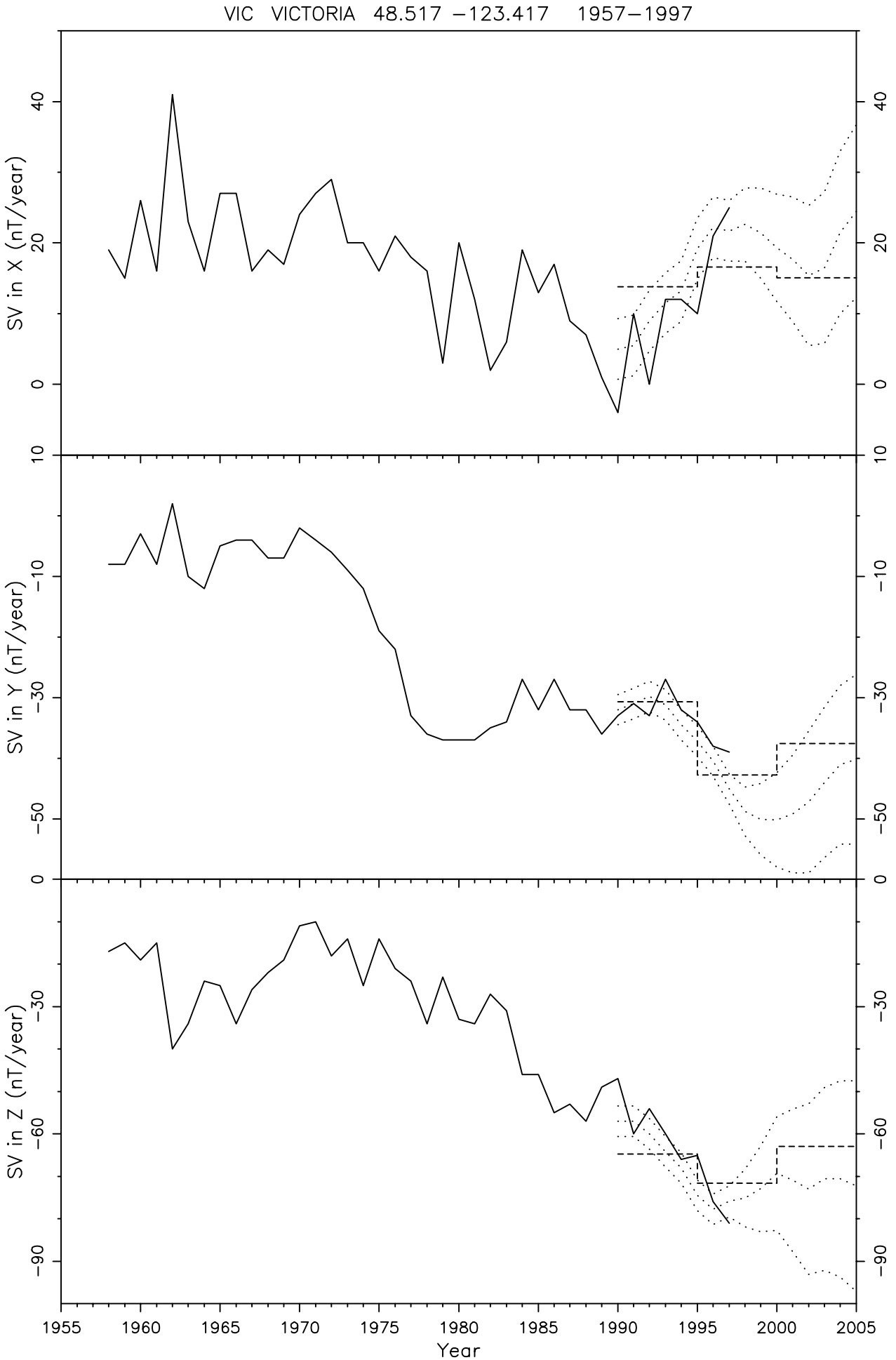
VIC VICTORIA 48.517 −123.417 1957−1997
SV in X (nT/year)
SV in Y (nT/year)
SV in Z (nT/year)
Year
1955
1960
1965
1970
1975
1980
1985
1990
1995
2000
2005

Figure 77

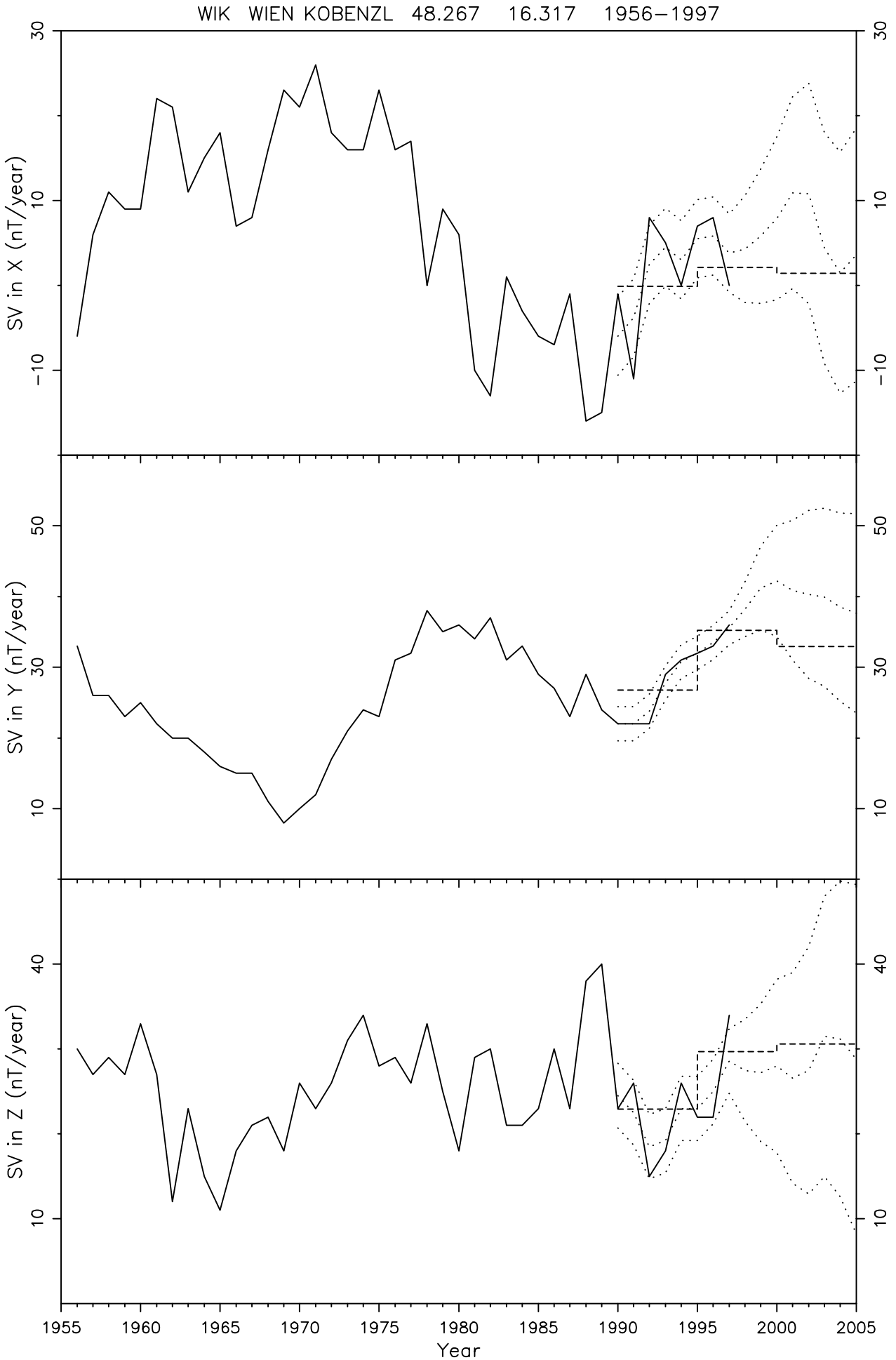
WIK WIEN KOBENZL 48.267 16.317 1956–1997
SV in X (nT/year)
SV in Y (nT/year)
SV in Z (nT/year)
Year
1955
1960
1965
1970
1975
1980
1985
1990
1995
2000
2005

Figure 78

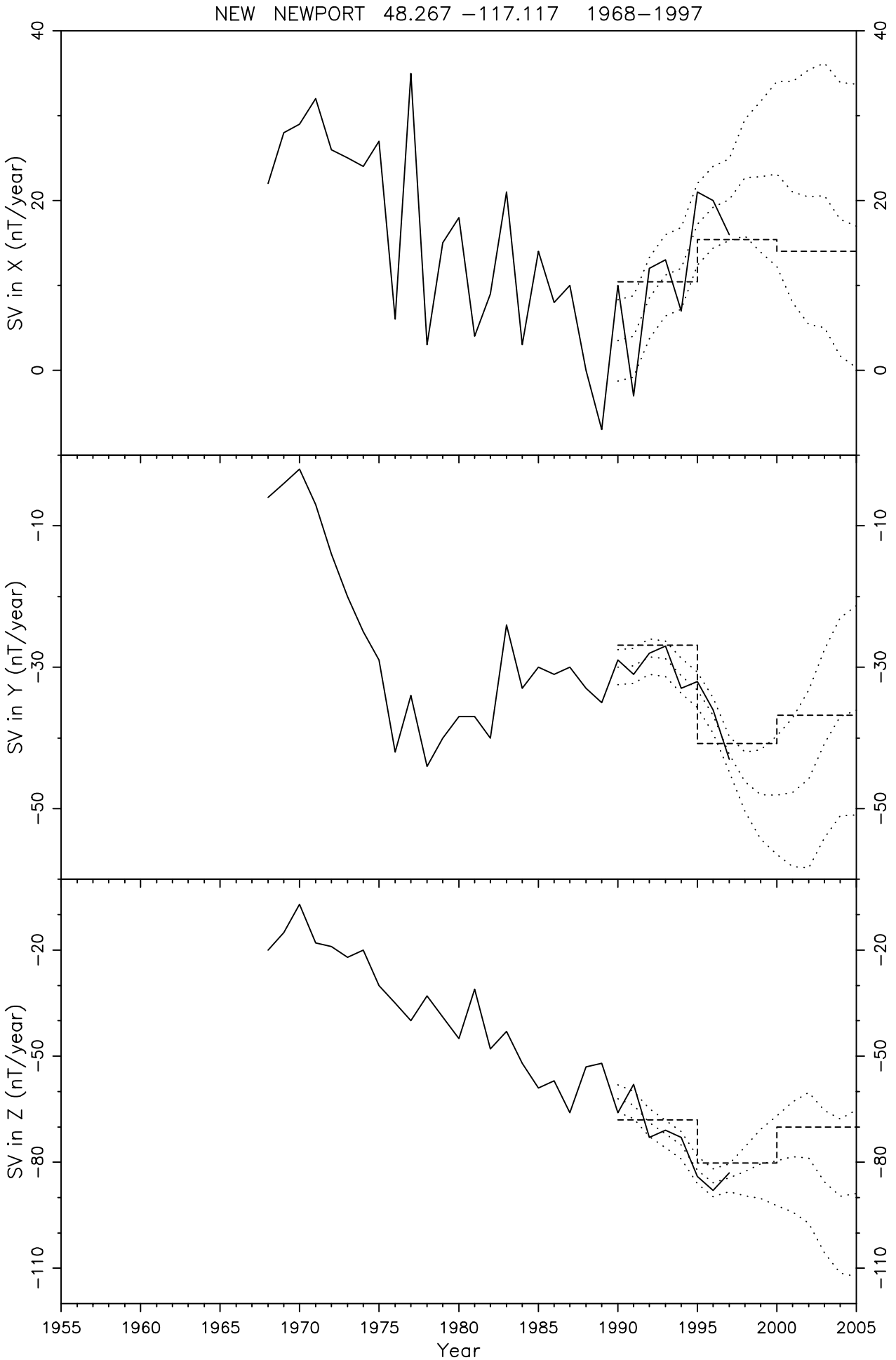
NEW NEWPORT 48.267 −117.117 1968−1997
SV in X (nT/year)
SV in Y (nT/year)
SV in Z (nT/year)
Year
1955
1960
1965
1970
1975
1980
1985
1990
1995
2000
2005

Figure 79

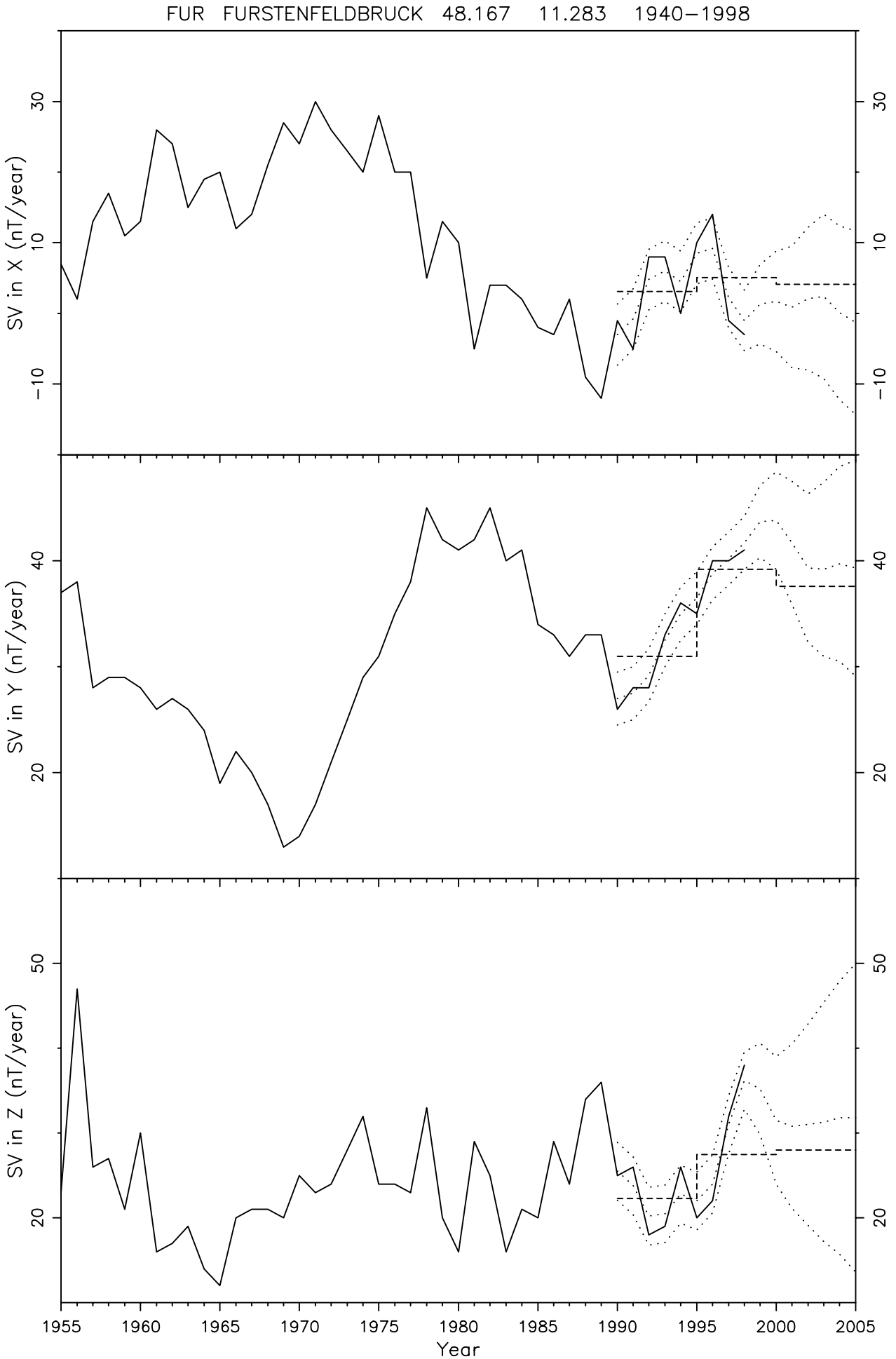
FUR FURSTENFELDBRUCK 48.167 11.283 1940–1998
SV in X (nT/year)
SV in Y (nT/year)
SV in Z (nT/year)
Year
1955
1960
1965
1970
1975
1980
1985
1990
1995
2000
2005

Figure 80

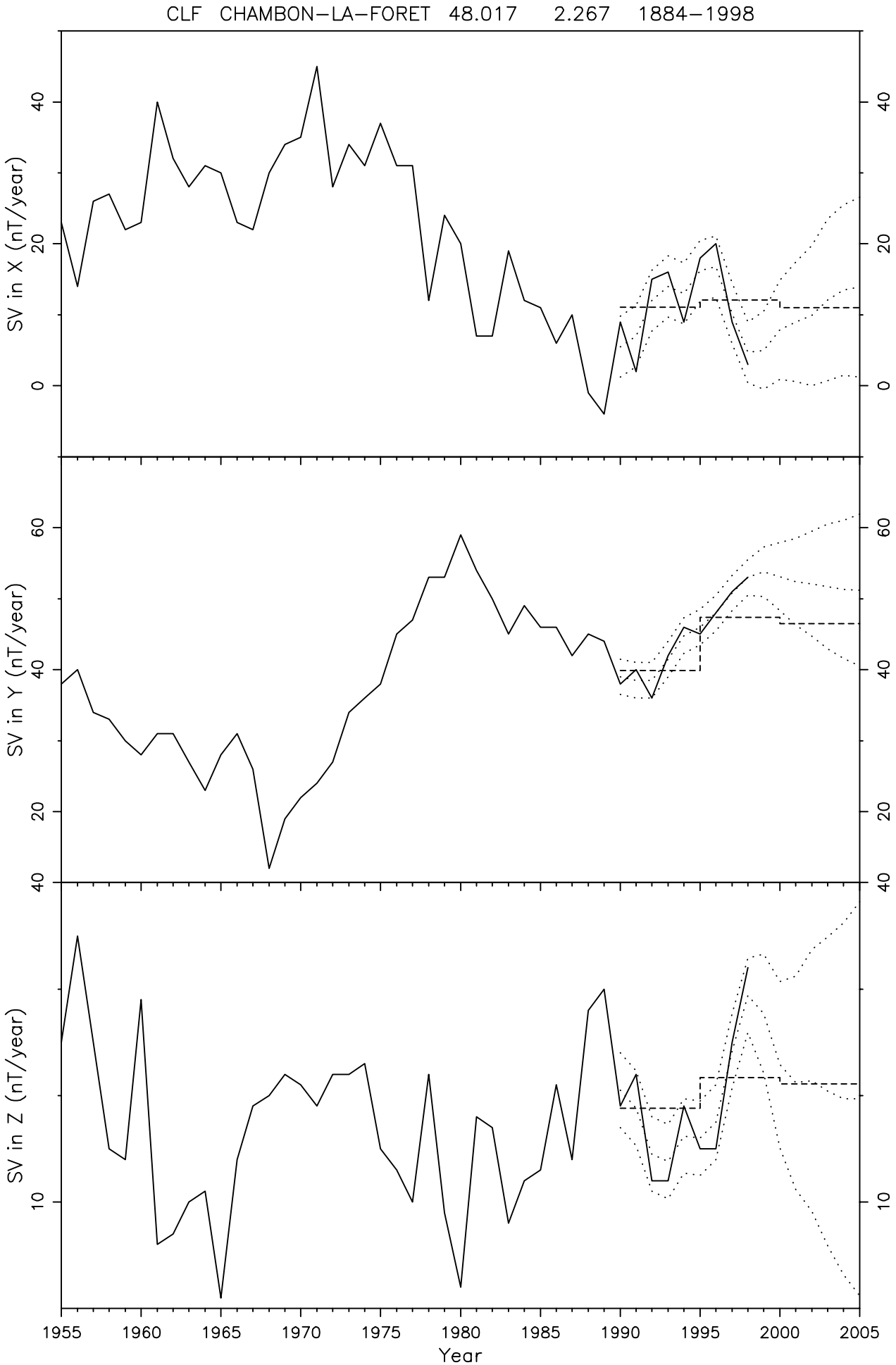
CLF CHAMBON−LA−FORET 48.017 2.267 1884−1998
SV in X (nT/year)
SV in Y (nT/year)
SV in Z (nT/year)
Year
1955
1960
1965
1970
1975
1980
1985
1990
1995
2000
2005

Figure 81

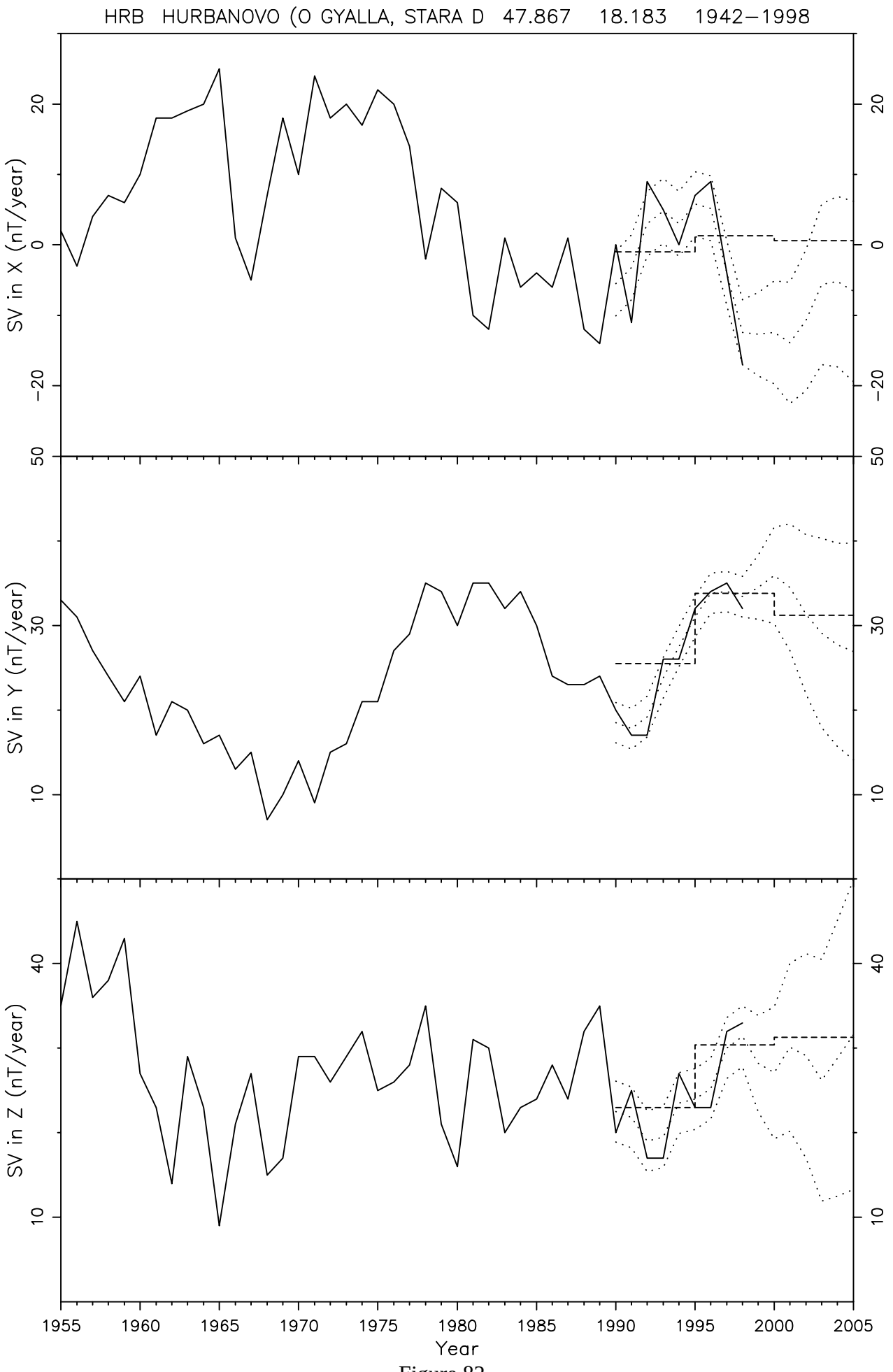
HRB HURBANOVO (O GYALLA, STARA D 47.867 18.183 1942–1998
SV in X (nT/year)
SV in Y (nT/year)
SV in Z (nT/year)
Year
1955
1960
1965
1970
1975
1980
1985
1990
1995
2000
2005

Figure 82

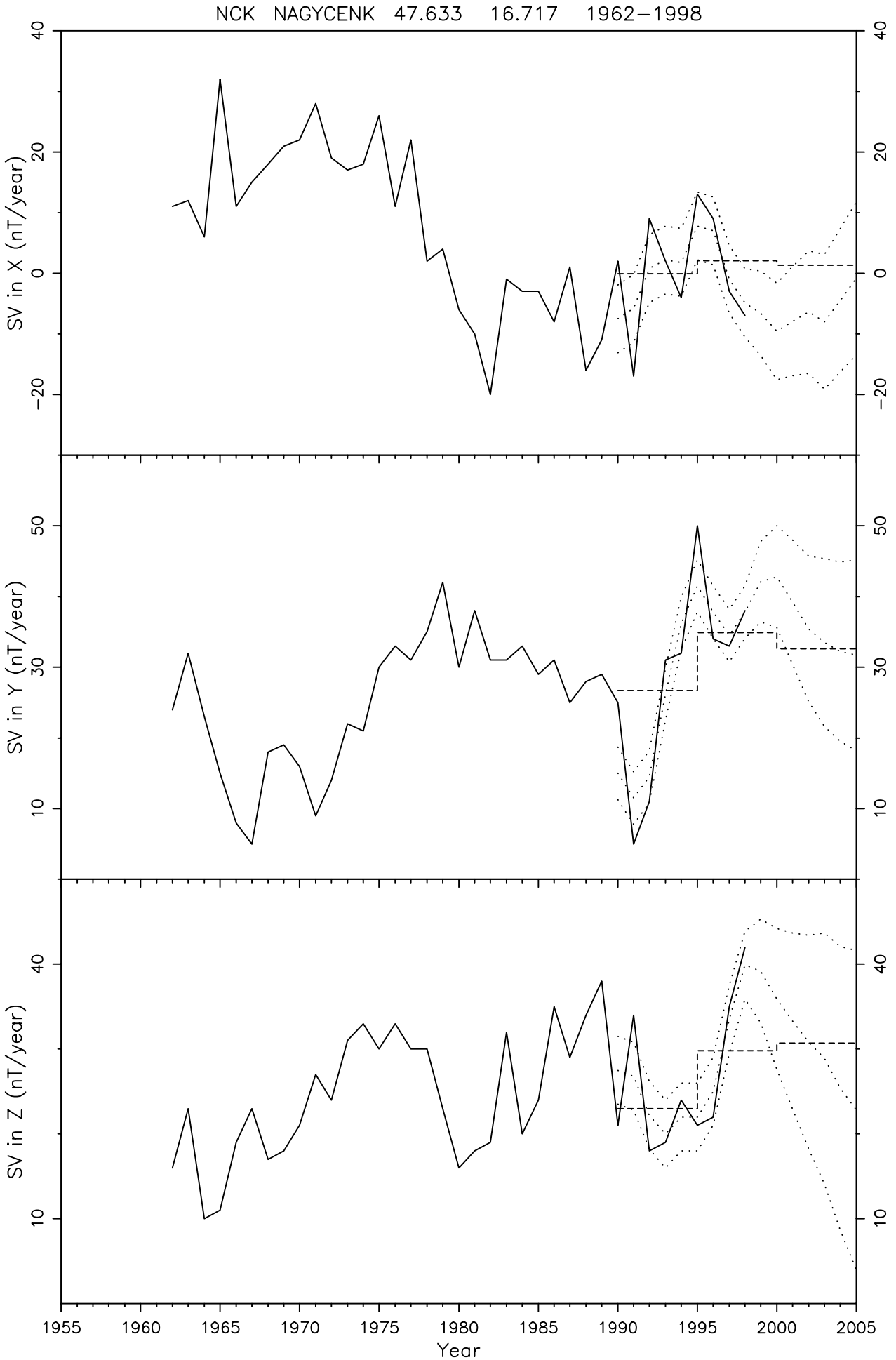
NCK NAGYCENK 47.633 16.717 1962–1998
SV in X (nT/year)
SV in Y (nT/year)
SV in Z (nT/year)
Year
1955
1960
1965
1970
1975
1980
1985
1990
1995
2000
2005

Figure 83

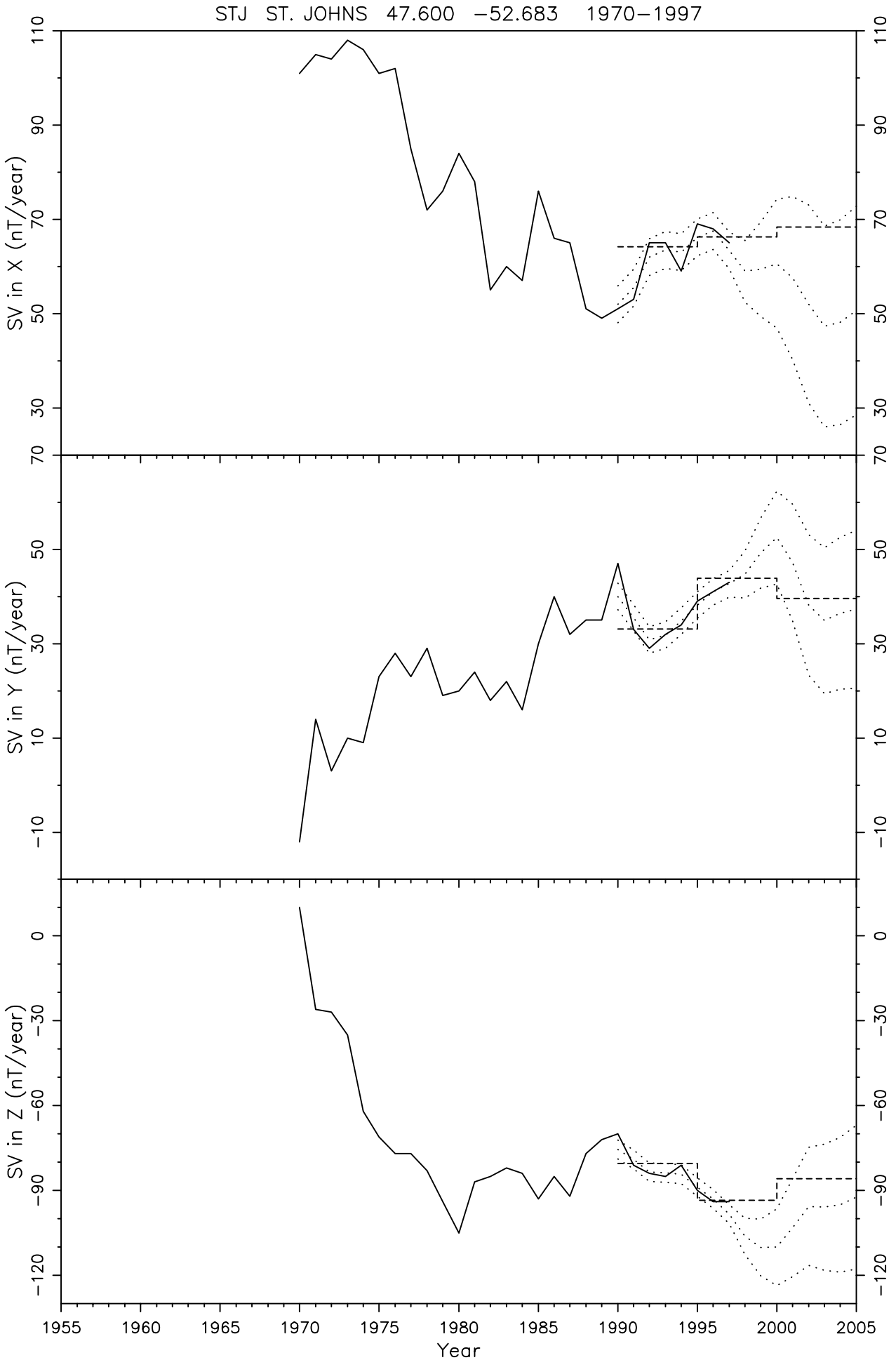
STJ ST. JOHNS 47.600 −52.683 1970−1997
SV in X (nT/year)
SV in Y (nT/year)
SV in Z (nT/year)
Year
1955
1960
1965
1970
1975
1980
1985
1990
1995
2000
2005

Figure 84

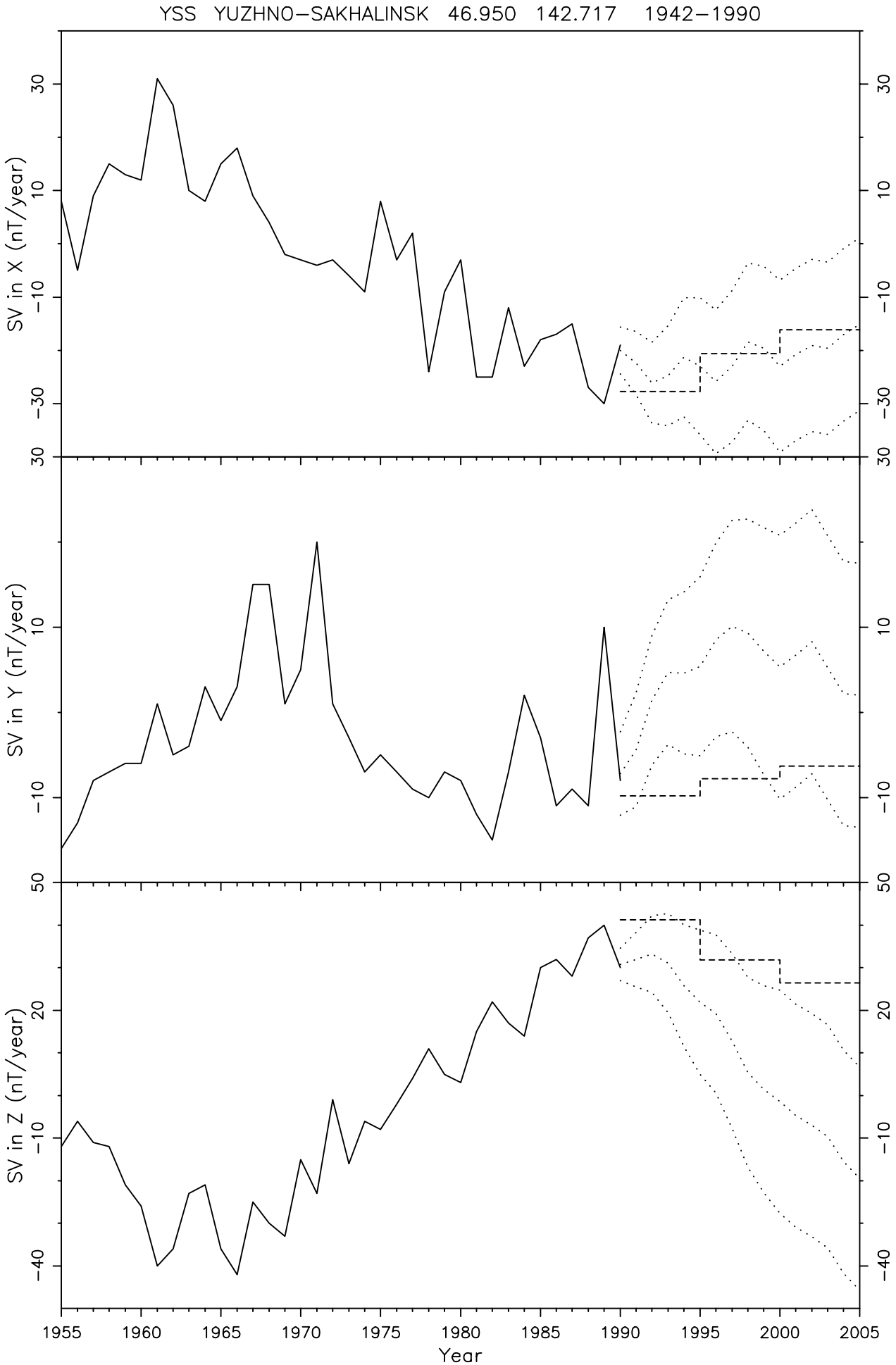
YSS YUZHNO−SAKHALINSK 46.950 142.717 1942−1990
SV in X (nT/year)
SV in Y (nT/year)
SV in Z (nT/year)
30
10
−10
−30
50
20
−40
1955
1960
1965
1970
1975
1980
1985
1990
1995
2000
2005
Year

Figure 85

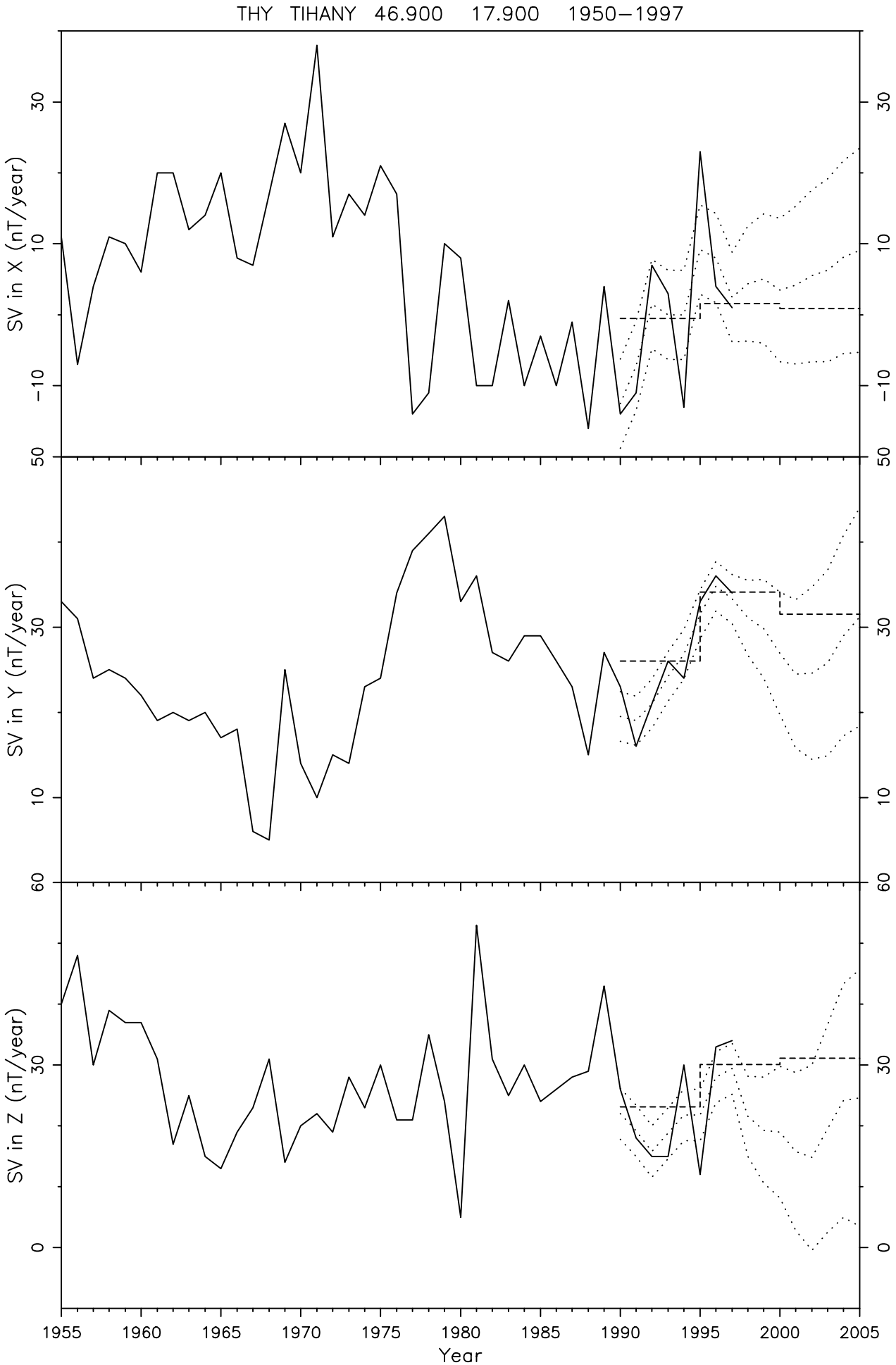
THY TIHANY 46.900 17.900 1950–1997
SV in X (nT/year)
SV in Y (nT/year)
SV in Z (nT/year)
Year
1955
1960
1965
1970
1975
1980
1985
1990
1995
2000
2005

Figure 86

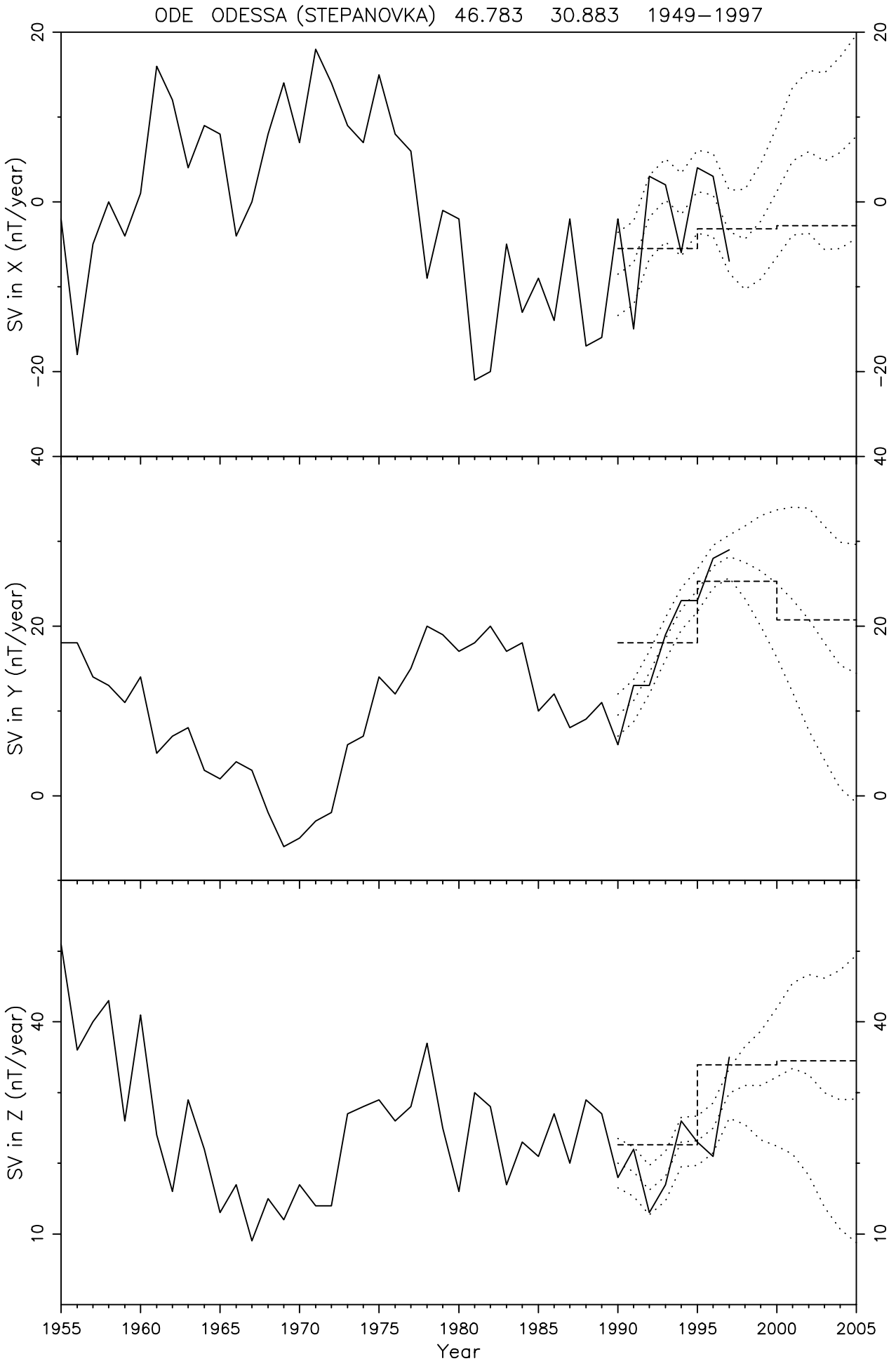
ODE ODESSA (STEPANOVKA) 46.783 30.883 1949–1997
SV in X (nT/year)
SV in Y (nT/year)
SV in Z (nT/year)
Year
1955
1960
1965
1970
1975
1980
1985
1990
1995
2000
2005

Figure 87

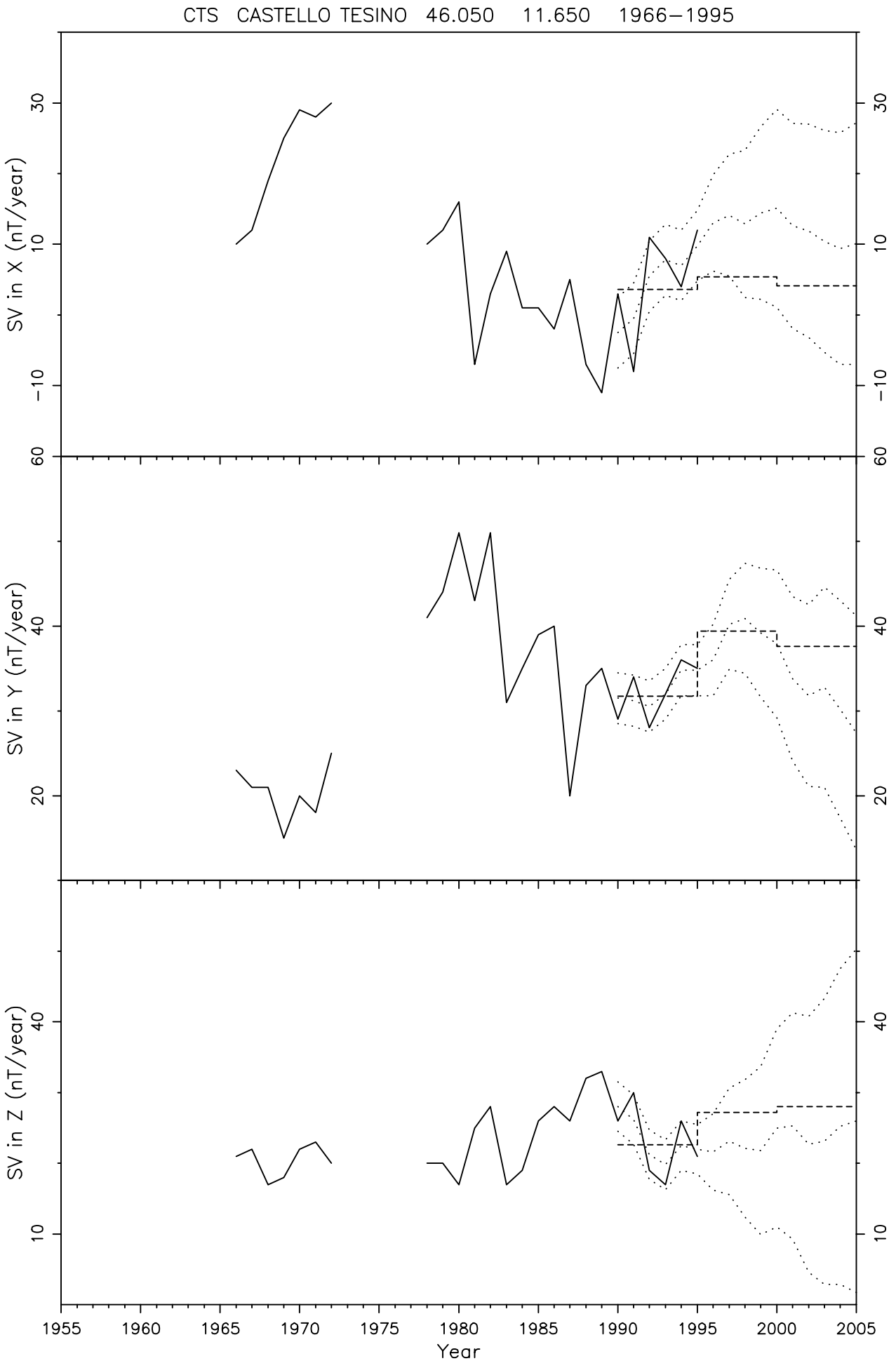
CTS CASTELLO TESINO 46.050 11.650 1966–1995
SV in X (nT/year)
SV in Y (nT/year)
SV in Z (nT/year)
Year
1955
1960
1965
1970
1975
1980
1985
1990
1995
2000
2005

Figure 88

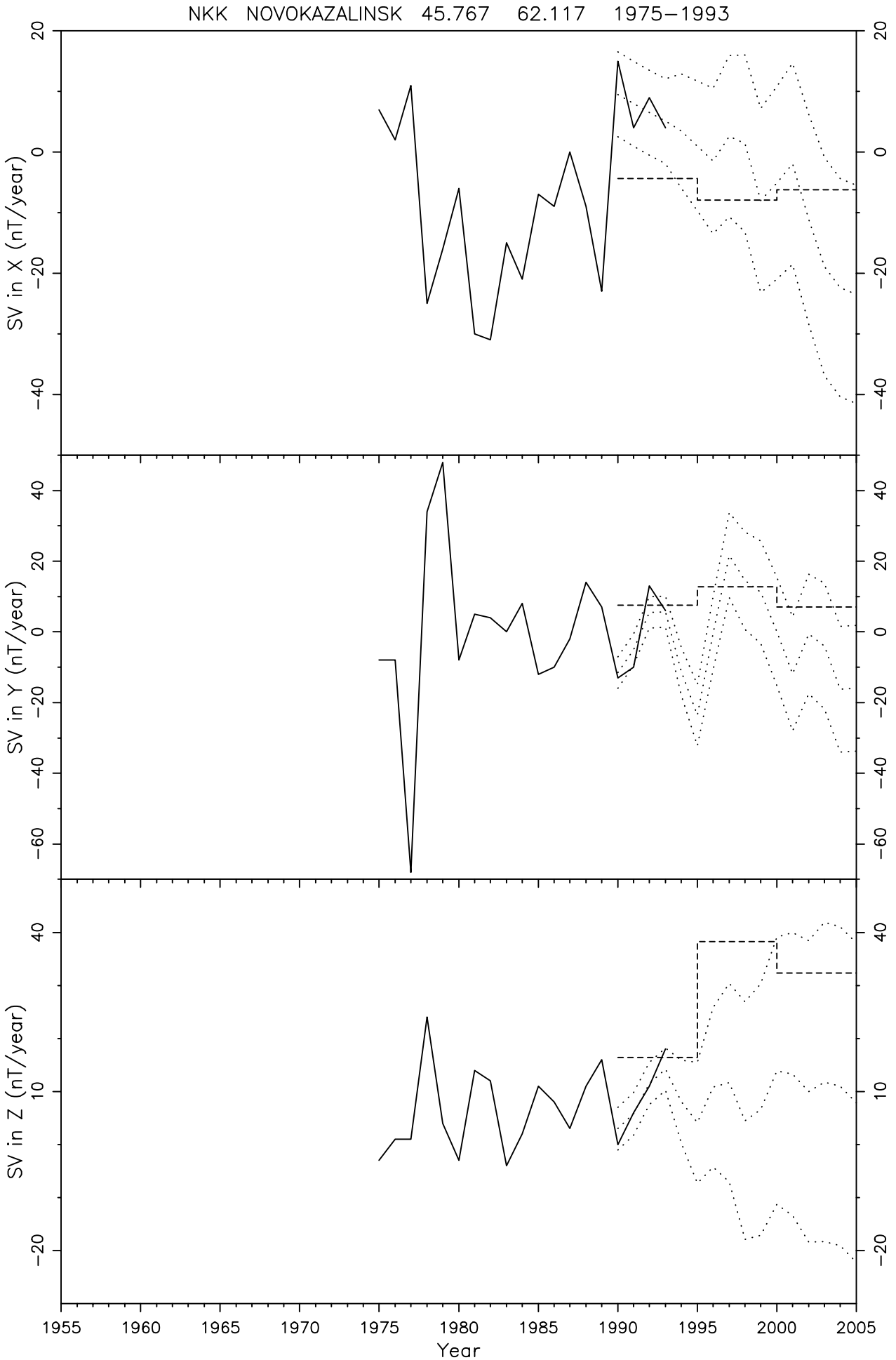
NKK NOVOKAZALINSK 45.767 62.117 1975–1993
SV in X (nT/year)
SV in Y (nT/year)
SV in Z (nT/year)
Year
1955
1960
1965
1970
1975
1980
1985
1990
1995
2000
2005

Figure 89

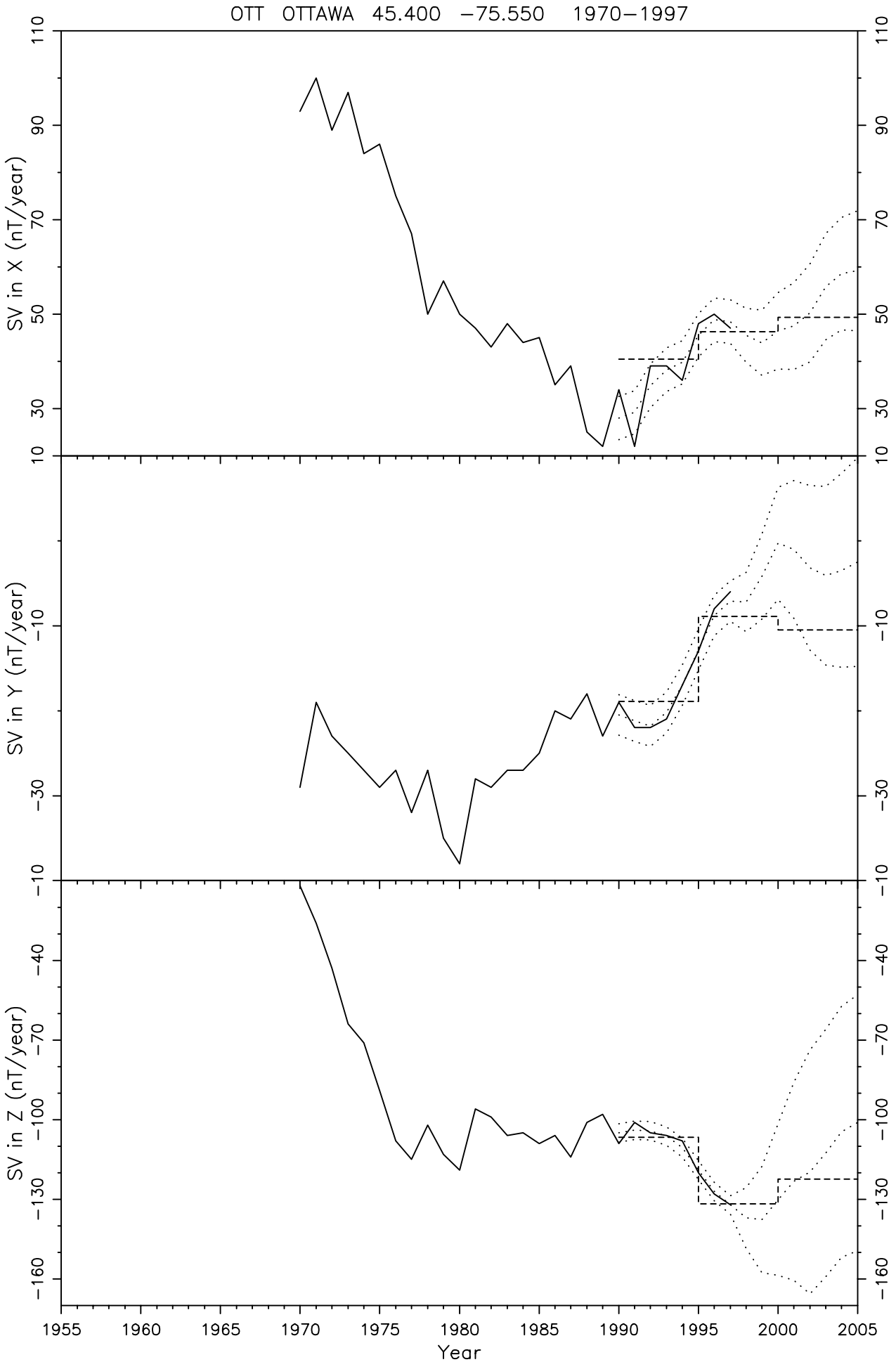
OTT OTTAWA 45.400 −75.550 1970−1997
SV in X (nT/year)
SV in Y (nT/year)
SV in Z (nT/year)
Year
1955
1960
1965
1970
1975
1980
1985
1990
1995
2000
2005

Figure 90

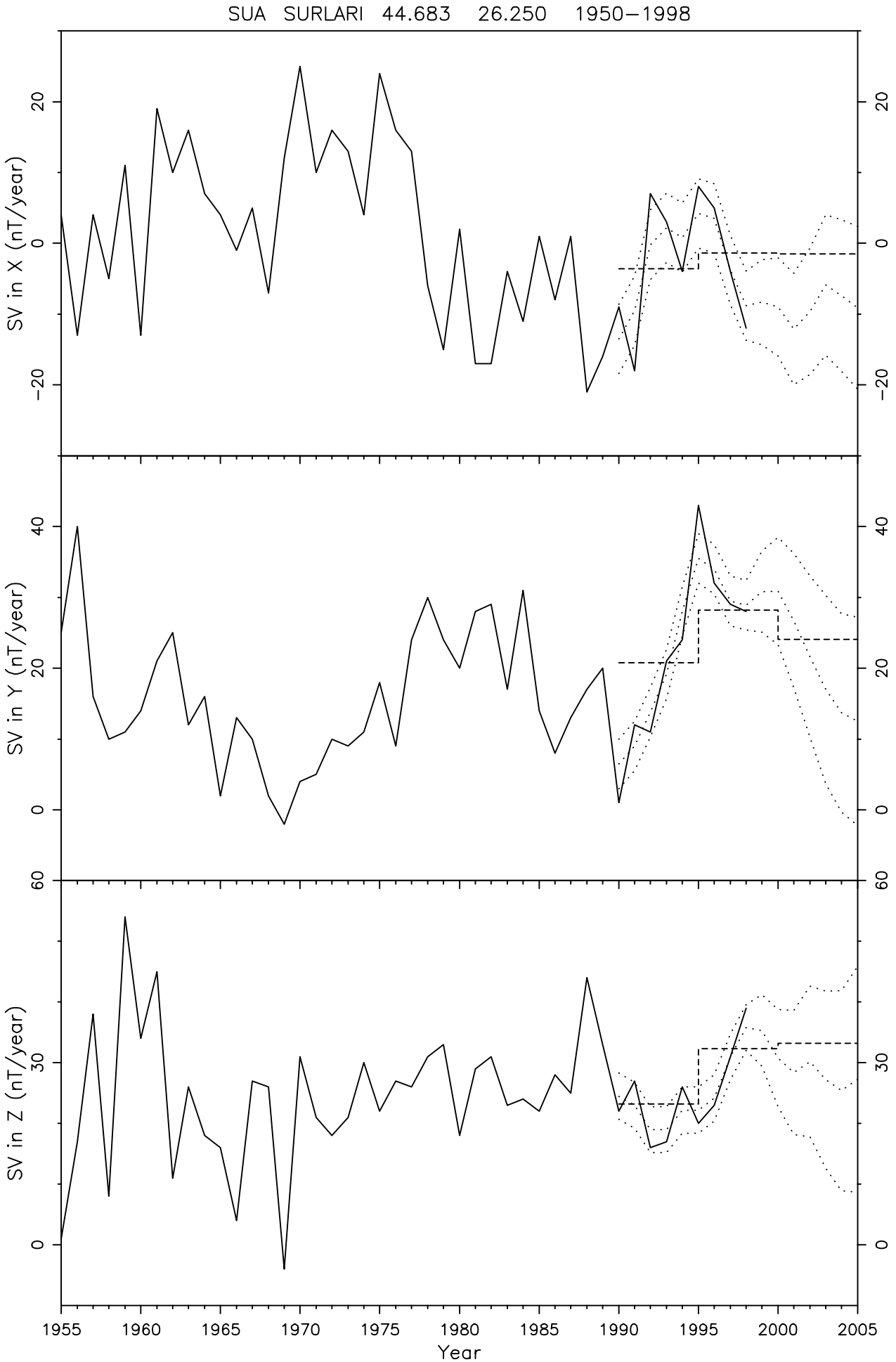
SUA SURLARI 44.683 26.250 1950–1998
SV in X (nT/year)
SV in Y (nT/year)
SV in Z (nT/year)
Year
1955
1960
1965
1970
1975
1980
1985
1990
1995
2000
2005

Figure 91

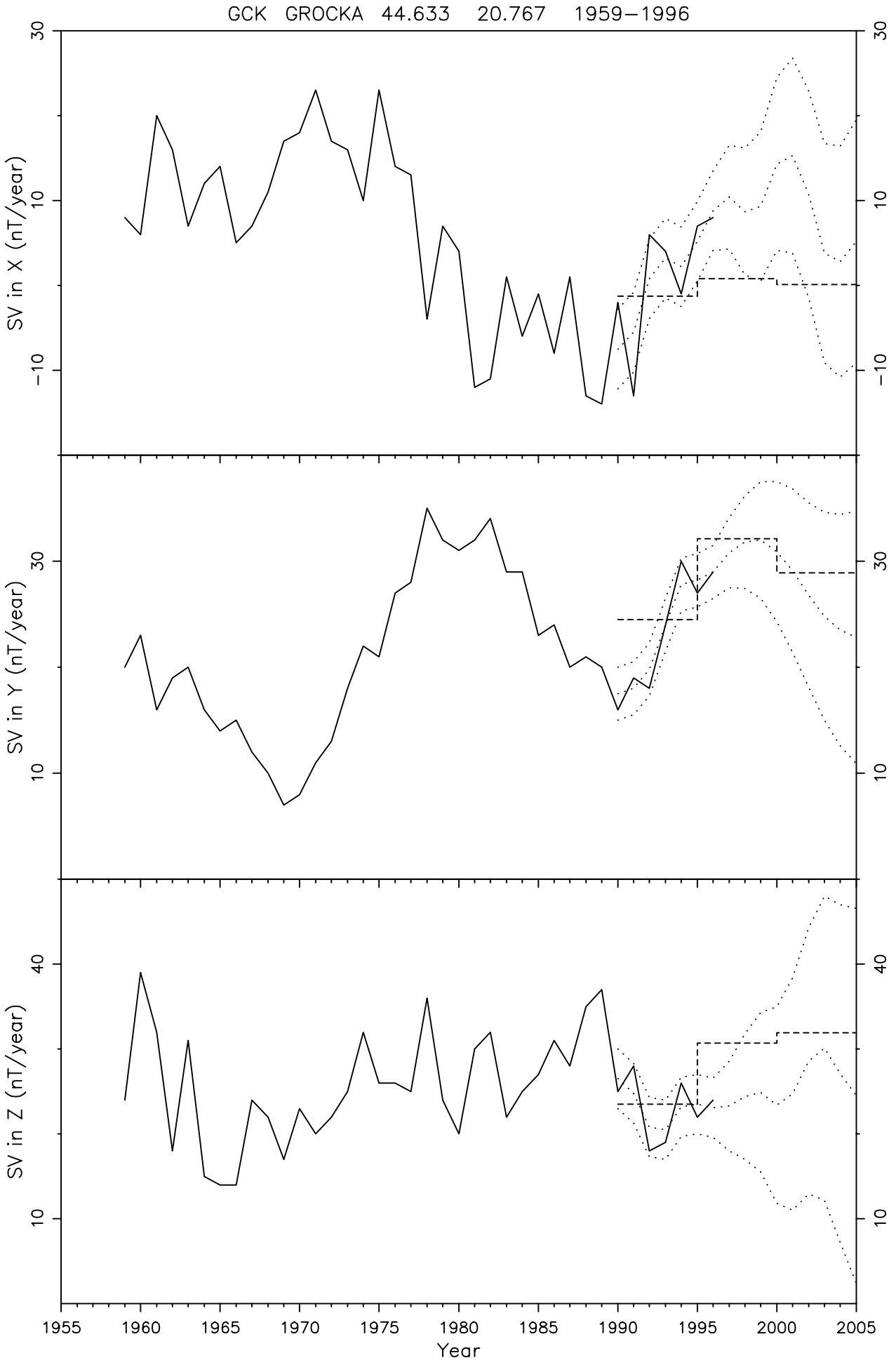
GCK GROCKA 44.633 20.767 1959–1996
SV in X (nT/year)
SV in Y (nT/year)
SV in Z (nT/year)
Year
1955
1960
1965
1970
1975
1980
1985
1990
1995
2000
2005

Figure 92

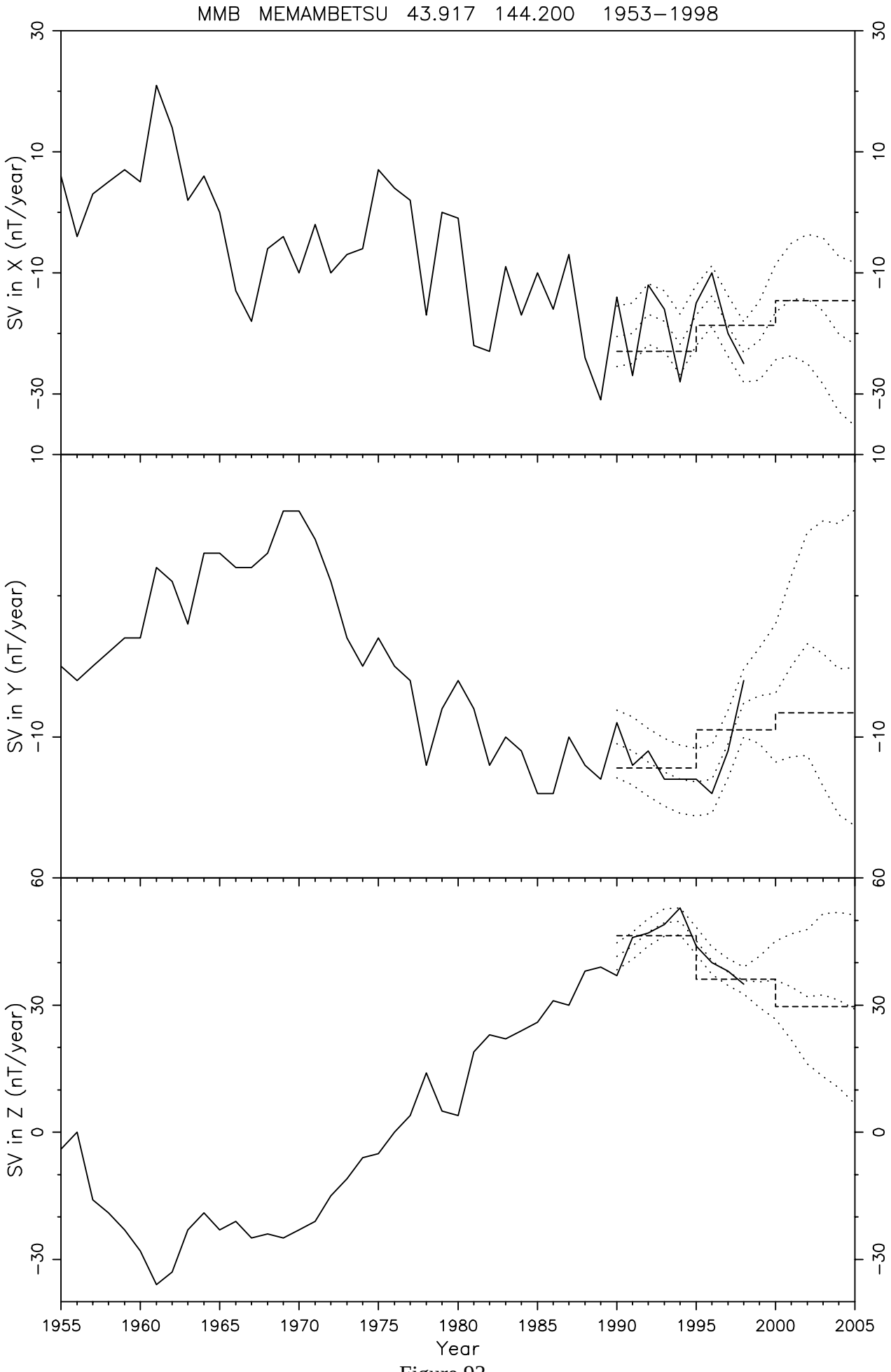
MMB MEMAMBETSU 43.917 144.200 1953–1998
SV in X (nT/year)
SV in Y (nT/year)
SV in Z (nT/year)
Year
1955
1960
1965
1970
1975
1980
1985
1990
1995
2000
2005

Figure 93

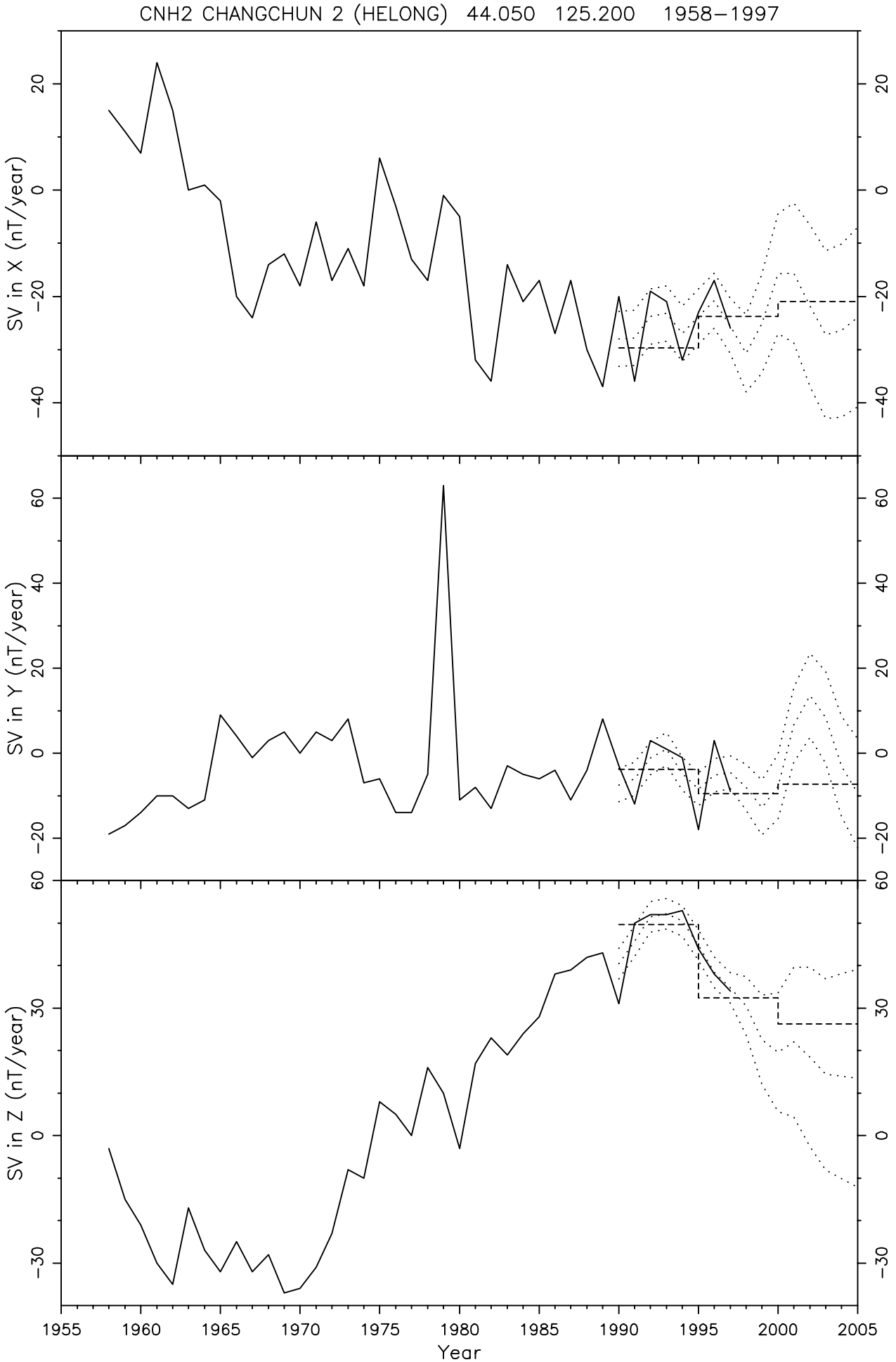
CNH2 CHANGCHUN 2 (HELONG) 44.050 125.200 1958–1997
SV in X (nT/year)
SV in Y (nT/year)
SV in Z (nT/year)
Year
1955
1960
1965
1970
1975
1980
1985
1990
1995
2000
2005

Figure 94

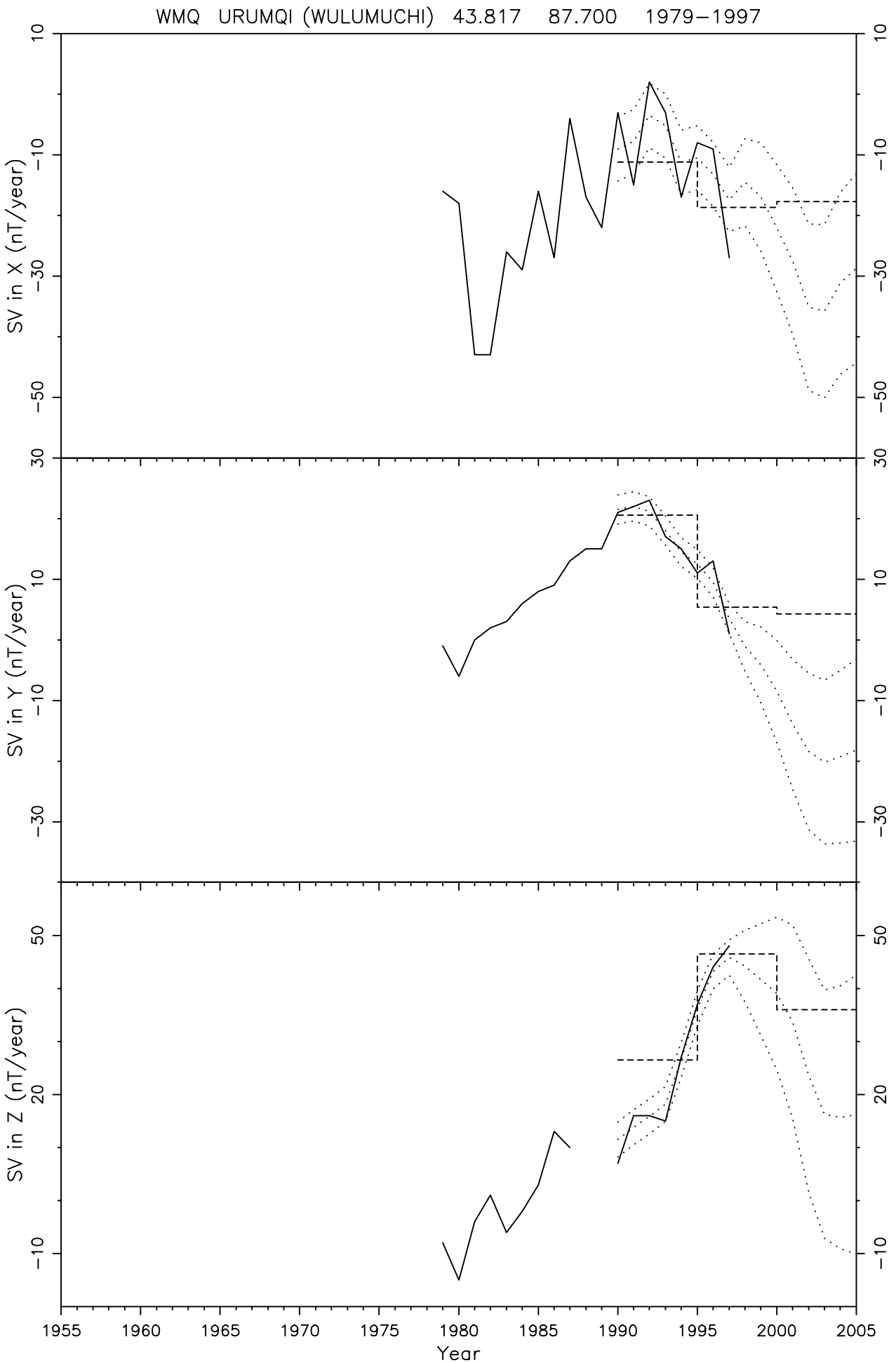
WMQ URUMQI (WULUMUCHI) 43.817 87.700 1979–1997
SV in X (nT/year)
SV in Y (nT/year)
SV in Z (nT/year)
10
−10
−30
−50
30
50
20
1955
1960
1965
1970
1975
1980
1985
1990
1995
2000
2005
Year

Figure 95

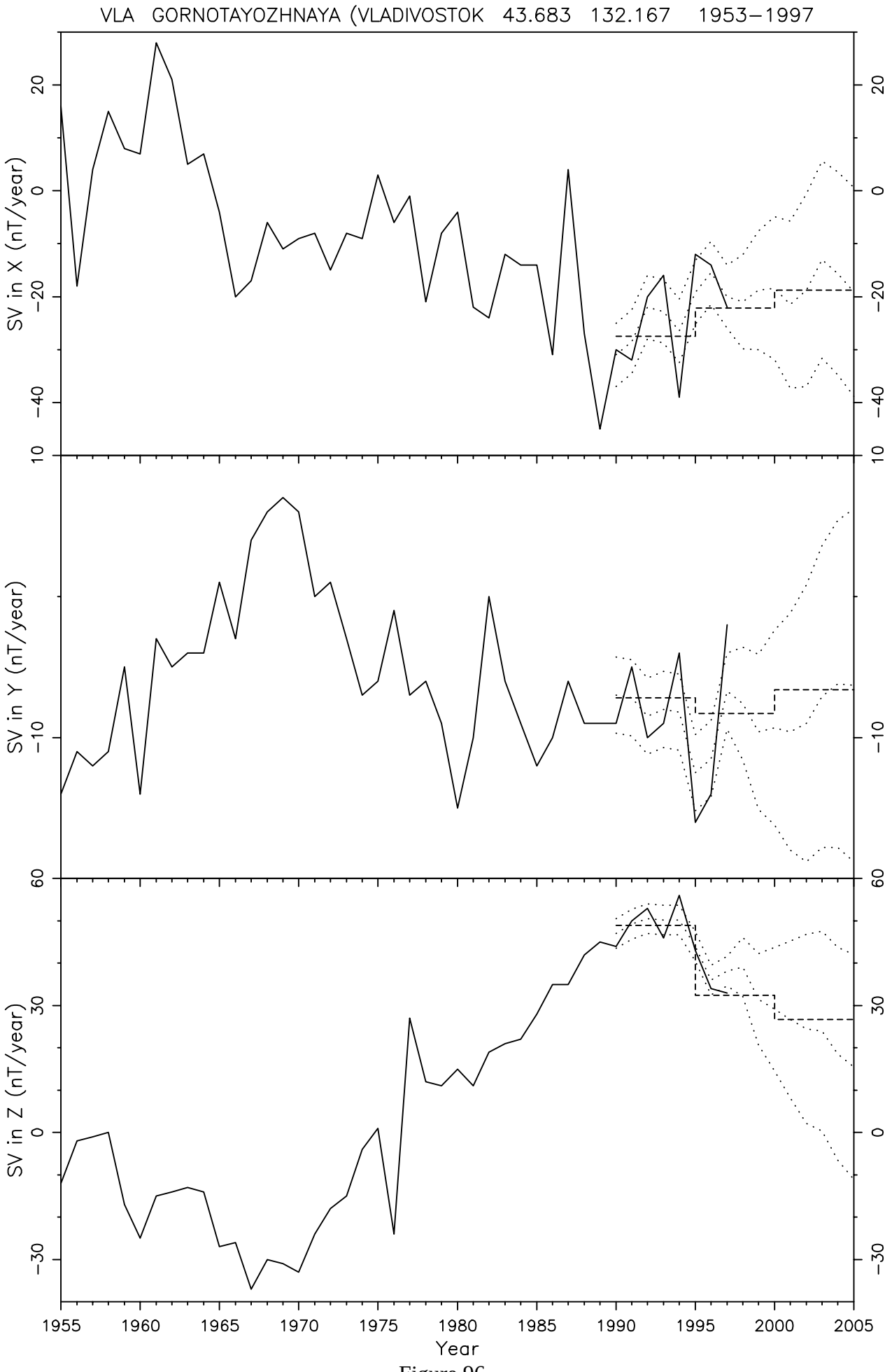
VLA GORNOTAYOZHNAYA (VLADIVOSTOK 43.683 132.167 1953–1997
SV in X (nT/year)
SV in Y (nT/year)
SV in Z (nT/year)
Year
1955
1960
1965
1970
1975
1980
1985
1990
1995
2000
2005

Figure 96

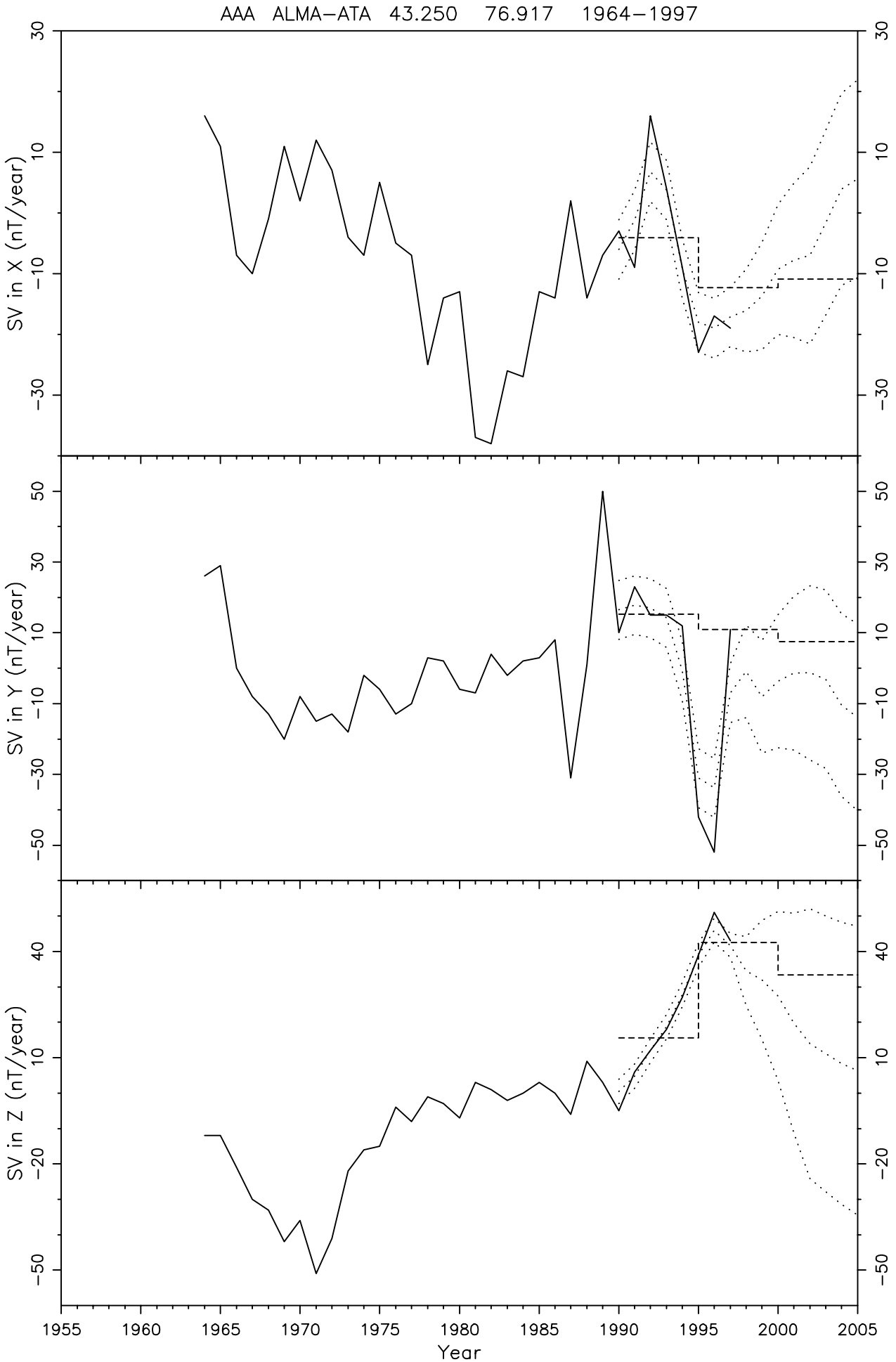
AAA ALMA−ATA 43.250 76.917 1964−1997
SV in X (nT/year)
SV in Y (nT/year)
SV in Z (nT/year)
Year
1955
1960
1965
1970
1975
1980
1985
1990
1995
2000
2005

Figure 97

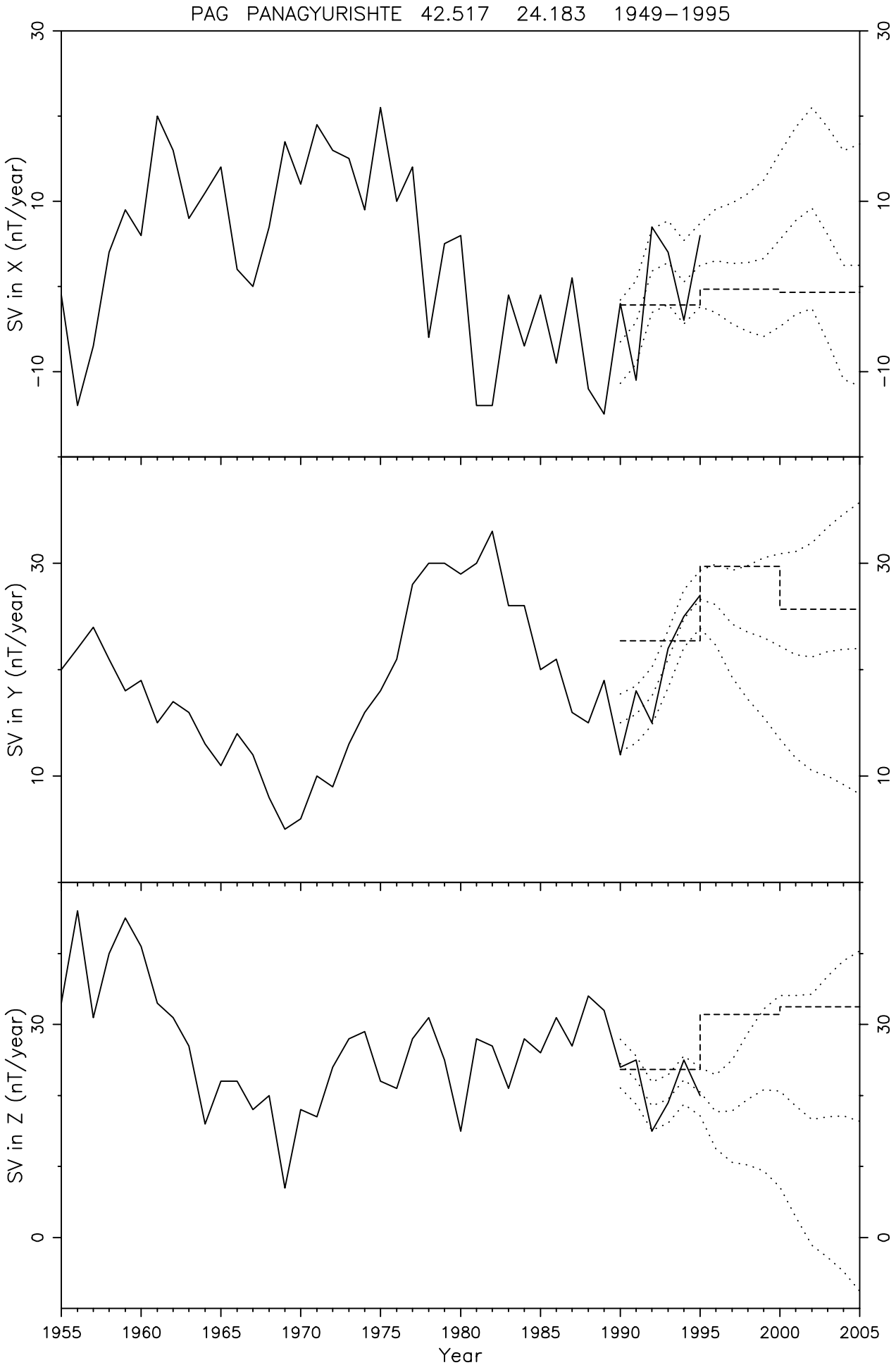
PAG PANAGYURISHTE 42.517 24.183 1949–1995
SV in X (nT/year)
SV in Y (nT/year)
SV in Z (nT/year)
30
10
−10
0
1955
1960
1965
1970
1975
1980
1985
1990
1995
2000
2005
Year

Figure 98

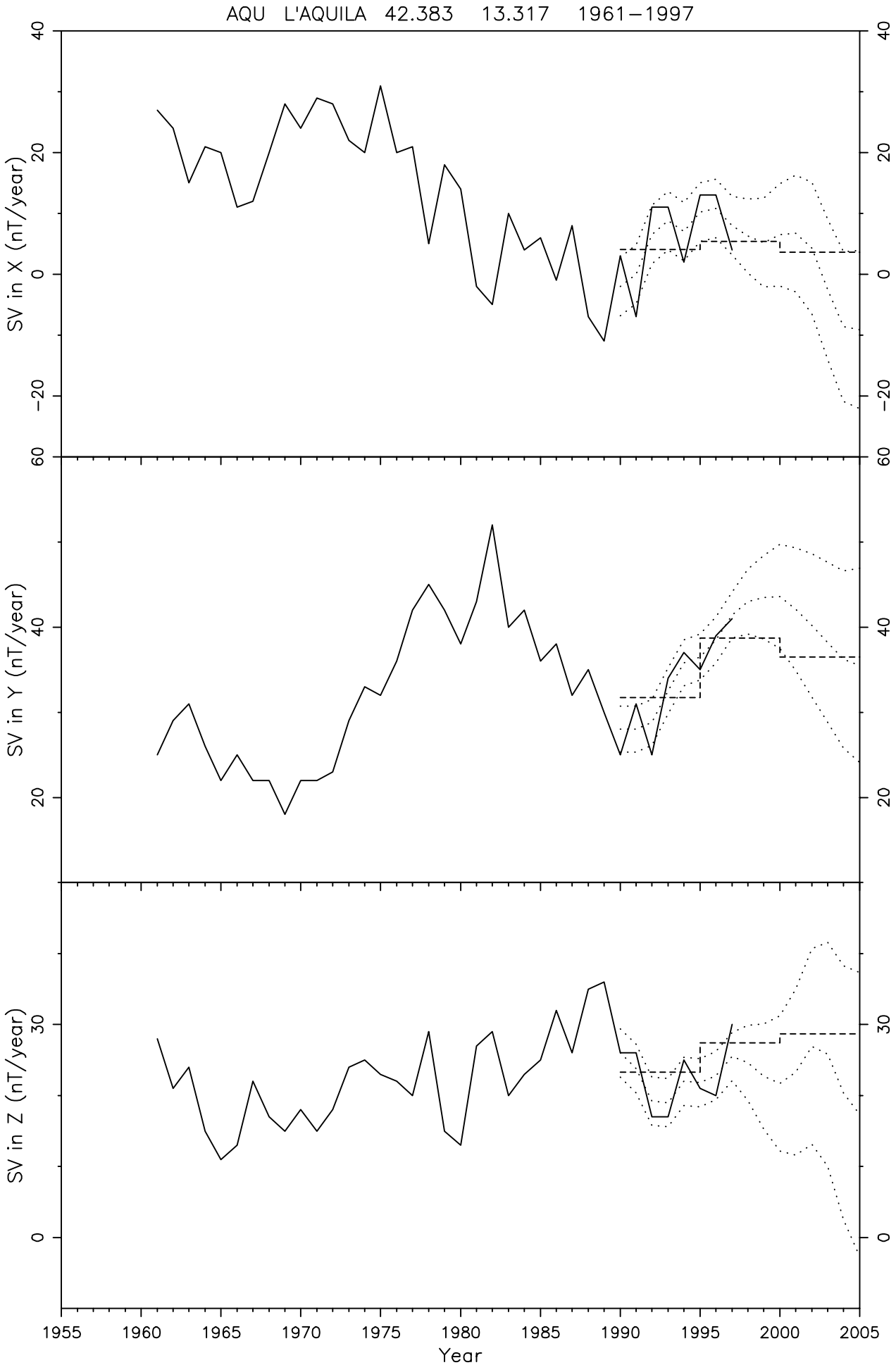
AQU L'AQUILA 42.383 13.317 1961−1997
SV in X (nT/year)
SV in Y (nT/year)
SV in Z (nT/year)
Year
1955
1960
1965
1970
1975
1980
1985
1990
1995
2000
2005

Figure 99

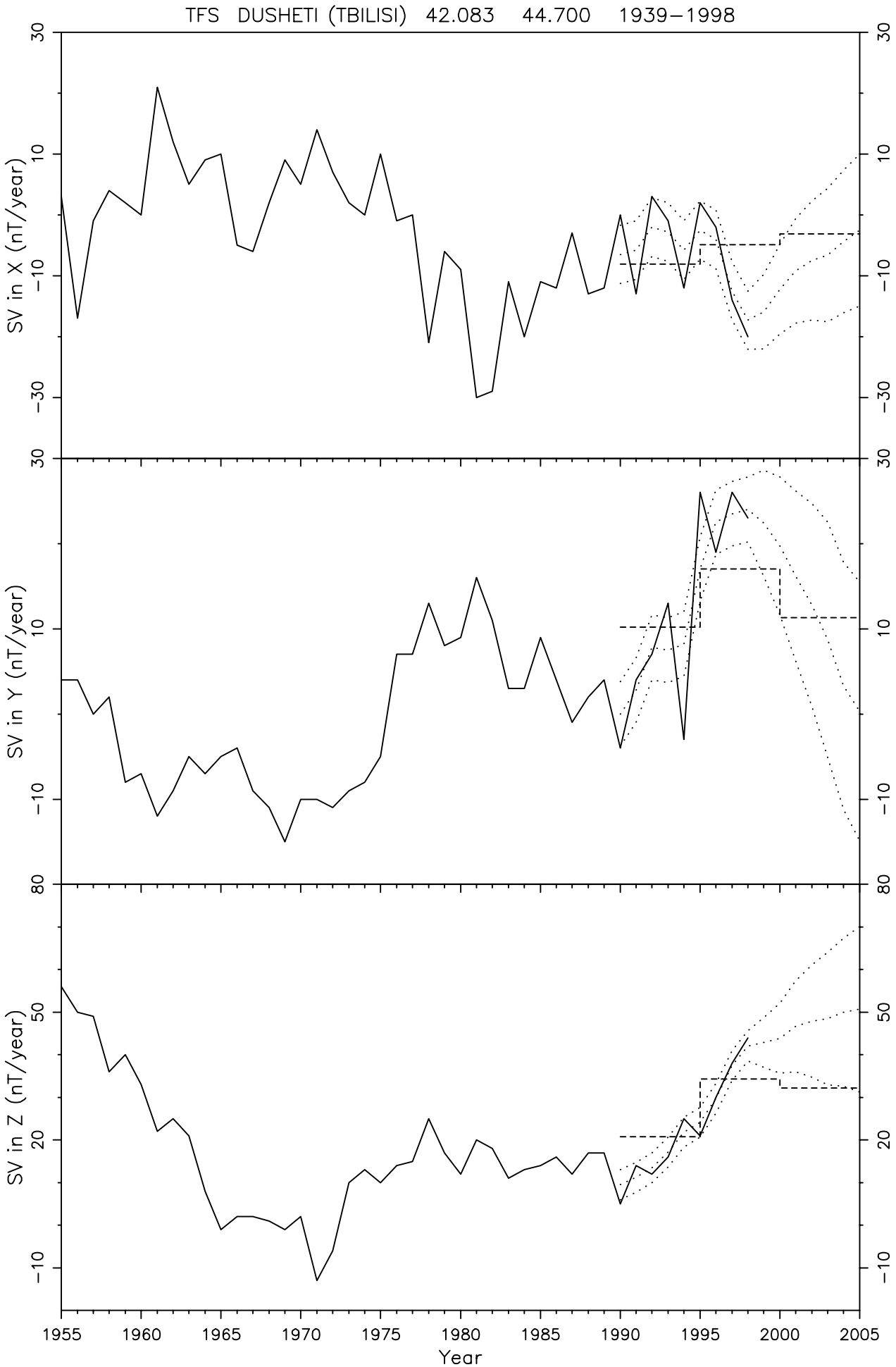
TFS DUSHETI (TBILISI) 42.083 44.700 1939–1998
SV in X (nT/year)
SV in Y (nT/year)
SV in Z (nT/year)
30
10
−10
−30
80
50
20
1955
1960
1965
1970
1975
1980
1985
1990
1995
2000
2005
Year

Figure 100

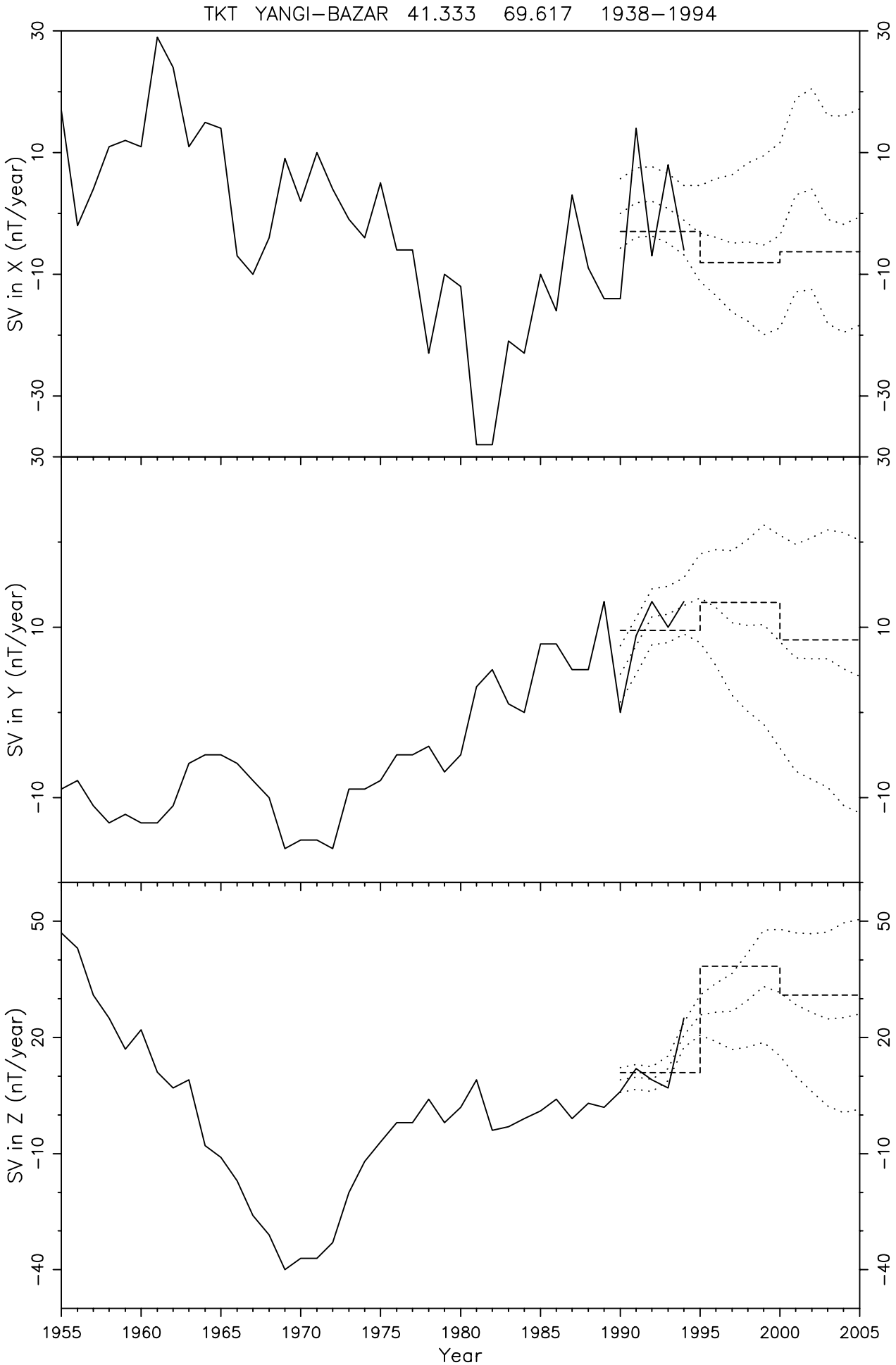
TKT YANGI−BAZAR 41.333 69.617 1938−1994
SV in X (nT/year)
SV in Y (nT/year)
SV in Z (nT/year)
30
10
−10
−30
50
20
−40
1955
1960
1965
1970
1975
1980
1985
1990
1995
2000
2005
Year

Figure 101

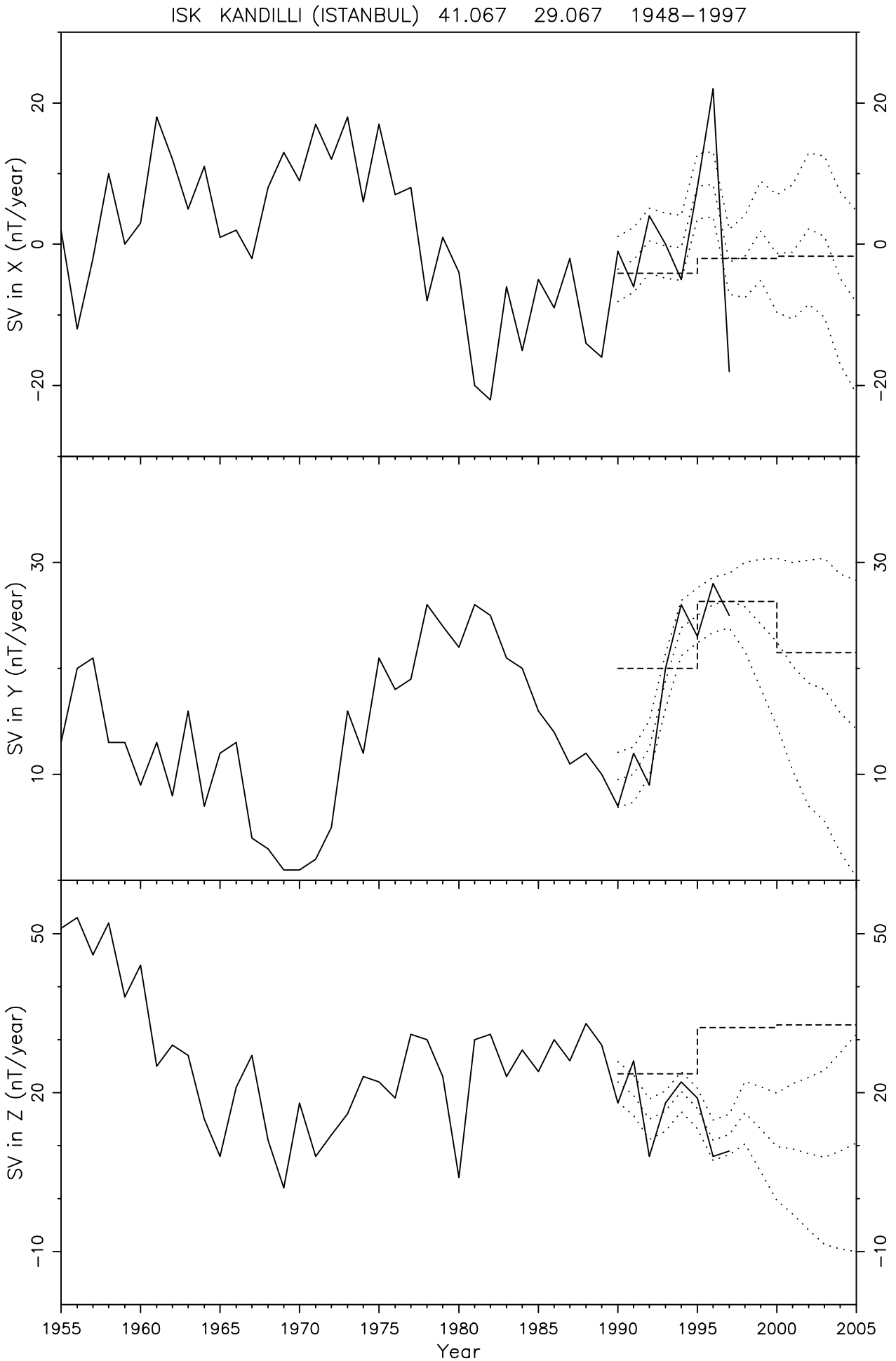
ISK KANDILLI (ISTANBUL) 41.067 29.067 1948–1997
SV in X (nT/year)
SV in Y (nT/year)
SV in Z (nT/year)
Year
1955
1960
1965
1970
1975
1980
1985
1990
1995
2000
2005

Figure 102

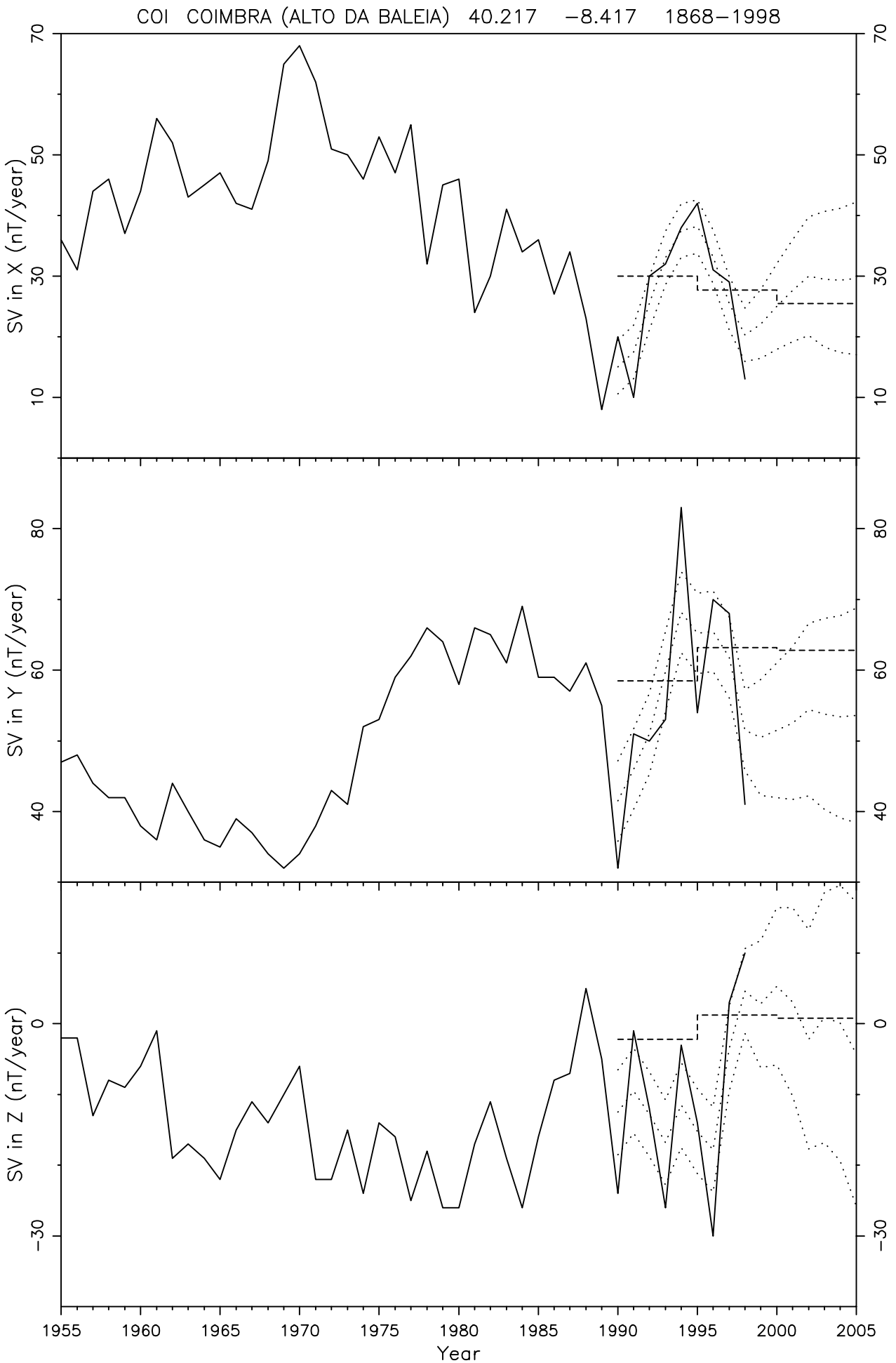
COI COIMBRA (ALTO DA BALEIA) 40.217 −8.417 1868−1998
SV in X (nT/year)
SV in Y (nT/year)
SV in Z (nT/year)
70
50
30
10
80
60
40
0
−30
1955
1960
1965
1970
1975
1980
1985
1990
1995
2000
2005
Year

Figure 103

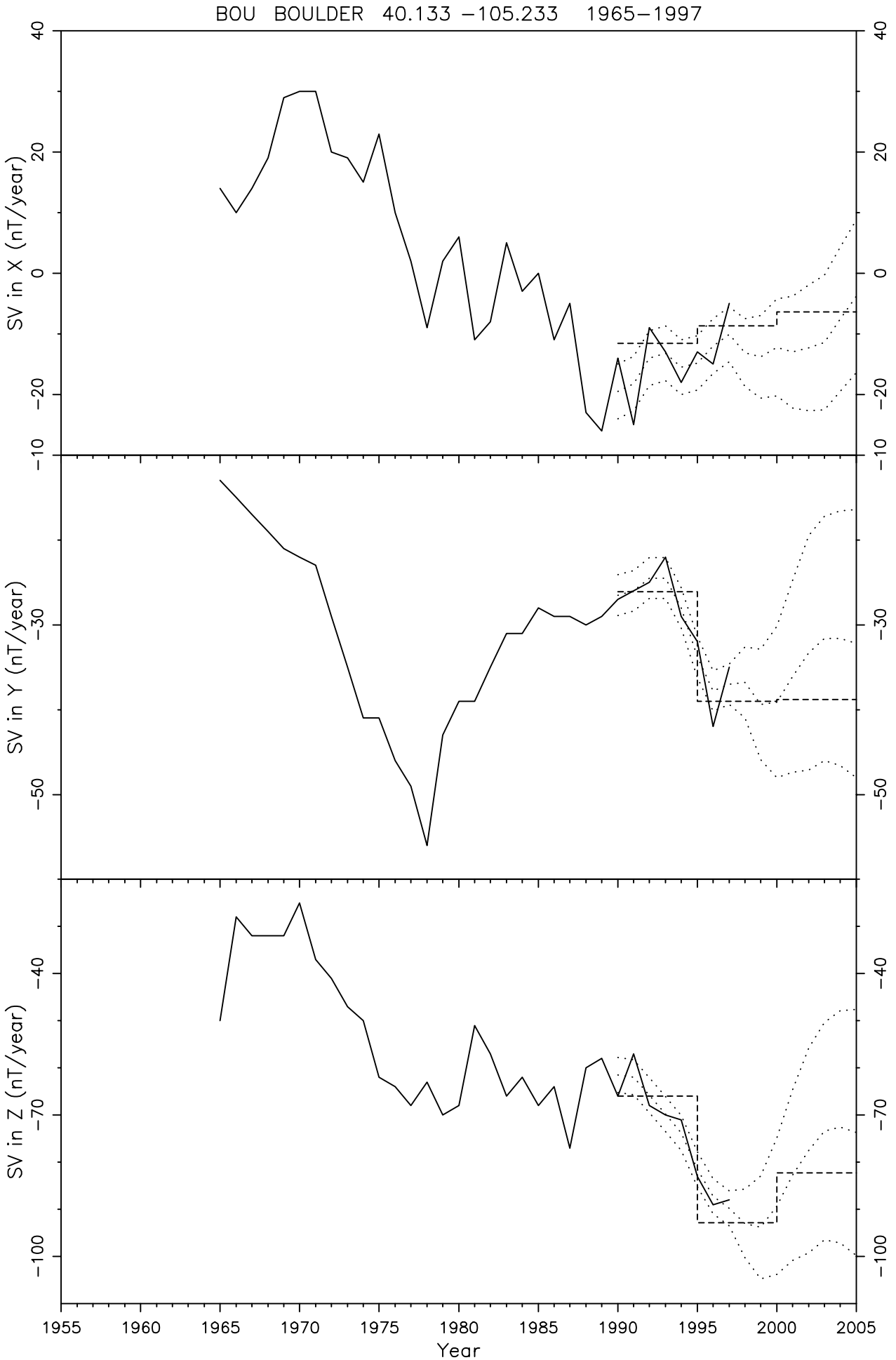
BOU BOULDER 40.133 −105.233 1965−1997
SV in X (nT/year)
SV in Y (nT/year)
SV in Z (nT/year)
40
20
0
−20
−10
−30
−50
−40
−70
−100
1955
1960
1965
1970
1975
1980
1985
1990
1995
2000
2005
Year

Figure 104

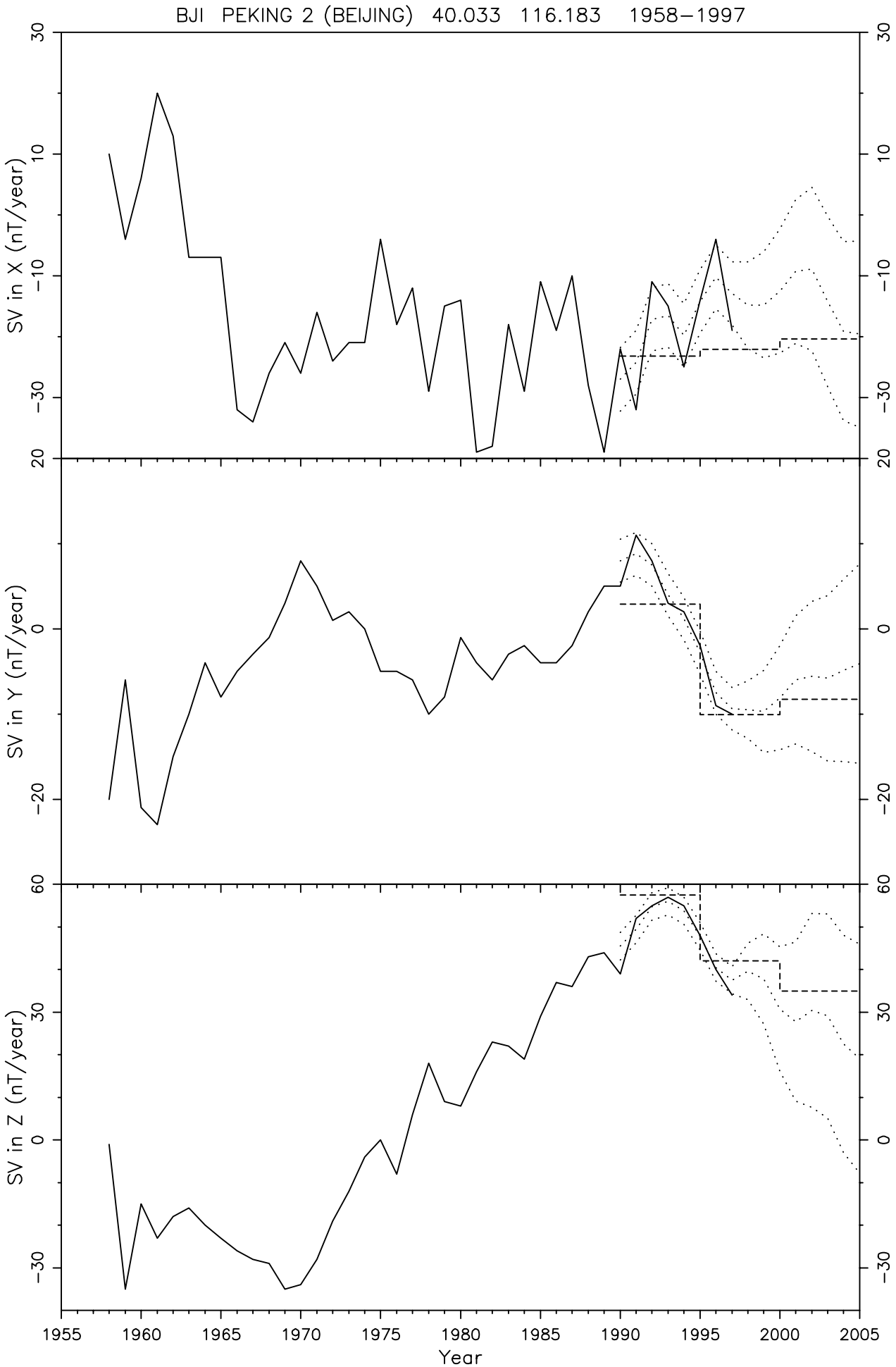
BJI PEKING 2 (BEIJING) 40.033 116.183 1958–1997
SV in X (nT/year)
SV in Y (nT/year)
SV in Z (nT/year)
30
10
−10
−30
20
0
−20
60
1955
1960
1965
1970
1975
1980
1985
1990
1995
2000
2005
Year

Figure 105

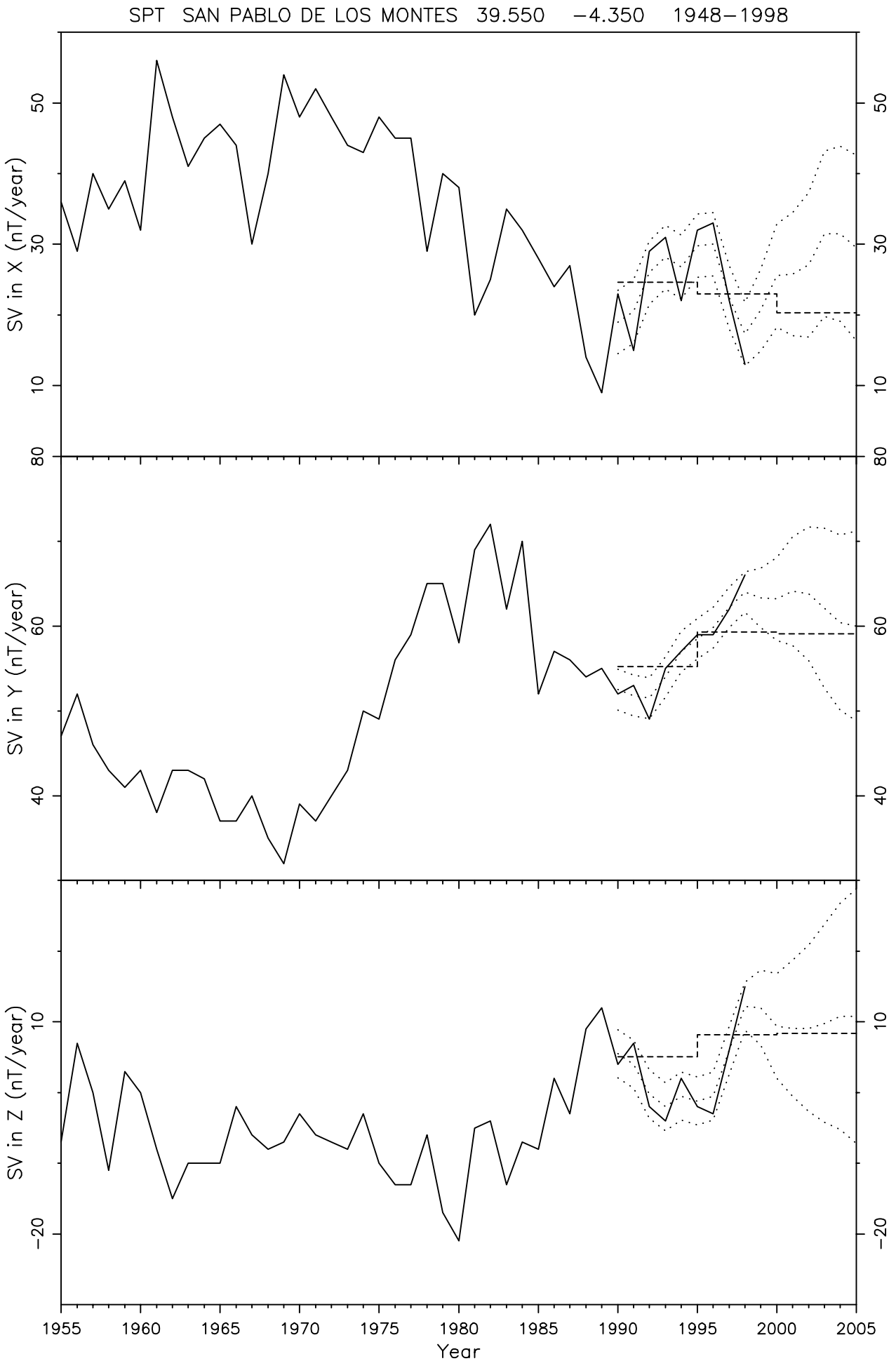
SPT SAN PABLO DE LOS MONTES 39.550 −4.350 1948−1998
SV in X (nT/year)
SV in Y (nT/year)
SV in Z (nT/year)
Year
1955
1960
1965
1970
1975
1980
1985
1990
1995
2000
2005

Figure 106

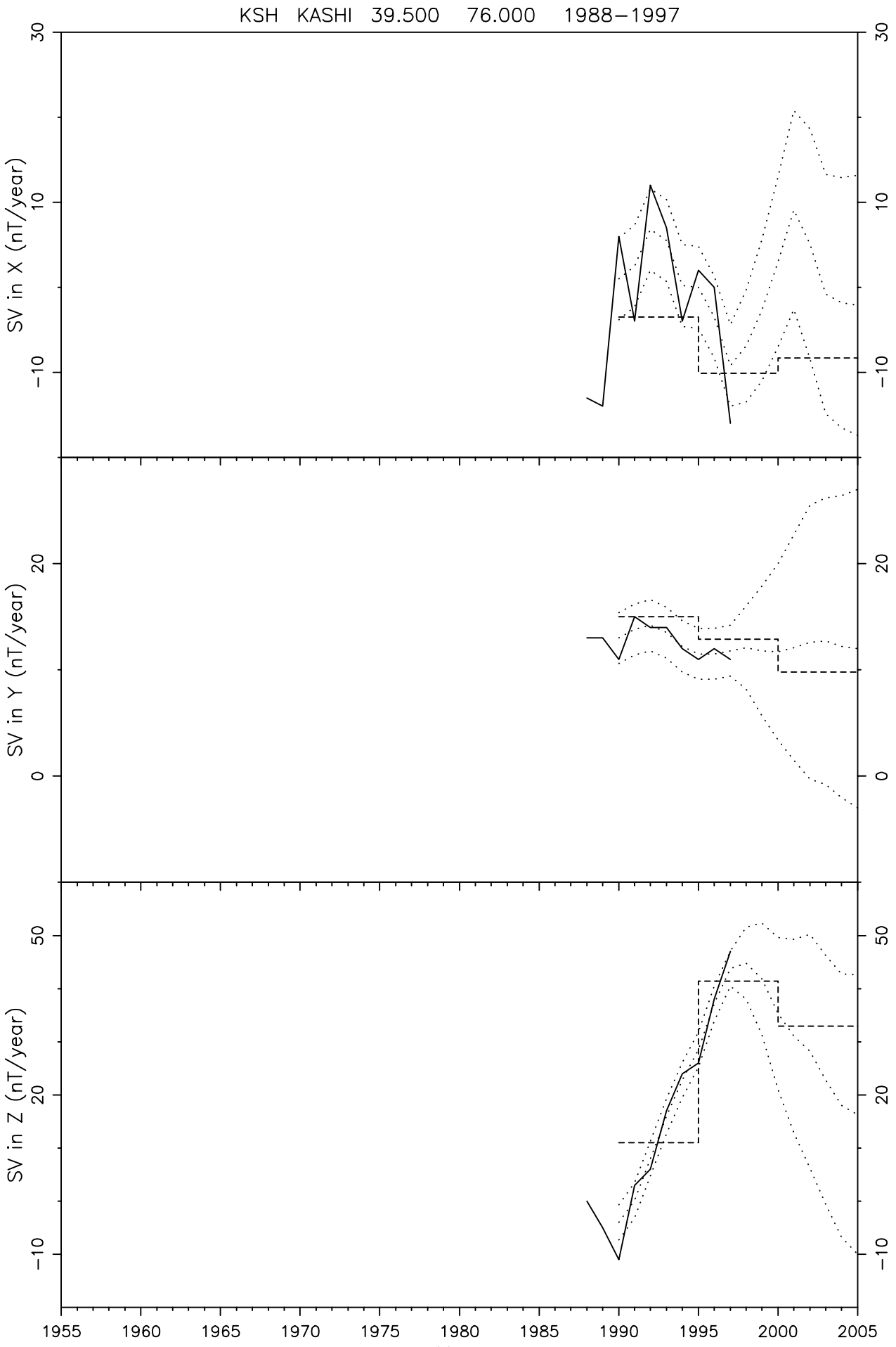
KSH KASHI 39.500 76.000 1988–1997
SV in X (nT/year)
SV in Y (nT/year)
SV in Z (nT/year)
30
10
−10
20
0
50
1955
1960
1965
1970
1975
1980
1985
1990
1995
2000
2005
Year

Figure 107

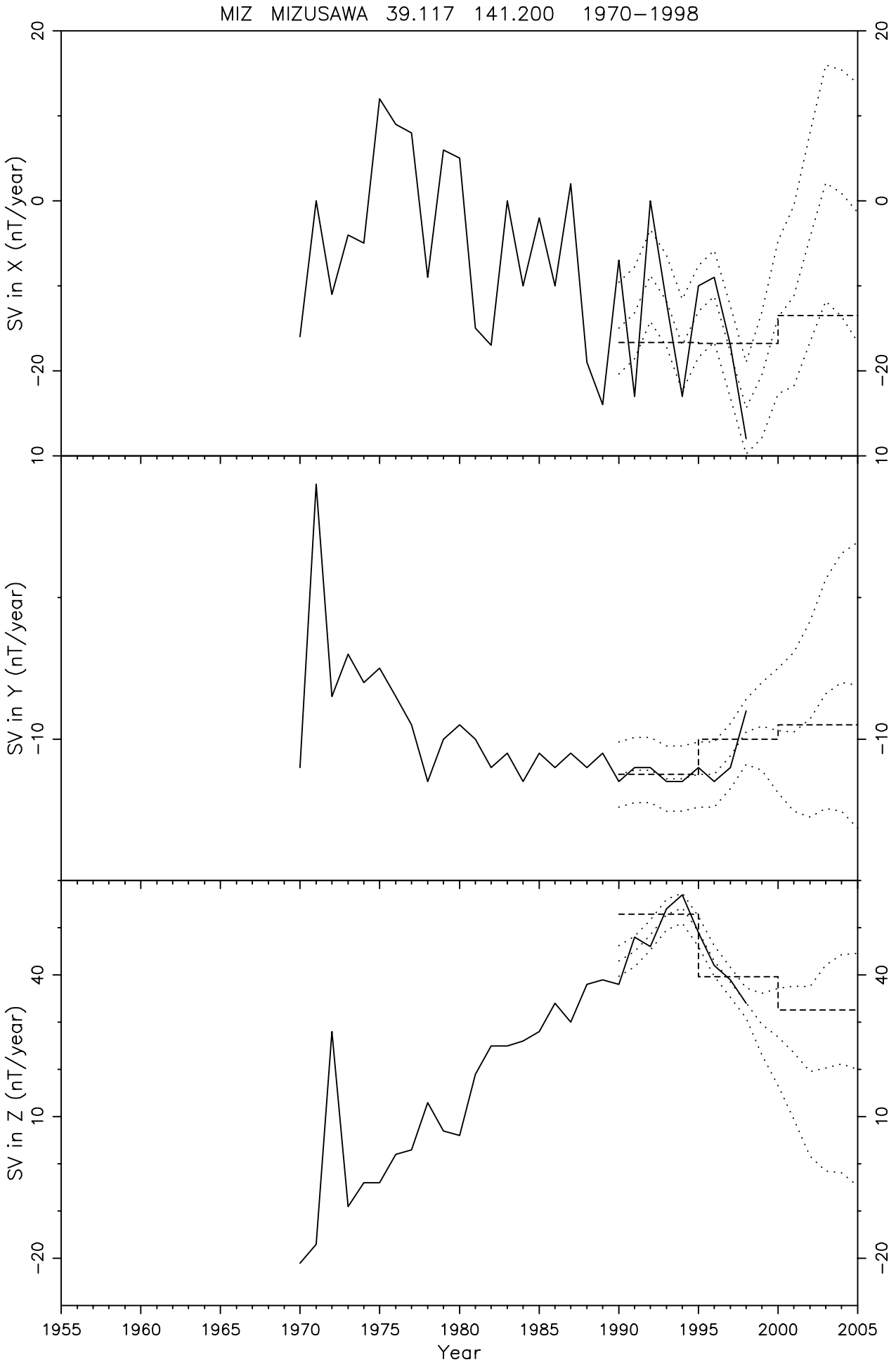
MIZ MIZUSAWA 39.117 141.200 1970–1998
SV in X (nT/year)
SV in Y (nT/year)
SV in Z (nT/year)
20
0
−20
10
−10
40
1955
1960
1965
1970
1975
1980
1985
1990
1995
2000
2005
Year

Figure 108

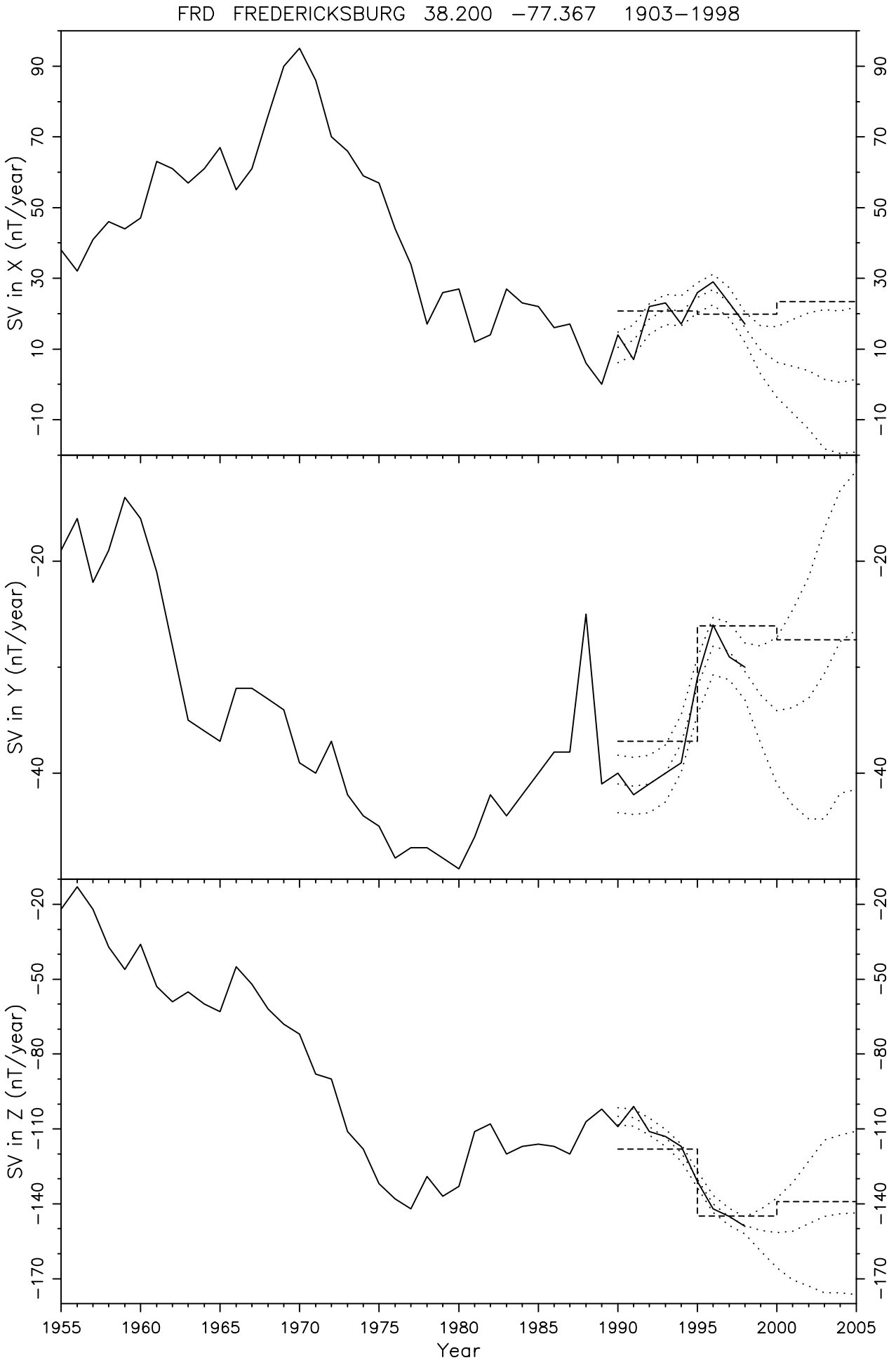
FRD FREDERICKSBURG 38.200 −77.367 1903−1998
SV in X (nT/year)
SV in Y (nT/year)
SV in Z (nT/year)
Year
1955
1960
1965
1970
1975
1980
1985
1990
1995
2000
2005

Figure 109

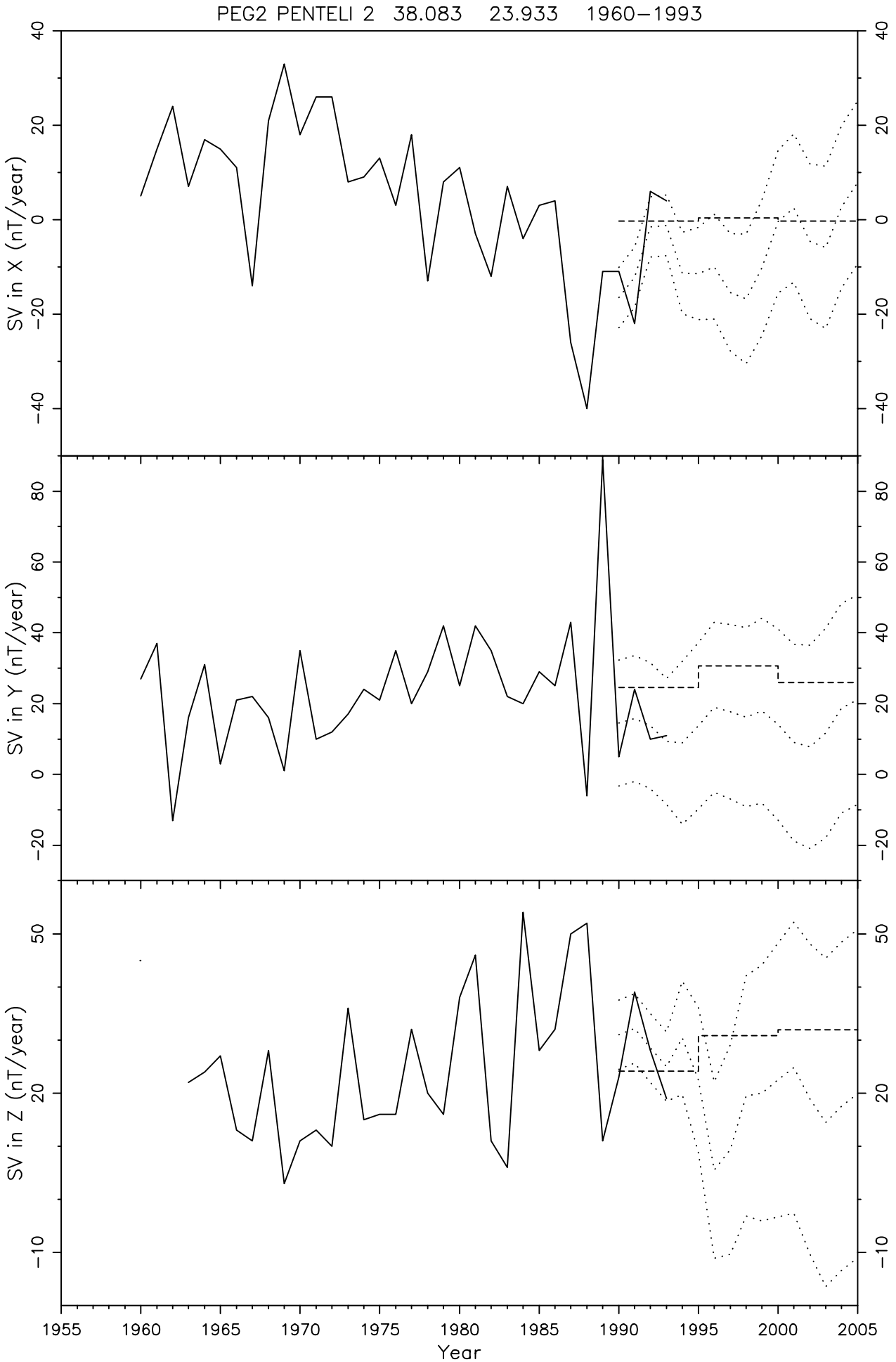
PEG2 PENTELI 2 38.083 23.933 1960−1993
SV in X (nT/year)
SV in Y (nT/year)
SV in Z (nT/year)
Year
1955
1960
1965
1970
1975
1980
1985
1990
1995
2000
2005

Figure 110

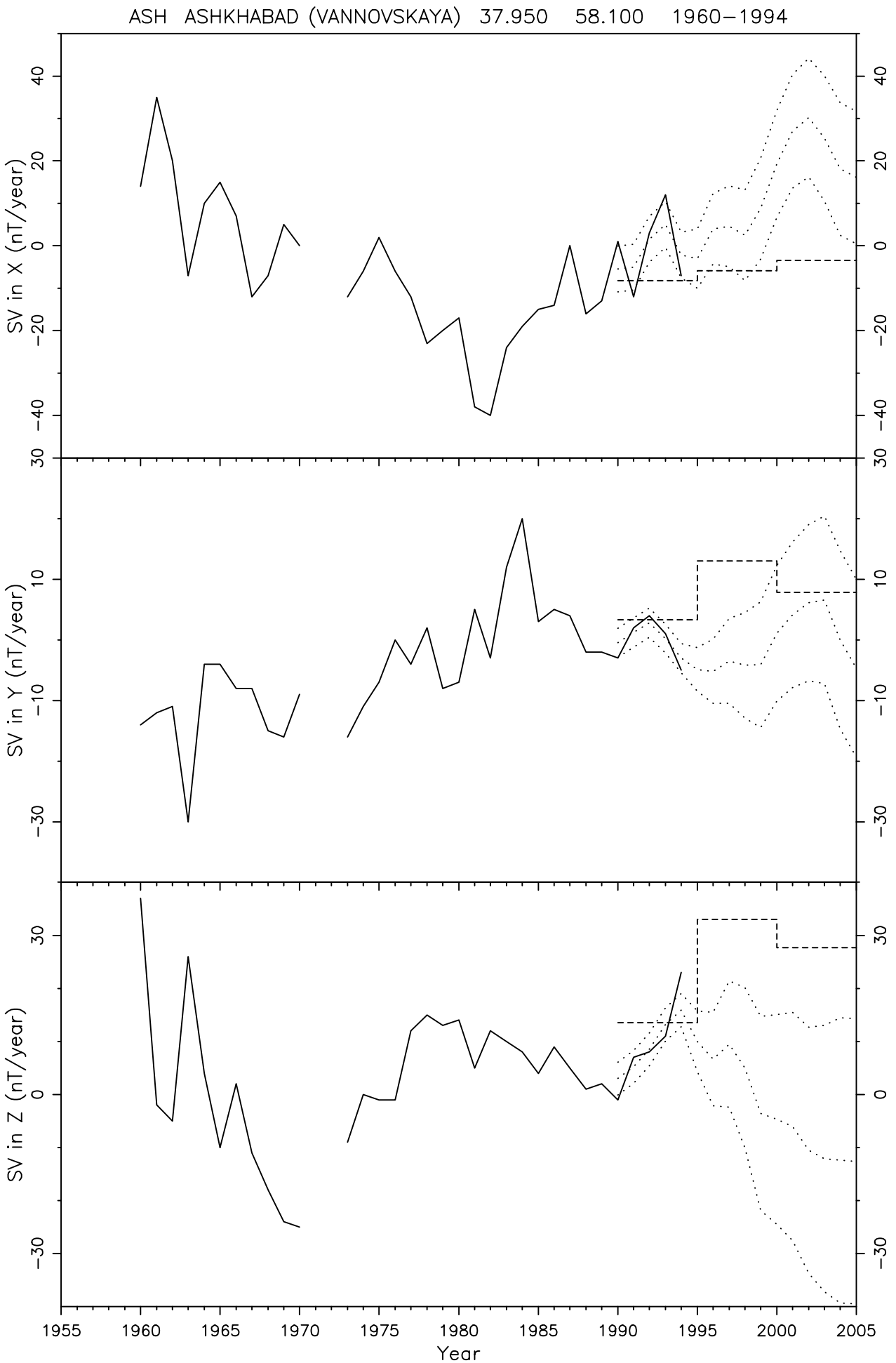
ASH ASHKHABAD (VANNOVSKAYA) 37.950 58.100 1960–1994
SV in X (nT/year)
SV in Y (nT/year)
SV in Z (nT/year)
Year
1955
1960
1965
1970
1975
1980
1985
1990
1995
2000
2005

Figure 111

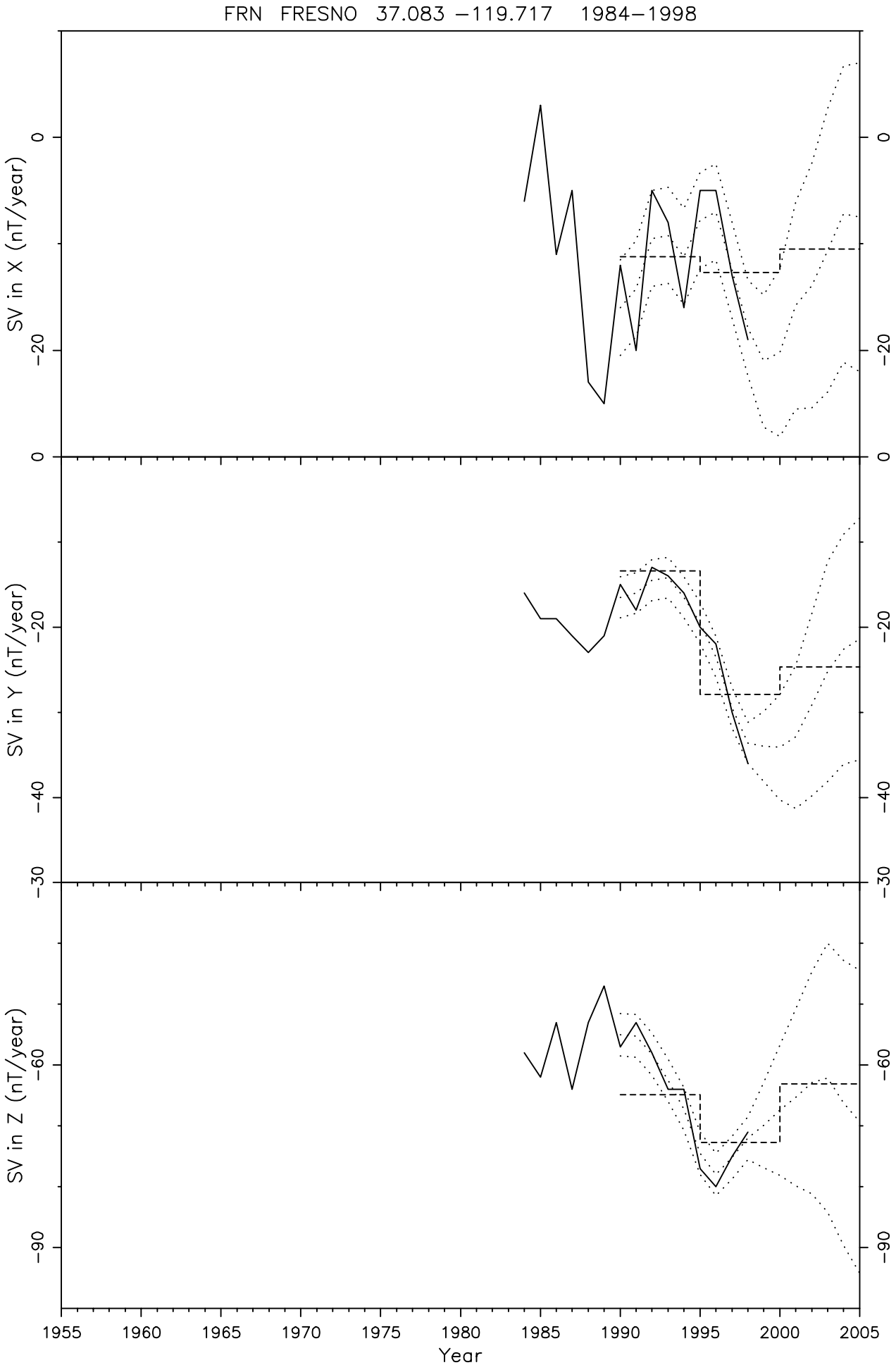
FRN FRESNO 37.083 −119.717 1984−1998
SV in X (nT/year)
SV in Y (nT/year)
SV in Z (nT/year)
0
−20
−40
−30
−60
−90
1955
1960
1965
1970
1975
1980
1985
1990
1995
2000
2005
Year

Figure 112

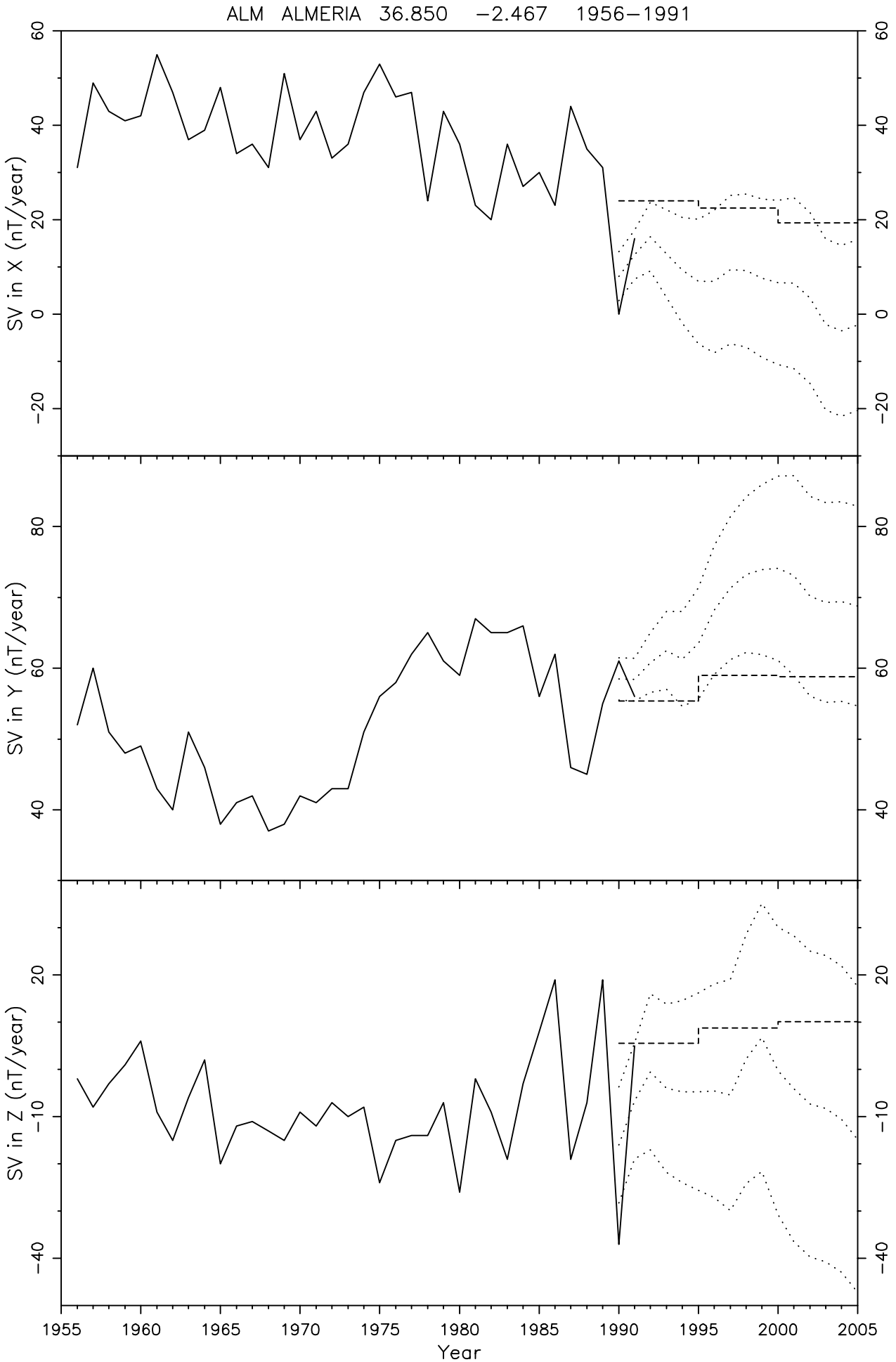
ALM ALMERIA 36.850 −2.467 1956−1991
SV in X (nT/year)
SV in Y (nT/year)
SV in Z (nT/year)
Year
1955
1960
1965
1970
1975
1980
1985
1990
1995
2000
2005

Figure 113

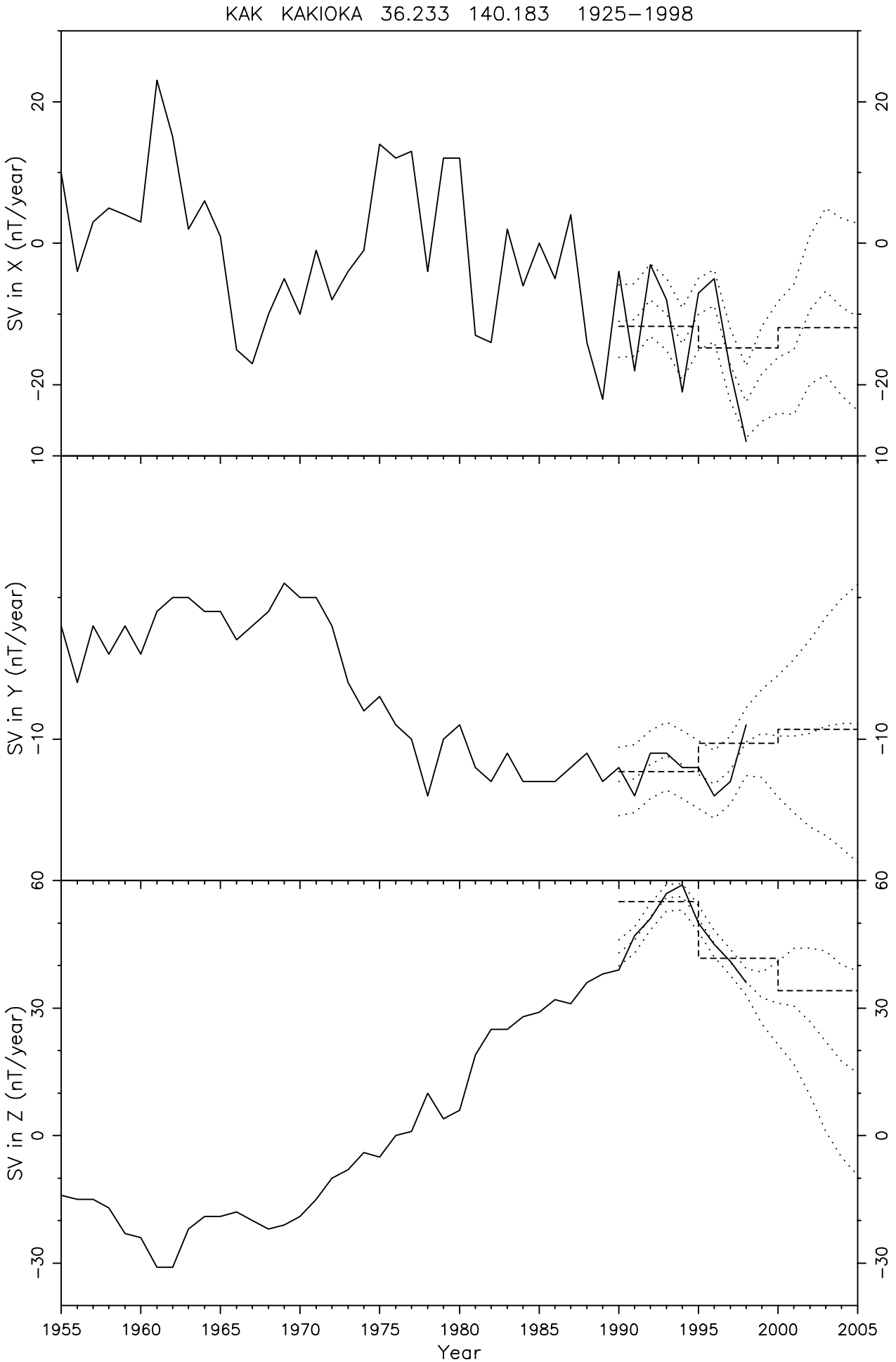
KAK KAKIOKA 36.233 140.183 1925–1998
SV in X (nT/year)
SV in Y (nT/year)
SV in Z (nT/year)
20
0
−20
10
−10
60
30
−30
1955
1960
1965
1970
1975
1980
1985
1990
1995
2000
2005
Year

Figure 114

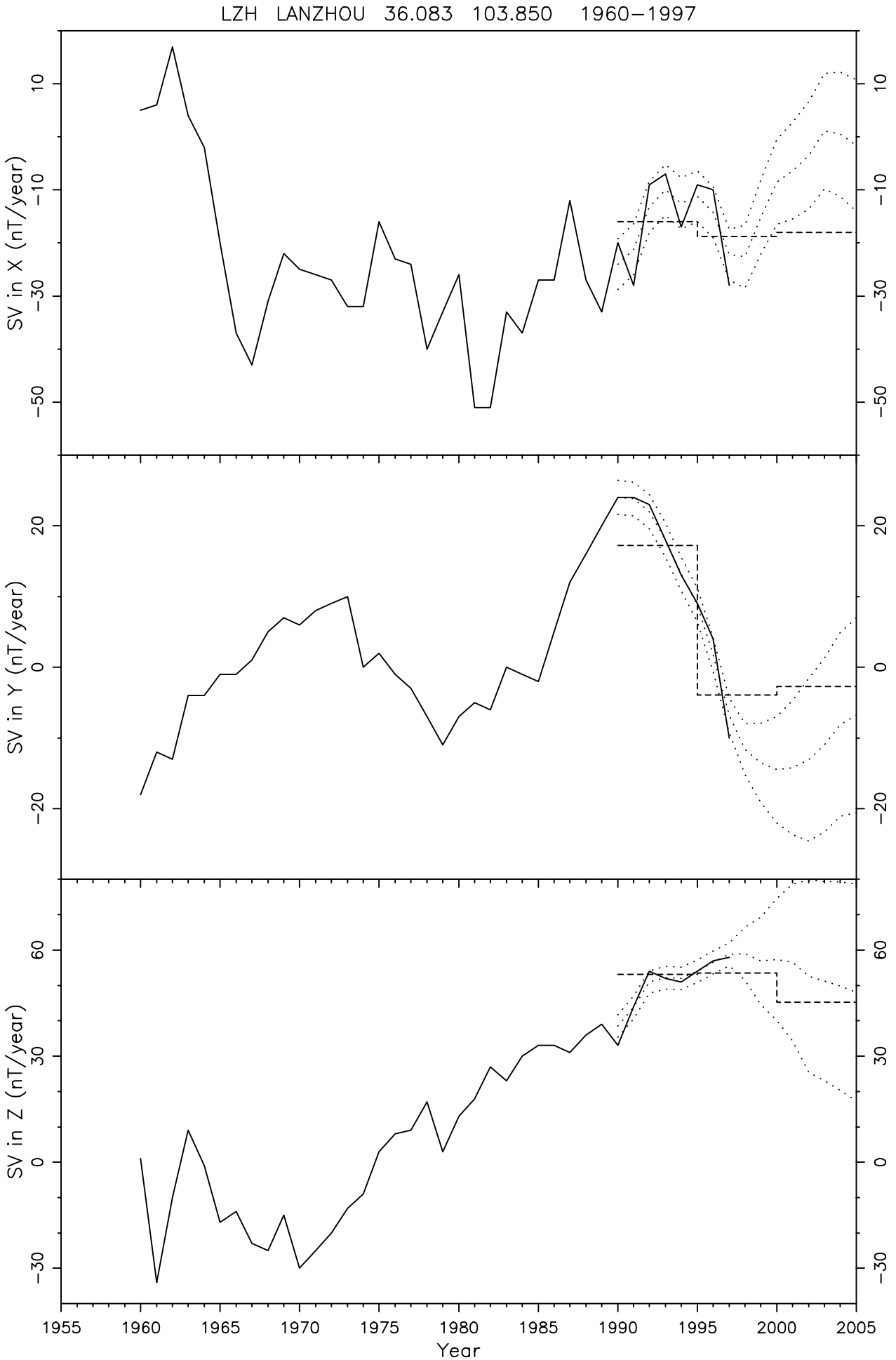
LZH LANZHOU 36.083 103.850 1960–1997
SV in X (nT/year)
SV in Y (nT/year)
SV in Z (nT/year)
Year
1955
1960
1965
1970
1975
1980
1985
1990
1995
2000
2005

Figure 115

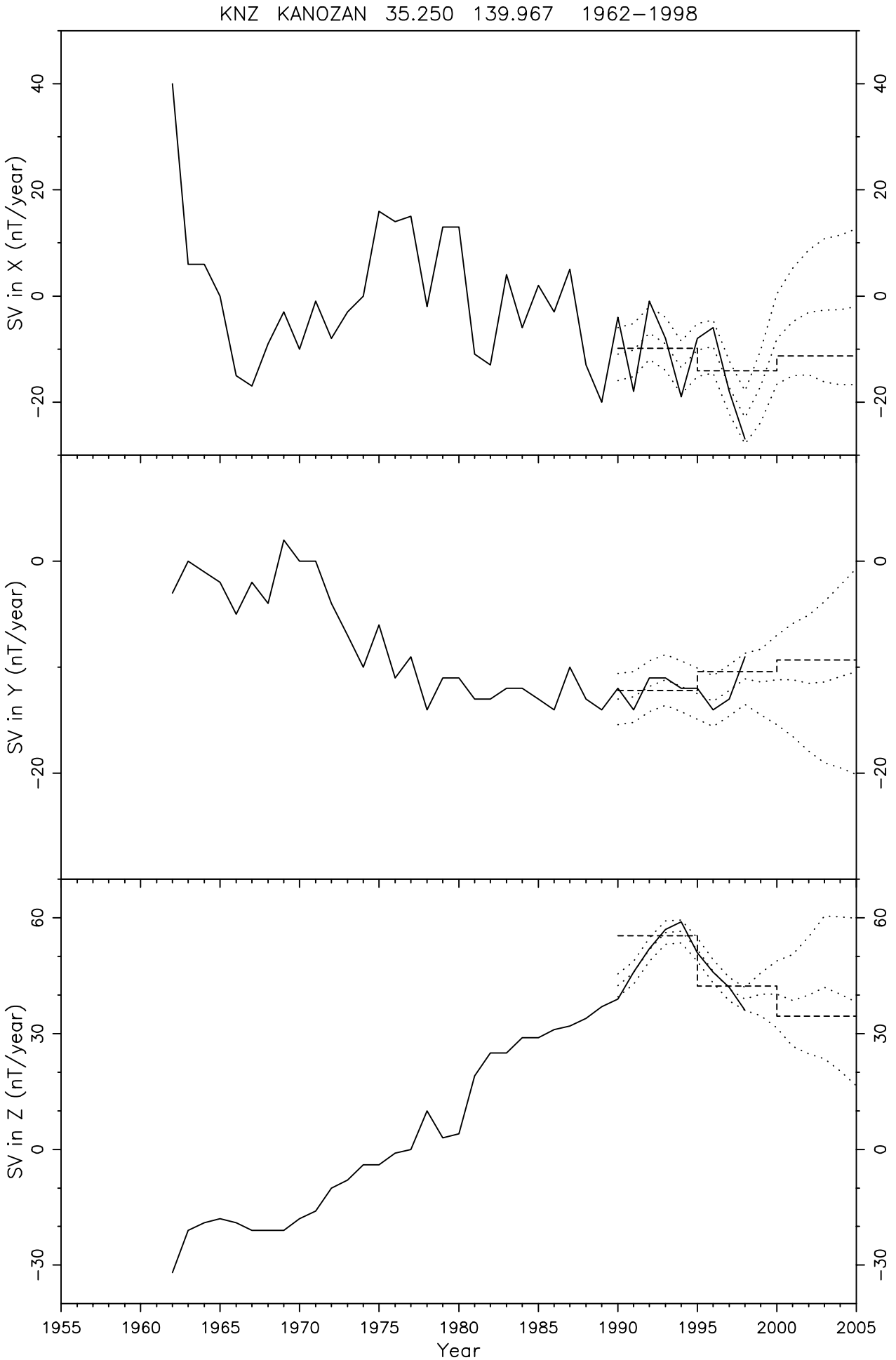
KNZ KANOZAN 35.250 139.967 1962–1998
SV in X (nT/year)
SV in Y (nT/year)
SV in Z (nT/year)
Year
1955
1960
1965
1970
1975
1980
1985
1990
1995
2000
2005

Figure 116

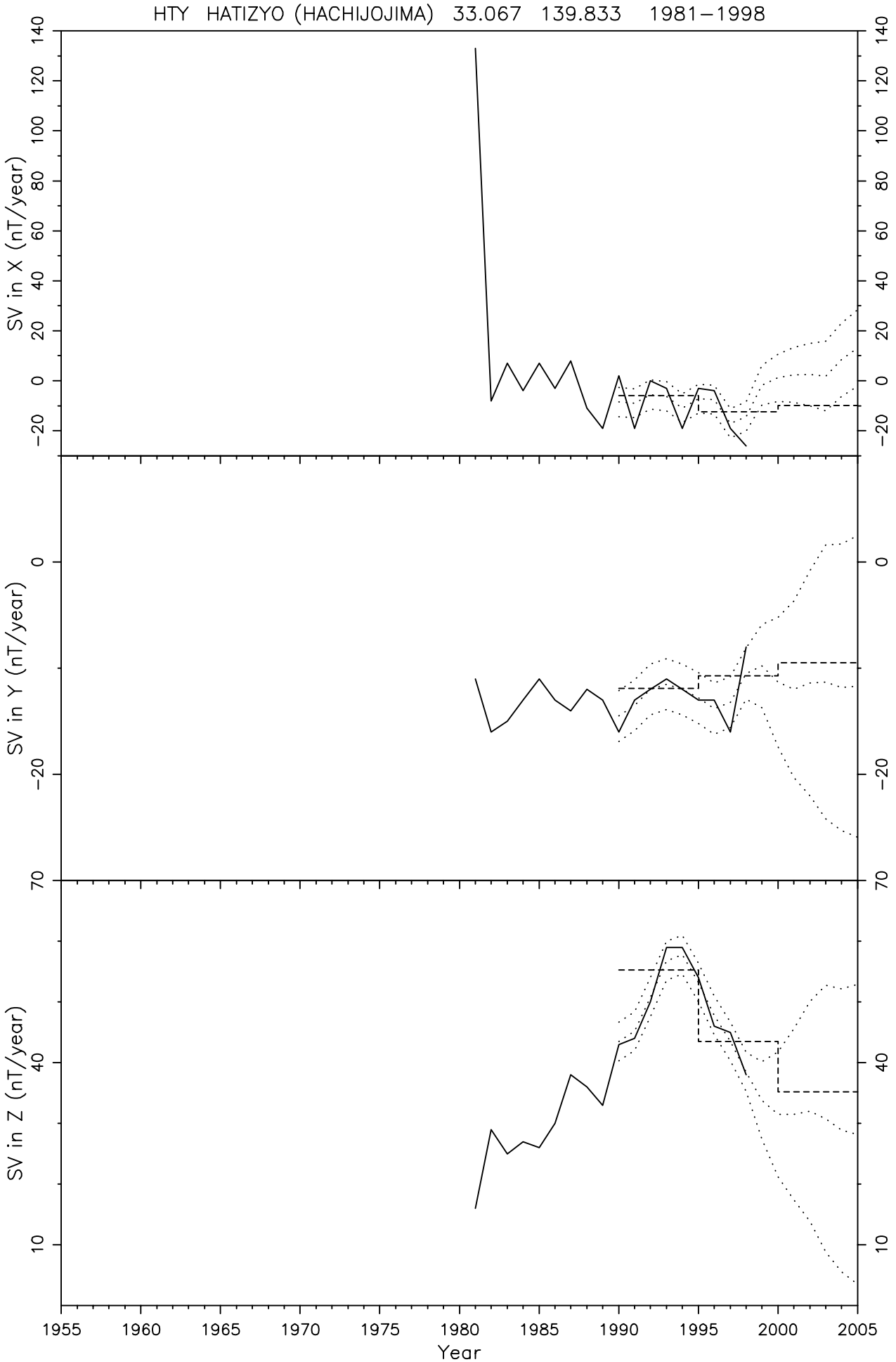
HTY HATIZYO (HACHIJOJIMA) 33.067 139.833 1981–1998
SV in X (nT/year)
SV in Y (nT/year)
SV in Z (nT/year)
Year
1955
1960
1965
1970
1975
1980
1985
1990
1995
2000
2005

Figure 117

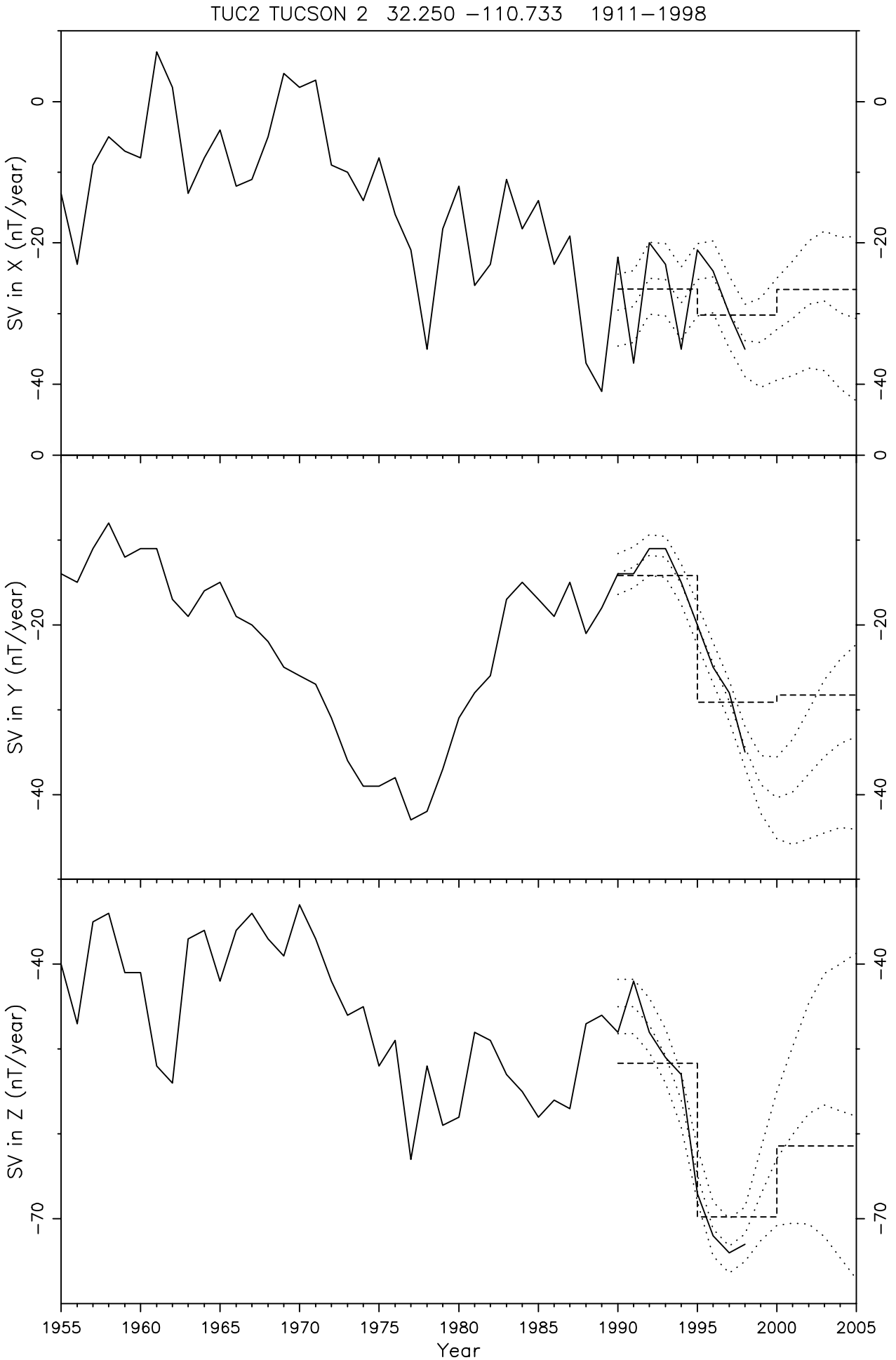
TUC2 TUCSON 2 32.250 −110.733 1911−1998
SV in X (nT/year)
SV in Y (nT/year)
SV in Z (nT/year)
0
−20
−40
−70
1955
1960
1965
1970
1975
1980
1985
1990
1995
2000
2005
Year

Figure 118

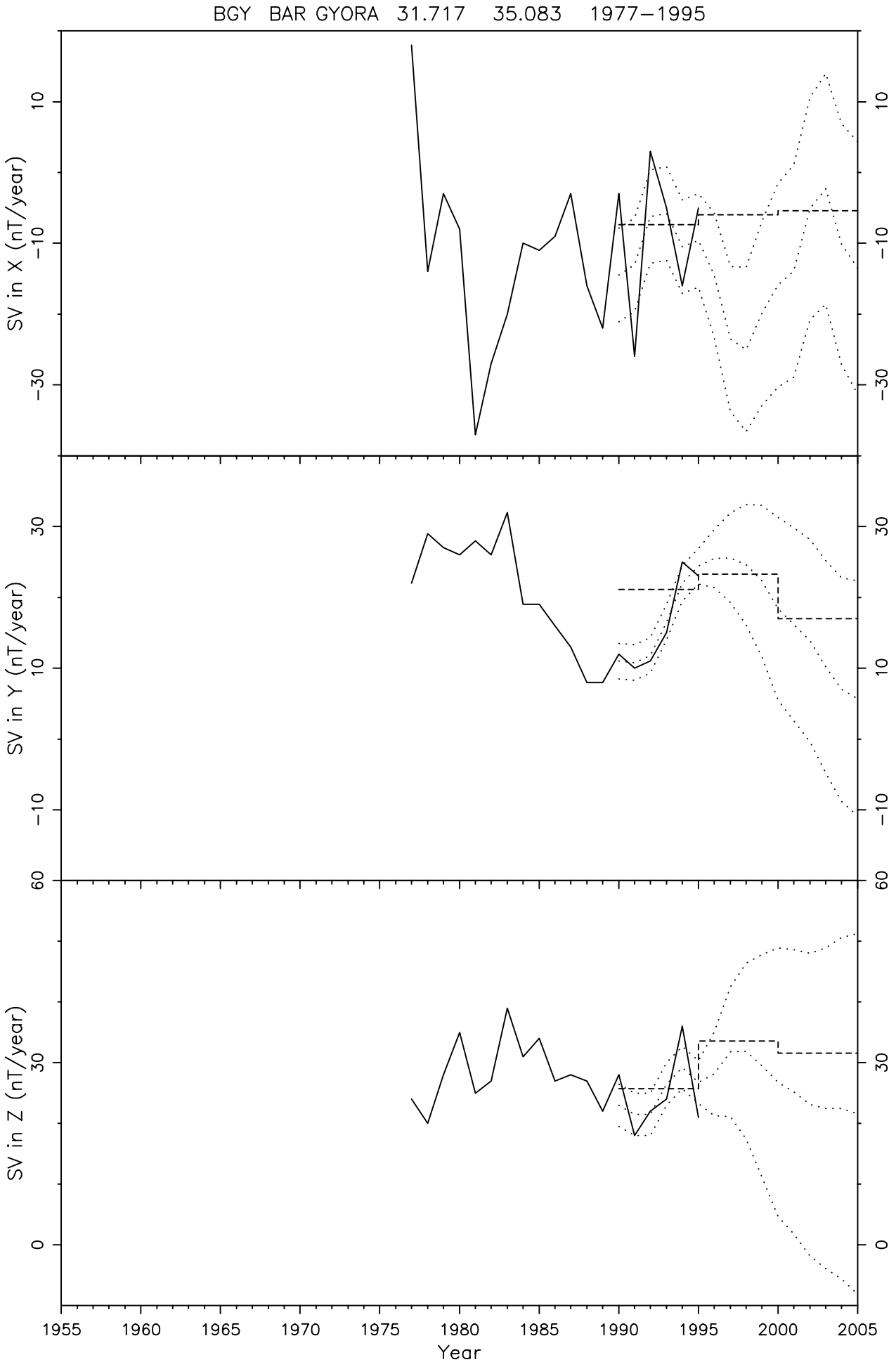
BGY BAR GYORA 31.717 35.083 1977–1995
SV in X (nT/year)
SV in Y (nT/year)
SV in Z (nT/year)
10
−10
−30
30
60
0
1955
1960
1965
1970
1975
1980
1985
1990
1995
2000
2005
Year

Figure 119

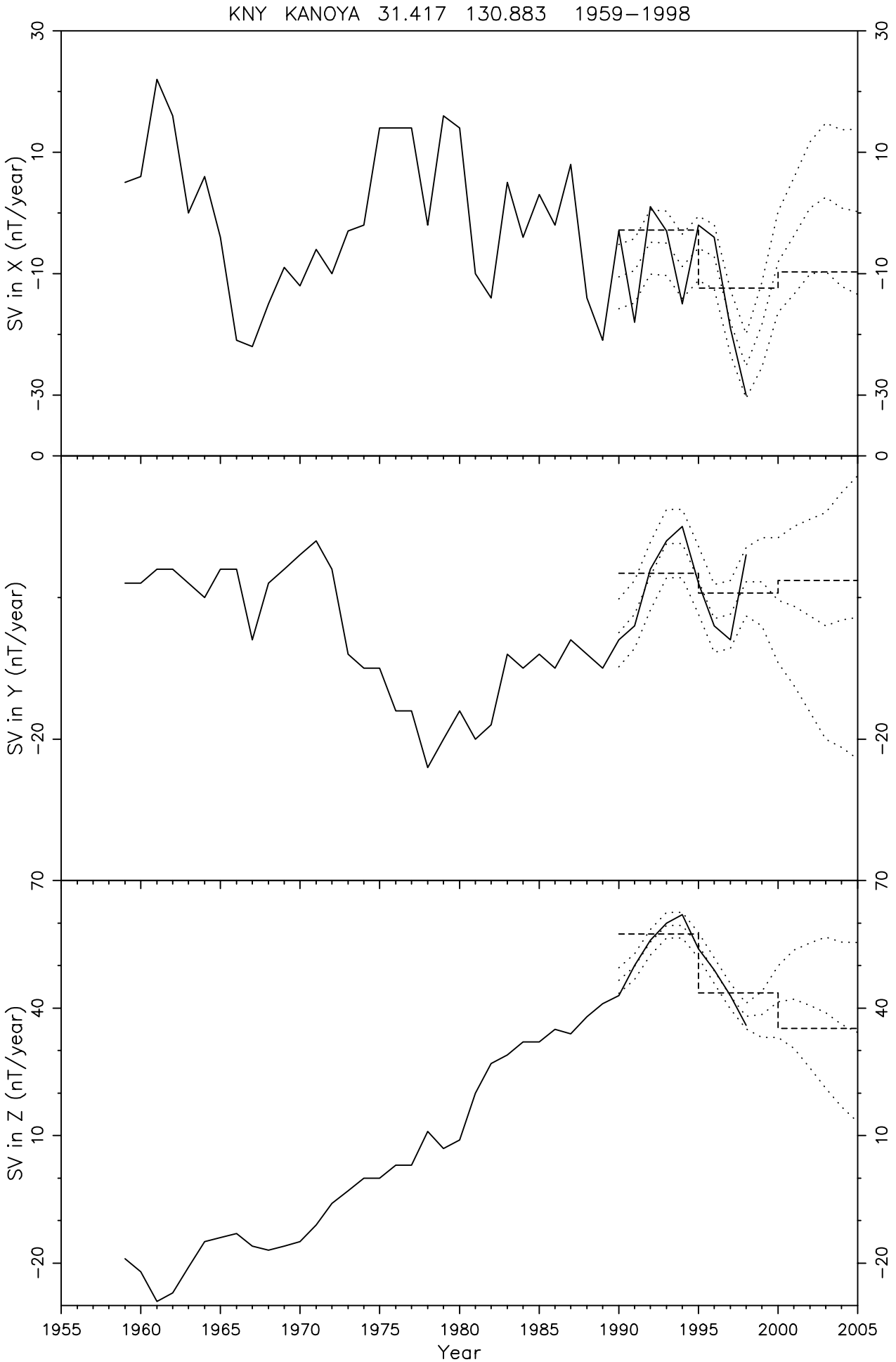
KNY KANOYA 31.417 130.883 1959−1998
SV in X (nT/year)
SV in Y (nT/year)
SV in Z (nT/year)
Year
1955
1960
1965
1970
1975
1980
1985
1990
1995
2000
2005

Figure 120

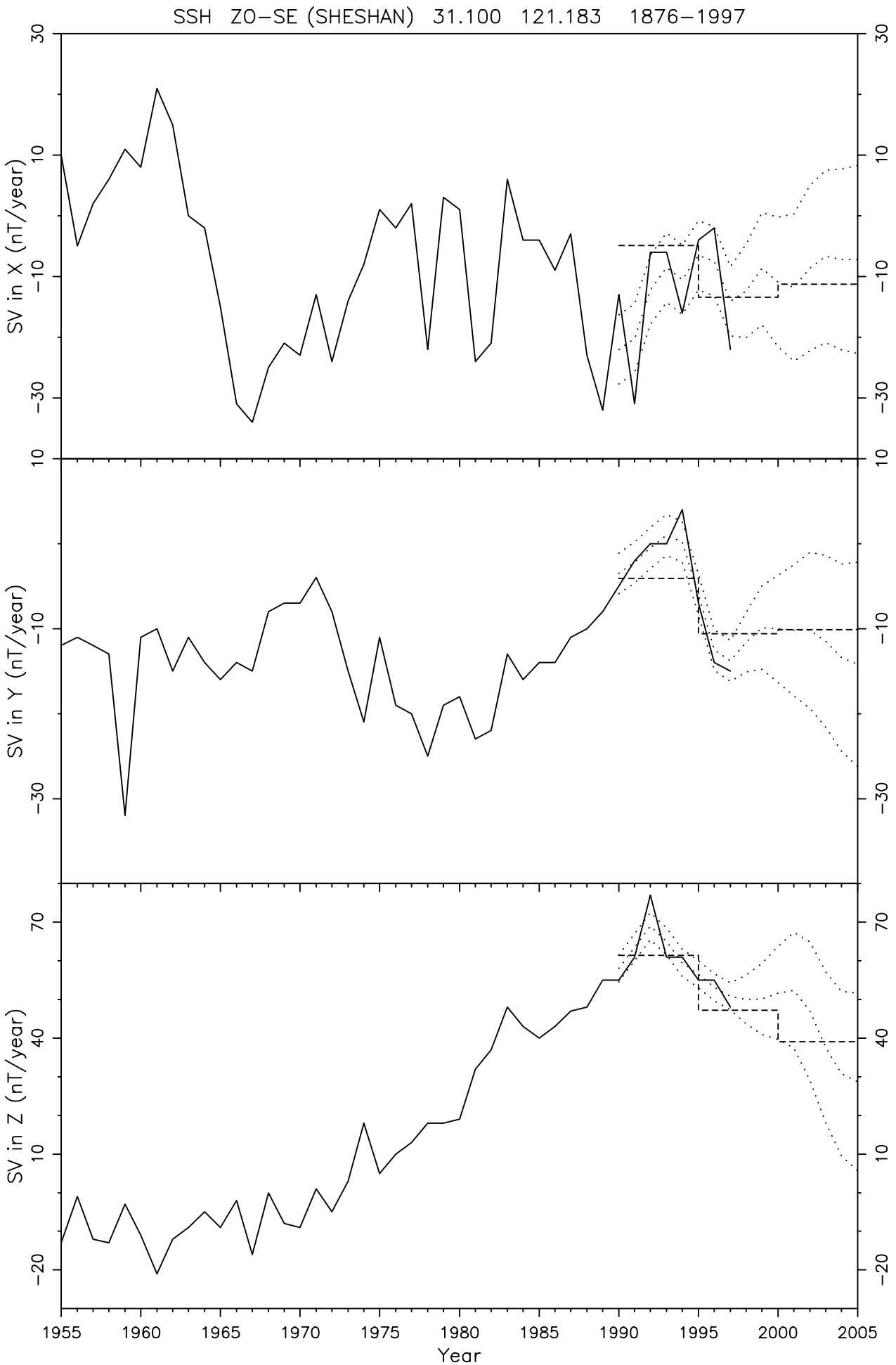
SSH ZO-SE (SHESHAN) 31.100 121.183 1876-1997
SV in X (nT/year)
SV in Y (nT/year)
SV in Z (nT/year)
Year
1955
1960
1965
1970
1975
1980
1985
1990
1995
2000
2005

Figure 121

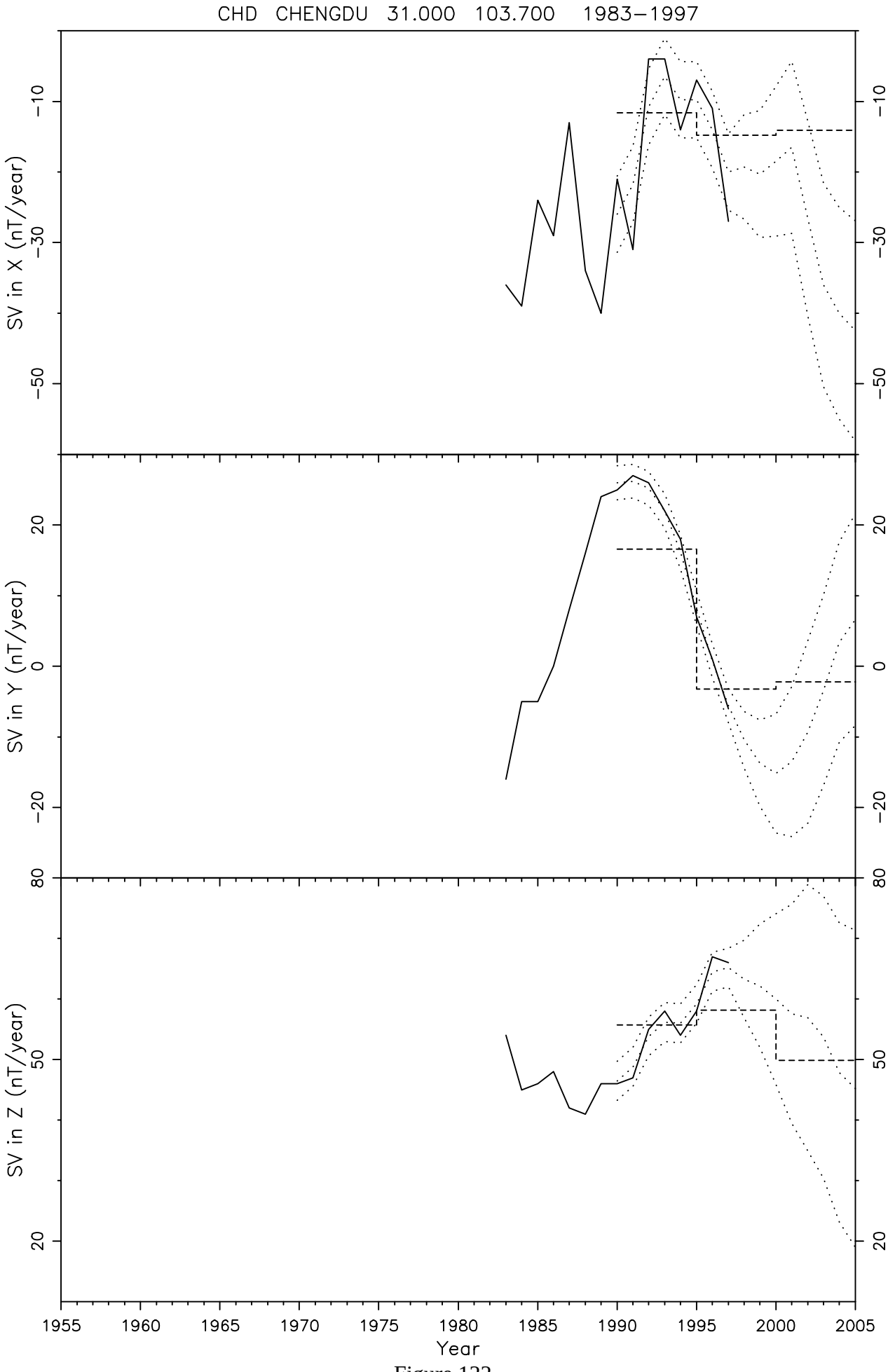
CHD CHENGDU 31.000 103.700 1983–1997
SV in X (nT/year)
−10
−30
−50
SV in Y (nT/year)
20
0
−20
80
SV in Z (nT/year)
50
20
1955
1960
1965
1970
1975
1980
1985
1990
1995
2000
2005
Year

Figure 122

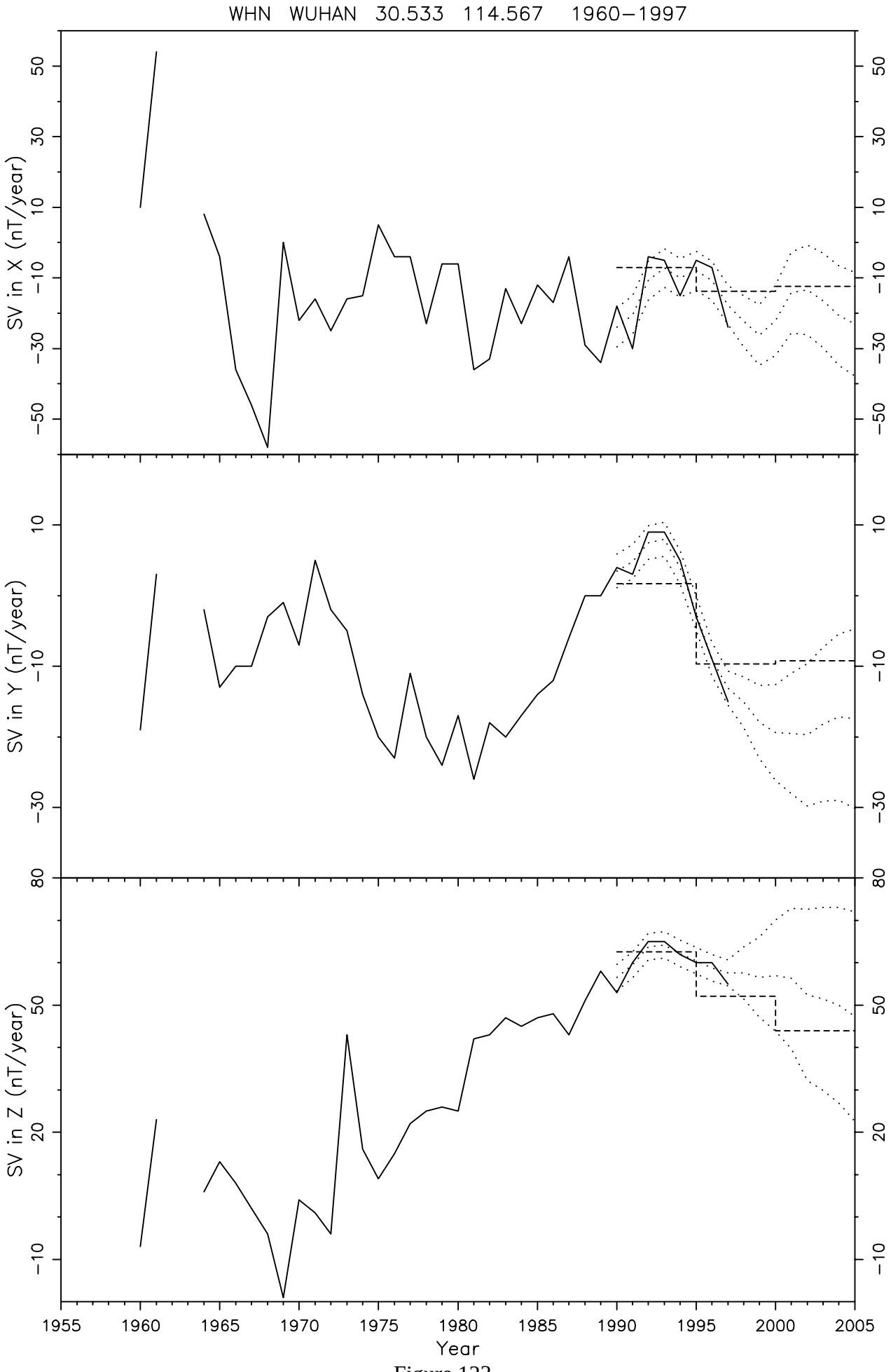
WHN WUHAN 30.533 114.567 1960−1997
SV in X (nT/year)
SV in Y (nT/year)
SV in Z (nT/year)
Year
1955
1960
1965
1970
1975
1980
1985
1990
1995
2000
2005

Figure 123

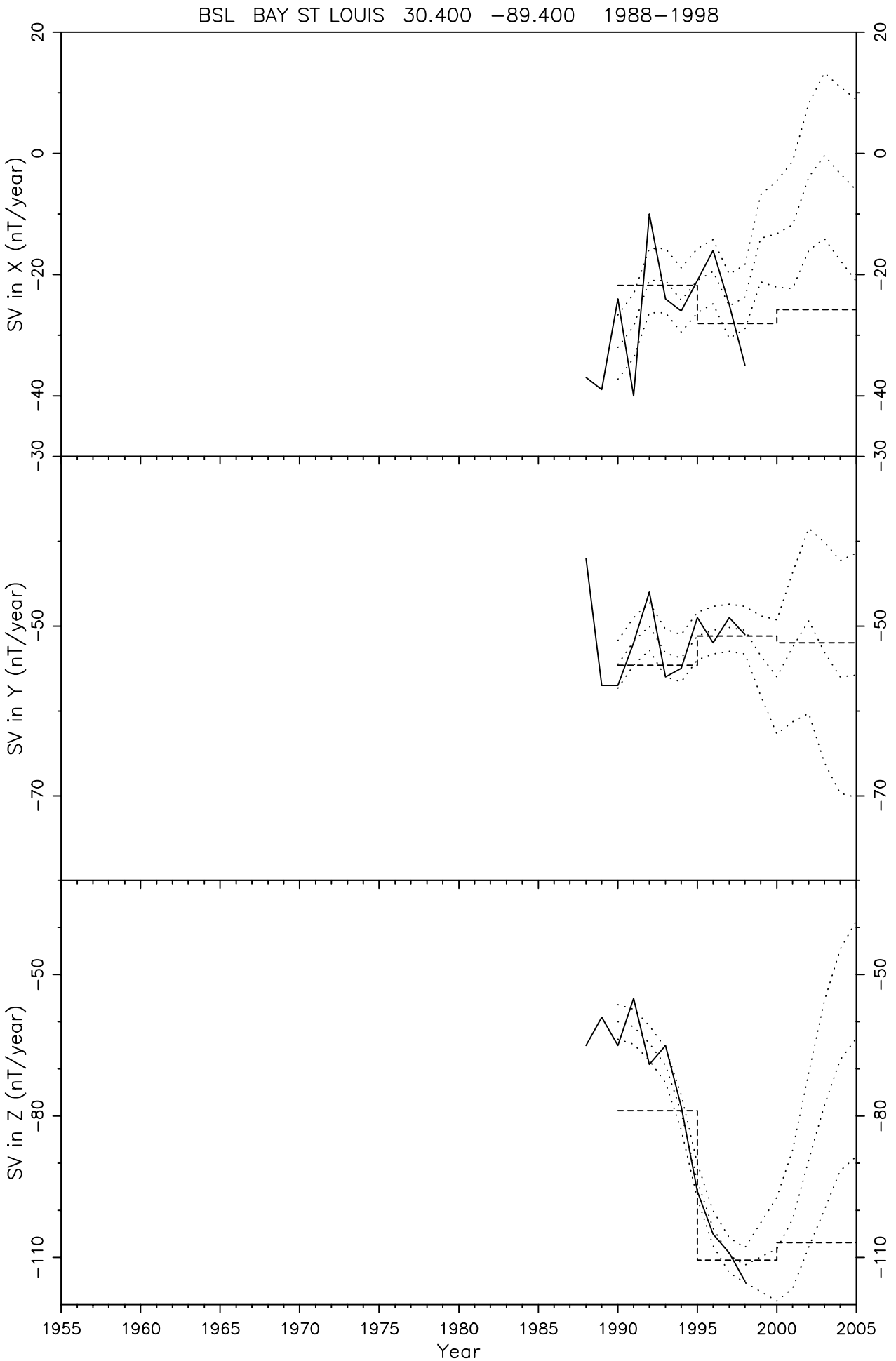
BSL BAY ST LOUIS 30.400 −89.400 1988−1998
SV in X (nT/year)
SV in Y (nT/year)
SV in Z (nT/year)
20
0
−20
−40
−30
−50
−70
−80
−110
1955
1960
1965
1970
1975
1980
1985
1990
1995
2000
2005
Year

Figure 124

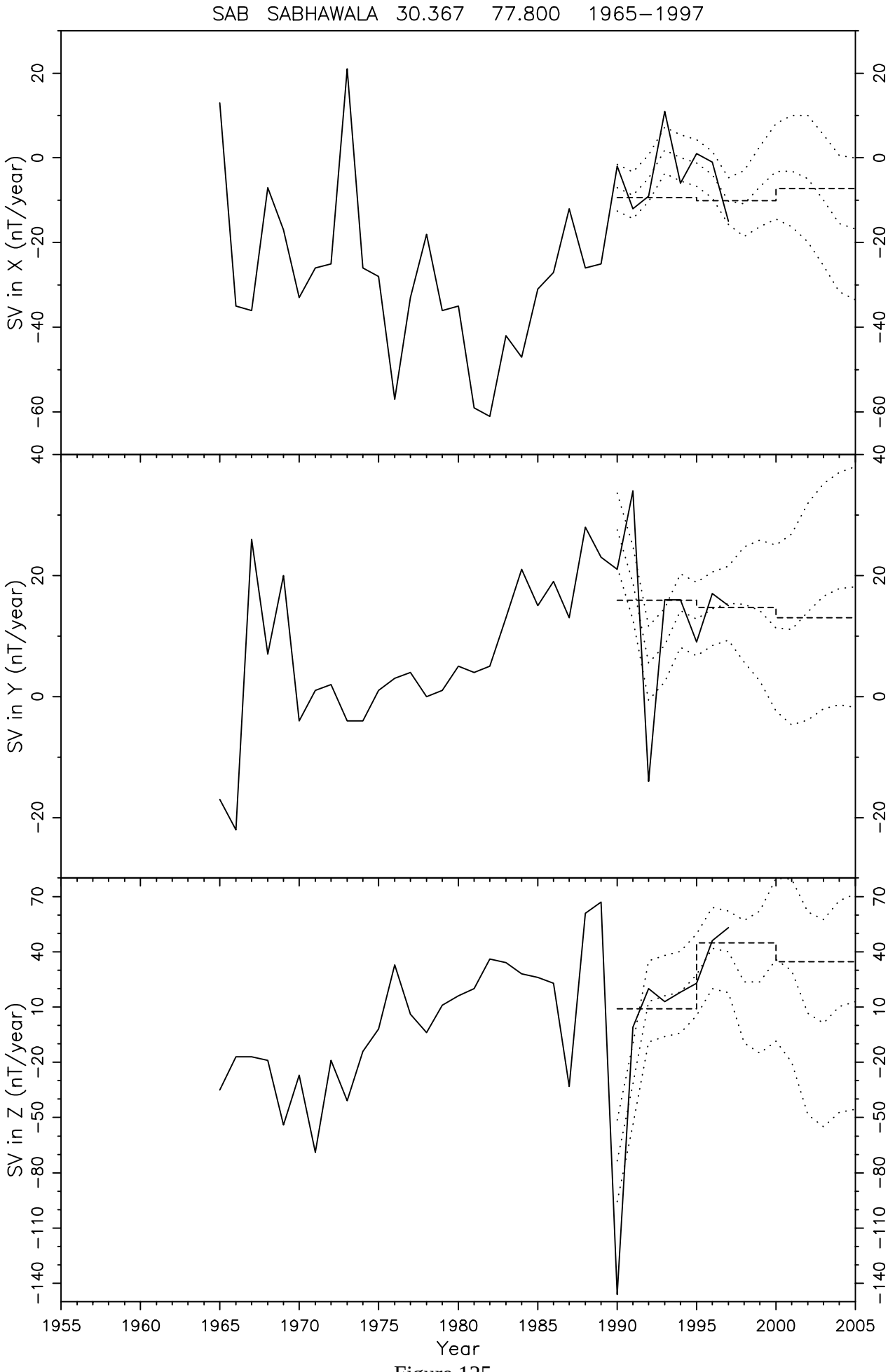
SAB SABHAWALA 30.367 77.800 1965–1997
SV in X (nT/year)
SV in Y (nT/year)
SV in Z (nT/year)
Year
1955
1960
1965
1970
1975
1980
1985
1990
1995
2000
2005

Figure 125

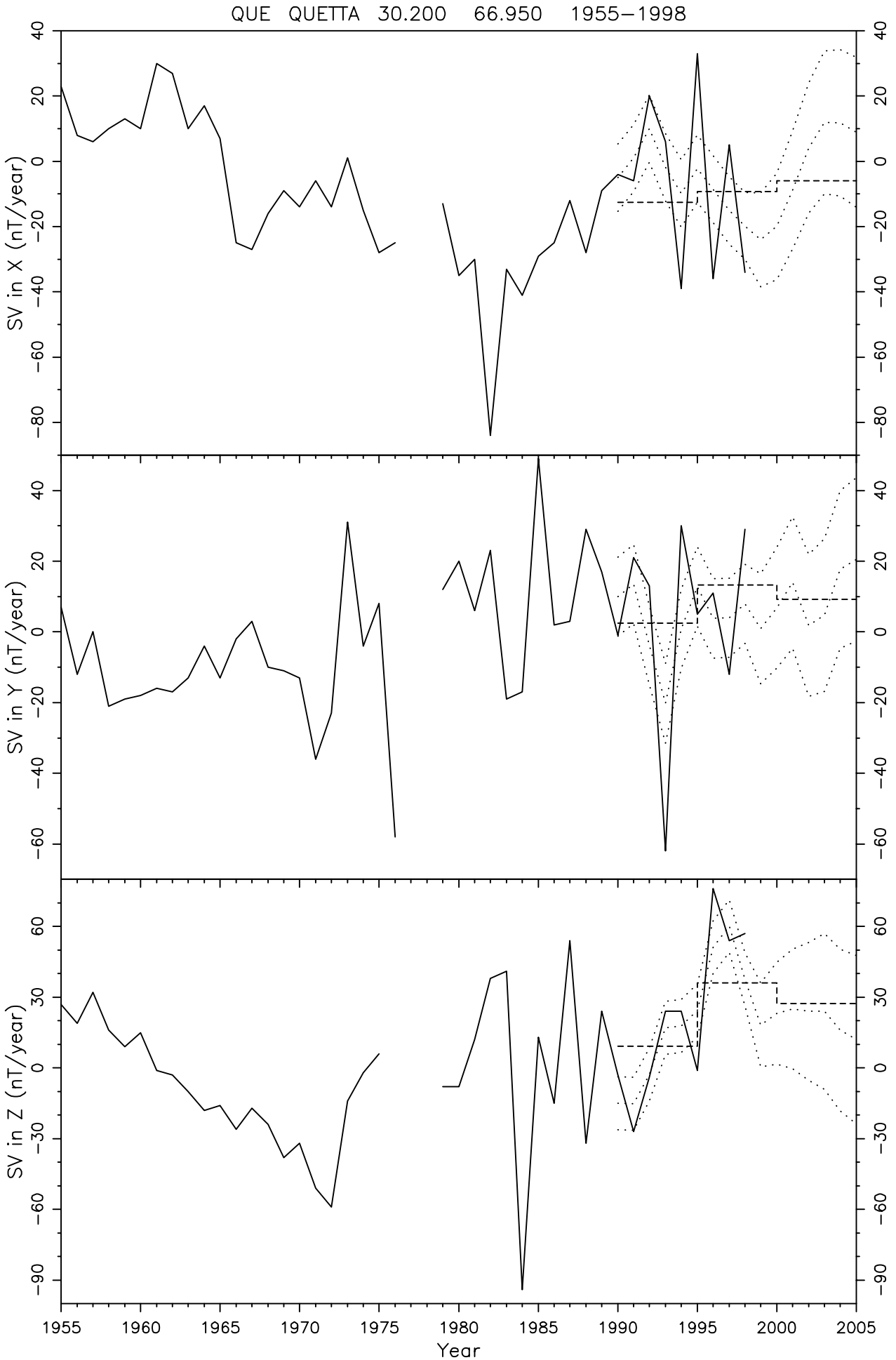
QUE QUETTA 30.200 66.950 1955–1998
SV in X (nT/year)
SV in Y (nT/year)
SV in Z (nT/year)
Year
1955
1960
1965
1970
1975
1980
1985
1990
1995
2000
2005

Figure 126

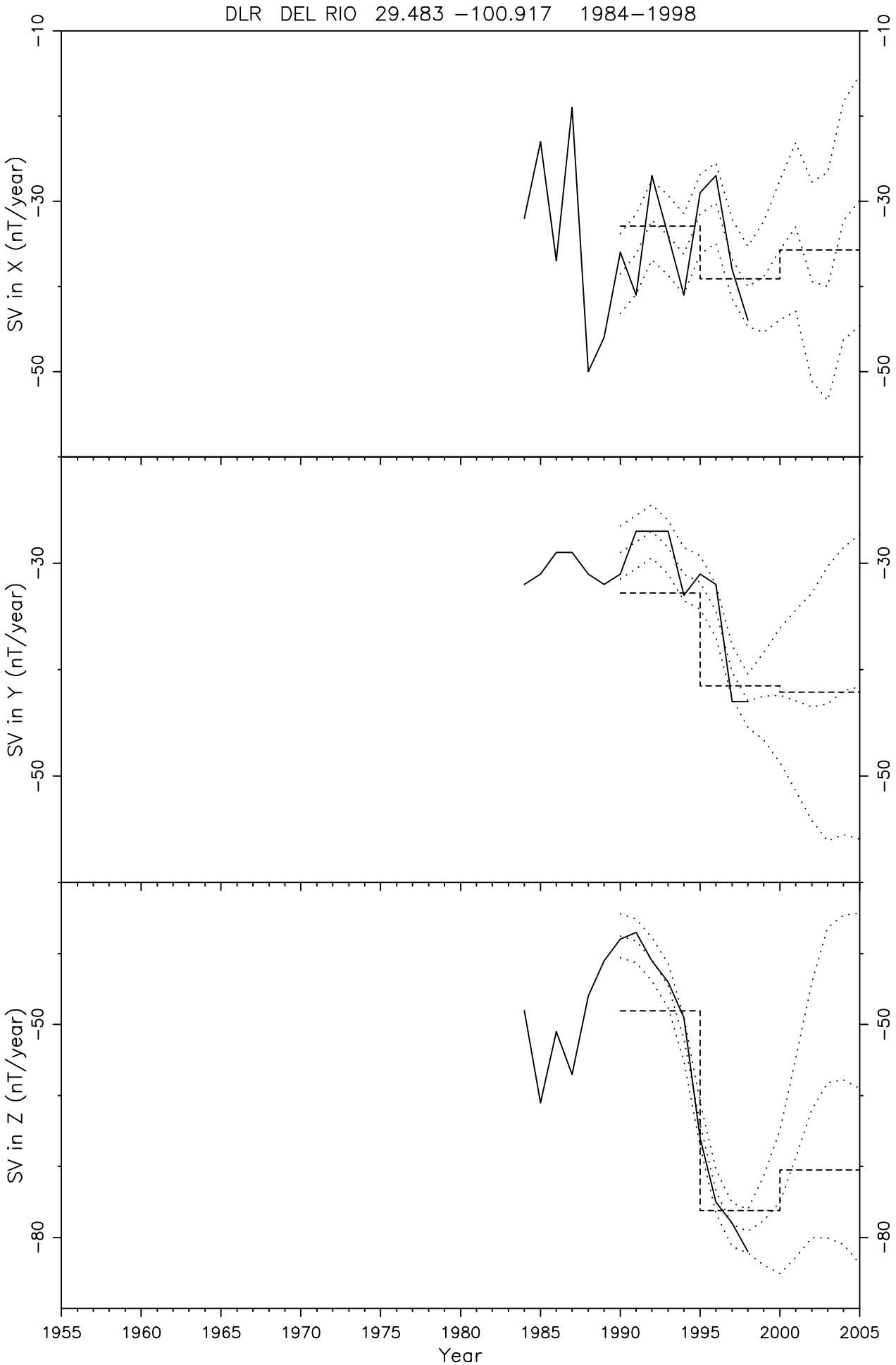
DLR DEL RIO 29.483 −100.917 1984−1998
SV in X (nT/year)
−10
−30
−50
SV in Y (nT/year)
−30
−50
SV in Z (nT/year)
−50
−80
1955
1960
1965
1970
1975
1980
1985
1990
1995
2000
2005
Year

Figure 127

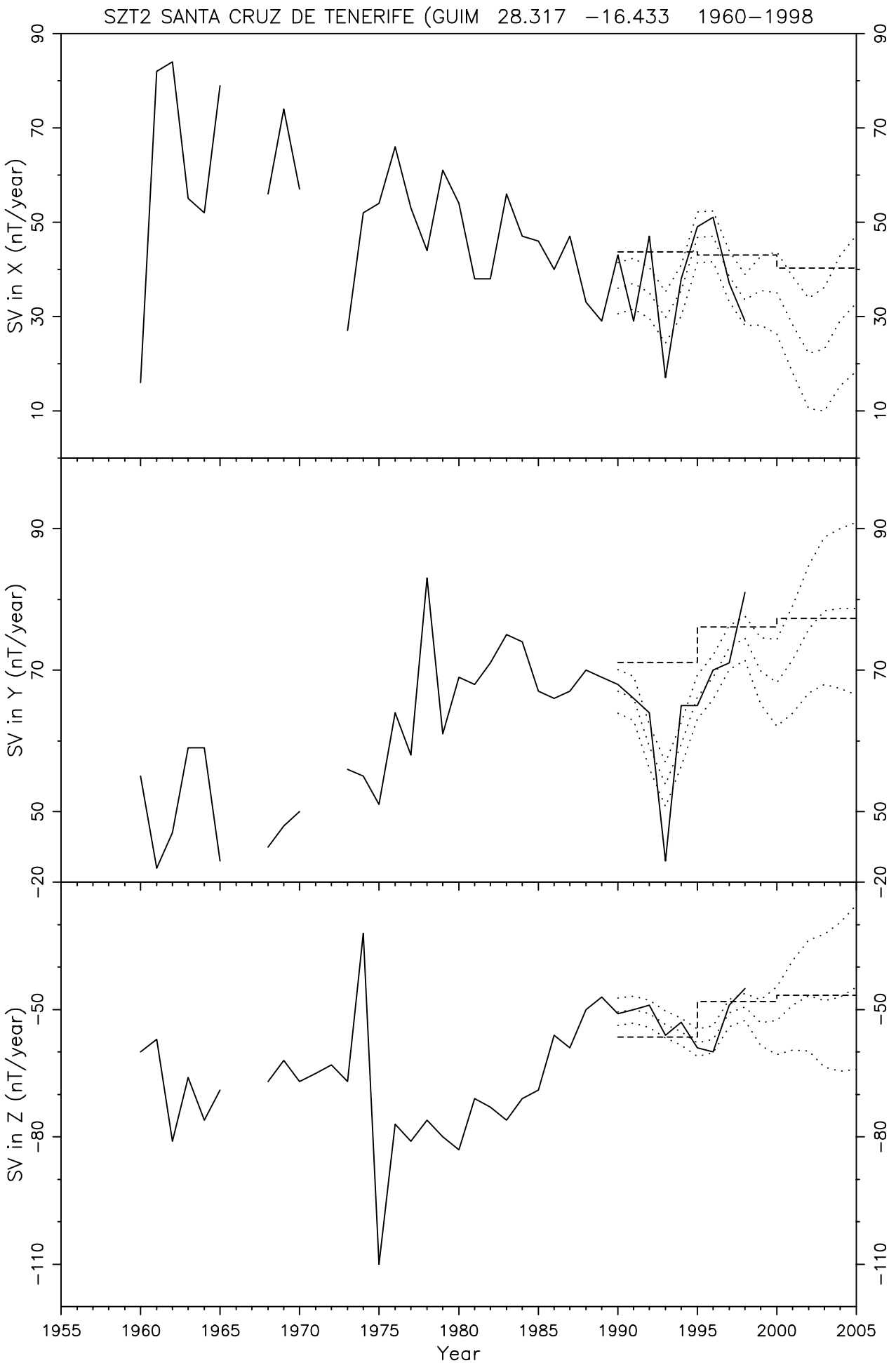
SZT2 SANTA CRUZ DE TENERIFE (GUIM 28.317 −16.433 1960−1998
SV in X (nT/year)
SV in Y (nT/year)
SV in Z (nT/year)
Year
1955
1960
1965
1970
1975
1980
1985
1990
1995
2000
2005

Figure 128

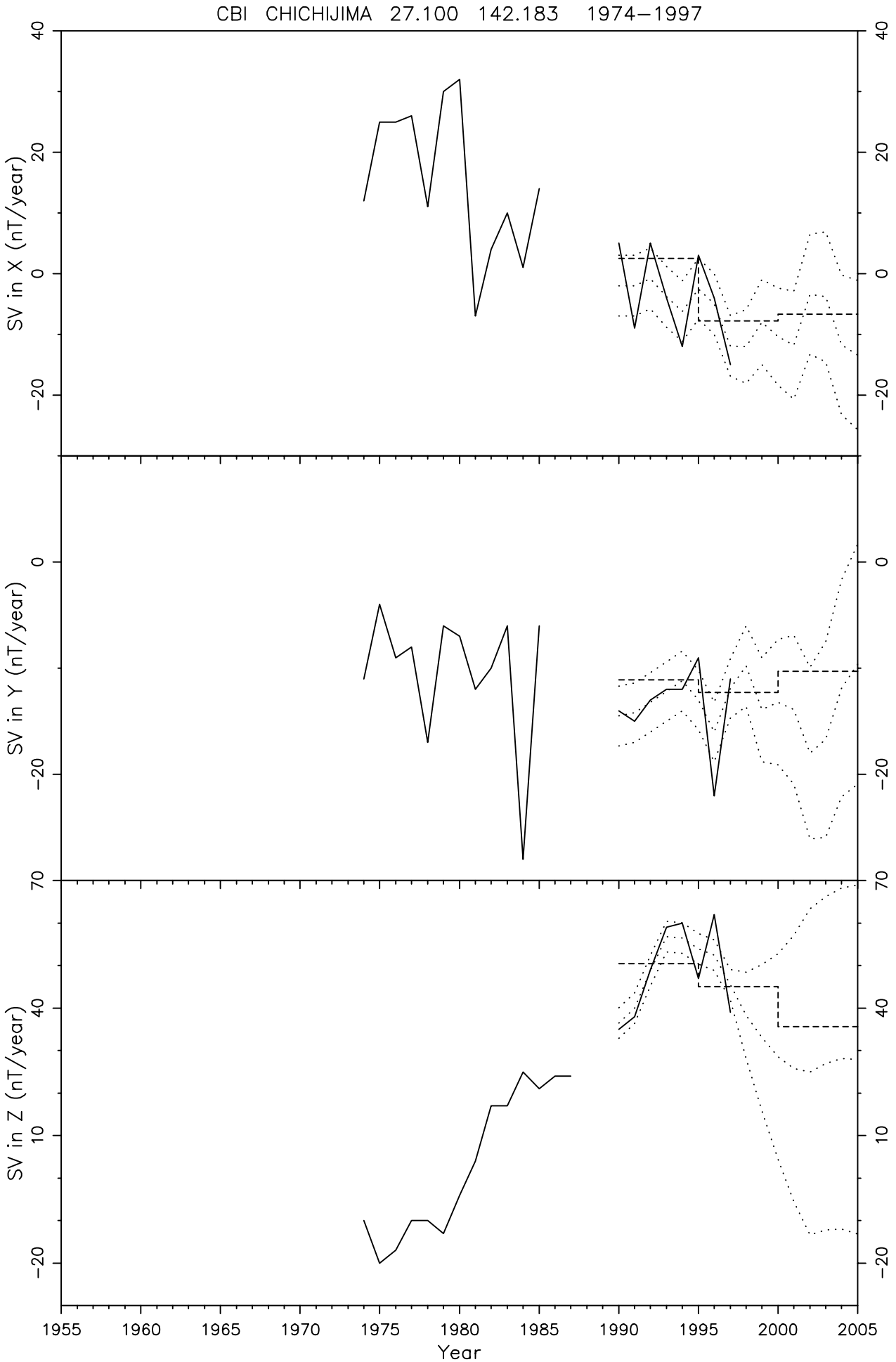
CBI CHICHIJIMA 27.100 142.183 1974–1997
SV in X (nT/year)
SV in Y (nT/year)
SV in Z (nT/year)
Year
1955
1960
1965
1970
1975
1980
1985
1990
1995
2000
2005

Figure 129

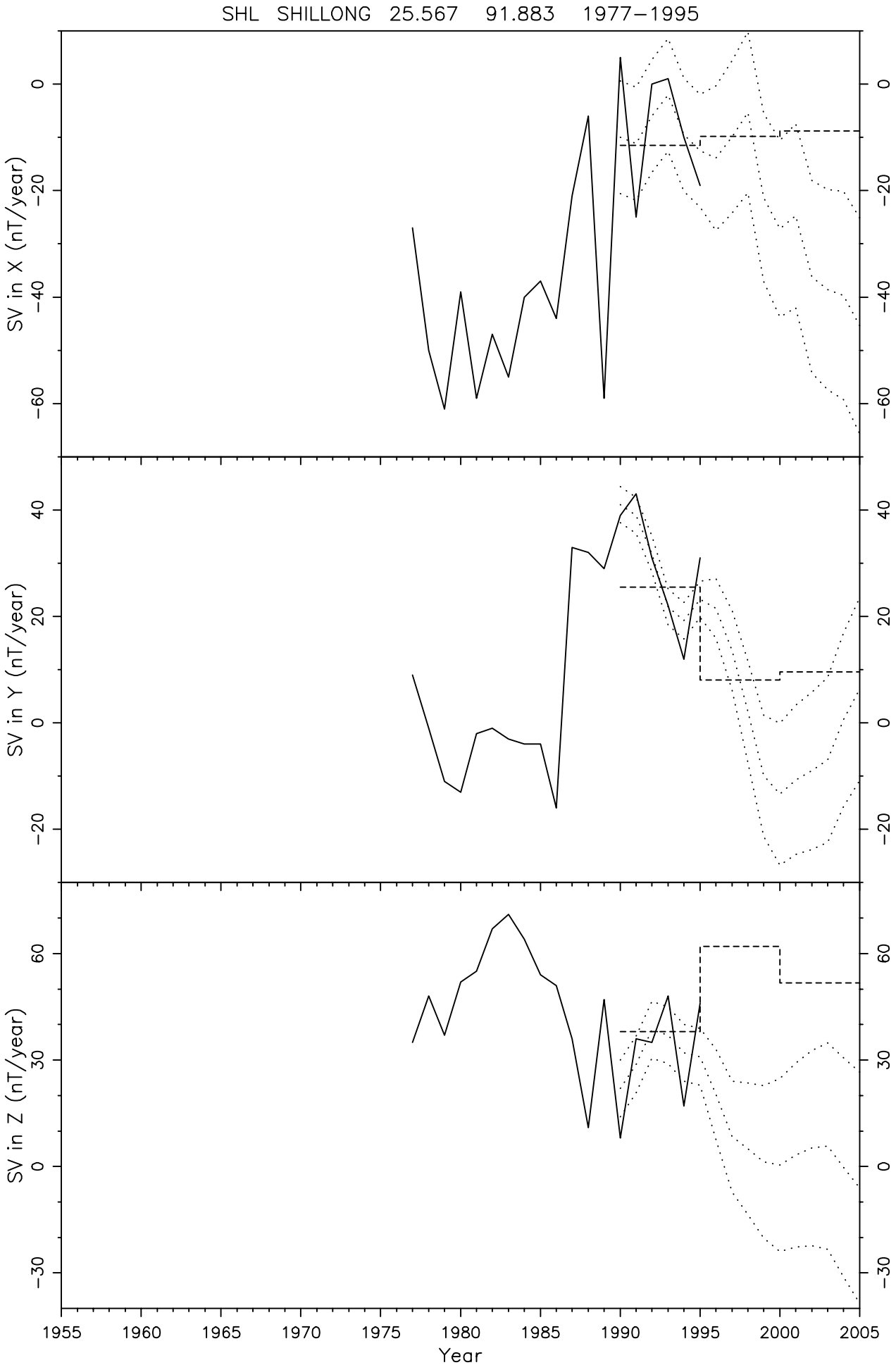
SHL SHILLONG 25.567 91.883 1977–1995
SV in X (nT/year)
SV in Y (nT/year)
SV in Z (nT/year)
Year
1955
1960
1965
1970
1975
1980
1985
1990
1995
2000
2005

Figure 130

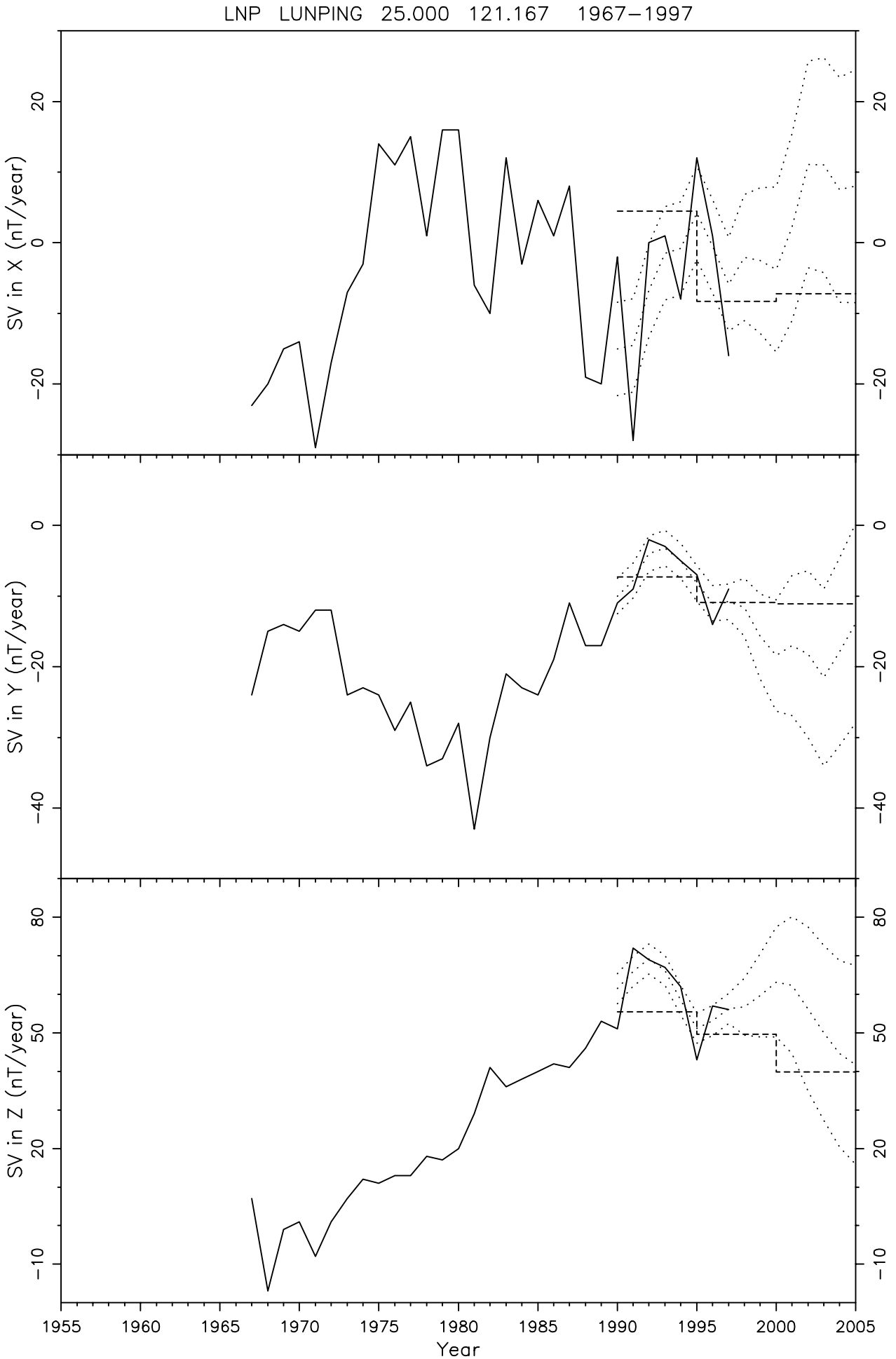
LNP LUNPING 25.000 121.167 1967–1997
SV in X (nT/year)
SV in Y (nT/year)
SV in Z (nT/year)
Year
1955
1960
1965
1970
1975
1980
1985
1990
1995
2000
2005

Figure 131

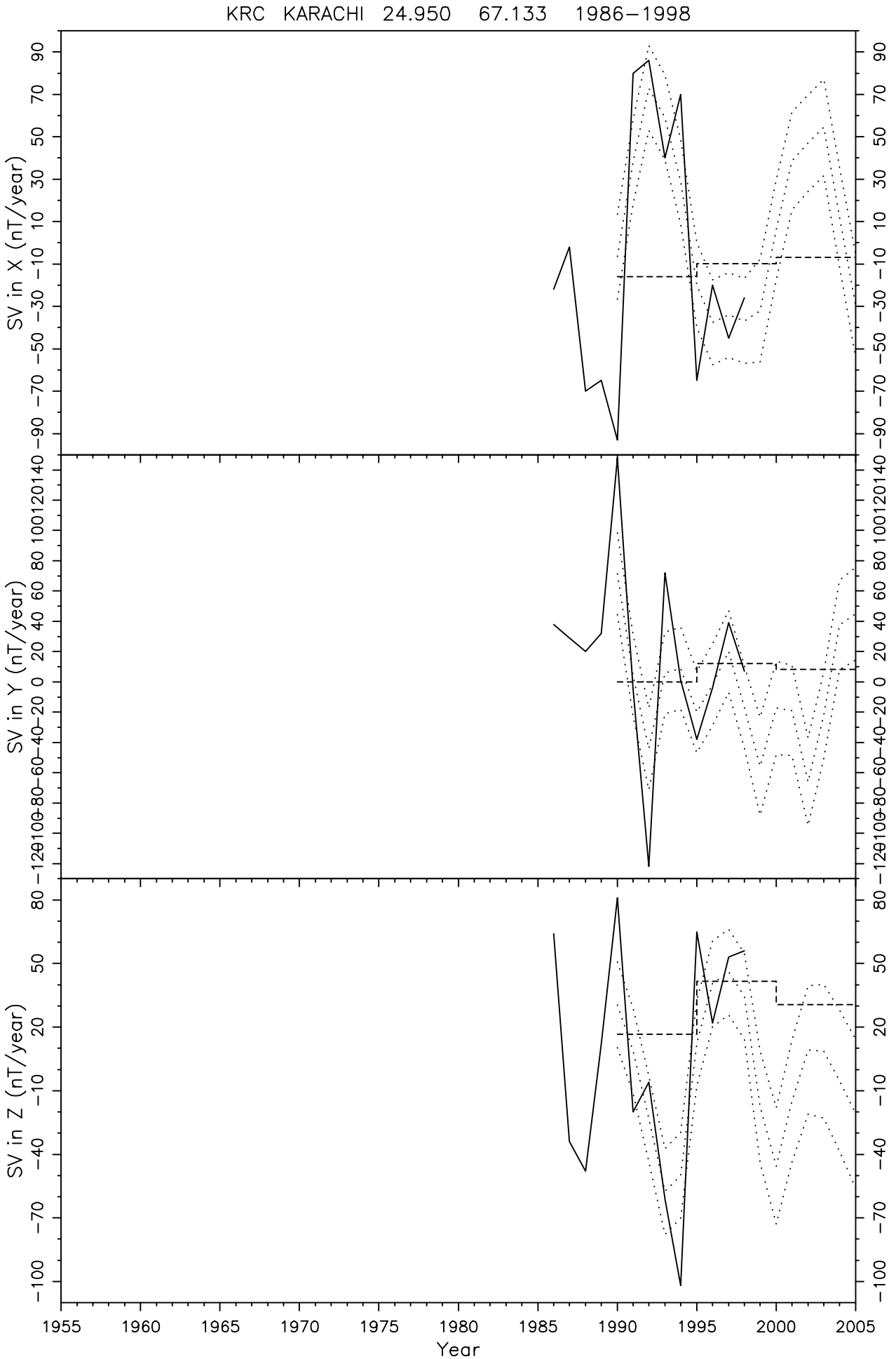
KRC KARACHI 24.950 67.133 1986–1998
SV in X (nT/year)
SV in Y (nT/year)
SV in Z (nT/year)
Year
1955
1960
1965
1970
1975
1980
1985
1990
1995
2000
2005

Figure 132

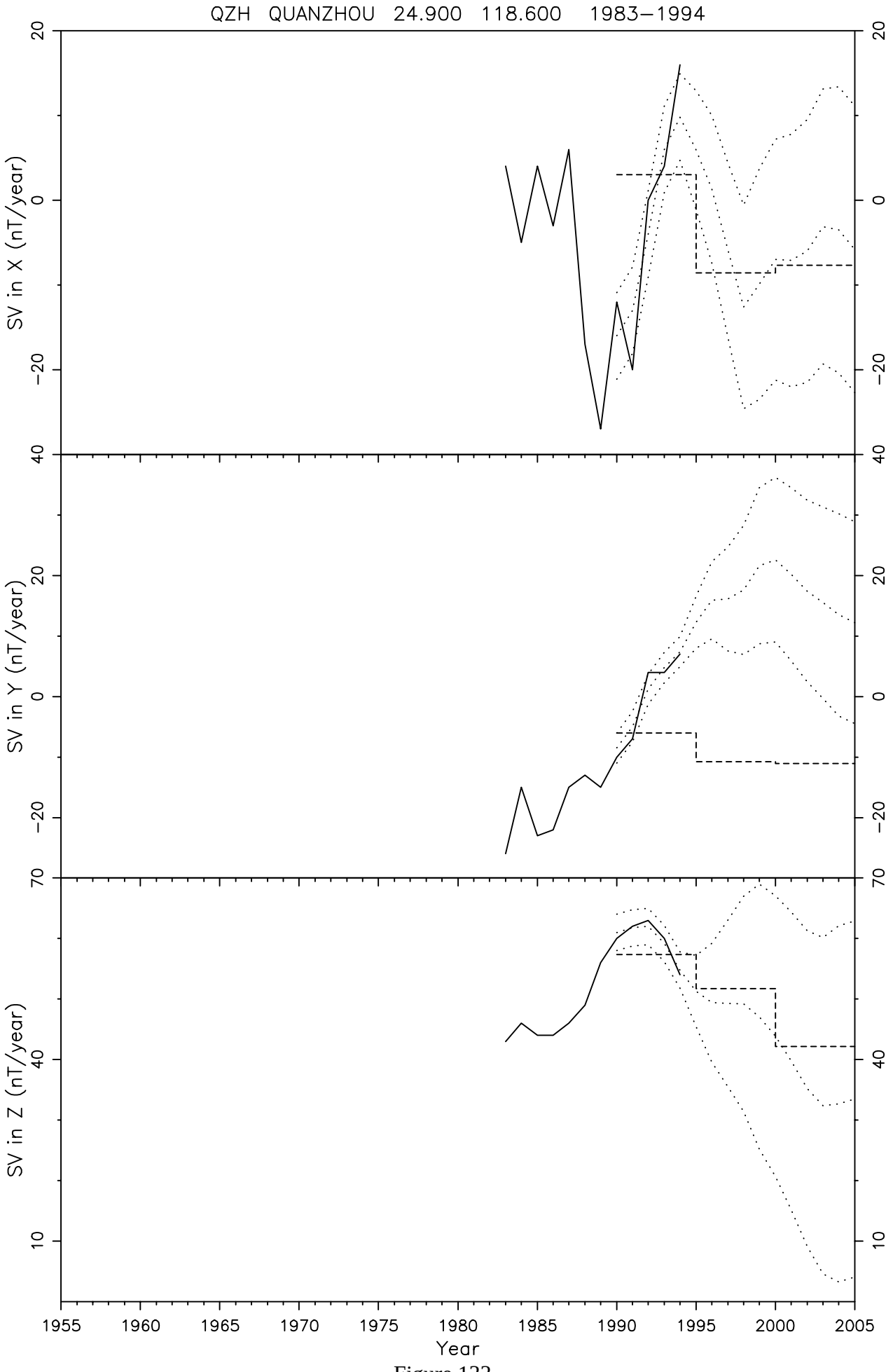
QZH QUANZHOU 24.900 118.600 1983–1994
SV in X (nT/year)
SV in Y (nT/year)
SV in Z (nT/year)
Year
1955
1960
1965
1970
1975
1980
1985
1990
1995
2000
2005

Figure 133

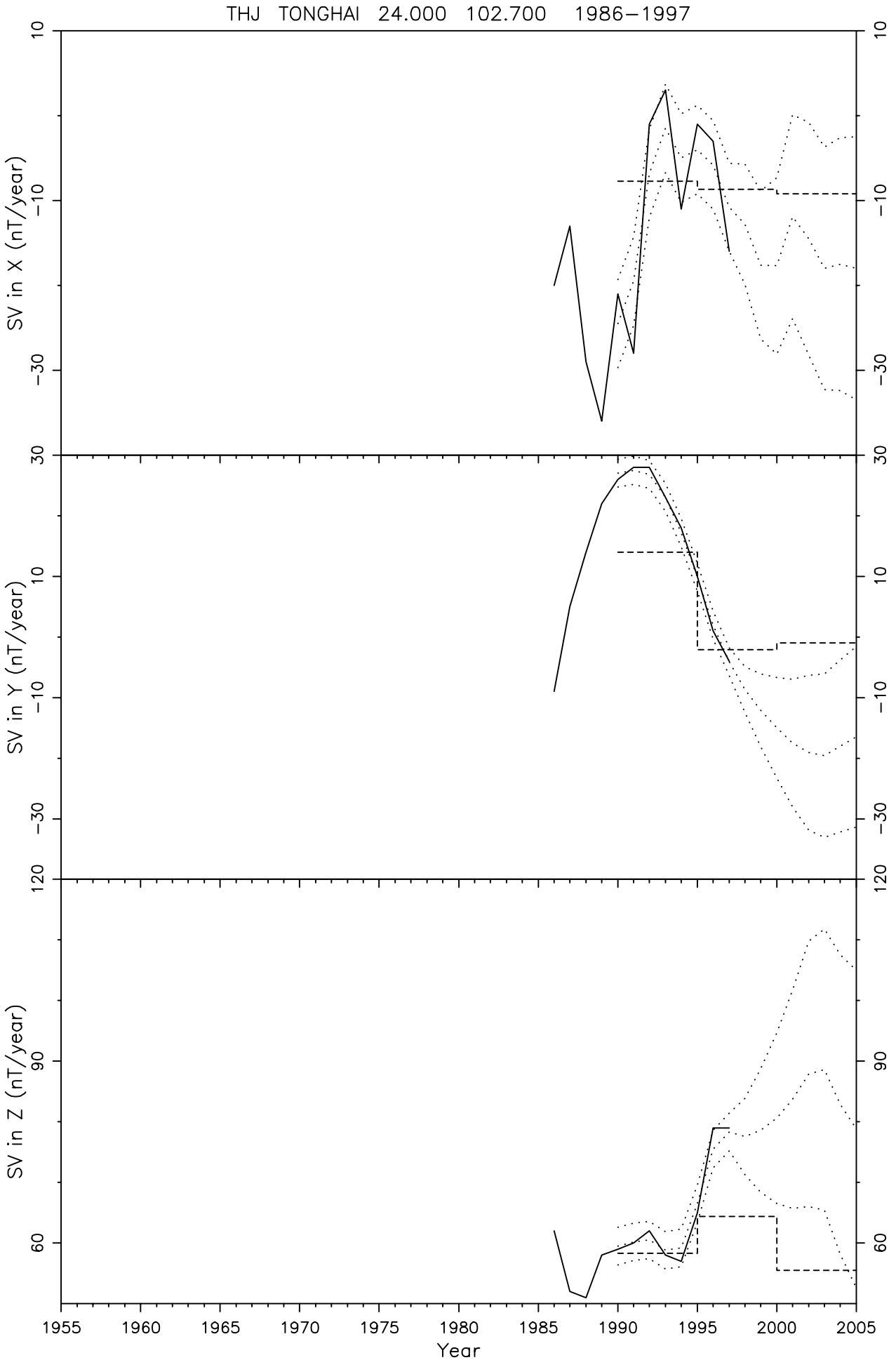
THJ TONGHAI 24.000 102.700 1986–1997
SV in X (nT/year)
SV in Y (nT/year)
SV in Z (nT/year)
10
−10
−30
30
10
−10
−30
120
90
60
1955
1960
1965
1970
1975
1980
1985
1990
1995
2000
2005
Year

Figure 134

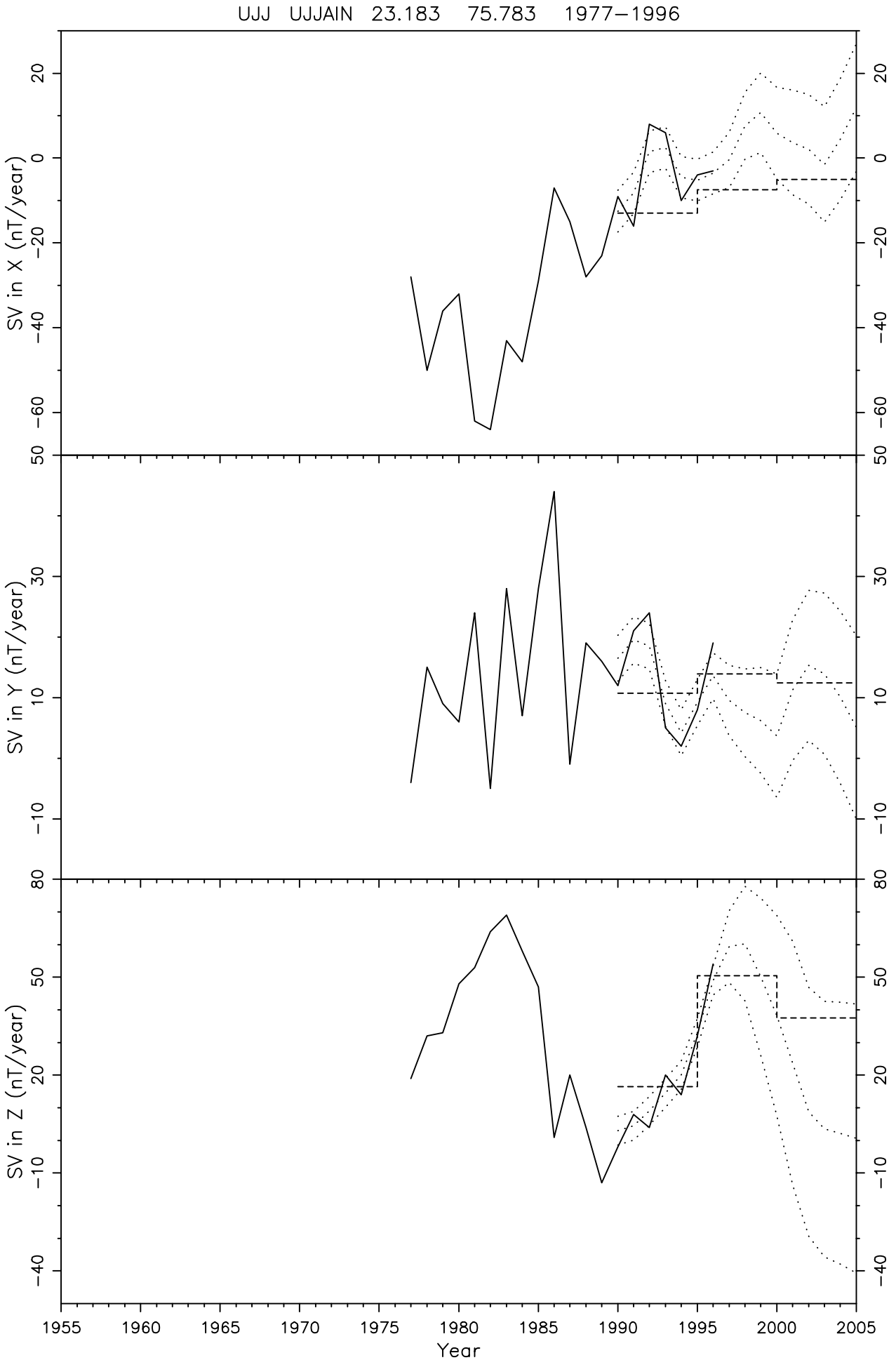
UJJ UJJAIN 23.183 75.783 1977–1996
SV in X (nT/year)
SV in Y (nT/year)
SV in Z (nT/year)
Year
1955
1960
1965
1970
1975
1980
1985
1990
1995
2000
2005

Figure 135

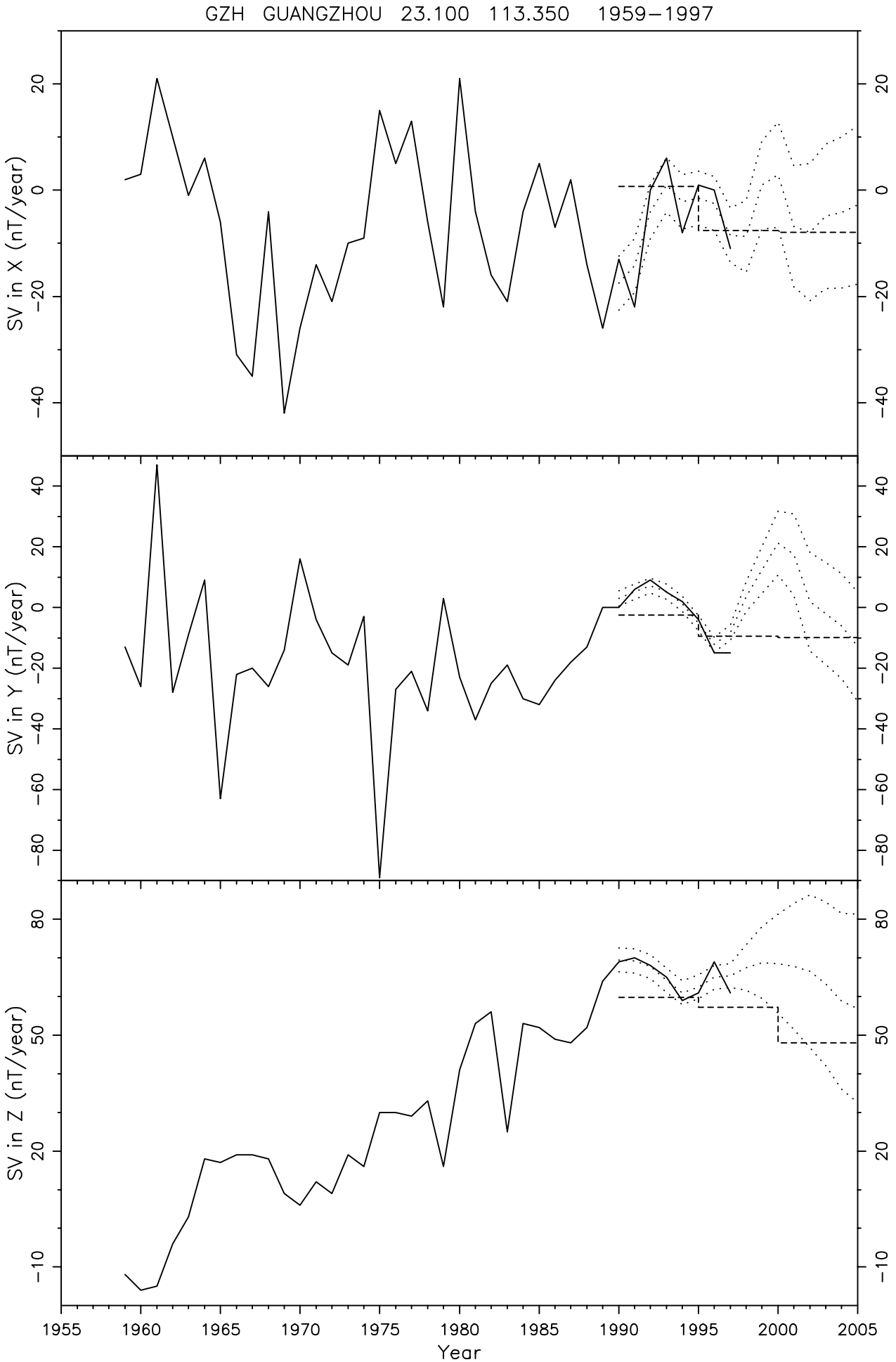
GZH GUANGZHOU 23.100 113.350 1959–1997
SV in X (nT/year)
SV in Y (nT/year)
SV in Z (nT/year)
Year
1955
1960
1965
1970
1975
1980
1985
1990
1995
2000
2005

Figure 136

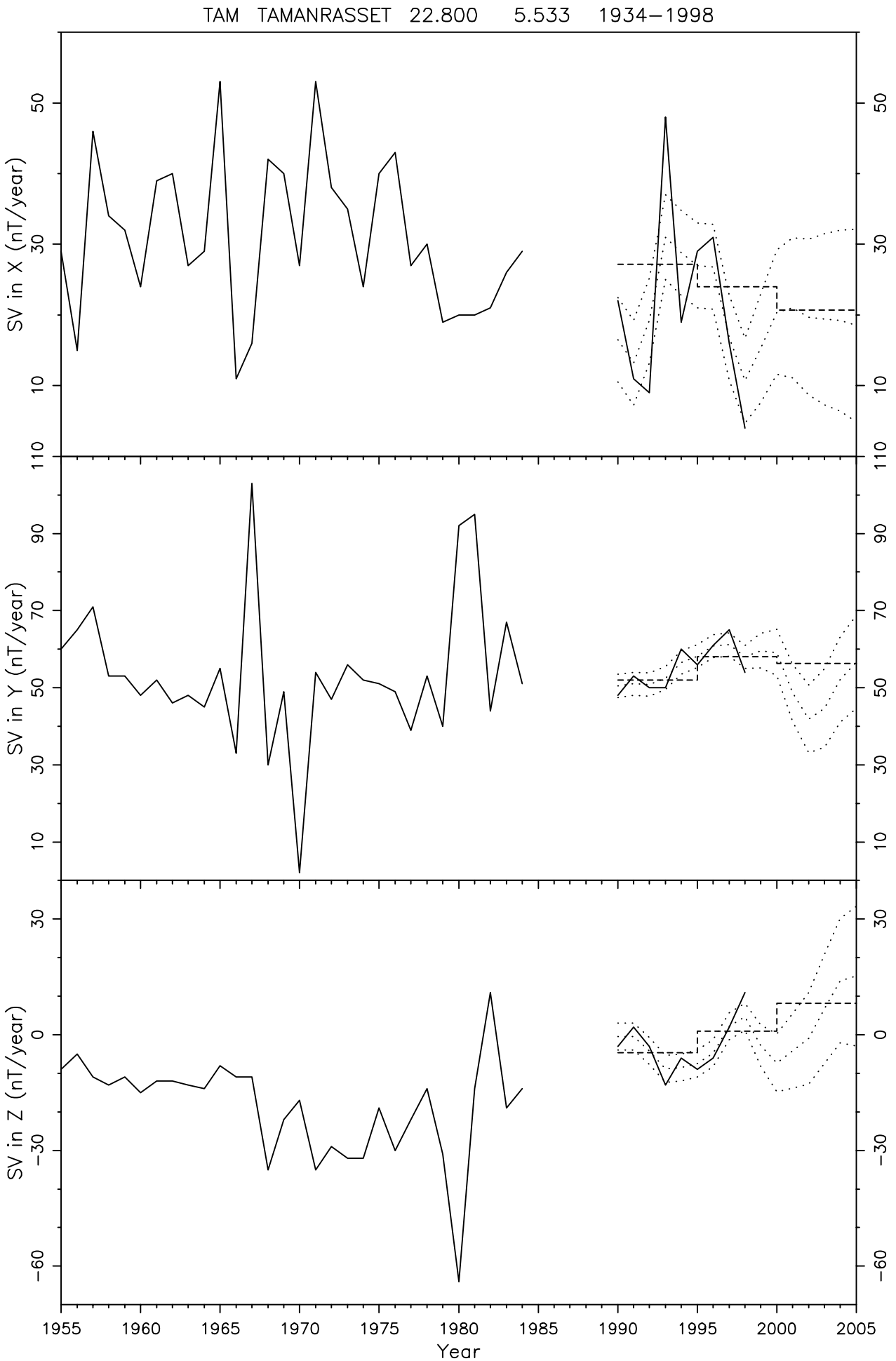
TAM TAMANRASSET 22.800 5.533 1934–1998
SV in X (nT/year)
SV in Y (nT/year)
SV in Z (nT/year)
Year
1955
1960
1965
1970
1975
1980
1985
1990
1995
2000
2005

Figure 137

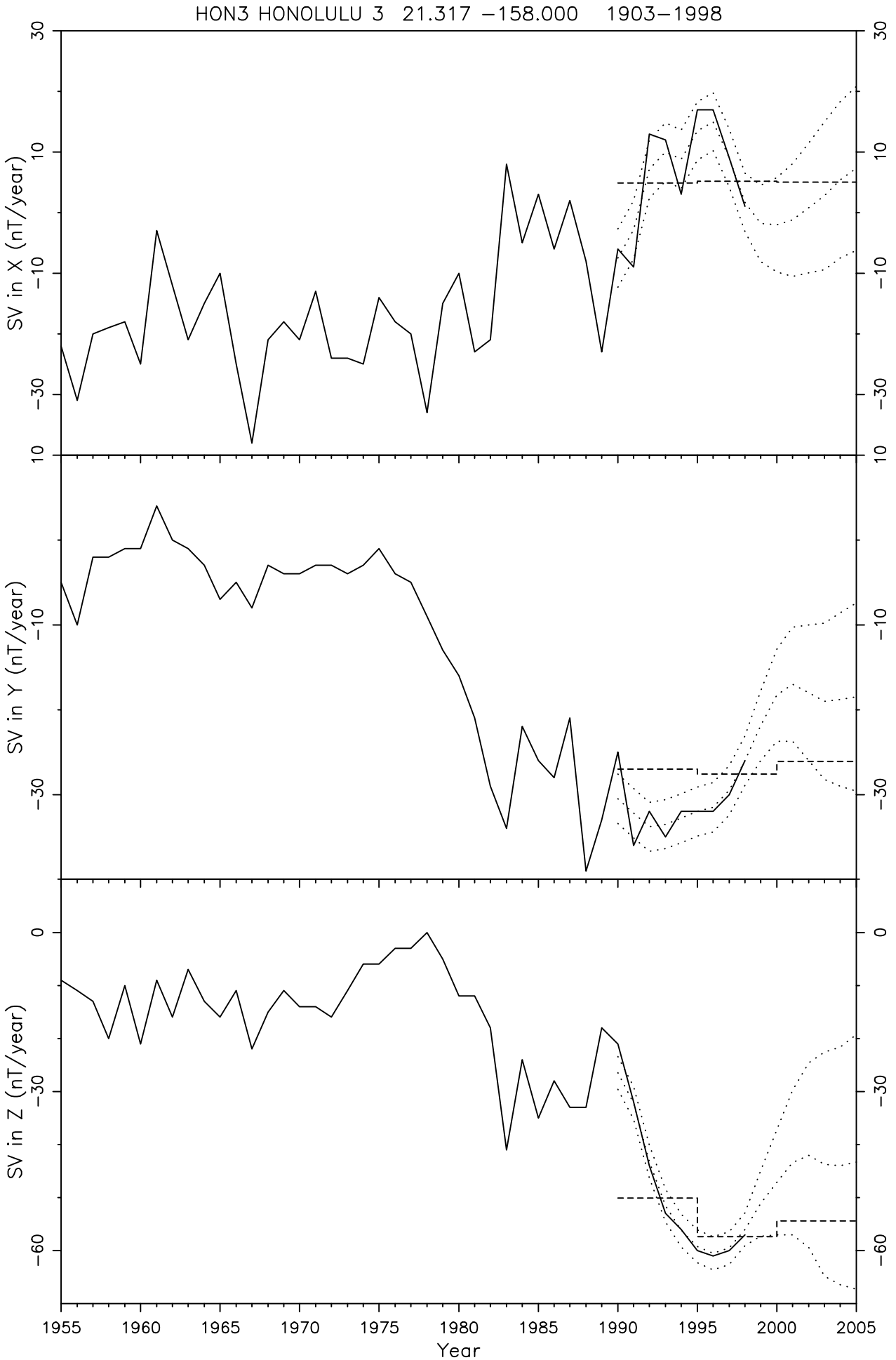
HON3 HONOLULU 3 21.317 −158.000 1903−1998
SV in X (nT/year)
SV in Y (nT/year)
SV in Z (nT/year)
30
10
−10
−30
−60
0
1955
1960
1965
1970
1975
1980
1985
1990
1995
2000
2005
Year

Figure 138

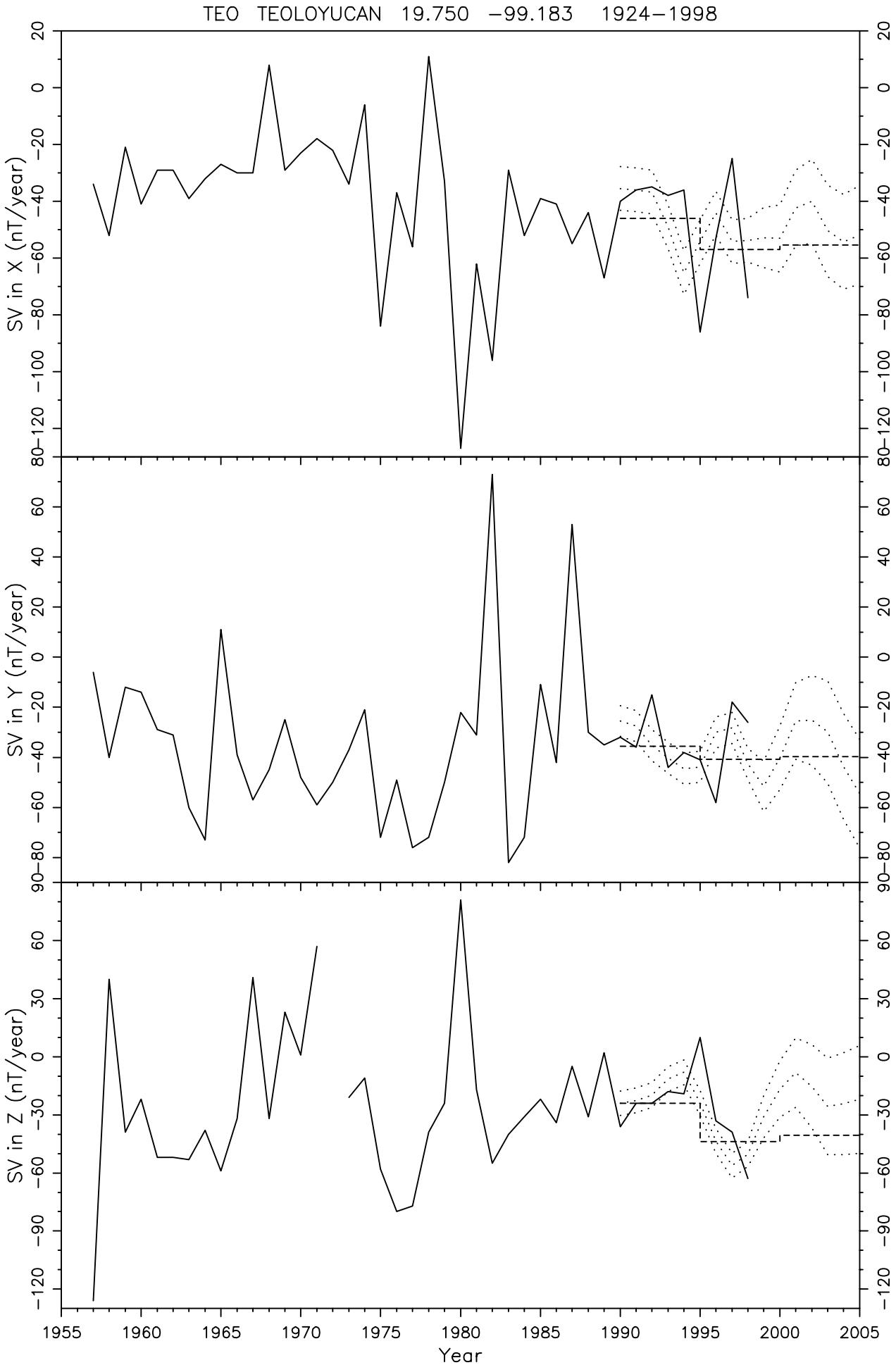
TEO TEOLOYUCAN 19.750 −99.183 1924−1998
SV in X (nT/year)
SV in Y (nT/year)
SV in Z (nT/year)
Year
1955
1960
1965
1970
1975
1980
1985
1990
1995
2000
2005

Figure 139

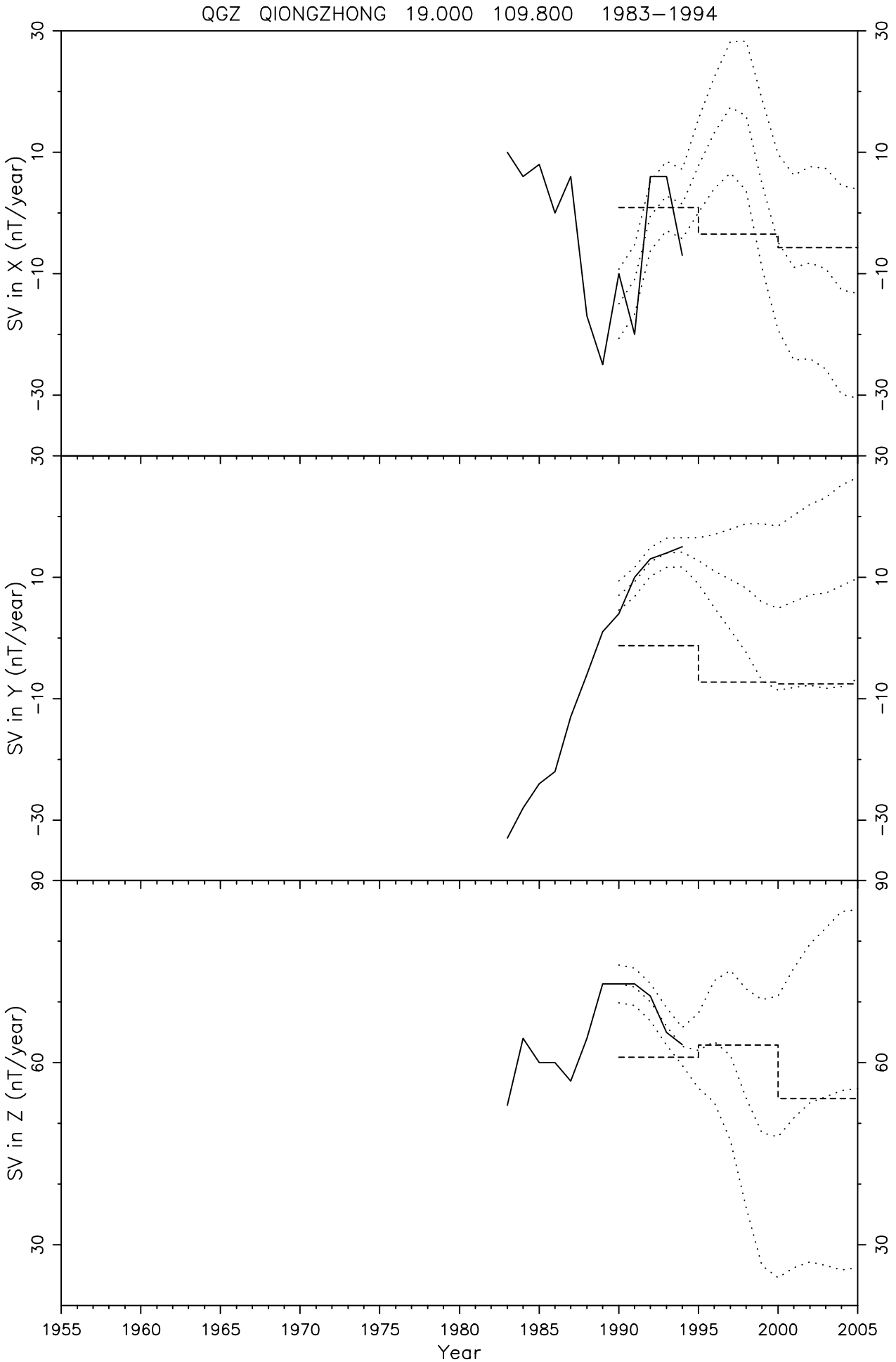
QGZ QIONGZHONG 19.000 109.800 1983–1994
SV in X (nT/year)
SV in Y (nT/year)
SV in Z (nT/year)
30
10
−10
−30
90
60
1955
1960
1965
1970
1975
1980
1985
1990
1995
2000
2005
Year

Figure 140

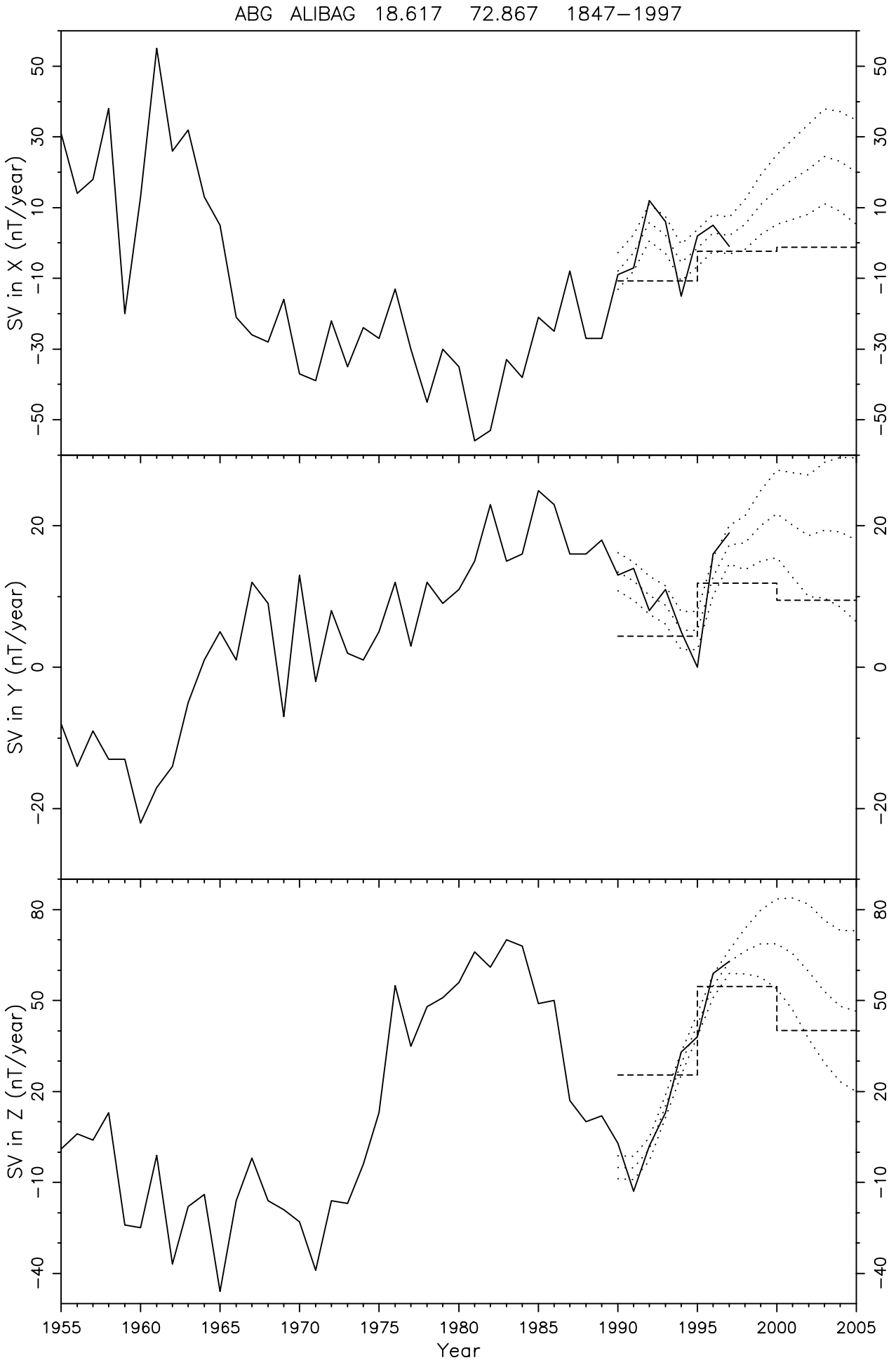
ABG ALIBAG 18.617 72.867 1847–1997
SV in X (nT/year)
SV in Y (nT/year)
SV in Z (nT/year)
Year
1955
1960
1965
1970
1975
1980
1985
1990
1995
2000
2005

Figure 141

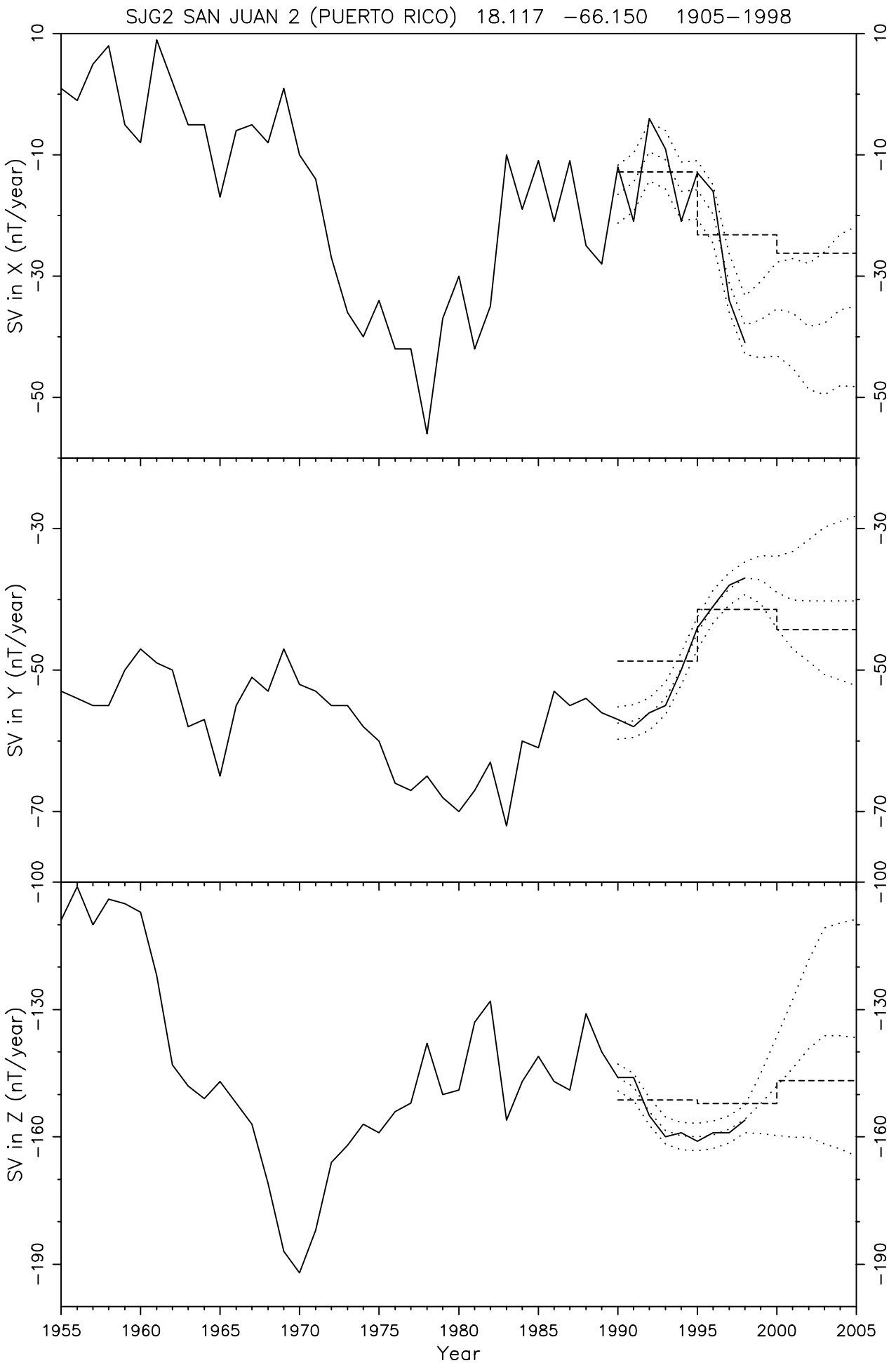
SJG2 SAN JUAN 2 (PUERTO RICO) 18.117 −66.150 1905−1998
SV in X (nT/year)
SV in Y (nT/year)
SV in Z (nT/year)
10
−10
−30
−50
−70
−100
−130
−160
−190
1955
1960
1965
1970
1975
1980
1985
1990
1995
2000
2005
Year

Figure 142

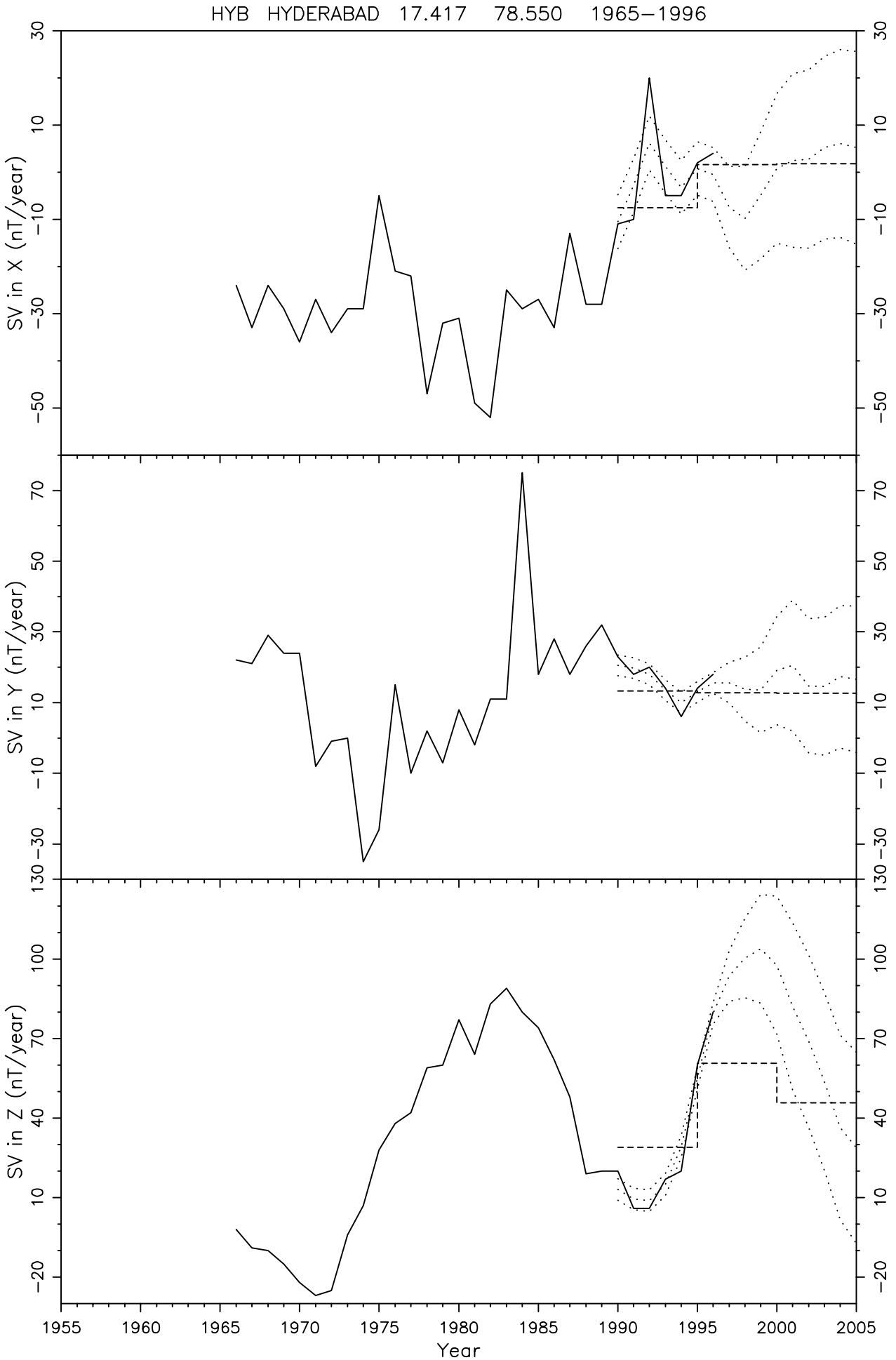
HYB HYDERABAD 17.417 78.550 1965–1996
SV in X (nT/year)
SV in Y (nT/year)
SV in Z (nT/year)
Year
1955
1960
1965
1970
1975
1980
1985
1990
1995
2000
2005

Figure 143

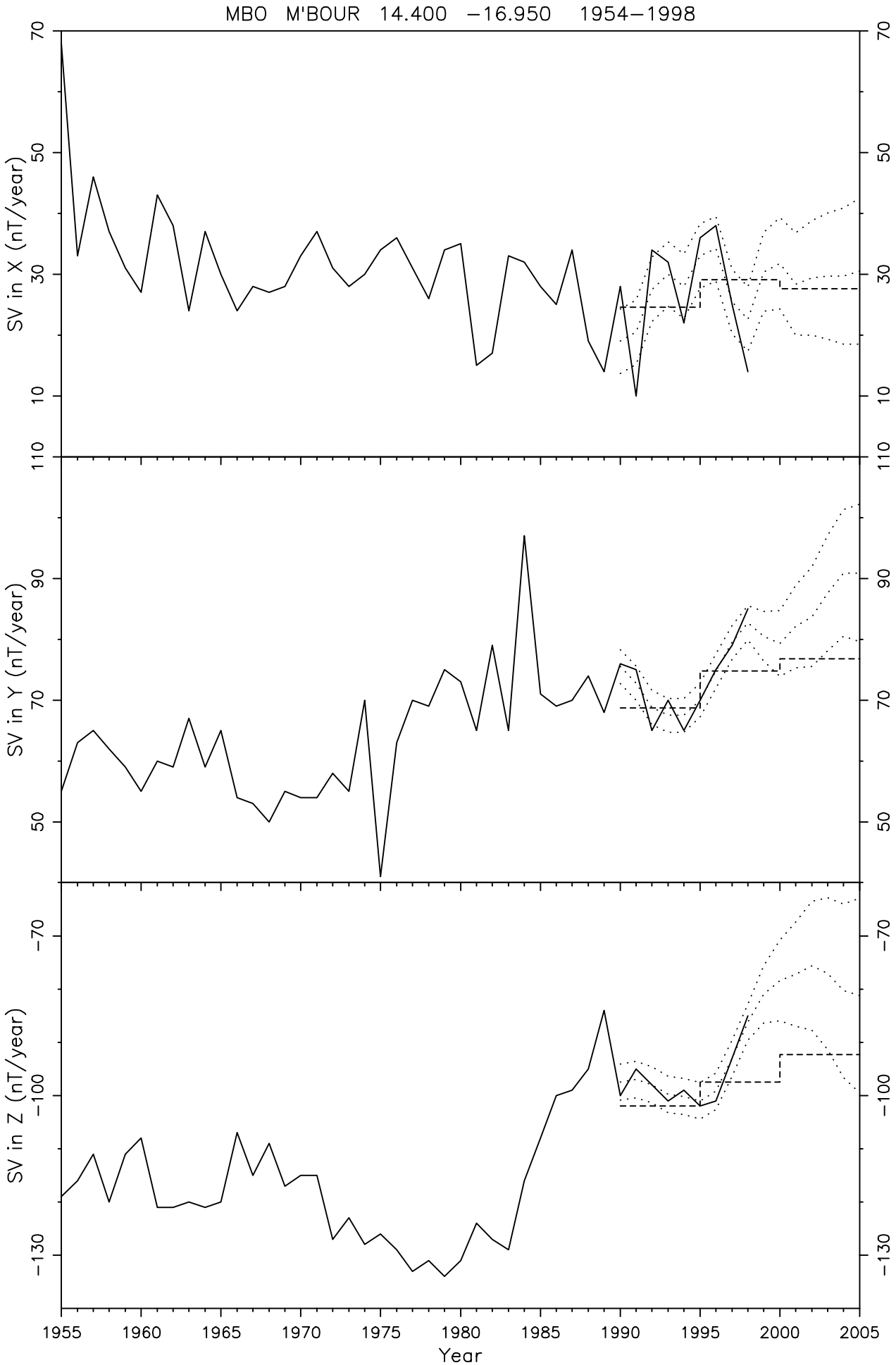
MBO M'BOUR 14.400 −16.950 1954−1998
SV in X (nT/year)
70
50
30
10
−10
SV in Y (nT/year)
90
70
50
SV in Z (nT/year)
−70
−100
−130
1955
1960
1965
1970
1975
1980
1985
1990
1995
2000
2005
Year

Figure 144

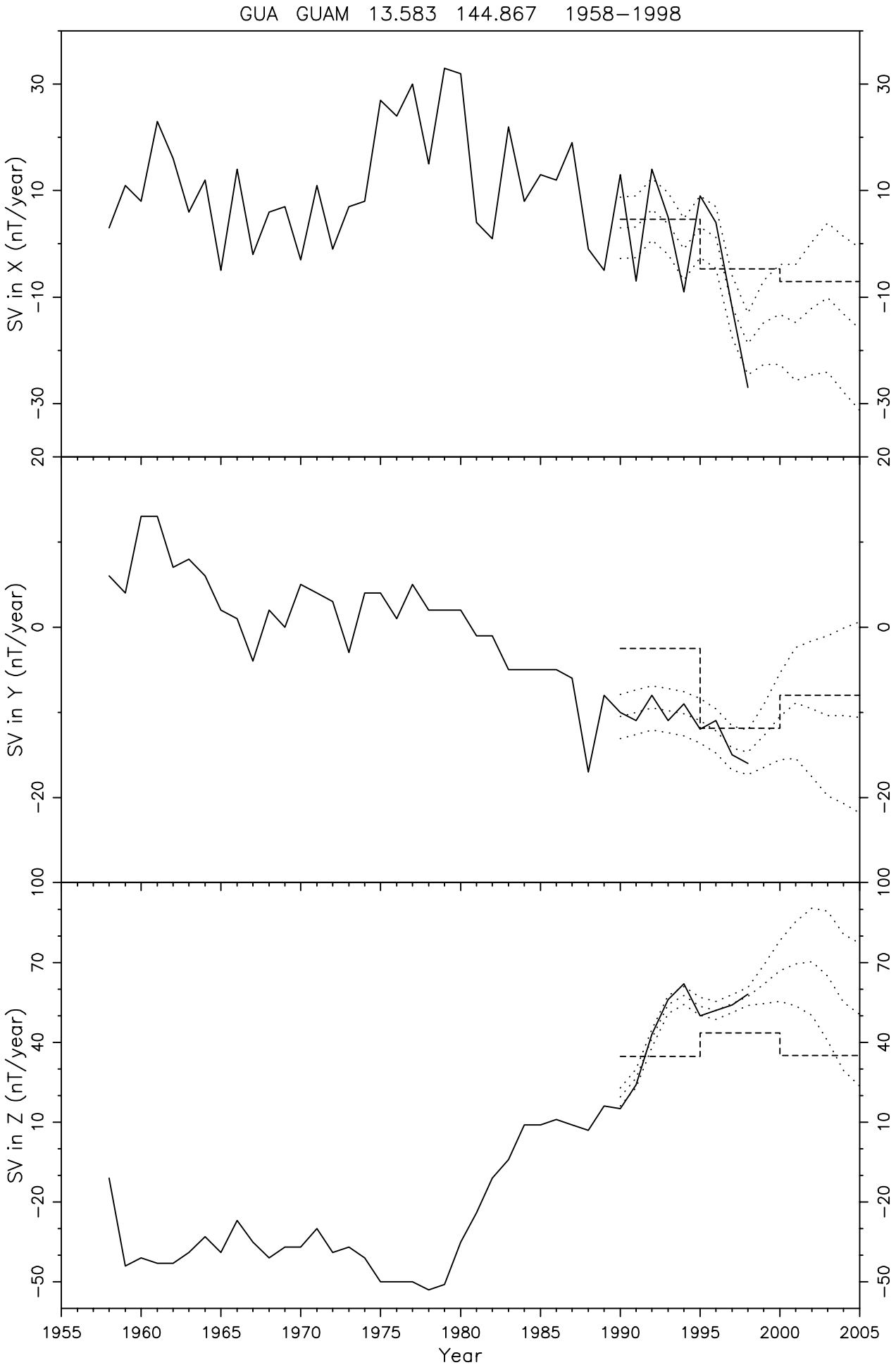
GUA GUAM 13.583 144.867 1958–1998
SV in X (nT/year)
SV in Y (nT/year)
SV in Z (nT/year)
Year
1955
1960
1965
1970
1975
1980
1985
1990
1995
2000
2005

Figure 145

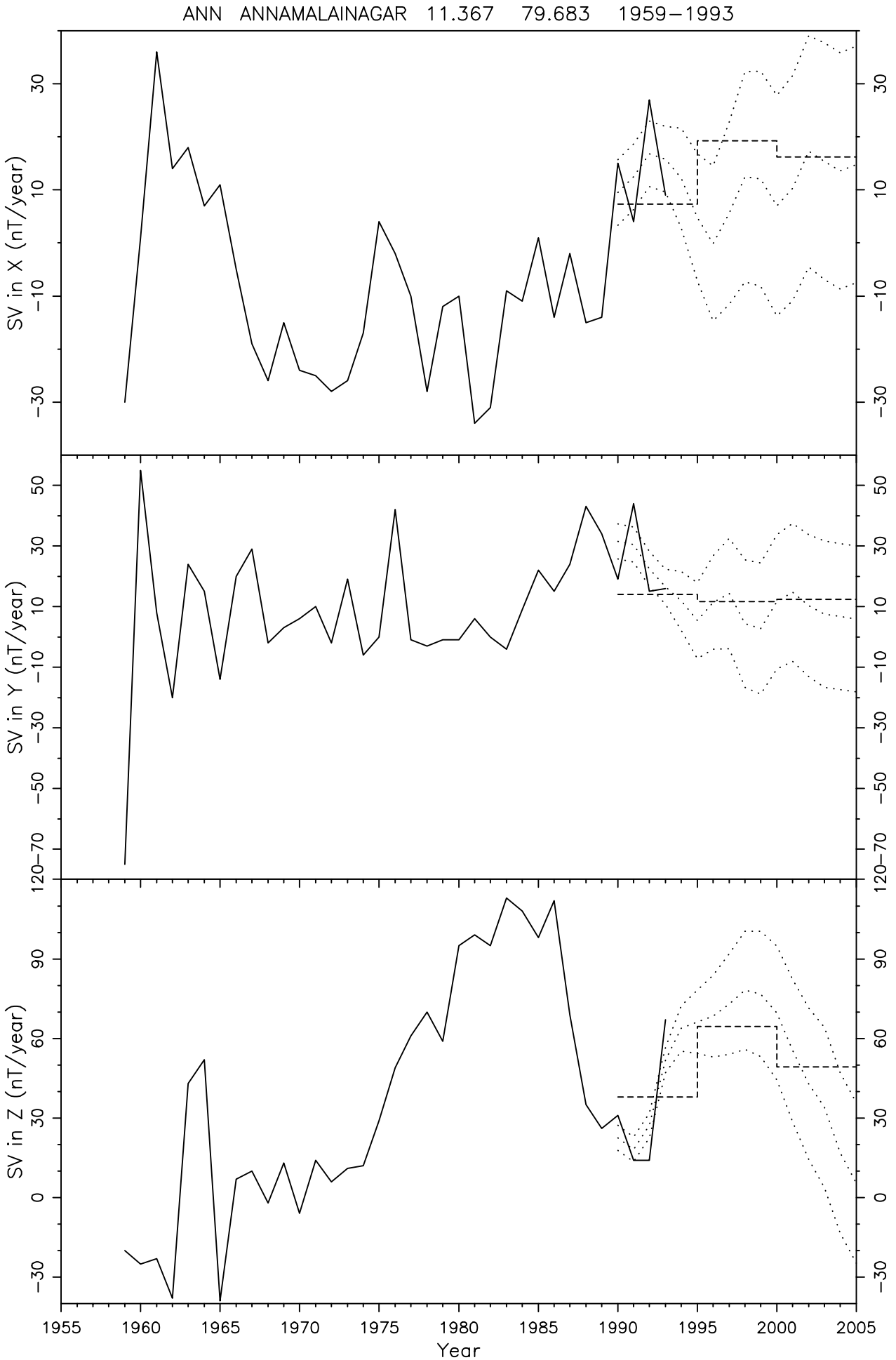
ANN ANNAMALAINAGAR 11.367 79.683 1959–1993
SV in X (nT/year)
SV in Y (nT/year)
SV in Z (nT/year)
Year
1955
1960
1965
1970
1975
1980
1985
1990
1995
2000
2005

Figure 146

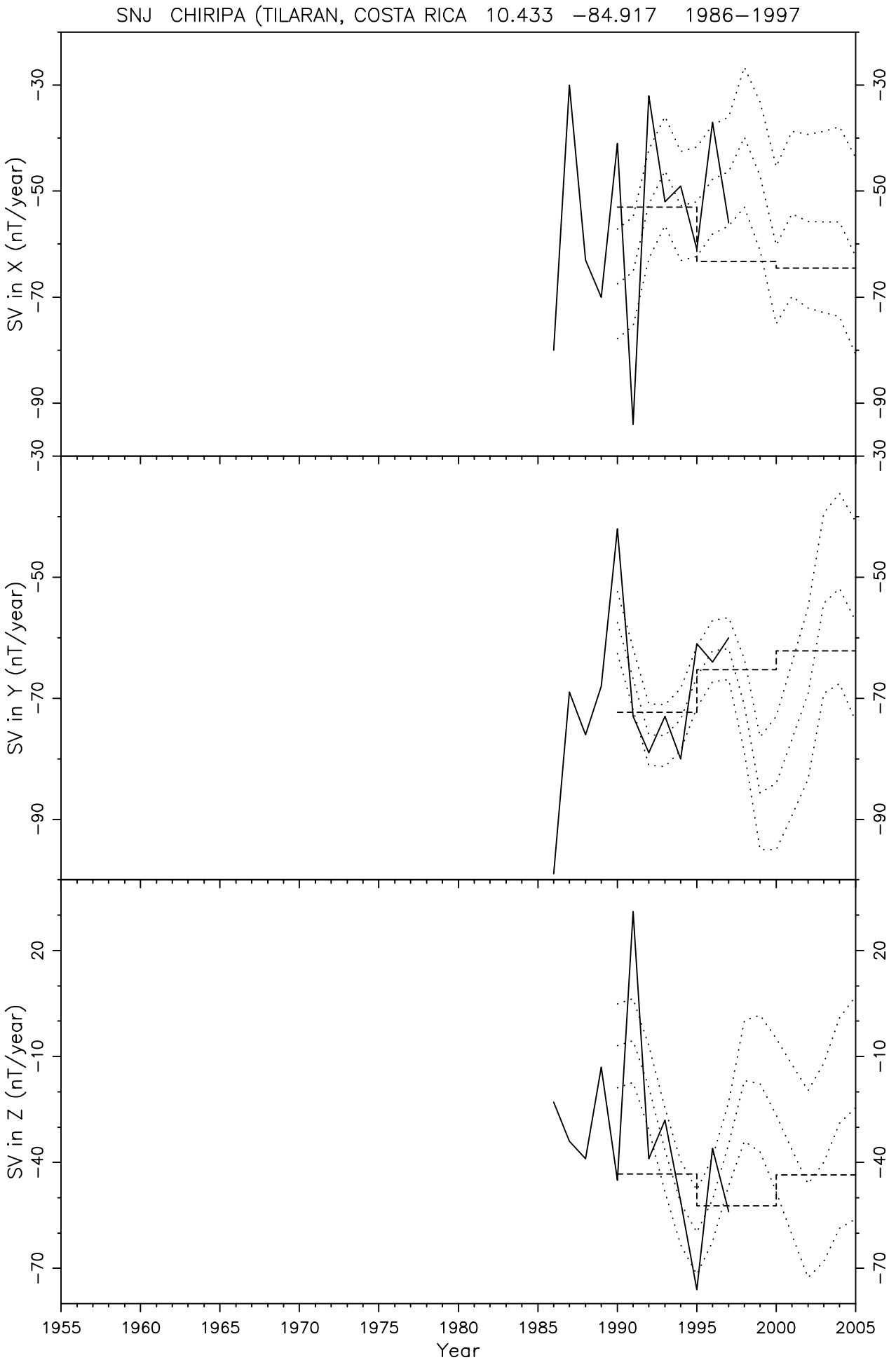
SNJ CHIRIPA (TILARAN, COSTA RICA 10.433 −84.917 1986−1997
SV in X (nT/year)
−30
−50
−70
−90
SV in Y (nT/year)
−50
−70
−90
SV in Z (nT/year)
20
−10
−40
−70
1955
1960
1965
1970
1975
1980
1985
1990
1995
2000
2005
Year

Figure 147

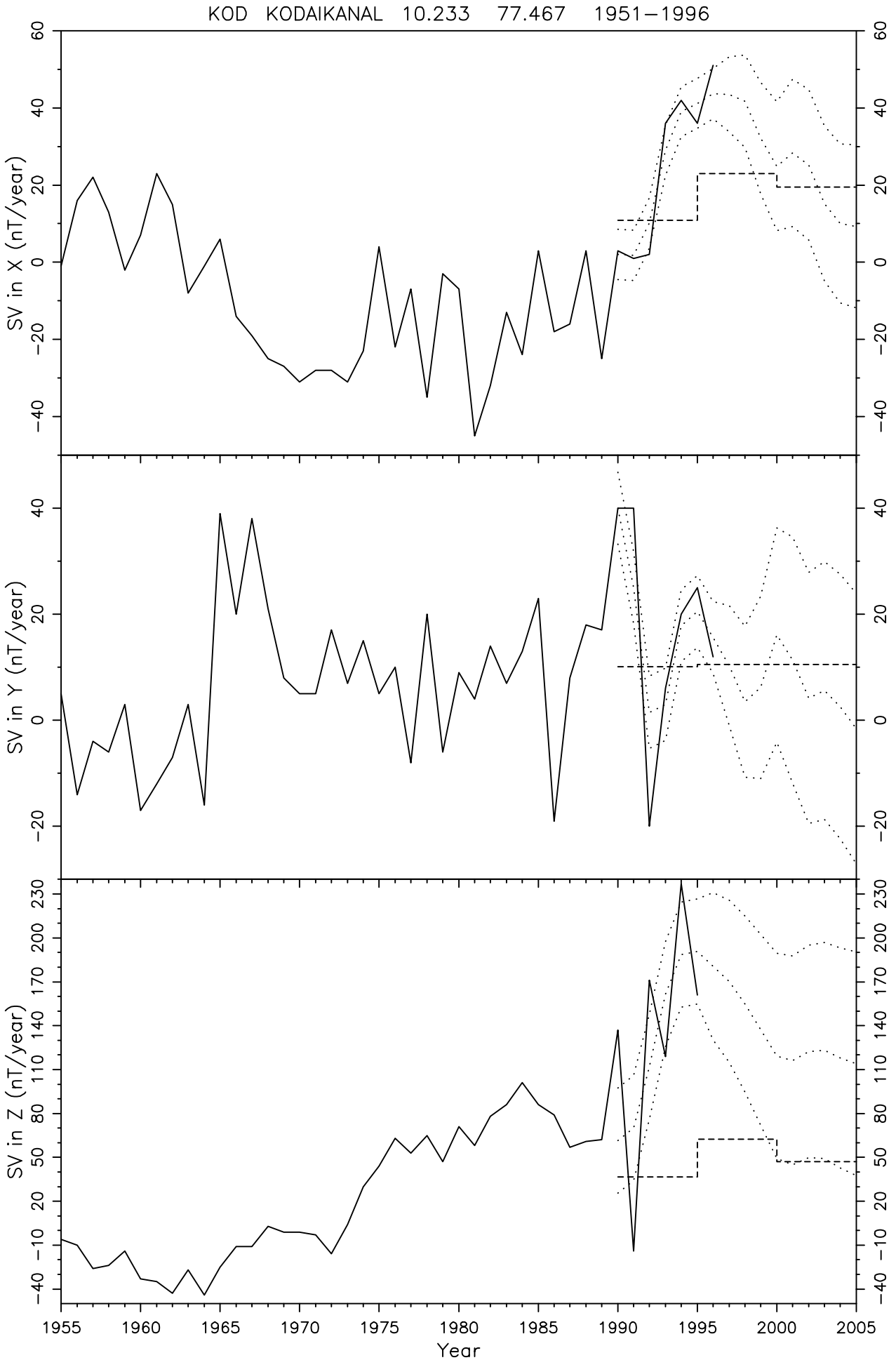
KOD KODAIKANAL 10.233 77.467 1951−1996
SV in X (nT/year)
SV in Y (nT/year)
SV in Z (nT/year)
Year
1955
1960
1965
1970
1975
1980
1985
1990
1995
2000
2005

Figure 148

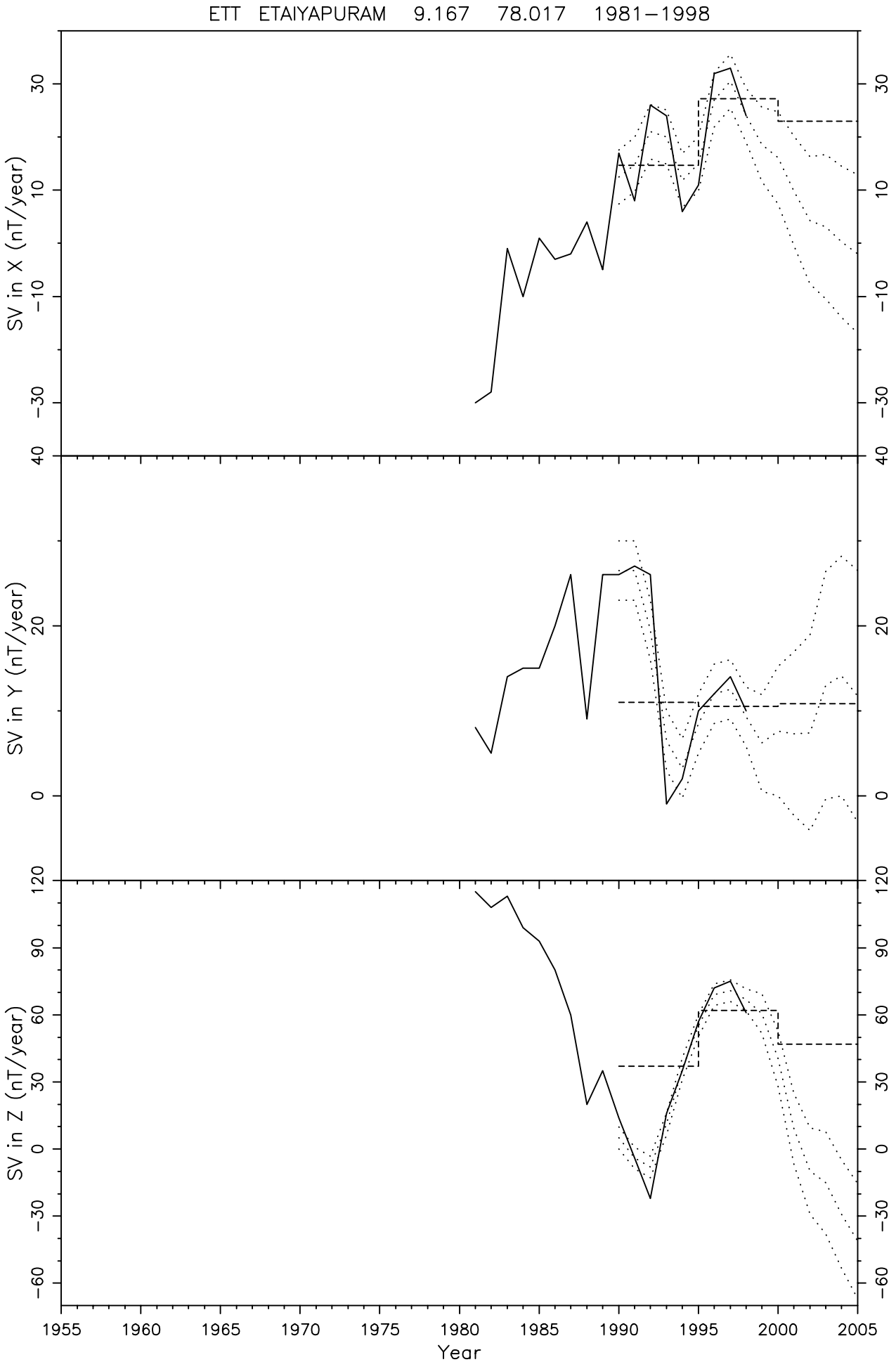
ETT ETAIYAPURAM 9.167 78.017 1981–1998
SV in X (nT/year)
SV in Y (nT/year)
SV in Z (nT/year)
Year
1955
1960
1965
1970
1975
1980
1985
1990
1995
2000
2005

Figure 149

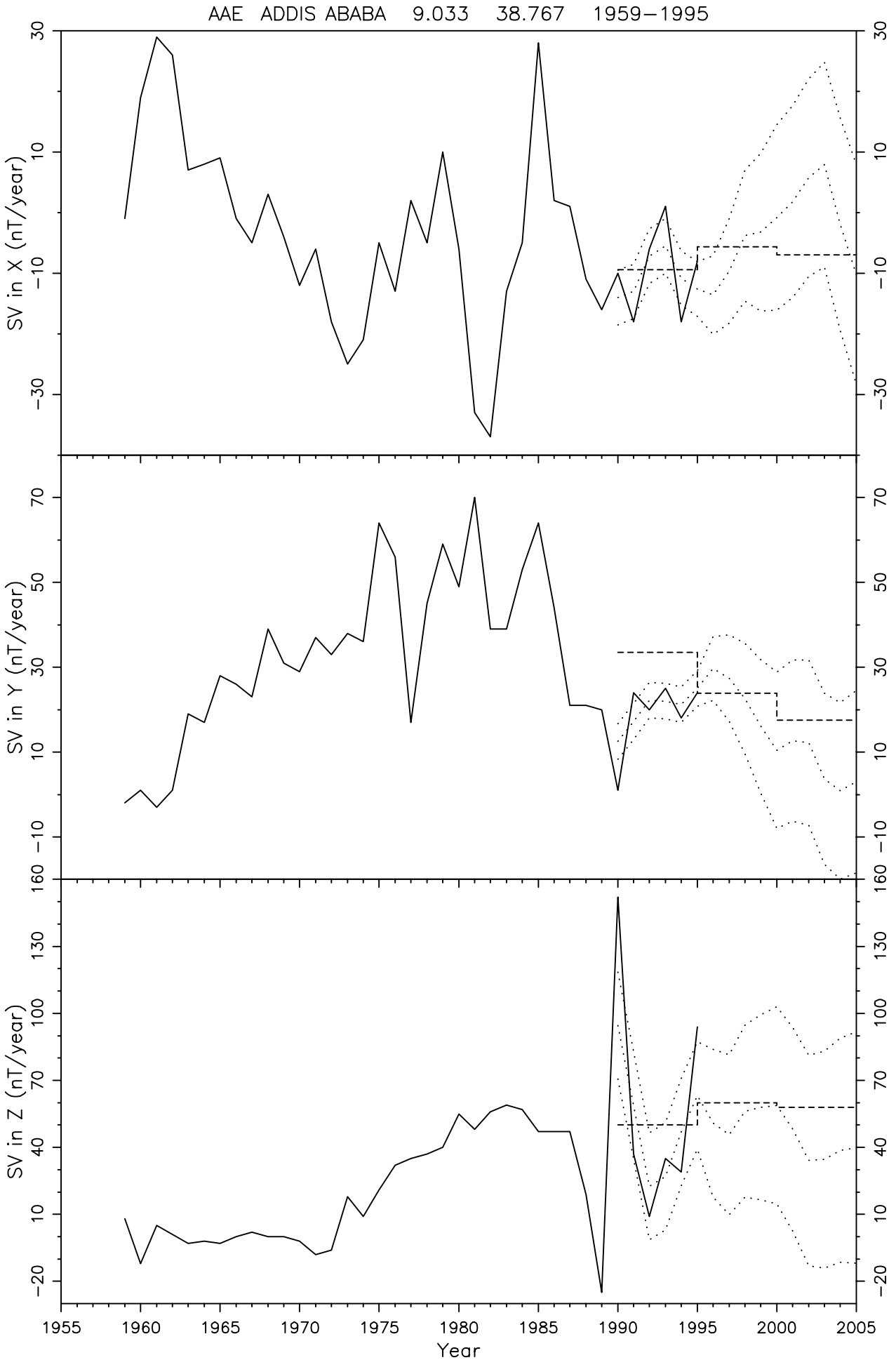
AAE ADDIS ABABA 9.033 38.767 1959–1995
SV in X (nT/year)
SV in Y (nT/year)
SV in Z (nT/year)
Year
1955
1960
1965
1970
1975
1980
1985
1990
1995
2000
2005

Figure 150

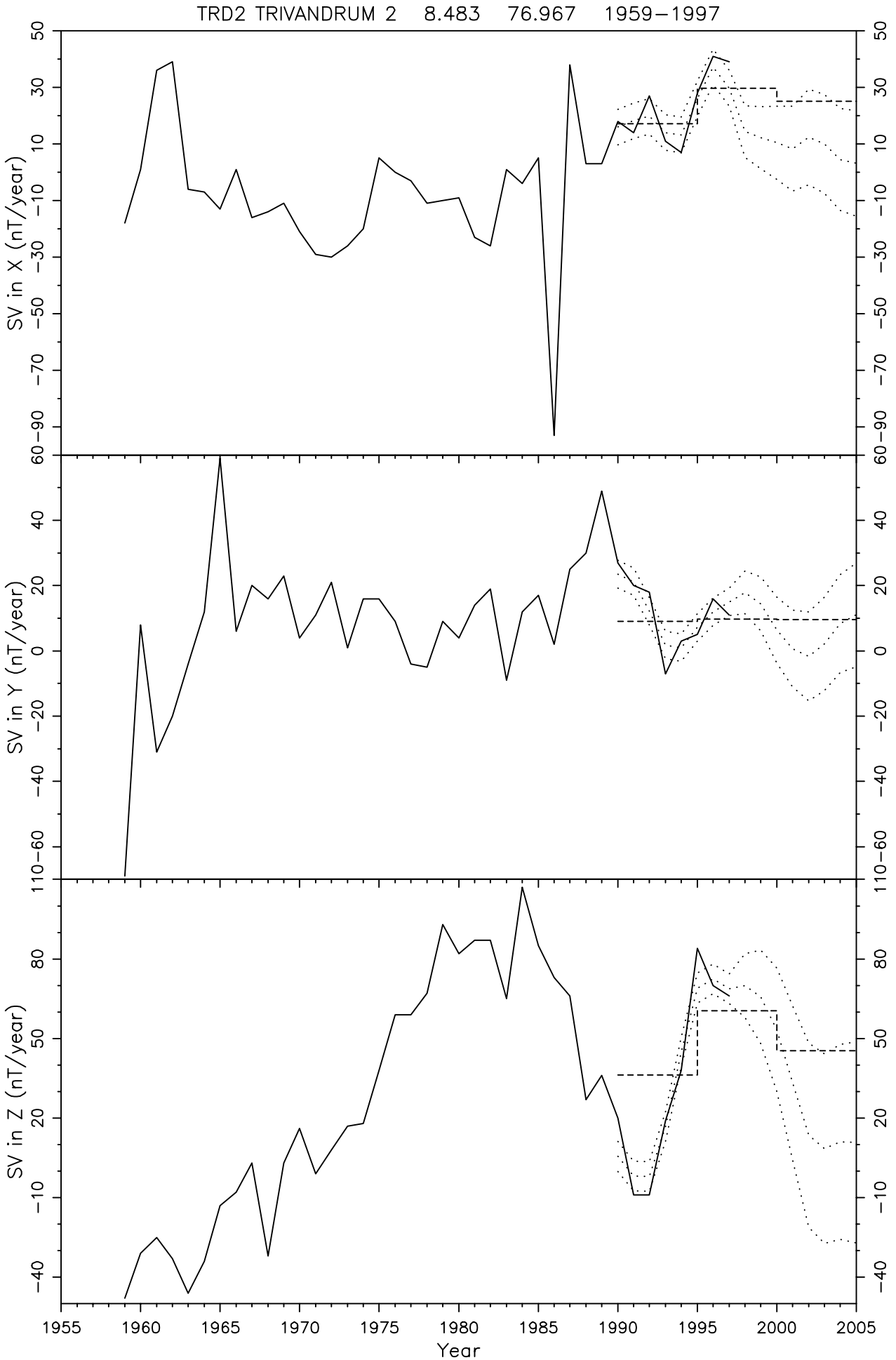
TRD2 TRIVANDRUM 2 8.483 76.967 1959–1997
SV in X (nT/year)
SV in Y (nT/year)
SV in Z (nT/year)
Year
1955
1960
1965
1970
1975
1980
1985
1990
1995
2000
2005

Figure 151

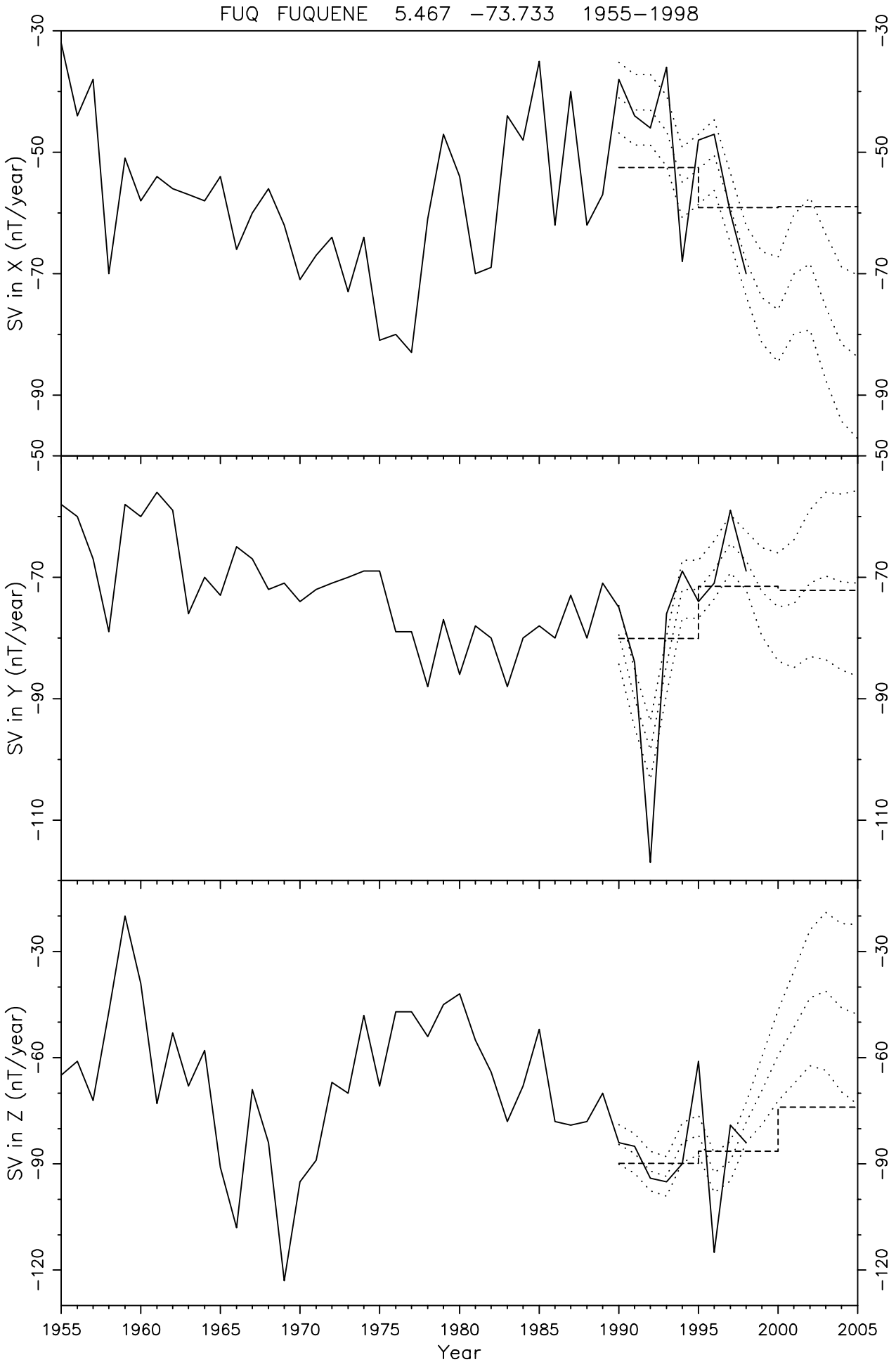
FUQ FUQUENE 5.467 −73.733 1955−1998
SV in X (nT/year)
SV in Y (nT/year)
SV in Z (nT/year)
Year
1955
1960
1965
1970
1975
1980
1985
1990
1995
2000
2005

Figure 152

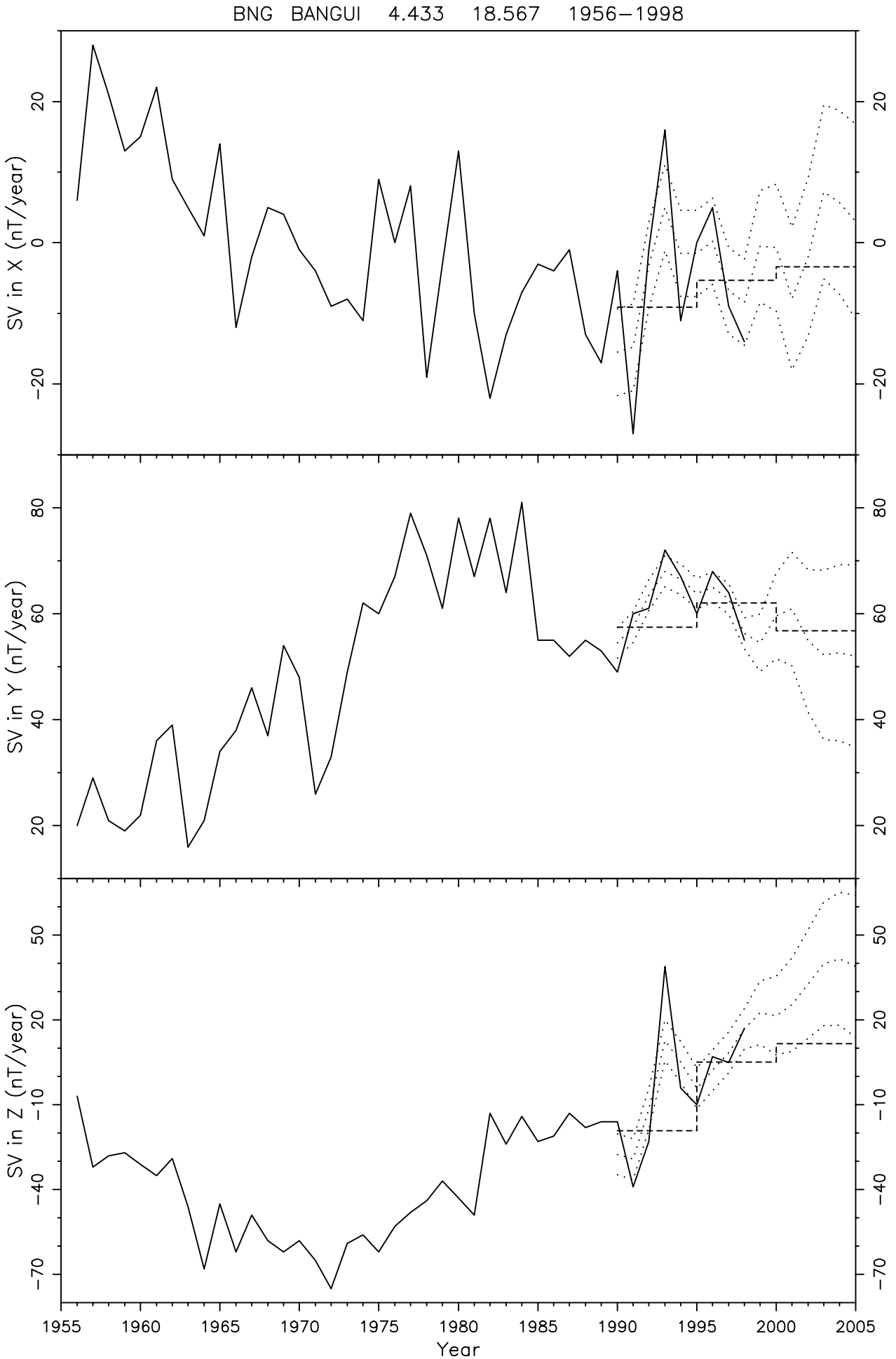
BNG BANGUI 4.433 18.567 1956–1998
SV in X (nT/year)
SV in Y (nT/year)
SV in Z (nT/year)
Year
1955
1960
1965
1970
1975
1980
1985
1990
1995
2000
2005

Figure 153

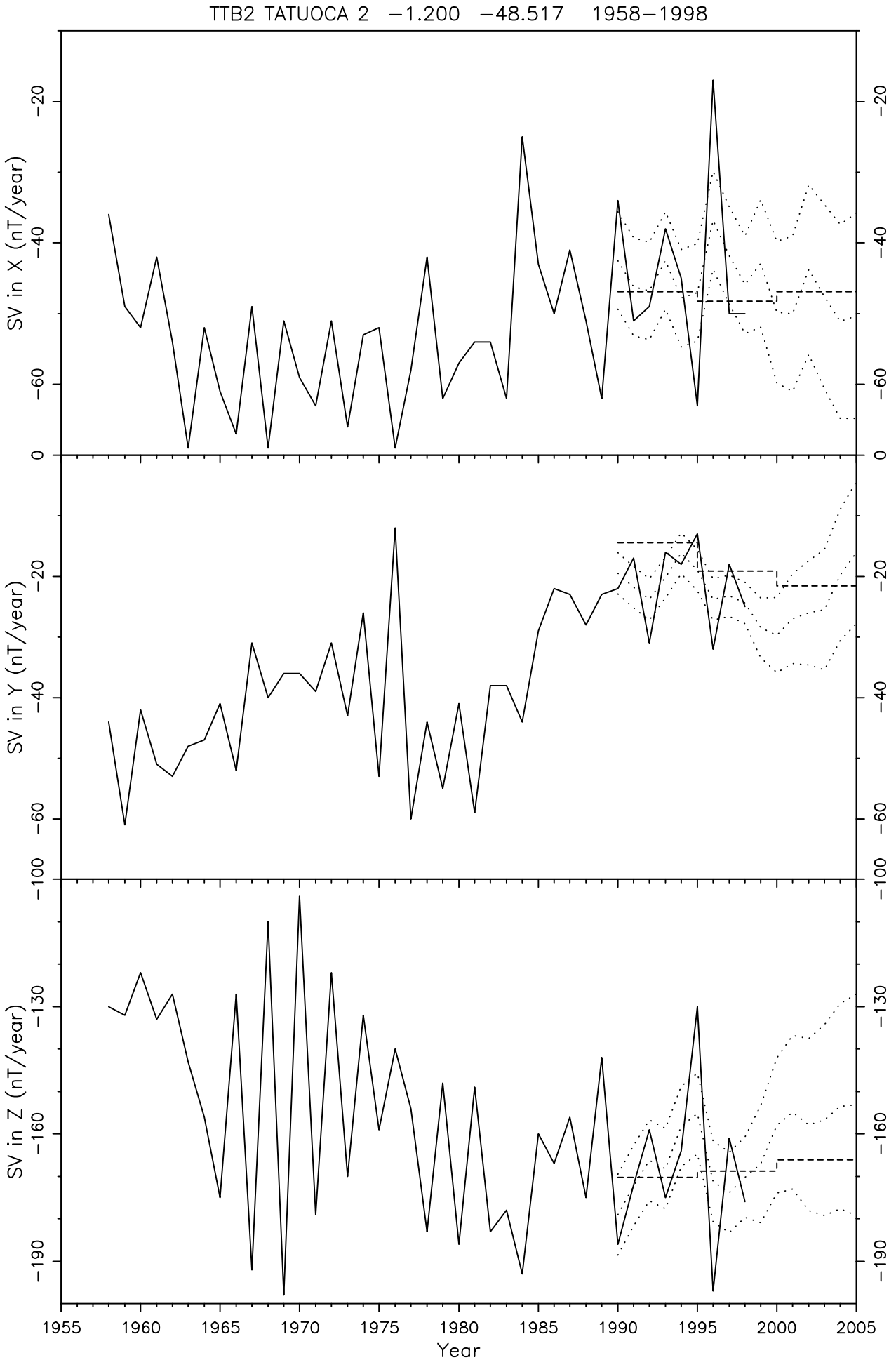
TTB2 TATUOCA 2 −1.200 −48.517 1958−1998
SV in X (nT/year)
SV in Y (nT/year)
SV in Z (nT/year)
0
−20
−40
−60
−100
−130
−160
−190
1955
1960
1965
1970
1975
1980
1985
1990
1995
2000
2005
Year

Figure 154

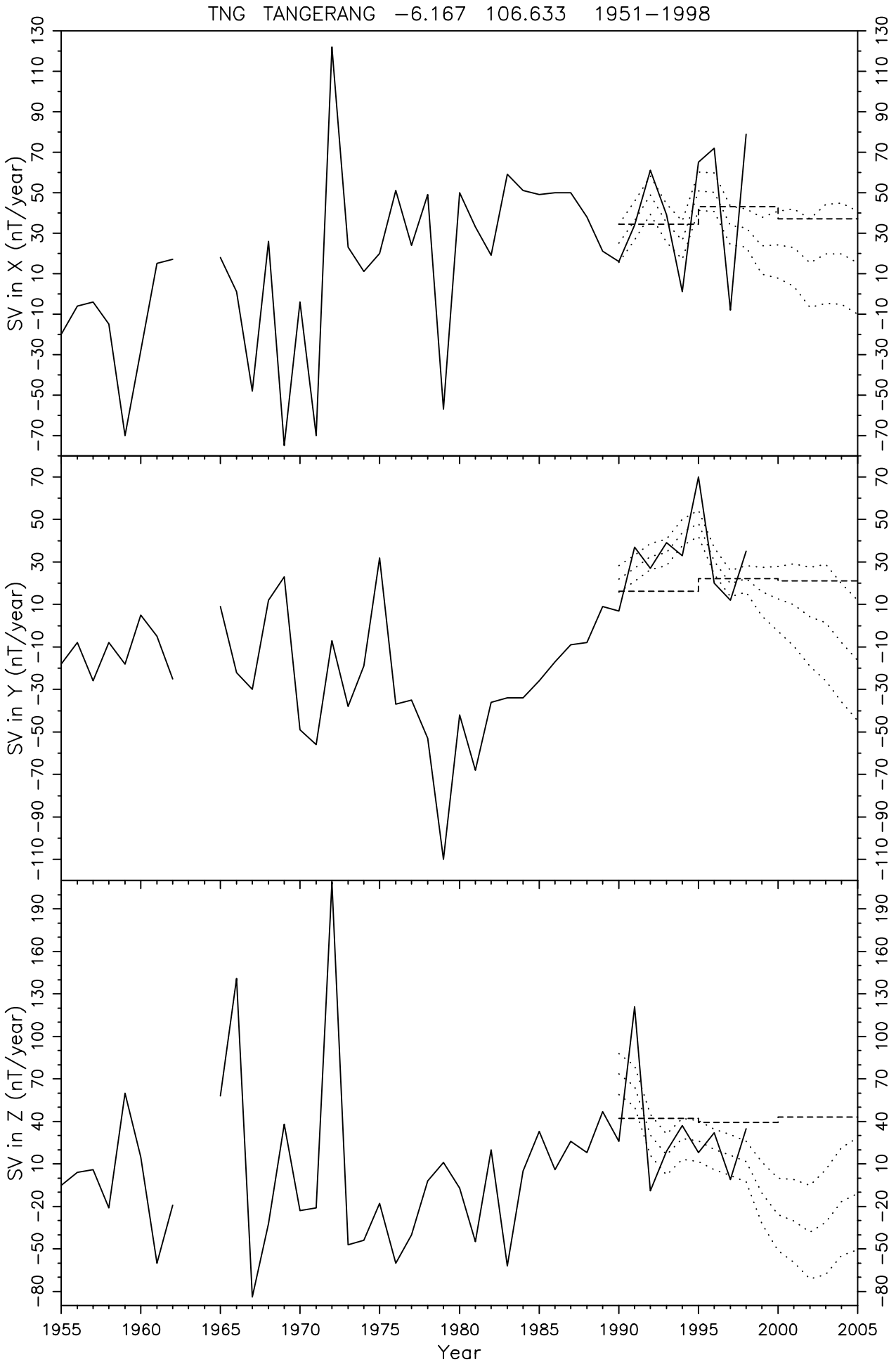
TNG TANGERANG −6.167 106.633 1951−1998
SV in X (nT/year)
SV in Y (nT/year)
SV in Z (nT/year)
Year
1955
1960
1965
1970
1975
1980
1985
1990
1995
2000
2005

Figure 155

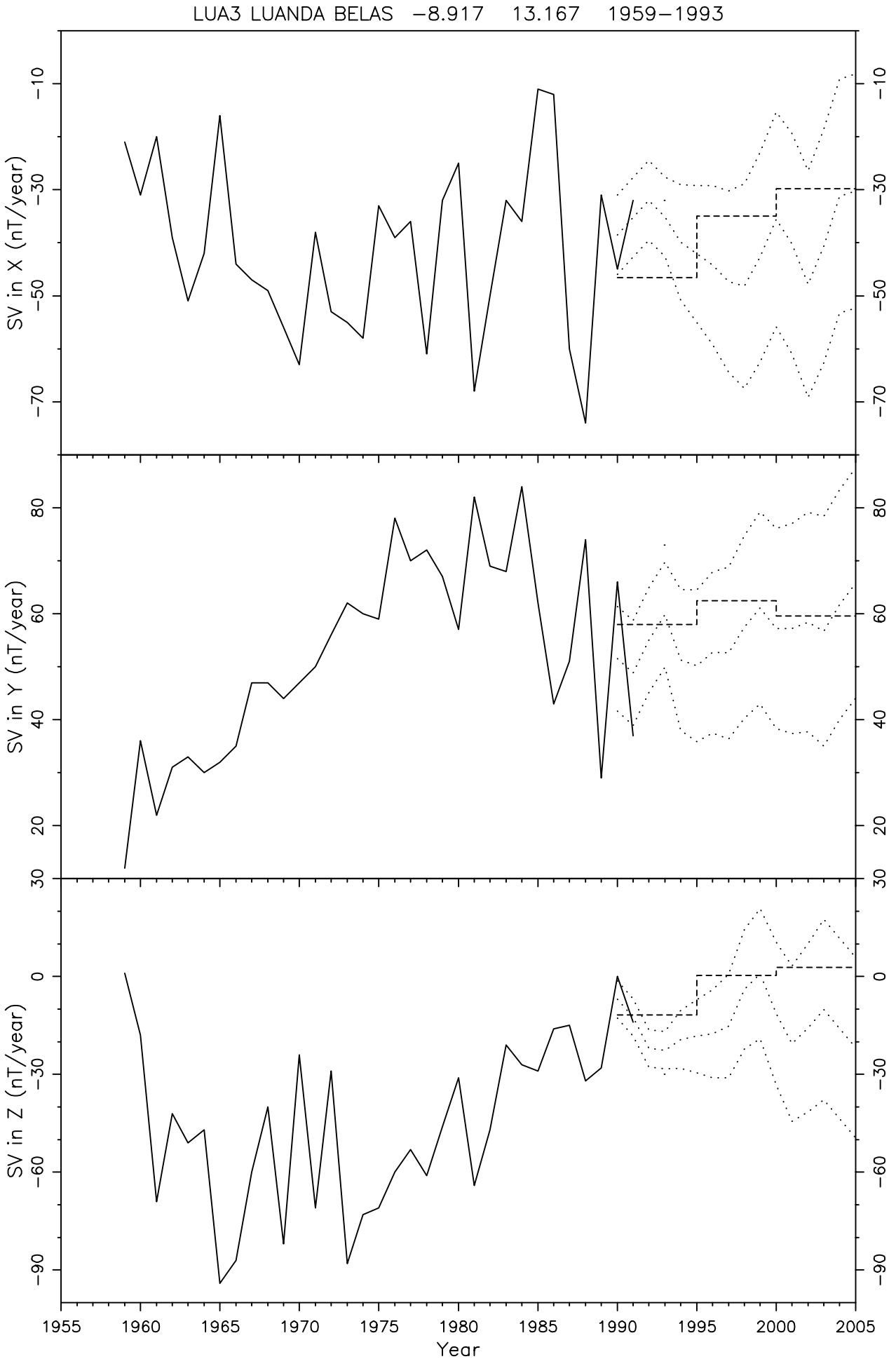
LUA3 LUANDA BELAS −8.917 13.167 1959−1993
SV in X (nT/year)
−10
−30
−50
−70
SV in Y (nT/year)
80
60
40
20
30
SV in Z (nT/year)
0
−30
−60
−90
1955
1960
1965
1970
1975
1980
1985
1990
1995
2000
2005
Year

Figure 156

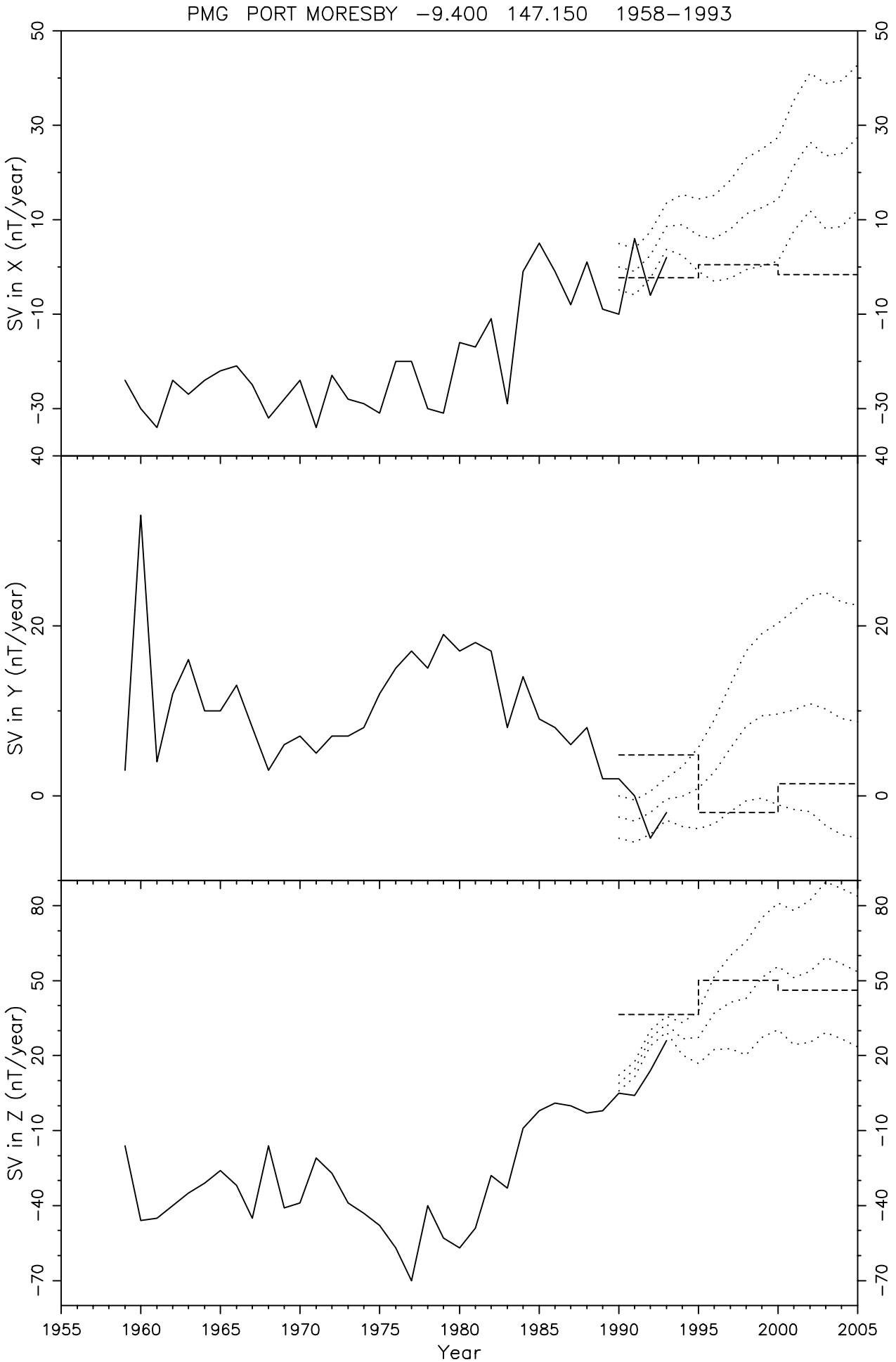
PMG PORT MORESBY −9.400 147.150 1958−1993
SV in X (nT/year)
SV in Y (nT/year)
SV in Z (nT/year)
Year
1955
1960
1965
1970
1975
1980
1985
1990
1995
2000
2005

Figure 157

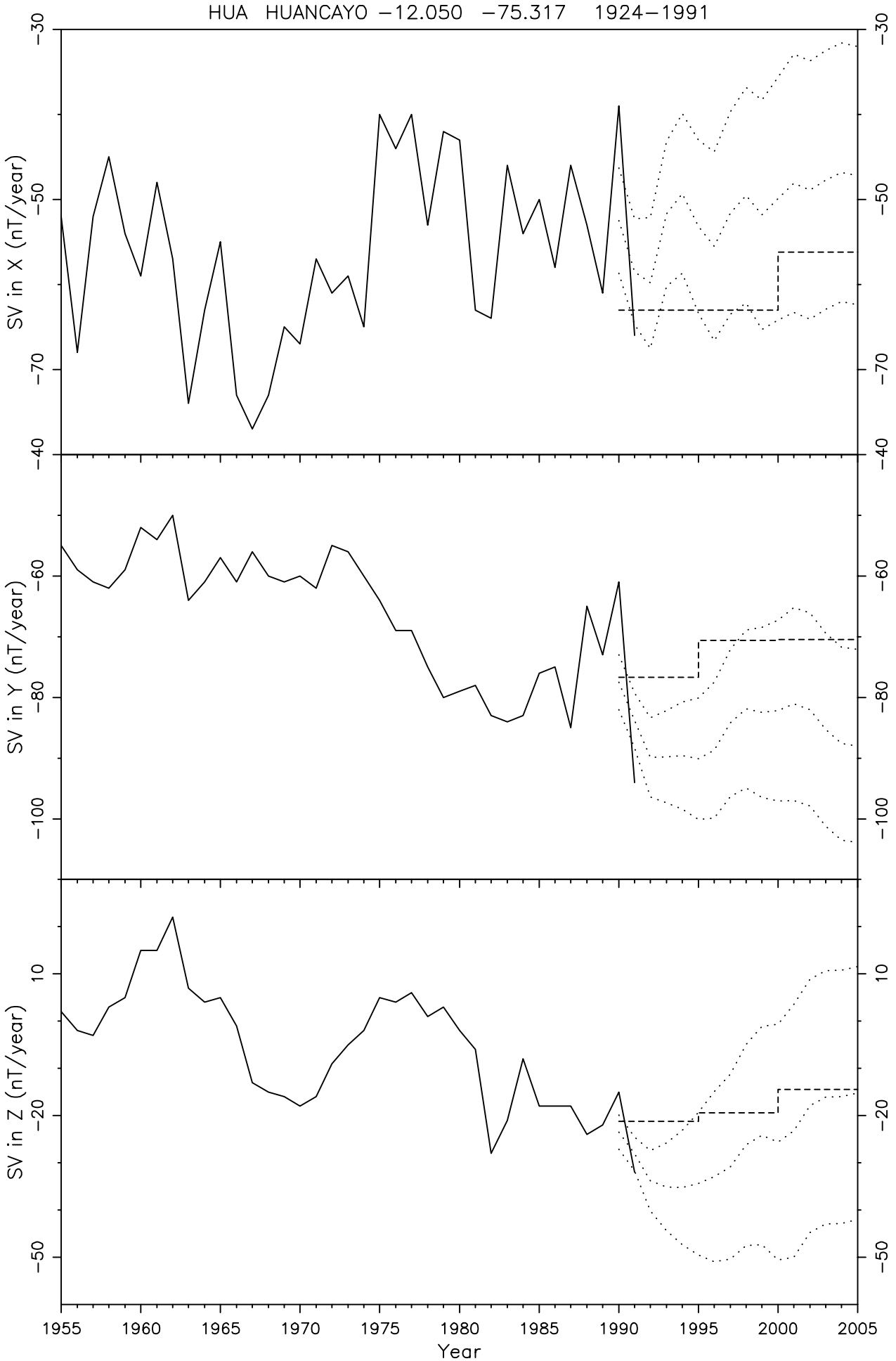
HUA HUANCAYO −12.050 −75.317 1924−1991
SV in X (nT/year)
−30
−50
−70
−40
SV in Y (nT/year)
−60
−80
−100
SV in Z (nT/year)
10
−20
−50
1955
1960
1965
1970
1975
1980
1985
1990
1995
2000
2005
Year

Figure 158

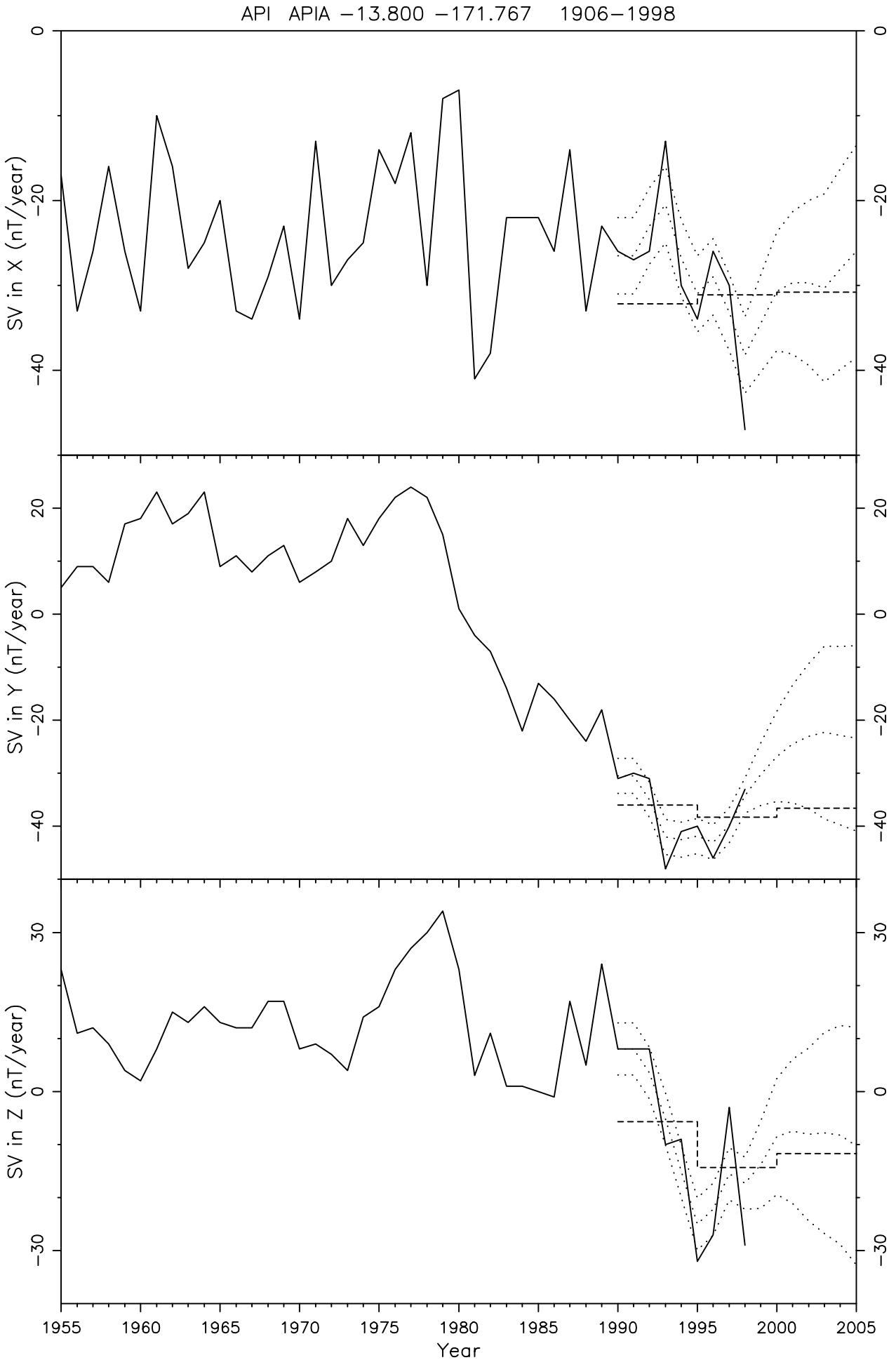
API APIA −13.800 −171.767 1906−1998
SV in X (nT/year)
SV in Y (nT/year)
SV in Z (nT/year)
0
−20
−40
20
30
−30
1955
1960
1965
1970
1975
1980
1985
1990
1995
2000
2005
Year

Figure 159

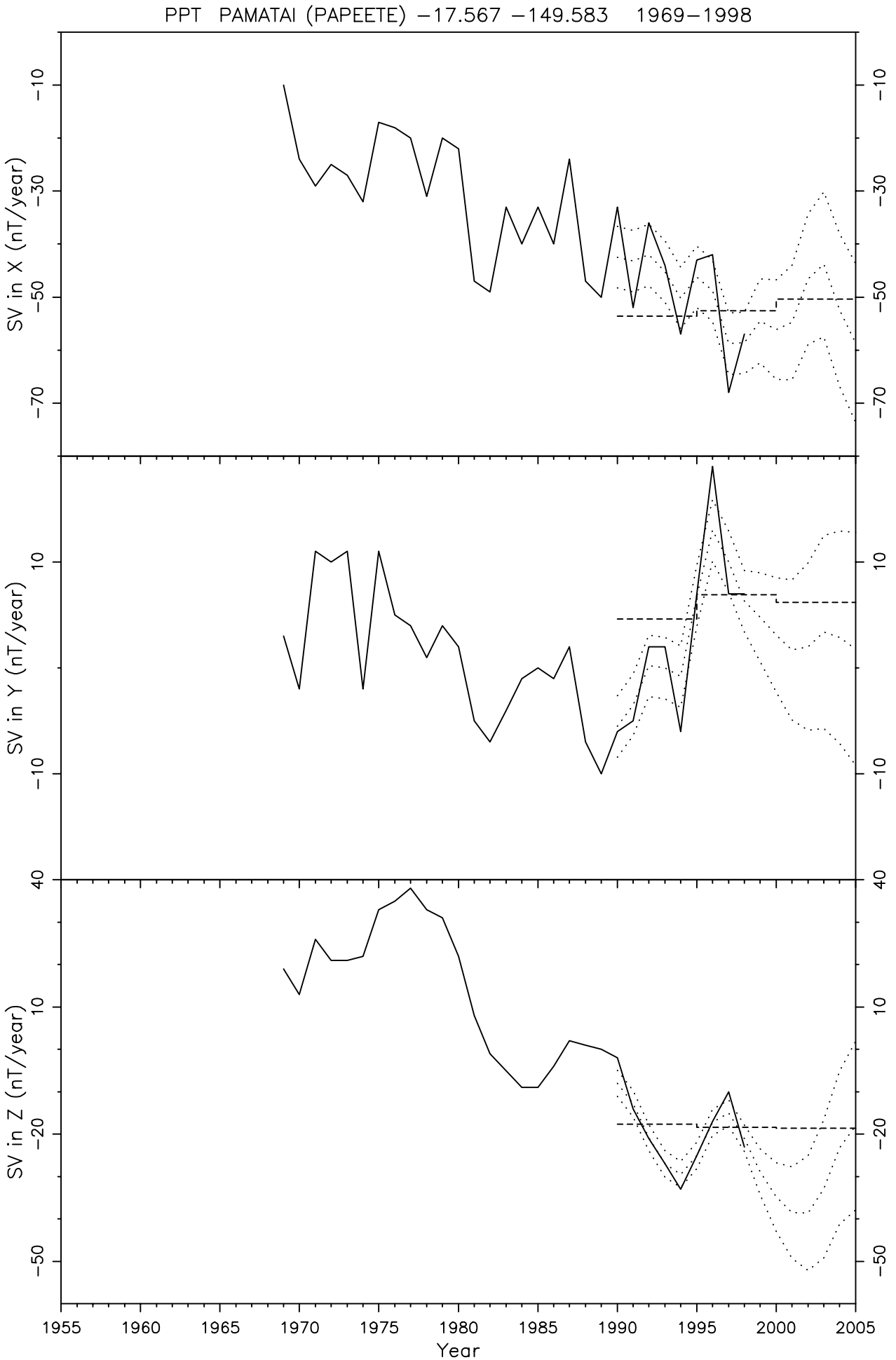
PPT PAMATAI (PAPEETE) −17.567 −149.583 1969−1998
SV in X (nT/year)
SV in Y (nT/year)
SV in Z (nT/year)
Year
1955
1960
1965
1970
1975
1980
1985
1990
1995
2000
2005

Figure 160

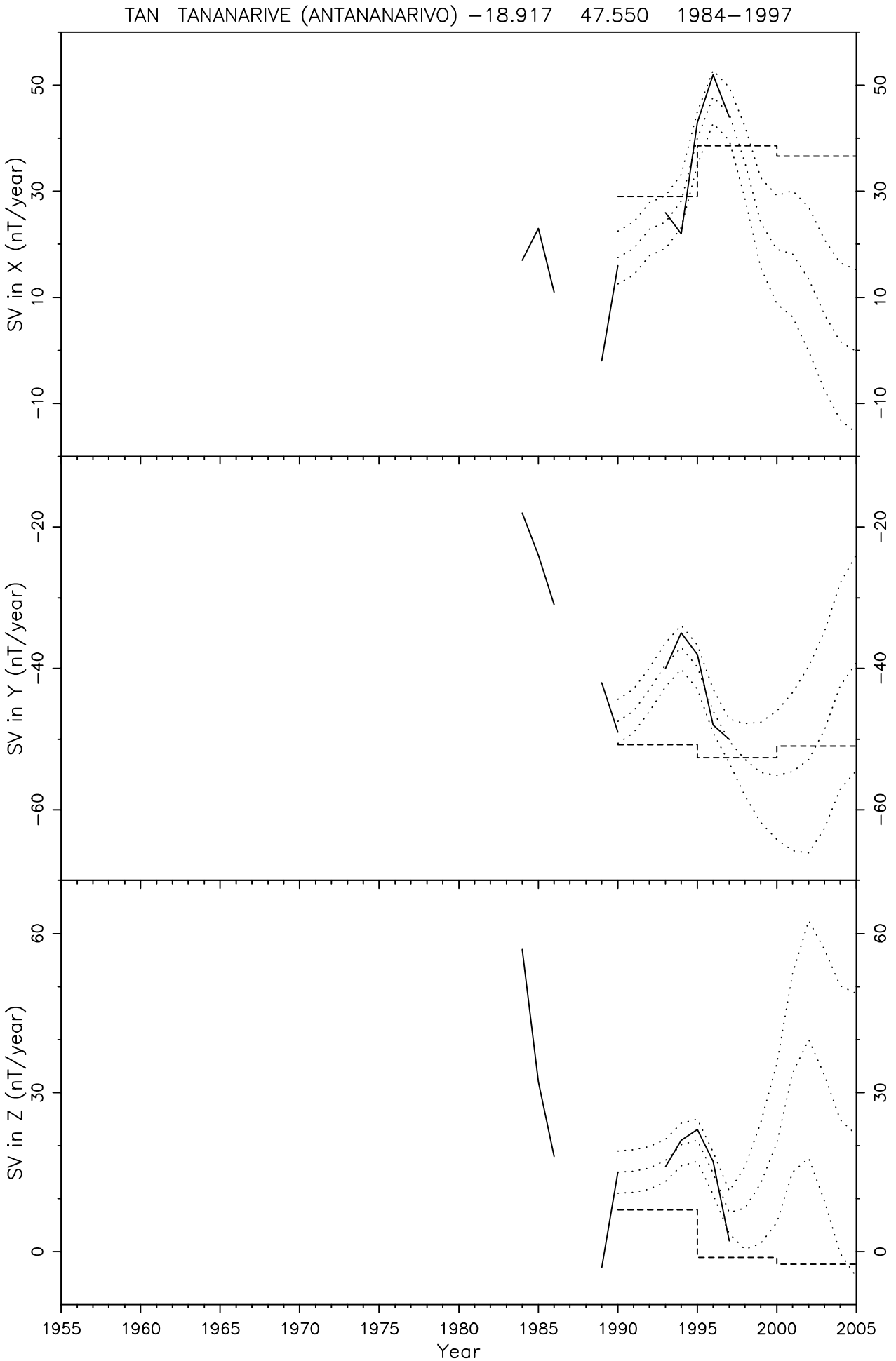
TAN TANANARIVE (ANTANANARIVO) −18.917 47.550 1984−1997
SV in X (nT/year)
SV in Y (nT/year)
SV in Z (nT/year)
Year
1955
1960
1965
1970
1975
1980
1985
1990
1995
2000
2005

Figure 161

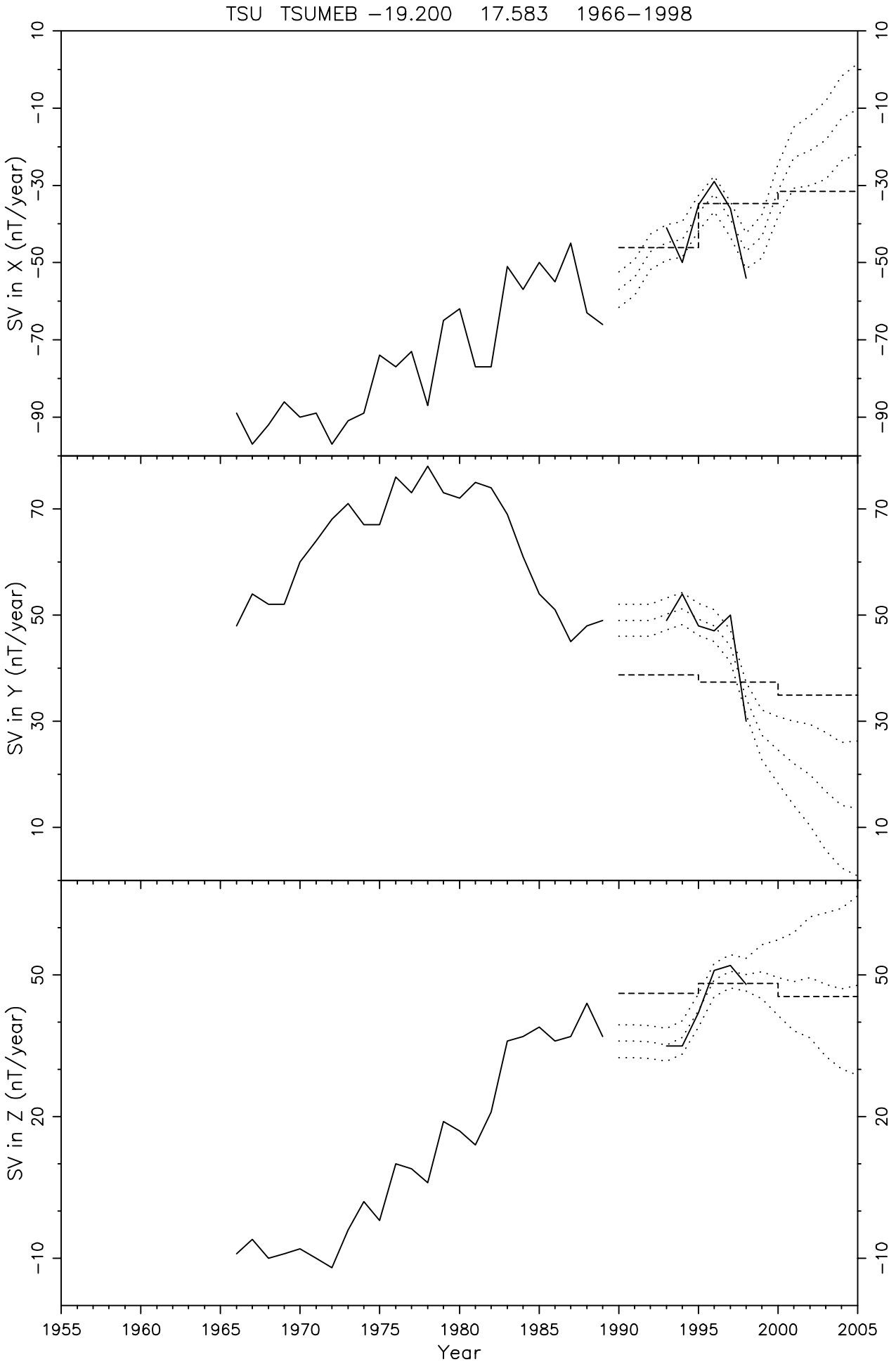
TSU TSUMEB −19.200 17.583 1966−1998
SV in X (nT/year)
SV in Y (nT/year)
SV in Z (nT/year)
Year
1955
1960
1965
1970
1975
1980
1985
1990
1995
2000
2005

Figure 162

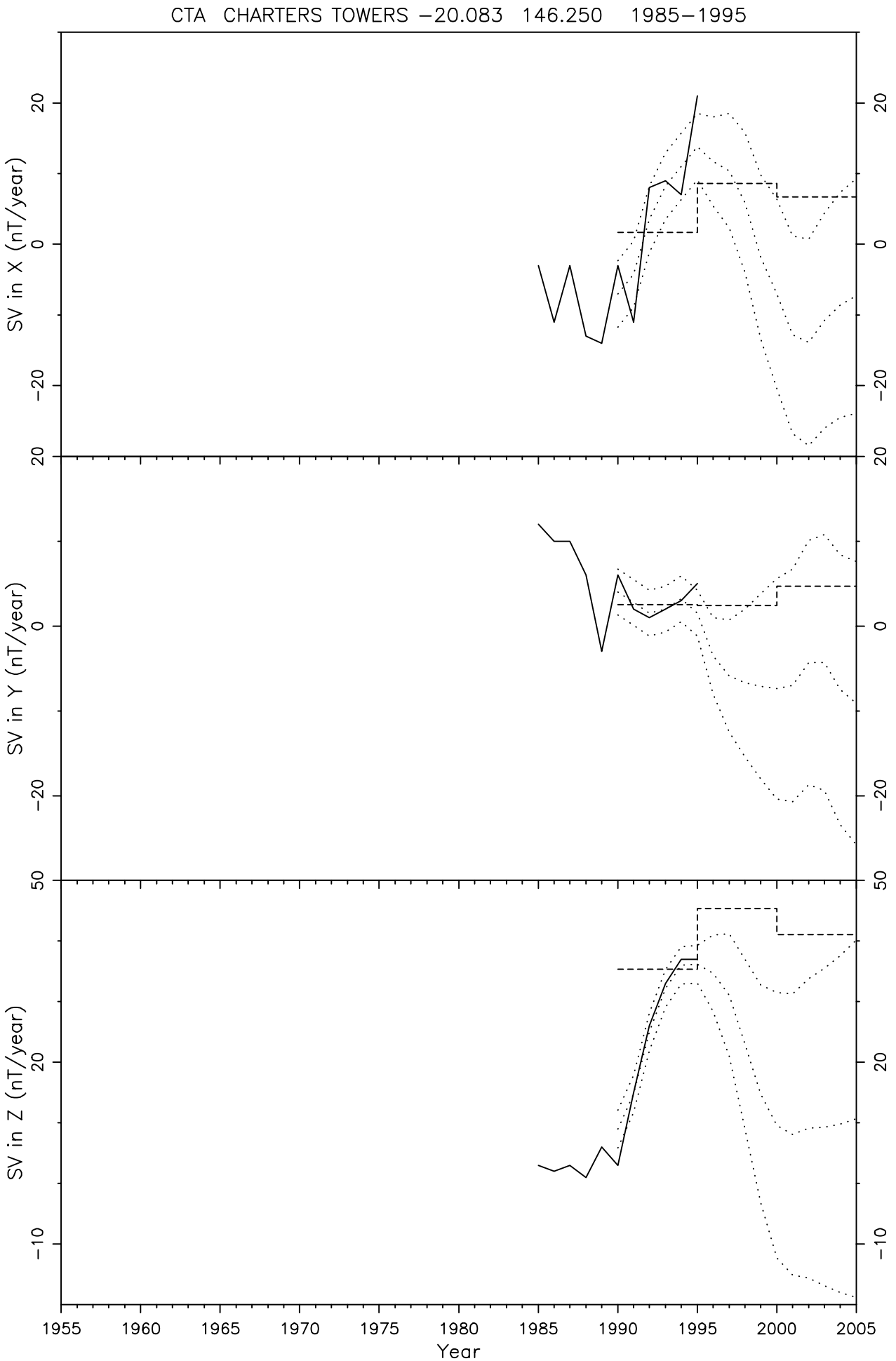
CTA CHARTERS TOWERS −20.083 146.250 1985−1995
SV in X (nT/year)
SV in Y (nT/year)
SV in Z (nT/year)
Year
1955
1960
1965
1970
1975
1980
1985
1990
1995
2000
2005

Figure 163

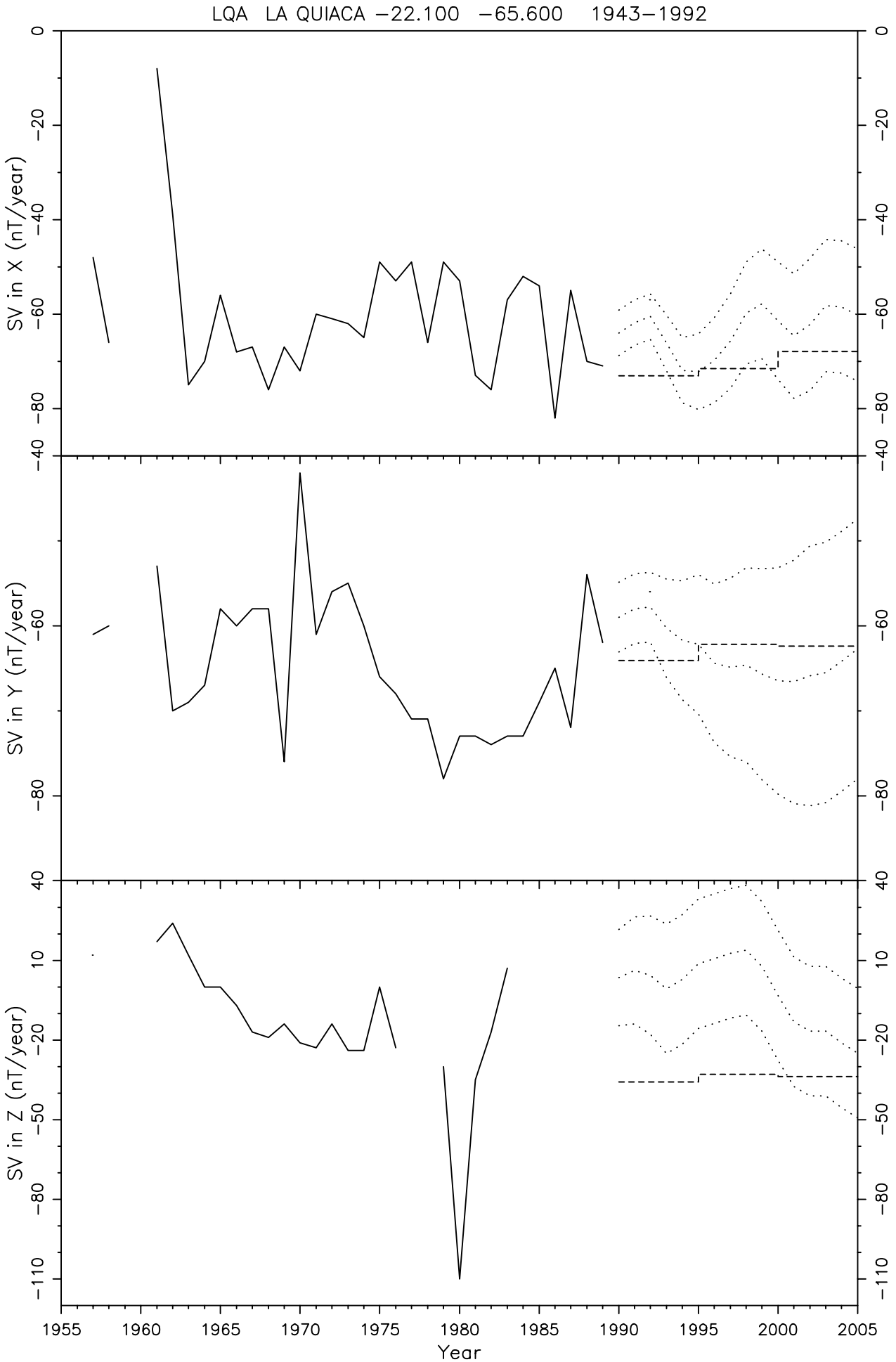
LQA LA QUIACA −22.100 −65.600 1943−1992
SV in X (nT/year)
SV in Y (nT/year)
SV in Z (nT/year)
Year
1955
1960
1965
1970
1975
1980
1985
1990
1995
2000
2005

Figure 164

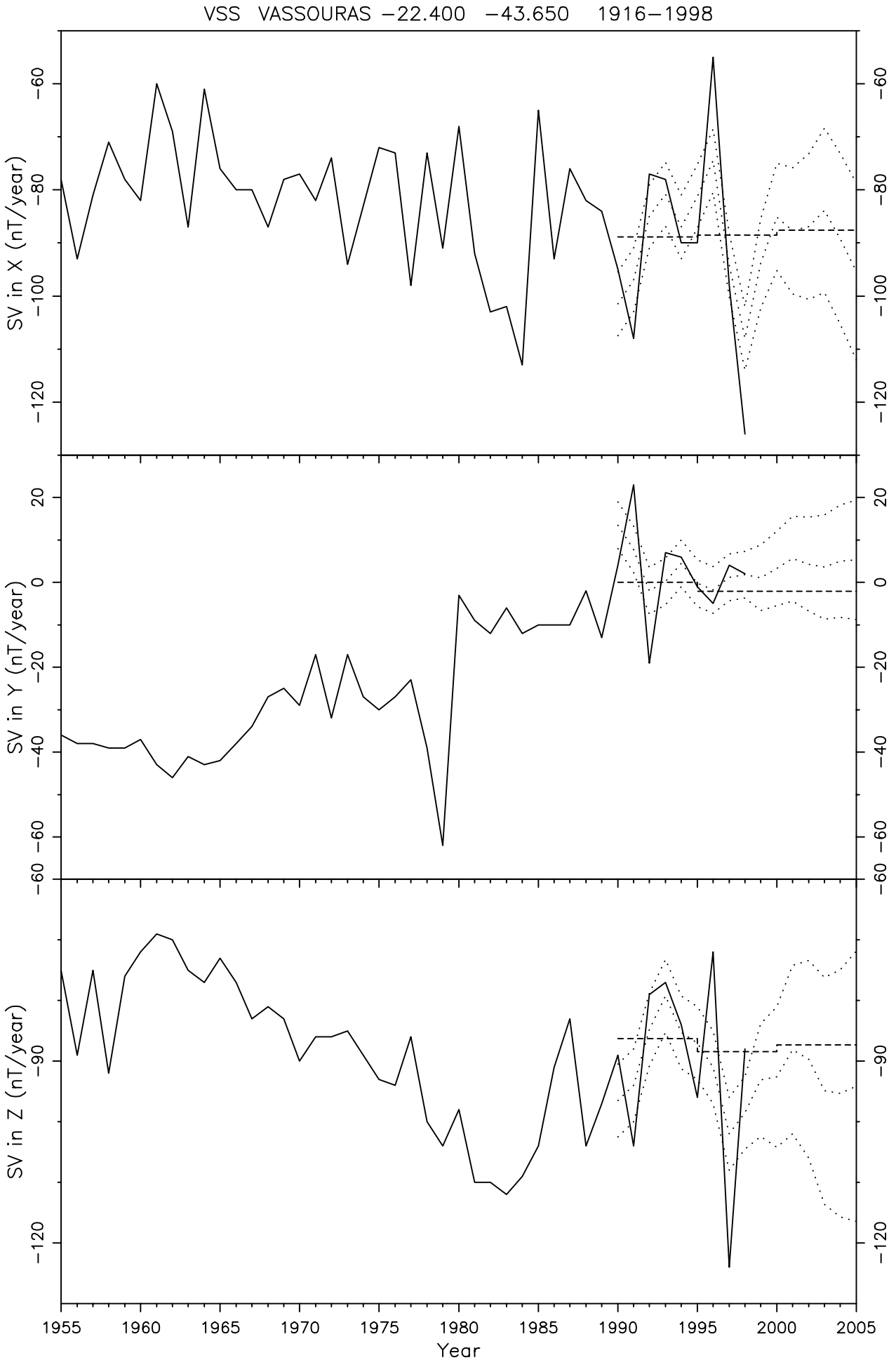
VSS VASSOURAS −22.400 −43.650 1916−1998
SV in X (nT/year)
SV in Y (nT/year)
SV in Z (nT/year)
Year
1955
1960
1965
1970
1975
1980
1985
1990
1995
2000
2005

Figure 165

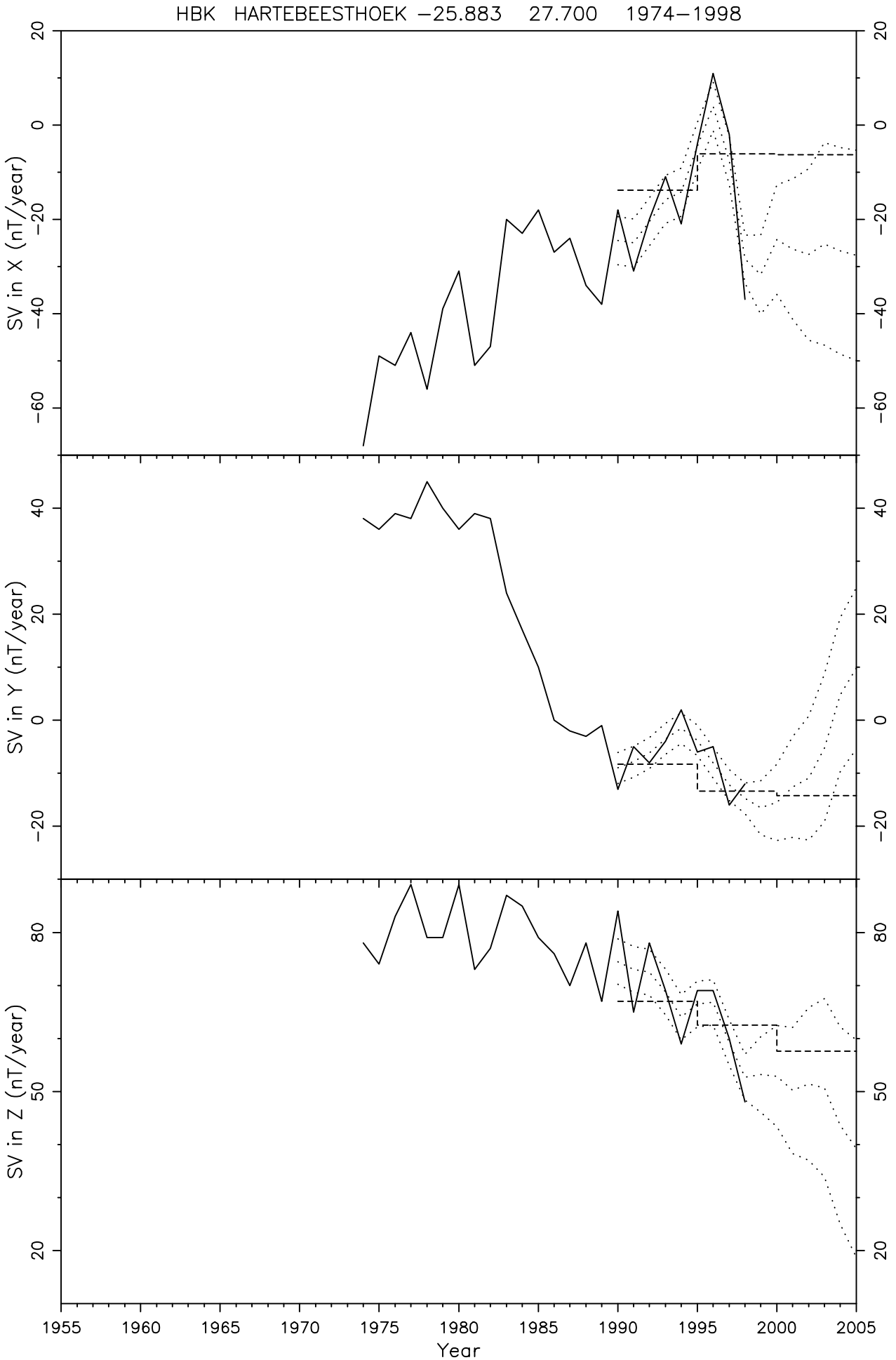
HBK HARTEBEESTHOEK −25.883 27.700 1974−1998
SV in X (nT/year)
SV in Y (nT/year)
SV in Z (nT/year)
Year
1955
1960
1965
1970
1975
1980
1985
1990
1995
2000
2005

Figure 166

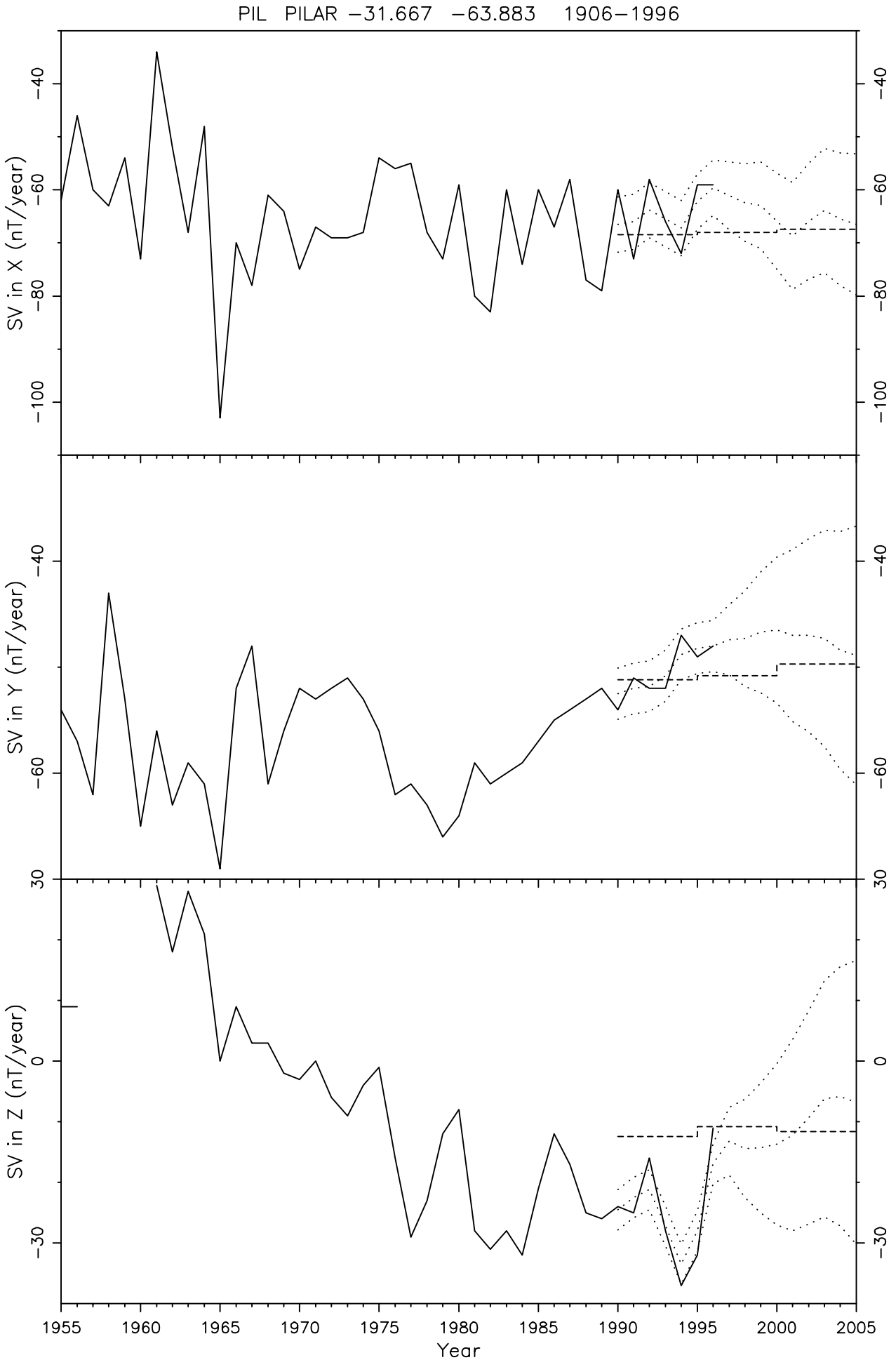
PIL PILAR −31.667 −63.883 1906−1996
SV in X (nT/year)
−40
−60
−80
−100
SV in Y (nT/year)
−40
−60
30
SV in Z (nT/year)
0
−30
1955
1960
1965
1970
1975
1980
1985
1990
1995
2000
2005
Year

Figure 167

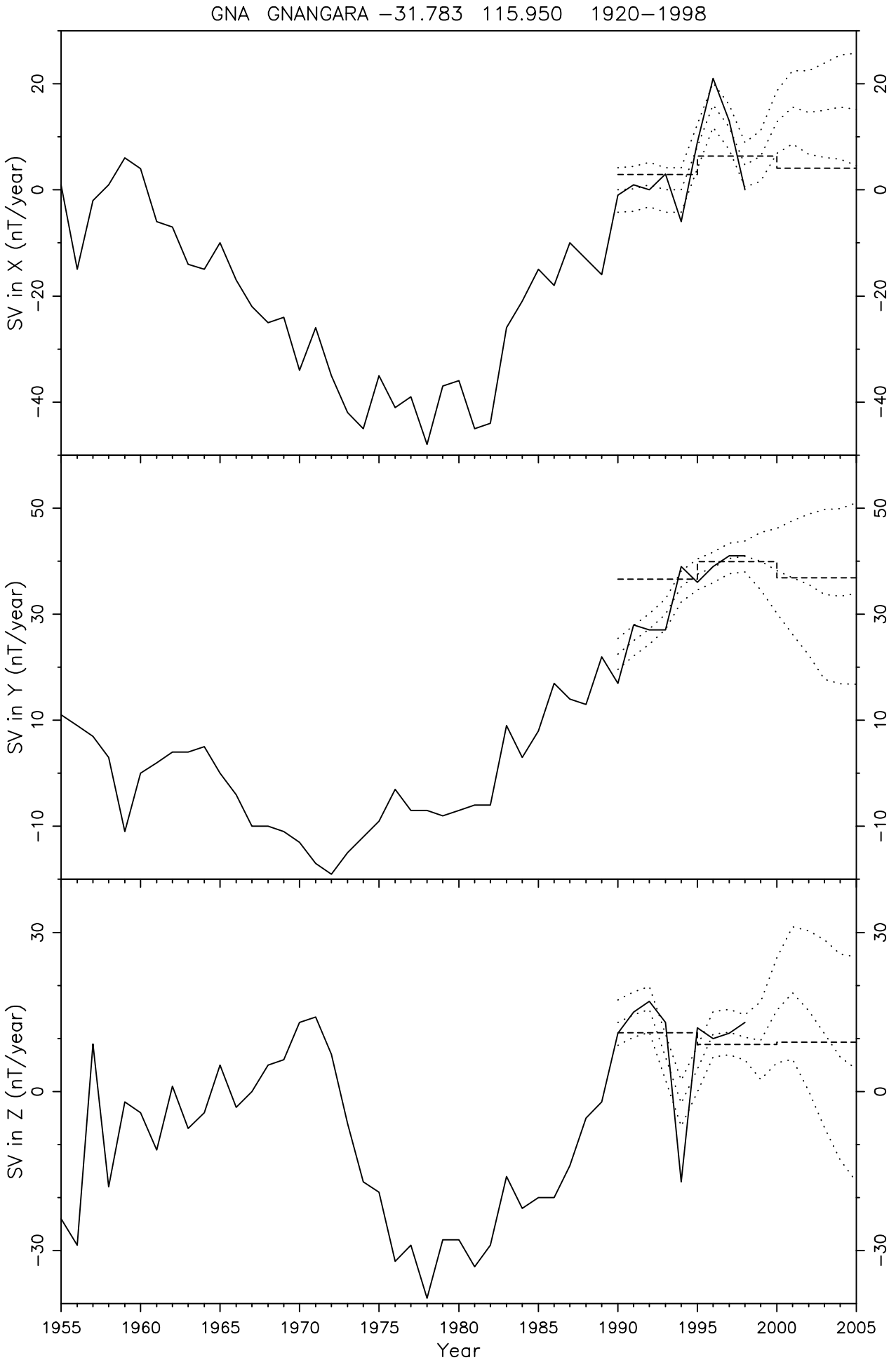
GNA GNANGARA −31.783 115.950 1920−1998
SV in X (nT/year)
SV in Y (nT/year)
SV in Z (nT/year)
Year
1955
1960
1965
1970
1975
1980
1985
1990
1995
2000
2005

Figure 168

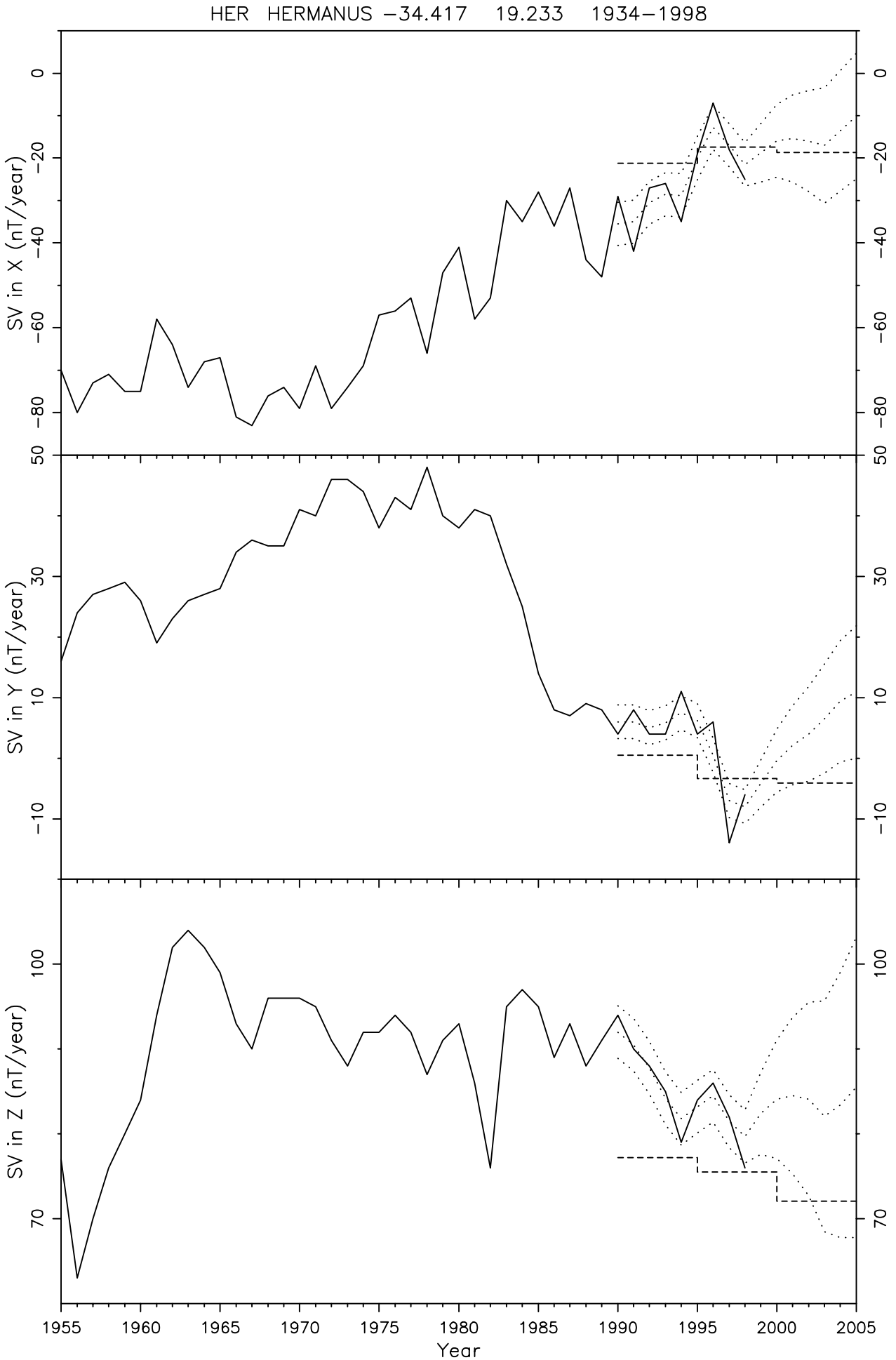
HER HERMANUS −34.417 19.233 1934−1998
SV in X (nT/year)
SV in Y (nT/year)
SV in Z (nT/year)
Year
1955
1960
1965
1970
1975
1980
1985
1990
1995
2000
2005

Figure 169

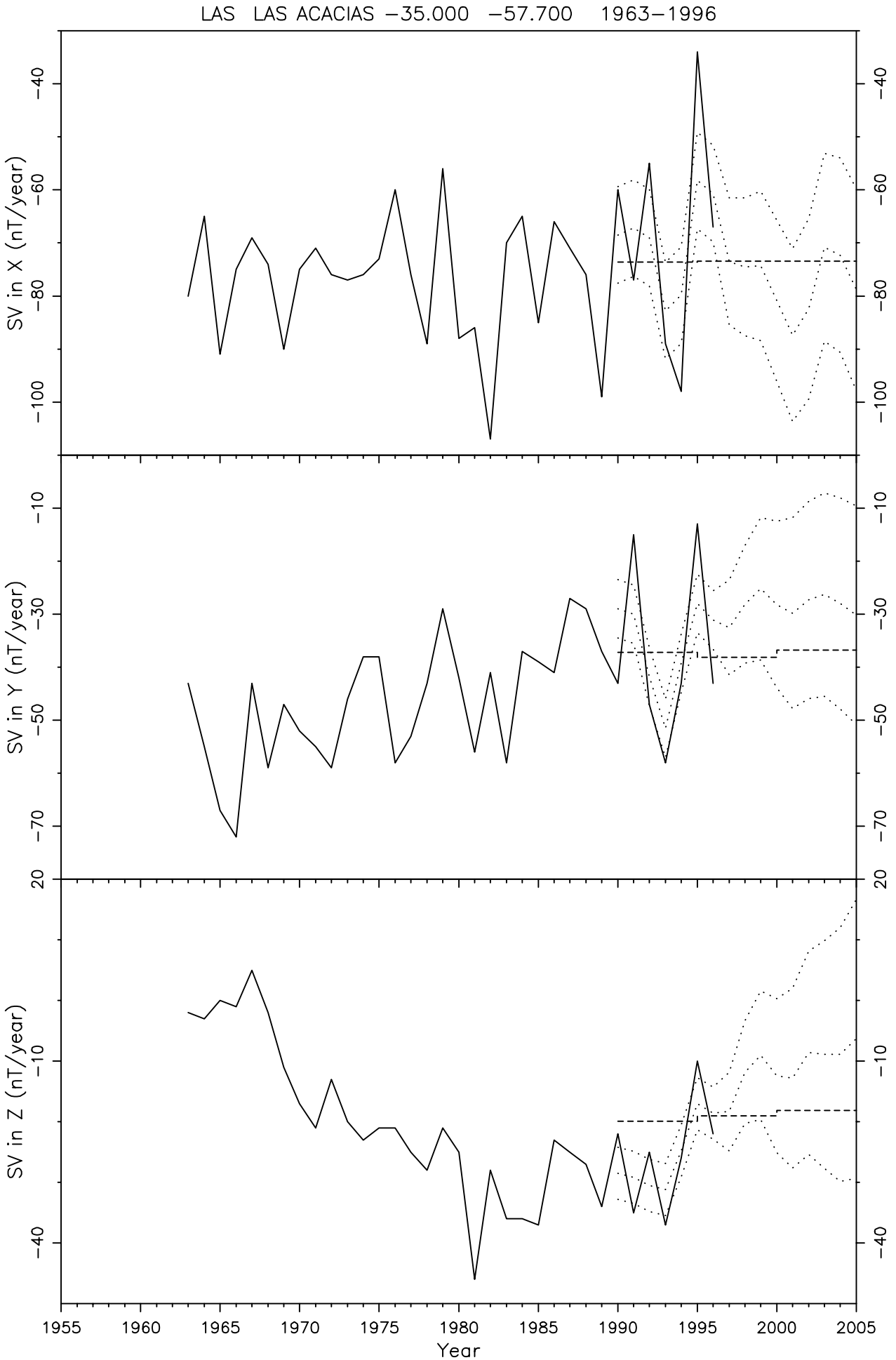
LAS LAS ACACIAS −35.000 −57.700 1963−1996
SV in X (nT/year)
SV in Y (nT/year)
SV in Z (nT/year)
Year
1955
1960
1965
1970
1975
1980
1985
1990
1995
2000
2005

Figure 170

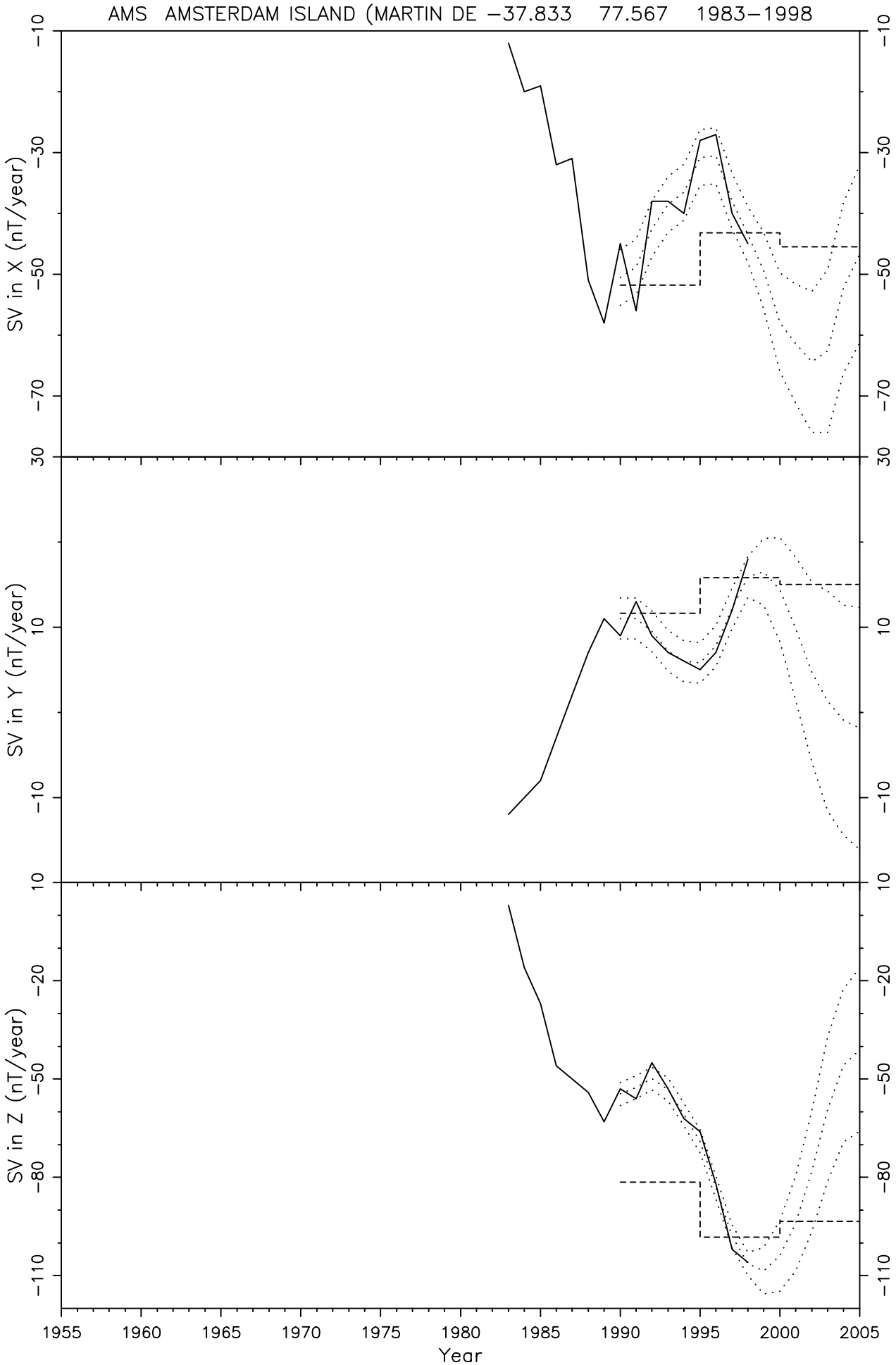
AMS AMSTERDAM ISLAND (MARTIN DE −37.833 77.567 1983−1998
SV in X (nT/year)
SV in Y (nT/year)
SV in Z (nT/year)
Year
1955
1960
1965
1970
1975
1980
1985
1990
1995
2000
2005

Figure 171

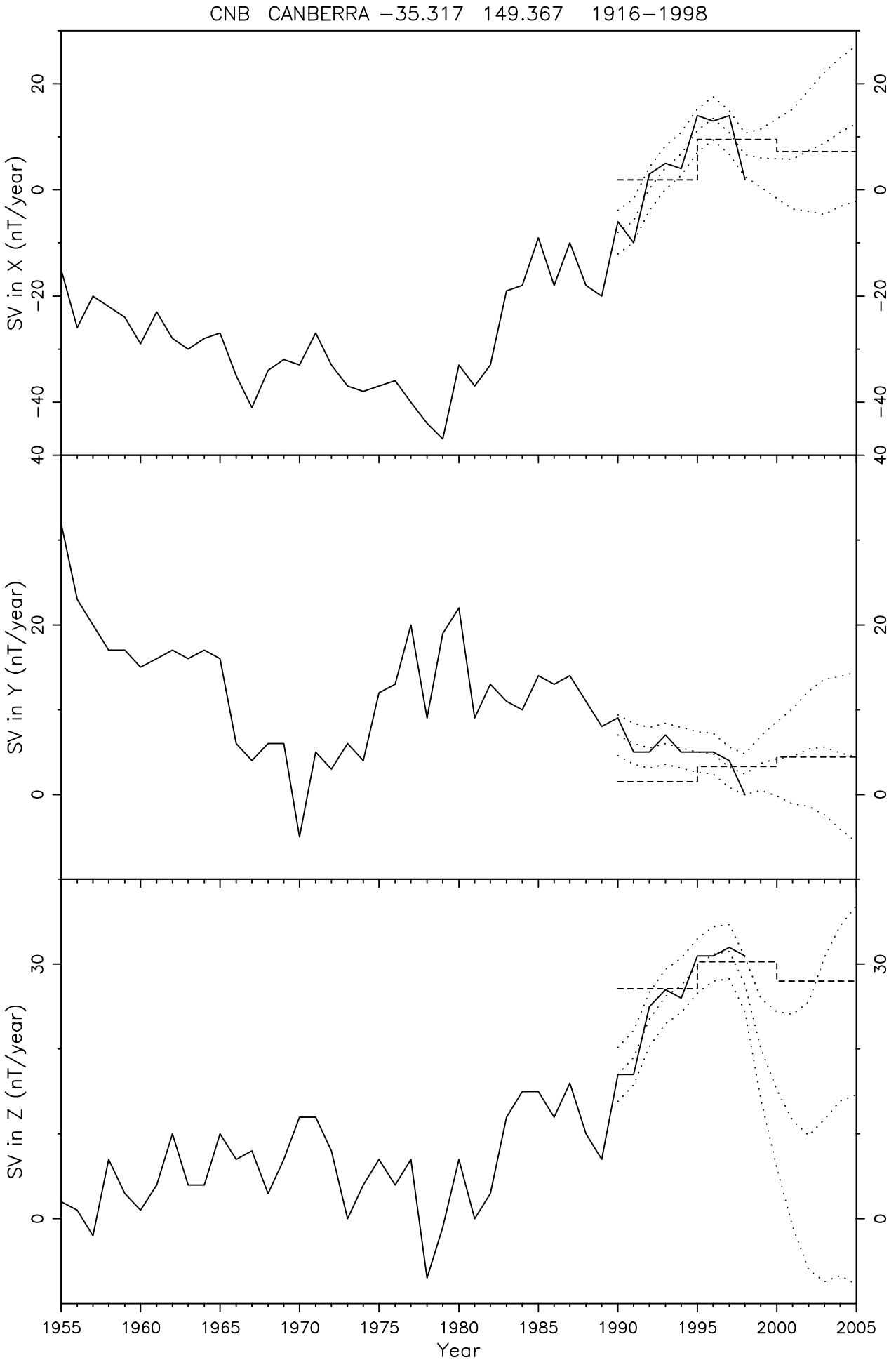
CNB CANBERRA −35.317 149.367 1916−1998
SV in X (nT/year)
SV in Y (nT/year)
SV in Z (nT/year)
20
0
−20
−40
40
30
1955
1960
1965
1970
1975
1980
1985
1990
1995
2000
2005
Year

Figure 172

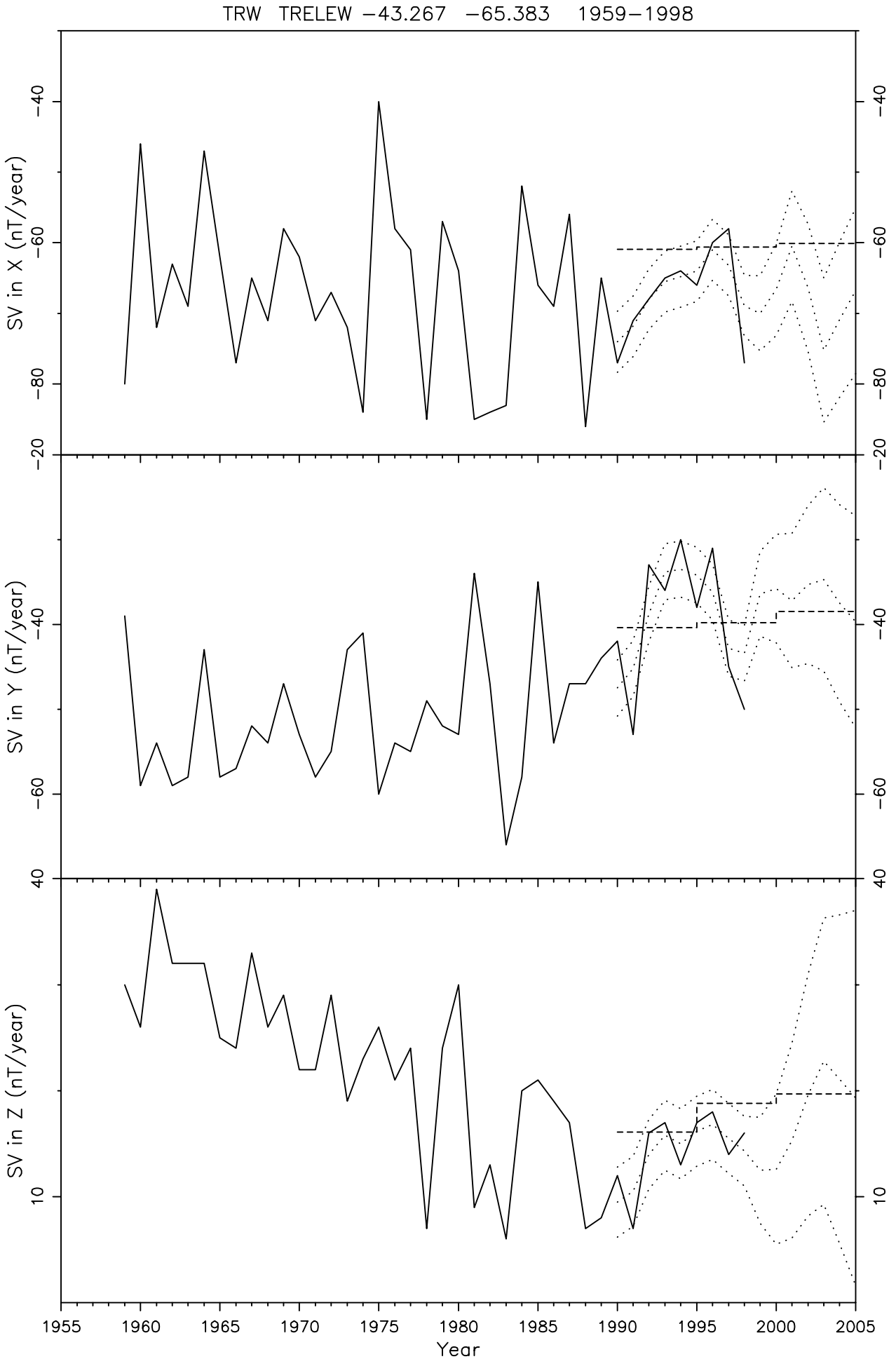
TRW TRELEW −43.267 −65.383 1959−1998
SV in X (nT/year)
SV in Y (nT/year)
SV in Z (nT/year)
−40
−60
−80
−20
40
10
1955
1960
1965
1970
1975
1980
1985
1990
1995
2000
2005
Year

Figure 173

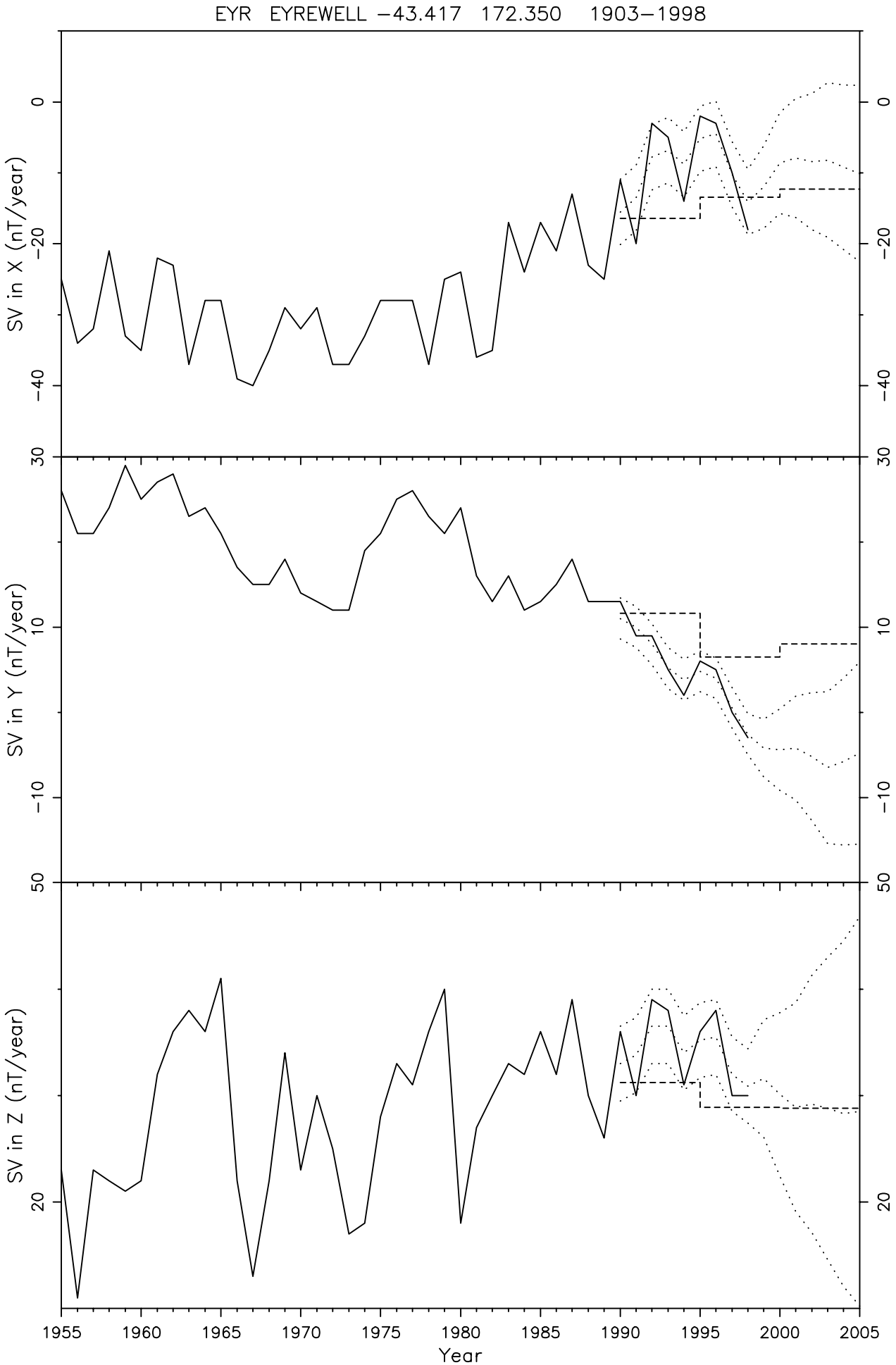
EYR EYREWELL −43.417 172.350 1903−1998
SV in X (nT/year)
SV in Y (nT/year)
SV in Z (nT/year)
0
−20
−40
30
10
−10
50
20
1955
1960
1965
1970
1975
1980
1985
1990
1995
2000
2005
Year

Figure 174

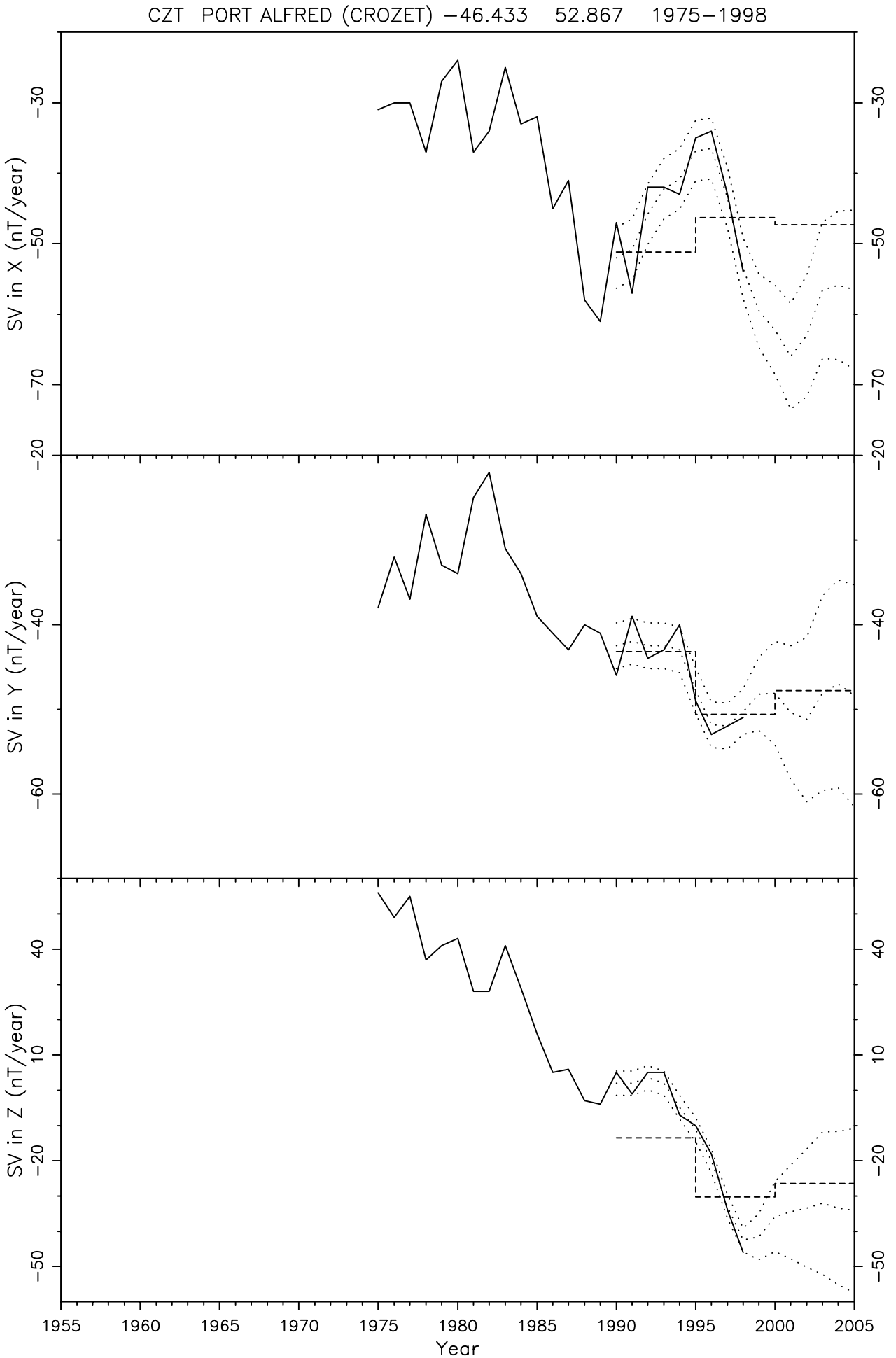
CZT PORT ALFRED (CROZET) −46.433 52.867 1975−1998
SV in X (nT/year)
−30
−50
−70
−20
SV in Y (nT/year)
−40
−60
SV in Z (nT/year)
40
10
−20
−50
1955
1960
1965
1970
1975
1980
1985
1990
1995
2000
2005
Year

Figure 175

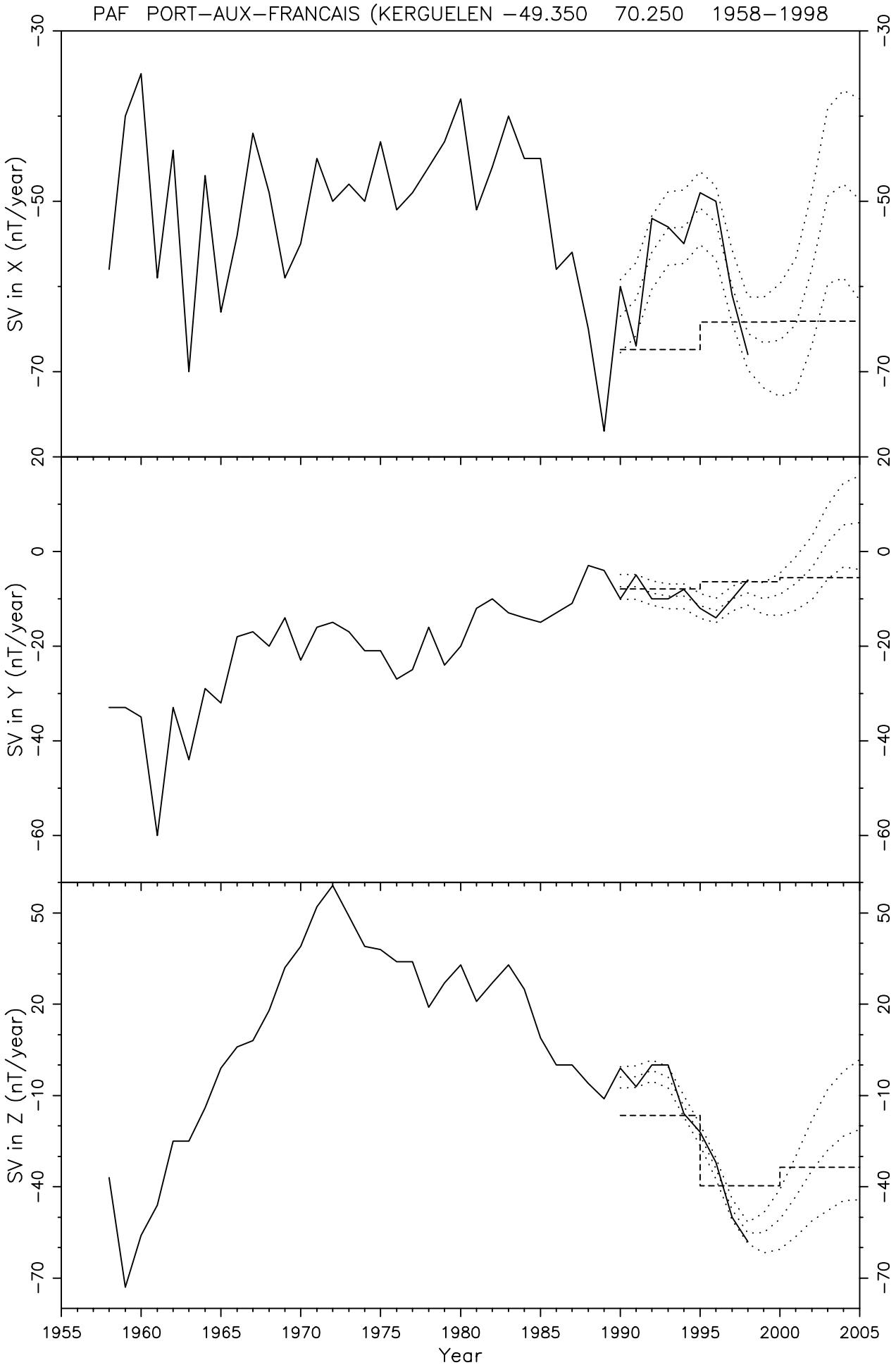
PAF PORT−AUX−FRANCAIS (KERGUELEN −49.350 70.250 1958−1998
SV in X (nT/year)
SV in Y (nT/year)
SV in Z (nT/year)
Year
1955
1960
1965
1970
1975
1980
1985
1990
1995
2000
2005

Figure 176

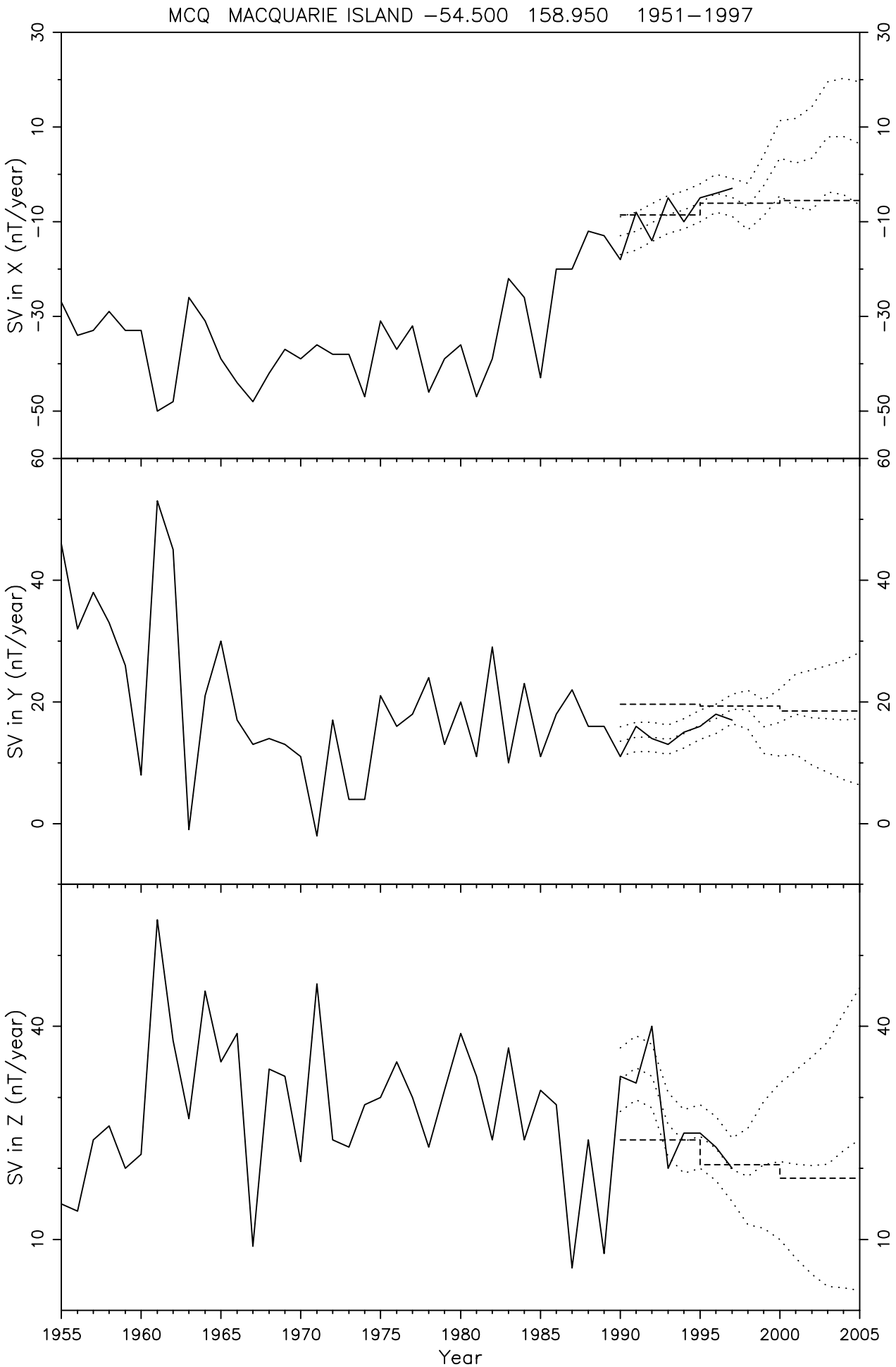
MCQ MACQUARIE ISLAND −54.500 158.950 1951−1997
SV in X (nT/year)
SV in Y (nT/year)
SV in Z (nT/year)
Year
1955
1960
1965
1970
1975
1980
1985
1990
1995
2000
2005

Figure 177

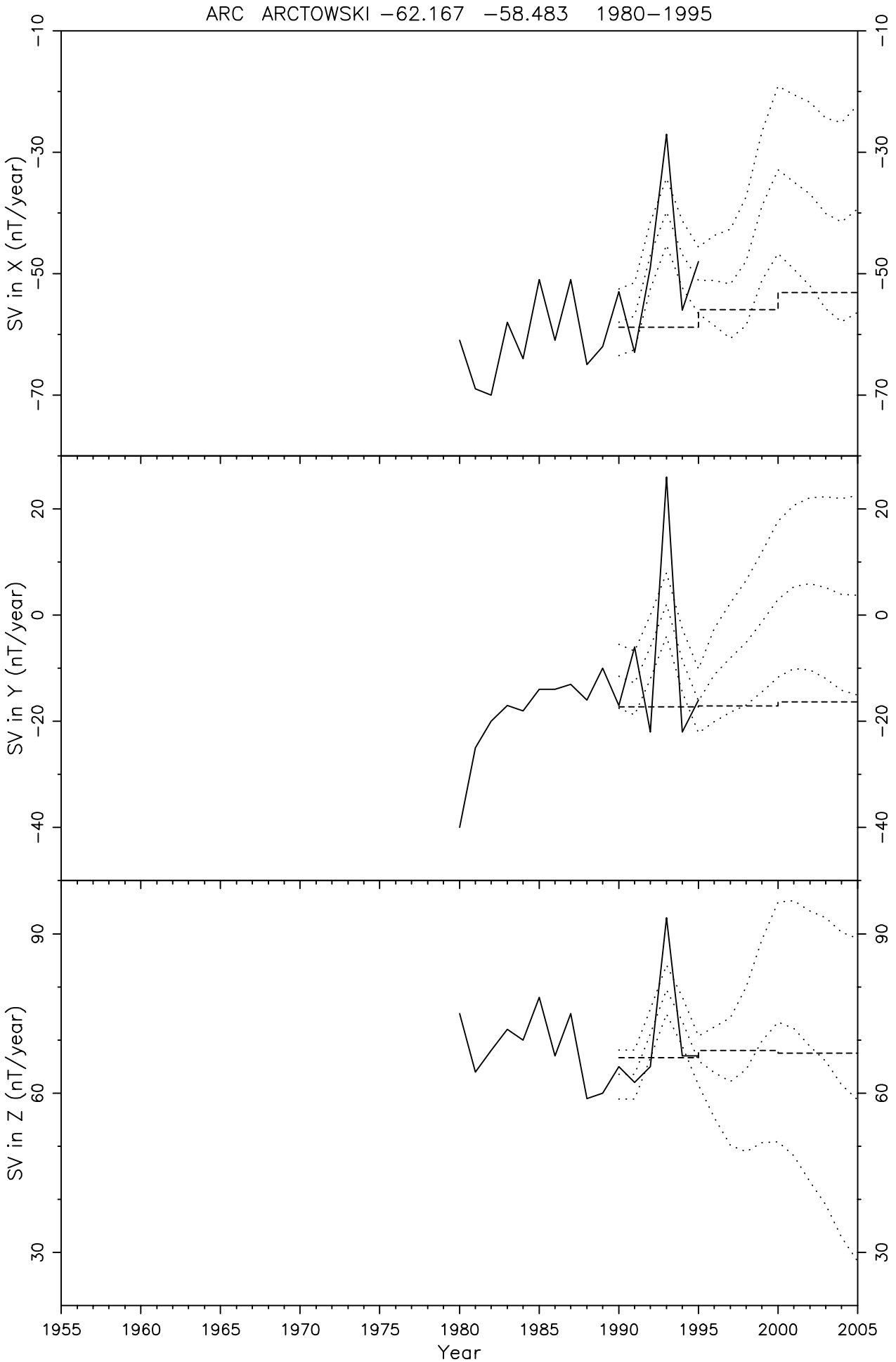
ARC ARCTOWSKI −62.167 −58.483 1980−1995
SV in X (nT/year)
−10
−30
−50
−70
SV in Y (nT/year)
20
0
−20
−40
SV in Z (nT/year)
90
60
30
1955
1960
1965
1970
1975
1980
1985
1990
1995
2000
2005
Year

Figure 178

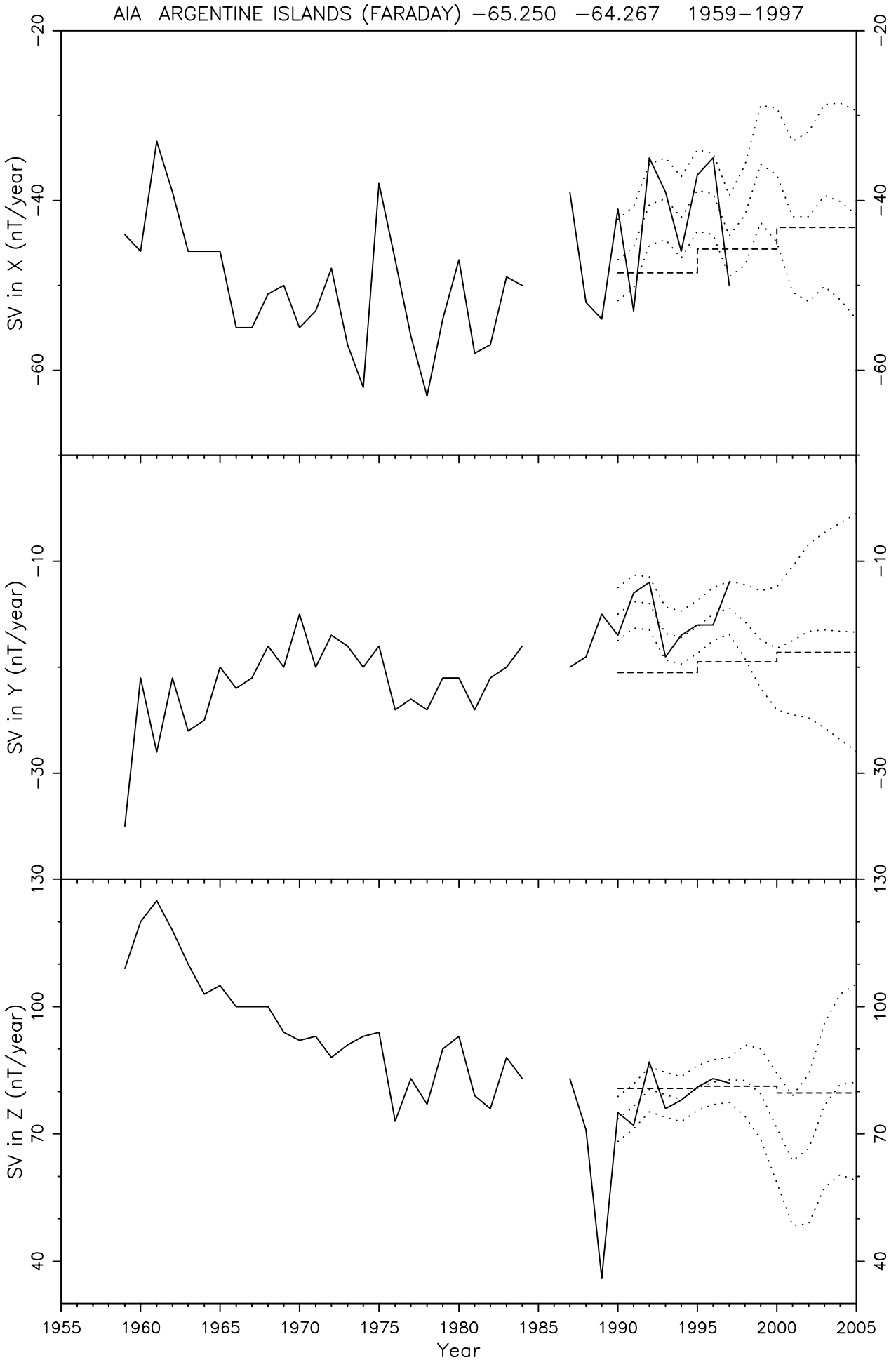
AIA ARGENTINE ISLANDS (FARADAY) −65.250 −64.267 1959−1997
SV in X (nT/year)
SV in Y (nT/year)
SV in Z (nT/year)
−20
−40
−60
−10
−30
130
100
70
40
1955
1960
1965
1970
1975
1980
1985
1990
1995
2000
2005
Year

Figure 179

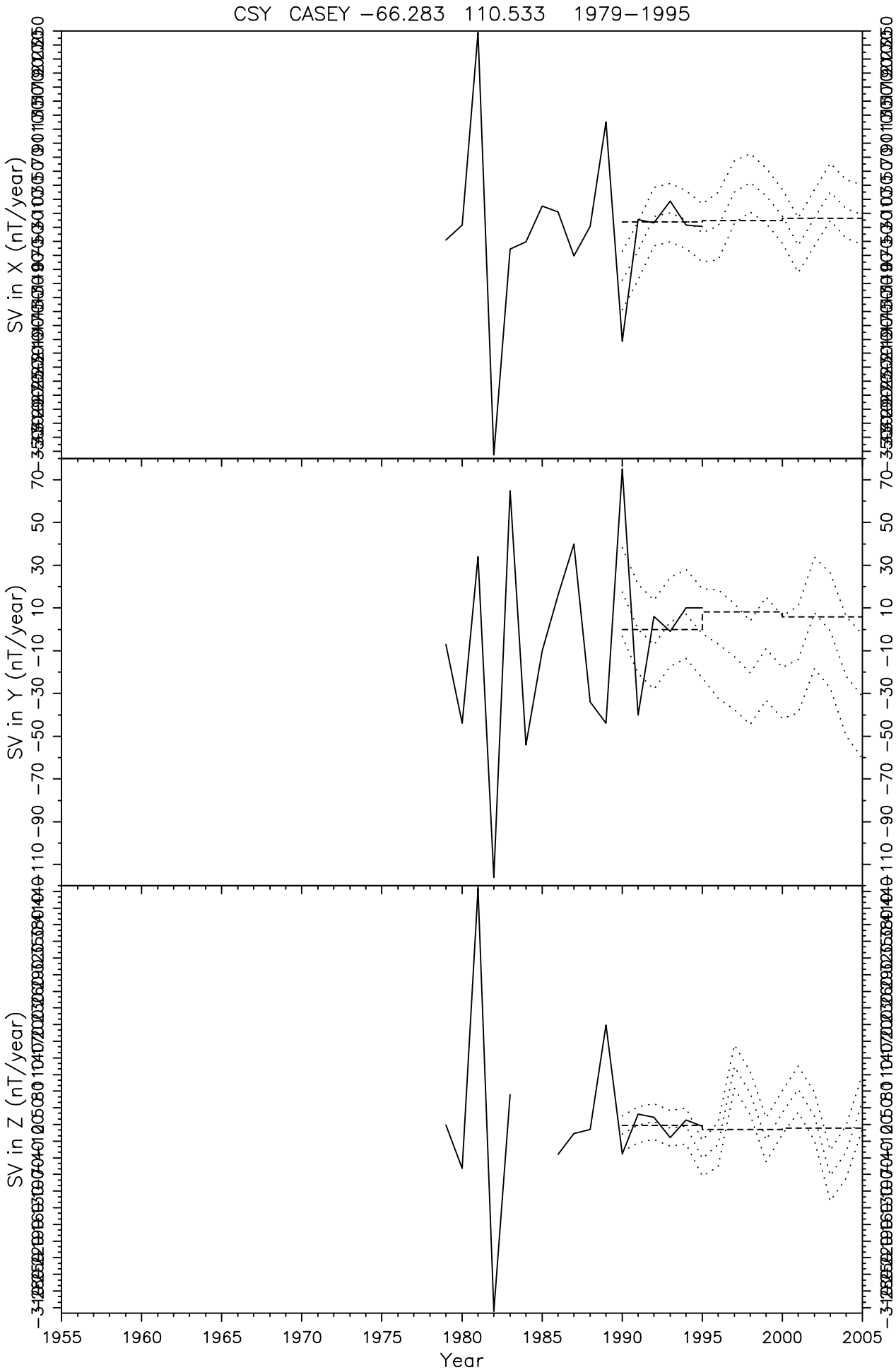
CSY CASEY −66.283 110.533 1979−1995
SV in X (nT/year)
SV in Y (nT/year)
SV in Z (nT/year)
1955
1960
1965
1970
1975
1980
1985
1990
1995
2000
2005
Year

Figure 180

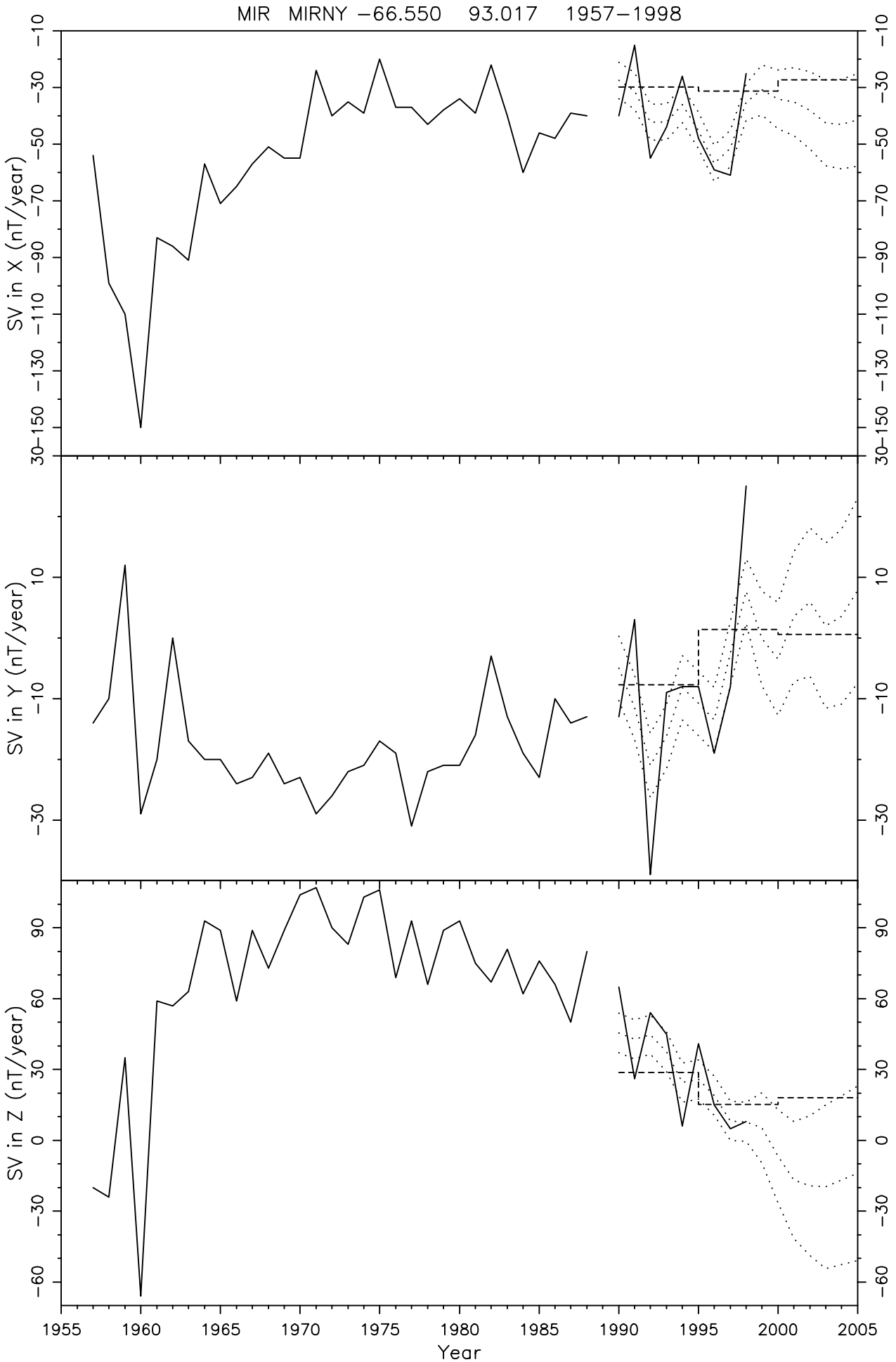
MIR MIRNY −66.550 93.017 1957−1998
SV in X (nT/year)
SV in Y (nT/year)
SV in Z (nT/year)
Year
1955
1960
1965
1970
1975
1980
1985
1990
1995
2000
2005

Figure 181

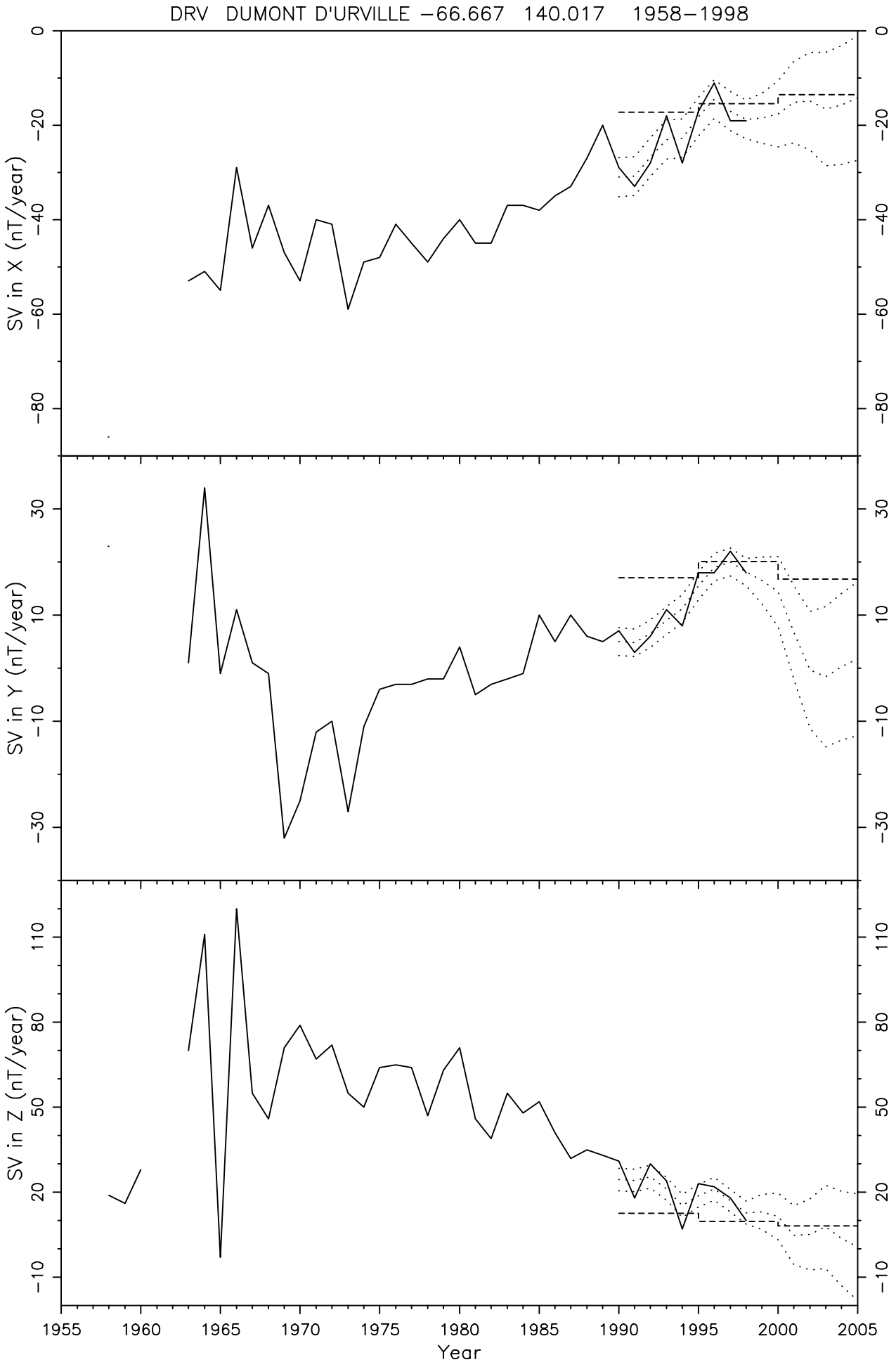
DRV DUMONT D'URVILLE −66.667 140.017 1958−1998
SV in X (nT/year)
SV in Y (nT/year)
SV in Z (nT/year)
Year
1955
1960
1965
1970
1975
1980
1985
1990
1995
2000
2005

Figure 182

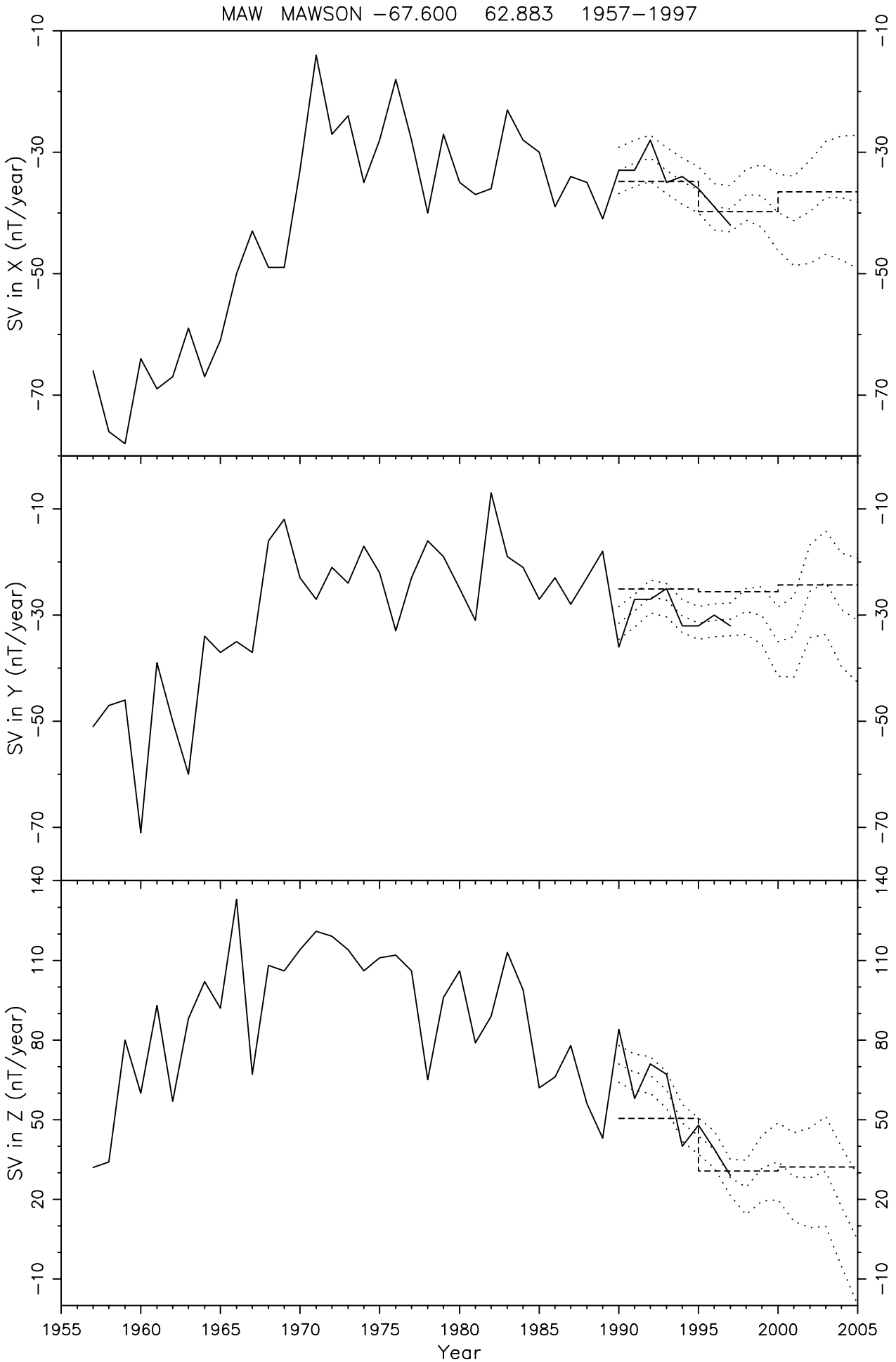
MAW MAWSON −67.600 62.883 1957−1997
SV in X (nT/year)
SV in Y (nT/year)
SV in Z (nT/year)
−10
−30
−50
−70
140
110
80
50
20
1955
1960
1965
1970
1975
1980
1985
1990
1995
2000
2005
Year

Figure 183

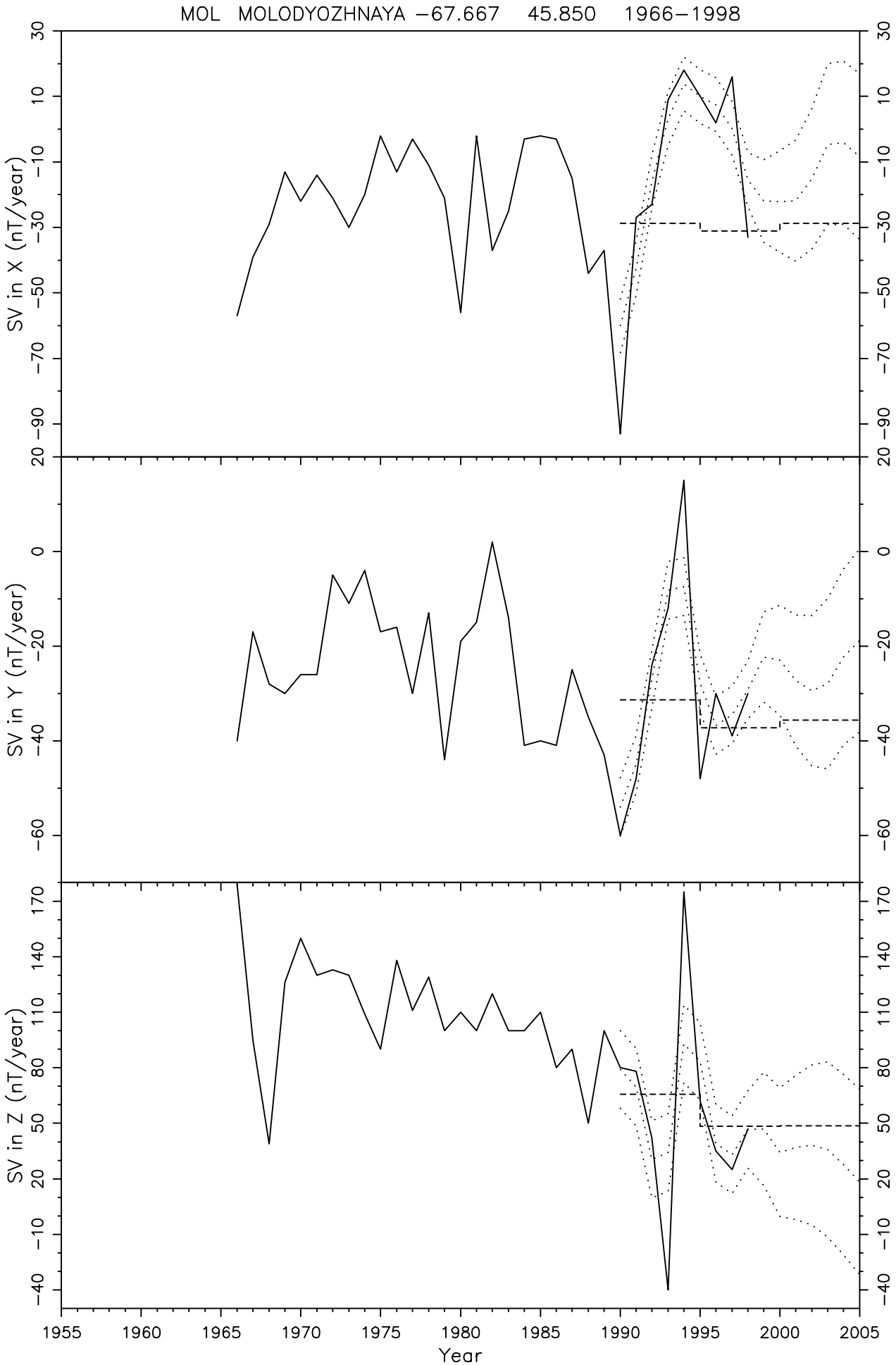
MOL MOLODYOZHNAYA −67.667 45.850 1966−1998
SV in X (nT/year)
SV in Y (nT/year)
SV in Z (nT/year)
Year
1955
1960
1965
1970
1975
1980
1985
1990
1995
2000
2005

Figure 184

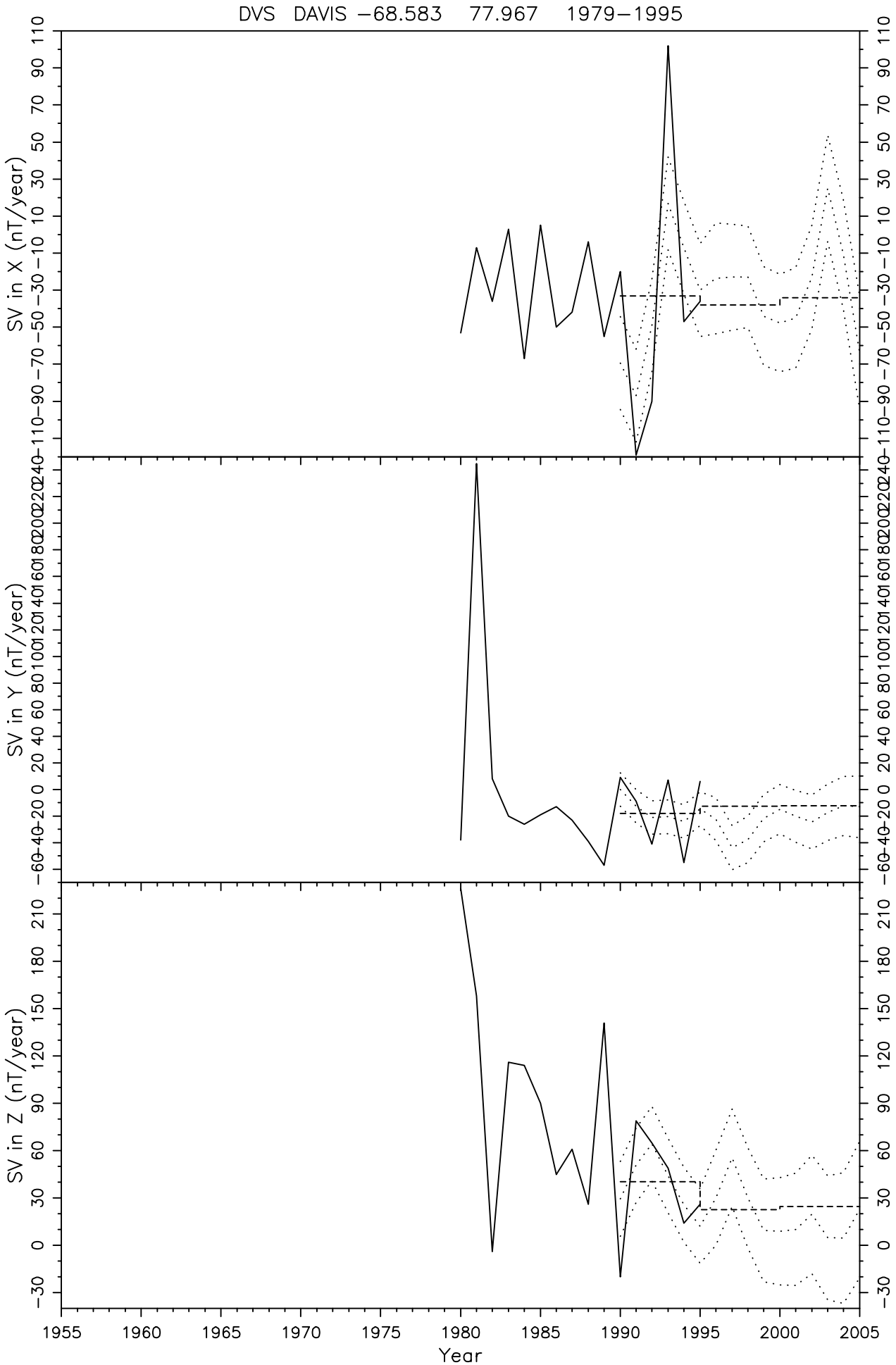
DVS DAVIS −68.583 77.967 1979−1995
SV in X (nT/year)
SV in Y (nT/year)
SV in Z (nT/year)
Year
1955
1960
1965
1970
1975
1980
1985
1990
1995
2000
2005

Figure 185

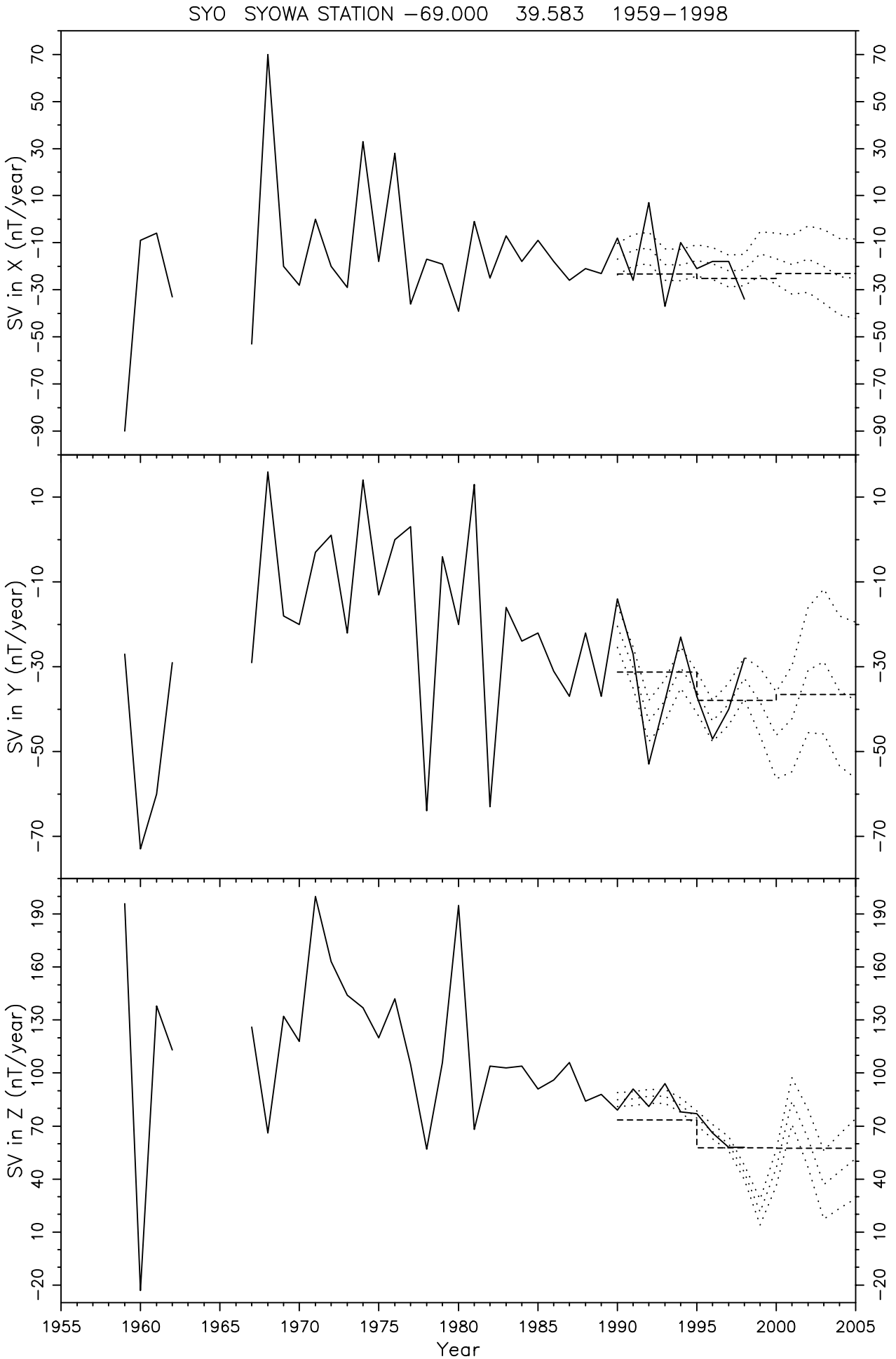
SYO SYOWA STATION −69.000 39.583 1959−1998
SV in X (nT/year)
SV in Y (nT/year)
SV in Z (nT/year)
Year
1955
1960
1965
1970
1975
1980
1985
1990
1995
2000
2005

Figure 186

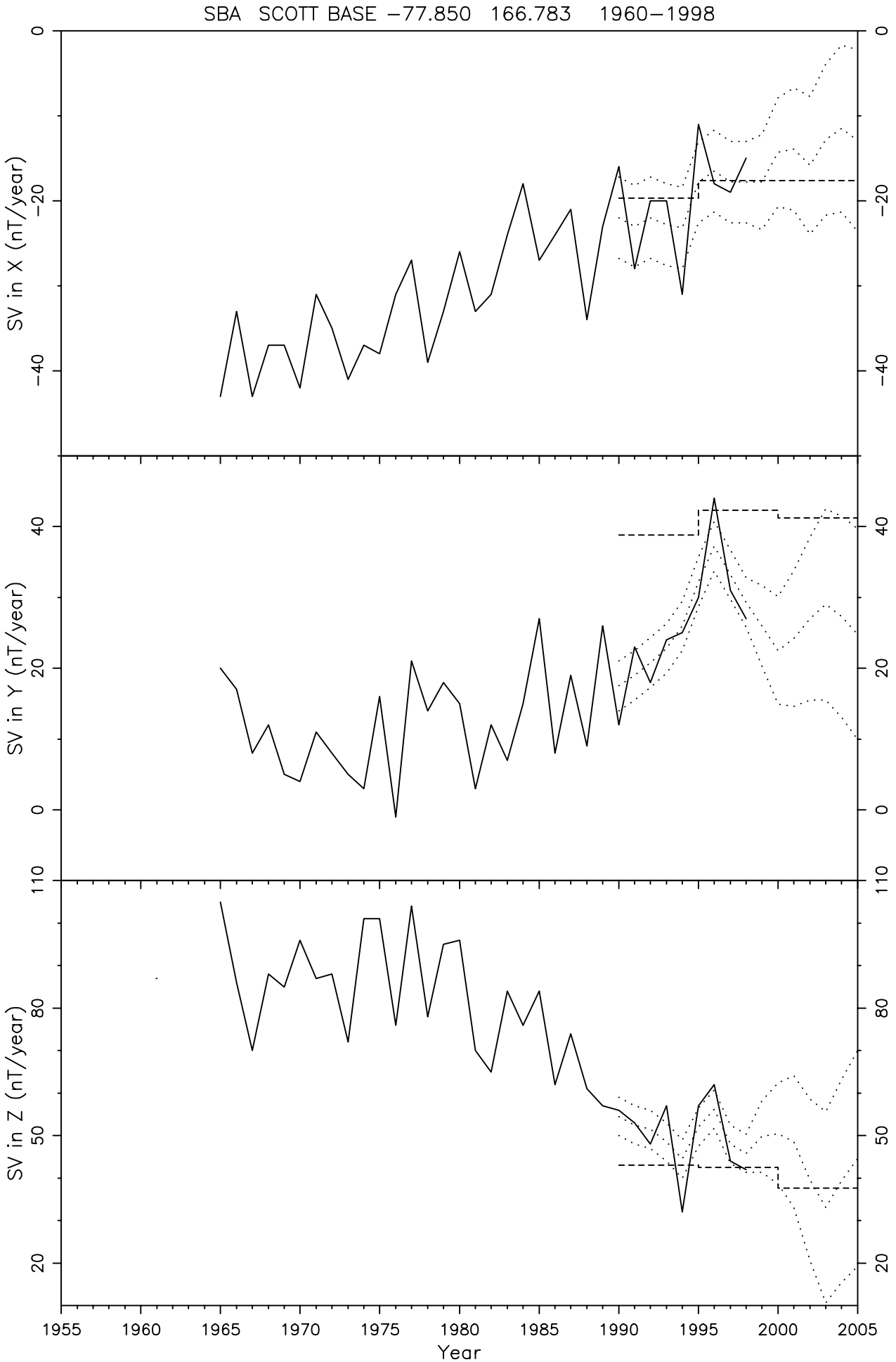
SBA SCOTT BASE −77.850 166.783 1960−1998
SV in X (nT/year)
SV in Y (nT/year)
SV in Z (nT/year)
Year
1955
1960
1965
1970
1975
1980
1985
1990
1995
2000
2005

Figure 187

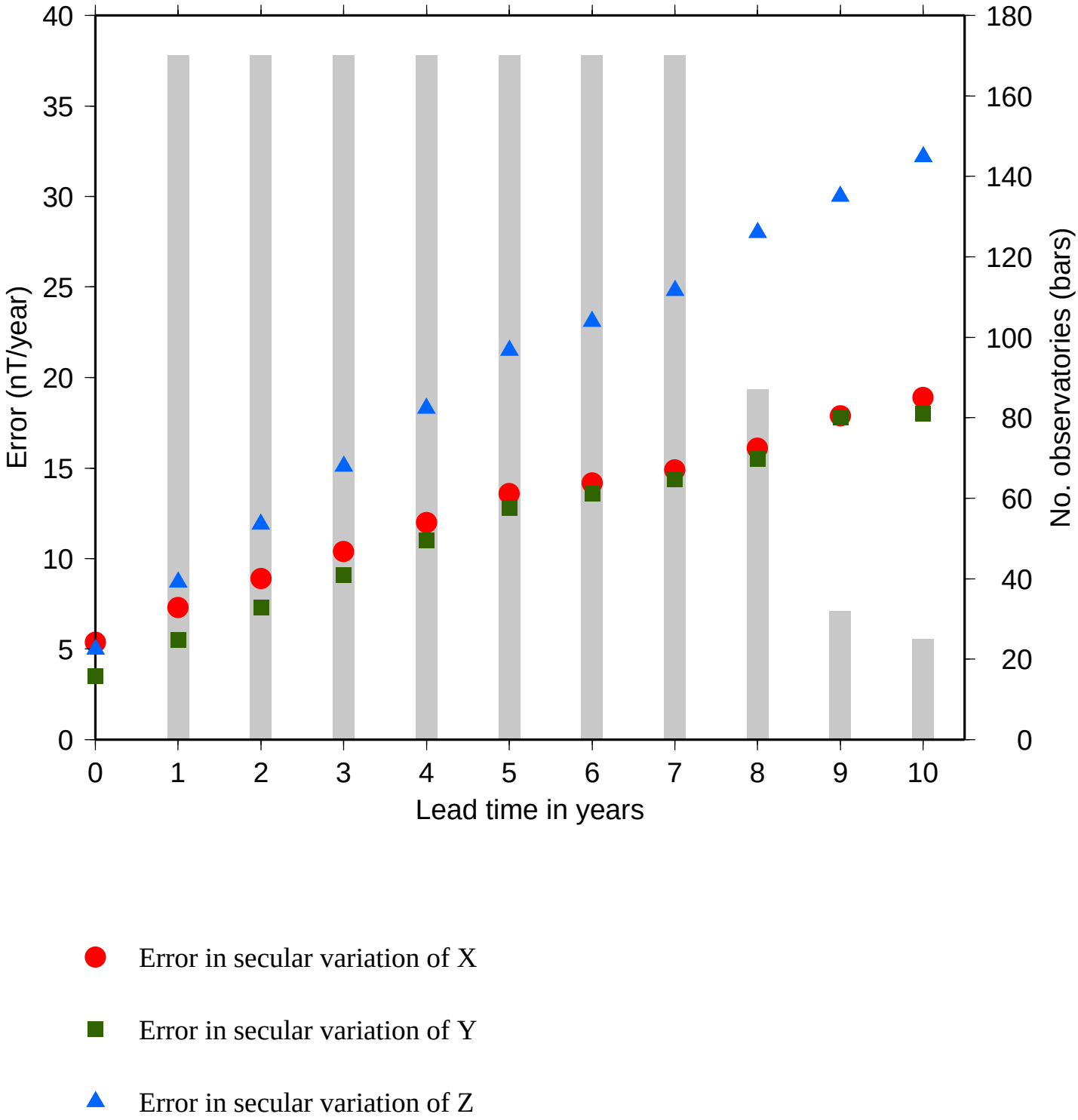
Error (nT/year)
No. observatories (bars)
Lead time in years
0
5
10
15
20
25
30
35
40
0
20
40
60
80
100
120
140
160
180
0
1
2
3
4
5
6
7
8
9
10
Error in secular variation of X
Error in secular variation of Y
Error in secular variation of Z

Figure 188

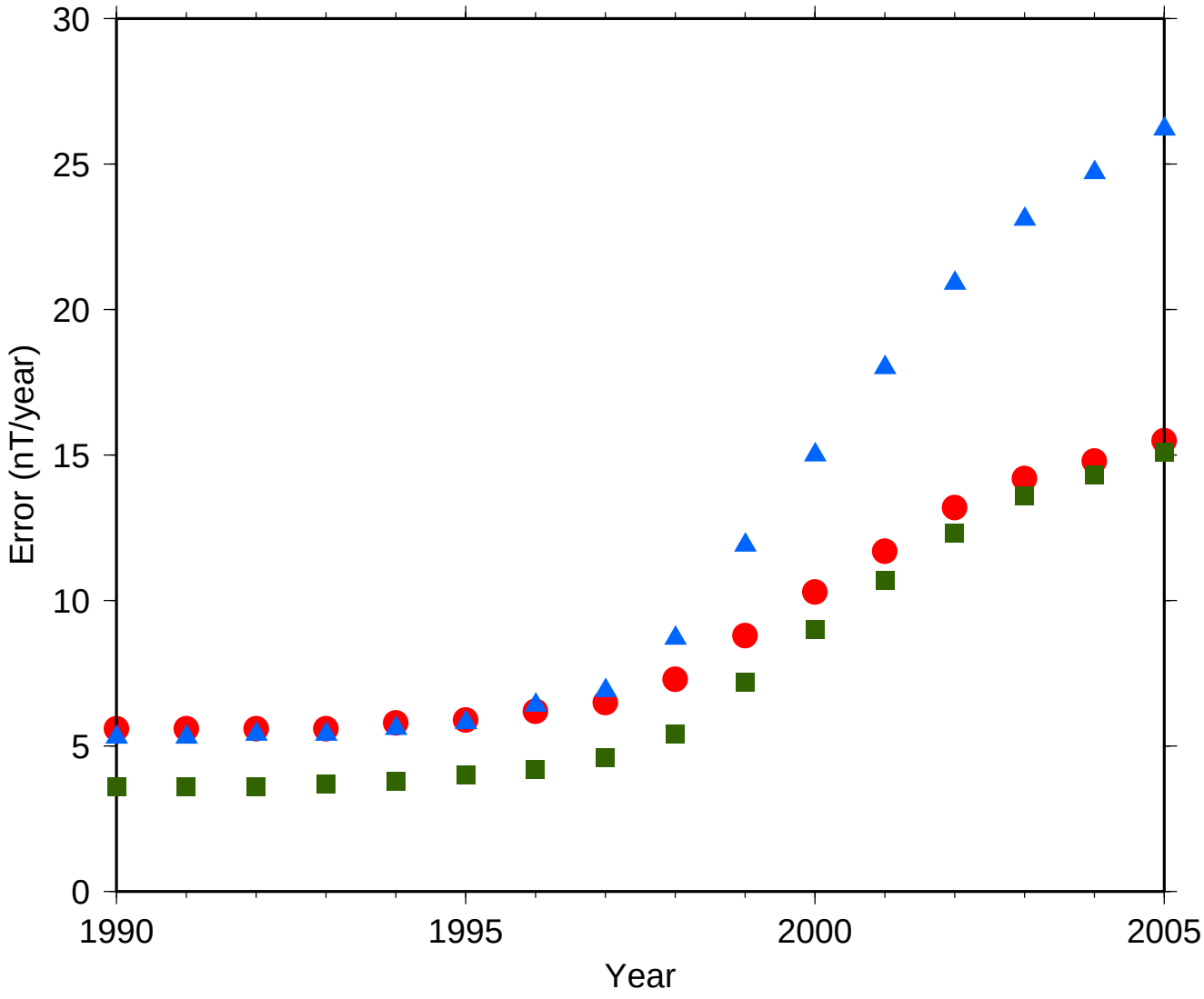
30
25
20
15
10
5
0
Error (nT/year)
1990
1995
2000
2005
Year
Error in secular variation of X
Error in secular variation of Y
Error in secular variation of Z

Figure 189

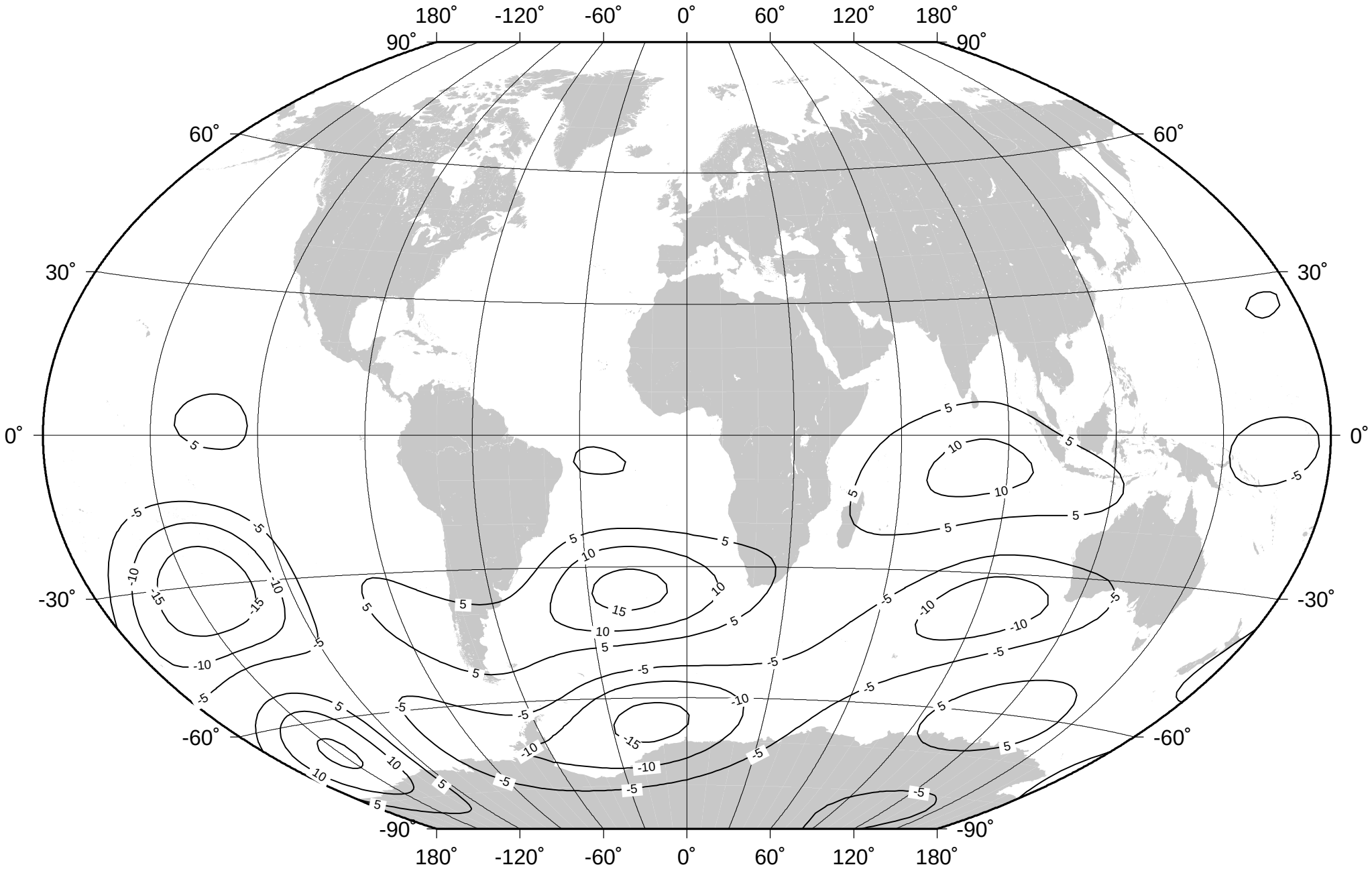

Differences between models (WMM (Sep 99) - WMM (Aug 99)) in their synthesis of secular variation in X for 1995.0-2000.0. Units: nT/year.

Figure 190

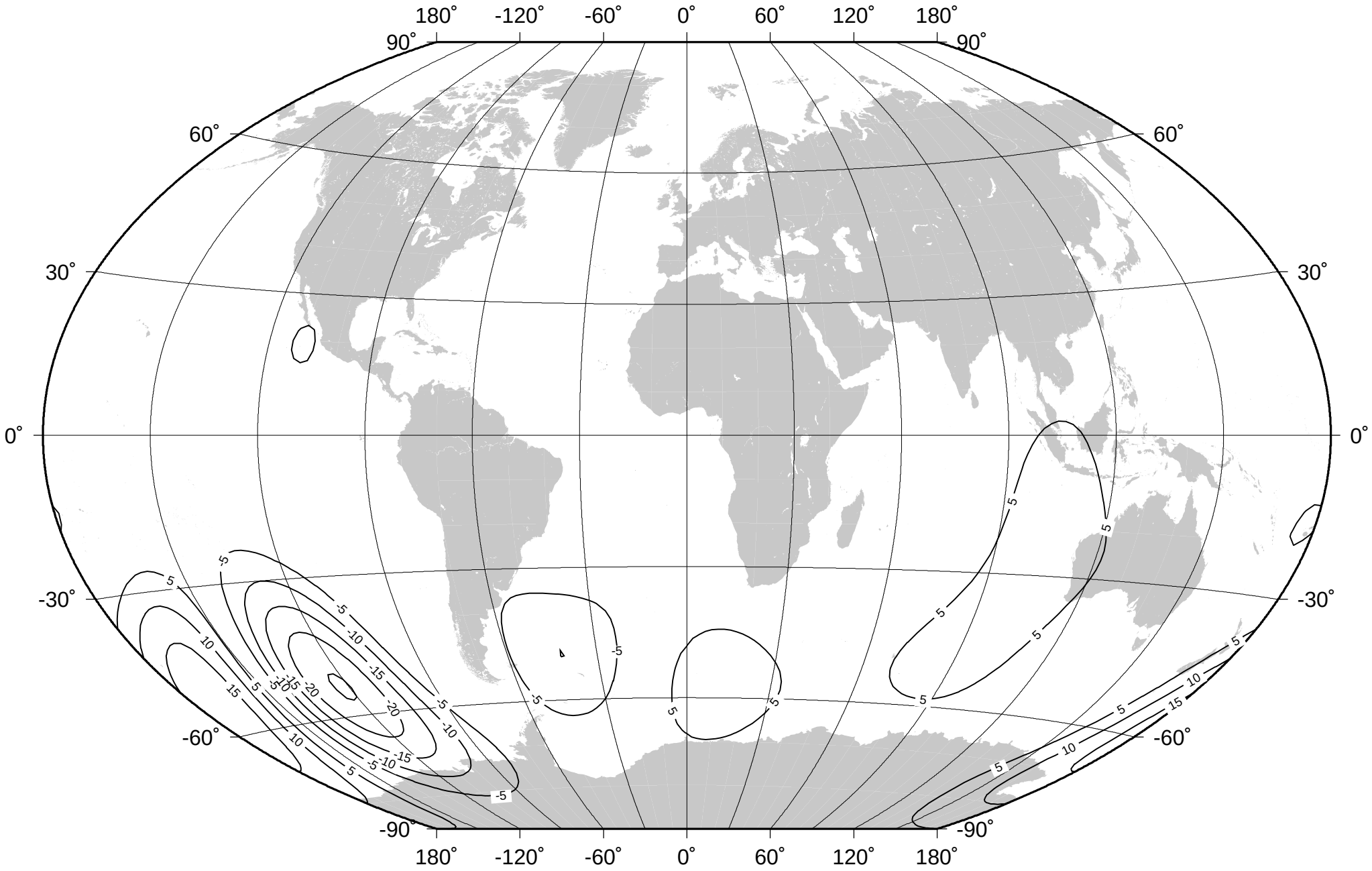

Differences between models (WMM (Sep 99) - WMM (Aug 99)) in their synthesis of secular variation in Y for 1995.0-2000.0. Units: nT/year.

Figure 191

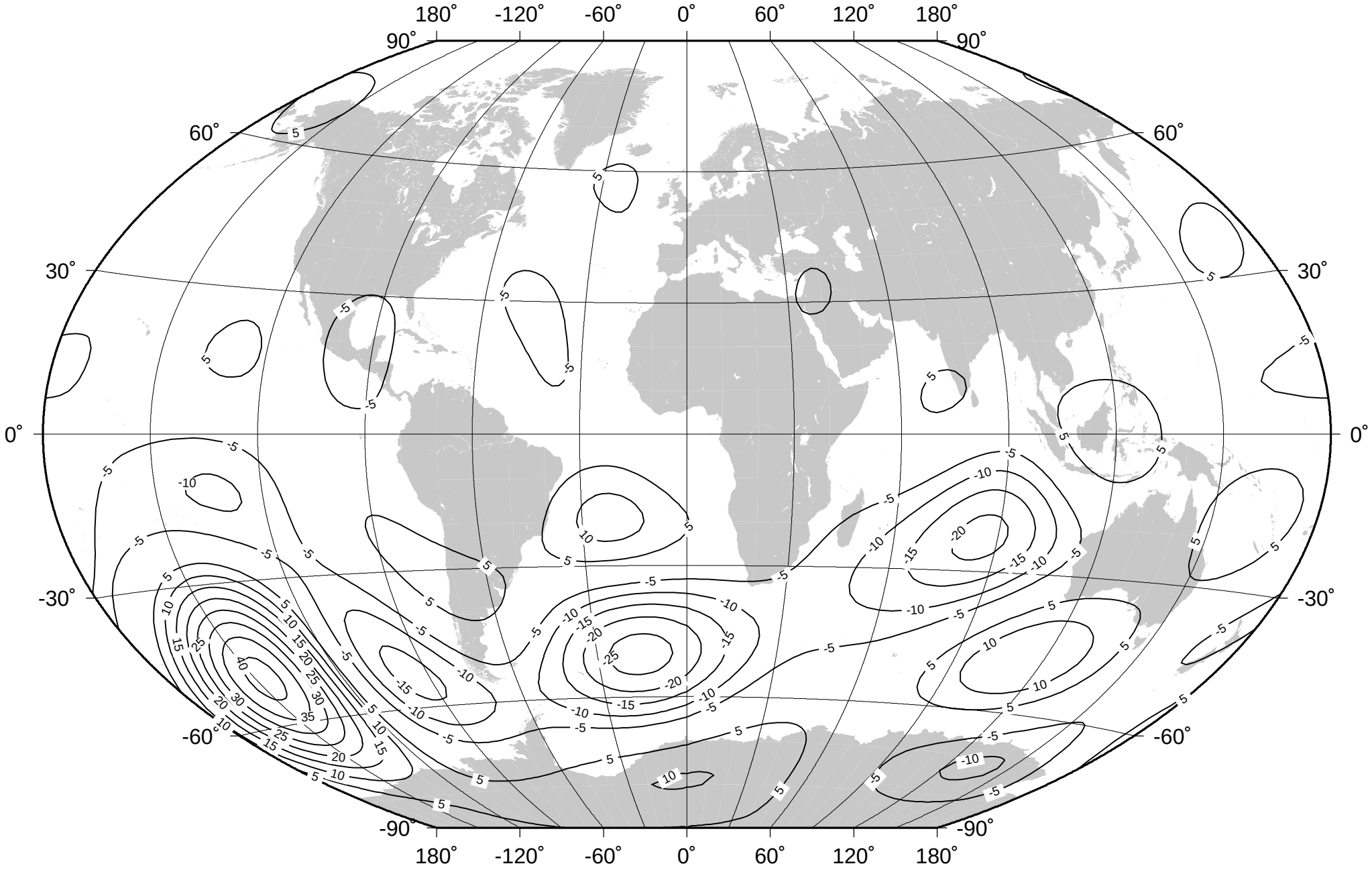

Differences between models (WMM (Sep 99) - WMM (Aug 99)) in their synthesis of secular variation in Z for 1995.0-2000.0. Units: nT/year.

Figure 192

WMM2000 (initial) - WMM2000 (final) differences at 2000.0 (C.I. = 10 nT for X and Y, 20 nT for Z and F)

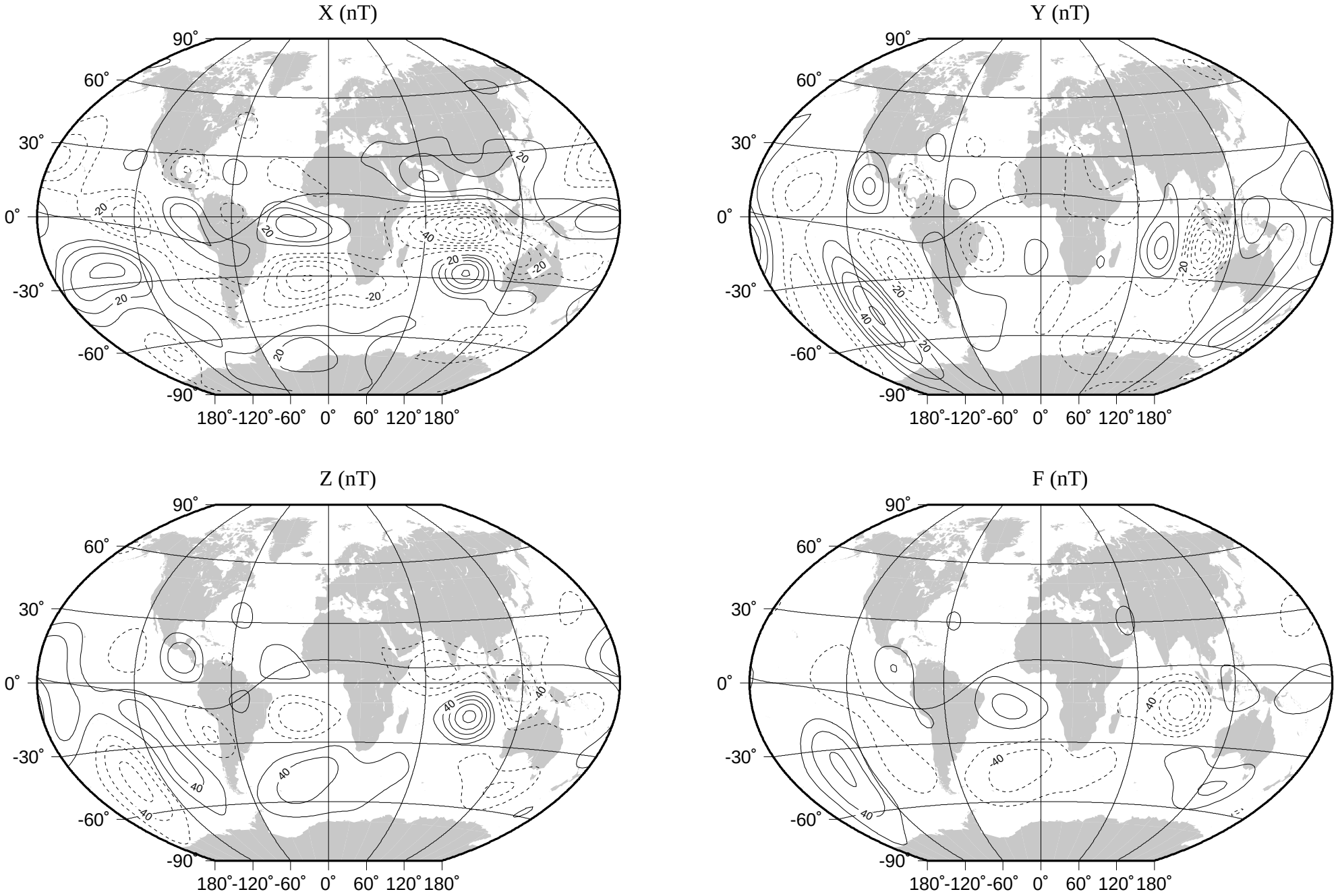

Figure 193

OERSTED MAGNETIC RESIDUAL CHART

(Overhauser)

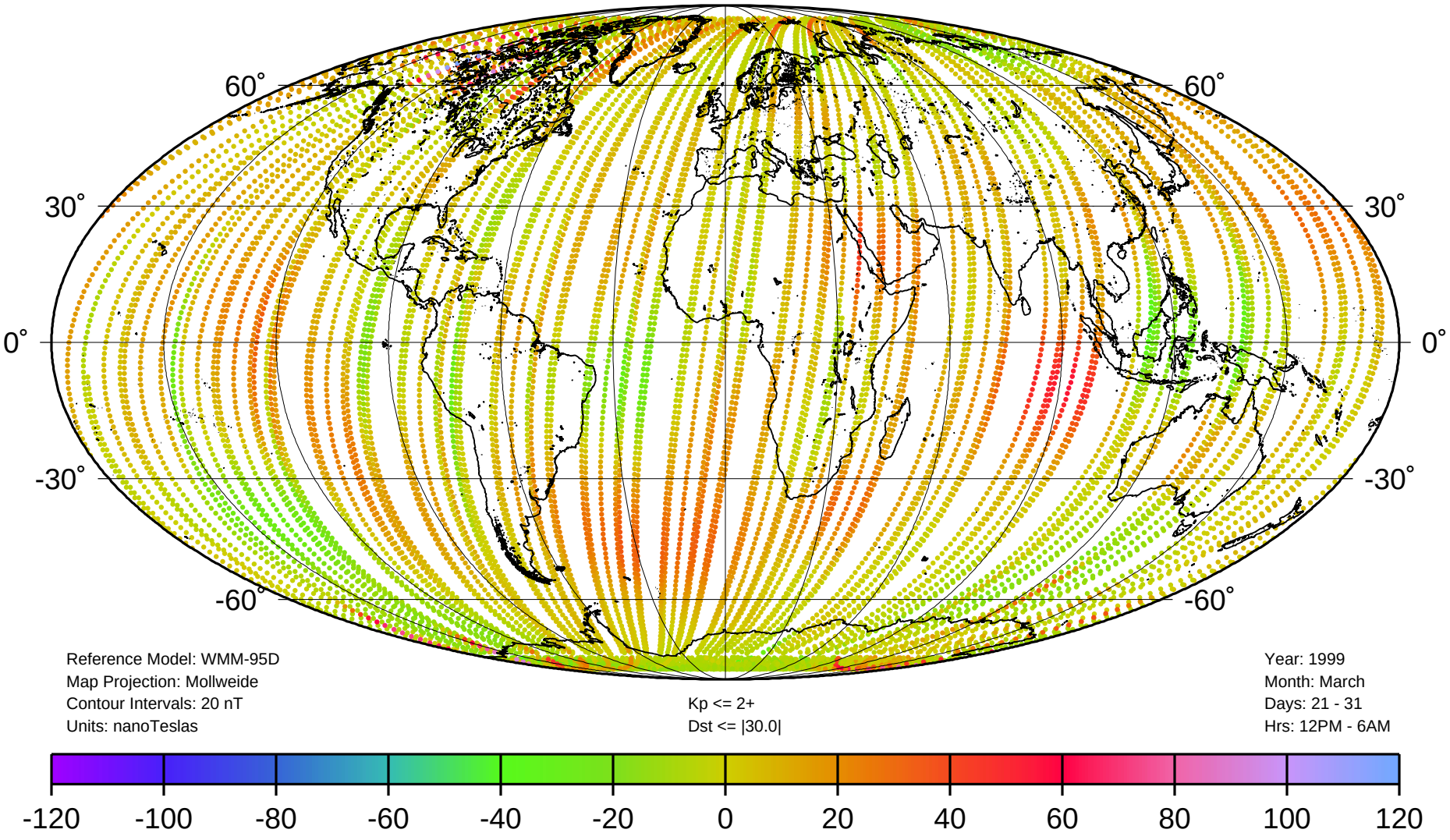

Figure 194

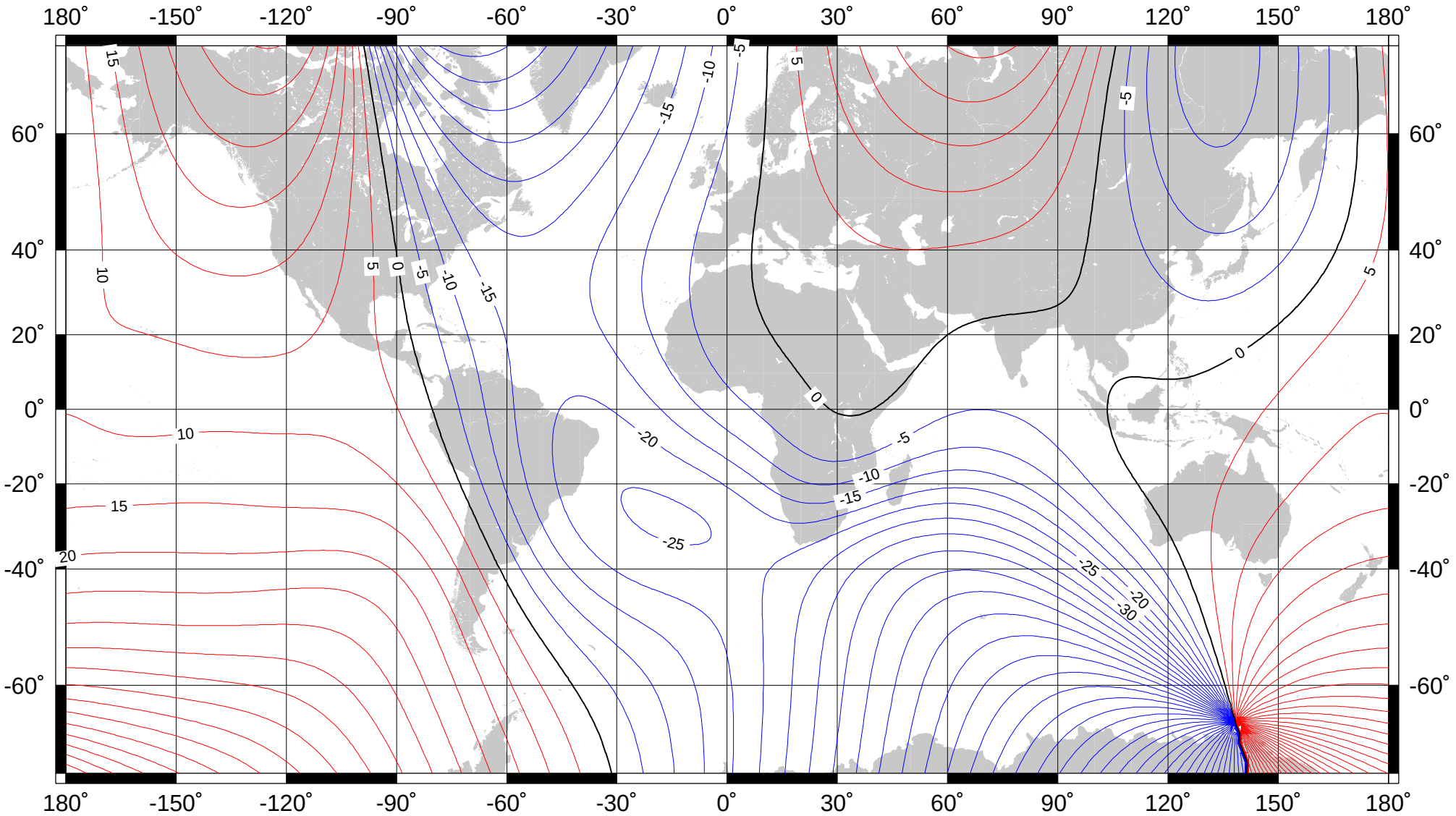

Declination (magnetic variation) at 2000.0 from the World Magnetic Model (WMM2000). Red - positive (east), blue - negative (west), black - zero (agonic line). Contour interval is 5˚ and projection is Mercator. This is an example of an isogonic chart.

Figure 195

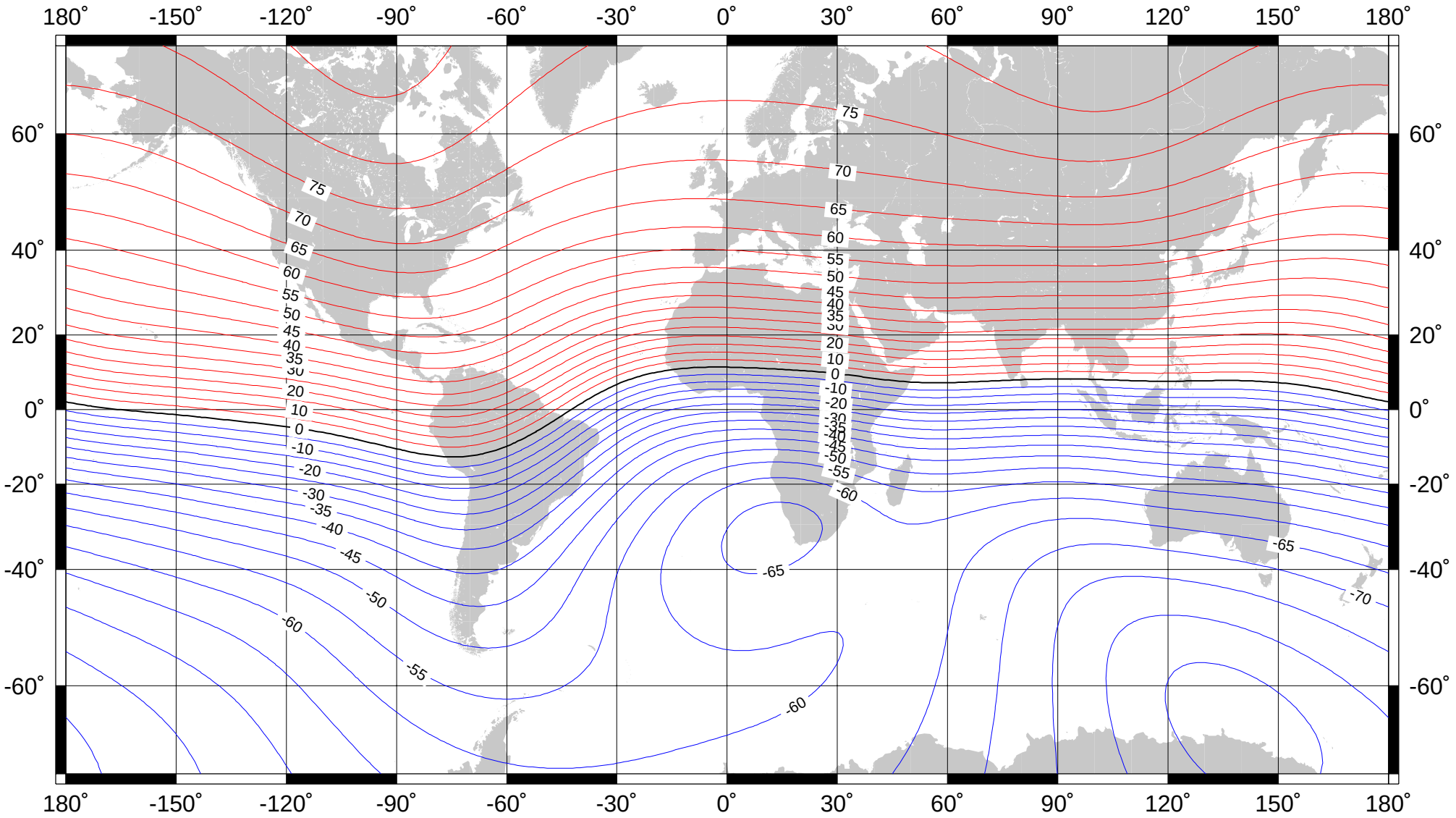

Inclination (magnetic dip) at 2000.0 from the World Magnetic Model (WMM2000). Red - positive (down), blue - negative (up), black - zero (dip equator). Contour interval is 5˚ and projection is Mercator. This is an example of an isoclinic chart.

Figure 196

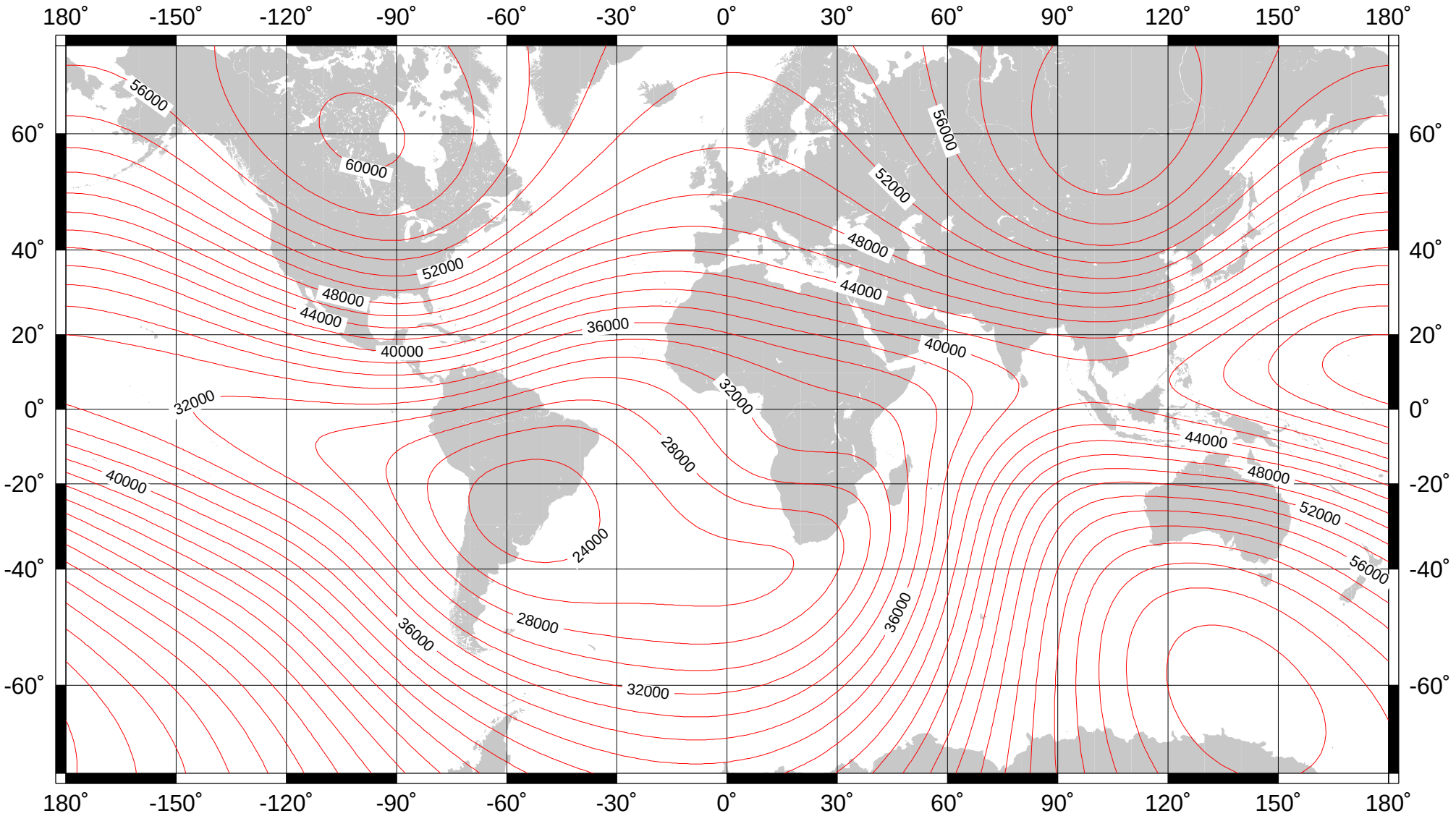

Total intensity (*F*) at 2000.0 from the World Magnetic Model (WMM2000). Contour interval is 2000 nT and projection is Mercator. This is an example of an isodynamic chart.

Figure 197

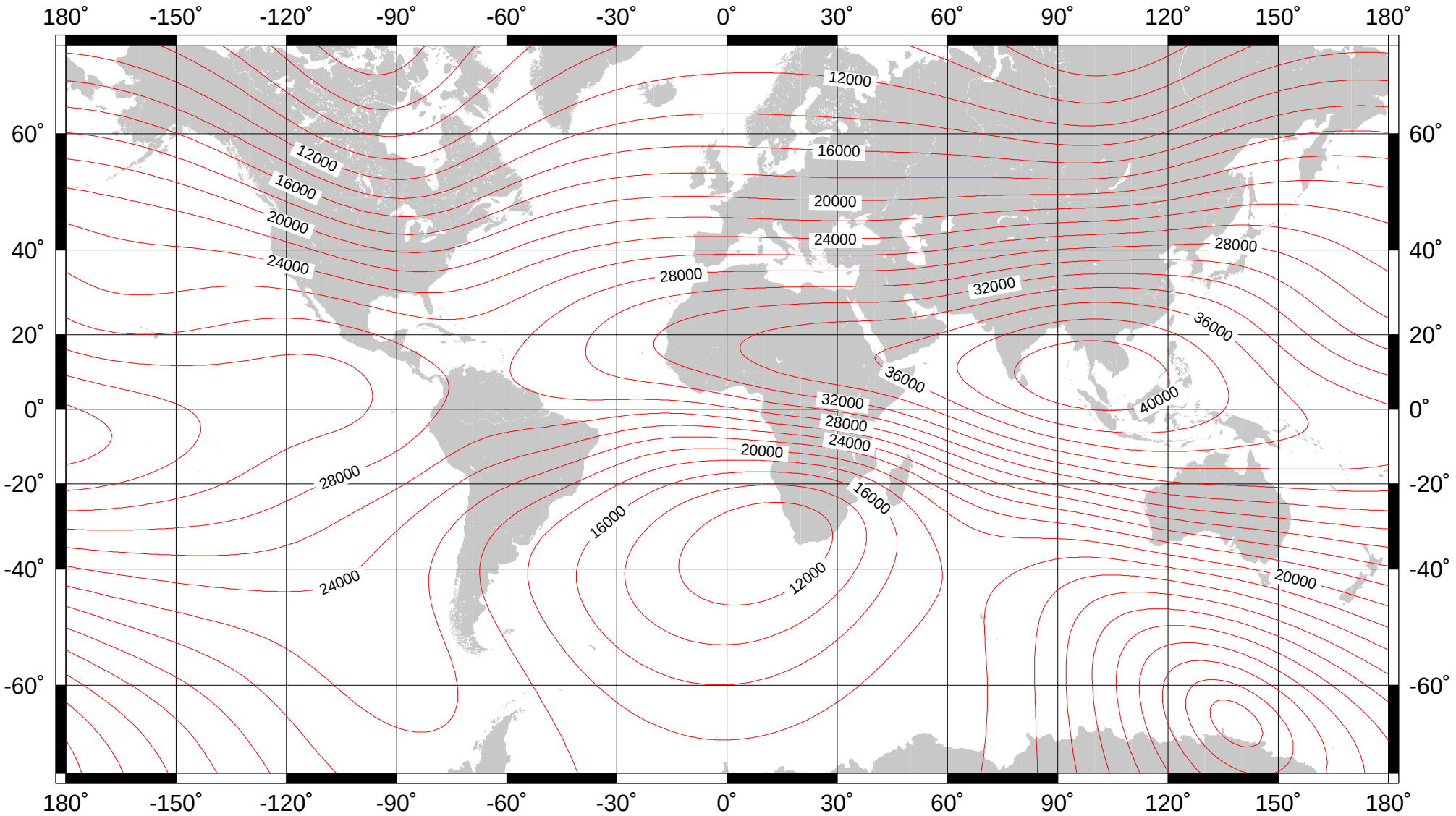

Horizontal intensity (*H*) at 2000.0 from the World Magnetic Model (WMM2000). Contour interval is 2000 nT and projection is Mercator. This is an example of an isodynamic chart.

Figure 198

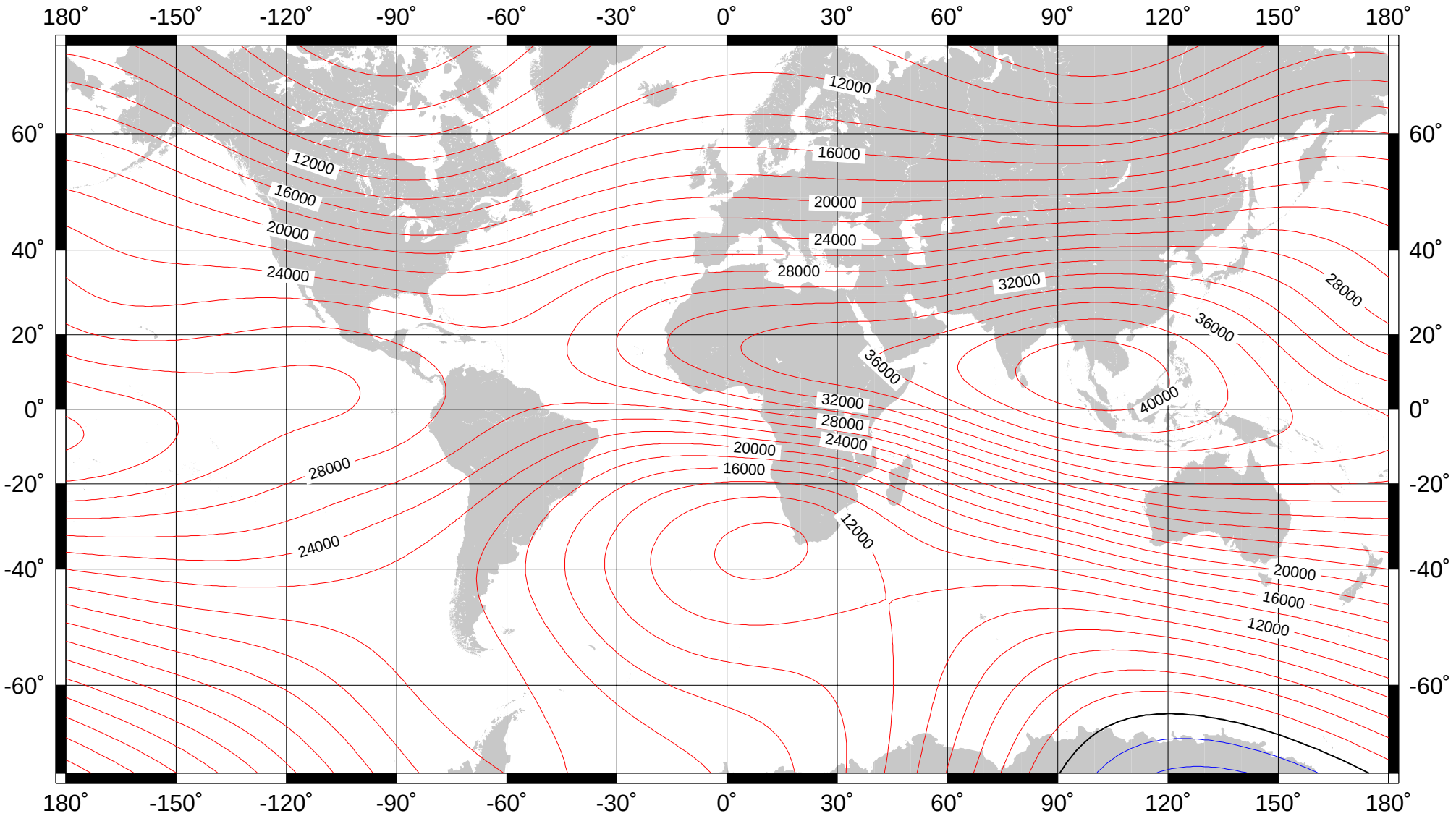

North component (X) at 2000.0 from the World Magnetic Model (WMM2000). Red - positive (north), blue - negative (south), black - zero. Contour interval is 2000 nT and projection is Mercator. This is an example of an isodynamic chart.

Figure 199

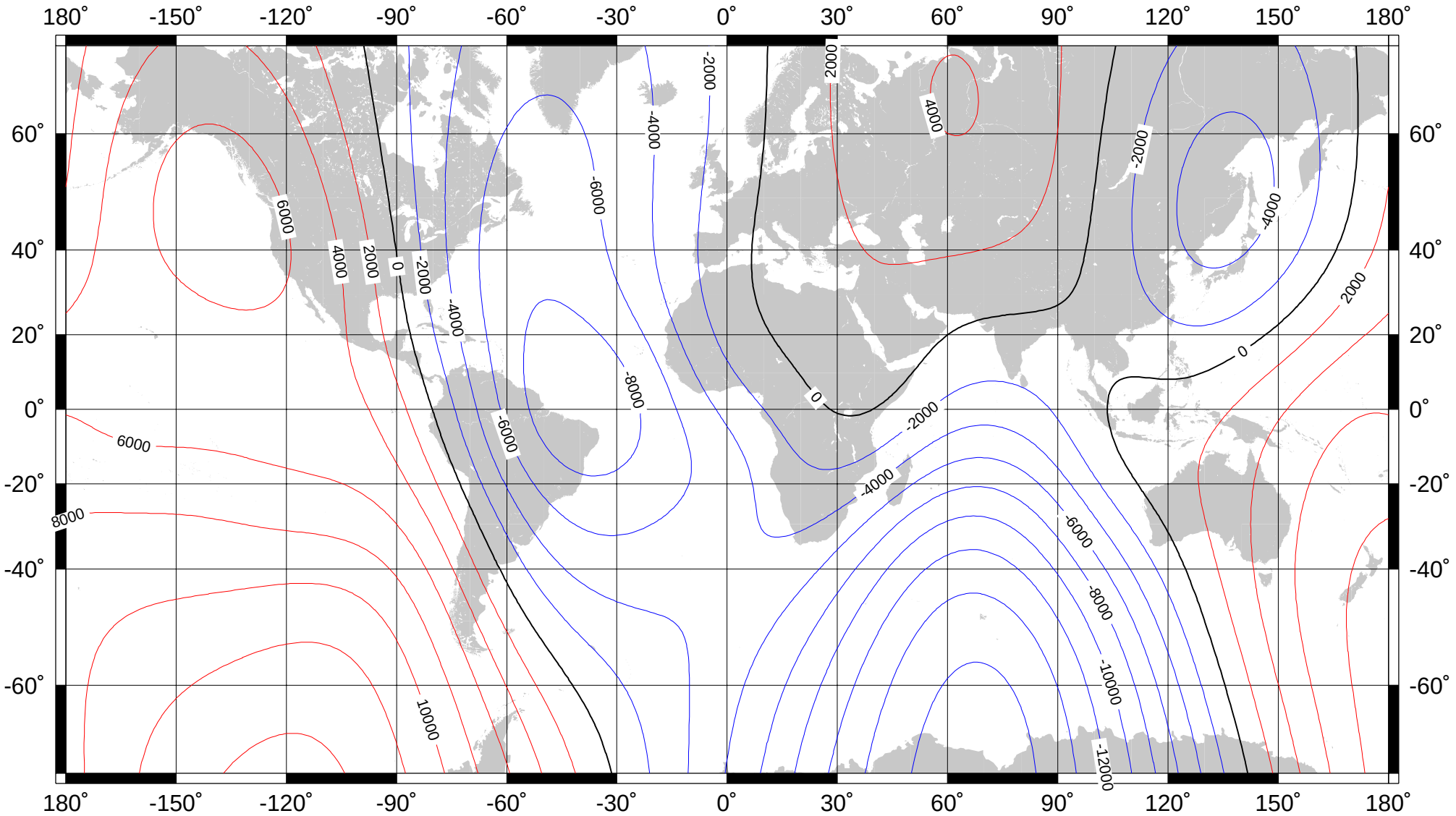

East component (*Y*) at 2000.0 from the World Magnetic Model (WMM2000). Red - positive (east), blue - negative (west), black - zero. Contour interval is 2000 nT and projection is Mercator. This is an example of an isodynamic chart.

Figure 200

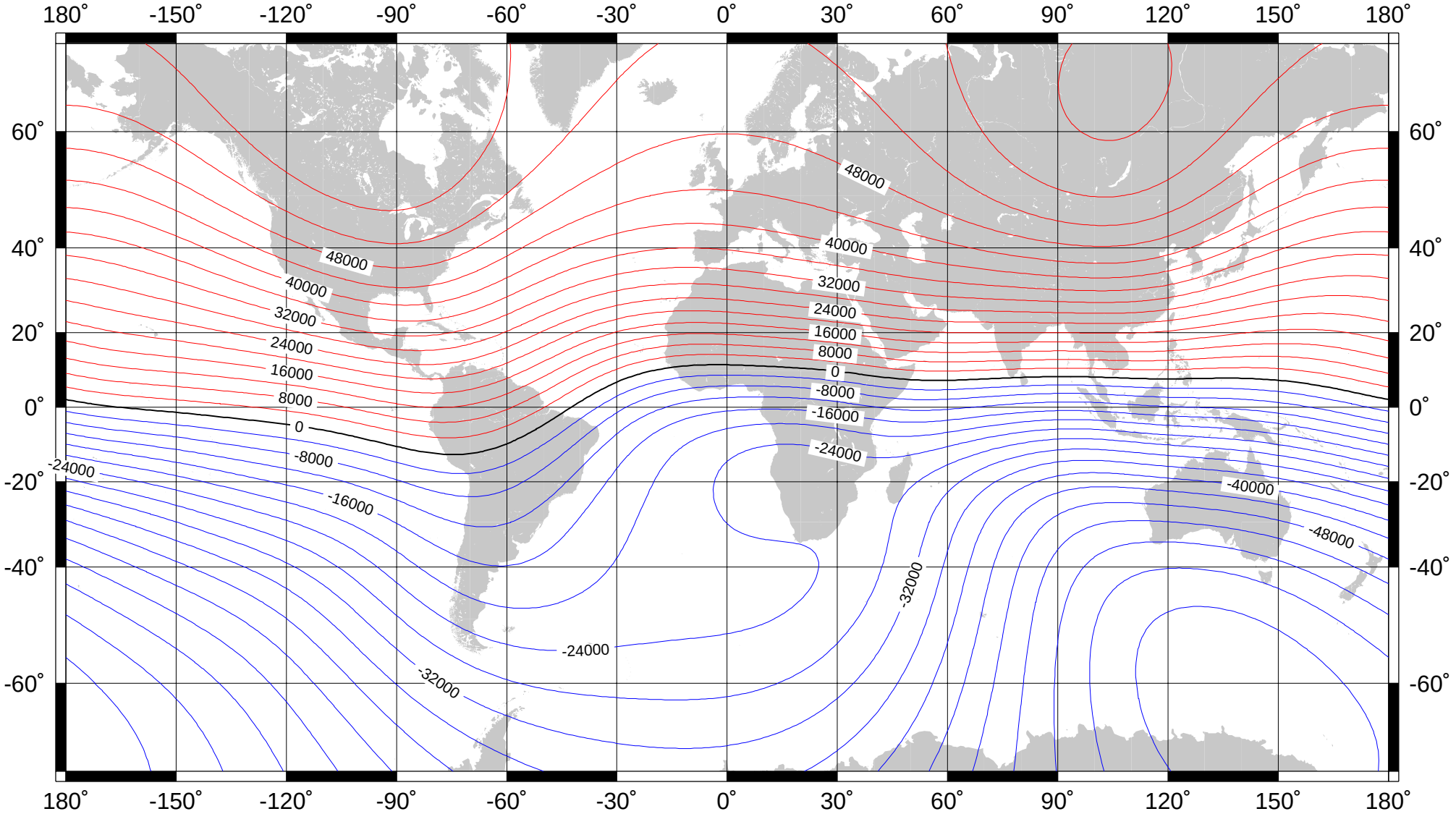

Vertical intensity (*Z*) at 2000.0 from the World Magnetic Model (WMM2000). Red - positive (down), blue - negative (up), black - zero. Contour interval is 4000 nT and projection is Mercator. This is an example of an isodynamic chart.

Figure 201

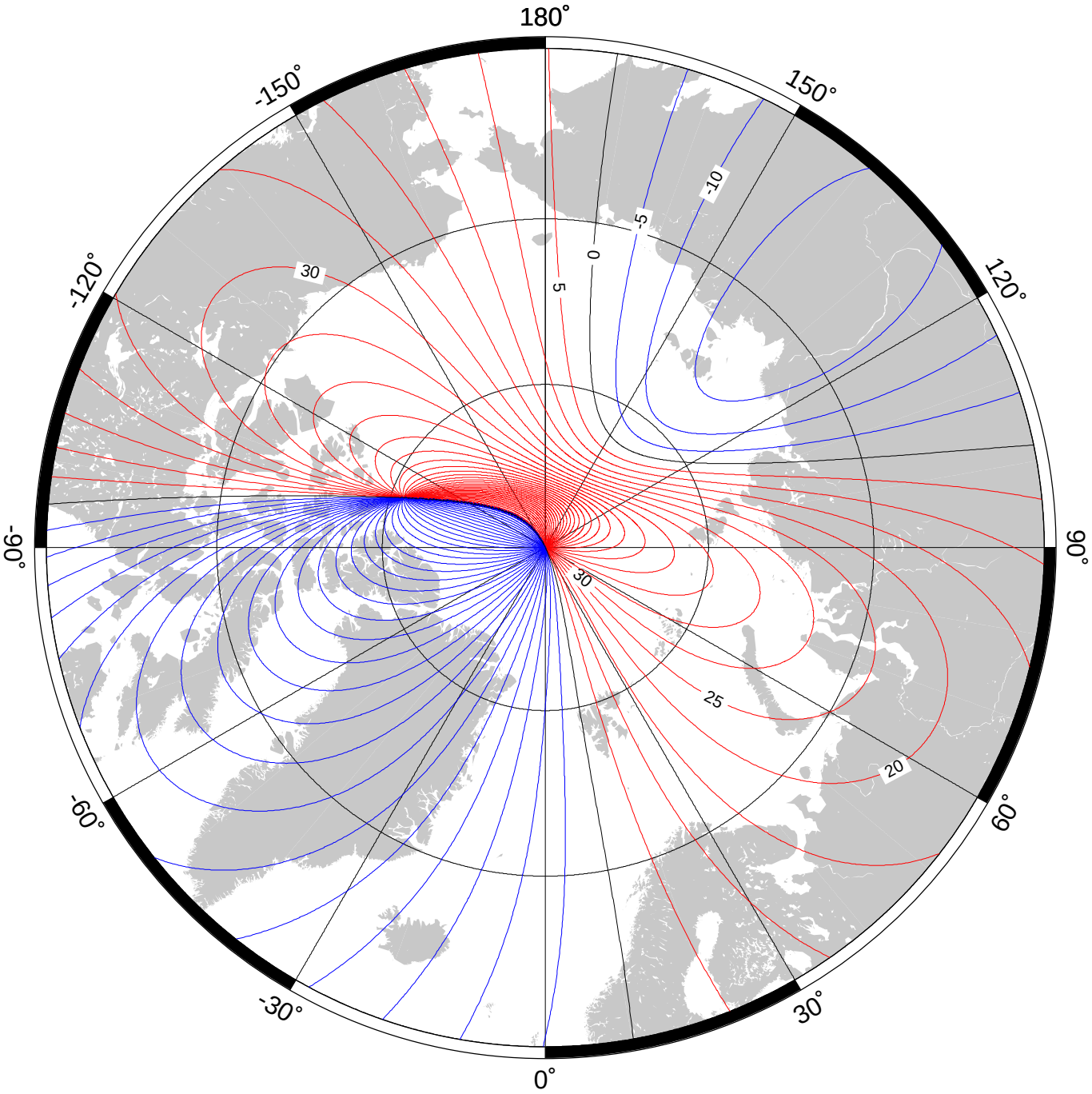

Declination (magnetic variation) in region of north pole at 2000.0 from the World Magnetic Model (WMM2000). Red - positive (east), blue - negative (west), black - zero. Contour interval is 5˚ and projection is Polar Stereographic.

Figure 202

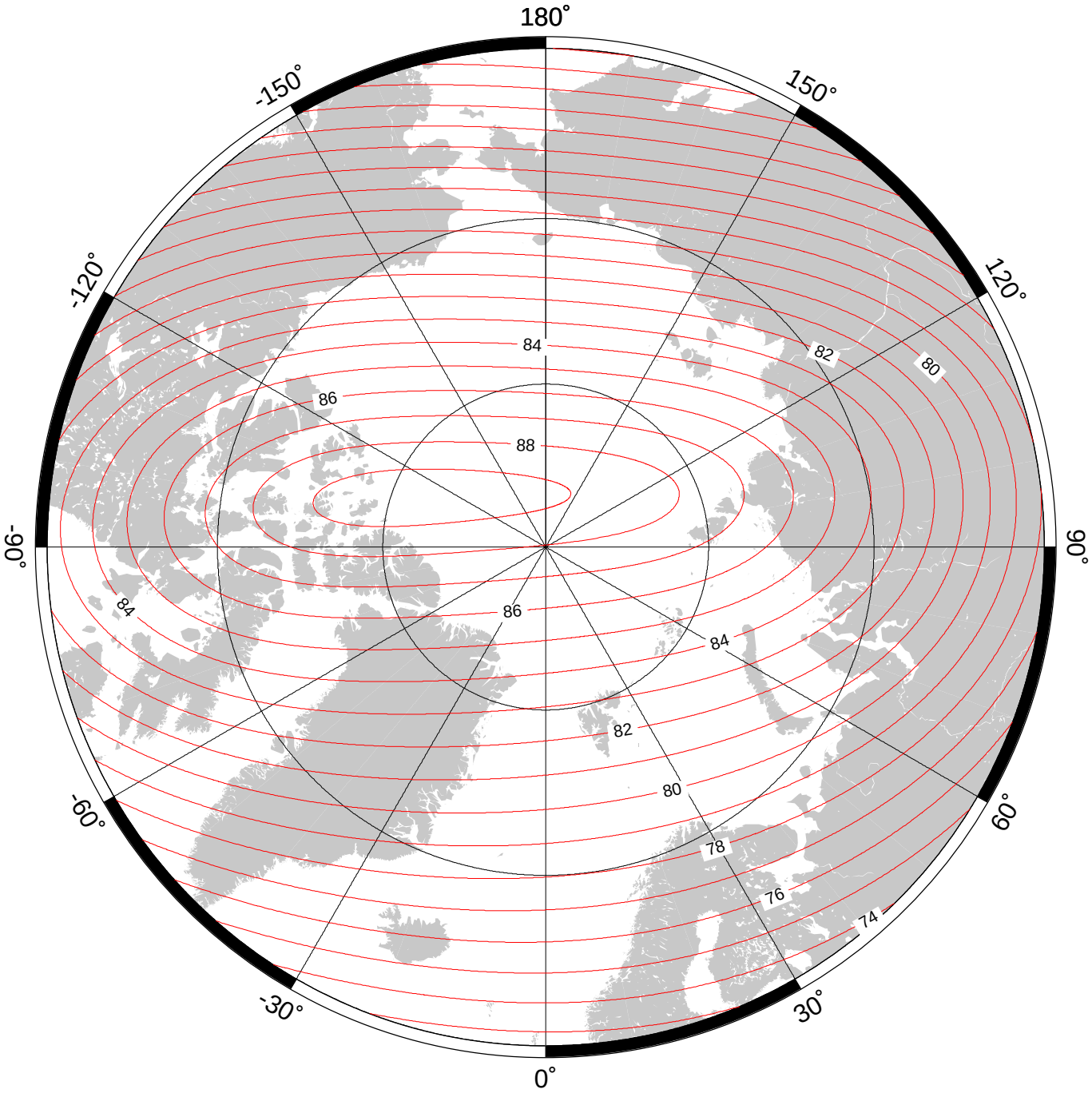

Inclination (magnetic dip) in region of north pole at 2000.0 from the World Magnetic Model (WMM2000). Contour interval is 1˚ and projection is Polar Stereographic.

Figure 203

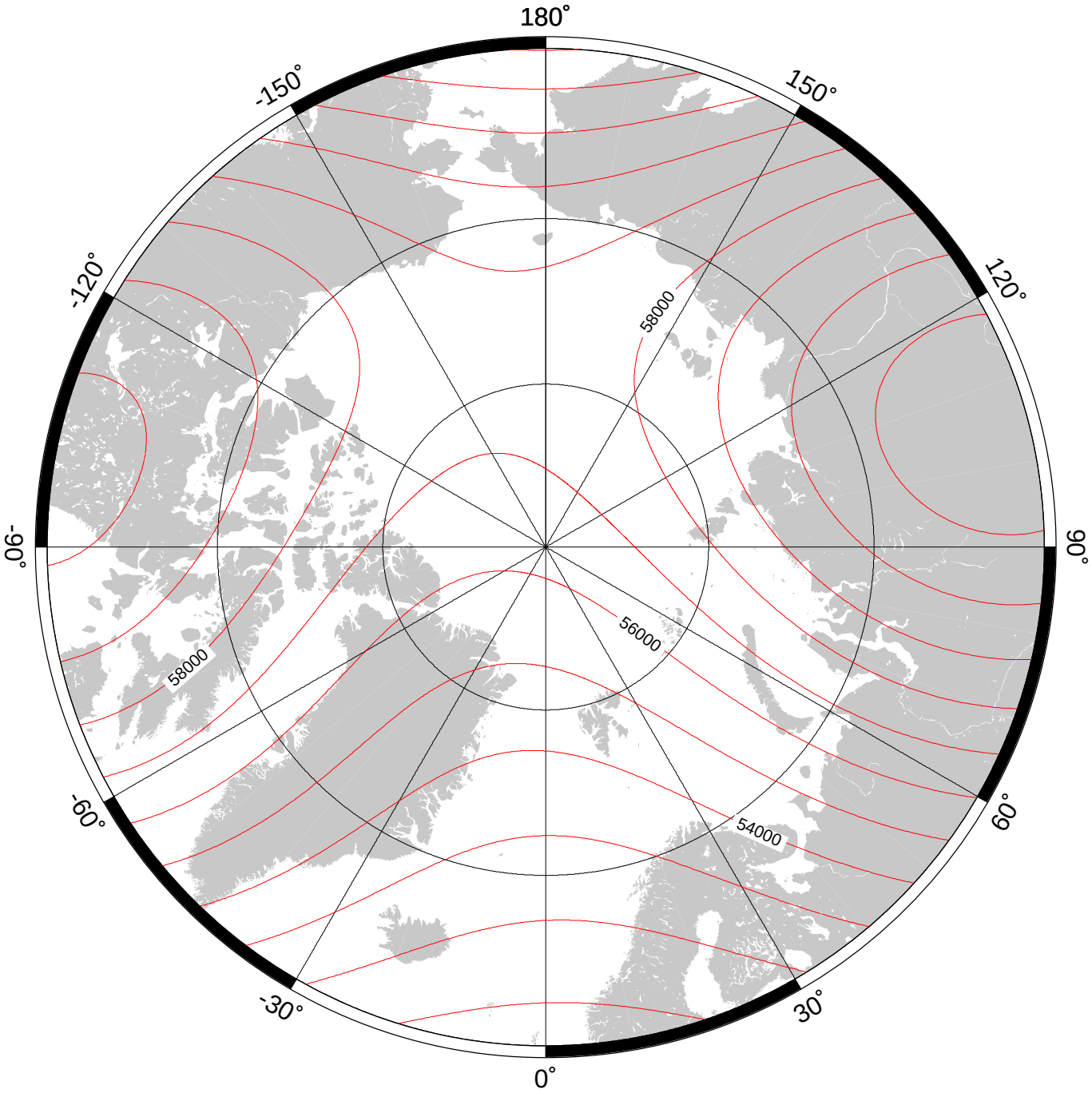

Total intensity (*F*) in region of north pole at 2000.0 from the World Magnetic Model (WMM2000). Contour interval is 1000 nT and projection is Polar Stereographic.

Figure 204

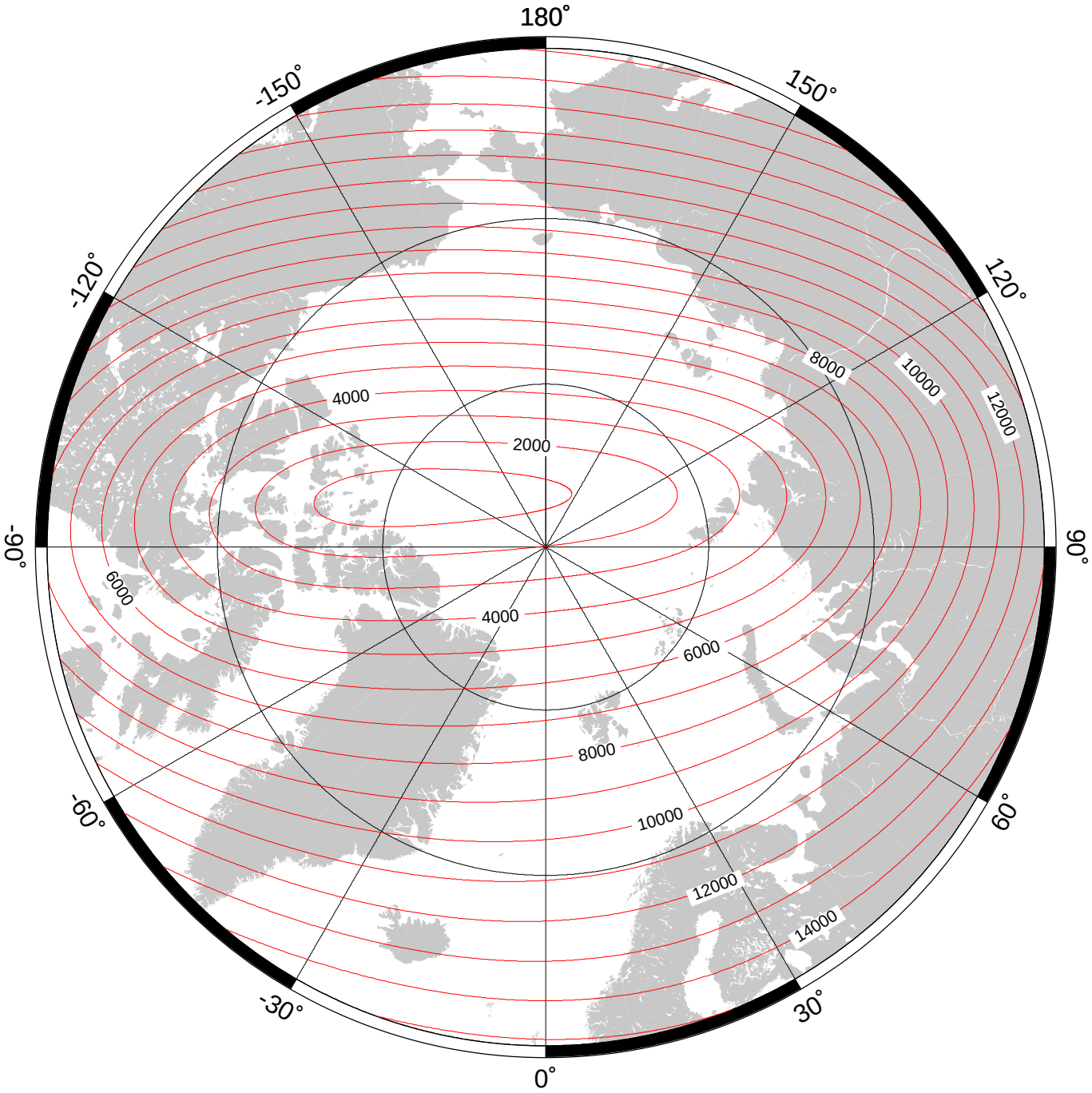

Horizontal intensity (*H*) in region of north pole at 2000.0 from the World Magnetic Model (WMM2000). Contour interval is 1000 nT and projection is Polar Stereographic.

Figure 205

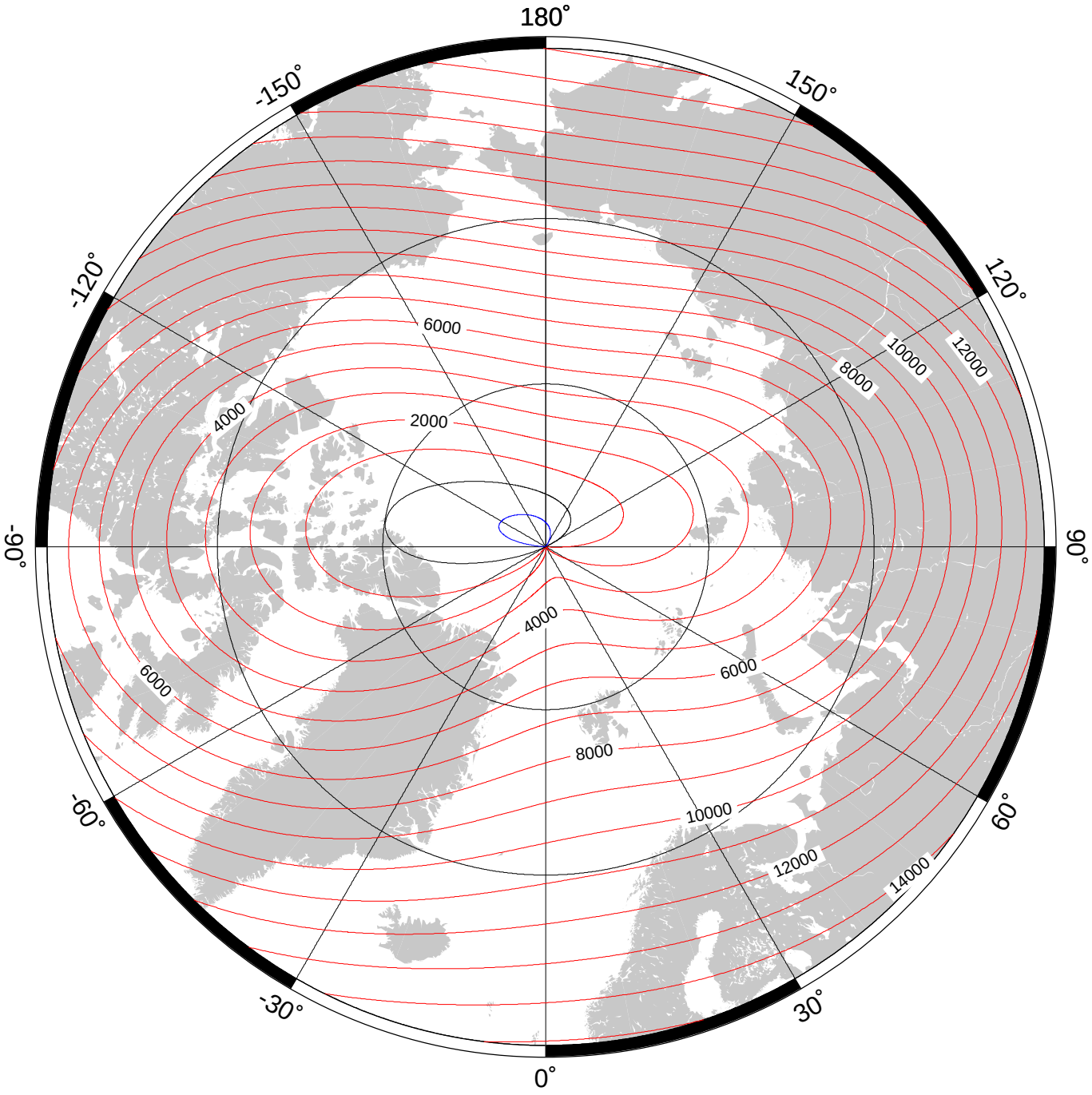

North component (X) in region of north pole at 2000.0 from the World Magnetic Model (WMM2000). Red - positive (north), blue - negative (south), black - zero. Contour interval is 1000 nT and projection is Polar Stereographic.

Figure 206

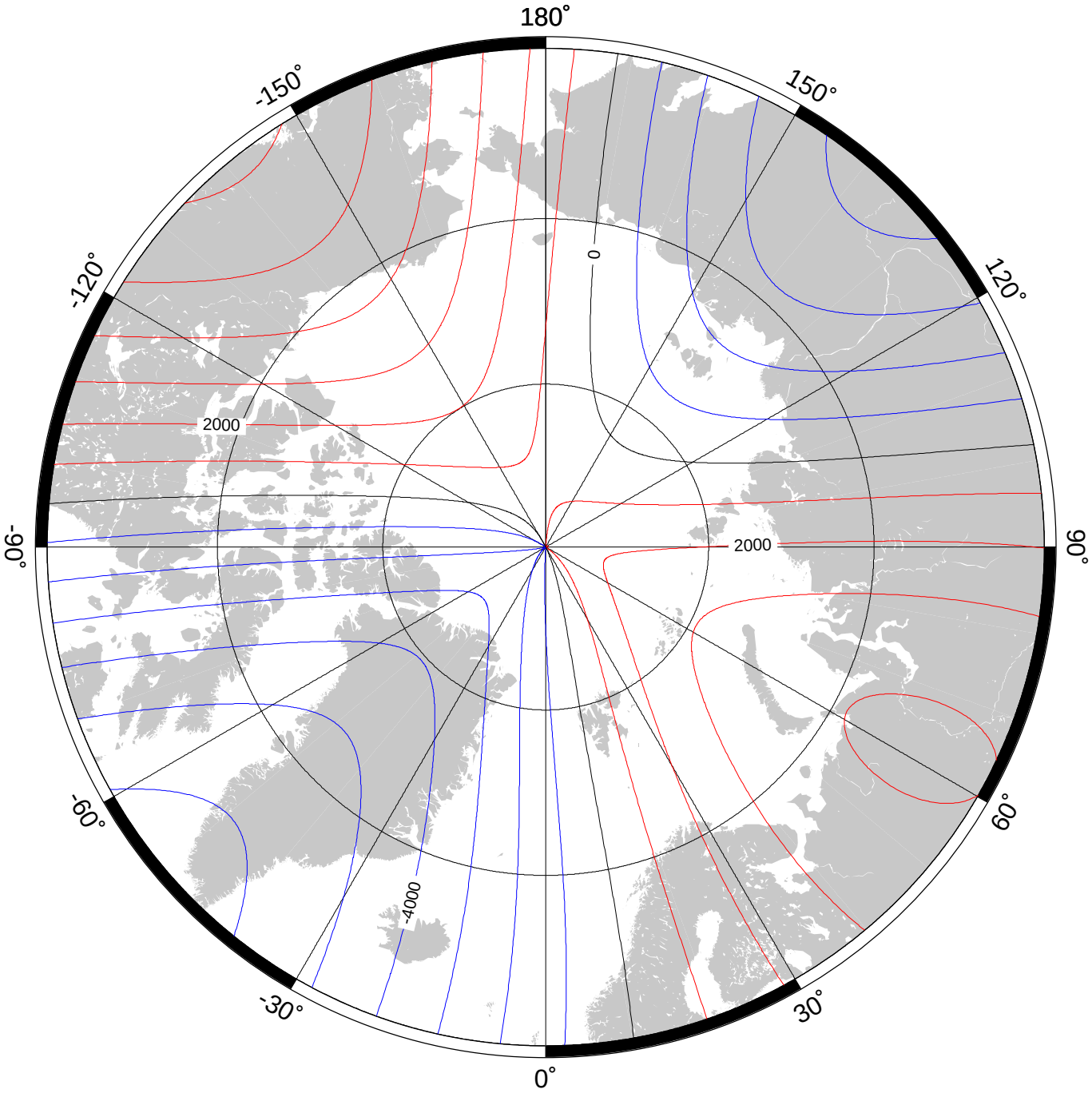

East component (*Y*) in region of north pole at 2000.0 from the World Magnetic Model (WMM2000). Red - positive (east), blue - negative (west), black - zero. Contour interval is 1000 nT and projection is Polar Stereographic.

Figure 207

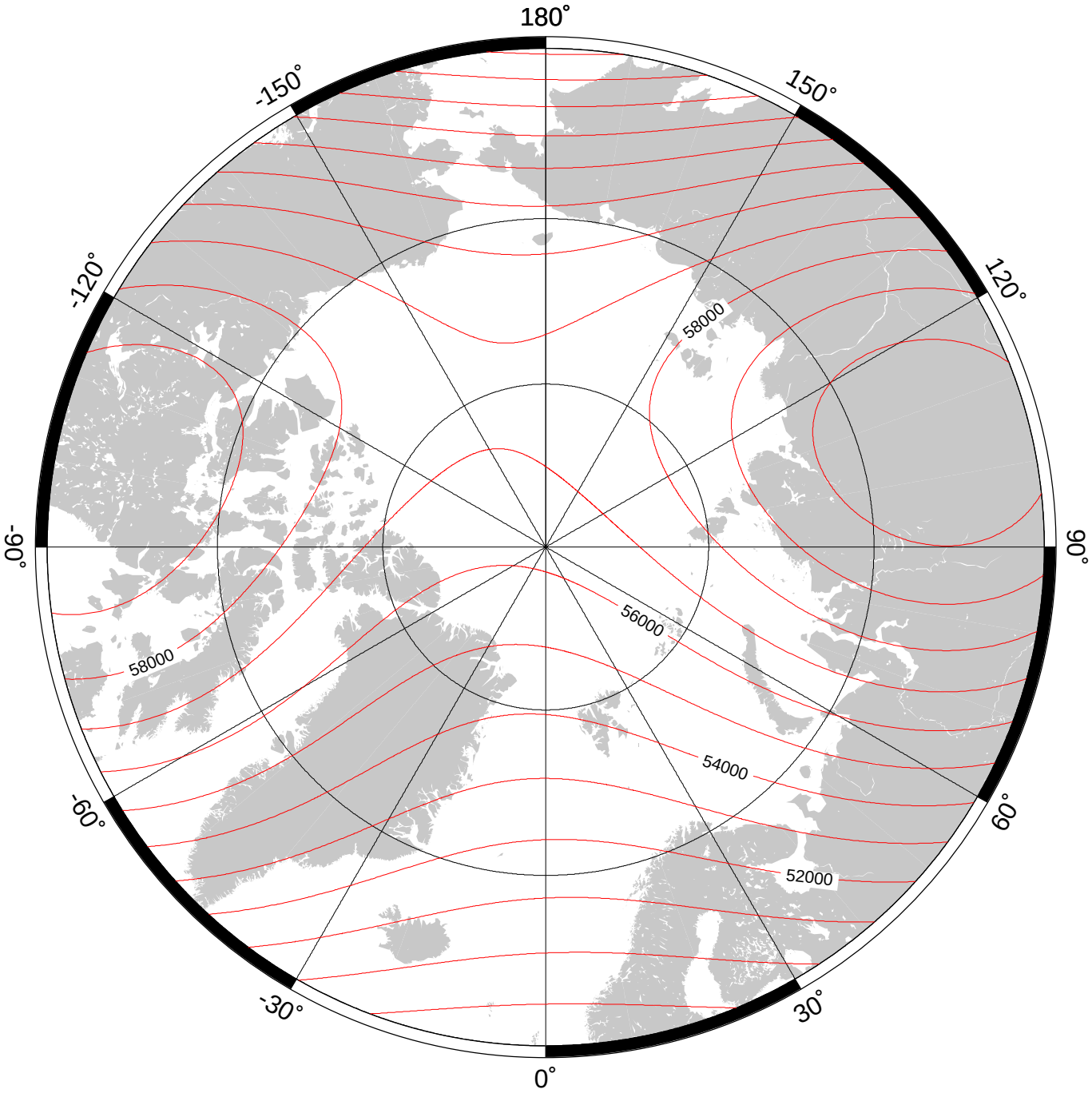

Vertical component (*Z*) in region of north pole at 2000.0 from the World Magnetic Model (WMM2000). Contour interval is 1000 nT and projection is Polar Stereographic.

Figure 208

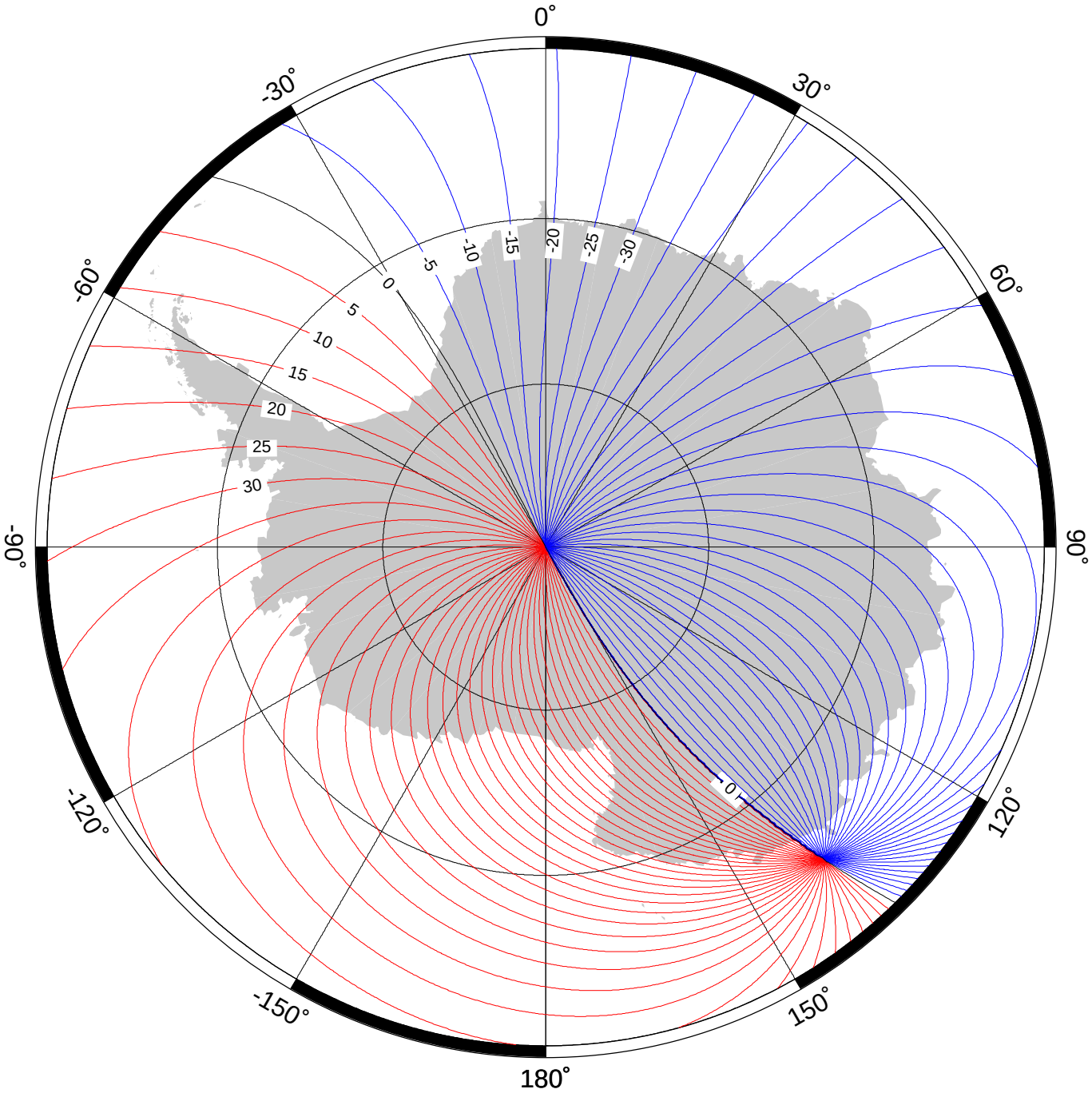

Declination (magnetic variation) in region of south pole at 2000.0 from the World Magnetic Model (WMM2000). Red - positive (east), blue - negative (west), black - zero. Contour interval is 5˚ and projection is Polar Stereographic.

Figure 209

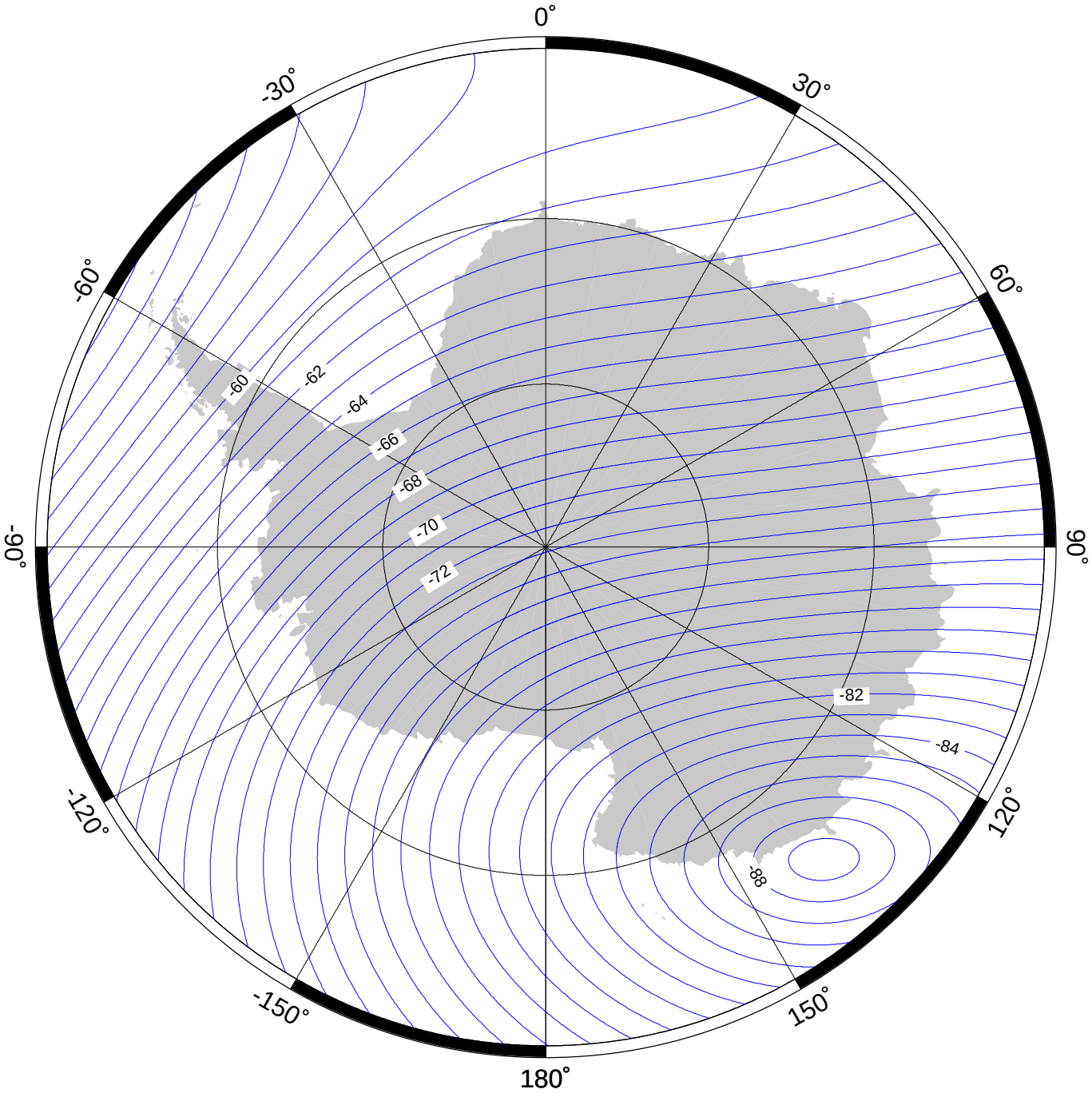

Inclination (magnetic dip) in region of south pole at 2000.0 from the World Magnetic Model (WMM2000). Contour interval is 1˚ and projection is Polar Stereographic.

Figure 210

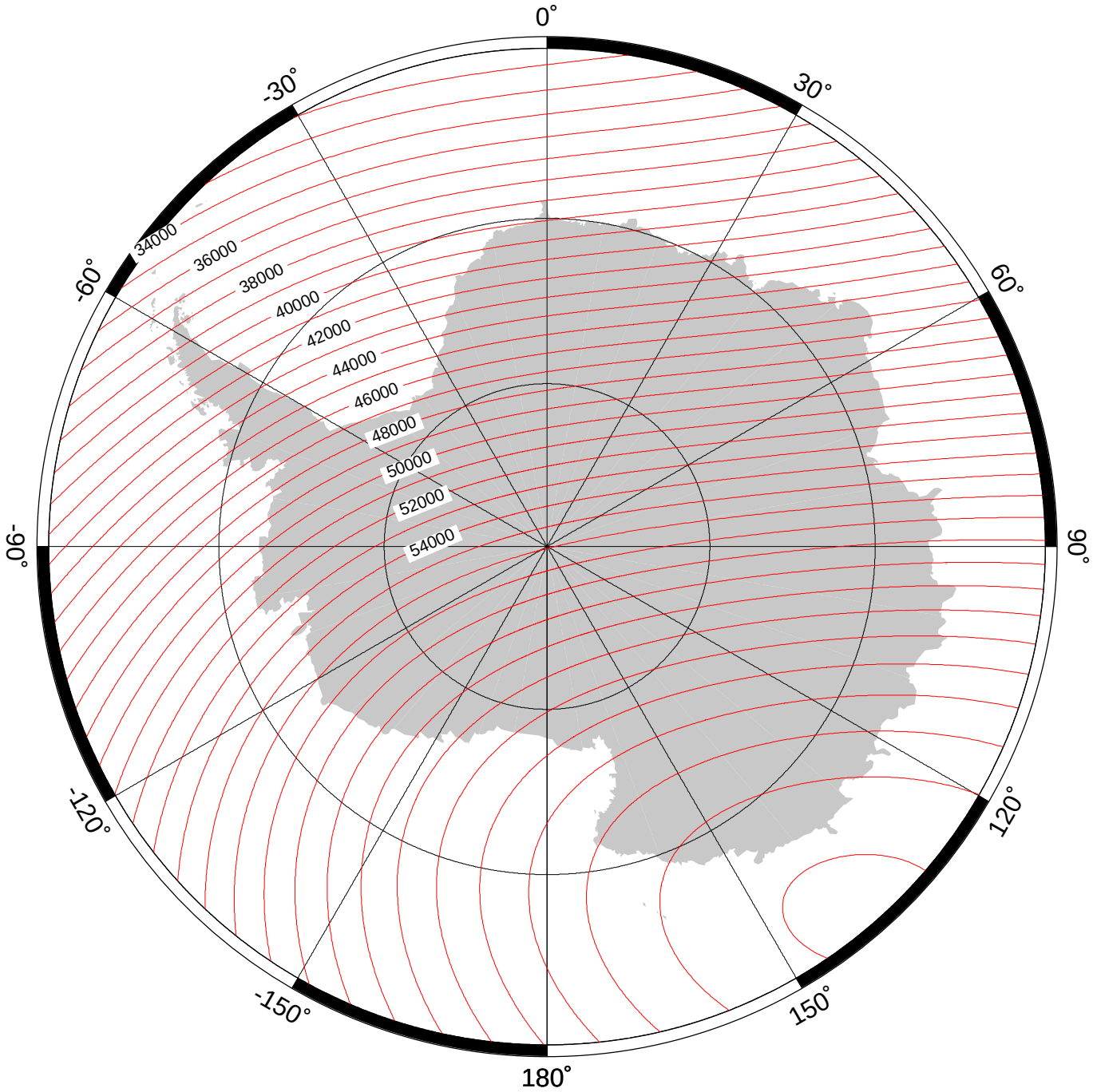

Total intensity (*F*) in region of south pole at 2000.0 from the World Magnetic Model (WMM2000). Contour interval is 1000 nT and projection is Polar Stereographic.

Figure 211

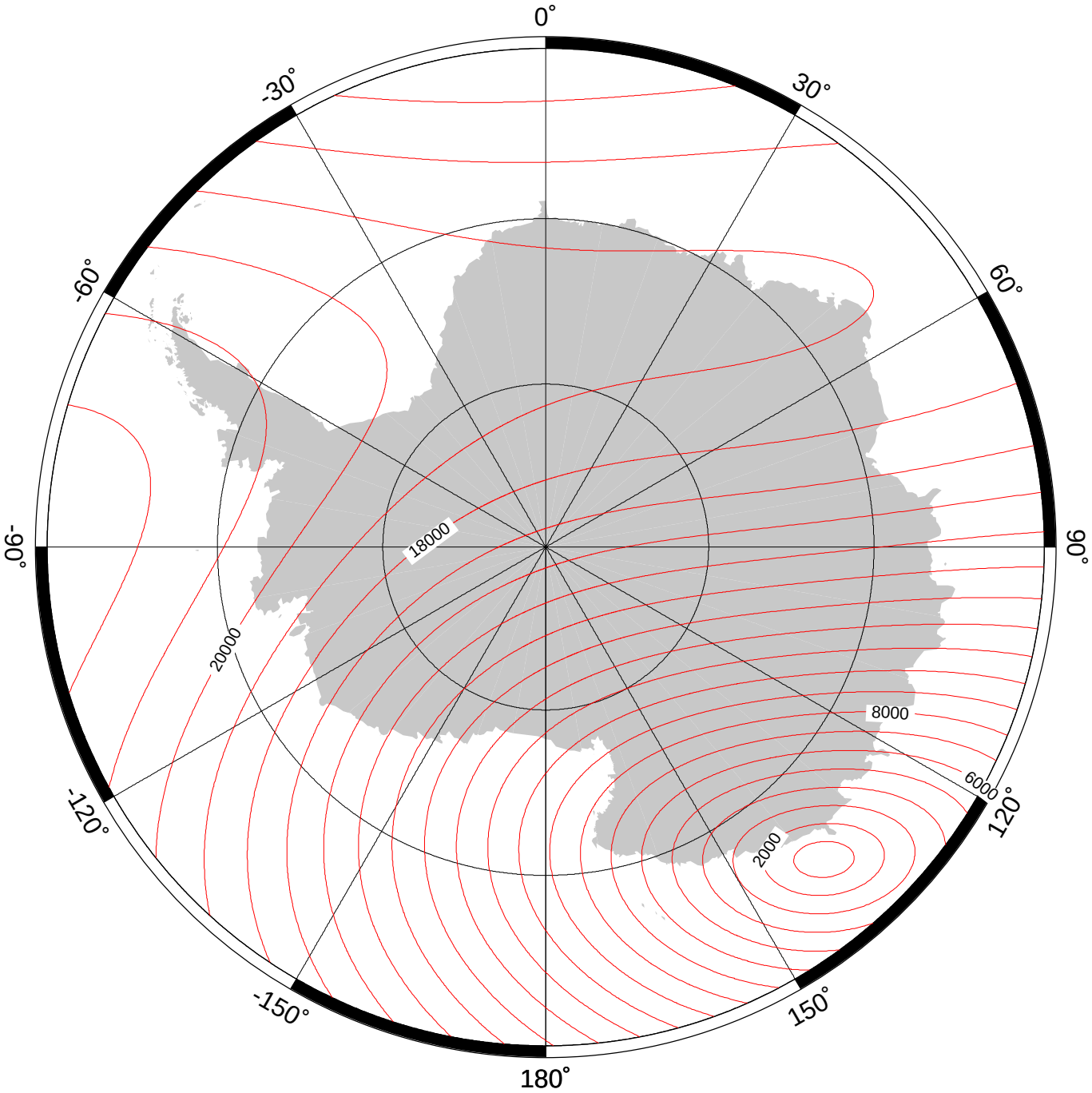

Horizontal intensity (*H*) in region of south pole at 2000.0 from the World Magnetic Model (WMM2000). Contour interval is 1000 nT and projection is Polar Stereographic.

Figure 212

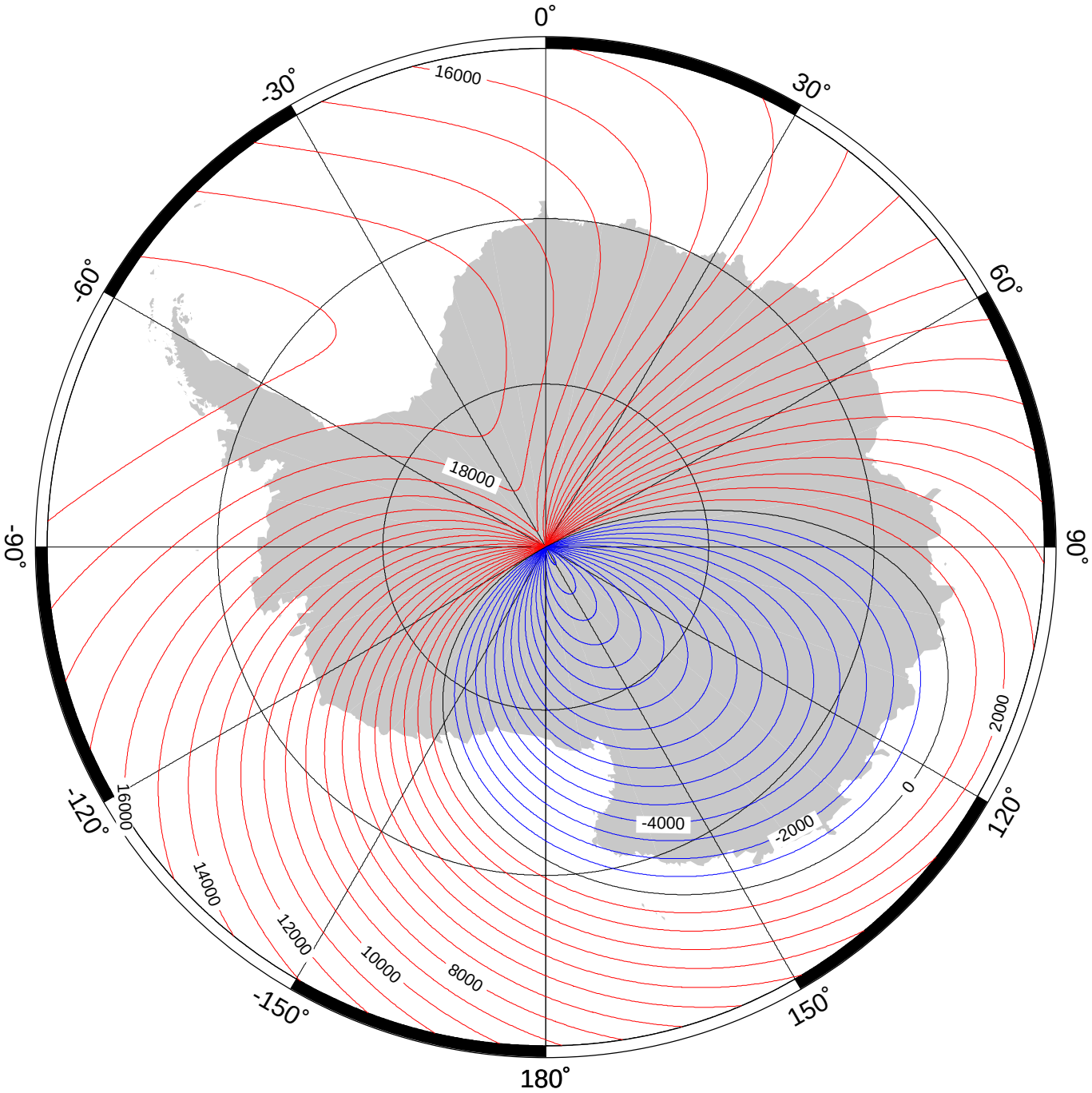

North component (X) in region of south pole at 2000.0 from the World Magnetic Model (WMM2000). Red - positive (north), blue - negative (south), black - zero. Contour interval is 1000 nT and projection is Polar Stereographic.

Figure 213

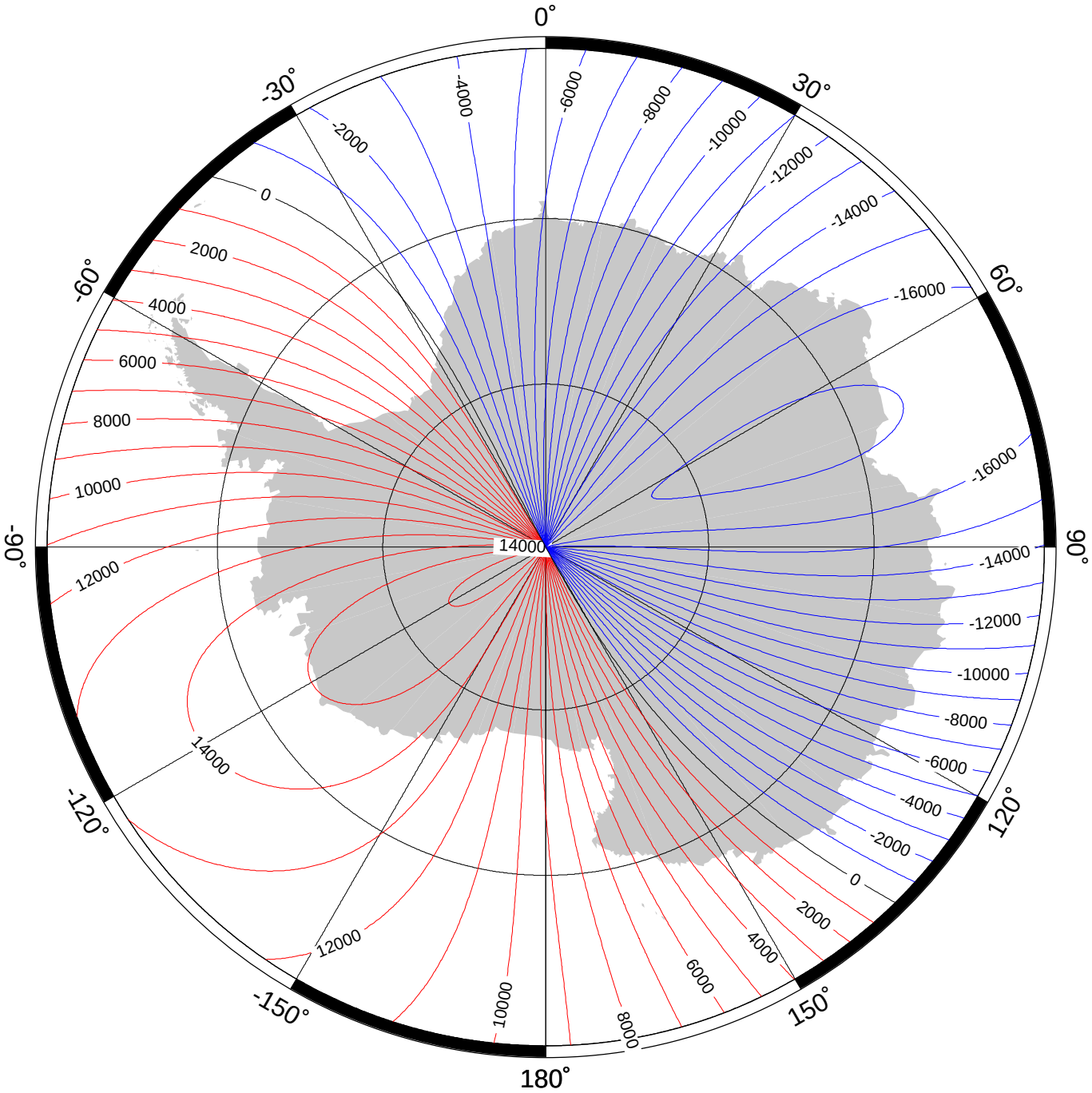

East component (*Y*) in region of south pole at 2000.0 from the World Magnetic Model (WMM2000). Red - positive (east), blue - negative (west), black - zero. Contour interval is 1000 nT and projection is Polar Stereographic.

Figure 214

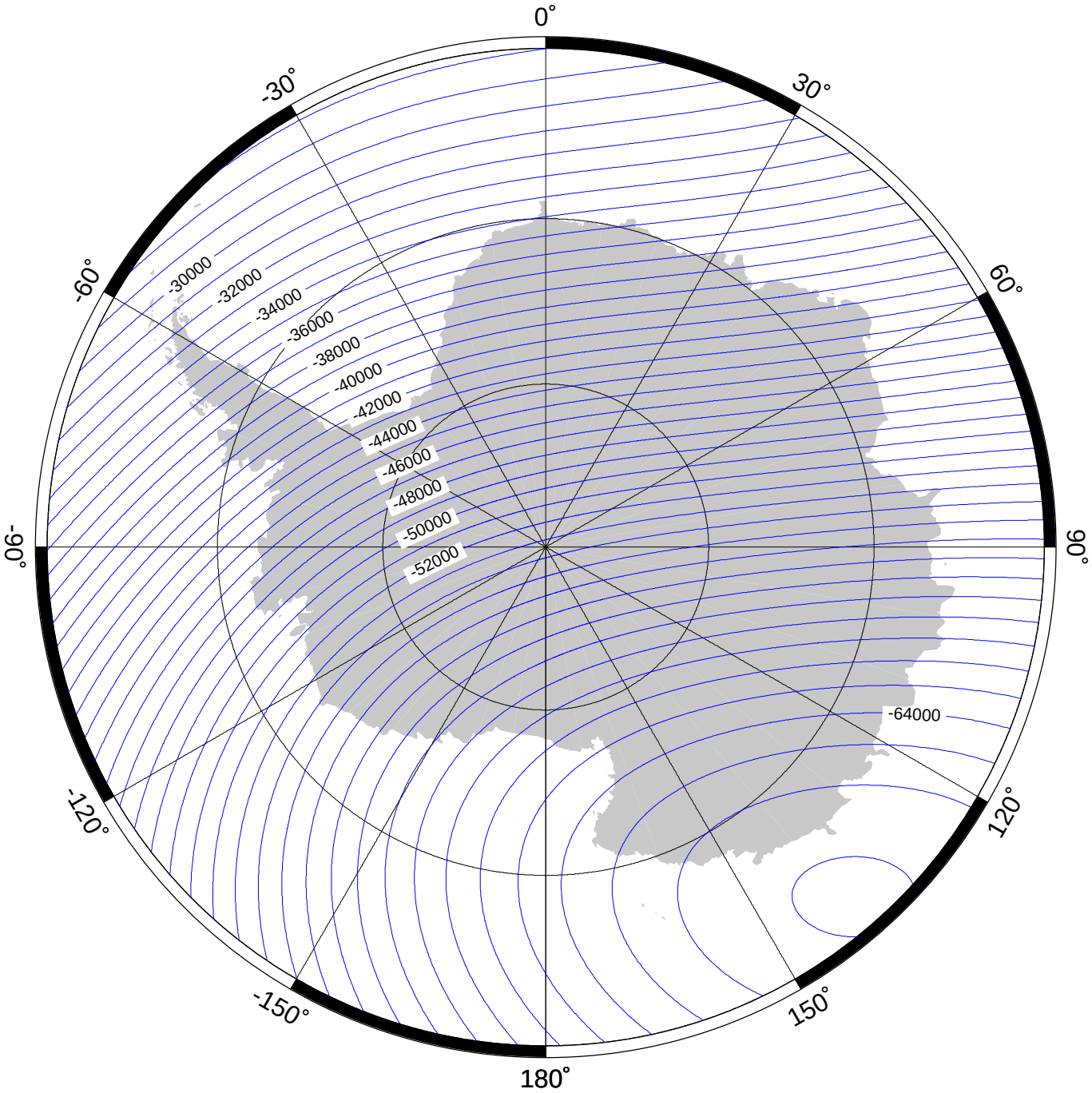

Vertical component (*Z*) in region of south pole at 2000.0 from the World Magnetic Model (WMM2000). Contour interval is 1000 nT and projection is Polar Stereographic.

Figure 215

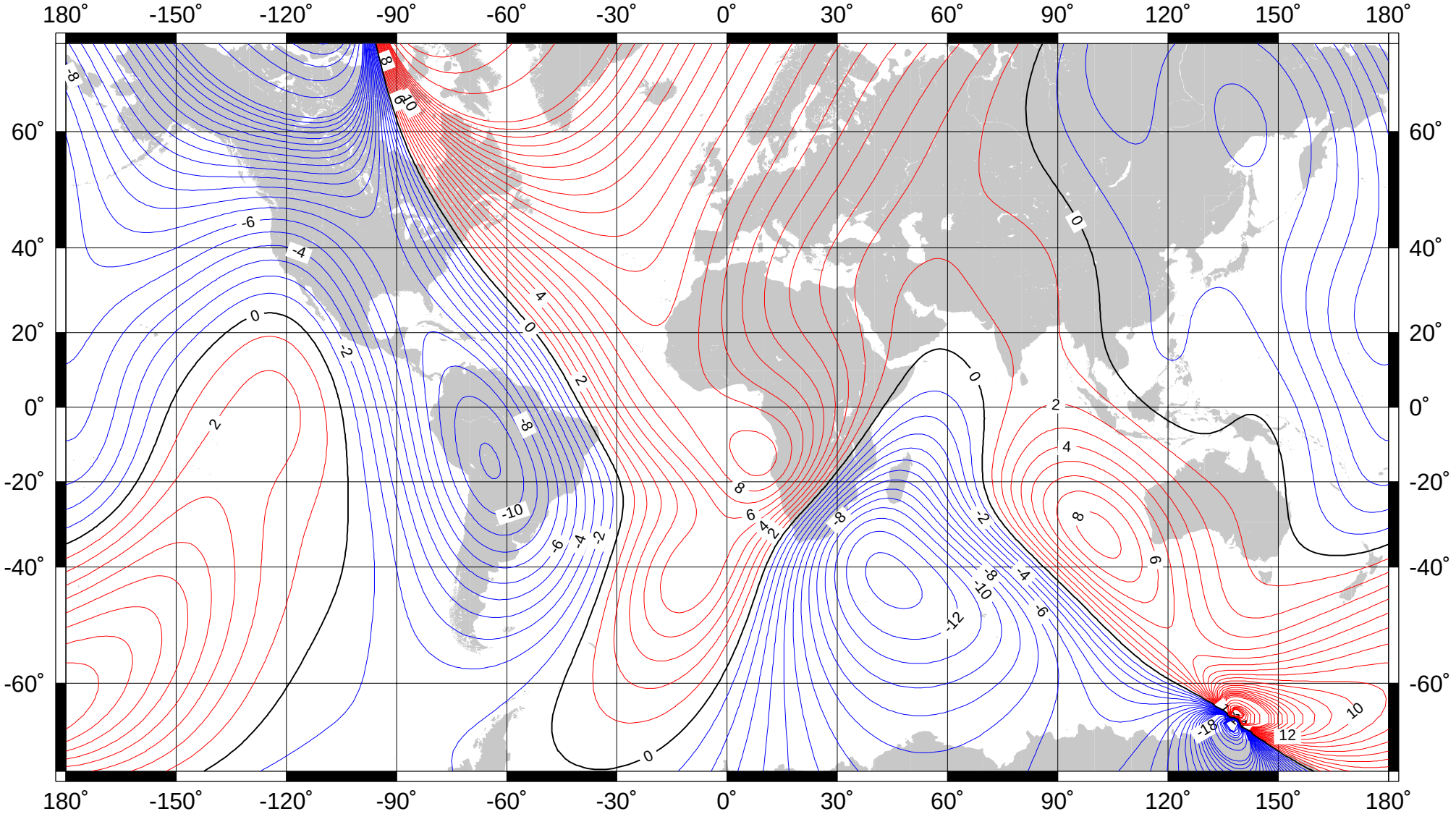

Annual rate of change of declination for 2000.0 to 2005.0 from the World Magnetic Model (WMM2000). Red - easterly change, blue - westerly change, black - zero change. Contour interval is 1´/year up to ±20´/year, thereafter 5´/year, and projection is Mercator. This is an example of an isoporic chart.

Figure 216

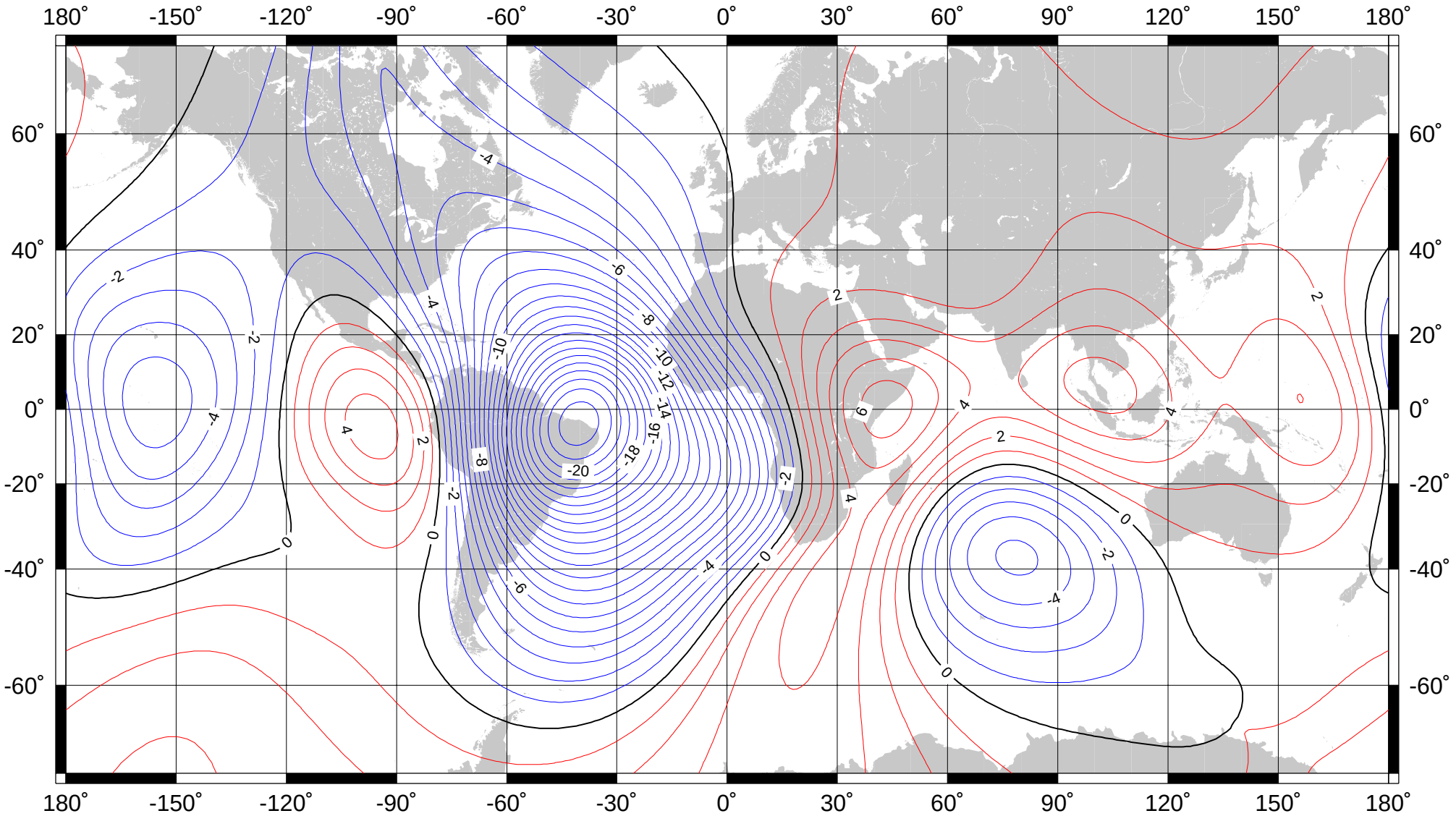

Annual rate of change of inclination for 2000.0 to 2005.0 from the World Magnetic Model (WMM2000). Red - positive (down) change, blue - negative (up) change, black - zero change. Contour interval is 1´/year and projection is Mercator. This is an example of an isoporic chart.

Figure 217

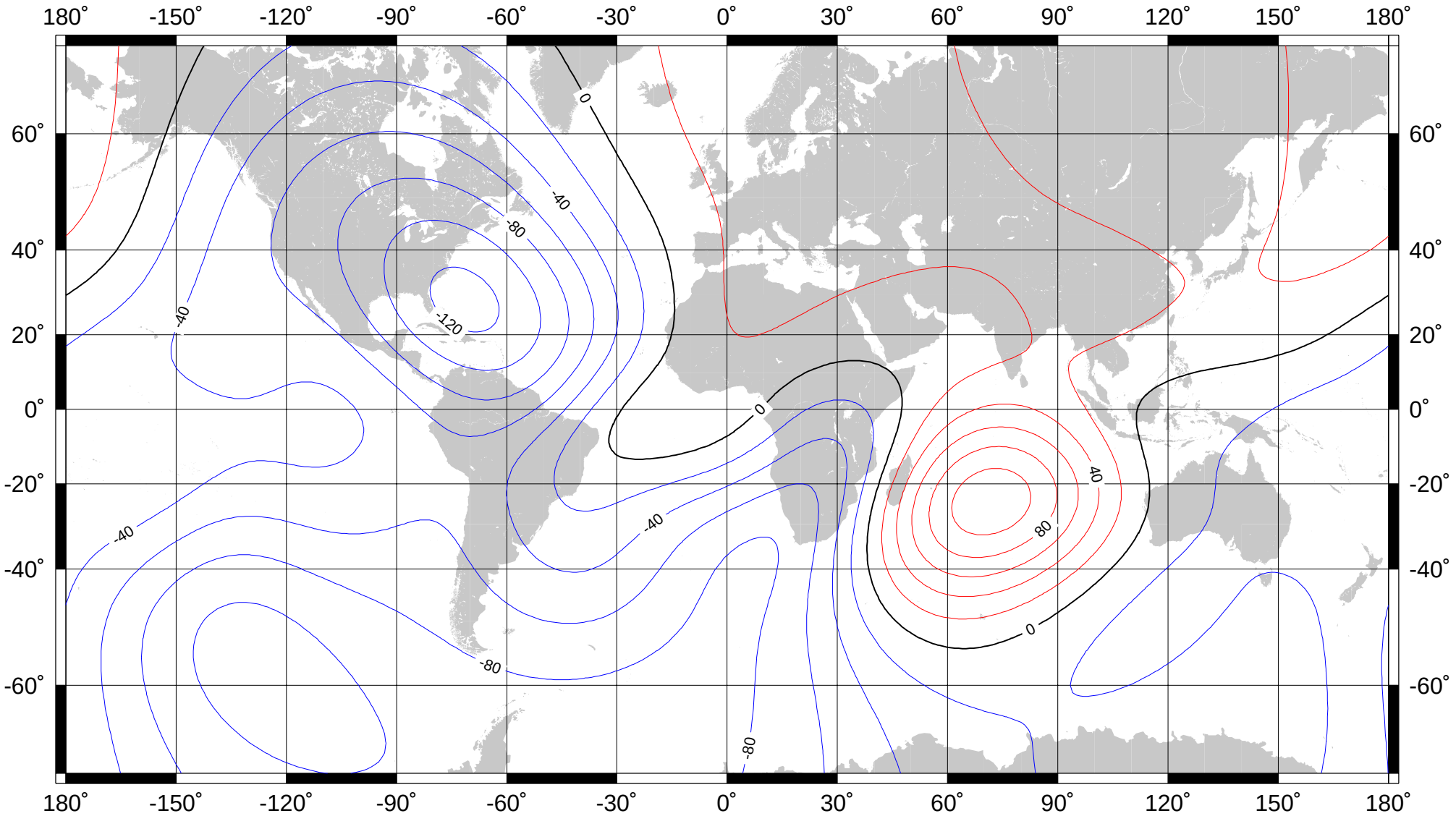

Annual rate of change of total intensity for 2000.0 to 2005.0 from the World Magnetic Model (WMM2000). Red - positive change, blue - negative change, black - zero change. Contour interval is 20 nT/year and projection is Mercator. This is an example of an isoporic chart.

Figure 218

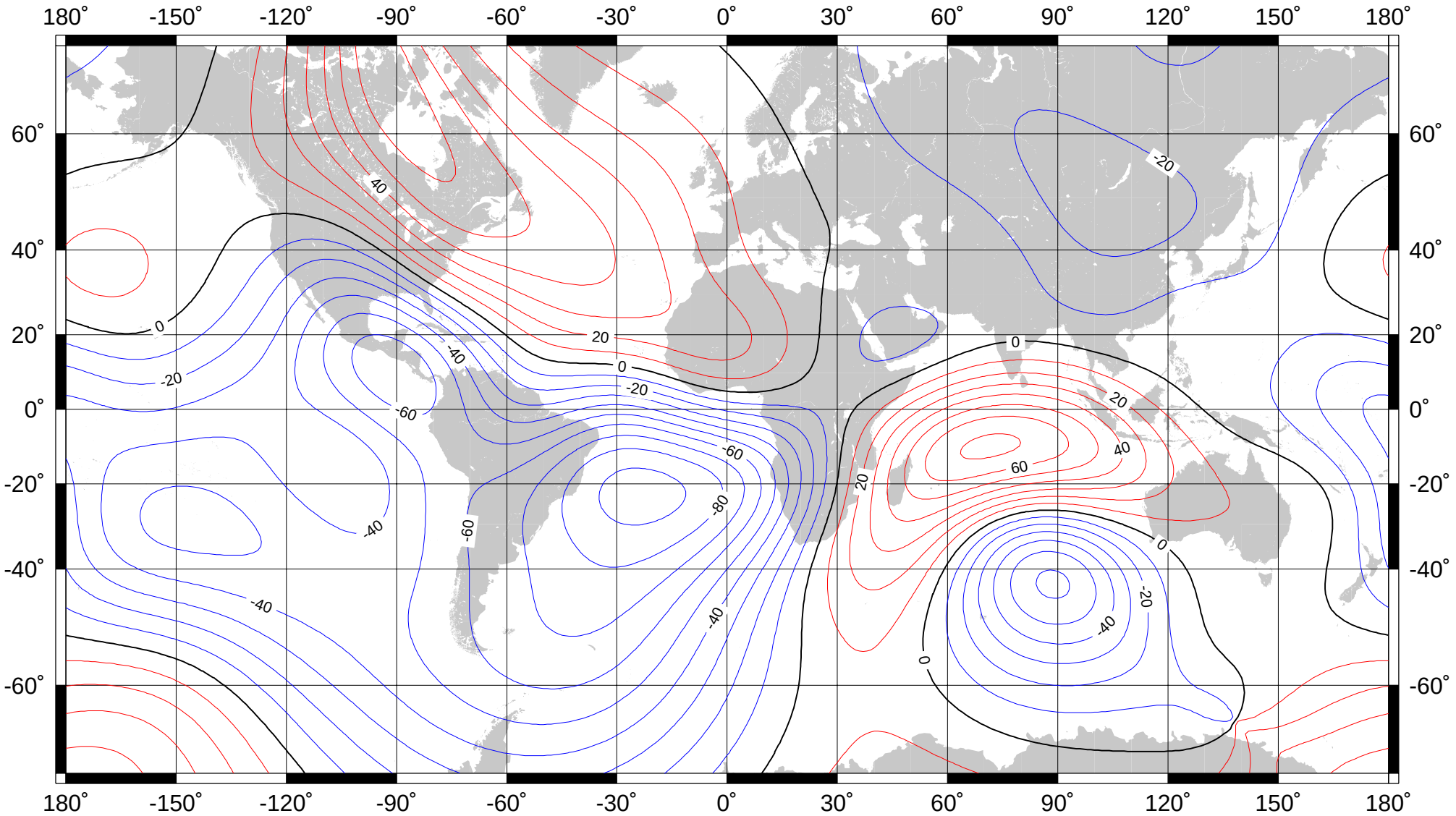

Annual rate of change of horizontal intensity for 2000.0 to 2005.0 from the World Magnetic Model (WMM2000). Red - positive change, blue - negative change, black - zero change. Contour interval is 10 nT/year and projection is Mercator. This is an example of an isoporic chart.

Figure 219

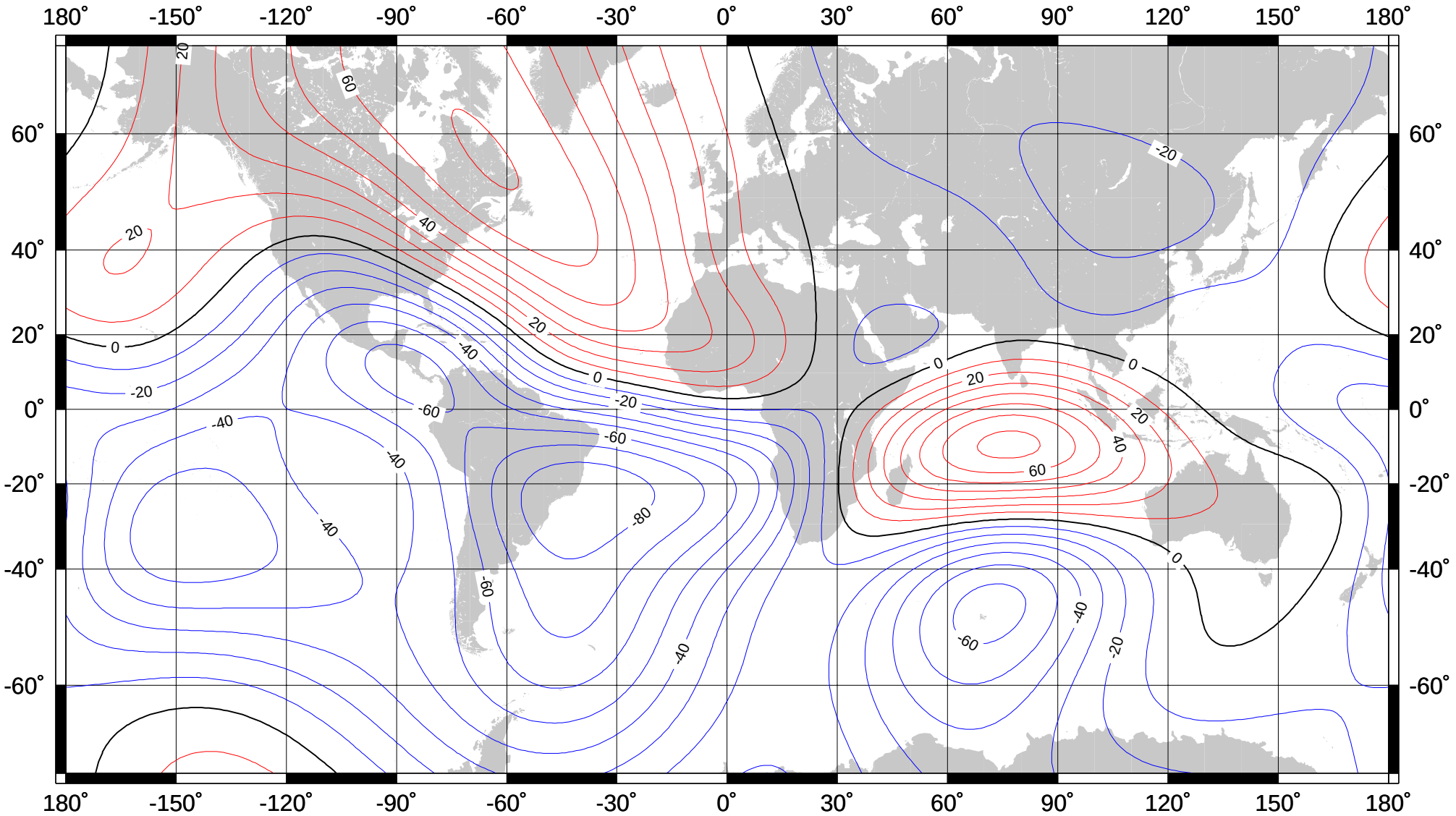

Annual rate of change of north component for 2000.0 to 2005.0 from the World Magnetic Model (WMM2000). Red - positive change, blue - negative change, black - zero change. Contour interval is 10 nT/year and projection is Mercator. This is an example of an isoporic chart.

Figure 220

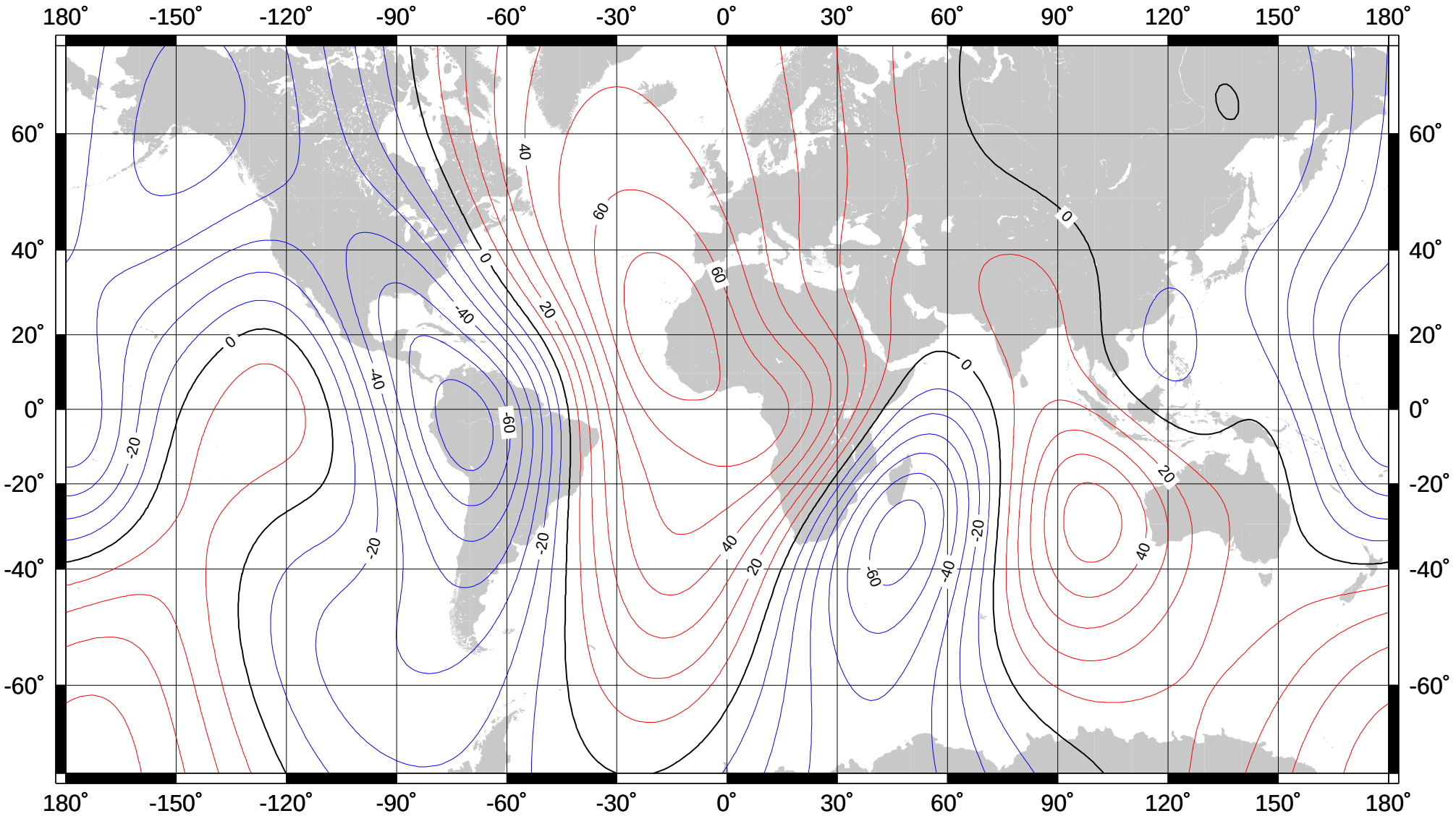

Annual rate of change of east component for 2000.0 to 2005.0 from the World Magnetic Model (WMM2000). Red - positive change, blue - negative change, black - zero change. Contour interval is 10 nT/year and projection is Mercator. This is an example of an isoporic chart.

Figure 221

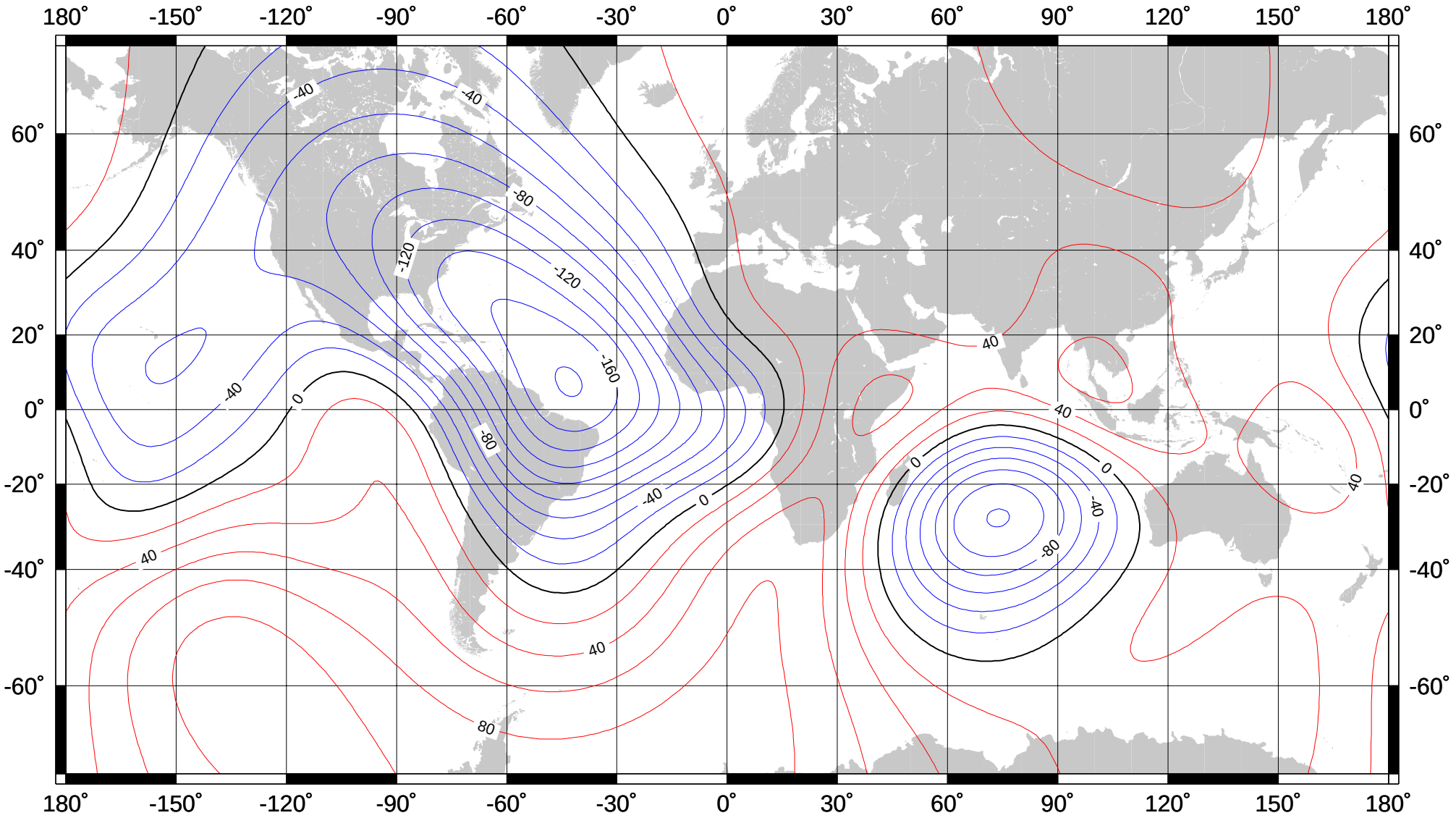

Annual rate of change of vertical intensity for 2000.0 to 2005.0 from the World Magnetic Model (WMM2000). Red - positive change (down), blue - negative change (up) , black - zero change. Contour interval is 20 nT/year and projection is Mercator. This is an example of an isoporic chart.

Figure 222

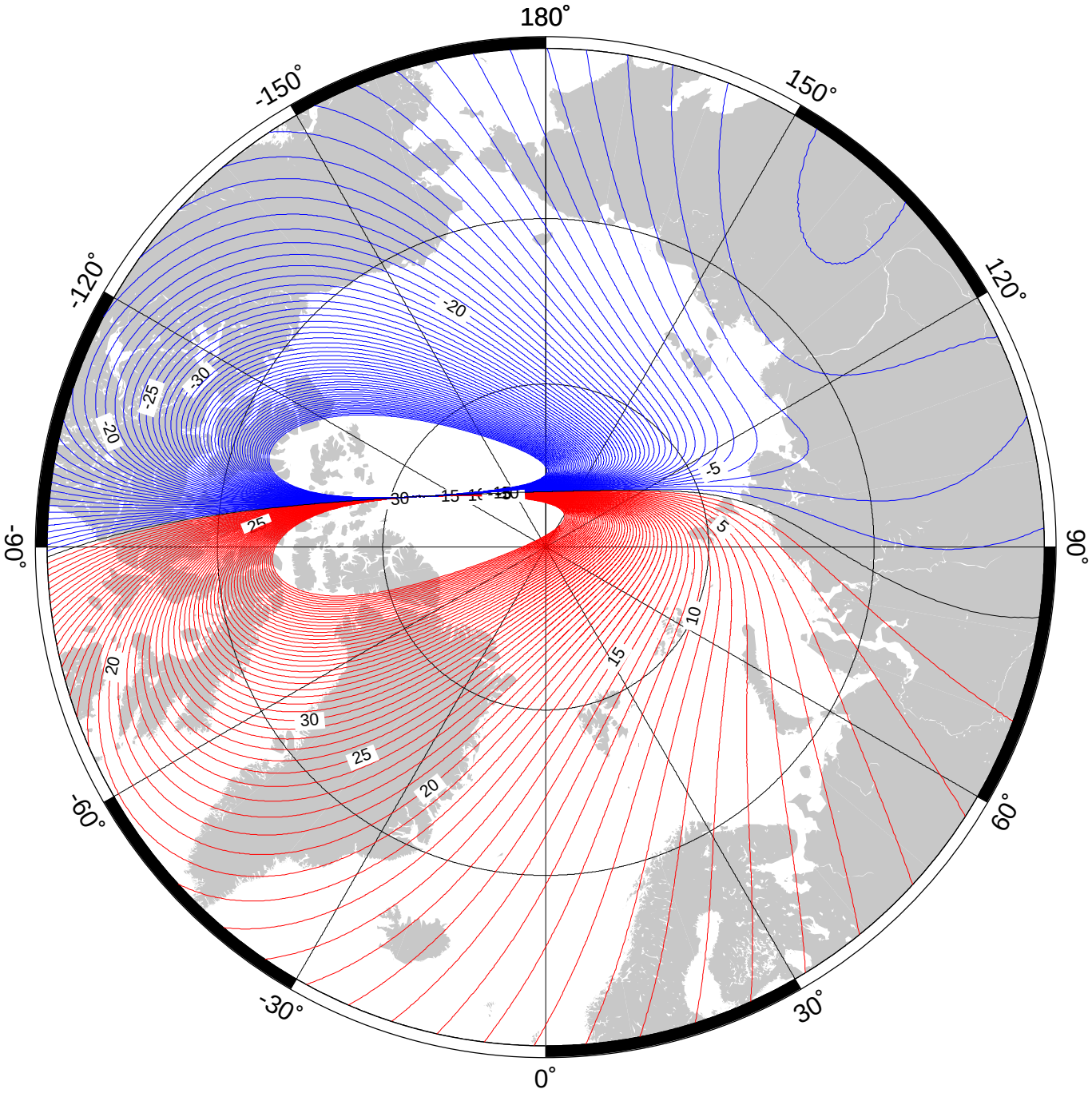

Annual rate of change of declination in region of north pole for 2000.0 to 2005.0 from the World Magnetic Model (WMM2000). Red - easterly change, blue - westerly change, black - zero change. Contour interval is 1´/year up to ±60´/year and projection is Polar Stereographic.

Figure 223

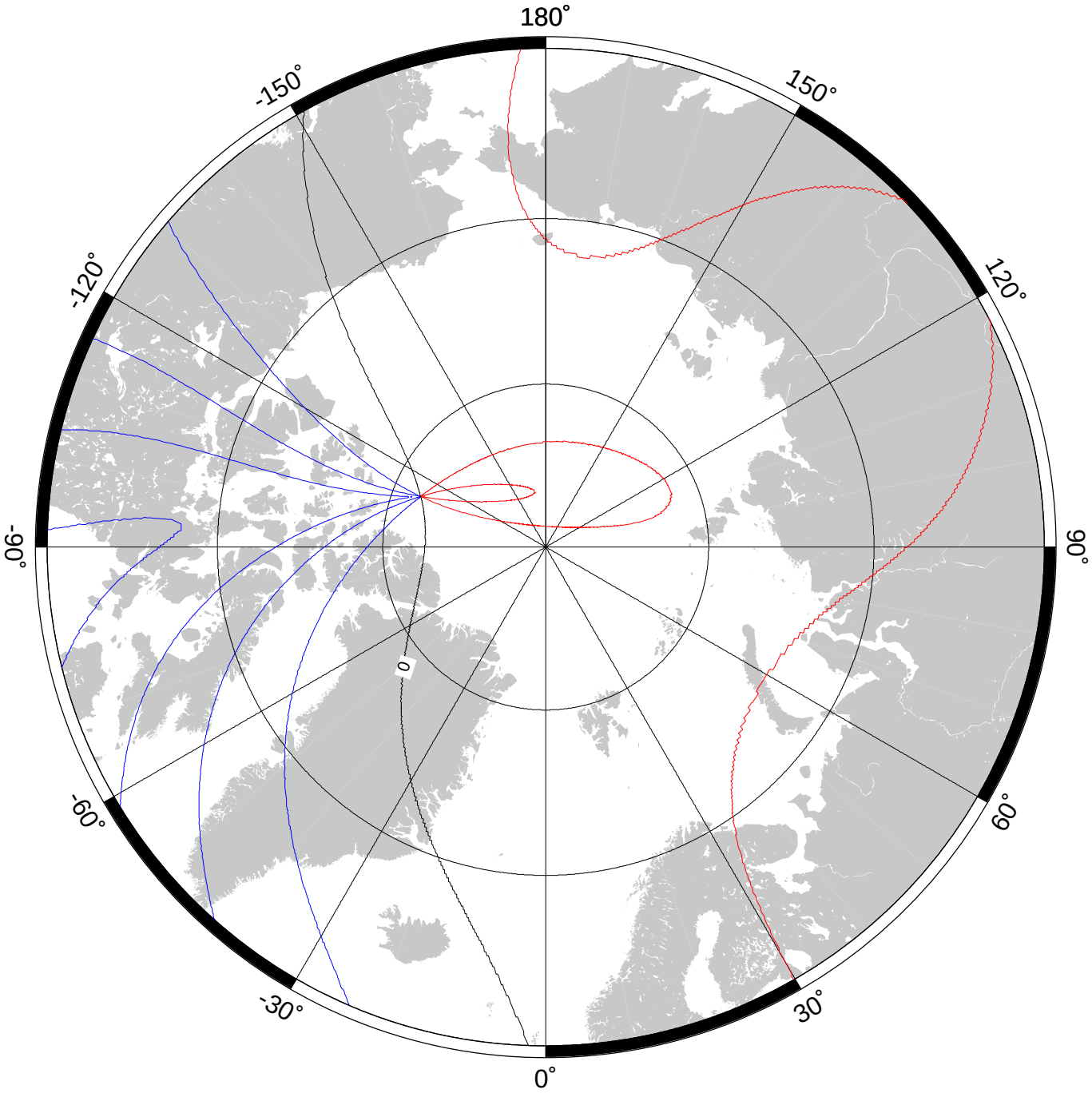

Annual rate of change of inclination in region of north pole for 2000.0 to 2005.0 from the World Magnetic Model (WMM2000). Red - positive change, blue - negative change, black - zero change. Contour interval is 1´/year and projection is Polar Stereographic.

Figure 224

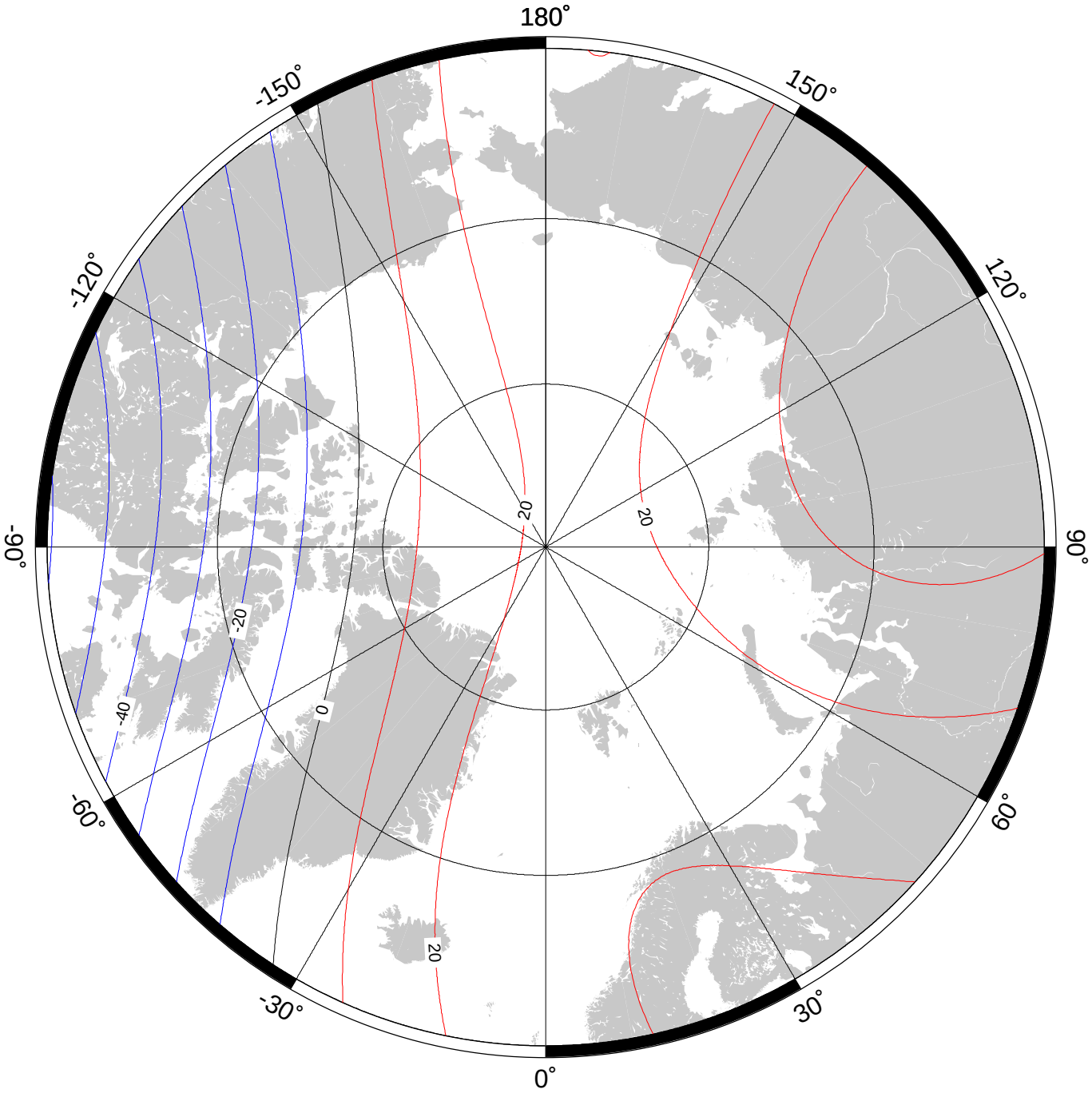

Annual rate of change of total intensity in region of north pole for 2000.0 to 2005.0 from the World Magnetic Model (WMM2000). Red - positive change, blue - negative change, black - zero change. Contour interval is 10 nT/year and projection is Polar Stereographic.

Figure 225

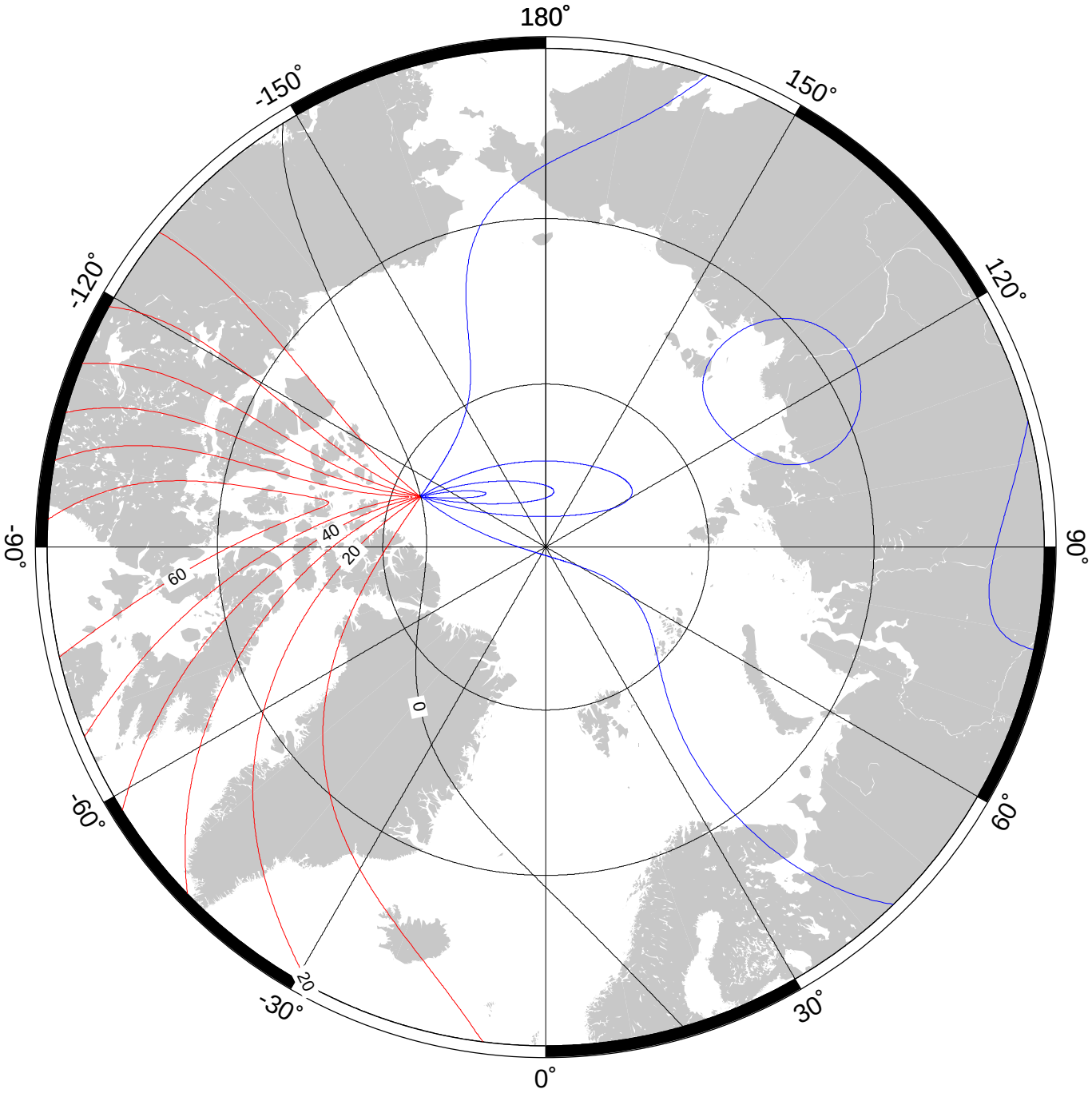

Annual rate of change of horizontal intensity in region of north pole for 2000.0 to 2005.0 from the World Magnetic Model (WMM2000). Red - positive change, blue - negative change, black - zero change. Contour interval is 10 nT/year and projection is Polar Stereographic.

Figure 226

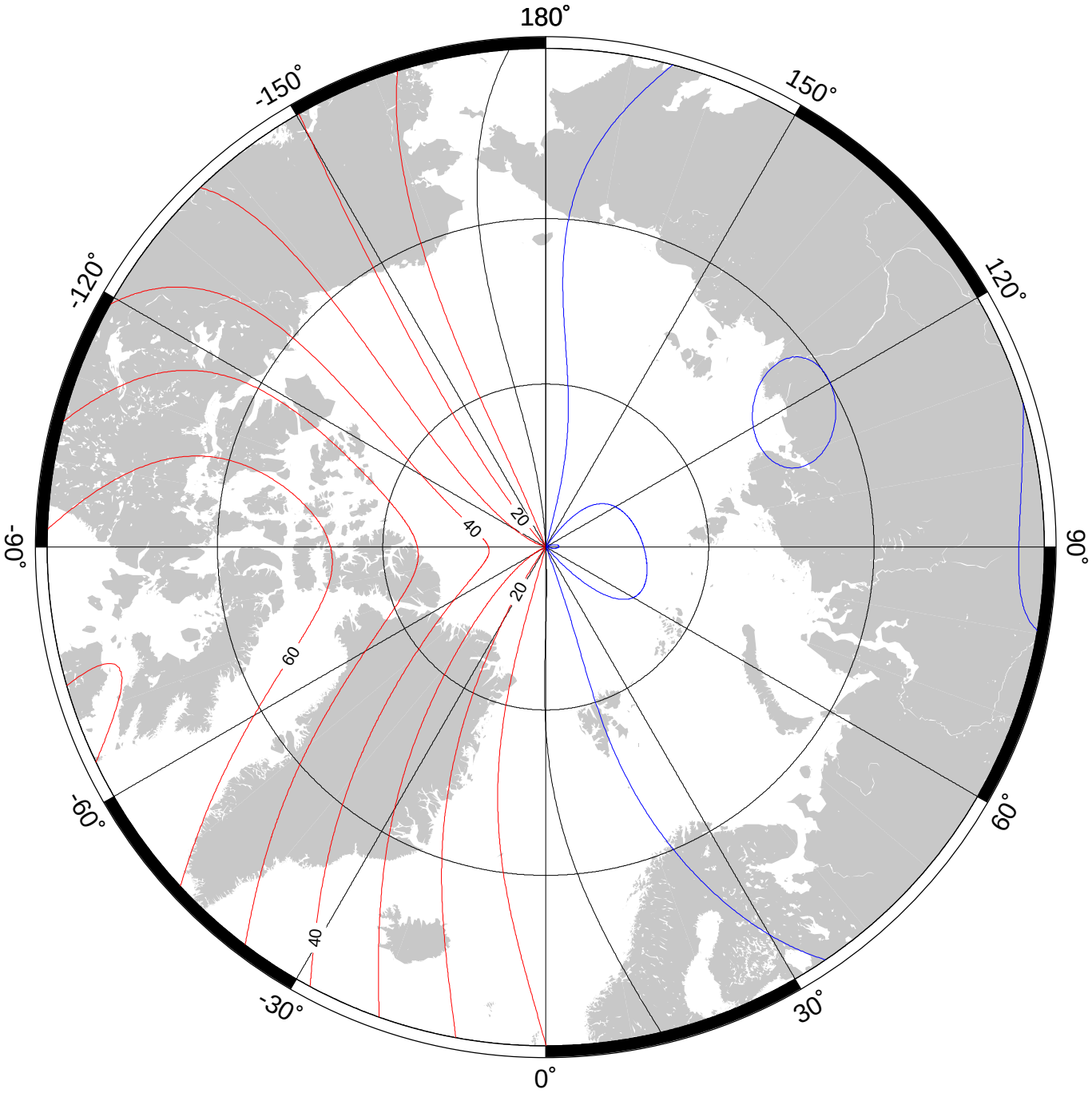

Annual rate of change of north component in region of north pole for 2000.0 to 2005.0 from the World Magnetic Model (WMM2000). Red - positive change, blue - negative change, black - zero change. Contour interval is 10 nT/year and projection is Polar Stereographic.

Figure 227

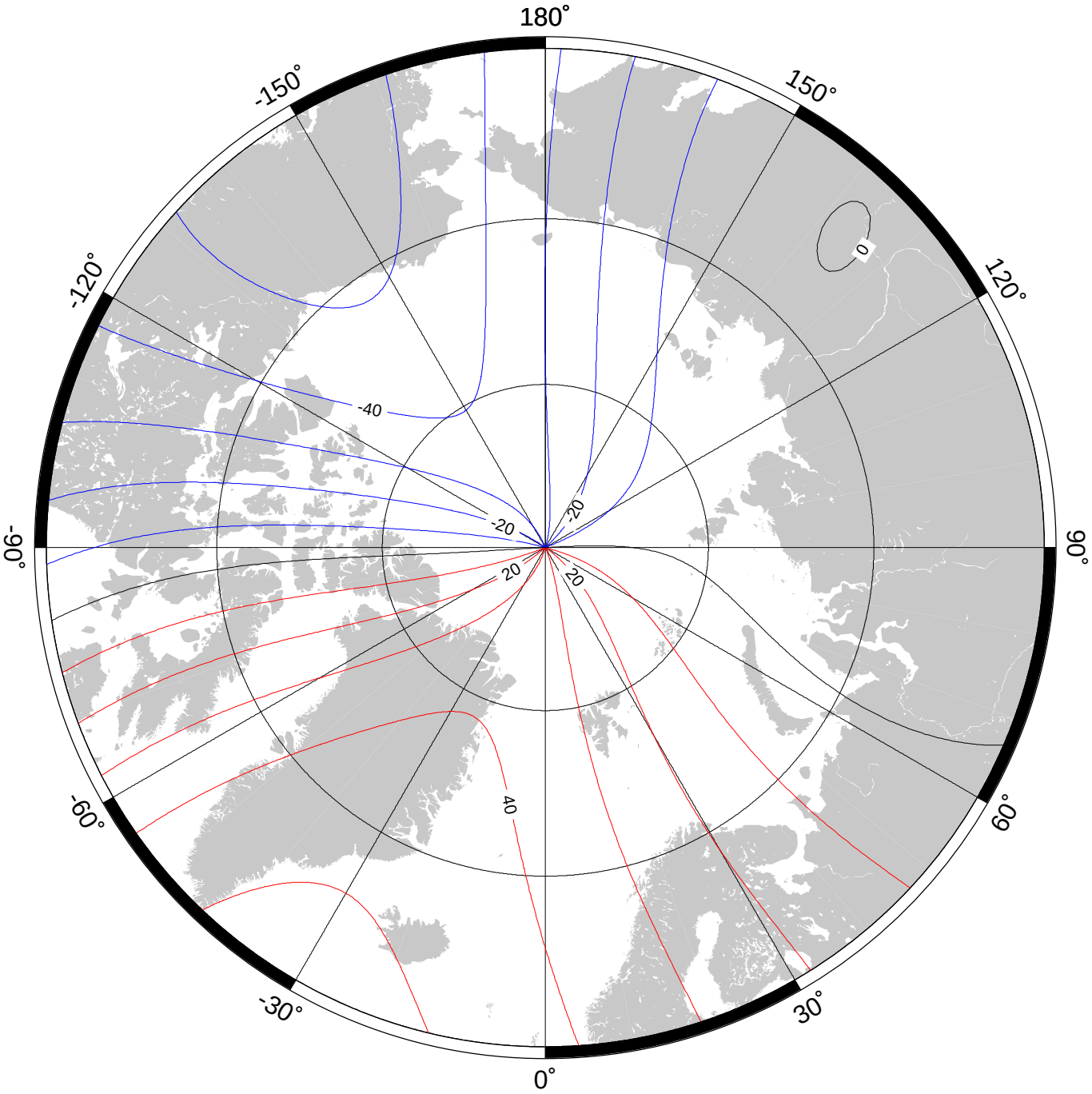

Annual rate of change of east component in region of north pole for 2000.0 to 2005.0 from the World Magnetic Model (WMM2000). Red - positive change, blue - negative change, black - zero change. Contour interval is 10 nT/year and projection is Polar Stereographic.

Figure 228

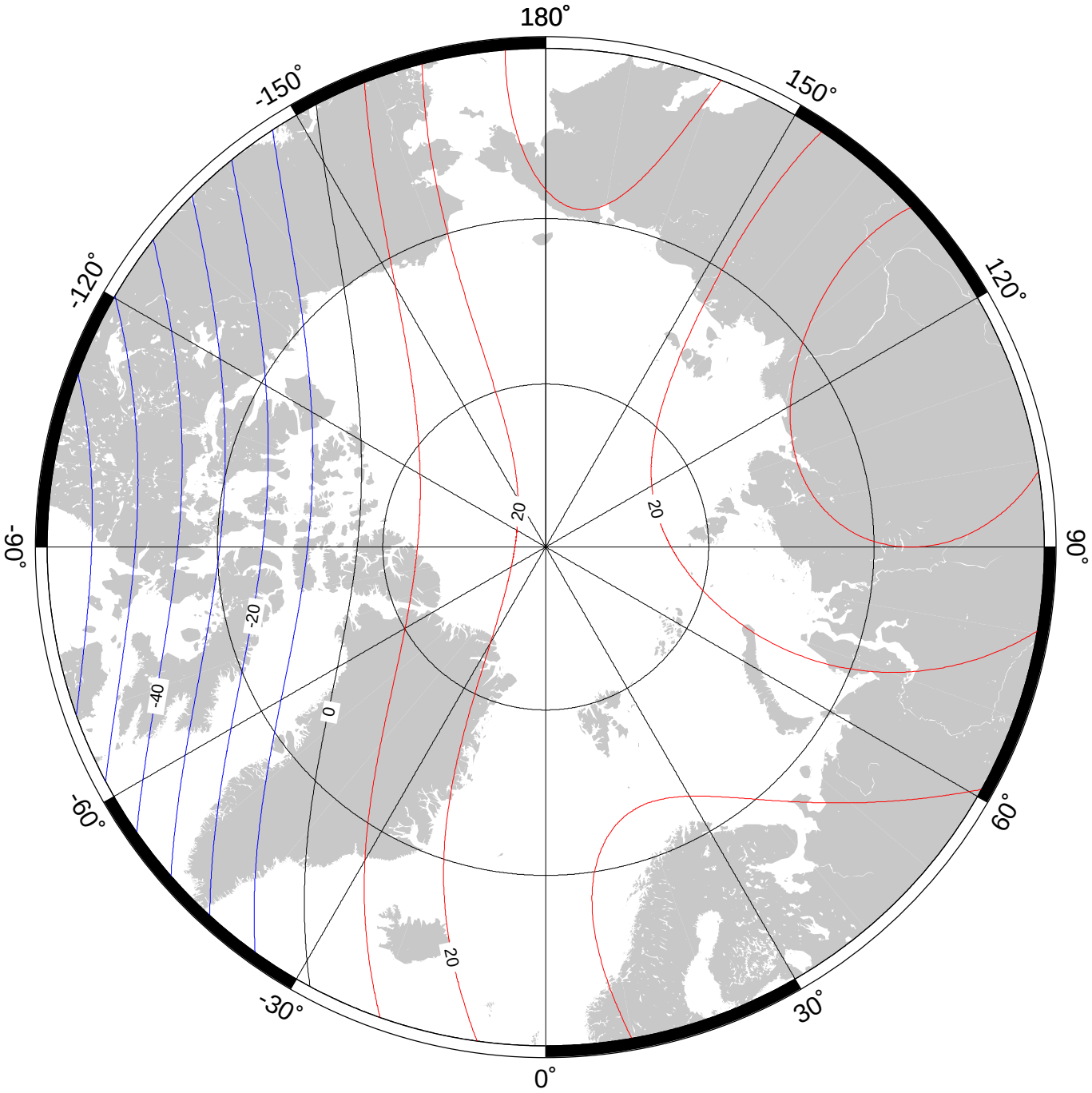

Annual rate of change of vertical component in region of north pole for 2000.0 to 2005.0 from the World Magnetic Model (WMM2000). Red - positive change, blue - negative change, black - zero change. Contour interval is 10 nT/year and projection is Polar Stereographic.

Figure 229

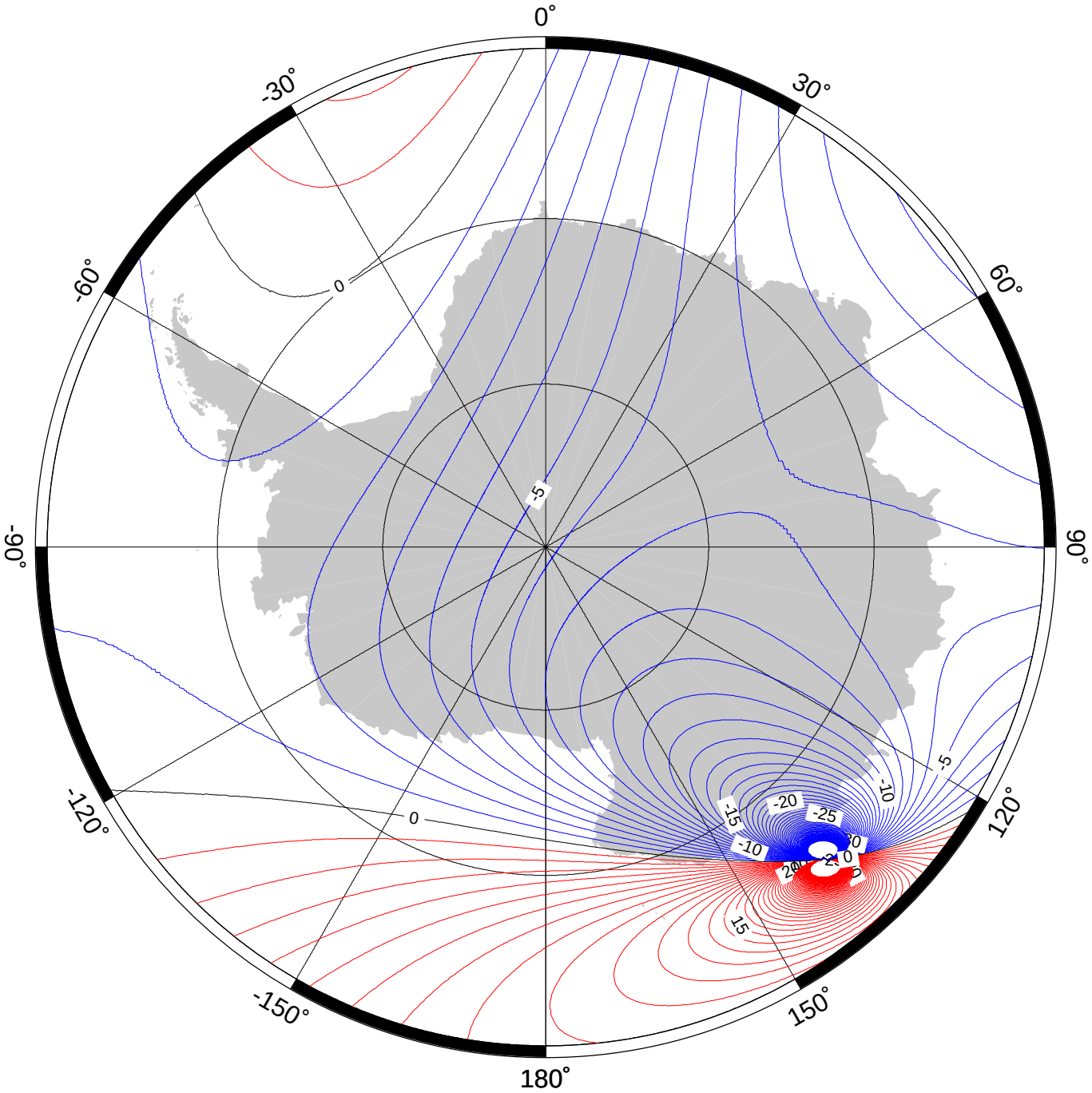

Annual rate of change of declination in region of south pole for 2000.0 to 2005.0 from the World Magnetic Model (WMM2000). Red - easterly change, blue - westerly change, black - zero change. Contour interval is 1´/year up to ±60´/year and projection is Polar Stereographic.

Figure 230

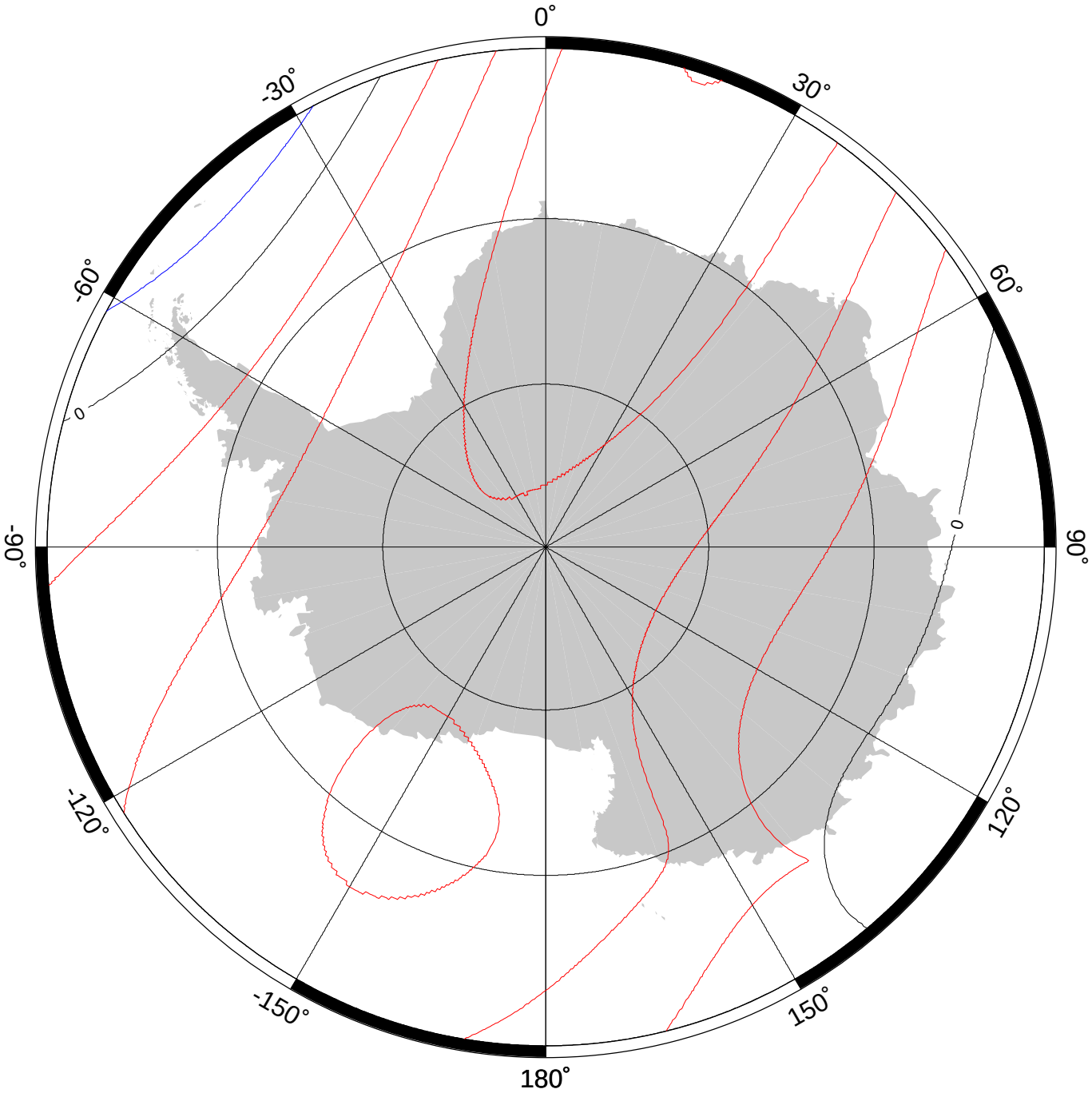

Annual rate of change of inclination in region of south pole for 2000.0 to 2005.0 from the World Magnetic Model (WMM2000). Red - positive change, blue - negative change, black - zero change. Contour interval is 1´/year and projection is Polar Stereographic.

Figure 231

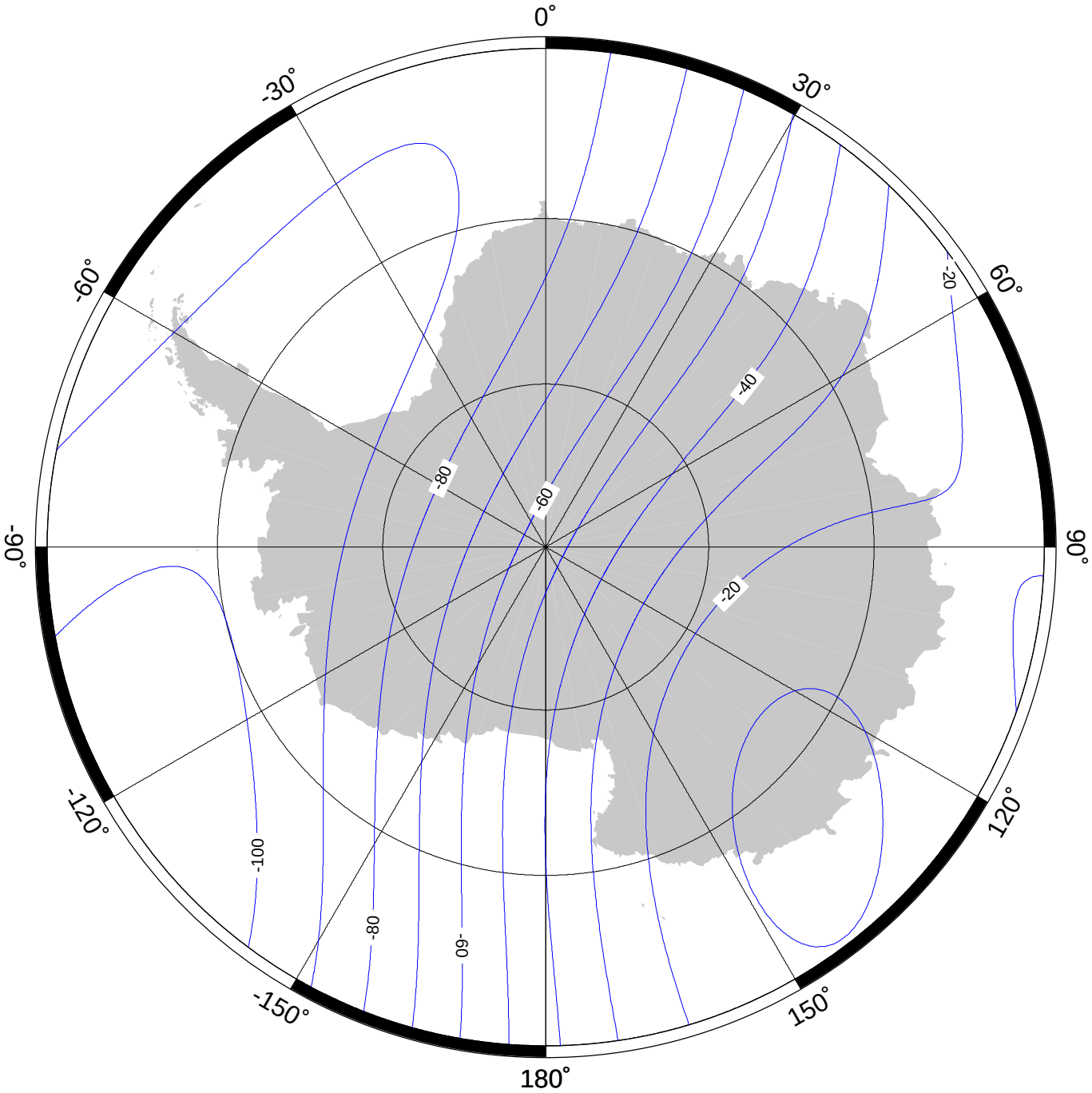

Annual rate of change of total intensity in region of south pole for 2000.0 to 2005.0 from the World Magnetic Model (WMM2000). Contour interval is 10 nT/year and projection is Polar Stereographic.

Figure 232

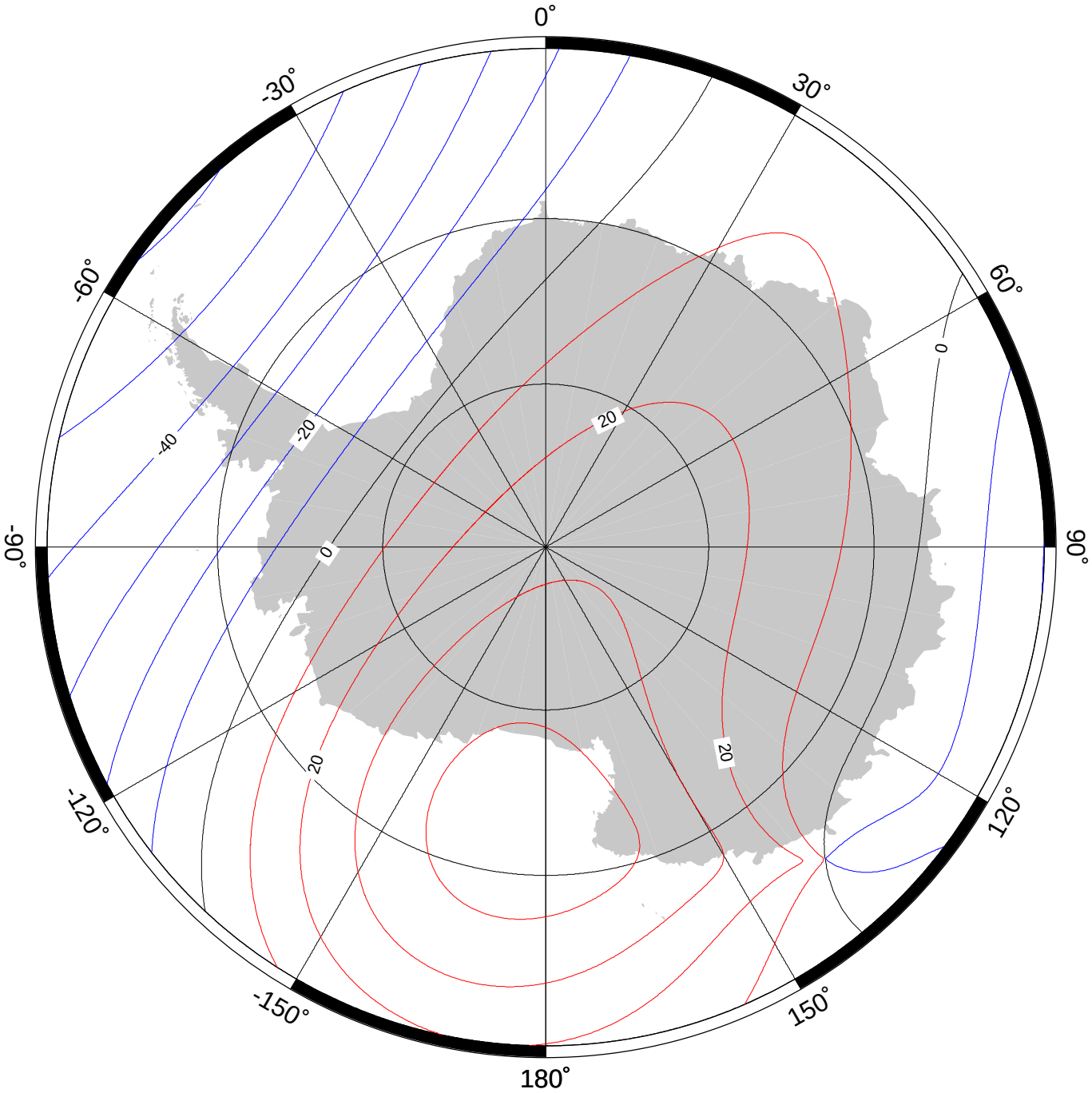

Annual rate of change of horizontal intensity in region of south pole for 2000.0 to 2005.0 from the World Magnetic Model (WMM2000). Red - positive change, blue - negative change, black - zero change. Contour interval is 10 nT/year and projection is Polar Stereographic.

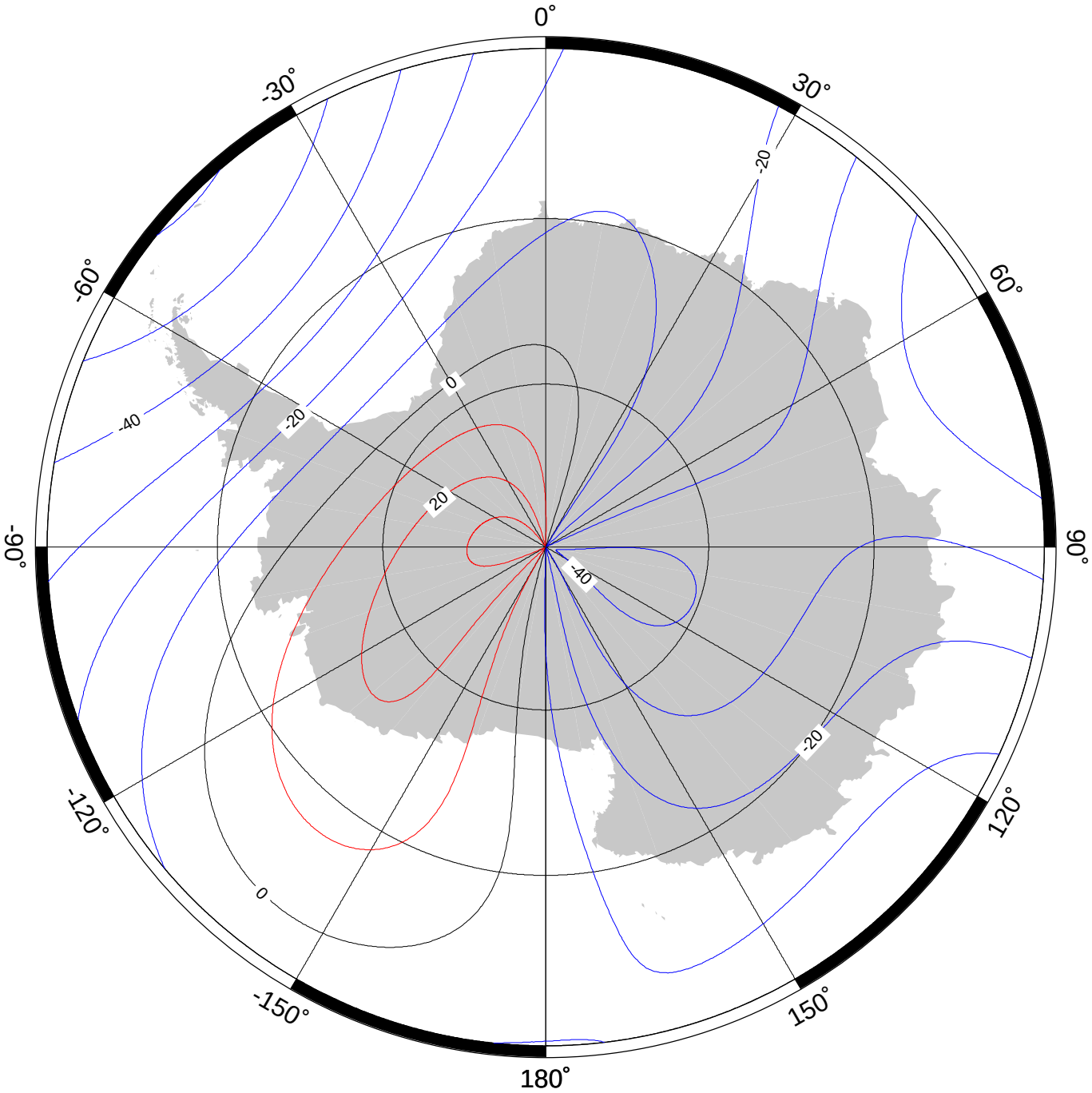

Annual rate of change of north component in region of south pole for 2000.0 to 2005.0 from the World Magnetic Model (WMM2000). Red - positive change, blue - negative change, black - zero change. Contour interval is 10 nT/year and projection is Polar Stereographic.

Figure 234

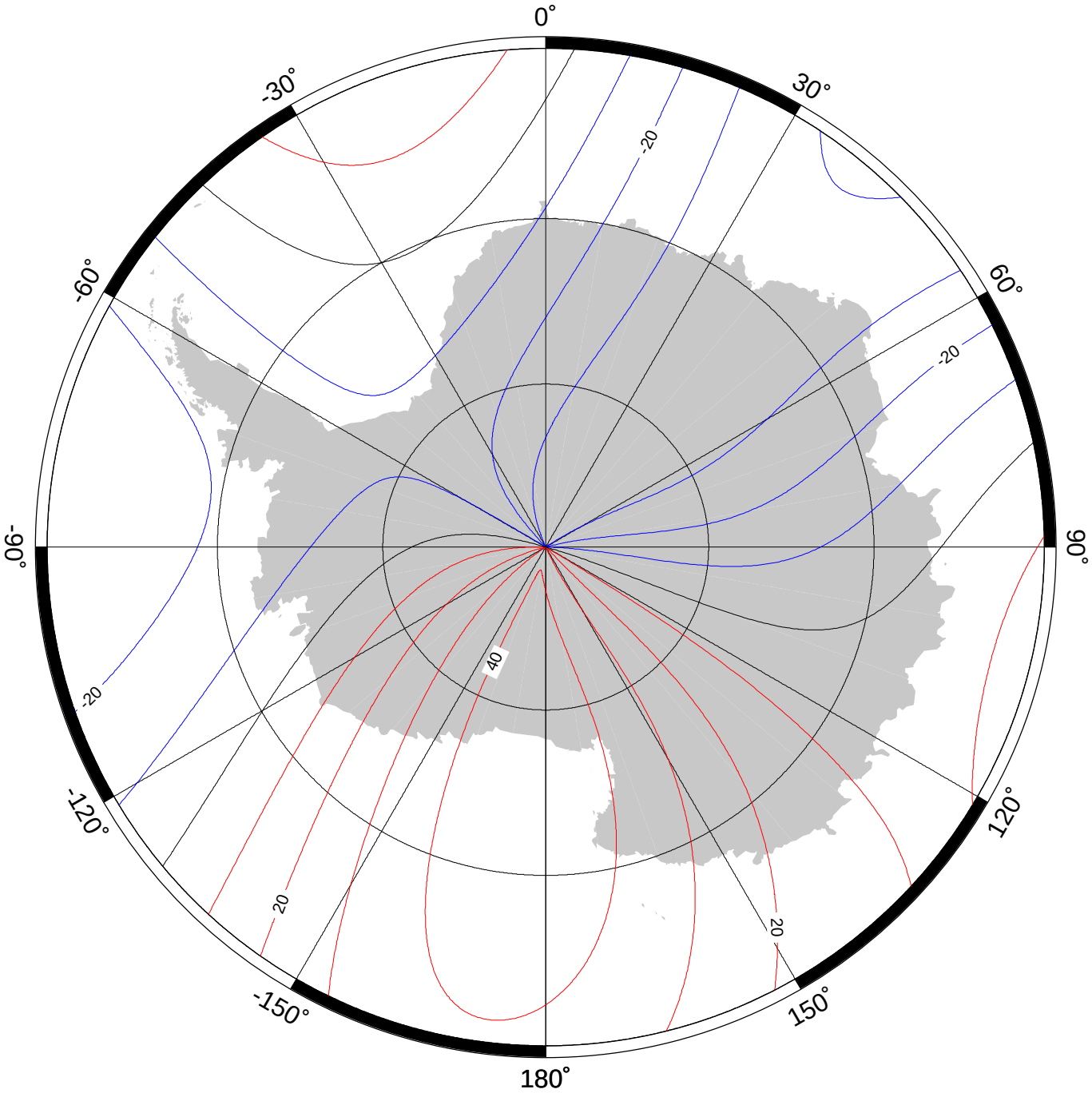

Annual rate of change of east component in region of south pole for 2000.0 to 2005.0 from the World Magnetic Model (WMM2000). Red - positive change, blue - negative change, black - zero change. Contour interval is 10 nT/year and projection is Polar Stereographic.

Figure 235

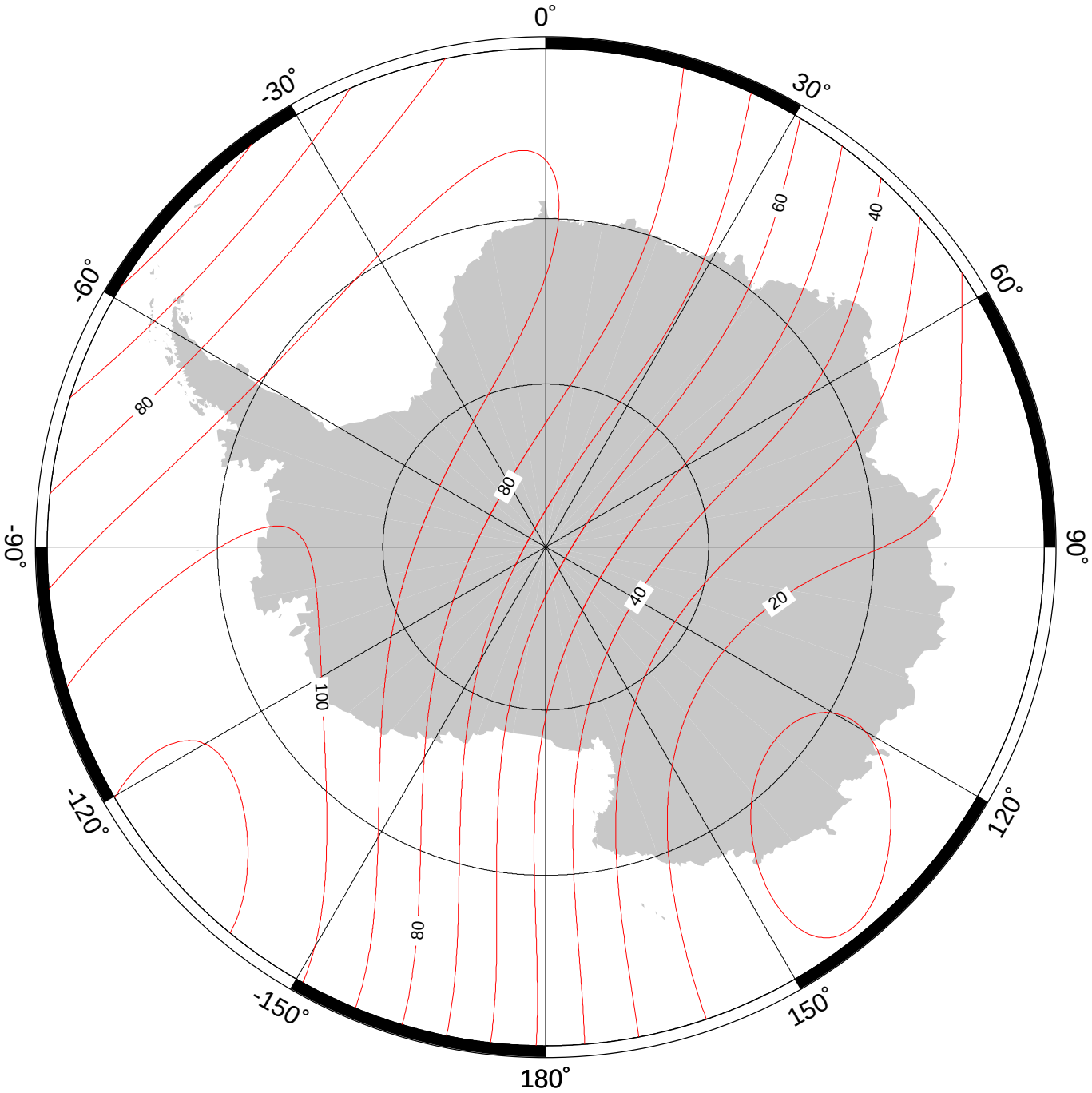

Annual rate of change of vertical component in region of south pole for 2000.0 to 2005.0 from the World Magnetic Model (WMM2000). Contour interval is 10 nT/year and projection is Polar Stereographic.

Figure 236